Syntheses and Structure-Activity Relationship Studies of Schwarzinicine Alkaloids as Vasorelaxant Agents

Lee Fong Kai

A dissertation submitted in fulfilment of the requirements for the degree of

Doctor of Philosophy

University of Nottingham Malaysia

Faculty of Science and Engineering

School of Pharmacy

March 2020

Acknowledgements

First and foremost, I would like to express my deepest gratitude to my main supervisor, Dr Lim Kuan Hon for giving me the opportunity to work on this interesting project and for all his support and guidance throughout the project. It has been a valuable experience to work alongside him and his enthusiasm, hard work and vision in his life served as a great inspiration for me to be a better researcher and a person in general. At the same time, I would like to thank my co-supervisor, Professor Ting Kang Nee for all her feedback in pharmacological aspects of my work. I am also greatly indebted to everyone who has contributed to my research; Mei Kee, Kayatri, Yin Ying and Leanne, who helped out in my organ bath experiments. I thank Premanand, who is a PhD student in our group, for his general assistance in laboratory related matters, particularly in chiral HPLC isolation work and also supplying natural schwarzinicine compounds to me as references and for biological studies. In addition, I would like to express my sincere gratitude to Dr Jason Loo Siau Ee from School of Pharmacy, Taylor's University for calculating the ECD spectra of several compounds that are reported in this dissertation. I thank Dr Low Yun Yee from Chemistry Department, University of Malaya for his advice in the organic synthetic aspects of my project and not forgetting Miss Dawn Sim and Mr Wong Soon Kit for their help in running NMR experiments for my compounds. Last but not least, I am grateful to my family and friends for supporting me in my studies.

Abstract

Hypertension has emerged as one of the leading risk factors responsible for global burden and mortality. Among the hypertensive patients, there is a segment of patients who are suffering from resistant hypertension, whose blood pressure cannot be controlled despite concurrently taking three or more classes of antihypertensive drugs. The adverse effects associated with the common classes of antihypertensive agents used have limited the combinations available to be used in treating resistant hypertension. Natural products play a vital role in drug discovery and development as they represent promising sources of useful lead molecules, in which they might be able to address the resistant hypertension issue. Our group has recently isolated from a previously uninvestigated *Ficus* species (*F. schwarzii*) a series of nine new phenethylamine alkaloids, namely, schwarzinicines A–G (**142–148**) and schwarzificusines A (**149**) and B (**150**). Schwarzinicine A (**142**), being the most abundant alkaloid of this series, was found to exhibit pronounced vasorelaxant effects in rat isolated aorta. In this study, we have successfully developed the total syntheses of schwarzinicines A (**142**), B (**143**) and F (**147**). In order to explore the active pharmacophore of schwarzinicine A (**142**) as a lead compound for vasorelaxation, several series of analogues were designed, synthesized and evaluated for their vasorelaxant activity for structure-activity relationship (SAR) analysis. In addition to the discovery of 13 synthetic analogues that were shown to be promising for further development, the SAR study revealed a few structural features that are associated with enhancement of vasorelaxant effects. These structural features could be useful to design better vasorelaxant agents in the future.

Abbreviations

ABSSSI	acute bacterial skin and skin structure infections
AcOH	acetic acid
ACE	angiotensin-converting enzyme
ARB	angiotensin-receptor blocker
AT_1-R	angiotensin II type I receptor
aq.	aqueous
Bn	benzyl
N-Boc	*N*-*tert*-butoxycarbonyl
BOP	(benzotriazol-1-yloxy)tris(dimethylamino)phosphonium hexafluorophosphate
CABP	community-acquired bacterial pneumonia
CCB	calcium channel blocker
CDI	carbonyldiimidazole
CE	Common Era
conc.	concentrated
COSY	correlation spectroscopy
CPCM	conductor-like polarizable continuum model
DCC	dicyclohexylcarbodiimide
DFT	density functional theory
DIBAL-H	diisobutylaluminium hydride
DMAP	4-dimethylaminopyridine
DMP	Dess-Martin periodinane
DMPEA	3,4-dimethoxyphenethylamine
DMSO	dimethyl sulfoxide
DBP	diastolic blood pressure

ECD	electronic circular dichroism
EDC	1-ethyl-3-(3-dimethylaminopropyl)carbodiimide
Et	ethyl
EtOH	ethanol
Et_2O	diethyl ether
Et_3N	triethylamine
equiv.	equivalent
EtOAc	ethyl acetate
FDA	Food and Drug Administration
h	hour
HDAC	histone deacetylase
HMBC	heteronuclear multiple bond correlation
HPLC	high performance liquid chromatography
HRESIMS	high resolution electrospray ionization mass spectrometry
HSQC	heteronuclear single quantum coherence
IN	integrase
IR	infrared
LDA	lithium diisopropylamide
Me	methyl
MeOH	methanol
min	minute
MS	molecular sieves
MW	molecular weight
m/z	mass-to-charge ratio
n-BuLi	*n*-butyllithium
NMO	4-methylmorpholine *N*-oxide
NMR	nuclear magnetic resonance

NOESY	nuclear Overhauser effect spectroscopy
PE	phenylephrine
PEA	phenethylamine
Ph	phenyl
PMHS	polymethylhydrosiloxane
ppm	parts per million
t_R	retention time
rt	room temperature
SAR	structure-activity relationship
SBP	systolic blood pressure
SCLC	small cell lung carcinoma
SD	Sprague Dawley
SEM	standard error of the mean
SHR	spontaneously hypertensive rat
TDDFT	time-dependent density functional theory
TFA	trifluoroacetic acid
THF	tetrahydrofuran
TLC	thin layer chromatography
TMS	tetramethylsilane
TPAP	tetrapropylammonium perruthenate

Contents

Acknowledgements I

Abstract II

Abbreviations III

1 Introduction

1.1 Hypertension 1

1.1.1 Antihypertensive agents 2

1.1.1.1 Angiotensin-converting enzyme (ACE) inhibitors 2

1.1.1.2 Angiotensin-receptor blockers (ARBs) 4

1.1.1.3 β-Blockers 5

1.1.1.4 Thiazide-type diuretics 7

1.1.1.5 Calcium channel blockers (CCBs) 8

1.1.2 Resistant hypertension 10

1.2 Natural products in drug development 11

1.2.1 Plant-based antihypertensive agents 14

1.3 Structure-activity relationship (SAR) studies and strategies in drug design 16

1.3.1 Simplification 17

1.3.2 Ring variations 19

1.3.3 Chain extension/contraction 21

1.3.4 Structural extension 23

1.3.5 Rigidification 24

1.3.6 Bioisosterism 27

1.3.7 Substituent variation 29

1.4 The genus *Ficus* 30

1.4.1 Alkaloids from the genus *Ficus* 31

1.4.2 Alkaloids from *Ficus schwarzii* 39

1.5 Research aims 41

2 Total syntheses of schwarzinicine alkaloids

2.1 Overview 43

2.1.1 Grignard reaction 44

2.1.2 Weinreb ketone synthesis 45

2.1.3 Reductive amination 47

2.2 Total syntheses of schwarzinicines A (**142**) and B (**143**) 50

2.2.1 Attempts to synthesize **142** and **143** 50

2.2.1.1 Retrosynthetic analysis 50

2.2.1.2 First attempt: Grignard reaction based on benzyl nitriles 51

2.2.1.3 Second attempt: Grignard reaction based on benzyl aldehydes 53

2.2.1.3.1 Synthesis of 3,4-dimethoxyphenylacetaldehyde (**177b**): Reduction of nitrile **177a** 53

2.2.1.3.2 Synthesis of 3,4-dimethoxyphenylacetaldehyde (**177b**): Oxidation of alcohol **183** 54

2.2.1.4 Third attempt: Weinreb ketone synthesis 57

2.2.2 Fourth approach to synthesize **142** and **143** 60

2.2.2.1 Retrosynthetic analysis 60
2.2.2.2 Full synthetic route to **142** and **143** 61
2.3 Total synthesis of schwarzinicine F (**147**) 68
2.3.1 First attempt to synthesize **147** 68
2.3.1.1 Retrosynthetic analysis 68
2.3.1.2 Synthetic studies to **147** 69
2.3.2 Second approach to synthesize **147** 76
2.3.2.1 Retrosynthetic analysis 76
2.3.2.2 Full synthetic route to **147** 77
2.4 Summary 86

3 Syntheses of schwarzinicine analogues

3.1 Overview 87
3.1.1 Strategies for analogue design for SAR studies 87
3.2 Preparation of analogues based on Weinreb ketone synthesis and/or reductive amination 90
3.3 Attempted *O*-demethylation of schwarzinicine analogue **215a** 95
3.4 Attempted preparation of schwarzinicine A isostere (**220**) 99
3.4.1 First attempt 99
3.4.2 Second attempt 100
3.5 Preparation of *N*-substituted schwarzinicine analogues 103
3.5.1 *N*-Alkylation of analogue **215b** 103
3.5.2 Quaternization of amines **215b** and **217b** 104
3.6 *N*-Boc deprotection of schwarzinicine analogue **215z** 107
3.7 Summary 112

4 Pharmacological evaluations and SAR studies of schwarzinicine alkaloids and synthetic analogues

4.1 Overview 113

4.1.1 Organ bath assay 113

4.1.2 Rationale for selecting rat aortic tissue for organ bath assay 114

4.1.3 Laboratory rats 115

4.2 *In vitro* vasorelaxant activity of schwarzinicines A–D (**142–145**) and F (**147d**) on SD rats 116

4.3 *In vitro* vasorelaxant activity of synthetic schwarzinicine analogues 119

4.3.1 SAR analysis 123

4.3.1.1 Aromatic methoxy substituents 123

4.3.1.2 Phenyl rings A, B and C 124

4.3.1.3 Ring variation 126

4.3.1.4 Chain length 130

4.3.1.5 Structural extension 132

4.3.1.6 Rigidification 133

4.3.1.7 Ionization state of central nitrogen atom 134

4.3.1.8 Electron withdrawing and donating substituents on phenyl rings 135

4.3.1.9 Stereochemistry 137

4.4 *In vitro* vasorelaxant activity of selected compounds on spontaneously hypertensive rats (SHRs) 138

4.5 Summary 141

5 Future work

5.1 Future studies 145

5.1.1 Proposed approach to total synthesis of schwarzinicine G

(**148**) 145

5.1.2 Perpetuation of SAR studies 146

5.1.3 Further studies on SHRs 149

6 Experimental

6.1 Chemistry 150

6.1.1 Total syntheses of schwarzinicines A (**142**) and B (**143**) 151

6.1.1.1 Synthesis of 3,4-dimethoxyphenylacetaldehyde (**177b**) 151

6.1.1.2 Full synthetic route to **142** and **143** 152

6.1.2 Total synthesis of schwarzinicine F (**147**) 157

6.1.2.1 First attempt 157

6.1.2.2 Second approach 164

6.1.3 Synthesis of schwarzinicine analogues 167

6.1.3.1 Preparation of Weinreb amides from carboxylic acids 167

6.1.3.2 Preparation of Weinreb amides from acyl chlorides 175

6.1.3.3 Weinreb ketone synthesis 178

6.1.3.4 Reductive amination 192

6.1.3.5 *O*-Demethylation of schwarzinicine analogue **215a** 228

6.1.3.6 Reduction of ketone **191a** 229

6.1.3.7 Tosylation of alcohol **221** 230

6.1.3.8 Formation of amides **230a–c** 231

6.1.3.9 Reduction of amides **230a–c** 234

6.1.3.10 Quaternization of amines **215b** and **217b** 236

6.1.3.11 *N*-Boc deprotection of schwarzinicine analogue **215z** 238

6.2 Computational analysis 239
6.3 Pharmacological testing 239
6.3.1 Chemicals and reagents 239
6.3.2 Tissue preparation 240
6.3.3 Effects of compounds against phenylephrine (PE)-induced contraction in aorta 241
6.3.4 Data analysis and statistics 241

References 243

Appendix 272

1

Introduction

1.1 Hypertension

Hypertension, also known as high blood pressure, is a medical condition in which the systolic blood pressure (SBP) and diastolic blood pressure (DBP) in the arteries are persistently elevated with SBP/DBP being at or above 140/90 mm Hg.[1] In 2000, about 26% of the adult population in the world had hypertension and this number is projected to increase to about 29% by 2025.[2] According to the Global Burden of Disease study, which is the largest and most comprehensive analysis of global health and disease, hypertension has emerged as one of the leading risk factors responsible for disease burden and mortality worldwide.[3] It is associated with a number of modern-day diseases such as stroke, renal failure and cardiovascular diseases.[4]

The causes of hypertension may be due to some of the lifestyle risk factors including obesity, high alcohol and salt intake.[4] Hypertension can be managed through nonpharmacological and/or pharmacological approaches. In the first case, lifestyle interventions such as weight loss (for patients who are obese), heart-healthy diet, increase physical exercise, reduce sodium and alcohol intake are recommended by experts to manage hypertension.[5] For the second case when lifestyle interventions are insufficient, antihypertensive drugs are used to significantly reduce the risk of contracting cardiovascular diseases, stroke and heart failure via reduction of high

blood pressure.[6,7] There are currently several classes of antihypertensive drugs in the market, namely, angiotensin-converting enzyme (ACE) inhibitors, angiotensin-receptor blockers (ARBs), β-blockers, calcium channel blockers (CCBs) and thiazide-type diuretics.[1,8] Each of these classes is briefly described in terms of their mechanism of actions, main uses, sub-classifications and complications/adverse effects in the following section.

1.1.1 Antihypertensive agents

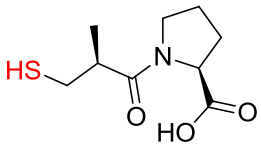
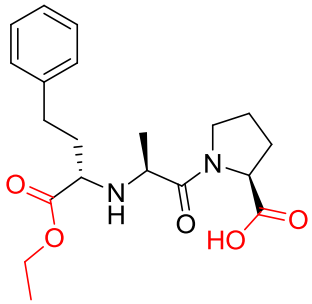
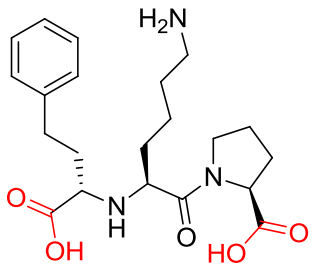
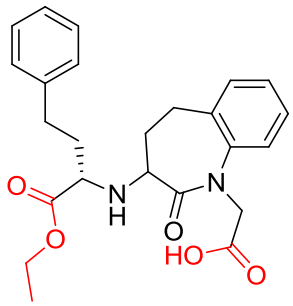
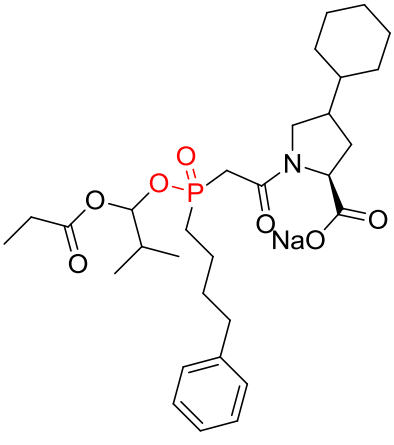
1.1.1.1 Angiotensin-converting enzyme (ACE) inhibitors

ACE inhibitors are primarily used to treat hypertension and also myocardial infarction, heart failure, renal failure and diabetic nephropathy.[9] This class of pharmacological agents works by blocking the conversion of angiotensin I to angiotensin II, an important component in the renin-angiotensin-aldosterone system responsible for the regulation of arterial blood pressure.[10,11]

ACE inhibitors can be divided into three classes as shown in Table 1.1 based on their structural differences.[9] The first ACE inhibitor, captopril[12] (**1**) was developed based on the known inhibitors of carboxypeptidase A, a zinc-containing metalloprotease and possessing a sulfhydryl group that acts as a ligand for the zinc moiety at the active site of ACE.[13] ACE inhibitors with a dicarboxyl group such as enalapril[12] (**2**), lisinopril[12] (**3**) and benazepril[14] (**4**) were later developed since captopril (**1**) was associated with unpleasant side effects such as skin rashes and loss of taste due to its sulfhydryl group.[15] The potency of these compounds is associated with the presence of the carboxyl group which has better binding to ACE and tissue penetration.[16] The –SH group of the sulfhydryl inhibitors, the –COOH group of the dicarboxylate compounds and the phosphonic acid group of the phosphorus-containing agents (fosinopril[17] (**5**)) are the key functional groups (Table 1.1) that

interact with the zinc ion of ACE to exhibit their inhibitory effects.[18] ACE inhibitors are associated with common side effects such as coughing, hypotension, hyperkalemia and angioedema.[10]

Table 1.1. Classes of ACE inhibitors with key functional groups for binding interaction highlighted in red

Class	ACE inhibitor
Sulfhydryl-containing agents	 **1** Captopril
Dicarboxyl-containing agents	 **2** Enalapril  **3** Lisinopril  **4** Benazepril
Phosphorus-containing agents	 **5** Fosinopril

1.1.1.2 Angiotensin-receptor blockers (ARBs)

Similar to ACE inhibitors, ARBs are used primarily for the treatment of hypertension. ARBs work by blocking the action of angiotensin II at the angiotensin II type I receptor (AT_1-R), which mediates most of the known actions that cause hypertension.[19,20] Development of ARBs began with the synthesis of losartan[20] (**6**, Figure 1.1), the first orally active, selective, potent, non-peptide and imidazole-type ARB.[11] Other ARBs that are synthesized (Figure 1.1) based on losartan (**6**) or its metabolites (as molecular templates) include valsartan[20] (**7**), irbesartan[21] (**8**) and telmisartan[22] (**9**).[23] Valsartan (**7**) that has an acylated amino acid instead of the imidazole in losartan (**6**), is as effective and well-tolerated in hypertensive patients as losartan (**6**).[24] Irbesartan (**8**) and telmisartan (**9**) may be more effective than both losartan (**6**) and valsartan (**7**) in providing better 24-hour control of blood pressure due to their longer-acting durations.[25]

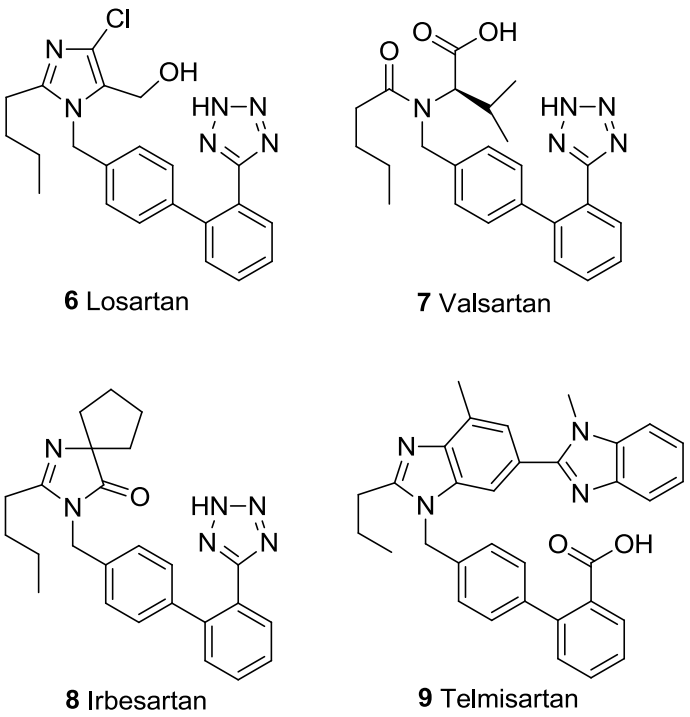


Figure 1.1. Chemical structures of selected ARBs

ARBs are mainly used in treatments where patients are intolerant to ACE inhibitor therapy.[26] For example, telmisartan (**9**) modestly decreased the risk of cardiovascular death, myocardial infarction or stroke in high-risk patients intolerant to ACE inhibitors, as telmisartan (**9**) is well tolerated in these patients.[26] The adverse effect of coughing due to the use of ACE inhibitors can be overcome with the use of ARBs instead, e.g., valsartan (**7**) showed comparable therapeutic efficacy as lisinopril (**3**) but induces significantly less cough in hypertensive patients.[27]On the other hand, ARBs shares some of the same adverse effects as ACE inhibitors, i.e., headache and dizziness.[28]

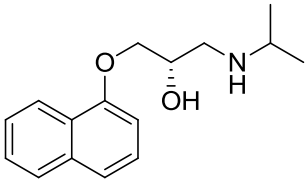
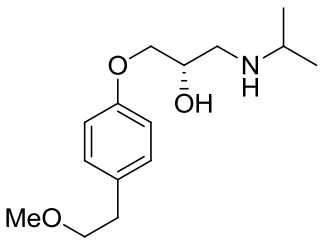
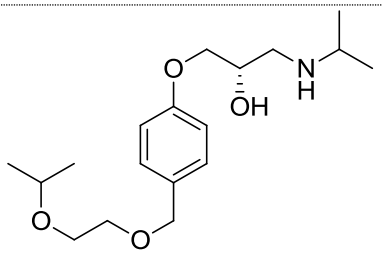
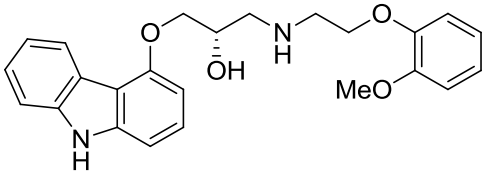
1.1.1.3 β-Blockers

β-Blockers are used in heart failure therapy particularly for long term secondary prevention after myocardial infarction.[29] Activation of the β_1-adrenergic receptors increases heart rate, therefore β-blockers work by binding preferentially and reversibly to β_1-adrenergic (as oppose to β_2-adrenergic) receptors, acting as competitive antagonists to endogenous catecholamines, noradrenaline and adrenaline, which can overstimulate the activity of the receptors.[30] On the other hand, the β_2-adrenergic receptors which are predominatly found in vascular and bronchial smooth muscle are responsible for smooth muscle relaxation in gastrointestinal tract and bronchi upon activation.[31]

β-Blockers that are available for clinical use can be grouped into three generations[32] and they are shown in Table 1.2.[33] Propranolol (**10**) represents the first clinically used β-blocker with its introduction in 1968 as an antianginal agent.[32] The first generation β-blockers are non-selective agents with equal affinities towards β_1- and β_2-adrenergic receptors.[32] The second-generation β-blockers, on the other hand,

are selective towards β_1-adrenergic receptors.[32] Selected examples of second-generation β-blockers include metoprolol (**11**) and bisoprolol (**12**), which were shown to reduce mortality in patients with chronic heart failure.[34,35] Third generation β-blockers may be selective or non-selective towards β-adrenergic receptors with favourable ancillary properties such as vasodilation which are desirable to treat hypertension.[32]

Table 1.2. Classification of β-blockers and selected examples

Generation	β-Blocker
First	 **10** Propranolol
Second	 **11** Metoprolol  **12** Bisoprolol
Third	 **13** Carvedilol

For example, carvedilol (**13**) is a β antagonist (prevents reflex tachycardia) with vasodilating properties (due to α_1-adrenergic receptor blockade).[36] As a result, the cardiac performance in patients with heart failure improved significantly when treated with carvedilol (**13**) compared to metoprolol (**11**) and the difference may be attributed to the greater antiadrenergic activity of carvedilol (**13**).[37] Some of the

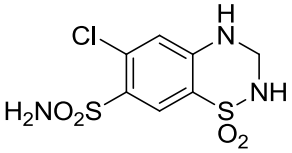
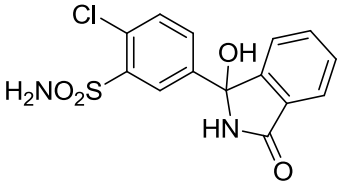
adverse effects of β-blockers are bronchospasm, heart failure, bradycardia, Raynaud's syndrome and fatigue.[38]

1.1.1.4 Thiazide-type diuretics

Thiazide and thiazide-type diuretics are recommended as the first-line drug treatment for patients with uncomplicated hypertension.[1] They exert their diuretic action via inhibition of the Na^+/Cl^- co-transporter in the renal distal convoluted tubule.[39–41] An increase in fluid loss to urine due to decreased Na^+ reabsorption leads to a reduction in extracellular fluid and plasma volume.[42] The volume loss is accompanied by reduced total peripheral resistance, increased renin stimulation and decreased blood pressure.[43,44]

Chlorothiazide[12] (**14,** Table 1.3) was the first thiazide diuretic used for the treatment of hypertension more than half a century ago[45] and since then related thiazide and thiazide-like diuretics (as shown in Table 1.3) are used for management of hypertension.[46] Although both thiazide and thiazide-like diuretics are structurally similar, they possess rather different pharmacokinetics.[47] For instance, hydrochlorothiazide[14] (**15**) has a half-life of 3.2–13.1 hours and its half-life is considered to be very short compared to chlorthalidone[48] (**16**), representing a thiazide-like diuretic, which has an extremely long half-life of 40–60 hours.[47] Thus, chlorthalidone (**16**) is more effective in lowering systolic blood pressure than hydrochlorothiazide (**15**), particularly related to overnight blood pressure reduction due to its longer elimination half-life.[49]

Table 1.3. Examples of thiazide and thiazide-like diuretics

Type	Compound
Thiazides	 **14** Chlorothiazide  **15** Hydrochlorothiazide
Thiazide-like diuretics	 **16** Chlorthalidone

Some adverse effects of thiazide and thiazide-like diuretics include electrolyte defects, metabolic abnormalities, hyponatremia and hyperuricemia.[50] Other adverse effects associated with diuretics including hypokalemia, hypomagnesemia and glucose intolerance may be countered with the combined administration of an ACE inhibitor or an ARB.[50]

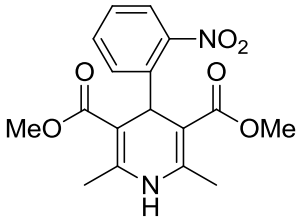
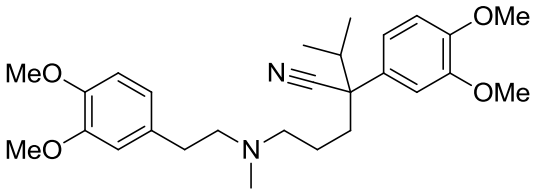
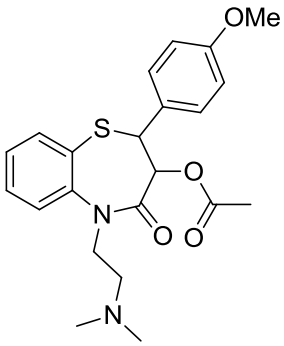
1.1.1.5 Calcium channel blockers (CCBs)

The fundamental role of CCBs is to inhibit L-type calcium channels in the vascular smooth muscle and the heart.[51] The L-type calcium channels are part of the voltage-gated calcium channel family that is responsible for the excitation-contraction coupling process of skeletal, smooth and cardiac muscles and are involved in aldosterone production in adrenocortical tissues.[52,53] Excessive plasma aldosterone levels will cause arterial hypertension, cardiac failure and its related disease processes.[52,53]

CCBs are divided into three classes as shown in Table 1.4 with distinctive structures and pharmacological properties.[54] Nifedipine[55] (**17**) is a long-acting

vasodilator in managing angina with the absence of myocardial depressant effects and antiarrhythmic properties.[56,57] Verapamil[55] (**18**) is used to treat re-entrant supraventricular arrhythmias, while only moderately effective as an antianginal agent.[56,57] Diltiazem[55] (**19**) is efficacious in treating angiospastic angina.[56]

Table 1.4. Classification of selected CCBs

Class	Compound
Dihydropyridines	 **17** Nifedipine
Phenylalkylamines	 **18** Verapamil
Benzothiazepines	 **19** Diltiazem

The side effects of nifedipine (**17**) include headache, flush, dizziness, fatigue, hypotension, tachycardia and ankle edema.[51] The side effects of verapamil (**18**) are less serious compared to those of nifedipine (**17**), which include headache, flush, constipation and impairment of atrioventricular conduction.[51] The side effects of

diltiazem (**19**) are somewhat intermediate between those of nifedipine (**17**) and verapamil (**18**), namely impairment of atrioventricular conduction.[51,57]

1.1.2 Resistant hypertension

Although antihypertensive medications are widely available to treat high blood pressure, there is a segment of patients who are suffering from resistant hypertension, whose blood pressure remains above goal (140/90 mm Hg) despite concurrent use of three or more antihypertensive drugs from different classes.[58] In addition to lifestyle factors, the underlying secondary causes of resistant hypertension include hyperaldosteronism, chronic kidney disease, renal artery stenosis and obstructive sleep apnoea.[59] These patients are exposed to a higher risk of cardiovascular complications and mortality.[60]

The current pharmacological treatment for resistant hypertension is the 3-drug regimen, which consists of an ACE inhibitor/ARB, a long-acting CCB and a long-acting thiazide-like diuretic.[60] This is coupled with a mineralocorticoid receptor agonist used as a fourth agent.[61] Despite the substantial increase in scientific studies in resistant hypertension, there is no single drug that has been approved specifically for the treatment of hypertension.[62] Moreover, the uses of drug combinations in the treatment of hypertension are often limited by adverse effects associated with the particular class of antihypertensive drug as mentioned in Section 1.1.1.[63] The current situation, therefore, reveals a significant gap in the antihypertensive arsenal, which requires an urgent expansion to include new agents that act via novel mechanism of action to address the resistant hypertension issue.

1.2 Natural products in drug development

Natural products play an important role in drug discovery as they often serve as useful leads in the development of pharmaceutical drug molecules and in some instances have been directly used as drug candidates in various therapeutic areas. About one-third of all Food and Drug Administration (FDA)-approved drug molecules are natural products or their derivatives.[64] In 2018, out of the 59 new FDA-approved drugs, 10 were inspired by natural products.[65] In the area of oncology, close to half of the 175 drug molecules approved for clinical use from 1940 to 2014, are either natural products or molecules derived from natural products.[66]

Natural products that have the desired pharmacological or biological activity have often attracted medicinal/synthetic chemists to produce and study them in the laboratory. In general, natural products possess rich structural diversity and complexity that are unsurpassed by any synthetic and combinatorial compound libraries.[67] With therapeutic applications in mind, medicinal chemists use natural products as lead compounds and have come up with biologically active mimics in the drug development process. The important chemical functional groups or elements of structural complementarity in natural product molecules to their biological targets are retained in these mimics.[68] In other words, natural products serve as templates in designing and synthesizing simpler analogues, which exhibit comparable or better activities than the parent natural products.

Selected recent examples of natural products (Figure 1.2) that have been successfully developed into useful therapeutic agents (approved for use in the clinic) include ingenol mebutate[66] (**20**) for the treatment of actinic keratosis,[69,70] homoharringtonine (**21**) for the treatment of chronic myeloid leukemia,[71,72]

cannabidiol (**22**) for the treatment of epilepsy,[73] fidaxomicin (**23**) for the treatment of *Clostridium difficile* infection[74] and trabectedin (**24**) for the treatment of advanced soft tissue sarcoma.[75]

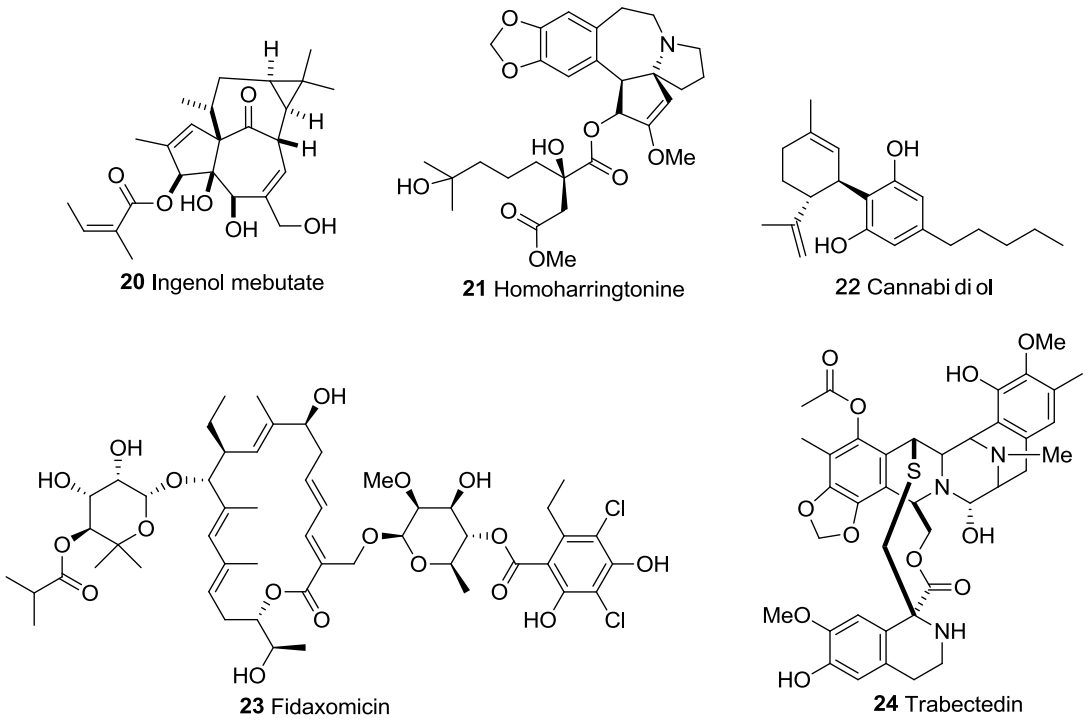


Figure 1.2. Selected examples of drugs available in the market that are originally natural products

An assessment of the source of natural product drugs revealed that plants (25%) are the best producers followed by bacteria (16%) and fungi (12%).[64] For instance, ingenol mebutate (**20**), homoharringtonine (**21**) and cannabidiol (**22**) were obtained from plants (i.e., *Euphorbia peplus, Cephalotaxus fortunei* and *Cannabis sativa*, respectively),[69,71,72,76] while fidaxomicin (**23**) and trabectedin (**24**) were obtained from a microbial source (i.e., *Dactylosporangium aurantiacum*)[74] and a marine source (i.e., *Ecteinascidia turbinata*)[77], respectively.

Selected examples of drug molecules (Figure 1.3) that were derived from natural products and recently approved for use in clinic include eravacycline (**25**) for

the treatment of complicated intra-abdominal infections, sarecycline (**26**) for the treatment of severe acne vulgaris, and omadacycline (**27**) for the treatment of community-acquired bacterial pneumonia (CABP) and acute bacterial skin and skin structure infections (ABSSSI).[73,78] These tetracycline antibiotics were developed based on naturally occurring tetracyclines (Figure 1.3), notably chlortetracycline (**28**) and oxytetracycline (**29**), which were isolated from the bacteria *Streptomyces aureofaciens* and *Streptomyces rimosus*, respectively.[79]

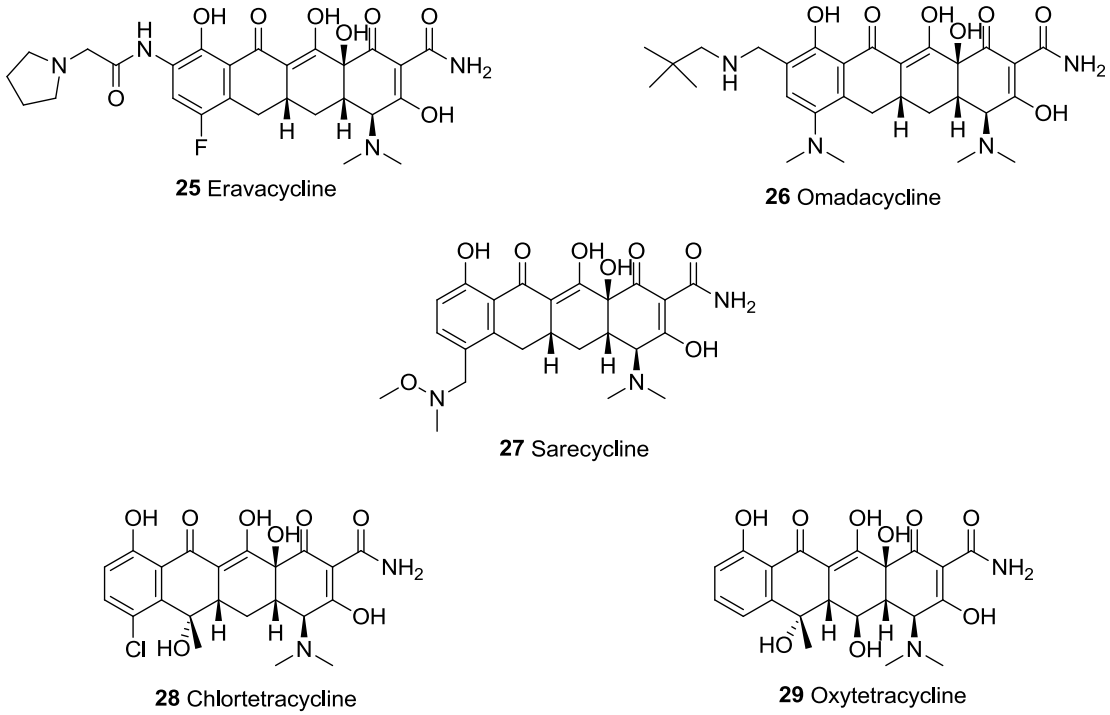


Figure 1.3. Synthetic tetracycline antibiotics (**25–27**) derived from naturally occurring tetracyclines (**28** and **29**)

Additionally, the development of topotecan (**30**, Figure 1.4), used for the treatment of small cell lung carcinoma (SCLC), and fingolimod (**31**, Figure 1.4), approved for the treatment of multiple sclerosis, are also inspired by natural products.[80–82] Topotecan (**30**) was derived based on camptothecin (**32**, Figure 1.4), an alkaloid isolated from the Chinese tree *Camptotheca acuminata*,[81] while fingolimod

(**31**) was designed and synthesized based on myriocin (**33**, Figure 1.4), a fungal metabolite isolated from *Isaria sinclairii*.[82]

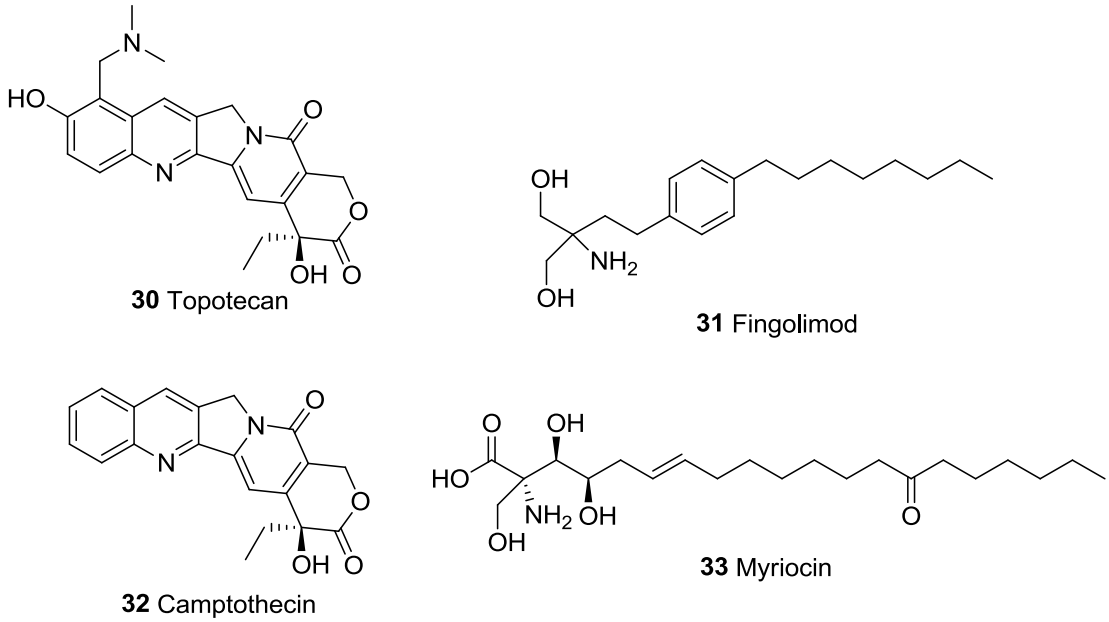


Figure 1.4. Examples of synthetic drugs derived from natural products (**30** and **31** derived from **32** and **33**, respectively)

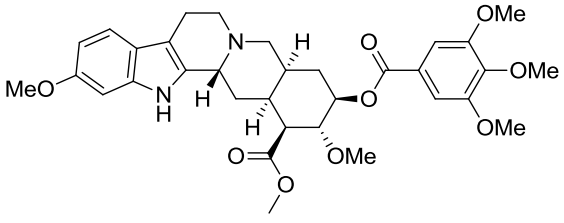
1.2.1 Plant-based antihypertensive agents

Medicinal plants have been used extensively for the treatment of diseases such as control of blood pressure since the dawn of human civilization. About 80% of the world's population depend on plant-based medicines for their primary healthcare.[83] In fact, phytotherapy is considered to be preferred over the use of conventional medicines (ACE inhibitors, ARBs, diuretics and CCBs) by rural dwellers in controlling hypertension due to the cost of current medication and adverse effects.[84]

The antihypertensive effects of some of the medicinal plants, including herbs, spices and basic cooking ingredients, have been investigated and validated.[85] Common herbs and spices that have antihypertensive potential include garlic (*Allium sativum*), lemongrass (*Cymbopogon citratus*), roselle (*Hibiscus sabdariffa*), Chinese

sage (*Salviae miltiorrhizae*) and ginger (*Zingiber officinale*).[86] It is not uncommon that hypertensive patients use these or other herbal remedies to help manage their blood pressure in addition to taking prescribed antihypertensive medication. Unfortunately, the risk of adverse interactions due to the concomitant use of these medicinal plants with conventional antihypertensive medicines is not entirely known.[87]

The common methods of investigating antihypertensive properties of medicinal plants include testing of the plant extracts or isolating and testing the pure compounds derived from the extracts. Most of the plants mentioned in the above paragraph were tested *in vivo* using their extracts from the different plant parts. Additionally, various pure secondary metabolites isolated from plants such as alkaloids (e.g., from *Uncaria rhynchophylla*[88] and *Stephania tetrandrae*[89]), flavonoids (e.g., from *Hibiscus sabdariffa*[90] and *Sedum sarmentosum*[91]), tannins (e.g., from Chinese herbs[92] and *Lumnitzera racemosa*[93]) and terpenoids (e.g., from *Andrographis paniculata*[94] and *Salvia cinnabarina*[95]) were also found to exhibit antihypertensive effects *in vivo*.



34 Reserpine

Figure 1.5. Reserpine as a drug to treat hypertension

One of the most well-known plant secondary metabolite that is used to treat hypertension is reserpine[12] (**34**, Figure 1.5), an alkaloid isolated from Indian snakeroot (*Rauwolfia serpentina*), which is a plant traditionally used in India to treat insanity, fever and snakebites.[96] Reserpine (**34**) was first approved by the FDA as a first-line

drug for the treatment of hypertension in the late 1950s.[96] However, it is now less commonly used as a second-line treatment due to the development of newer antihypertensive agents with superior side effect profiles.[97]

1.3 Structure-activity relationship (SAR) studies and strategies in drug design

One of the main aims of undertaking SAR studies of a biologically active molecule is to determine its pharmacophore, which broadly refers to the key chemical/functional groups and their disposition in 3-D space within the molecule, that are responsible for the observed biological activity.[12] Ideally, SAR studies will also reveal the parts of the structure that are dispensable, which potentially enable simpler, cost- and time-effective analogues to be designed and synthesized.[12] Simplistically, SAR can be done by synthesizing a number of analogues where only one particular part of the lead molecule is altered each time.[12] This is followed by the evaluation of biological activities of the analogues synthesized and the results obtained are compared to those of the lead compound. For example, a diminished activity for an analogue compared to the lead molecule may suggest that a particular chemical group in the lead molecule prior to alteration is essential/important for activity.[12] On the other hand, a particular chemical group may be regarded as nonessential if the activity of the analogue is comparable to that of the lead compound.[12]

Pharmacophoric determination based on SAR studies essentially serves as a crucial guide in designing analogues with improved therapeutic properties (e.g., greater potency and efficacy, lower toxicity and side effects) compared to the lead compound.[98] There are a number of strategies that are commonly used in drug design, which include simplification, ring variations, chain extension/contraction, structural

extension, rigidification, bioisosterism and substituent variation.[12] Each of these strategies will be explained and illustrated with relevant examples in the following sections.

1.3.1 Simplification

The simplification strategy broadly aims to address the question of whether the entire skeleton of the lead molecule is necessary for activity and if not how can it be simplified to make analogue synthesis more accessible and cost-efficient.[12] Therefore, this strategy involves removal of groups that are not part of the pharmacophore, which may include removal of non-essential functional groups, replacing cyclic structures with acyclic ones or removal of chiral centres from a complex lead compound.[12] As such, simpler analogues can be synthesized while retaining a good level of activity as the lead molecule. Furthermore, it was found that structurally less complex drug molecules have a higher chance of achieving market success.[99] Hence, this strategy is often applied to complex natural product leads. Selected examples of clinical drugs derived based on the simplification of complex natural products include bicyclol (**35**, Figure 1.6), vorinostat (**36**, Figure 1.7), and eribulin (**37**, Figure 1.8).[100] These examples are used to illustrate the application of simplification in SAR studies in the following paragraphs.

Schisandrin C (**38**, Figure 1.6), a dibenzocyclooctadiene lignan isolated from traditional Chinese medicine *Fructus Schizandrae*, was found to display promising antihepatitis B virus activity.[101] Its chemical structure was initially incorrectly determined as **39** (Figure 1.6).[100] A total synthesis was also performed based on the incorrect structure of **39**.[100] An intermediate of the synthesis, which is devoid of the eight-membered ring was serendipitously found to possess similar antihepatitis B

virus activity as the target compound. As a result, bicyclol (**35**), which is more synthetically accessible, was discovered and approved for the treatment of chronic viral hepatitis.[101] Furthermore, bicyclol (**35**) has improved solubility, *in vivo* absorption, bioavailability and biological activity.[102]

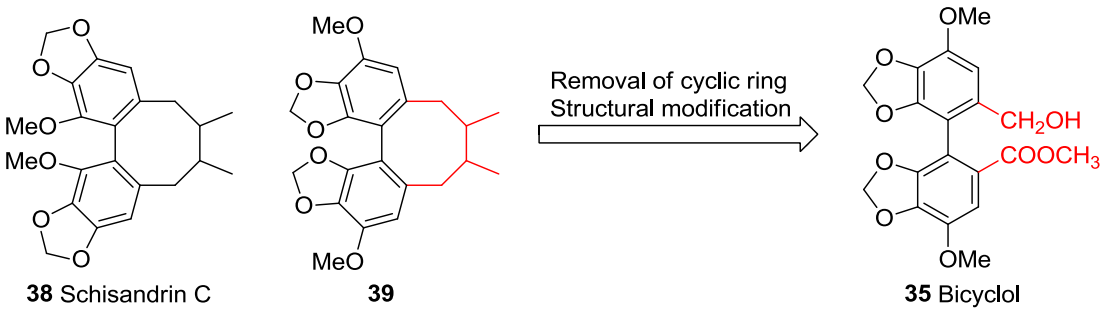


Figure 1.6. Structural simplification of schisandrin C (**38**)

Trichostatin A (**40**, Figure 1.7), a natural product isolated from the actinomycete *Streptomyces hygroscopicus*, exhibited inhibition of histone deacetylase (HDAC).[103] Abnormal expressions of HDACs are generally associated with tumour growth.[104] SAR studies showed that the molecule inhibited HDAC by chelating to the zinc ion in the active site of the HDAC enzyme via its hydroxamic acid group.[100] Its activity was not affected by the presence of the conjugated *trans* double bonds as well as the chiral center.[100] By eliminating the conjugated double bonds and the chiral center, a simpler analogue, namely vorinostat (**36**), was discovered and was approved for the treatment of cutaneous T-cell lymphoma.[105]

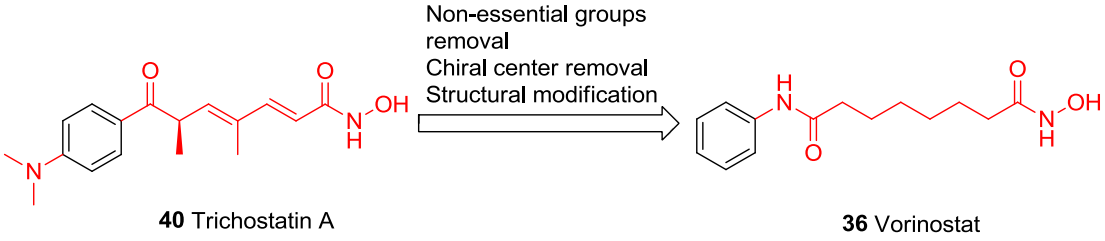


Figure 1.7. Structural simplification of trichostatin A (**40**)

Halichondrin B (**41**, Figure 1.8), a polyether macrolide isolated from the marine sponge *Halichondria okadai*, was shown to display promising antitumor properties.[106] However, its complex structure and scare supply from natural source present a huge challenge in total synthesis and drug development.[100] As a result, a molecule that has a major part of the molecule in halichondrin B (**41**) excluded was synthesized, giving rise to the discovery of eribulin (**37**), which was approved for the treatment of refractory metastatic breast cancer.[107]

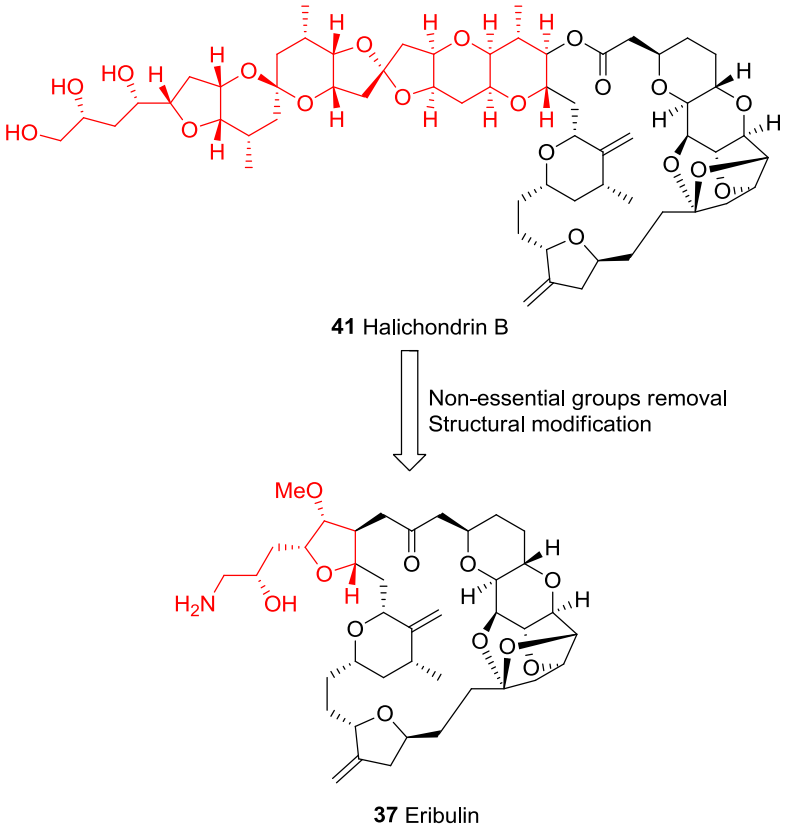


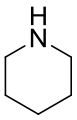
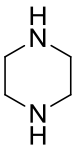
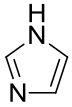
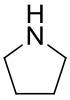
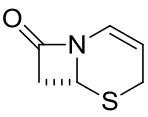
Figure 1.8. Structural simplification of halichondrin B (**41**)

1.3.2 Ring variations

Ring systems constitute the main components of the molecular framework present in most drug molecules available in the market.[108] They are widely used by medicinal chemists in drug design to manipulate the molecular properties of drugs (such as electronic, steric, lipophilicity and polarity) with the aim to affect therapeutic

properties, including absorption, distribution, metabolism and clearance of the drug molecules in a positive way.[109] With many different ring systems available for medicinal chemists to utilize in designing their desired molecules, the top 10 most frequently encountered ring systems (inclusive of aromatic/heteroaromatic/heterocyclic rings) in drug molecules are shown in Table 1.5.[108] While the list is not exhaustive, it is found that certain rings are generally more manipulable than others for the discovery of novel and bioactive drugs.[110]

Table 1.5. Top 10 most frequently used ring systems in drug molecules

1	**2**	**3**	**4**	**5**
				
Benzene	Pyridine	Piperidine	Piperazine	Cyclohexane
6	**7**	**8**	**9**	**10**
				
Oxane	Imidazole	Pyrrolidine	Cephem	Cyclopropane

The ring variation strategy involves the replacement of existing rings with other ring systems in the lead compound with the aim to improve its activity and selectivity profile.[12] The strategy of ring variation in drug design may be exemplified by the effort to develop an antifungal drug starting from the imidazole-containing compound tioconazole (**42**, Figure 1.9).[111] Based on the structure of tioconazole (**42**), molecule **43**[111] (Figure 1.9) emerged as one of the possible drug candidates to be developed into an antifungal agent.[112] It was later found that the imidazole group in **43** was susceptible to metabolic inactivation leading to poor oral bioavailability.[113] In

order to mitigate this problem, a range of substituted imidazoles as well as other heterocyclic systems were used to replace the imidazole group in **43**.[111] Subsequently, the 1,2,4-triazole derivative (**44**, Figure 1.9) was identified as the best candidate for further drug development as it was less susceptible to metabolic inactivation.[111]

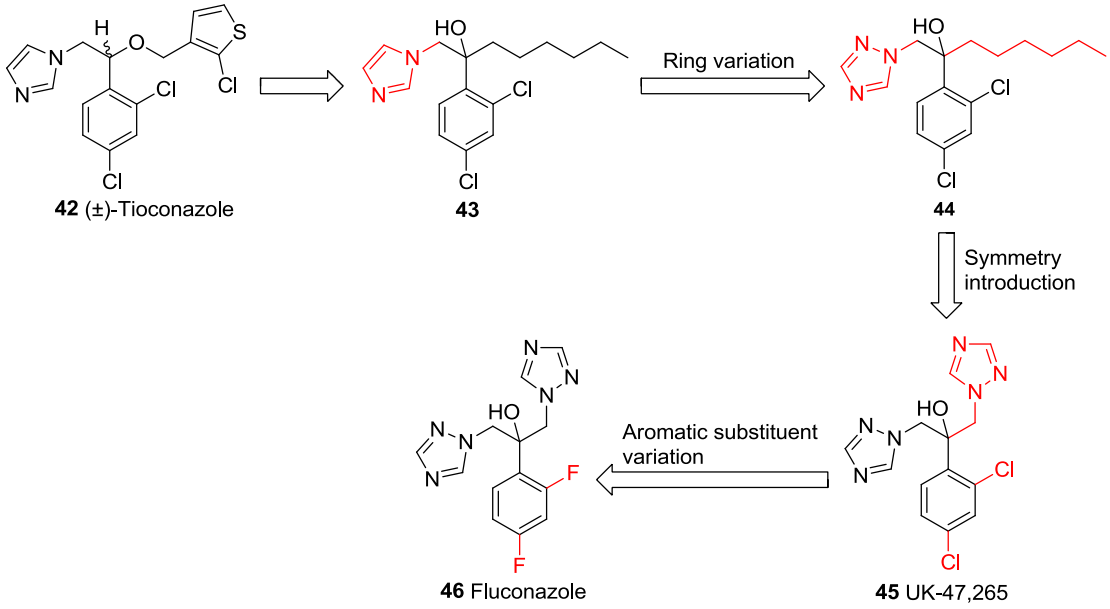


Figure 1.9. Development of tioconazole (**42**) into fluconazole (**46**)

At a later stage of the development, an element of symmetry was introduced to the molecule by replacing the hexyl side chain in **44** with a 1-methyl-1,2,4-triazole moiety to yield the symmetrical bis-triazole UK-47,265 (**45**, Figure 1.9).[111] Subsequently, the two aromatic chloro substituents in UK-47,265 (**45**) were replaced with two fluoro groups to finally yield fluconazole (**46**), an antifungal medication used for the treatment of a variety of fungal infections, particularly *Candida* infections.[111,114]

1.3.3 Chain extension/contraction

Chain extension/contraction may be a useful tactic in drug optimization when two binding groups are connected by a chain. The chain length may not be optimum in the

lead structure for the best interaction to occur between the binding groups on the ligand and the biological target site.[12] Thus, lengthening or shortening of the chain length may result in an overall stronger interaction between the ligand and receptor (Figure 1.10).[12]

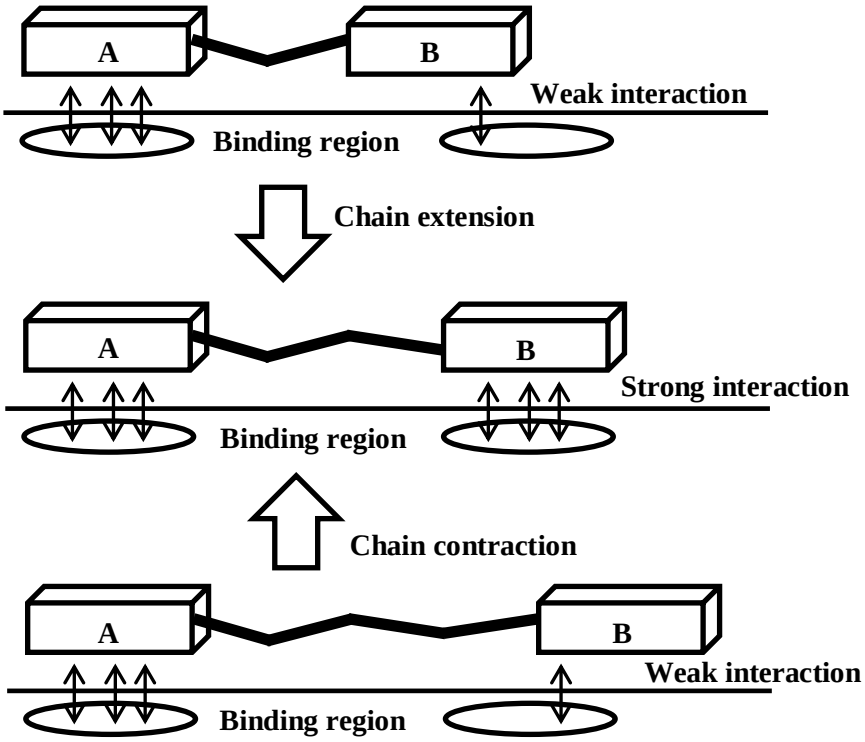


Figure 1.10. Chain extension/contraction involving two binding groups A and B on a ligand interacting with the binding region within a biological target site

The chain extension strategy can be illustrated by the development of enalaprilat (**47**, Figure 1.11), which is the active metabolite of enalapril (**2**), used as an ACE inhibitor for the treatment of hypertension and congestive heart failure.[115] Molecule **48** (Figure 1.11) was first recognised as one of the useful analogues that eventually led to the development of enalaprilat (**47**).[12] A chain extension strategy was applied to **48** in attempts to improve its potency. When the benzyl group in **48** was converted into a phenethyl group in **49** (Figure 1.11), a significant increase in

activity was observed, i.e., **49** is 10 times more potent than **48**.[12] Enalaprilat (**47**) represents the active epimer of the diastereoisomeric mixture of **49**.[12]

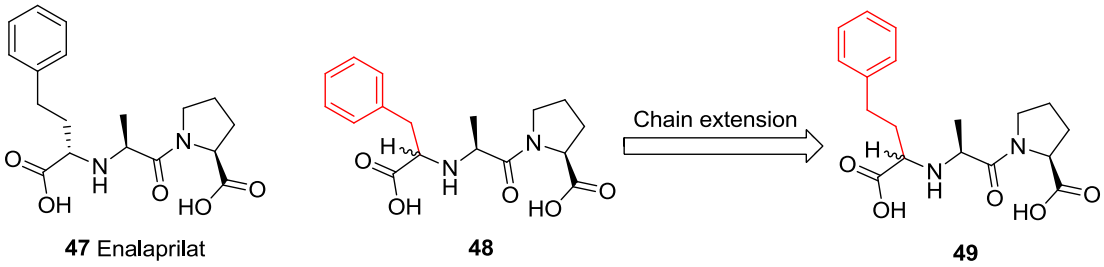


Figure 1.11. Chain extension of **48**

1.3.4 Structural extension

Structural extension is a strategy where the lead molecule is 'extended' by the addition of extra chemical/functional groups to probe for potential extra binding regions within the target site, which may lead to enhancement of the desired effect.[12] This strategy is often used to reveal extra hydrophobic interactions within the binding site by the addition of extra alkyl or arylalkyl groups to the lead molecule.[12] On the other hand, chemical groups with polar functional groups can also be added to the lead molecule to probe for extra hydrogen bonding or polar interactions within the binding site.[12]

The strategy of structural extension is exemplified by the anticancer drug imatinib (CGP 57148) (**50**, Figure 1.12), which represents the first protein kinase inhibitor to hit the market for the treatment of chronic myeloid leukemia.[116,117] In the process of discovering imatinib (**50**) as an anticancer drug, CGP 53716 (**51**, Figure 1.12) emerged as one of the intermediates that showed promising protein kinase inhibiting activity.[118,119] However, there were significant discrepancies between the *in vitro* and *in vivo* activities showed by **51**.[118,119] In attempts to improve selectivity, the structure of **51** was extended at the *para*-position of the benzamide phenyl ring to

include a 1-methylene-4-methylpiperazine moiety to give imatinib (**50**), which was found to show equal potency *in vitro* and *in vivo* and eventually approved as a clinical drug.[116,117]

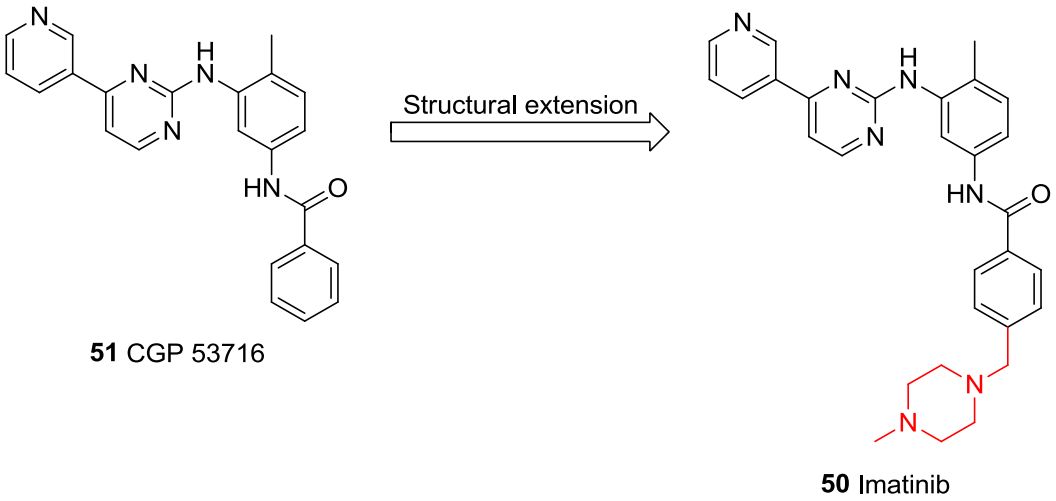


Figure 1.12. Structural extension of CGP 53716 (**51**)

1.3.5 Rigidification

A flexible drug molecule can adopt a large number of conformations due to the presence of several rotatable bonds. However, possibly only one of these conformations can effectively bind to the biological target site, triggering the desired biological effect, and this conformation is known as the active conformation.[12] In general, the molecule/ligand will suffer a loss in entropy upon binding to the target site, as prior to binding the molecule is more flexible (higher entropy) and the molecule becomes rigidified when it is bound to the target site (lower entropy). The strategy of rigidification, also known as conformational restriction, may be able to increase the selectivity of a ligand by locking its otherwise flexible molecular framework to the specific active conformation for binding, thus reducing the possibility of off-target effect.[12] Thermodynamically, rigidification also contributes

favourably to the overall ligand-target binding affinity since a more rigid ligand contributes to a lower entropy loss when bound to its target site.[120,121]

The major approach for structural rigidification is by the formation of cyclic structures to reduce the number of rotatable bonds present in the molecule, and the rigidified molecule must be locked in the desired active conformation.[12] The rigidification strategy has been applied in various areas of drug development, including human immunodeficiency viruses (HIV) inhibitors, anticancer agents, Alzheimer's disease therapeutic agents, antiinfluenza agents, as well as antibacterial and antifungal agents.[122]

An example of a drug that made it into the market through the rigidification strategy is dolutegravir (**52**, Figure 1.13), an FDA-approved drug to treat HIV infection.[123,124] Carbamoyl pyridone HIV-1 integrase (IN) inhibitor **53** (Figure 1.13) emerged as one of the intermediates in the development of novel IN inhibitors.[124] To improve metabolic stability, the methyl ester group in **53** was converted to amide **54** (Figure 1.13).[124] However, the presence of an unfavourable intramolecular H-bonding between the central hydroxyl and amide NH moieties in **54** resulted in a substantial reduction in activity.[124] To mitigate this issue, the conformation adopted by the amide group in **54** must be in such a way where the carbonyl function is located nearest to the hydroxyl group. This was eventually achieved by employing an intramolecular tethering technique, which saw the discovery of dolutegravir (**52**) as an HIV inhibitor.[124]

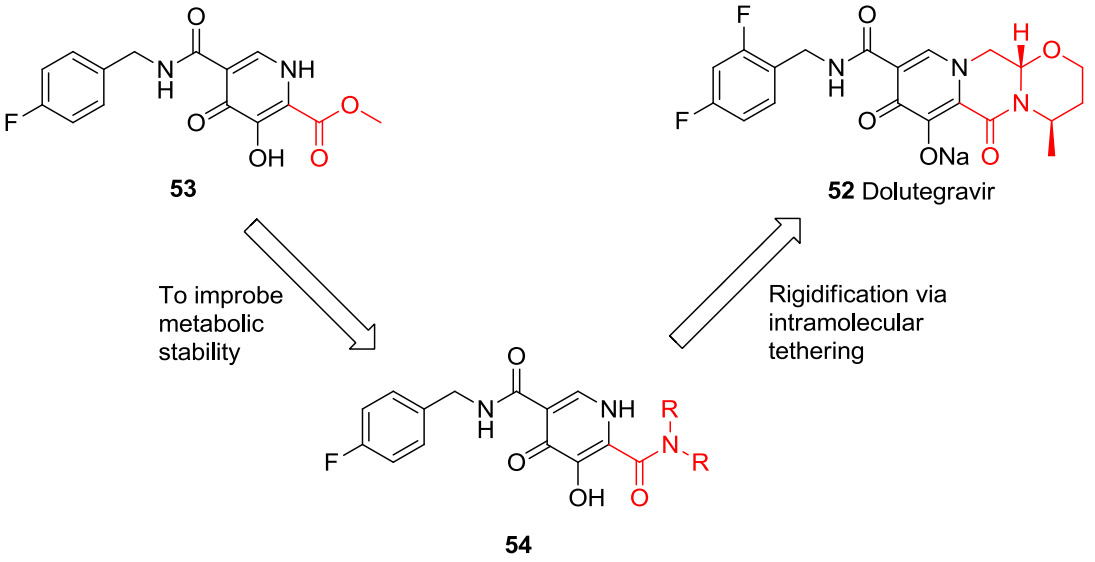


Figure 1.13. Rigidification of IN inhibitor (**53**)

The rigidification strategy can also be illustrated by the structural modification of morphine (**55**, Figure 1.14) in the development of analogues with stronger analgesic effects.[12] Morphine (**55**) is a well-known analgesic drug which relieves pain via mediation through the μ-opioid receptors.[125] Etorphine[126] (**56**, Figure 1.14) is a rigidified analogue of morphine (**55**), where an extra ring with a branched group is introduced to rigidify and subsequently limit the number of conformations the molecule can adopt.[127] As a result, etorphine (**56**) is 3200 times more potent than morphine (**55**) in terms of its analgesic activity.[127]

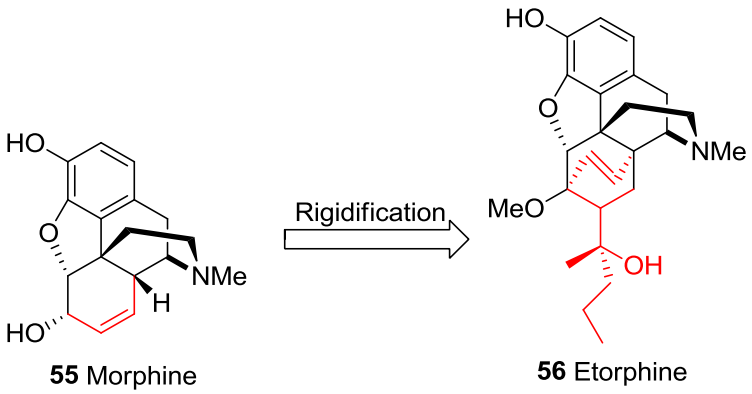
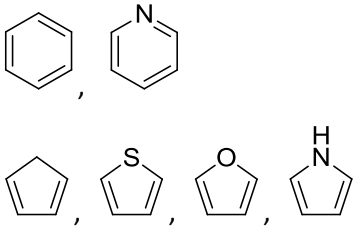


Figure 1.14. Rigidification of morphine (**55**)

1.3.6 Bioisosterism

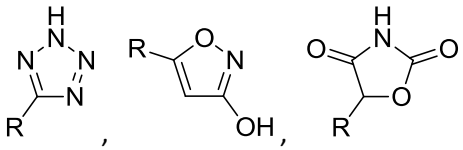
Bioisosteres are chemical groups that have similar chemical or physical properties and produce roughly similar biological effects to another compound.[128] Bioisosterism is an important approach in drug design especially in decreasing the level of toxicity and/or improving the level of potency, selectivity and pharmacokinetics of a lead compound.[98] Bioisosteres can be divided into the classical and non-classical categories.[98] Classical bioisosteres refer to the replacement of a functional group/atom/partial structure with a group that has the same valency (mono-, di-, tri-, tetra-valent) and ring equivalents.[98] A few examples of classical bioisosteres are shown in Table 1.6.[12,129]

Table 1.6. Examples of classical isosteres

Monovalent	–OH, $–NH_2$, $–CH_3$ –F, –Cl, –Br, –I, –SH
Divalent	$–CH_2–$, –NH–, –O–, –S– $–COCH_2–$, –CONH–, –COO–, –COS–
Trivalent	=CH–, =N–
Tetravalent	=C=, $=N^+=$
Ring equivalent	

On the other hand, non-classical bioisosteres refer to the replacement of a chemical group with one that is structurally distinct, possessing different steric and electronic properties but retains similar biological activities.[98] Selected examples of non-classical isosteres are shown in Table 1.7 for carboxylic acid (–COOH) isosteres.[130]

Table 1.7. Selected examples of carboxylic acid (–COOH) isosteres

Acyclic	$–SO_3H$, $–PO_3H$, $–SO_2NH_2$
Cyclic	

The concept of bioisosterism can be illustrated by the discovery of ixabepilone (**57**, Figure 1.15), an anticancer agent used to treat breast cancer, based on the structure of epothilone B (**58**, Figure 1.15).[131,132] Epothilone B (**58**), which was isolated from the myxobacterium *Sorangium cellulosum*, was found to possess potent *in vitro* anticancer activity against breast and colon tumour cell lines.[132] However, epothilone B (**58**) showed only modest *in vivo* antitumour activity due to its poor metabolic stability and unfavourable pharmacokinetics.[133] A range of semisynthetic analogues were designed and evaluated, which eventually led to the discovery of ixabepilone (**57**).[133] The lactone oxygen atom in epothilone B (**58**) was replaced with a nitrogen atom (classical isostere) in ixabepilone (**57**), to give a lactam analogue. The lactam ring in ixabepilone (**57**) is not susceptible to hydrolysis by esterases, resulting in improved metabolic stability.[134]

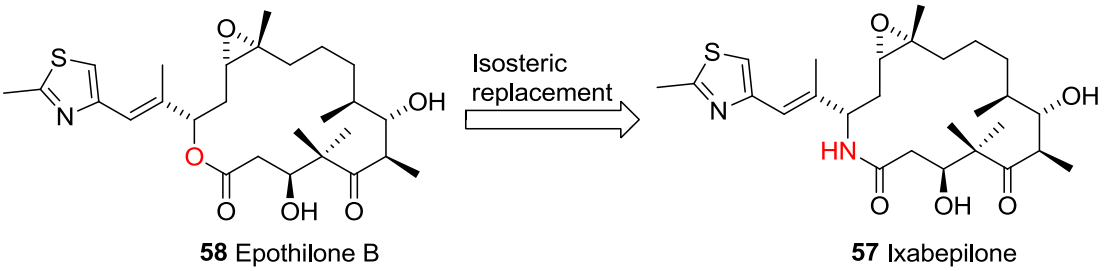


Figure 1.15. Isosteric replacement of epothilone B (**58**)

Another drug that made it into the market based on bioisosterism is losartan (**6**), an ARB that is used for the treatment of hypertension.[135] EXP-7711 (**59**, Figure 1.16), which is one of the candidates in the drug development pipeline, suffered from

relatively weak potency despite being orally active and possesses a long-lasting effect for lowering blood pressure.[135] As a result, the carboxylic acid moiety in EXP-7711 (**59**) was replaced by its non-classical cyclic isostere, i.e., tetrazole, in losartan (**6**) and this modification improved the oral absorption and potency by 1000 times.[135]

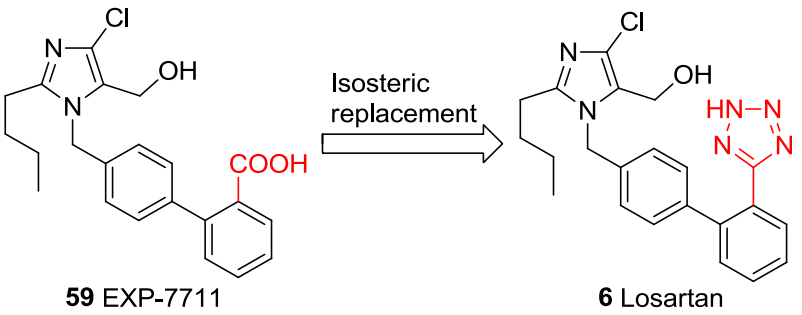


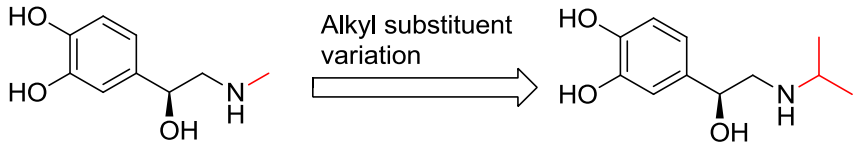
Figure 1.16. Isosteric replacement of EXP-7711 (**59**)

1.3.7 Substituent variation

Substituent variation refers to the alteration of alkyl or aromatic substituents of a lead in order to improve its binding interaction.[12] For example, if an alkyl group interacts with a hydrophobic region in a binding site, the length and bulkiness of the alkyl group can be varied for better fitting into the binding site to give improved interaction.[12] Variation of substituents on an aromatic ring may affect binding interaction and activity since different substituents possess different steric, hydrophobic, and electronic properties.[12]

The substituent variation strategy can be highlighted by the development of isoprenaline (**60**, Figure 1.17) as a selective β-adrenergic agonist.[12] Isoprenaline (**60**) was obtained by replacement of the *N*-methyl group in adrenaline (**61**) with the bulkier *N*-isopropyl group.[12,136] This simple modification resulted in a significant change in the activity observed, whereby adrenaline (**61**) is a non-selective

adrenoreceptor agonist while isoprenaline (**60**) shows selectivity for β-adrenergic receptors over α-adrenergic receptors.[137]



61 Adrenaline **60** Isoprenaline

Figure 1.17. Alkyl substituent variation of adrenaline (**61**)

As mentioned in Section 1.3.2, aromatic substituent variation strategy was applied on UK-47,265 (**45**) where the aromatic chloro substituents were replaced with fluoro substituents to yield fluconazole (**46**) that has superior water solubility for intravenous administration.[111]

On a side note, it is common for different drug design strategies to be employed in combination (as reflected in the case of fluconazole (**46**)) to discover biologically active drugs with optimum effects with regards to pharmacological and pharmacokinetic properties.

1.4 The genus *Ficus*

The genus *Ficus* belongs to the tribe Ficeae (figs) in the mulberry family Moraceae.[138] This genus is well represented by over 735 species worldwide and approximately 367 species in Malesia, i.e., the region covering countries of Malaysia, Indonesia, Brunei Darussalam, Singapore, the Philippines and Papua New Guinea.[139]

The figs are trees, shrubs and vines occurring as part of the vast range of ecological niches throughout the tropics.[140] Their leaves are usually spirally arranged, distichous, subopposite or sometimes subverticillate.[139] A unique trait of the *Ficus*

species is the fruit, sometimes referred to as a syconium, an enclosed inflorescence in which internal flowers are exclusively pollinated by female agaonine wasps.[141]

Ficus species have extensive usage in ethnomedicine to cure a number of cancer-related diseases conditions since the 1st century CE in the West.[142] In Asia, specifically in Malaysia, the leaves of *F. deltoidea* are used to treat diabetes, skin diseases, hypertension and regulate menstrual cycle.[143–145] In Malaysia and India, various parts of *F. hispida* are used to treat a number of disease conditions such as ulcers, psoriasis, anemia, jaundice and more.[144–146]

1.4.1 Alkaloids from the genus *Ficus*

Alkaloids are nitrogen-containing organic compounds of natural origin with a greater or lesser degree of basic character.[147] By extension, certain neutral compounds including amides may be considered as alkaloids.[148] To date, the occurrence of alkaloids in *Ficus* is limited to eight species and is summarized in Table 1.8. The structures of alkaloids isolated from *Ficus* species are shown in Figure 1.18.

....

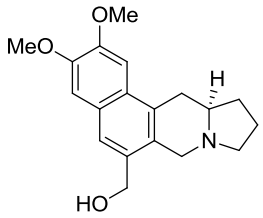
Table 1.8. Occurrence of alkaloids in *Ficus*

Plant	Plant part	Alkaloids	References
F. fistulosa Reinw. ex Blume	Stem-bark	Fistulosine (**62**) (–)-13aα-Antofine (13a*R*-antofine) (**63**) (–)-14β-Hydroxyantofine (**64**) (–)-13aα-Secoantofine ((–)-Secoantofine) (**65**)	[149]
	Bark	Fistulopsine A (**66**) (+)-Septicine (**67**) (+)-Tylocrebrine (**68**)	[150]
	Leaf	Fistulopsine B (**69**) (+)-Tylophorine (**70**) (–)-3,6-Didemethylisotylocrebrine (**71**)	
	Leaves and stem-bark	Aurantiamide acetate (**72**) Indole-3-carboxaldehyde (**73**) Palmanine (**74**) 3,4-Dihydro-6,7-dimethoxyisocarbostyril (**75**)	[151]
F. fistulosa var. *tengerensis*	Leaves	(+)-Antofine (**76**) (±)-Fistulosine (**77**) (–)-Secoantofine (**65**) (+)-Tengechlorenine (**78**) (+)-Tengerensine (**79**)	[152]
F. hirta Vahl.	Fruits	Methyl 1-methyl-1,2,3,4-tetrahydro-β-carboline-3-carboxylate (**80**) 1-Methyl-1,2,3,4-tetrahydro-β-carboline-3-carboxylic acid (**81**)	[153]
F. hispida Linn.	Stem-bark	(+)-Deoxypergularinine (**82**) Hispidacine (**83**)	[154]
	Leaves	Hispidine (**84**) Hispiloscine (**85**) 3,6,7-Trimethoxy-14-hydroxyphenanthroindolizidine (*O*-Methyltylophorinidine) (**86**) 3,6,7-Trimethoxyphenanthroindolizidine ((–)-Deoxypergularinine) (**87**)	[154,155]
	Leaves-twig	*O*-Methyltylophorinidine (**86**)	[156]

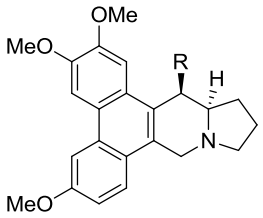
....

	Twigs	Ficushispimine A (**88**) Ficushispimine B (**89**) Ficushispimine C (**90**) Ficushispidine (**91**) 1-(4-Hydroxyphenyl)-2-(2-pyrrolidinyl)ethanone (**92**)	[157]
F. nota (Blanco) Merr.	Leaves	Ficusnotin A (**93**) Ficusnotin B (**94**) Ficusnotin F (**95**)	[158]
F. pachyrhachis	Leaves	(+)-Nor-reticuline (**96**) (–)-Reticuline (**97**)	[159]
F. pantoniana King	(Not specified)	Ficine (**98**) Isoficine (**99**)	[160]
F. septica Burm f.	Twigs	Dehydroantofine (**100**) Dehydrotylophorine (**101**) Secodehydroantofine (**102**) Tylophoridicine D (**103**)	[161]
	Leaves	Antofine (**104**) (+)-Antofine (**76**) Dehydrotylophorine (**101**) Ficuseptamine A (**105**) Ficuseptamine B (**106**) Ficuseptamine C (**107**) Ficuseptine A (**108**) (+)-Isotylocrebrine (**109**) Norruspoline (**110**) Phyllosterone (**111**) Septicine (**112**) (–)-Secoantofine (**65**) Tylocrebrine (**113**) (–)-Tylophorine (13a*R*-Tylophorine) (**114**) (+)-Tylocrebrine (**68**) (+)-Tylophorine (**70**) (+)-Tylophorine *N*-oxide (**115**) 14α-Hydroxyisocrebrine *N*-oxide (**116**) 14α-Hydroxyisotylocrebrine *N*-oxide (**117**) 14-Hydroxy-2,3,4,6,7-pentamethoxyphenanthroindolizidine (**118**) 14-Hydroxy-3,4,6,7-tetramethoxyphenanthroindolizidine (**119**)	[162,163]

Stem	Dehydrotylophorine (**101**) Ficuseptine B (**120**) Ficuseptine C (**121**) Ficuseptine D (**122**) (+)-Isotylocrebrine (**109**) Tylocrebrine (**113**) (–)-Tylophorine (**114**) 10*S*,13a*R*-Antofine *N*-oxide (**123**) 10*S*,13a*R*-Isotylocrebrine *N*-oxide (**124**) 10*S*,13a*S*-Isotylocrebrine *N*-oxide (**125**) 10*R*,13a*R*-Tylocrebrine *N*-oxide (**126**) 10*S*,13a*R*-Tylocrebrine *N*-oxide (**127**) 10*R*,13a*R*-Tylophorine *N*-oxide (**128**) 10*S*,13a*R*-Tylophorine *N*-oxide (**129**)	[164]
Roots	Dehydrotylophorine (**101**) Ficuseptine A (**108**) Ficuseptine B (**120**) Ficuseptine E (**130**) Ficuseptine F (**131**) Ficuseptine G (**132**) Ficuseptine H (**133**) Ficuseptine I (**134**) Ficuseptine J (**135**) Ficuseptine K (**136**) Ficuseptine L (**137**) Ficuseptine M (**138**) Ficuseptine N (**139**) 13a*R*-Antofine (**63**) 13a*R*-Isotylocrebrine (**140**) 13a*R*-Tylophorine (**114**) 13a*R*-Tylocrebrine (**141**) 10*S*,13a*R*-Isotylocrebrine *N*-oxide (**124**) 10*S*,13a*R*-Tylocrebrine *N*-oxide (**127**) 10*R*,13a*R*-Tylophorine *N*-oxide (**128**)	[165]

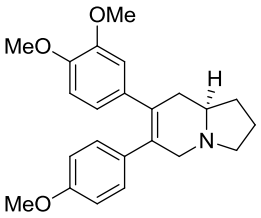


62 Fistulosine

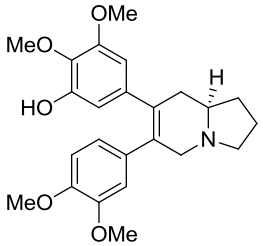


63 (–)-13aα-Antofine: R = H

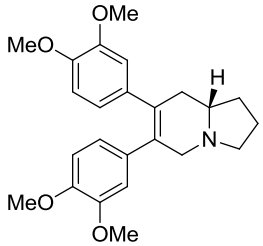
64 (–)-14ß-Hydroxyantofine: R = OH



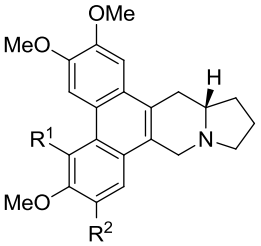
65 (–)-13aα-Secoantofine



66 Fistulopsine A



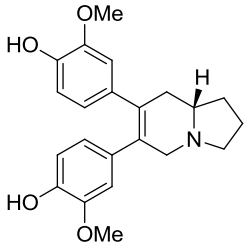
67 (+)-Septicine



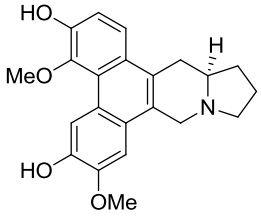
68 (+)-Tylocrebrine: R^1 = OMe, R^2 = H

70 (+)-Tylophorine: R^1 = H, R^2 = OMe

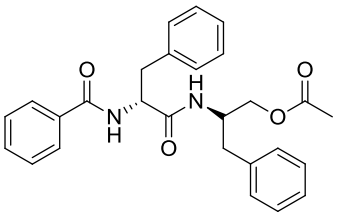
76 (+)-Antofine: R^1 = R^2 = H



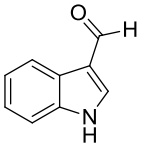
69 Fistulopsine B



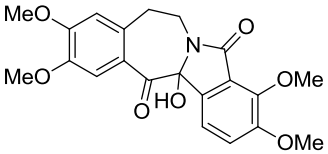
71 (–)-3,6-Dimethylisotylocrebrine



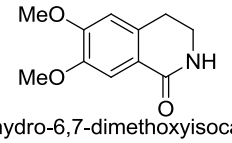
72 Aurantiamide acetate



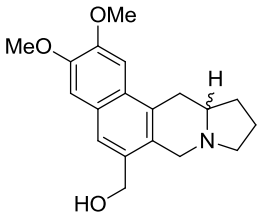
73 Indole-3-carboxaldehyde



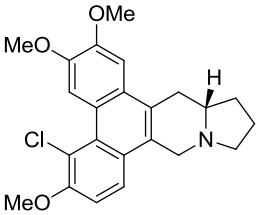
74 Palmanine



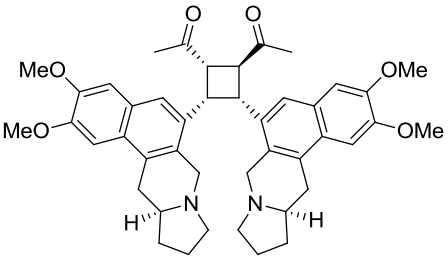
75 3,4-Dihydro-6,7-dimethoxyisocarbostyril



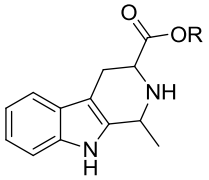
77 (±)-Fistulosine



78 (+)-Tengechlorenine

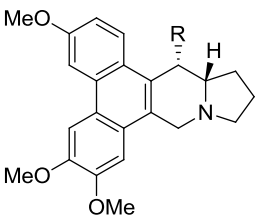


79 (+)-Tengerensine



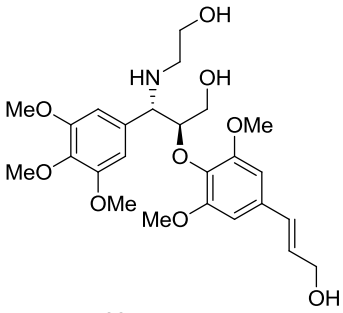
80 Methyl 1-methyl-1,2,3,4-tetrahydro-ß-carboline-3-carboxylate: R = Me

81 1-Methyl-1,2,3,4-tetrahydro-ß-carboline-3-carboxylic acid: R = H

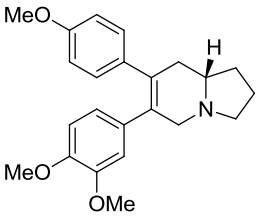


82 (+)-Deoxypergularinine: R = H

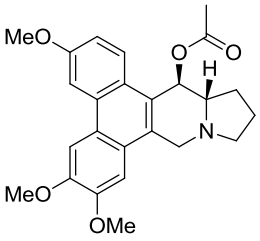
86 3,6,7-Trimethoxy-14-hydroxyphenanthroindolizidine: R = OH



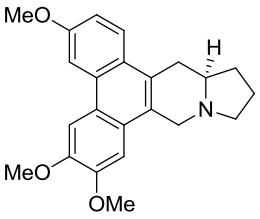
83 Hispidacine



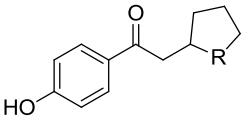
84 Hispidine



85 Hispilosine



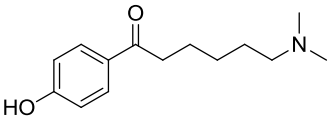
87 3,6,7-Trimethoxyphenanthroindolizidine



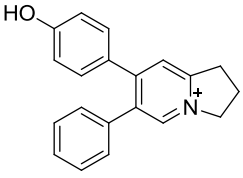
88 Ficushispimine A: R = N^+Me_2

89 Ficushispimine B: R = NMe

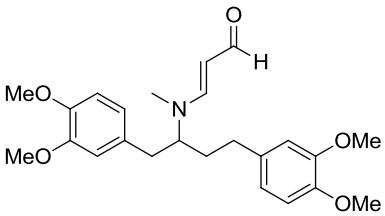
92 1-(4-Hydroxyphenyl)-2-(2-pyrrolidinyl)ethanone: R = NH



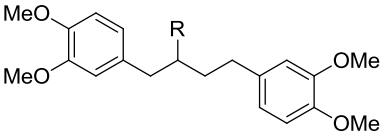
90 Ficushispimine C



91 Ficushispidine

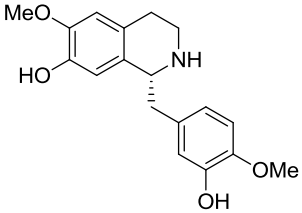


93 Ficusnotin A

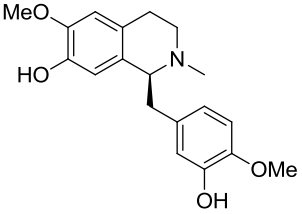


94 Ficusnotin B: R = NHAc

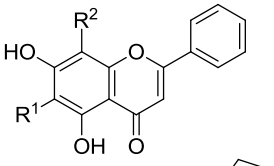
95 Ficusnotin F: R = NHCHO



96 (+)-Nor-reticuline

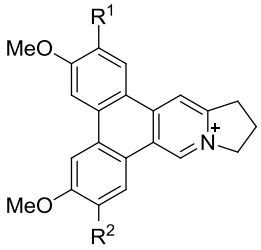


97 (–)-Reticuline



98 Ficine: R^1 = H, R^2 =

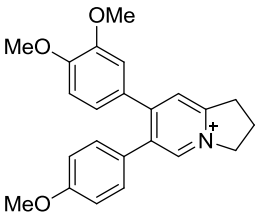
99 Isoficine: R^1 = , R^2 = H



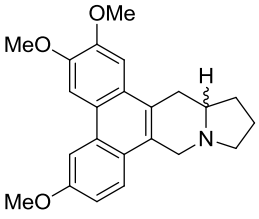
100 Dehydroantofine: R^1 = OMe, R^2 = H

101 Dehydrotylophorine: R^1 = OMe, R^2 =OMe

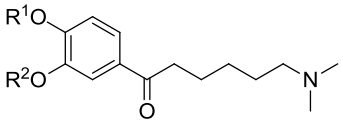
103 Tylophoridicine D: R^1 = H, R^2 =OMe



102 Secodehydroantofine

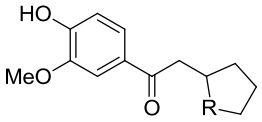


104 Antofine



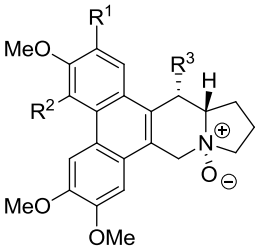
105 Ficuseptamine A: R^1 = H, R^2 = Me

106 Ficuseptamine B: R^1 = Me, R^2 = H

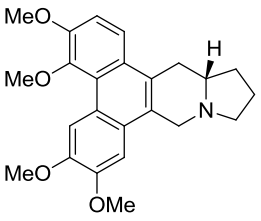


107 Ficuseptamine C: R = $^+N(CH_3)_2$

111 Phyllosterone: R = NCH_3



108 Ficuseptine A: R^1 = R^2 = OMe, R^3 = OH

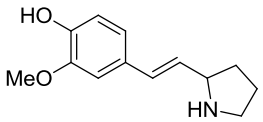


109 (+)-Isotylocrebrine

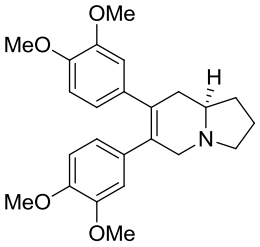
115 (+)-Tylophorine *N*-oxide: R^1 = OMe, R^2 = R^3 = H

116 14α-Hydroxyisocrebrine *N*-oxide: R^1 = H, R^2 = OMe, R^3 = OH

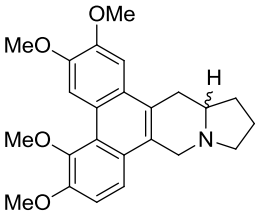
117 14α-Hydroxyisotylocrebrine *N*-oxide: R^1 = H, R^2 = OMe, R^3 = OH



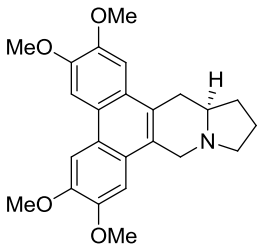
110 Norruspoline



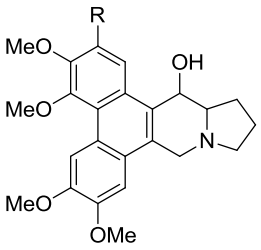
112 Septicine



113 Tylocrebrine

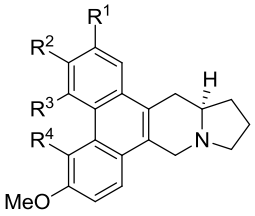


114 (–)-Tylophorine



118 14-Hydroxy-2,3,4,6,7-pentamethoxyphenanthroindolizidine: R = OMe

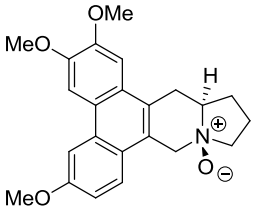
119 14-Hydroxy-3,4,6,7-tetramethoxyphenanthroindolizidine: R = H



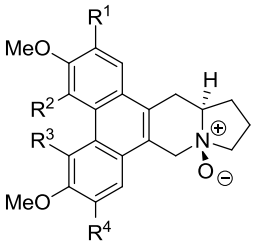
120 Ficuseptine B: R^1, R^2 = OCH_2O, R^3 = H, R^4 = OMe

121 Ficuseptine C: R^1, R^2 = OCH_2O, R^3 = R^4 = H

122 Ficuseptine D: R^1 = R^4 = H, R^2 = R^3 = OMe

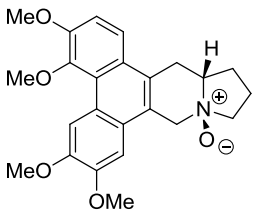


123 10*S*,13a*R*-Antofine *N*-oxide

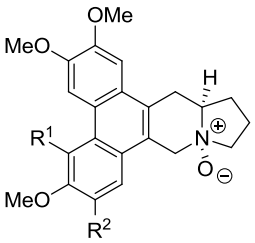


124 10*S*,13a*R*-Isotylocrebrine *N*-oxide: R^1 = R^3 = H, R^2 = R^4 = OMe

127 10*S*,13a*R*-Tylocrebrine *N*-oxide: R^1 = R^3 = OMe, R^2 = R^4 = H

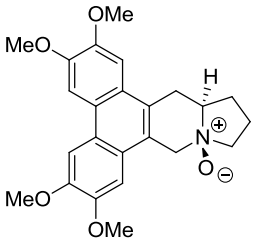


125 10*S*,13a*S*-Isotylocrebrine *N*-oxide

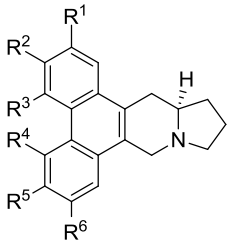


126 10*R*,13a*R*-Tylocrebrine *N*-oxide: R^1 = OMe, R^2 = H

128 10*R*,13a*R*-Tylophorine *N*-oxide: R^1 = H, R^2 = OMe



129 10*S*,13a*R*-Tylophorine *N*-oxide



130 Ficuseptine E: R^1 = R^3 = OH, R^2 = R^5 = OMe, R^4 = R^6 = H

131 Ficuseptine F: R^1 = R^2 = R^3 = R^4 = R^5 = OMe, R^6 = H

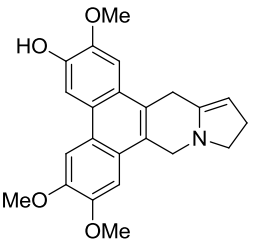
132 Ficuseptine G: R^1 = R^4 = H, R^2 = R^3 = R^6 = OMe, R^5 = OH

133 Ficuseptine H: R^1 = R^4 = R^5 = OMe, R^2 = OH, R^3 = R^6 = H

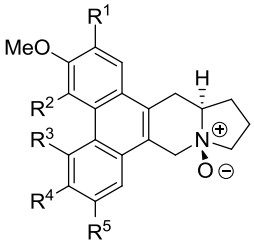
135 Ficuseptine J: R^1 = R^2 = R^4 = OMe, R^3 = R^6 = H, R^5 = OH

140 13a*R*-Isotylocrebrine: R^1 = R^4 = H, R^2 = R^3 = R^5 = R^6 = OMe

141 13a*R*-Tylocrebrine: R^1 = R^2 = R^4 = R^5 = OMe, R^3 = R^6 = H

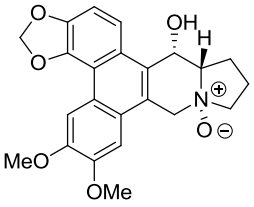


134 Ficuseptine I

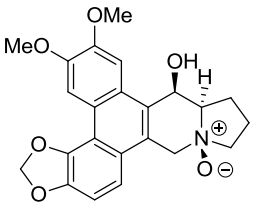


136 Ficuseptine K: R^1 = R^3 = OMe, R^2 = R^5 = H, R^4 = OH

137 Ficuseptine L: R^1 = R^3 = R^5 = H, R^2 = R^4 = OMe



138 Ficuseptine M



139 Ficuseptine N

Figure 1.18. Alkaloids from *Ficus* species

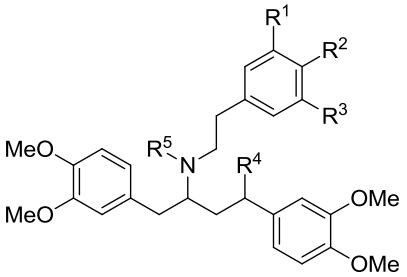
From Table 1.8, it is apparent that alkaloid-producing *Ficus* species predominantly produce phenanthroindolizidine-type alkaloids in the leaf, bark, stem and root parts. Phenanthroindolizidine alkaloids are known to possess interesting pharmacological properties, particularly anticancer activities.[166,167] This class of alkaloids has attracted many organic chemists to develop total syntheses of these compounds, such as tylophorine (**70** and **114**), antofine (**104**), tylocrebrine (**113**).[166,168] Extensive SAR studies on the phenanthroindolizidines for their potential anticancer effects were also carried out.[166,168] The next common class of alkaloids isolated from this genus is *seco*-phenanthroindolizidines that include fistulopsine B (**69**), ficushispidine (**91**), septicine (**67** and **112**), (–)-secoantofine (**65**), secodehydroantofine (**102**) and hispidine (**84**).

To date, our group has reported the phytochemical investigations of three *Ficus* plant species, namely *F. fistulosa*, *F. fistulosa* var. *tengerensis* and *F. hispida*, which yielded the discovery of six novel alkaloids including fistulopsines A (**66**) and B (**69**), (+)-tengechlorenine (**78**), (+)-tengerensine (**79**), hispidacine (**83**) and hispiloscine (**85**).[150,152,154] However, alkaloidal investigations of other *Ficus* species are still very limited considering the fact that there is a large number of species within this genus. Given the fact that alkaloids represent one of the most important classes of natural products for drug discovery,[169] scientists should continue to work on other uninvestigated *Ficus* species to explore and discover potentially useful biologically active alkaloids.

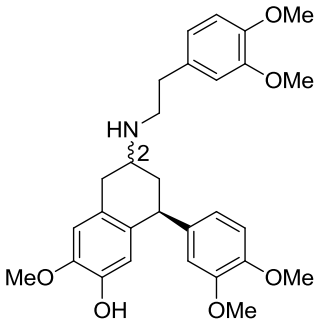
1.4.2 Alkaloids from *Ficus schwarzii*

In continuation of our studies of biologically active alkaloids from Malaysian *Ficus*, we have recently isolated a series of nine novel alkaloids from the leaves of *Ficus*

schwarzii Koord., namely, schwarzinicines A–G (**142–148**),[170] schwarzificusines A (**149**) and B (**150**) (unpublished) (Figure 1.19). The basic backbone of the schwarzinicine structures constitute an unprecedented 1,4-diarylbutanoid-phenethylamine adduct. On the other hand, schwarzificusines are characterized by a phenylaminotetralin core structure incorporating a phenethylamine moiety.



142 Schwarzinicine A: $R^1 = R^4 = R^5 = H$, $R^2 = R^3 = OMe$
143 Schwarzinicine B: $R^1 = R^4 = H$, $R^2 = R^3 = OMe$, $R^5 = Me$
144 Schwarzinicine C: $R^1 = R^4 = R^5 = H$, R^2, $R^3 = OCH_2O$
145 Schwarzinicine D: $R^1 = OH$, R^2, $R^3 = OCH_2O$, $R^4 = R^5 = H$
146 Schwarzinicine E: $R^1 = OH$, $R^2 = R^3 = OMe$, $R^4 = R^5 = H$
147 Schwarzinicine F: $R^1 = R^5 = H$, $R^2 = R^3 = OMe$, $R^4 = OH$
148 Schwarzinicine G: $R^1 = H$, $R^2 = R^3 = OMe$, $R^4 = OH$, $R^5 = Me$



149 Schwarzificusine A: 2α-$NHCH_2CH_2Ar$
150 Schwarzificusine B: 2ß-$NHCH_2CH_2Ar$

Figure 1.19. Structures of schwarzinicines A–G (**142–148**), schwarzificusines A (**149**) and B (**150**)

Schwarzinicine A (**142**), which was obtained as the most abundant alkaloid from the leaves of *F. schwarzii*, was found to possess pronounced vasorelaxant activity in male Sprague Dawley (SD) rat isolated aorta pre-contracted with phenylephrine (PE) in an organ bath setup. Although the potency of **142** was comparable to that of dobutamine (a known phenylalkylamine vasorelaxant agent), it showed a significantly higher efficacy (see Section 4.2). Additionally, **142** exhibited selective relaxant effect in rat aorta tissue compared to trachea and bronchus tissues (Figure 1.20). Furthermore, unlike the phenanthroindolizidine alkaloids, **142** showed no apparent cytotoxicity towards selected human cancer cell lines (neutral red assay).

While mechanistic study for the vasorelaxant effect of **142** is currently underway, the preliminary biological data strongly suggest that **142** represents a promising lead that can be further developed into useful therapeutic agents, particularly to complement the existing classes of antihypertensive drugs available in the market.

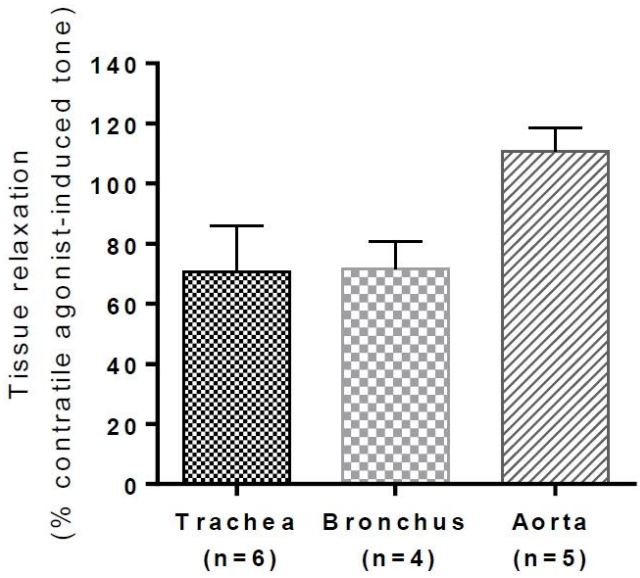


Figure 1.20. Vasorelaxation induced by schwarzinicine A (**142**) at 30μM in rat isolated trachea, bronchus and aorta. The data represents mean ± SEM of (*n*) determinations

1.5 Research aims

It is imperative that a sustainable source of the schwarzinicine alkaloids is the key to further investigations into their potential development for therapeutic use. The project, therefore, aimed to develop sustainable and scalable syntheses of the schwarzinicine alkaloids, particularly schwarzinicine A (**142**), from commercially available building blocks. This is because the isolation yield of **142** from its natural source is very low, ca. 0.0005% (or 50 mg obtained from 10 kg of dried leaves) despite that **142** was isolated as the most abundant alkaloid from the leaves of *F. schwarzii*. Synthetic

routes to schwarzinicines B (**143**) and F (**147**) would also be developed in the present project.

Additionally, we also aimed to explore and better understand the SAR around the structure of schwarzinicine A (**142**) as a lead compound in promoting vasorelaxant effects in rat isolated aorta. This was achieved by carefully designing and synthesizing various **142** analogues using the analogue design strategies described in Section 1.3, followed by evaluation of their vasorelaxant effects using the organ bath setup (see Section 4.1.1). Subsequently, a detailed analysis of SAR provided useful information to facilitate further structural optimization of the molecular scaffold of **142** for better activity.

2

Total syntheses of schwarzinicine alkaloids

2.1 Overview

It was highlighted in Chapter 1 that schwarzinicine A (**142**) exhibited promising vasorelaxant effect in SD rat isolated aorta. In order to explore the biological activity of schwarzinicine A (**142**) and other schwarzinicine alkaloids, which may facilitate the development of possible antihypertensive agents, it is desirable that the schwarzinicine alkaloids can be prepared in the laboratory considering the fact that the leaves of *Ficus schwarzii* are not in any way a sustainable source of the alkaloids. In this chapter, we describe the total syntheses of schwarzinicines A (**142**), B (**143**) and F (**147**). Schwarzinicine F (**147**) was obtained in minute amounts and its relative stereochemistry could not be ascertained due to the lack of material as well as decomposition. Therefore, it was also our aim that the synthesis of schwarzinicine F (**147**) would enable us to resolve the stereochemical issue related to its structure. Brief introductions to Grignard reaction and Weinreb ketone synthesis are presented in this chapter as these reactions were employed in the synthetic route to schwarzinicines A (**142**) and B (**143**). The reductive amination reaction, which represents a common and key step in the syntheses of schwarzinicines A (**142**), B (**143**) and F (**147**), is discussed in this chapter. The stereoselectivity aspect of the reductive amination reaction associated with the 3-hydroxyketone system present in the ketone

intermediate for the preparation of schwarzinicine F (**147**) is also discussed. These three main reactions mentioned above were also conveniently employed for the preparation of various schwarzinicine analogues designed for SAR studies.

2.1.1 Grignard reaction

First discovered by Victor Grignard in 1900, the Grignard reaction remains as one of the most influential organometallic chemical reactions in the formation of C–C bonds.[171,172] Grignard reagents are usually prepared in diethyl ether (Et_2O) or tetrahydrofuran (THF), although various other solvents, such as dimethoxyethane, tetrahydropyran, anisole, di-*n*-propyl ether, may also be used but are often associated with the problem of solubility of magnesium halide (MgX_2).[173] Precipitation of MgX_2 will shift the Schlenk equilibrium to the right, leaving R_2Mg in solution and thus affecting the reactivity of Grignard reagent (RMgX) as a whole (Scheme 2.1).[173]

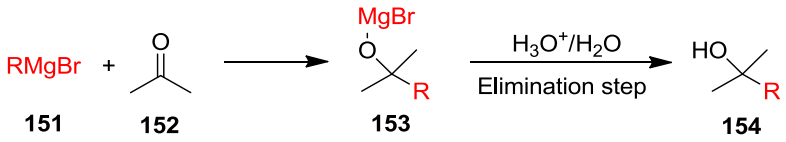
$$2RMgX \rightleftharpoons R_2Mg + MgX_2$$

Scheme 2.1. Schlenk equilibrium of Grignard reagent (RMgX)

The formation of Grignard reagent involves the insertion of a magnesium metal into an alkyl–halide (R–X) bond and the resulting compound (RMgX) is stabilized by coordination to solvent molecules or other coordinating ligands.[173] In general, the ease of formation of Grignard reagent follows the relative reactivity of halogens, i.e., I > Br > Cl >> F; and allyl, benzyl > primary alkyl > secondary alkyl, cycloalkyl = tertiary alkyl, aromatic > vinyl.[174]

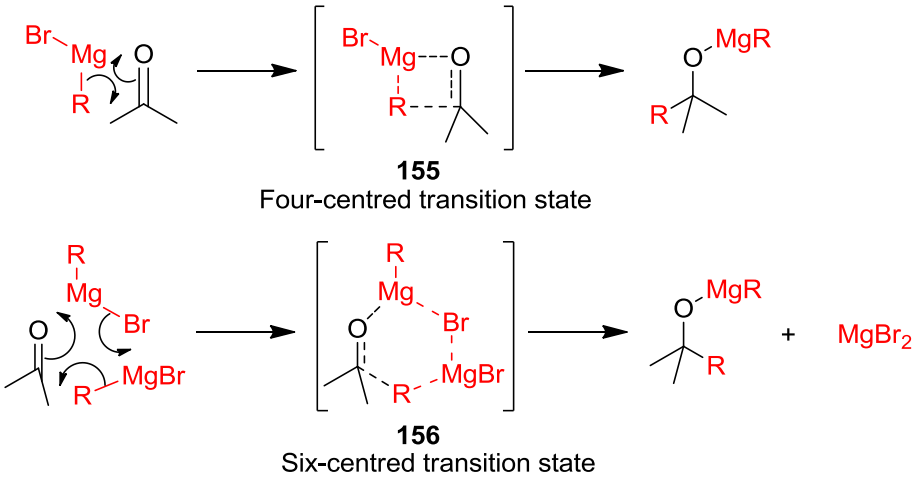
The reaction begins with a nucleophilic attack of the carbon attached to magnesium in Grignard reagent **151** onto the electrophilic carbon of the carbonyl group in **152** (e.g., ketone) (Scheme 2.2).[175] This addition reaction involves the

formation of intermediate **153**, which on subsequent elimination step (quenching with acid) produces the desired alcohol product **154**.



Scheme 2.2. A typical Grignard reaction between a Grignard reagent and a ketone

Many possible mechanisms have been proposed for the Grignard reaction.[176,177] The two most common ones are those that involve the formation of a four-centred transition state (**155**) and a six-membered transition state (**156**) (Scheme 2.3).[176,177] A range of electrophiles including nitriles, aldehydes and Weinreb amides can be used as coupling partners in the Grignard reaction.[174]



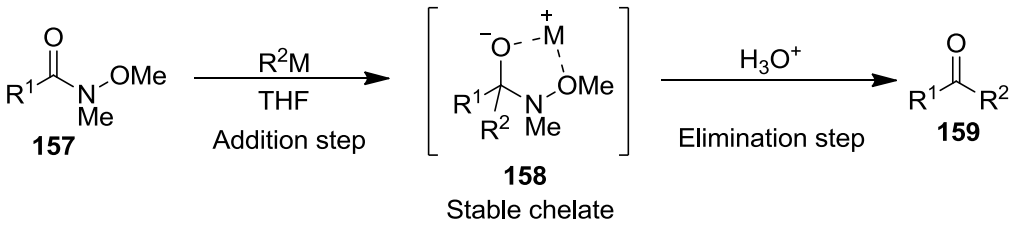
Scheme 2.3. Possible transition states for Grignard reaction

2.1.2 Weinreb ketone synthesis

Discovered by Steven Weinreb and Steven Nahm in 1981, the Weinreb ketone synthesis reaction is a method to make ketones from *N*-methoxy-*N*-methylamides (Weinreb amides) and organometallic reagents.[178] It is a powerful chemical reaction in forming C–C bonds and has increasingly gained popularity for its uses in organic synthesis.[179] Weinreb amides, which essentially are acylating agents, can be used to

make various ketones, aldehydes or cyclic compounds through many reactions, making them very versatile in the synthesis of complex natural product molecules.[179,180] A Weinreb amide is typically made from *N,O*-dimethylhydroxylamine with either an acid chloride or a carboxylic acid.[181] When a carboxylic acid is used, an acid activating agent such as 1-ethyl-3-(3-dimethylaminopropyl)carbodiimide (EDC), carbonyldiimidazole (CDI), dicyclohexyl-carbodiimide (DCC) or (benzotriazol-1-yloxy)tris(dimethylamino)-phosphonium hexafluorophosphate (BOP) is normally required for the successful conversion of the carboxylic acid into the corresponding Weinreb amide.[179]

Scheme 2.4 shows a reaction mechanism for the coupling reaction between a Weinreb amide (**157**) and a Grignard or other organometallic reagent that gives rise to a ketone *en route* to the synthesis of more complex molecules. The reaction proceeds via the formation of the stable metal-chelated intermediate **158** from a nucleophilic addition step of an organometallic reagent onto **157**, followed by an elimination step (quenching with acid) to produce the desired ketone product **159**.[178,182] The formation of the metal-chelated intermediate **158** has the advantage of preventing over-addition of the nucleophilic coupling reagent when used in excess.[181] As a result, yields of ketones produced from Weinreb amides are usually higher.[181]

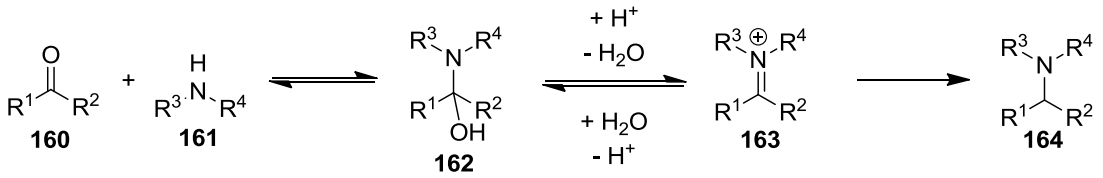


Scheme 2.4. Mechanism of Weinreb ketone synthesis

2.1.3 Reductive amination

Reductive amination is one of the most important chemical reactions in the formation of primary, secondary and tertiary amines from aldehydes or ketones with ammonia, primary or secondary amines. This also corresponds to the fact that a majority of drug molecules and derivatives made in the process of drug discovery and development are amines.[172] Compared to other C–N bond formation reactions, such as direct alkylation of nitrogen with alkyl halides, reductive amination reaction represents a favourable strategy in making amines as it does not give rise to significant over-alkylation and thus offers a greater degree of control over reactivity issue.[172]

The reaction proceeds via condensation of carbonyl compound **160** with amine **161** to form hemiaminal **162**, which subsequently undergoes dehydration to form an iminium ion intermediate **163** (Scheme 2.5).[183] Subsequent reduction of the iminium ion by a suitable reducing agent affords the desired amine **164** as a racemic mixture due to prochiral carbonyl carbon of **160**.



Scheme 2.5. Mechanism of reductive amination

Reductive amination reaction can be carried out using the direct method, whereby the reaction is performed *in situ* (one-pot reaction) with the carbonyl compound and amine being mixed together with a suitable reducing agent without prior formation of the iminium ion.[183] On the other hand, the indirect method involves the formation of the iminium ion intermediate followed by a separate reduction step.[183] The direct reductive amination method requires a highly selective reducing

agent such as sodium triacetoxyborohydride ($NaBH(OAc)_3$)[184] or sodium cyanoborohydride ($NaBH_3CN$)[185] as shown in Figure 2.1. $NaBH(OAc)_3$, being a milder reducing agent than $NaBH_3CN$, is more selective compared to $NaBH_3CN$.[184]Additionally, $NaBH(OAc)_3$ is also a greener reagent than $NaBH_3CN$ since the latter is associated with the issue of cyanide waste products.[184] However, $NaBH(OAc)_3$ tends to be unstable under aqueous condition due to the nature of the triacetoxyborohydride group and reactions done in a polar protic solvent such as methanol (MeOH) were generally less successful as compared to $NaBH_3CN$, which tolerates protic solvents well.[185,186]

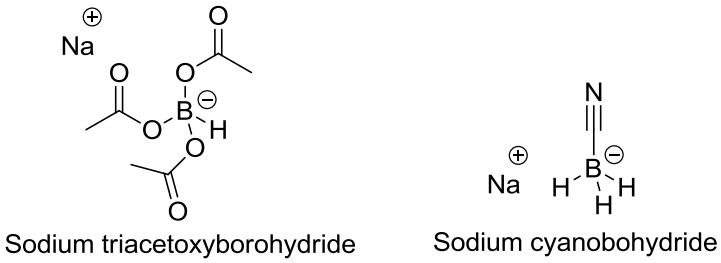
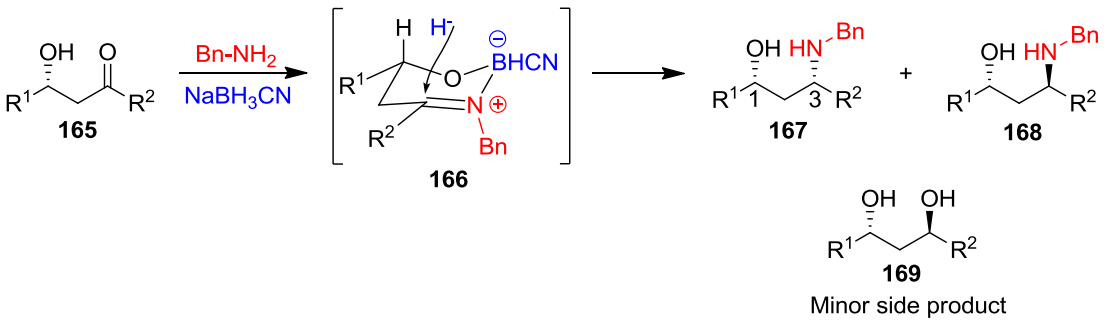


Figure 2.1. Two common reducing agents used in reduction amination

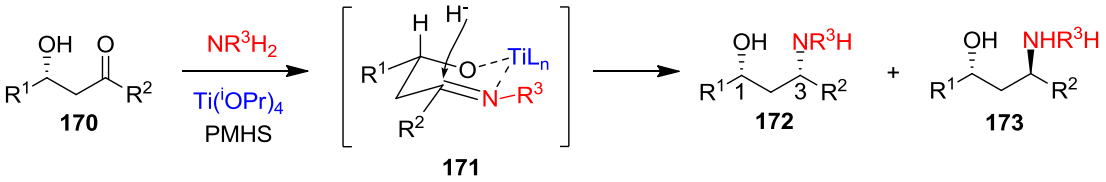
There were two previous reports that described the stereoselective preparation of 1,3-*syn*-aminoalcohols via reductive amination reaction of 3-hydroxyketones.[187,188] 1,3-Aminoalcohol is an important chemical group that is present in many bioactive molecules.[188] This includes the ketone intermediate for the preparation of schwarzinicine F (**147**) (see Section 2.3). Firstly, Haddad *et al.*[187] reported that the reductive amination between 3-hydroxyketone **165** and benzylamine (Bn-NH_2) in the presence of either $NaBH(OAc)_3$ or $NaBH_3CN$ produced 1,3-*syn*-aminoalcohol **167** in high diastereomeric excess when compared to the 1,3-*anti* product **168**, while a small amount of 1,3-diol **169** was also obtained as a minor product (Scheme 2.6).[187] It was also reported that the use of $NaBH_3CN$, in contrast to $NaBH(OAc)_3$, as the reducing agent resulted in the best stereoselectivity effect giving the 1,3-*syn* product **167** in the

highest yield. It was proposed that the reaction proceeded via the formation of transition state **166**, which adopted a chair conformation during the attack by an external hydride species on **166** from the axial position (Scheme 2.6).[187]



Scheme 2.6. Reductive amination reported by Haddad *et al.*[187]

On the other hand, Menche *et al.*[188] reported that the reductive amination reaction between 3-hydroxyketone **170** and NR^3H_2 in the presence of $Ti(^iOPr)_4$ gave rise to intermediate **171** in a chair-like conformation, while polymethylhydrosiloxane (PMHS) was used as the reducing agent and eventually produced predominantly 1,3-*syn*-aminoalcohol **172** over the 1,3-*anti* product **173** (Scheme 2.7).



Scheme 2.7. Reductive amination reported by Menche *et al.*[188]

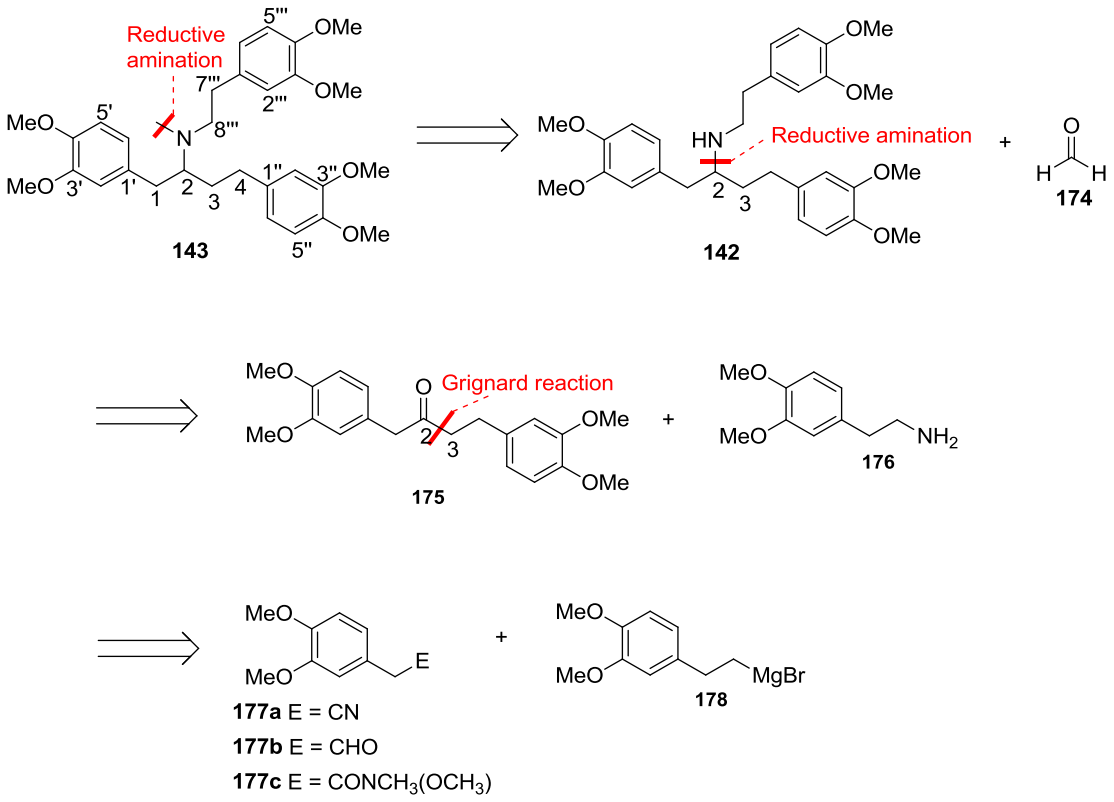
It is apparent that there is a high resemblance between the transition states proposed by Haddad *et al.*[187] (i.e., **166**) and Menche *et al.*[188] (i.e., **171**). Additionally, both the reported procedures afforded 1,3-*syn*-aminoalcohol as the major product as opposed to the diastereomeric 1,3-*anti* product.

2.2 Total syntheses of schwarzinicines A (142) and B (143)

2.2.1 Attempts to synthesize 142 and 143

2.2.1.1 Retrosynthetic analysis

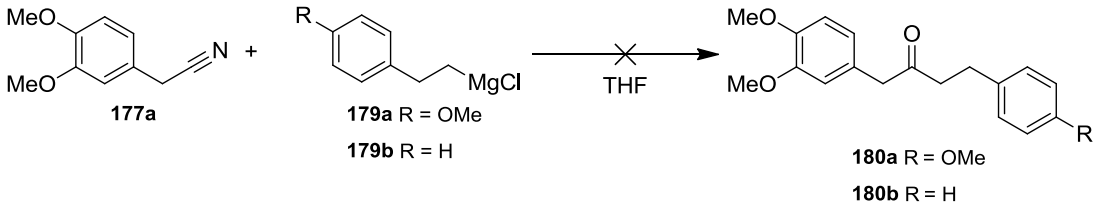
A retrosynthetic analysis of schwarzinicines A (**142**) and B (**143**) was carried out and one possible route is presented in Scheme 2.8. Retrosynthetically, **143** can be prepared via a reductive amination reaction between formaldehyde (**174**) and **142**. The C-2–N bond in **142** could be forged through a reductive amination reaction between ketone **175** and 3,4-dimethoxyphenethylamine (DMPEA, **176**). The requisite precursor **175** could in turn be made from a Grignard reaction between electrophile **177** (bearing an electrophilic functional group (E)) and Grignard reagent **178**. The potential functional groups for making reagent **177** an effective electrophile for reaction with Grignard reagent **178** include nitrile **177a**, aldehyde **177b** and Weinreb amide **177c**.



Scheme 2.8. Retrosynthesis analysis of schwarzinicines A (**142**) and B (**143**)

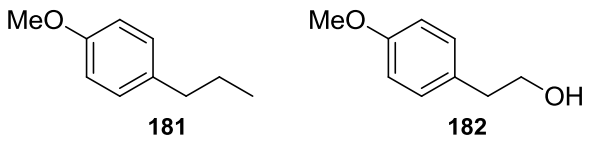
2.2.1.2 First attempt: Grignard reaction based on benzyl nitriles

In the syntheses of schwarzinicines A (**142**) and B (**143**), the synthetic route based on nitrile as the required electrophile to produce the relevant ketone precursor was attempted. Based on the procedure reported by Zhang *et al.*,[189] a model reaction was first carried out between (3,4-dimethoxyphenyl)acetonitrile (**177a**) and the commercially available 4-methoxyphenethylmagnesium chloride (**179a**) (Scheme 2.9), which unfortunately did not lead to the formation of the desired ketone **180a** after stirring the reaction mixture at room temperature for 23 hours.



Scheme 2.9. Attempted Grignard reaction between nitrile and Grignard reagents

Instead, alkane **181** and alcohol **182** (Figure 2.2) were isolated as the degradation products of Grignard reagent **179a** alongside starting material **177a** following purification of the crude reaction mixture. This appeared to suggest that the Grignard reagent could have been deactivated or have degraded into alkane **181** and alcohol **182** before use. Thus, the Grignard reagent could not perform a nucleophilic attack onto the nitrile group. This is also supported by the observation that the thin layer chromatography (TLC) profile of the supposedly pure Grignard reagent itself showed the presence of two spots with similar R_f values to those of the alkane **181** and alcohol **182** isolated.



181 **182**

Figure 2.2. Alkane and alcohol products of Grignard reagent **179a**

Another commercially available Grignard reagent, phenethylmagnesium chloride (**179b**) was then used in place of **179a** in the reaction with nitrile **177a** (Scheme 2.9). Based on the procedure reported by Fürstner *et al.*,[190] the reaction mixture was allowed to reflux for 3 hours prior to workup. Analysis of the TLC after workup showed the presence of four spots, one of which corresponded to that of the starting material **177a**. The crude mixture was subjected to chromatographic purification and ^{1}H NMR analysis showed that the starting material **177a** was indeed recovered, while the side products isolated have complex ^{1}H NMR spectra and could not be identified. The formation of side products might be attributed to the harsh reaction condition used. The mild set of reaction condition in which we adapted for the previous model reaction between nitrile **177a** and Grignard reagent **179a** (Scheme 2.9) was subsequently reutilized in next trial reaction.

Hence, based on the procedure reported by Zhang *et al.*,[189] the reaction was carried out under milder condition by stirring the reaction mixture at room temperature for 26 hours prior to workup. Analysis of the TLC after workup showed a profile that was similar to that of the previous trial, indicating the presence of spots due to the starting material **177a** along with several side products. It seemed that the formation of side products was not due to the harsh reaction conditions used.

Weiberth *et al.*[191] reported that the product yield from reactions between Grignard reagents and nitriles can be greatly improved by the use of catalytic amount of copper (I) salts. Therefore, CuBr was used in the subsequent trial as a catalyst and the reaction mixture was refluxed for 5 hours prior to workup. As with the previous two cases, the TLC profile of the reaction mixture again showed the presence of starting material **177a** along with four unidentified side products with complex ^{1}H NMR. The synthetic route based on nitrile as the required electrophile was thus far unsuccessful.

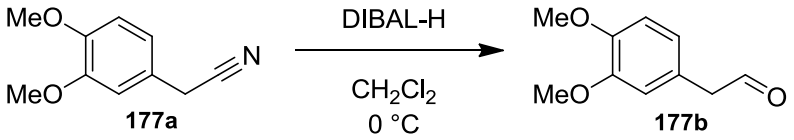
2.2.1.3 Second attempt: Grignard reaction based on benzyl aldehydes

2.2.1.3.1 Synthesis of 3,4-dimethoxyphenylacetaldehyde (177b): Reduction of nitrile 177a

The other potential electrophilic functional group that could react with a Grignard reagent was aldehyde. The alcohol formed from this Grignard reaction could then be oxidized into the desired ketone intermediate. Since aldehyde **177b** was not commercially available, we attempted to prepare it by reduction of nitrile **177a** (Table 2.1). In the first trial (entry 1, Table 2.1), the reaction conditions reported by Henrion *et al.*[192] were used and aldehyde **177b** was obtained in 6% yield. The yield was unacceptably low considering the fact that it was isolated together with an

unidentified major side product. It was thought that the addition of diisobutylaluminium hydride (DIBAL-H) all at once into the reaction mixture might have caused a rapid increase in the temperature (exothermic reaction) of the reaction solution, which in turn might have negatively affected the product yield.

Table 2.1. Reduction reactions of nitrile **177a**



Entry	Method	Time (h)	Yield (%)
1.	I	0.5	6[a]
2.	II[b]	0.2	8

[a]Yield determined based on ^{1}H NMR analysis. [b]DIBAL-H was added dropwise into the stirring solution of nitrile **177a** in CH_2Cl_2.

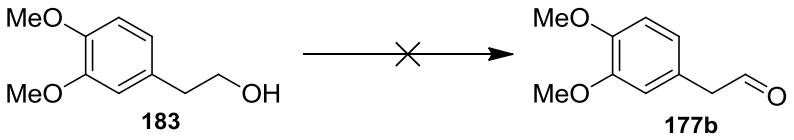
In the second trial of the same reaction (entry 2, Table 2.1), DIBAL-H was added dropwise into a stirring solution of the nitrile **177a** in CH_2Cl_2 in an ice bath. The reaction was worked up after 10 minutes and a product yield of 8% was obtained. This second attempt has also failed to increase the reaction yield. Alternative reactions to produce aldehyde **177b** in high yield must be considered following the unsuccessful optimization of reduction of nitrile **177a**.

2.2.1.3.2 Synthesis of 3,4-dimethoxyphenylacetaldehyde (177b): Oxidation of alcohol 183

Another possible route to synthesize the aldehyde precursor **177b** is selective oxidation of 3,4-dimethoxyphenethyl alcohol (**183**, Table 2.2) using two methods commonly employed to oxidize primary alcohols to aldehydes, i.e., Ley-Griffith and Dess-Martin oxidation reactions. The series of reaction conditions used in the attempt

to optimize the synthesis of aldehyde **177b** from oxidation of 3,4-dimethoxyphenethyl alcohol (**183**) are presented in Table 2.2.

Table 2.2. Attempted oxidation reactions of alcohol **183**



Entry	Method	Time (h)
1.	I[a]	6
2.	II[a]	0.75
3.	III[b]	4
4.	IV[b]	0.5
5.	V	24.5
6.	VI	3

Methods: I. $ClCH_2CH_2Cl$, tetrapropylammonium perruthenate (TPAP) (0.08 eq.), 4-methylmorpholine *N*-oxide (NMO) (1.5 eq.) and molecular sieves (MS) with addition of more TPAP (0.16 eq.), NMO (1.5 eq.) and MS after 3 hours at rt; II. CH_2Cl_2, TPAP (0.15 eq.), NMO (5 eq.) and MS at rt; III. CH_2Cl_2, TPAP (0.06 eq.), NMO (1.6 eq.) and MS with addition of more TPAP (0.09 eq.) and NMO (1.5 eq.) after 2 hours at rt; IV. CH_2Cl_2, TPAP (0.1 eq.), NMO (5 eq.) and MS at rt; V. CH_2Cl_2 and Dess-Martin periodinane (DMP) (1.2 eq.) with addition of pyridine (11 eq.), water (1.2 eq.) and acetonitrile (0.5 eq.) after 2 hours at rt; VI. CH_2Cl_2, DMP (5.5 eq.), pyridine (2.2 eq.) and water (3 eq.) at rt.
[a]Reaction workup with 0.1 M $Na_2S_2O_3$ solution, brine and saturated $CuSO_4$ solution.
[b]Filtration of reaction mixture through Celite without workup.

By using the method adapted from the procedure reported by Griffith *et al.*,[193] only an unidentified side product was obtained (similar to that previously obtained from entry 1, Table 2.1) in the first trial (entry 1, Table 2.2). Optimization of the reaction condition was thus carried out to favour the formation of the desired product.

Subsequently, excess NMO (5 equiv.) as the co-oxidant was used and the reaction time was substantially reduced (45 minutes) (entry 2, Table 2.2) since it was thought that a long reaction time (6 hours) in the first trial might have resulted in decomposition of the initially formed aldehyde product. However, no desired product was obtained for this trial. Instead, several unidentified side products were isolated

from the reaction. This suggested that the possibility of decomposition of the aldehyde due to long reaction time may not be true.

The reaction workup method was then checked to find out if it was the cause for product decomposition since aldehyde is considered as a relatively reactive functional group. Thus, the reaction mixture was only filtered through a microcolumn of Celite without workup at the end of the reaction for the third trial (entry 3, Table 2.2). Again, the desired product was not detected. Instead, several unidentified side products were obtained after purification. The result, therefore, ruled out the possibility that the workup method is problematic.

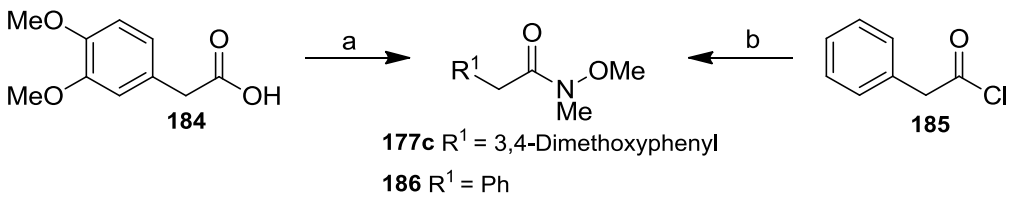
The fourth trial (entry 4, Table 2.2) combined the changes made in the second and third trials by halting the reaction after a short period of time (30 minutes) and filtering the reaction mixture through a microcolumn of Celite without workup. No formation of product was observed in this reaction. This outcome provided further confirmation that long reaction time and the workup step were not the cause for the unsuccessful formation of aldehyde **177b**.

With the failure to optimize the Ley-Griffith oxidation reaction in the previous four trials, another oxidation method involving the use of DMP was attempted. The reaction was first carried out based on the reaction condition reported by Kraus *et al.*[194] However, after 2 hours, there was little evidence that the desired product was formed based on TLC (entry 5, Table 2.2). Pyridine, water and acetonitrile were then added into the reaction mixture since Meyer *et al.*[195] reported that water was found to be able to accelerate the Dess-Martin oxidation reaction. However, the formation of the product was still not observed after 24.5 hours. Another trial (entry 6, Table 2.2)

based on the procedure reported by the same group[195] was carried out and formation of product **177b** was also not observed at the end of the reaction.

2.2.1.4 Third attempt: Weinreb ketone synthesis

The third electrophile we used for the Grignard reaction was Weinreb amide. We started off by synthesizing the relevant Weinreb amides as shown in Scheme 2.10. The treatment of carboxylic acid **184** with *N,O*-dimethylhydroxylamine hydrochloride, EDC and 4-dimethylaminopyridine (DMAP) in CH_2Cl_2 at room temperature afforded Weinreb amide **177c**.[196,197] On the other hand, treatment of phenethylacetyl chloride (**185**) with *N,O*-dimethylhydroxylamine hydrochloride and pyridine in CH_2Cl_2 from 0 °C to room temperature gave Weinreb amide **186** as a model substrate.[198]

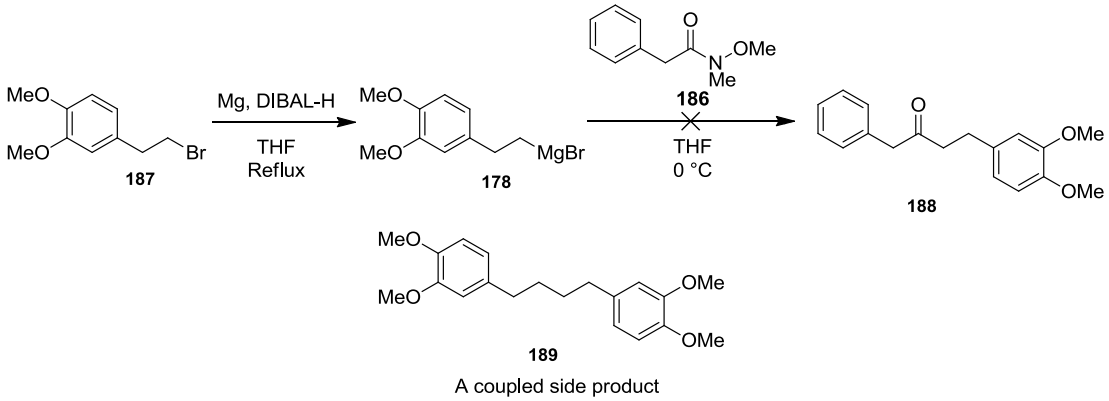


Reagents and conditions: (a) *N,O*-Dimethylhydroxylamine hydrochloride, EDC, DMAP, CH_2Cl_2, rt, 21 h, 89%; (b) *N,O*-Dimethylhydroxylamine hydrochloride, pyridine, CH_2Cl_2, 0 °C to rt, 2.5 h, 96%.

Scheme 2.10. Preparation of Weinreb amides **177c** and **186**

The model reaction first required the preparation of the Grignard reagent 3,4-dimethoxyphenethylmagnesium bromide (**178**) from 3,4-dimethoxyphenethyl bromide (**187**) (Scheme 2.11) based on the procedure reported by Chuang *et al.*[199] This was followed by addition of the Grignard reagent onto Weinreb amide **186** in an attempt to prepare ketone **188**. However, the formation of the desired product was not detected. Instead, several unidentified side products and a minute amount of 1,4-bis(3,4-dimethoxyphenyl)butane (**189**) were obtained based on ^{1}H NMR analysis. The detection of the Grignard reagent coupled product (**189**) after but not before the

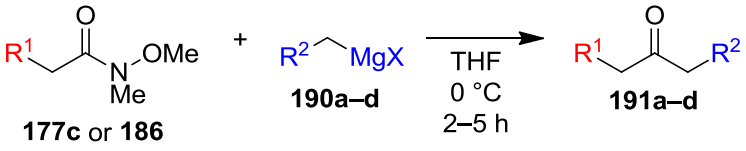
reaction was carried out, indicated that the Grignard reagent **178** was successfully formed in the reaction mixture. However, the absence of the desired product suggested that the reaction between **178** and Weinreb amide **186** did not happen.



Scheme 2.11. Attempted synthesis of ketone precursor **188**

However, when several other Grignard reagents (**190a–c**) were used in place of **178** to react with amide **186**, the reactions proceeded smoothly in THF at 0 °C to produce ketones **191a–c** (Table 2.3).[200] Interestingly, the reaction involving Weinreb amide **177c** and 4-methoxyphenethylmagnesium bromide (**190d**) was also successful, giving the desired product **191d** in good yield (Table 2.3).

Table 2.3. Weinreb ketone synthesis using different Grignard reagents



R^1	R^2	X	Yield (%)	Product
Ph (**186**)	3,4-Dimethoxybenzyl	Br (**178**)	-	Nil
Ph (**186**)	Bn	Cl (**190a**)	59	**191a**
Ph (**186**)	Et	Cl (**190b**)	62	**191b**
Ph (**186**)	Ph	Br (**190c**)[a]	45	**191c**
3,4-Dimethoxyphenyl (**177c**)	4-Methoxybenzyl	Cl (**190d**)	70	**191d**

[a]Prepared from benzyl bromide and Mg turnings in THF at room temperature.

In an attempt to work out a possible explanation of why the reaction involving 3,4-dimethoxyphenethylmagnesium bromide (**178**) was unsuccessful, the mechanism previously established for the reaction between a Weinreb amide and an organometallic reagent was considered (Scheme 2.4).[178,182] Based on the proposed reaction mechanism (mentioned in Section 2.1.2), we postulated that the reason why **178** was unreactive towards the Weinreb amide is because the Mg metal centre in **178** was too strongly chelated to the 3,4-dimethoxy group of another molecule of **178** (Figure 2.3), unlike the usual chelation to ethereal solvent molecules.[173,201,202] Therefore, the crucial metal-chelated intermediate as presented in Scheme 2.4 could not be formed, thus prevented Weinreb ketone synthesis. A search in the literature has only showed four previous reports that recorded reactions involving **178**,[199,203–205] which suggests that this particular Grignard reagent was rarely used in reactions compared to other Grignard reagents. This could be because **178** is not particularly reactive and therefore it has very limited uses.

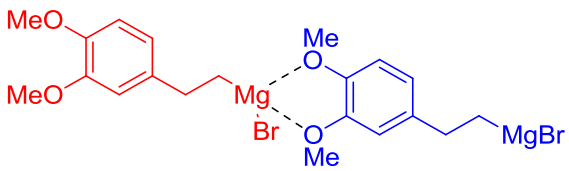


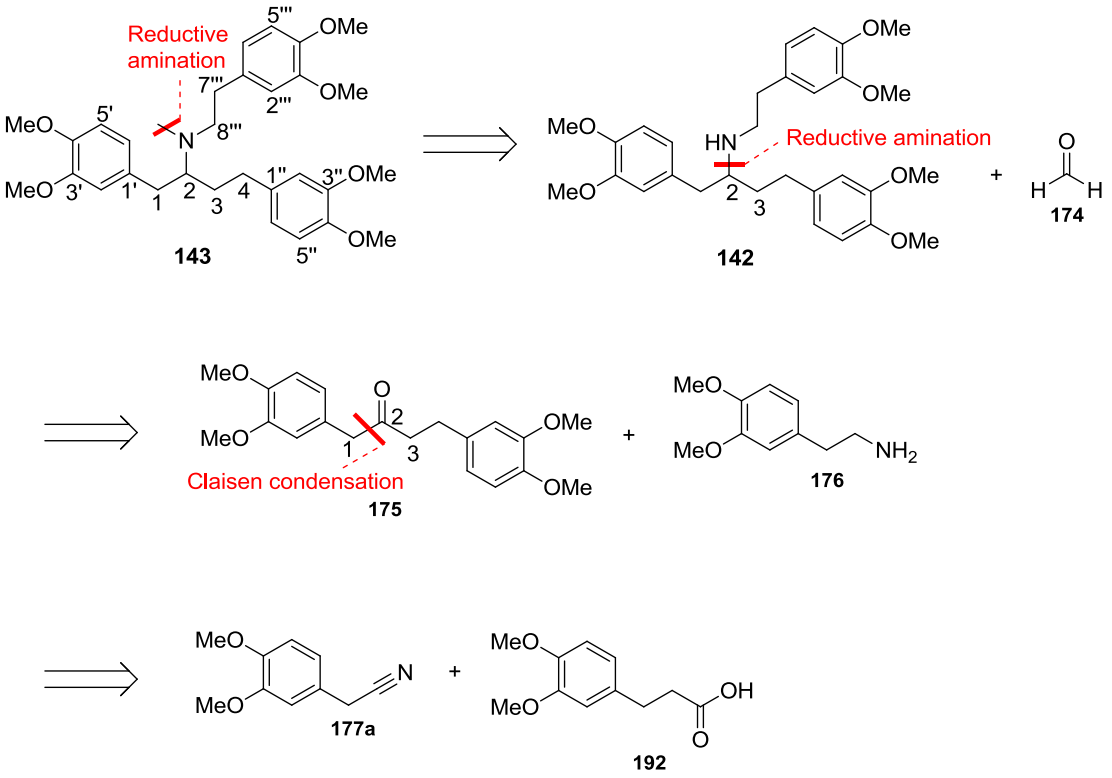
Figure 2.3. Possible formation of a chelated complex between two molecules of **178**

It is worth noting that the reaction involving Weinreb amide **177c**, which consists of the 3,4-dimethoxy moiety, and Grignard reagent **190d** was unexpectedly successful. This may be because the excess Grignard reagent **190d** used (4.5 equiv.) overcame the chelation effect due to the 3,4-dimethoxy moiety present in **177c**. In any case, with the unsuccessful synthesis of ketone **188**, it was thought that another synthetic route to schwarzinicines A (**142**) and B (**143**) must be considered.

2.2.2 Fourth approach to synthesize 142 and 143

2.2.2.1 Retrosynthetic analysis

An alternative retrosynthetic analysis of schwarzinicines A (**142**) and B (**143**) is depicted in Scheme 2.12. Compared to the initial retrosynthetic route (Scheme 2.8), the requisite ketone precursor **175** would now be constructed from a Claisen condensation between nitrile **177a** and an ester derivative of (3,4-dimethoxyphenyl)propionic acid (**192**).



Scheme 2.12. An alternative retrosynthetic analysis of **142** and **143**

Notably, the disconnection in **175** was made at the C-1–C-2 bond in the alternative retrosynthetic route (Scheme 2.12), while the initial route (Scheme 2.8) involved a C-2–C-3 bond disconnection. Additionally, nitrile **177a** would react as a nucleophile in Scheme 2.12 (Claisen reaction), whereas in Scheme 2.8, nitrile **177a** would react as an electrophile (Grignard reaction).

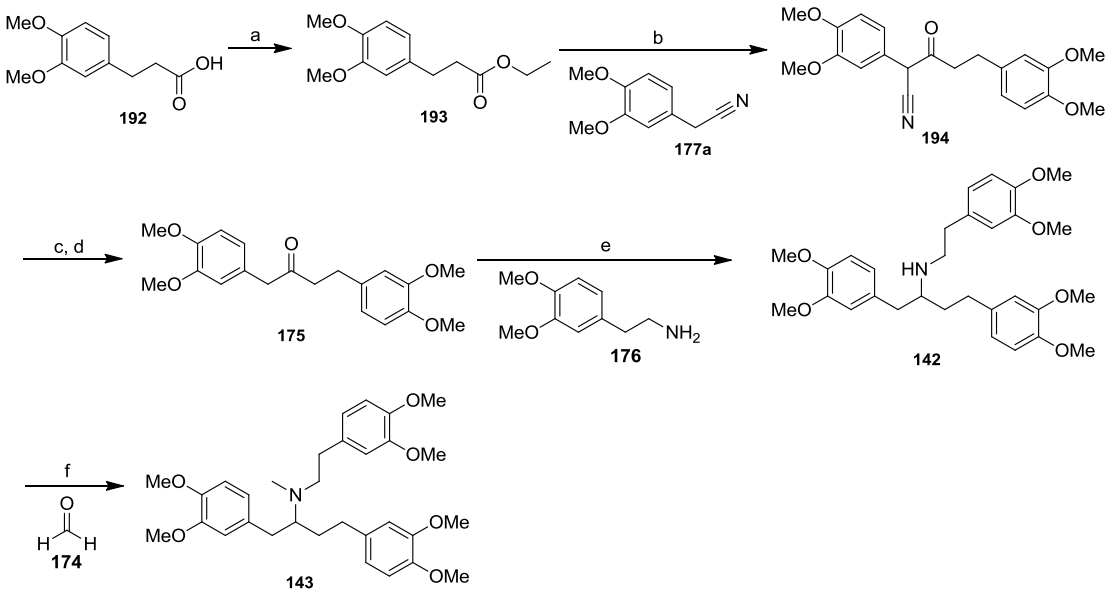
2.2.2.2 Full synthetic route to 142 and 143

Schwarzinicines A (**142**) and B (**143**) were successfully synthesized based on the synthetic route shown in Scheme 2.13. First of all, ester **193** was prepared in excellent yield via a Steglich esterification[206] of the commercially available carboxylic acid **192** with EtOH in the presence of EDC and DMAP. Subsequently, ester **193** underwent a Claisen condensation with nitrile **177a**, which was first treated with *n*-BuLi in THF at 0 °C, to furnish ketonitrile **194**.

Hydrolysis of ketonitrile **194** with a mixture of AcOH and concentrated HCl at 60 °C produced the expected amide, which was further hydrolyzed and decarboxylated *in situ* after the reaction mixture was diluted with water and refluxed to furnish ketone **175**. It is worth noting that this reaction procedure was adapted from the one initially reported by Carroll *et al.*[207] Our initial attempt following the exact procedure, whereby stirring of ketonitrile **194** in a mixture of AcOH and concentrated HCl for four days followed by addition of water into the mixture and allowing it to stand at room temperature for 24 hours, gave the desired amide product in 27% yield, which was comparable to the reported yield of 25%.[207] Unexpectedly, we also detected a minute amount of ketone **175** in addition to the amide product, an observation that was not previously reported by Carroll *et al.*[207] This inspired us to optimize the synthetic procedure to favour the formation of ketone **175** by possibly avoiding long hours of reaction and the need to isolate the amide intermediate. A one-pot *in situ* synthetic strategy was eventually devised and it proved to be quite successful. To our delight, ketone **175** was obtained as the sole product in 61% yield based on the optimized procedure, i.e., three-hour, one-pot reaction constituting nitrile hydrolysis cum *in situ* decarboxylation of ketonitrile **194**. Our modified procedure in the preparation of ketone **175** was superior over the original procedure reported by

Carroll *et al.* (two reaction steps, over five days), which only yielded a meagre 13% overall yield of **175**.[207] Interestingly, ketone **175** was recently isolated as a natural product from the leaves of *Ficus nota* and assigned the trivial name ficusnotin E.[158] To date, only one group has reported the total synthesis of ficusnotin E.[208] The spectroscopic data of our synthetic ketone **175** are in complete agreement with those reported for ficusnotin E.[158]

Finally, a reductive amination reaction[183,186] of ketone **175** with $NaBH(OAc)_3$ in the presence of DMPEA (**176**) furnished **142** in 38% yield. A second reductive amination reaction between formaldehyde (**174**) and **142** in the presence of $NaBH_3CN$ and AcOH in MeOH provided **143** in 50% yield. $NaBH_3CN$ was used instead of $NaBH(OAc)_3$ in the second reductive amination step as the reaction was carried out under aqueous condition due to the use of formaldehyde (**174**) solution (37% in water) and $NaBH_3CN$ is known to tolerate aqueous conditions better.



Reagents and conditions: (a) EtOH, EDC, DMAP, CH_2Cl_2, 0 °C to rt, 2.5 h, 82%; (b) **177a**, *n*-BuLi, THF, 0 °C, 5 min, 23%; (c) AcOH, conc. HCl, 60 °C, 2 h; (d) H_2O, reflux, 1 h, 61%; (e) **176**, $NaBH(OAc)_3$, AcOH, $ClCH_2CH_2Cl$, rt, 30 h, 38%; (f) **174**, $NaBH_3CN$, AcOH, MeOH, rt, 23 h, 50%.

Scheme 2.13. Synthetic route to schwarzinicines A (**142**) and B (**143**)

The ^{1}H and ^{13}C NMR data of synthetic **142** and **143** are in complete agreement with those of the natural compounds,[170] as shown in Figures 2.4–2.7. Both synthetic **142** and **143** were obtained as racemic mixtures and they are optically inactive. This is consistent with their chiral HPLC profiles with each profile showing two peaks in a ratio of 1:1. In contrast, chiral HPLC showed natural schwarzinicine A (**142**) to be a scalemic mixture (ratio of 4:1), while schwarzinicine B (**143**) is enantiomerically pure.[170] The chiral HPLC profiles for natural and synthetic **142** and **143** are shown in Appendix (Figures S13–S16). In short, the first total syntheses of schwarzinicines A (**142)** and B (**143**) via ketone **175** as the key intermediate were accomplished in four and five steps with overall yields of 4.4% and 2.2%, respectively.

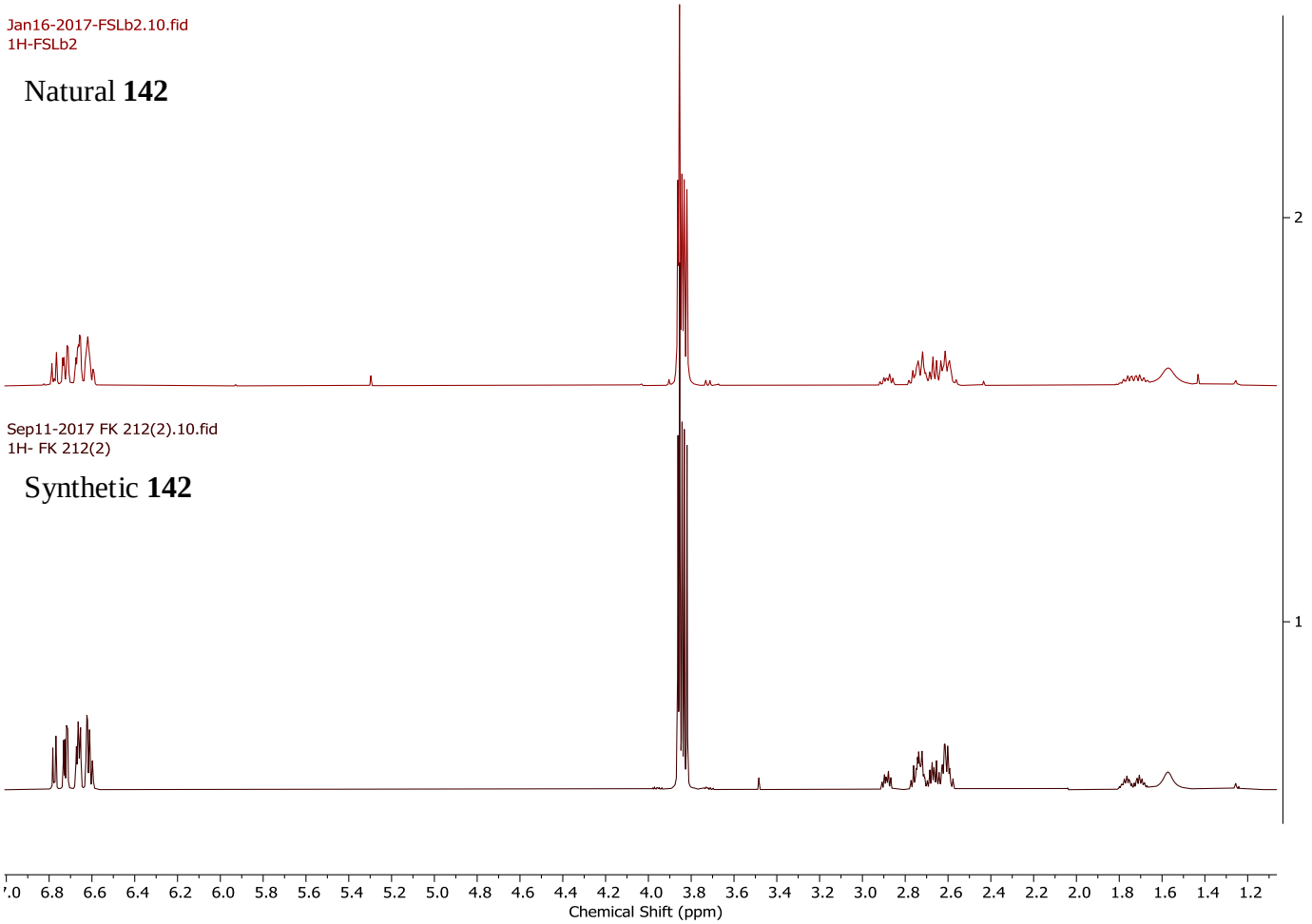


Figure 2.4. ^{1}H NMR spectra of natural and synthetic schwarzinicine A (**142**) ($CDCl_3$, 600 MHz)

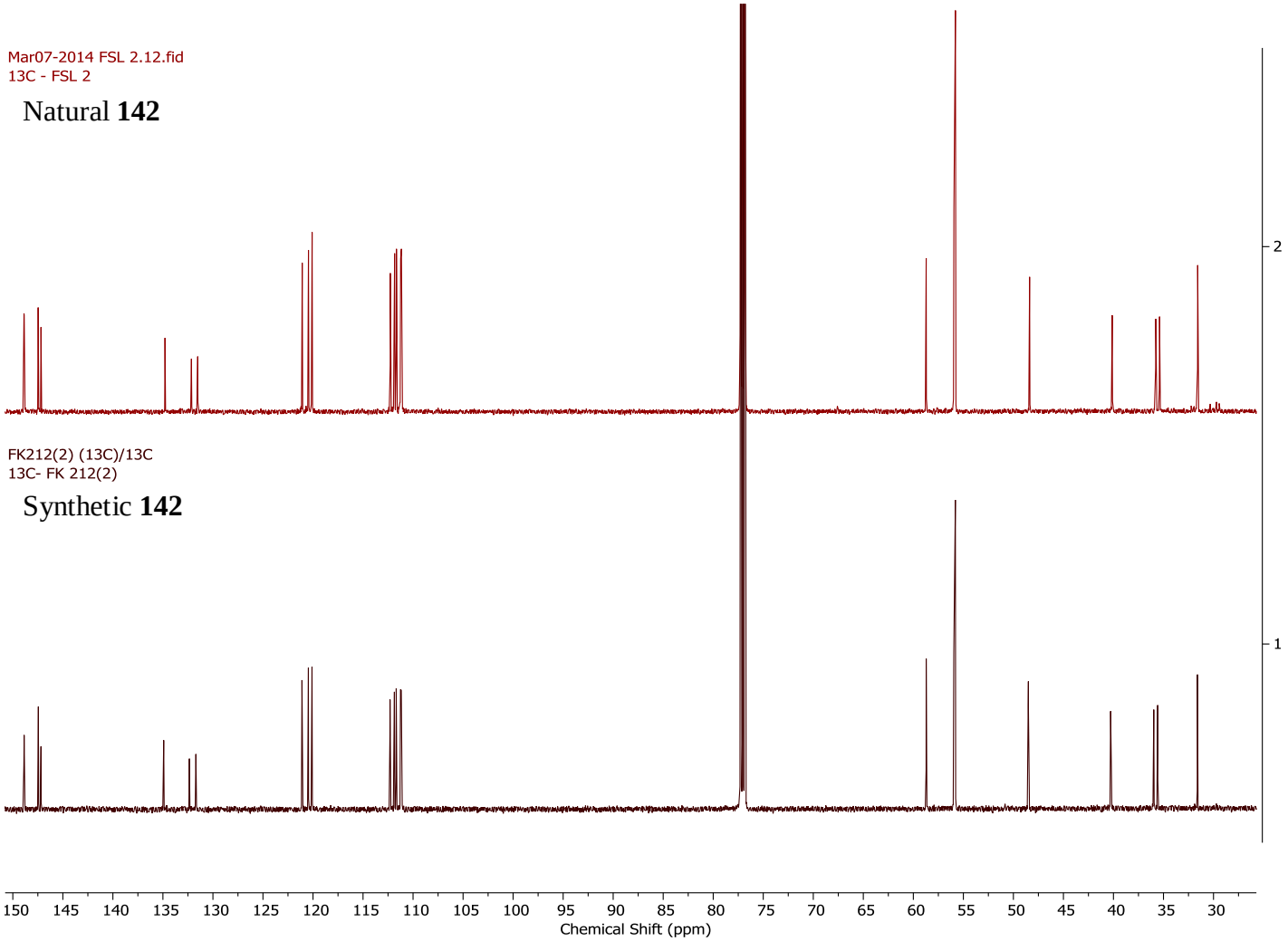


Figure 2.5. ^{13}C NMR spectra of natural and synthetic schwarzinicine A (**142**) ($CDCl_3$, 150 MHz)

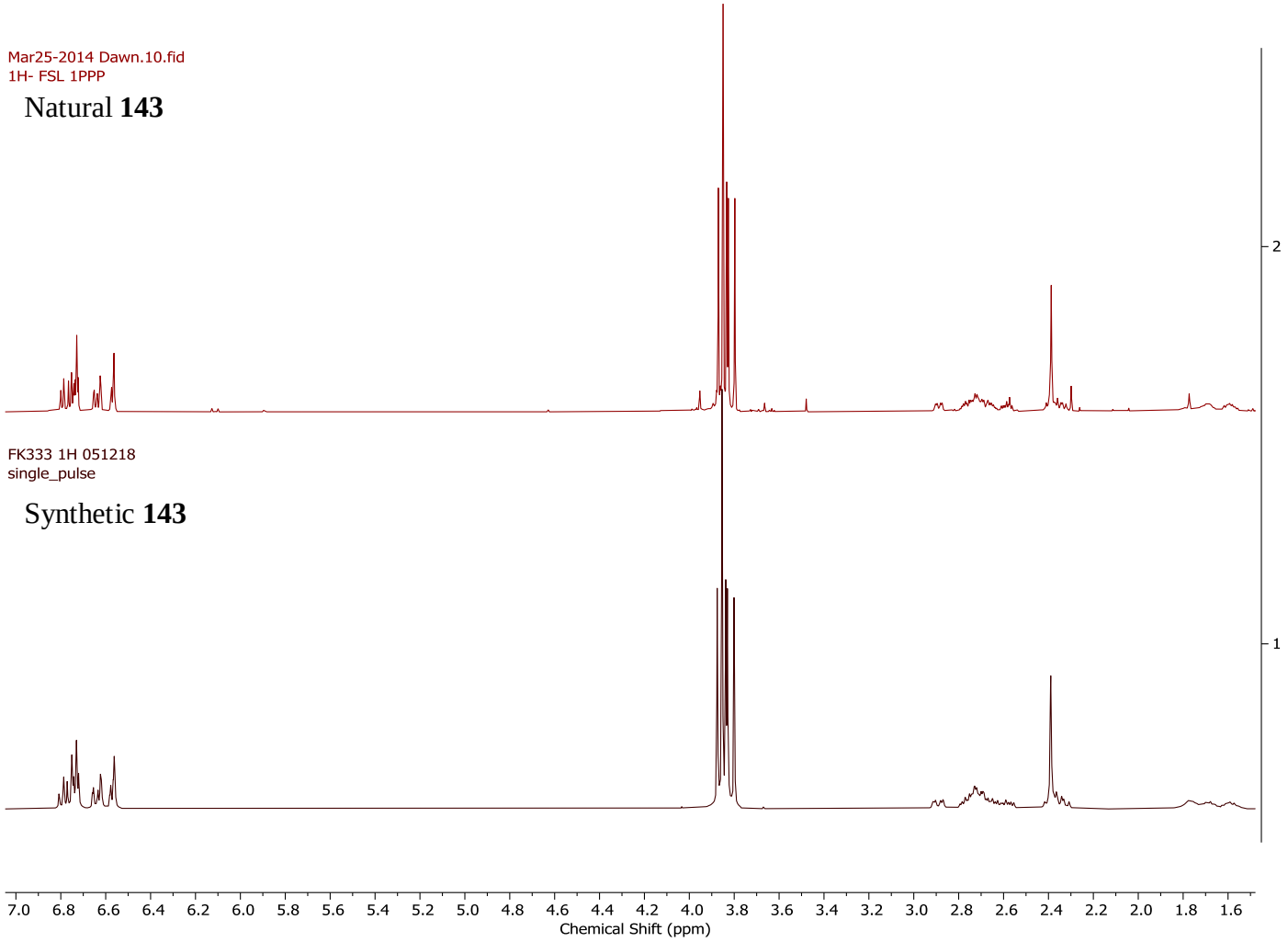


Figure 2.6. ^{1}H NMR spectra of natural and synthetic schwarzinicine B (**143**) in ($CDCl_3$, 400 MHz)

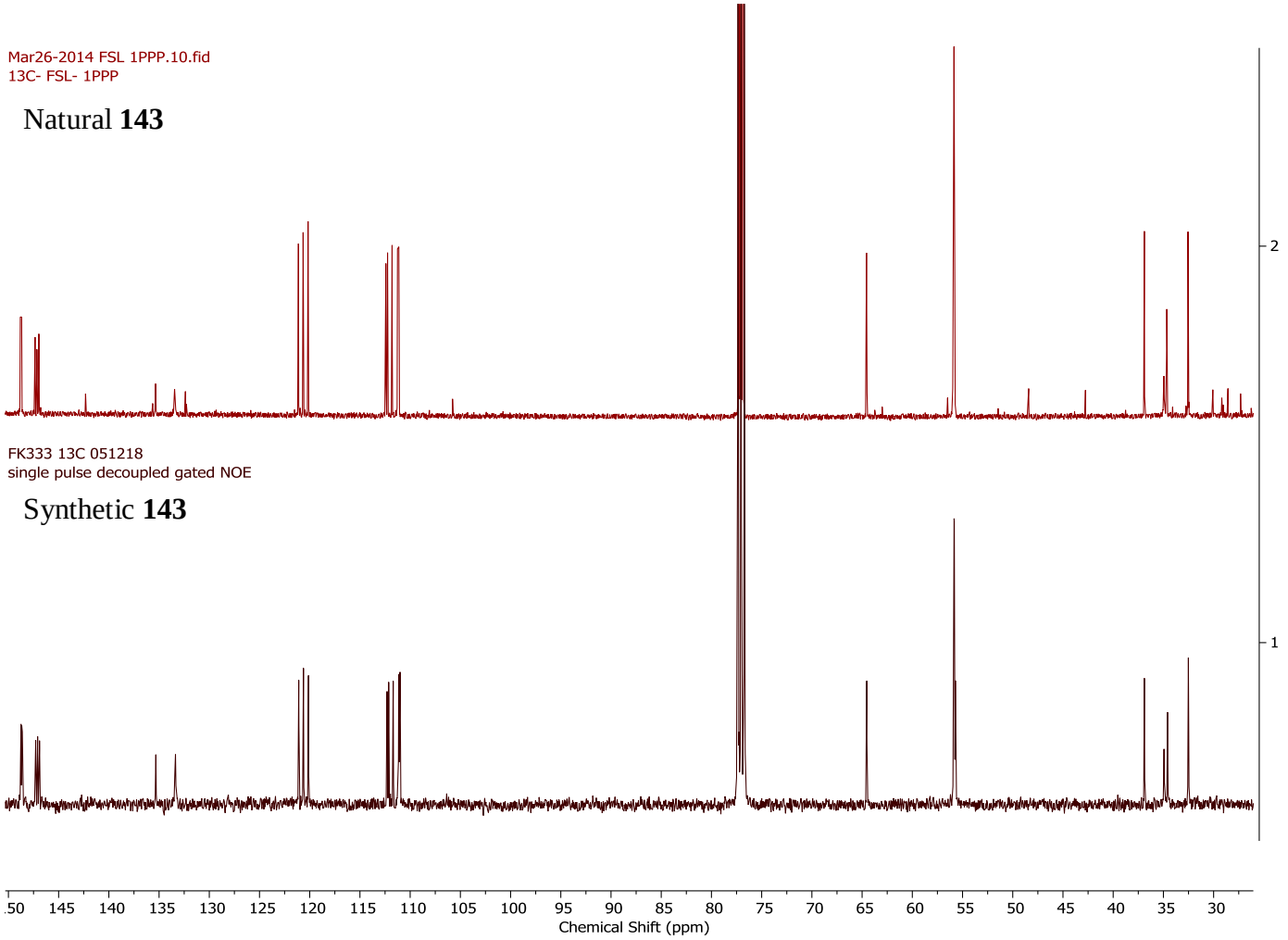


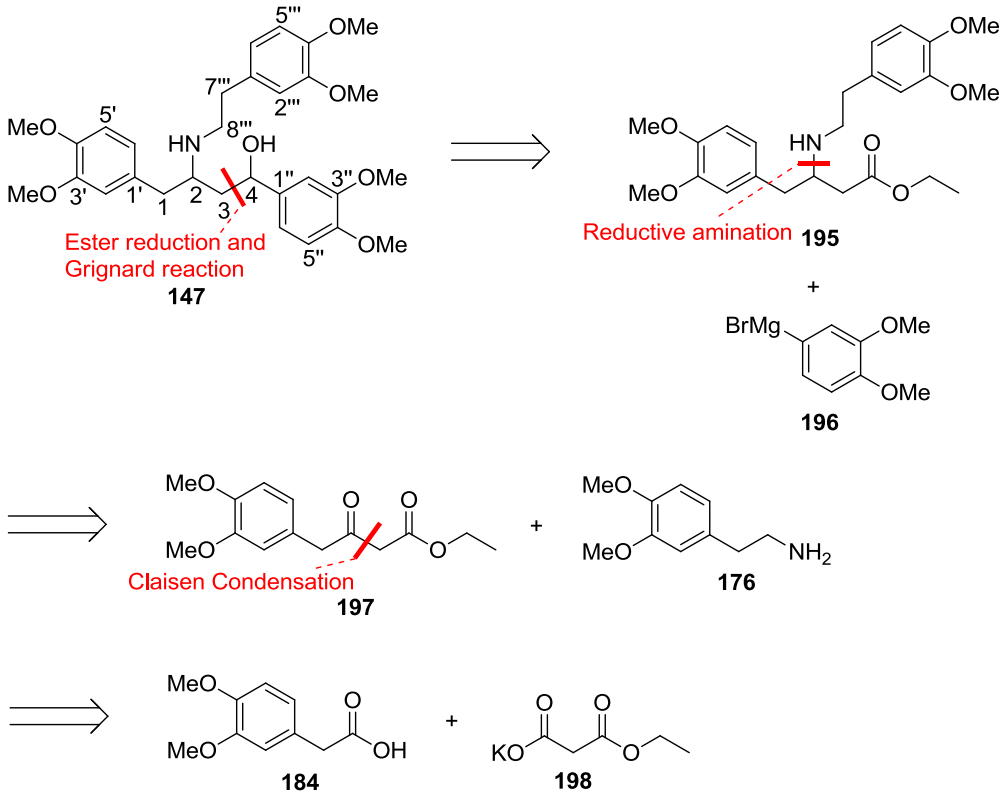
Figure 2.7. ^{13}C NMR spectra of natural and synthetic schwarzinicine B (**143**) in ($CDCl_3$, 100 MHz)

2.3 Total synthesis of schwarzinicine F (147)

2.3.1 First attempt to synthesize 147

2.3.1.1 Retrosynthetic analysis

Compared to schwarzinicines A (**142**) and B (**143**), the challenge in synthesizing schwarzinicine F (**147**) lay in the presence of a benzylic hydroxyl group in the molecule of **147**. The retrosynthetic analysis of **147** is shown in Scheme 2.14. Retrosynthetically, the C-3–C-4 bond in **147** could be forged by a Grignard reaction between the aldehyde analogue of **195** and Grignard reagent **196**. Amine **195** could be prepared from a reductive amination reaction between DMPEA (**176**) and β-ketoester **197**, which could in turn be constructed from a Claisen condensation reaction between carboxylic acid **184** and ethyl potassium malonate (**198**).

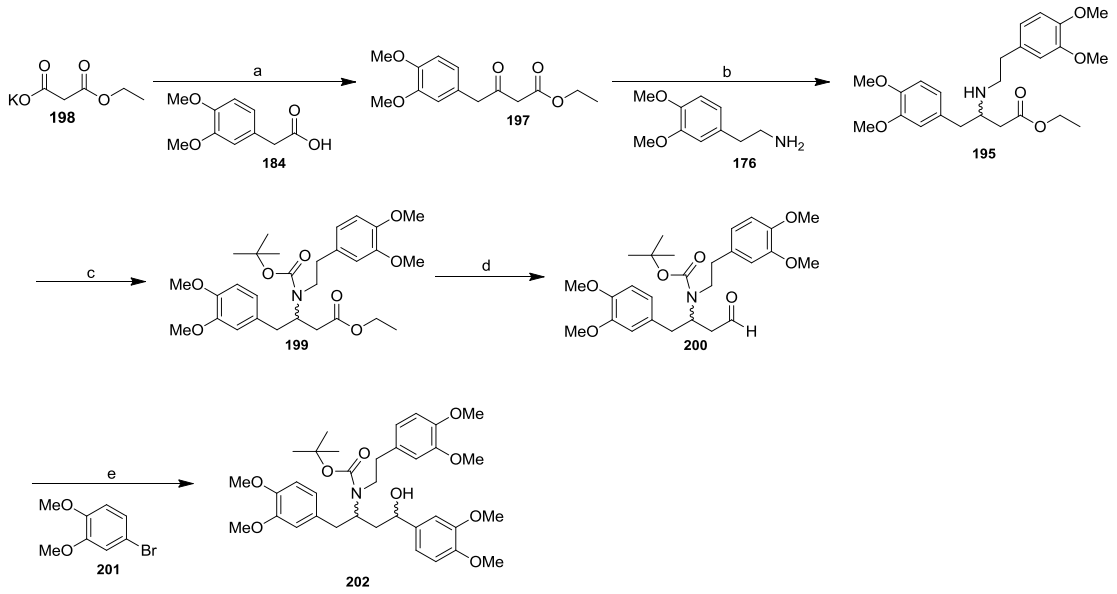


Scheme 2.14. Retrosynthetic analysis of schwarzinicine F (**147**)

It was anticipated that this synthetic route would give rise to four stereoisomeric products, or, in other words, i.e., two pairs of diastereomeric enantiomers. This route was advantageous as it gave access to both diastereomeric enantiomer pairs required for confirmation of the structure of natural schwarzinicine F (**147**); one of these four stereoisomers was expected to correspond to natural **147**, assuming it to be enantiomerically pure.

2.3.1.2 Synthetic studies to 147

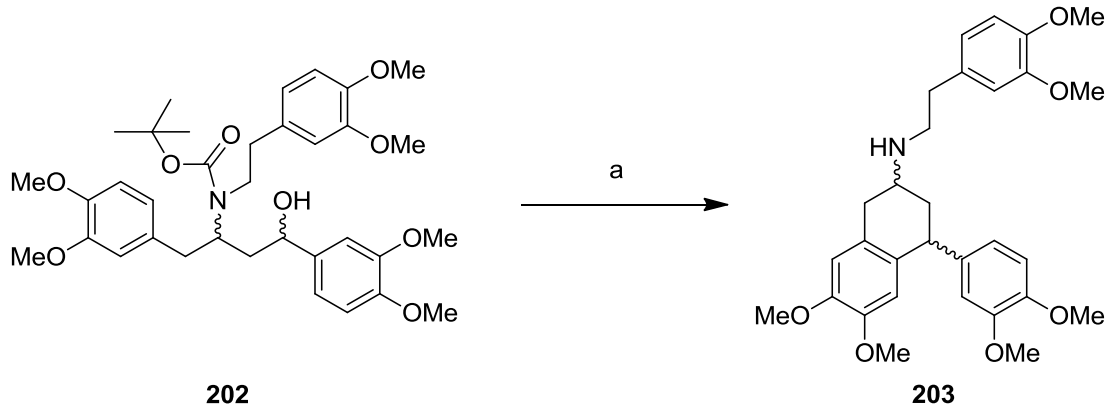
As illustrated in Scheme 2.15, our first attempted synthesis to **147** started with a Claisen condensation between carboxylic acid **184** and ethyl potassium malonate (**198**) in the presence of $MgCl_2$ in THF under reflux condition,[209,210] which smoothly afforded β-ketoester **197** in 87% yield. Reductive amination of **197** with $NaBH(OAc)_3$ in the presence of DMPEA (**176**) gave amine **195** in 45% yield. The NH group in **195** was then protected with a Boc group[211] in amine **199** to ensure that it would not interfere with the subsequent reaction steps. The ethyl ester group in **199** was smoothly reduced to an aldehyde group in **200** with DIBAL-H.[212] Aldehyde **200** was then reacted with the Grignard reagent of aryl bromide **201** to yield **202** as a mixture of four stereoisomers in 68% combined yield. By using chromatographic separation on silica, the mixture was separated into the two diastereomeric pairs of **202** in 1:1 ratio. Without determining their relative configurations, one of these diastereomeric pairs was subjected to an *N*-Boc deprotection step. We intended to only probe the feasibility of the *N*-Boc deprotection step, while the relative/absolute configurations of the final target products if obtained, could be determined at a later stage.



Reagents and conditions: (a) $MgCl_2$, THF, reflux, 3 h; **184**, CDI, THF, rt, 45 min; rt, 18 h, 87%; (b) **176**, $NaBH(OAc)_3$, AcOH, $ClCH_2CH_2Cl$, rt, 27 h, 45%; (c) Di-*tert*-butyl dicarbonate, Et_3N, DMAP, THF, rt, 6 h, 68%; (d) DIBAL-H, CH_2Cl_2, -78 °C, 20 min, 86%; (e) **201**, Mg, THF, reflux, 2 h; THF, rt, 1.5 h, 68% for two pairs of diastereomeric enantiomers.

Scheme 2.15. Synthesis of **202**

Attempt to deprotect the *N*-Boc group in **202** with trifluoroacetic acid (TFA) as shown in Scheme 2.16 based on the procedure reported by Alonso *et al.*,[213] however, yielded the cyclized products **203a–d** (four stereoisomers, Figure 2.8), rather than the expected stereoisomeric products of **147a–d**.



Reagents and conditions: (a) TFA, CH_2Cl_2, 0 °C to rt, 50 min, 12% for two pairs of diastereomeric enantiomers.

Scheme 2.16. Attempted *N*-Boc deprotection of compound **202**

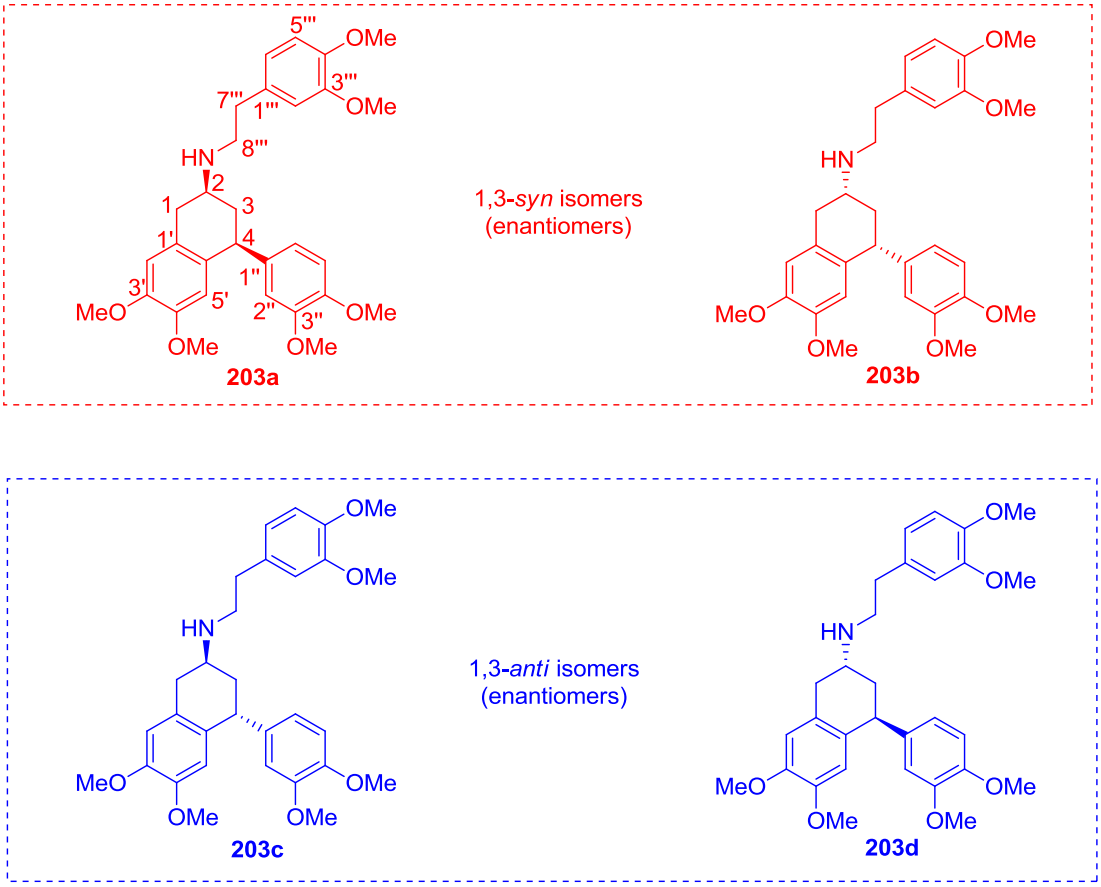


Figure 2.8. The structures of four stereoisomers of **203**

The two diastereomeric pairs of enantiomers of **203** were separated using silica chromatography and the 2D structure of the two racemic diastereomers (i.e., **203a/203b** and **203c/203d**), as shown in Figure 2.8, was established by HRESIMS, 1D (^{1}H and ^{13}C) and 2D (HSQC, COSY and HMBC) NMR data. The NMR data for both diastereomers are shown in Table 2.4. Since their relative configurations were not established, the two sets of NMR data were only assigned to 'Diastereomeric pair 1' and 'Diastereomeric pair 2'. As expected, the ^{1}H and ^{13}C spectra for both diastereomers were significantly different as shown in Figures 2.9 and 2.10. No further attempt was made to resolve the stereochemical issue of the cyclized products **203** since it is not the aim of the present project.

Table 2.4. ^{1}H (700 MHz) and ^{13}C (175 MHz) NMR data of the diastereomers of **203** in $CDCl_3$

Position	Diastereomeric pair 1		Diastereomeric pair 2	
	δ_H	δ_C	δ_H	δ_C
1	3.23 m[a]	32.7	3.34 m[a]	32.7
	3.37 m		3.46 m	
2	3.43 m	55.2	3.34 m[a]	51.6
3	2.24 q (12.3)	36.5	2.45 d (12.1)	34.2
	2.76 d (12.1)		2.53 td (12.0, 5.7)	
4	3.96 dd (12.4, 5.7)	45.1	4.29 m	42.7
1'	-	124.2	-	127.9
2'	6.50 s	111.3	6.42 s[b]	112.3[a]
3'	-	147.9[a]	-	148.2[b]
4'	-	147.8[a]	-	149.0[b]
5'	6.21 s	111.9	6.47 s[b]	124.8[a]
6'	-	130.1	-	110.9
1''	-	136.8	-	137.7
2''	6.58 d (2.1)	111.3	6.54 d (1.5)	111.4
3''	-	147.8	-	147.7[c]
4''	-	148.1	-	148.1[c]
5''	6.65 m[b]	111.4	6.70 d (8.3)	111.0
6''	6.65 m[b]	120.6	6.33 dd (8.5, 2.1)	120.5
1'''	-	128.8	-	128.8
2'''	6.77 d (7.9)	111.7	6.71 m[c]	111.8
3'''	-	149.1[b]	-	149.2[d]
4'''	-	148.9[b]	-	148.2[d]
5'''	6.70 m[c]	112.0	6.75 d (8.7)[b]	111.5
6'''	6.70 m[c]	120.7	6.71 m[c]	120.7
7'''	3.23 m[a]	32.4	3.21 t (8.5)	32.2
8'''	3.23 m[a]	46.8	3.04 m	47.1
			3.13 m	
3'-, 4'-,	3.57 (3H, s)[d]	55.7–56.0[c]	3.71 (2 x 3H, s)[d]	55.7–56.0[e]
3''-, 4''-,	3.73 (3H, s)[d]		3.79 (3H, s)[d]	
3'''-, 4'''-	3.756 (3H, s)[d]		3.81 (3H, s)[d]	
OMe	3.762 (3H, s)[d]		3.82 (3H, s)[d]	
	3.84 (3H, s)[d]		3.84 (3H, s)[d]	
	3.86 (6H, s)[d]			

[a–e]Assignments may be interchanged within each column due to severe or partial overlapped of signals.

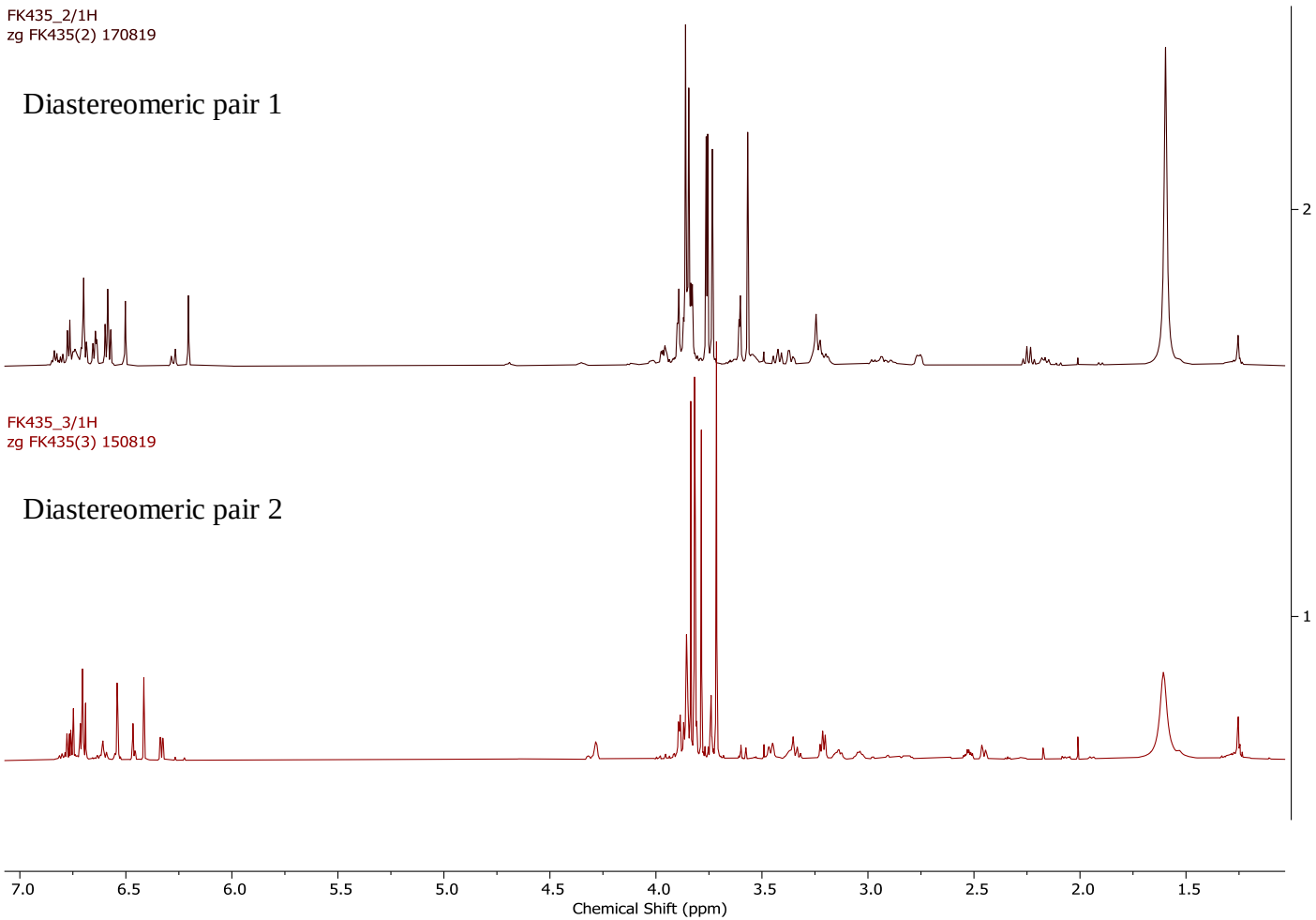


Figure 2.9. ^{1}H NMR spectra of the two diastereomers of **203** ($CDCl_3$, 700 MHz)

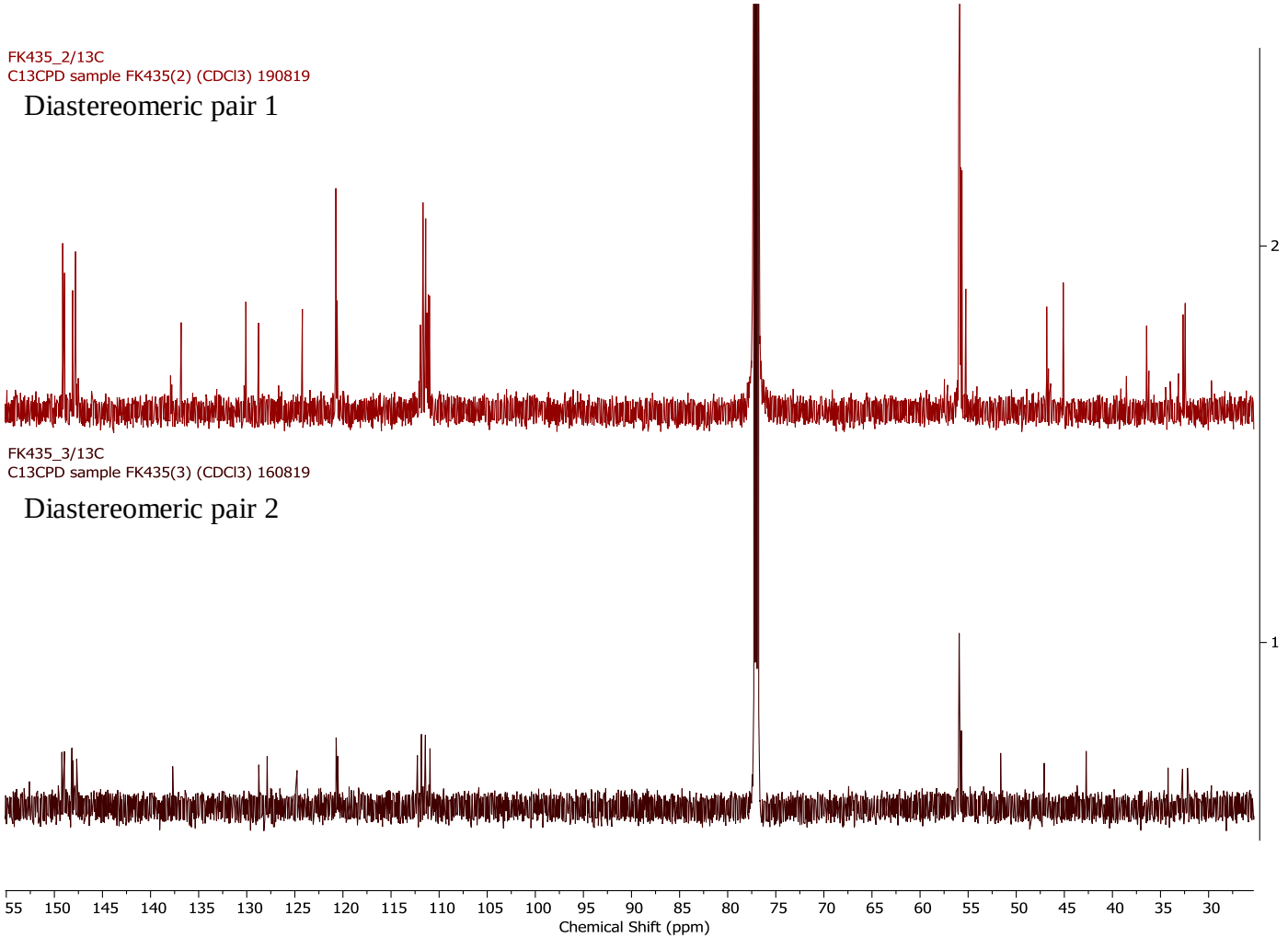
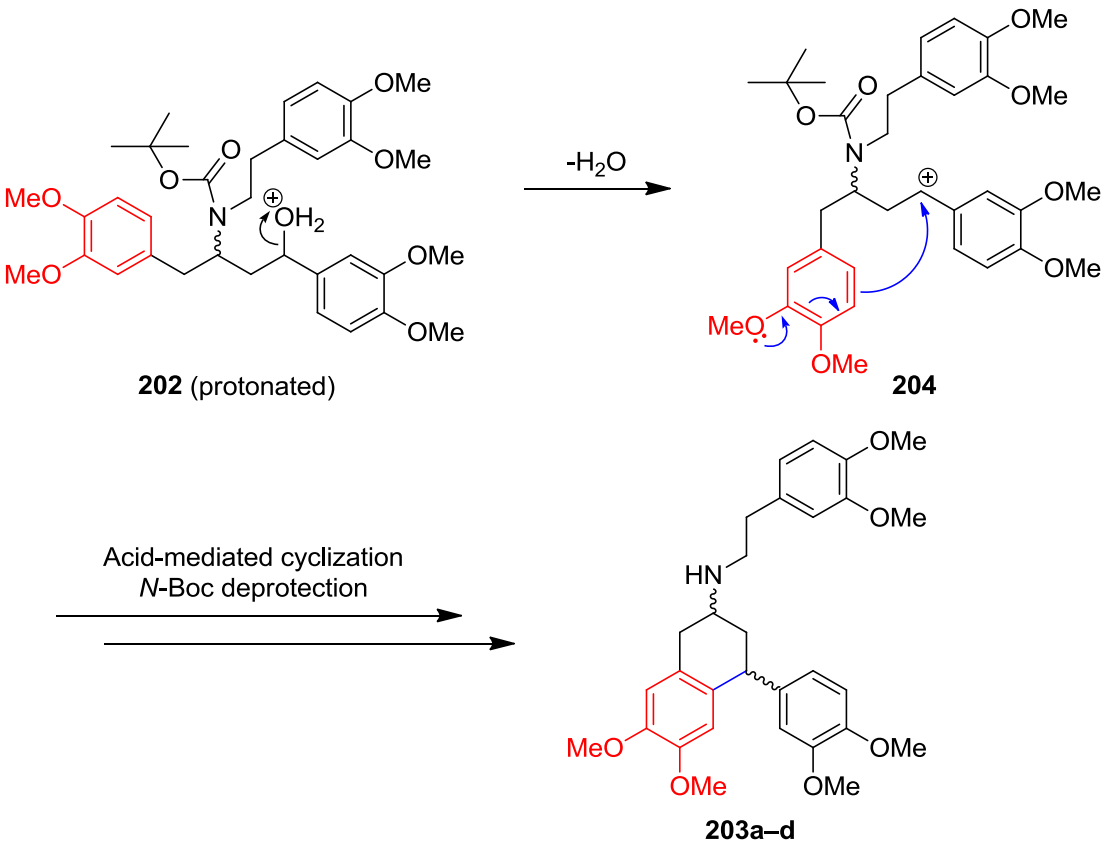


Figure 2.10. ^{13}C NMR spectra of the two diastereomers of **203** ($CDCl_3$, 175 MHz)

Nonetheless, the cyclization reaction may be explained by the mechanism proposed in Scheme 2.17. It is envisaged that in addition to the intended *N*-Boc deprotection step, the benzylic alcohol function in **202** readily undergoes a dehydroxylation under acidic conditions. As a result, when **202** was treated with TFA, the resonance stabilized benzylic carbocation **204** was formed, which was subsequently trapped by the 3,4-dimethoxyphenyl group that is located at the other end of the butanoid chain (directed by *para*-positioned methoxy group). This eventually gave rise to the *N*-Boc deprotected cyclized products **203**. A similar acid-mediated cyclization reaction involving 1-(3,4-dimethoxyphenyl)-4-hydroxy-4-(4-methoxyphenyl)-butan-2-one and polyphosphoric acid, reported previously by Bertolini *et al.*[214], provided support for the cyclization mechanism proposed in Scheme 2.17.



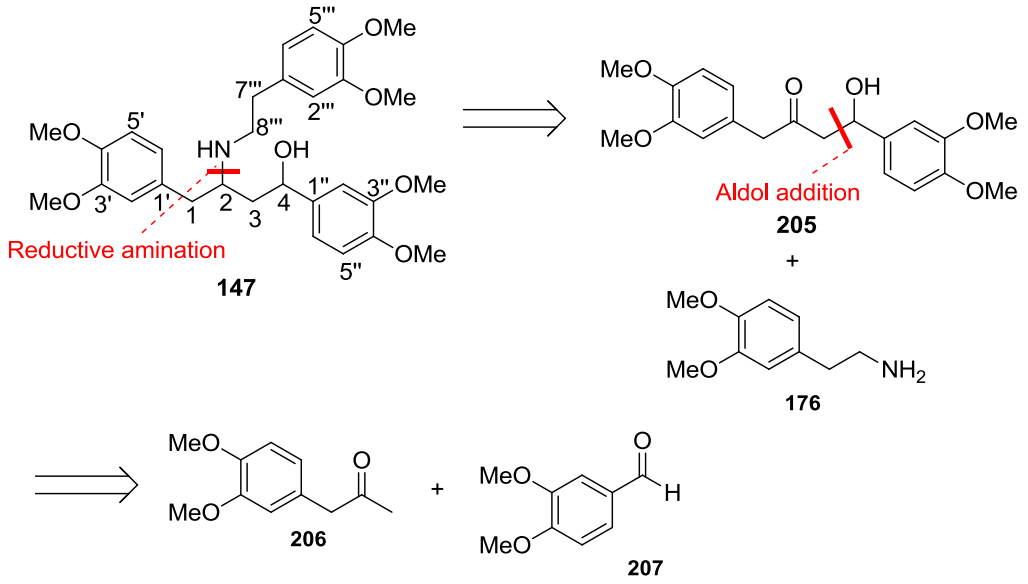
Scheme 2.17. Postulated mechanism for the conversion of **202** to **203a–d**

Interestingly, the planar structure of **203** possesses an identical C-N skeleton to two alkaloids, namely, schwarzificusines A (**149**) and B (**150**), that were obtained from the leaves of *Ficus schwarzii* (unpublished). Specifically, **203** represents the *O*-methyl derivative of **149** and **150**.

2.3.2 Second approach to synthesize 147

2.3.2.1 Retrosynthetic analysis

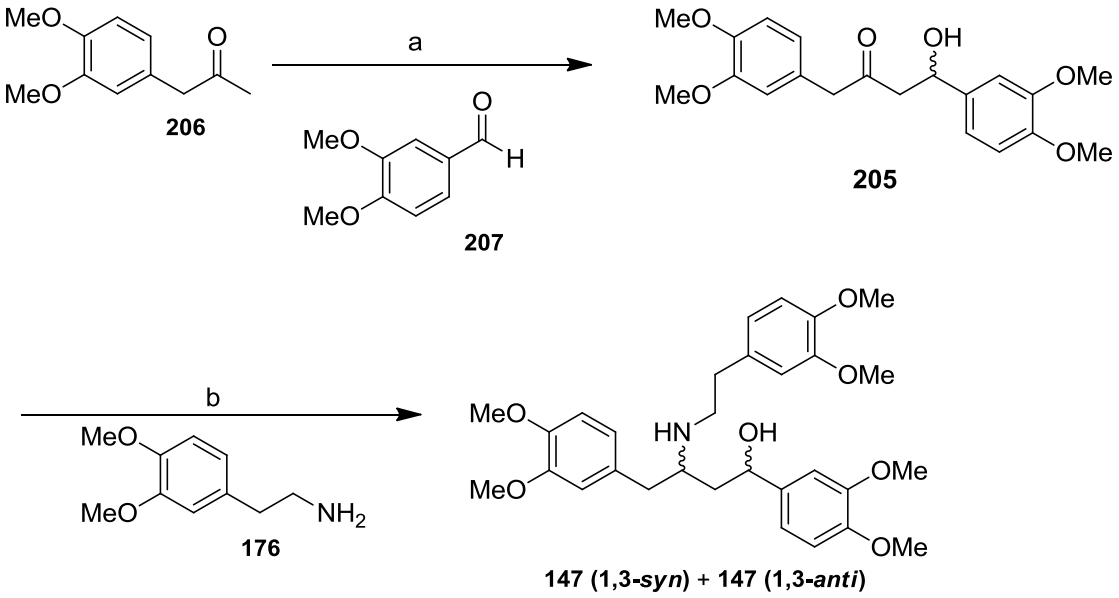
Since the first synthetic approach failed to produce isolable schwarzinicine F (**147**) due to the presence of the labile benzylic alcohol function, a different synthetic route was considered. An alternative retrosynthetic analysis to **147** was devised as shown in Scheme 2.18, featuring a shorter route compared to the first approach. Retrosynthetically, **147** could be formed by a reductive amination reaction between 3-hydroxyketone **205** and DMPEA (**176**). 3-Hydroxyketone **205** could be prepared by an aldol addition reaction between 3,4-dimethoxyphenylacetone (**206**) and veratraldehyde (**207**). As with the first synthetic attempt, this synthetic plan would also give rise to four stereoisomeric products.



Scheme 2.18. Retrosynthetic analysis of schwarzinicine F (**147**)

2.3.2.2 Full synthetic route to 147

As illustrated in Scheme 2.19, the synthesis of 3-hydroxyketone **205** commenced with an aldol addition reaction between ketone **206** and veratraldehyde (**207**) using lithium diisopropylamide (LDA) as a base to afford the desired aldol product **205**.[214] This was followed by a reductive amination reaction of 3-hydroxyketone **205** with $NaBH_3CN$ in the presence of DMPEA (**176**). $MgSO_4$ was added into the reaction mixture to ensure that the reaction was carried out under anhydrous condition. The reaction afforded a major (41% yield) and a minor product (7% yield). Analyses of the HRESIMS, 1D (^1H and ^{13}C) and 2D (HSQC, COSY and HMBC) NMR spectroscopic data suggested the two products to be diastereomeric.



Reagents and conditions: (a) LDA, **207**, THF, -78 °C, 4.5 h, 47%; (b) **176**, $NaBH_3CN$, AcOH, $MgSO_4$, THF, 0 °C to rt, 23 h, 41% 1,3-*syn* and 7% 1,3-*anti*.

Scheme 2.19. Second approach to schwarzinicine F (**147**)

Based on the work of Haddad *et al.* (see Section 2.1.3),[187] the major product (**147a**/**147b**) corresponds to the 1,3-*syn*-aminoalcohol pair of enantiomers, while the minor product (**147c**/**147d**) corresponds to the 1,3-*anti*-aminoalcohol pair of

enantiomers (Figure 2.11). The ^{1}H and ^{13}C NMR data of natural schwarzinicine F (**147**) and the major product (**147a/147b**) were compared (Table 2.5, Figures 2.12 and 2.13). Although there are many similarities between the NMR data of **147a/147b** and those of natural **147**, there are also significant deviations, particularly for the chemical shifts associated with the butanoid chain (H/C-1–H/C-4). This inferred that **147a/147b** is diastereomerically related to natural **147**.

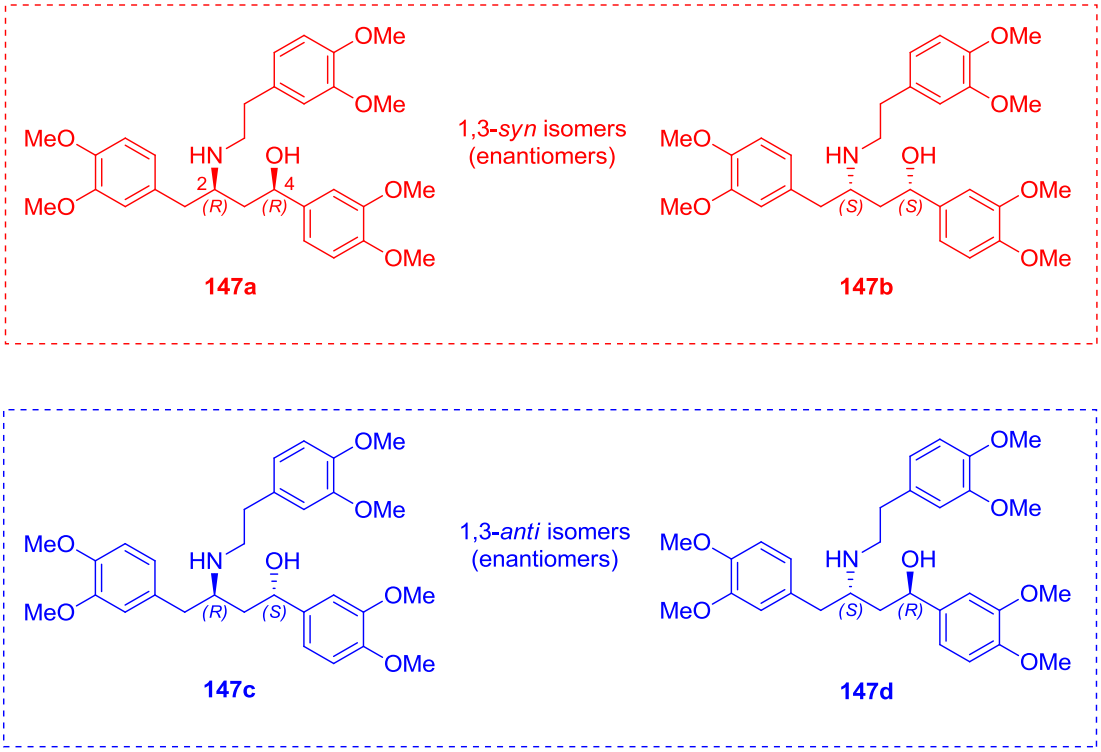


Figure 2.11. The structures of the 1,3-aminoalcohol stereoisomers **147a–d**

Table 2.5. ^{1}H (700 MHz) and ^{13}C NMR (175 MHz) NMR data of natural **147** and **147a/147b** in $CDCl_3$

Position	δ_H		δ_C	
	147*	**147a/147b**	**147***	**147a/147b**
1	2.72 dd (13.8, 6.2)	2.57 dd (13.6, 7.1)	39.3	40.0
	2.82 dd (13.7, 7.9)	2.79 dd (13.8, 4.8)		
2	3.00 m	3.13 m[a]	57.6	60.4
3	1.69 ddd (14.5, 5.8, 2.8)	1.47 dt (14.3, 10.9)	39.0	42.3
	1.96 ddd (14.5, 8.3, 3.2)	1.70 dt (14.3, 2.3)		
4	5.07 dd (8.3, 2.8)	4.81 dd (10.6, 2.1)	71.6	75.2
1'	-	-	130.6	130.6
2'	6.56 d (1.8)	6.55 d (2.0)	112.0	112.4
3'	-	-	149.0	149.0
4'	-	-	147.7[a]	147.9[a]
5'	6.70 d (8.1)[a]	6.70 d (8.1)	111.2[b]	111.3
6'	6.54 dd (8.1, 1.8)	6.48 dd (8.1, 2.0)	120.9	121.4
1"	-	-	138.0	138.0
2"	6.90 br s	6.92 s	108.8	108.8
3"	-	-	148.8	148.8[b]
4"	-	-	147.6	147.9[a]
5"	6.82 m	6.81 m[b]	110.9	110.8[c]
6"	6.82 m	6.81 m[b]	117.4	117.7
1'"	-	-	131.6	131.9
2'"	6.63 d (1.8)	6.75 d (2.0)	111.7	111.9
3'"	-	-	149.0	148.8[b]
4'"	-	-	147.8[a]	147.6
5'"	6.74 dd (8.1)[a]	6.81 m[b]	111.2[b]	111.2[c]
6'"	6.60 dd (8.1, 1.8)	6.73 d (2.0)	120.5	120.6
7'"	2.65 m	2.73 m	35.7	36.4
	2.99 m	2.89 m[c]		
8'"	2.78 m	2.89 m[c]	48.4	47.9
	3.00 m	3.13 m[a]		
3'-, 4'-,	3.81 s[b]	3.81 s[d]	55.8–55.9[c]	55.8–55.9[c]
3"-, 4"-,	3.85 s[b]	3.85 s[d]		
3'"-, 4'"-	3.87 s[b]	3.86 s[d]		
OMe	3.87 s[b]	3.88 s[d]		
	3.87 s[b]	3.88 s[d]		
	3.87 s[b]	3.89 s[d]		
*N*H	1.67 br s			

[a-d]Assignments may be interchanged within each column due to severe or partial overlapped of signals. ***147c/147d** have identical ^{1}H and ^{13}C NMR data as natural **147**.

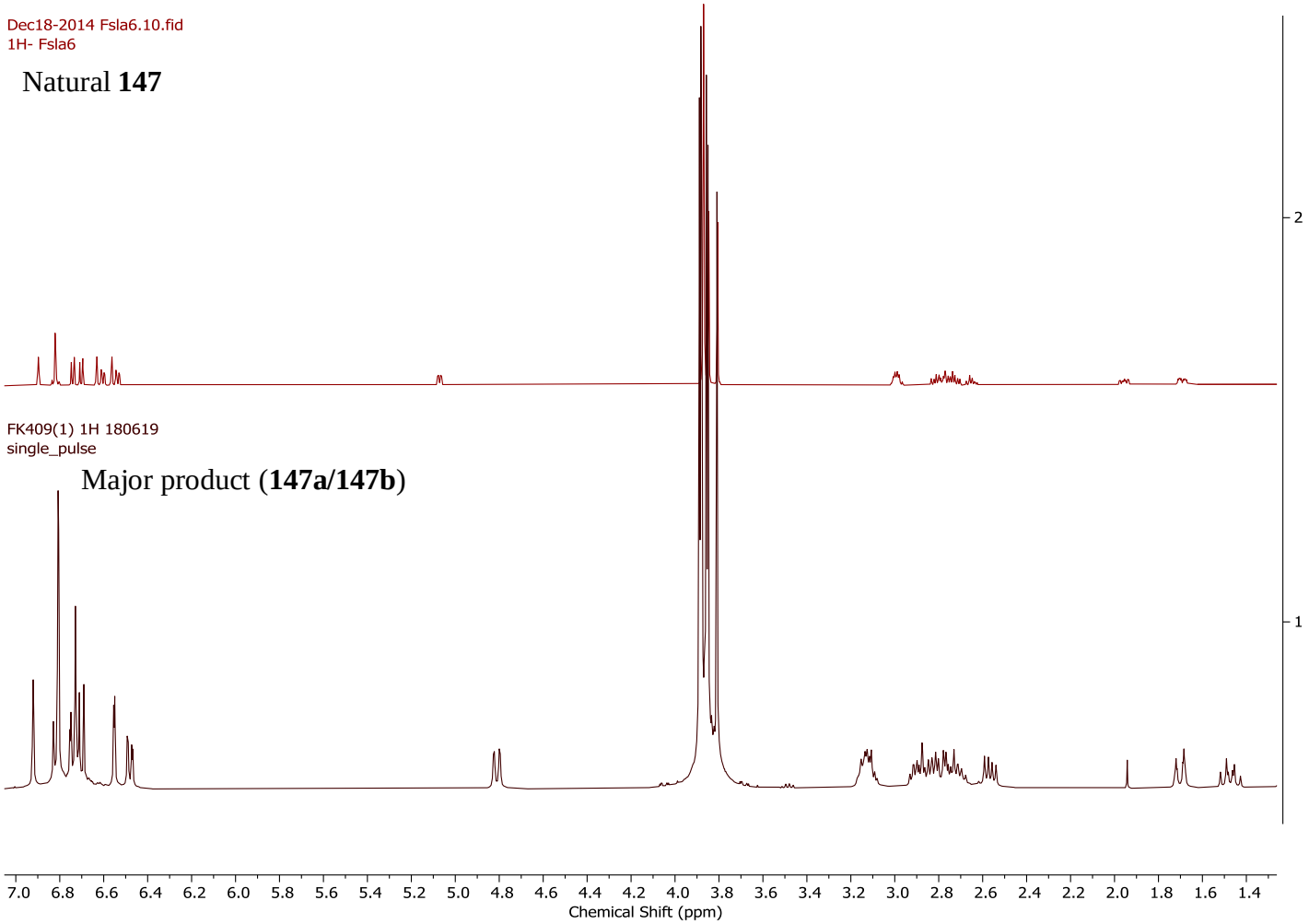


Figure 2.12. ^{1}H NMR spectra of natural schwarzinicine F (**147**) and **147a/147b** in ($CDCl_3$, 400 MHz)

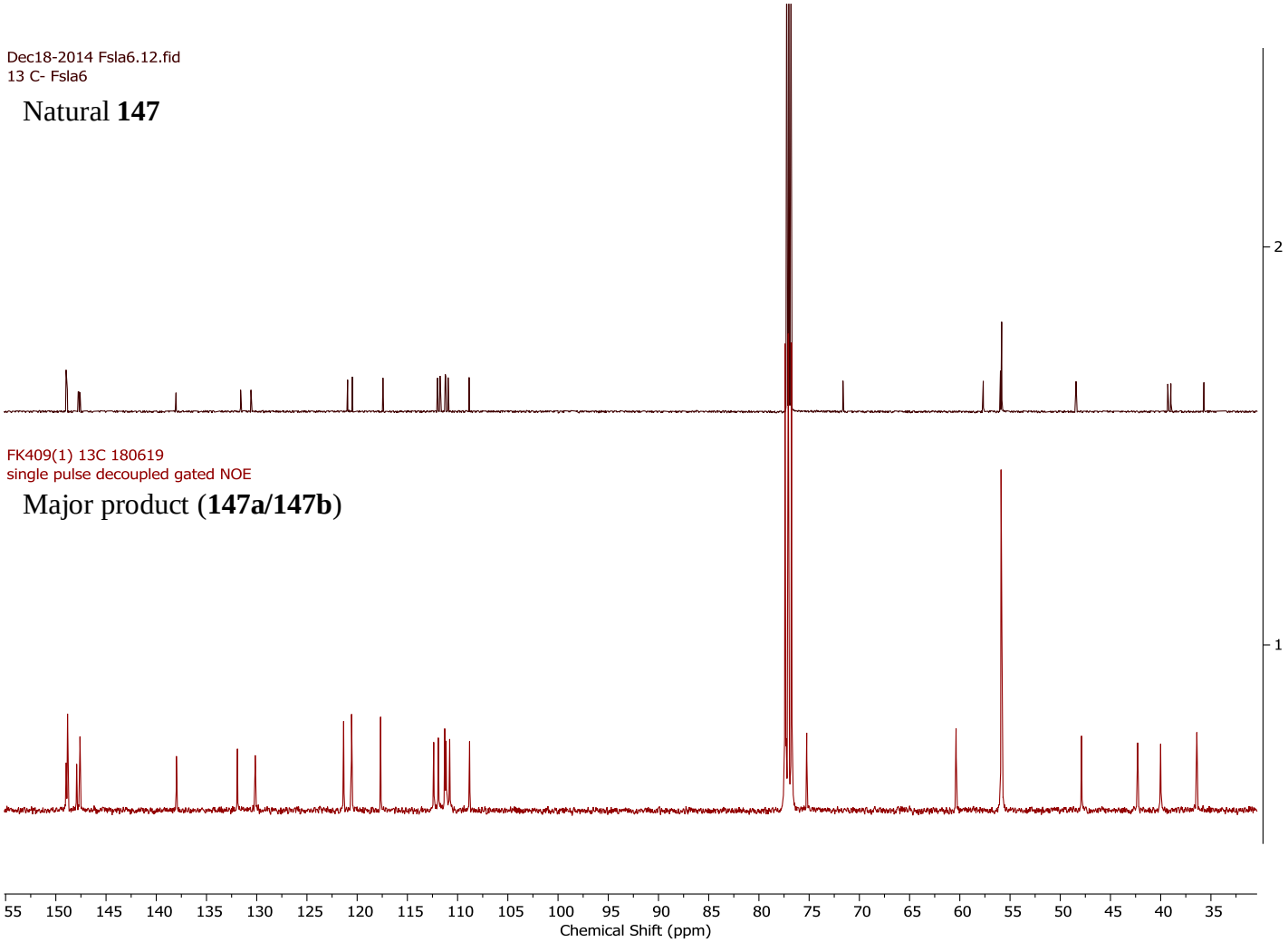


Figure 2.13. ^{13}C NMR spectra of natural schwarzinicine F (**147**) and **147a/147b** ($CDCl_3$, 100 MHz)

The racemic mixture **147a/147b** was subjected to chiral HPLC resolution. The chiral HPLC profile displayed two peaks in a ratio of 1:1 (Figure S58 in Appendix). The enantiomers **147a** and **147b** were successfully separated through repeated chiral HPLC isolation (Figures S59 and S60 in Appendix). Subsequently, the ECD spectra of both **147a** and **147b** were acquired and as expected, they showed opposite Cotton effects (Figure 2.14). In addition, the specific optical rotations obtained for both the enantiomers were opposite to each other ($[\alpha]_D^{25}$ +9 (*c* 0.22, $CHCl_3$) *vs* $[\alpha]_D^{25}$ –10 (*c* 0.28, $CHCl_3$)). The experimental ECD spectra of **147a** and **147b** were compared to those calculated for the 1,3-*syn* enantiomers (2*R*,4*R* and 2*S*,4*S*; Figure 2.14). The absolute configurations of **147a** and **147b** were therefore determined as 2*R*,4*R* and 2*S*,4*S*, respectively.

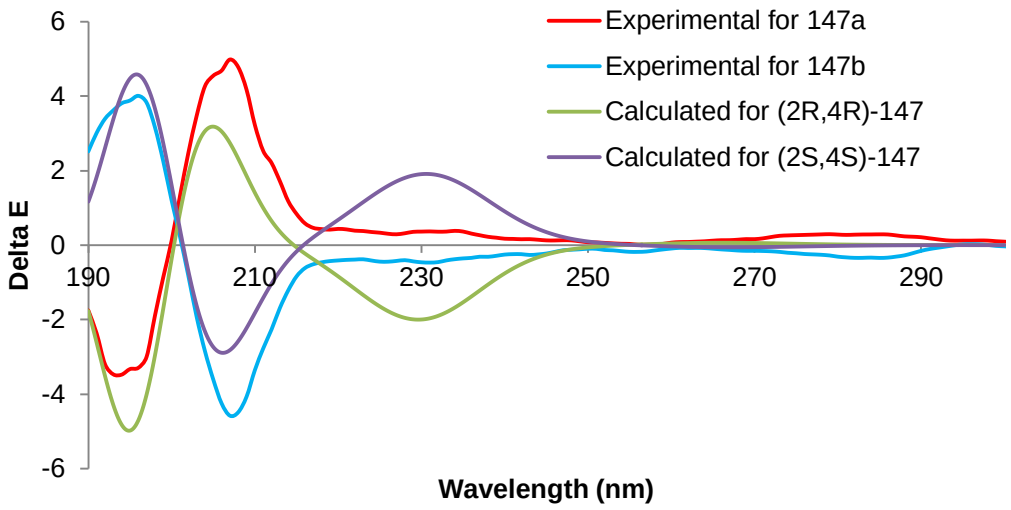


Figure 2.14. Experimental and calculated ECD spectra of **147a** and **147b**

On the other hand, comparison of the NMR data of the minor product (**147c/147d**) with that of natural **147** revealed that they are essentially identical (Figures 2.15 and 2.16). Therefore, natural **147** is deduced to assume the 1,3-*anti* relative configuration, i.e., natural **147** possesses an absolute configuration that is identical to either that of **147c** or **147d**.

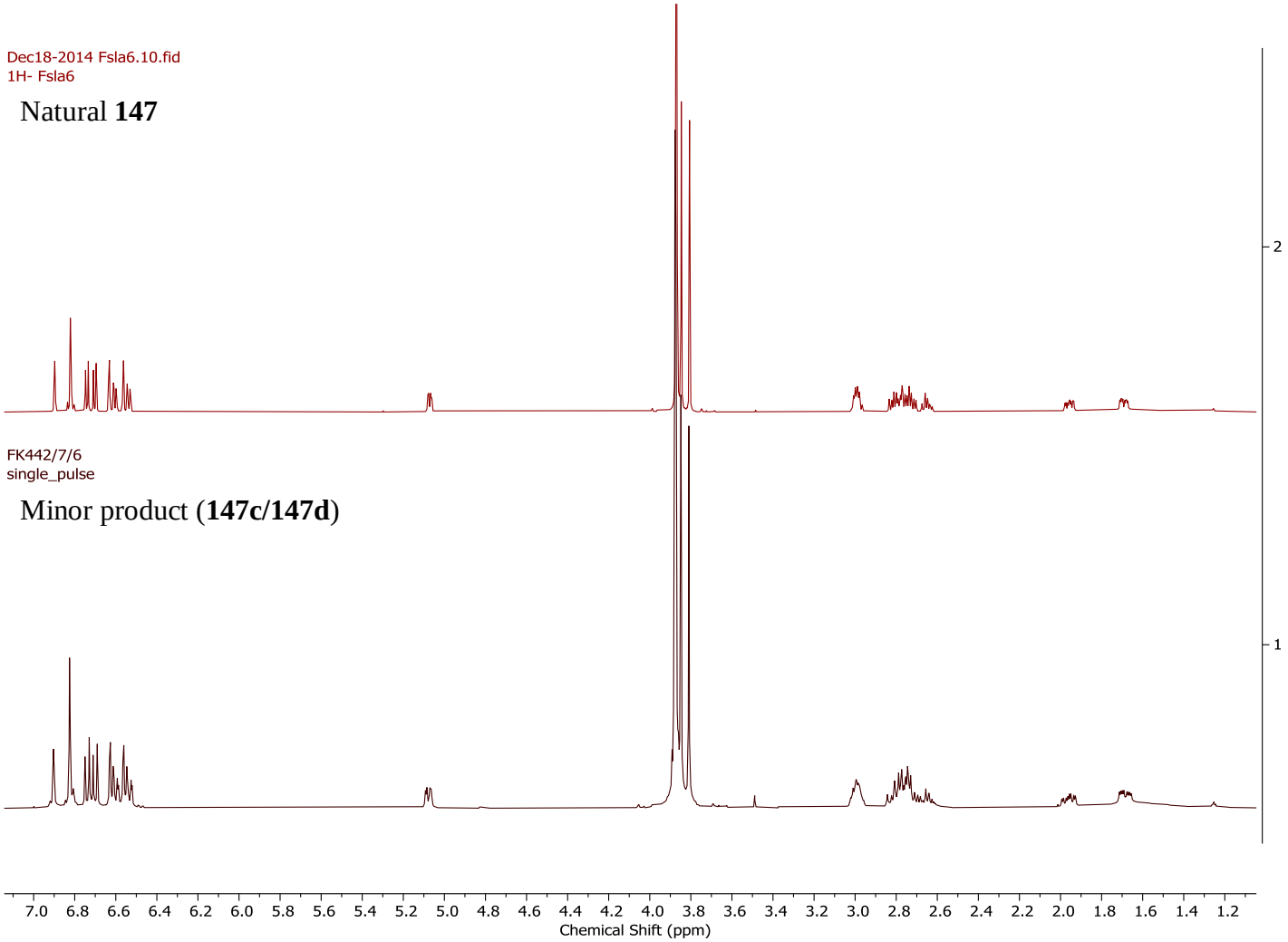


Figure 2.15. ^{1}H NMR spectra of natural schwarzinicine F (**147**) and **147c/147d** ($CDCl_3$, 400 MHz)

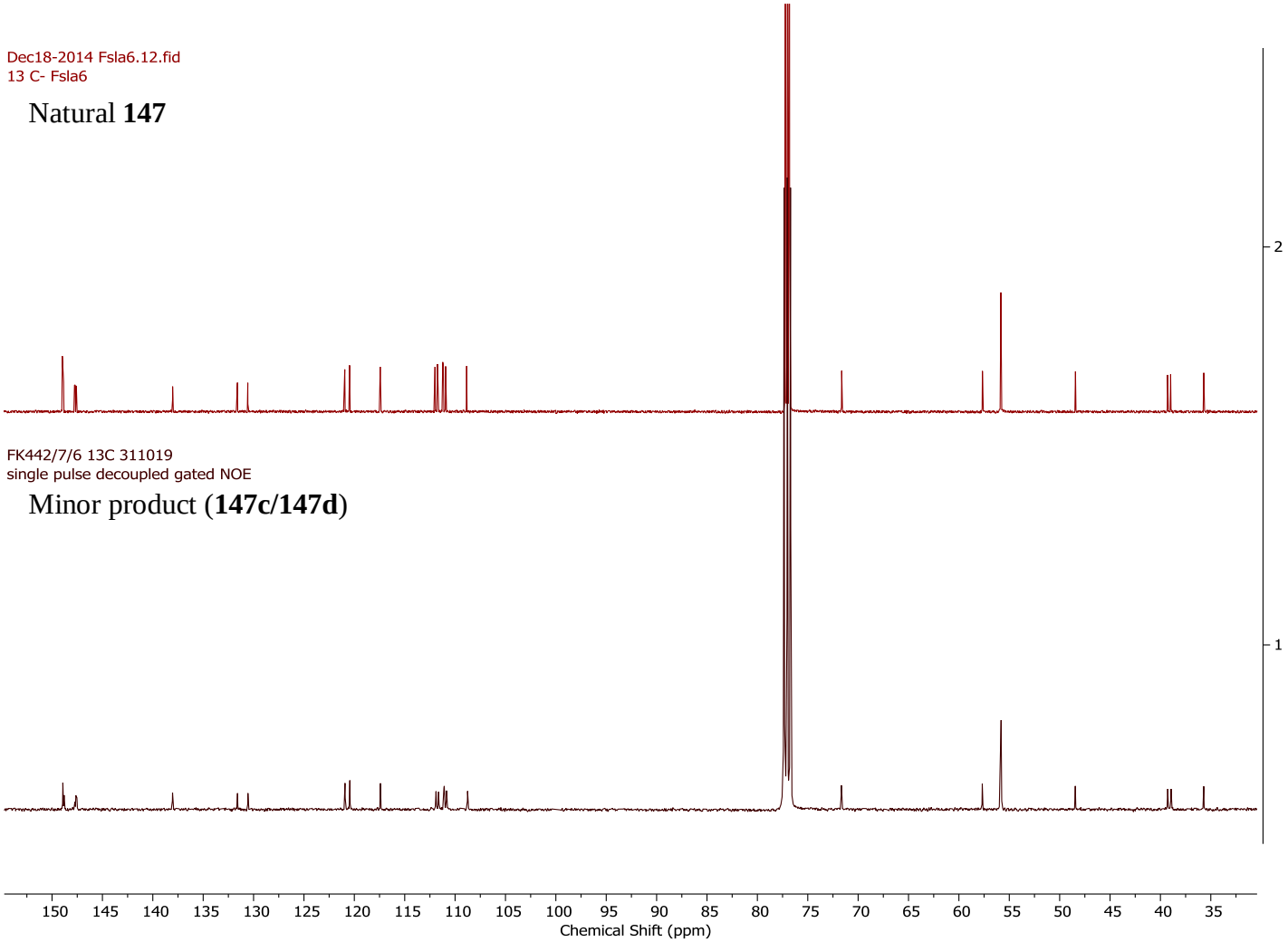


Figure 2.16. ^{13}C NMR spectra of natural schwarzinicine F (**147**) and **147c/147d** in ($CDCl_3$, 100 MHz)

To determine the absolute configuration of natural schwarzinicine F (**147**), the **147c/147d** racemic mixture was subjected to chiral HPLC resolution. As expected, the chiral HPLC profile revealed the presence of two peaks in 1:1 ratio (Figure S61 in Appendix). In contrast, the chiral HPLC profile of natural schwarzinicine F (**147**) showed only one peak indicating that it is enantiomerically pure as a natural product.[170] Through repeated chiral HPLC isolation, the enantiomers **147c** and **147d** were successfully separated (Figures S62 and S63 in Appendix). The retention time (t_R) of **147d** (14.08 min) closely matches that of **147** (14.26 min) (Figure S57 in Appendix). The experimental ECD spectra of **147**, **147c**, and **147d** were compared to the calculated ECD spectra for the 1,3-*anti* enantiomers (2*R*,4*S* and 2*S*,4*R*; Figure 2.17). The absolute configuration of **147** was therefore determined as 2*S*,4*R*, which corresponds to **147d**. Furthermore, the optical rotation obtained for **147d** ($[\alpha]_D^{25}$ +19 (*c* 0.14, $CHCl_3$)) is consistent with that for natural **147** ($[\alpha]_D^{25}$ +25 (*c* 0.22, $CHCl_3$)).[170]

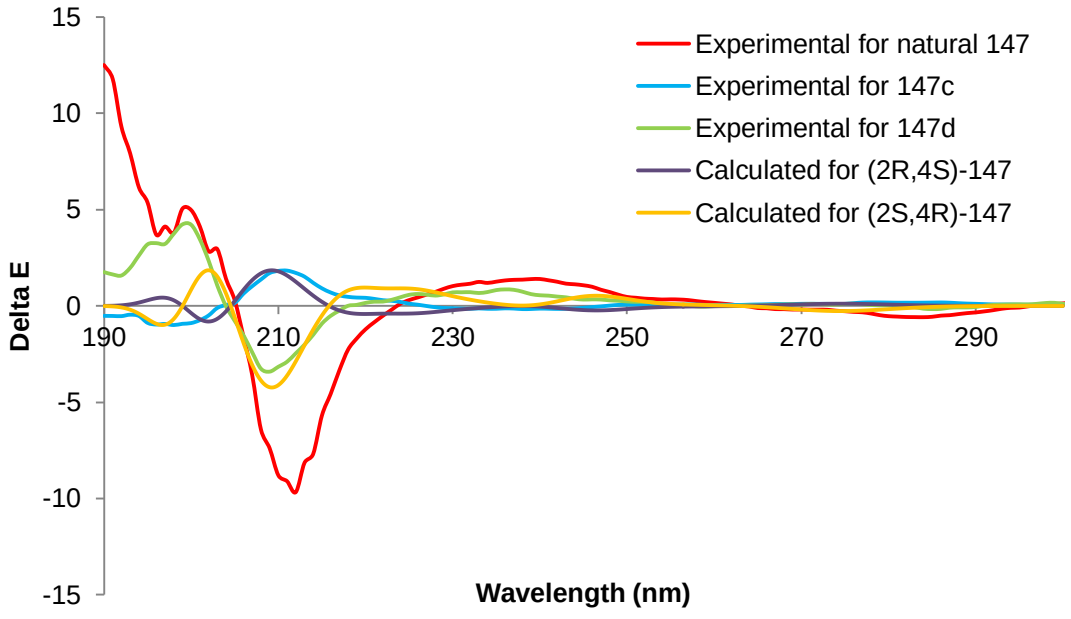


Figure 2.17. Experimental and calculated ECD spectra of natural schwarzinicine F (**147**), **147c** and **147d**

2.4 Summary

After multiple attempts, schwarzinicines A (**142**) and B (**143**) were successfully synthesized via a 4- and 5-step linear sequence, respectively. The key synthetic steps include Claisen condensation, nitrile hydrolysis cum *in situ* decarboxylation and reductive amination. Even though the first attempted synthesis to schwarzinicine F (**147**) was unsuccessful, it unexpectedly afforded the *O*-methyl derivative of a pair of previously undescribed diastereomers, i.e., schwarzificusines A and B (**149** and **150**), which were recently isolated from the leaves from *Ficus schwarzii*. This serendipitous discovery may prove to be useful in future attempts to accomplish the total syntheses of **149** and **150**. The total synthesis of schwarzinicine F (**147**) was successfully achieved on the second attempt, employing aldol addition and reductive amination as key synthetic steps. The absolute configuration of natural schwarzinicine F (**147**) was also established (2*S*,4*R*) on the basis of chemical correlations, chiral HPLC resolution and ECD calculations.

3

Syntheses of schwarzinicine analogues

3.1 Overview

Having successfully synthesized schwarzinicines A (**142**), B (**143**) and F (**147**), we now turned our focus to the preparation of various schwarzinicine analogues in the effort to explore and better understand the SAR around the structure of schwarzinicine A (**142**) in promoting its vasorelaxant effect in rat isolated aorta. We have previously demonstrated that both the Weinreb ketone synthesis and reductive amination are useful methods in constructing the core skeleton of schwarzinicine alkaloids, as described in Chapter 2. As expected, both these synthetic methods have been successfully utilized to synthesize a majority of the schwarzinicine analogues designed for SAR studies. Other reactions employed for the synthesis and modification of schwarzinicine analogues include formation and reduction of amide, quaternization of secondary amine, *O*-demethylation, reduction of ketone, tosylation of alcohol and Williamson ether synthesis.

3.1.1 Strategies for analogue design for SAR studies

The structure of schwarzinicine A (**142**) (Figure 3.1) consists of three aromatic rings (labelled A, B and C), with each substituted with two methoxy groups at positions-3 and -4. Ring A is connected to the central nitrogen atom via an ethylene (–CH_2CH_2–)

fragment, which when taken together constitute the phenethylamine partial structure. Rings B and C, on the other hand, are connected with each other via an *n*-butylene chain with branching at C-2, which connects to the phenethylamine nitrogen atom.

For the purpose of SAR studies, the structure of schwarzinicine A (**142**) was altered in stages/sequentially with the aim to afford a series of synthetic analogues that possess an array of functionalities or chemical groups, which would enable us to probe the active pharmacophore and possibly the mode of binding (Figure 3.1). The analogue design strategies employed in the present study include simplification, chain extension/contraction, substituent variation, ring variation, structural extension, isosterism and rigidification.

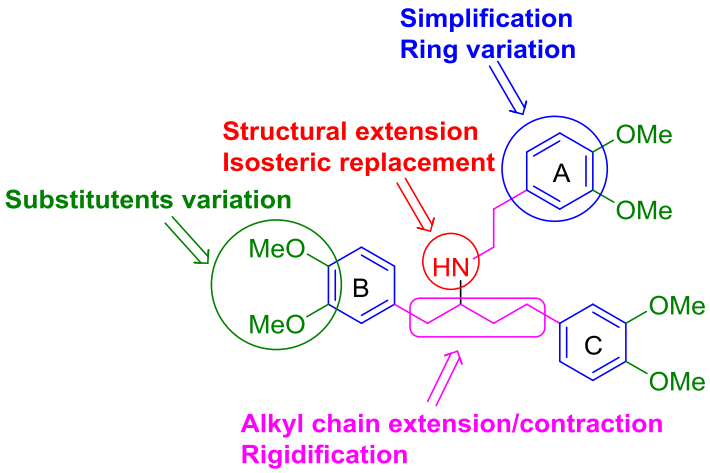


Figure 3.1. Possible sites for structural modification of **142**

For the simplification strategy, the three aromatic rings A–C in **142** were removed (in one instance a benzyl group was removed) sequentially to allow us to investigate the importance of each ring for vasorelaxant activity. The chain extension/contraction strategy was employed to probe the optimum carbon chain length between the amine nitrogen and the aromatic rings for vasorelaxant activity. Substituent variations involving aromatic rings A–C of **142** were carried out whereby the methoxy groups on the rings were replaced by electron donating, electron

withdrawing or neutral chemical groups. This strategy would allow us to determine the importance of the methoxy groups in **142** for activity as well as discover other substituents that may alter the activity of the molecule. The aromatic rings A–C were also replaced with various other heteroaromatic, heterocyclic and carbocyclic moieties based on the ring variation strategy.

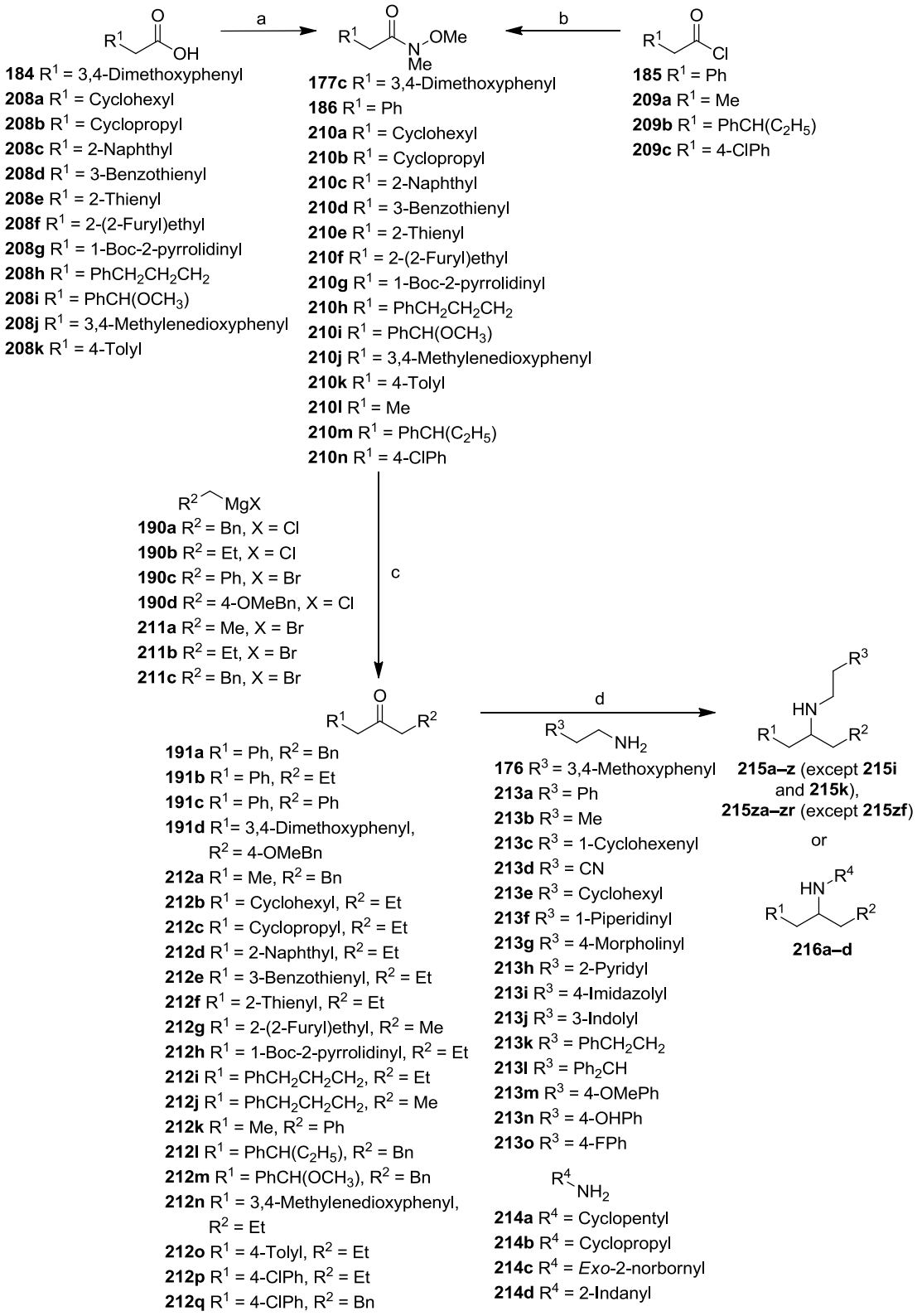
Selected alkyl groups of various lengths and sizes were coupled to the nitrogen atom present in **142** to extend the structure of the molecule. This strategy has the benefit of probing for any additional hydrophobic interaction within the binding site. The importance of the central nitrogen atom for activity was investigated by substituting it with an isosteric group/atom, i.e., to prepare analogues with similar structures as **142** but with the absence of the nitrogen atom. Furthermore, the chemical state of the NH group was varied by means of amide formation, alkylation and quaternization. This would enable us to probe for the chemical state in which the amine group in **142** shows optimum interaction with the target site.

For the rigidification strategy, an additional cyclic structure was incorporated in **142** to restrict the number of rotatable bonds present in the molecule, which thus reduces the number of conformations that the molecule can adopt. If the molecule is locked in the correct conformation, the activity/selectivity of the molecule for the binding site may increase.

3.2 Preparation of analogues based on Weinreb ketone synthesis and/or reductive amination

The syntheses of Weinreb amides **177c** and **186** and ketone precursors **191a–d** were described in Section 2.2.1.4. In addition to these, numerous other ketone precursors were prepared based on the Weinreb ketone synthesis approach, while reductive amination between these ketones and the various primary amines gave rise to a series of schwarzinicine analogues (Scheme 3.1 and Table 3.1).

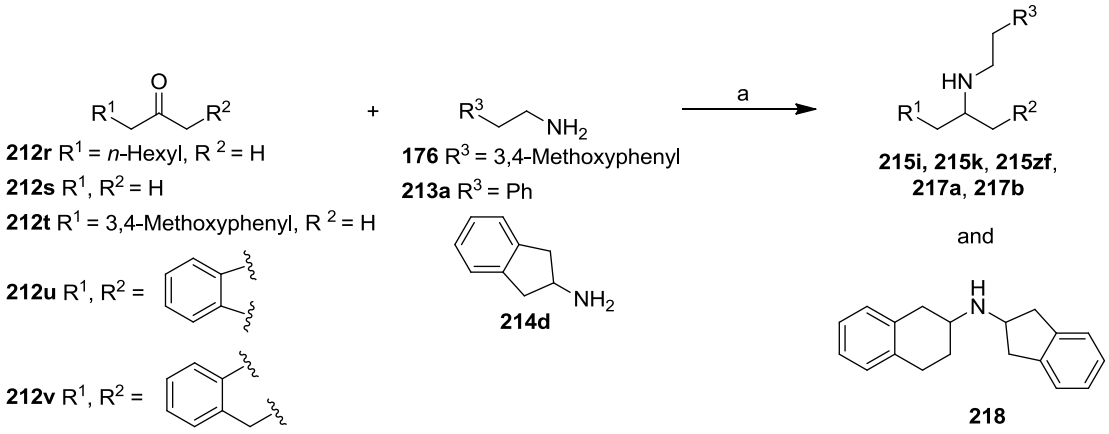
In the first part of the synthesis, Weinreb amides **177c** and **210a–k** were made from carboxylic acids **184** and **208a–k**,[196,197] whereas Weinreb amides **186** and **210l–n** were prepared from acid chlorides **185** and **209a–c**.[198] Subsequently, Weinreb amides **177c**, **186** and **210a–n** were successfully coupled with Grignard reagents **190a–d** and **211a–c** in THF at 0 °C to afford ketones **191a–d** and **212a–q**,[200] which then underwent reductive amination reaction[183,186] with primary amines **176**, **213a–o** and **214a–d**, in the presence of STAB and AcOH in $ClCH_2CH_2Cl$ at room temperature to afford the desired analogues **215a–z** (except for **215i** and **215k**), **215za–zr** (except for **215zf**) and **216a–d** (Scheme 3.1 and Table 3.1). Analogues **215i**, **215k** and **215zf** were made from reductive amination between commercially available ketones **212r–t** and amines **176** and **213a** (Scheme 3.2 and Table 3.1).



Reagents and conditions: (a) *N,O*-Dimethylhydroxylamine hydrochloride, EDC, DMAP, CH_2Cl_2, rt; (b) *N,O*-Dimethylhydroxylamine hydrochloride, pyridine, CH_2Cl_2, 0 °C to rt; (c) THF, 0 °C; (d) $NaBH(OAc)_3$, AcOH, $ClCH_2CH_2Cl$, rt.

Scheme 3.1. Synthesis of schwarzinicine analogues based on Weinreb amides

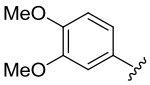
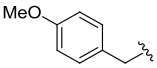
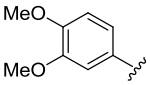
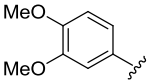
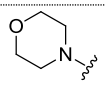
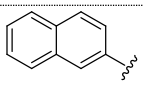
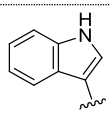
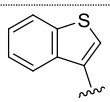
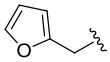
For rigidification strategy, we aimed to reduce the number of rotatable bonds in schwarzinicine A (**142**) to potentially lock it in its active conformation for improved potency. With that in mind, compound **203** as described in Section 2.3.1.2 appeared to be a perfect candidate as it consists of an aminotetralin structural skeleton, in which the butanoid chain connecting rings B and C is more conformationally restricted due to a reduction in the number of rotatable bonds. However, the poor reaction yield obtained for **203** has hindered the pharmacological evaluation of its vasorelaxant effect. We decided to look for alternatives to **203** where the designed molecules should have high structural similarity to **203** and can be easily prepared. As a result, **216d, 217a, 217b** and **218** were designed and synthesized. Analogues **217a**, **217b** and **218** were made from reductive amination between commercially available ketones (**212u** and **212v**) and amines (**213a** and **214d**) (Scheme 3.2 and Table 3.1).

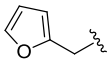
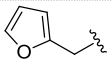
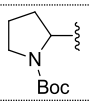
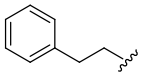
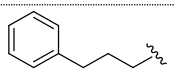
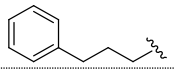
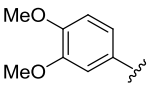
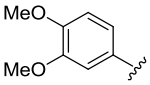
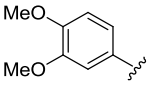
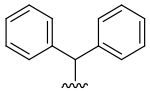
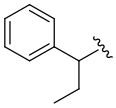
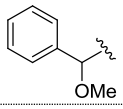
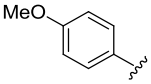
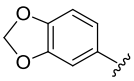
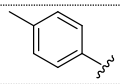
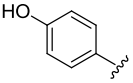
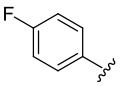
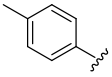
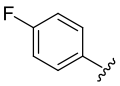
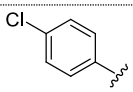
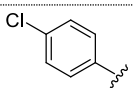
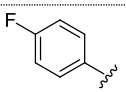


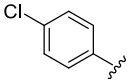
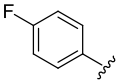
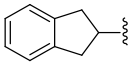
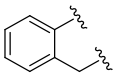
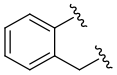
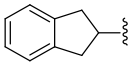
Reagents and conditions: (a) $NaBH(OAc)_3$, AcOH, $ClCH_2CH_2Cl$, rt.

Scheme 3.2. Synthesis of schwarzinicine analogues based on reductive amination between commercially available ketones and amines

Table 3.1. List of schwarzinicine analogues synthesized based on Schemes 3.1 and 3.2

Compound	R^1	R^2	R^3	R^4	Yield (%)
215a					48
215b	Ph	Bn	Ph		83
215c	Ph	Bn	Me		49
215d	Me	Bn	Ph		72
215e	Ph	Et	Ph		26
215f	Ph	Et			24
215g		Et	Ph		59
215h		Et	Ph		69
215i[a]	*n*-Hexyl	Et	Ph		72
215j	Ph	Et	CN		58
215k[b]	H	H			5
215l		Et			23
215m		Et			14
215n		Et			65
215o	Ph	Et			30
215p	Ph	Et			33
215q	Ph	Et			36
215r	Ph	Et			14
215s		Et	Ph		69
215t	Ph	Et			16
215u		Et	Ph		68
215v		Et	Ph		46
215w		Me	Ph		47

Compound	R^1	R^2	R^3	R^4	Yield (%)
215x		Me			27
215y		Me			29
215z		Et	Ph		73
215za	Ph	Et			51
215zb		Et	Ph		80
215zc		Me	Ph		77
215zd	Ph	Ph			43
215ze	Me	Ph	Ph		61
215zf[c]		H			50
215zg	Ph	Et			37
215zh		Bn	Ph		8
215zi		Bn	Ph		50
215zj	Ph	Et			26
215zk		Et	Ph		67
215zl		Et	Ph		39
215zm	Ph	Et			13
215zn	Ph	Et			44
215zo		Et			46
215zp		Et	Ph		70
215zq		Et			72

Compound	R^1	R^2	R^3	R^4	Yield (%)
215zr		Bn			61
216a	Ph	Et			22
216b	Ph	Et			60
216c	Ph	Et			22
216d	Ph	Et			20
217a[d]			Ph		11
217b[e]			Ph		78
218[f]					11

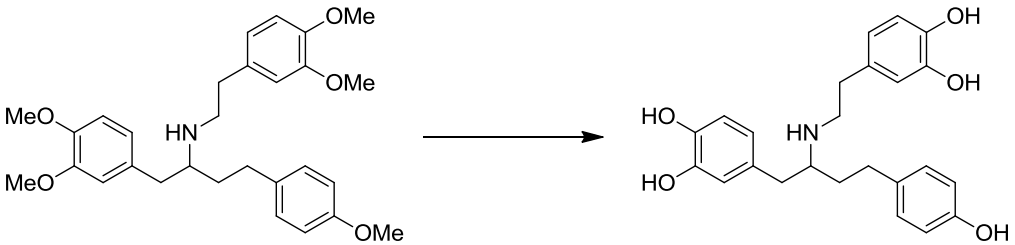
[a]Reaction between 4-undecanone (**212r**) and phenethylamine (PEA, **213a**). [b]Reaction between acetone (**212s**) and DMPEA (**176**). [c]Reaction between 3,4-dimethoxyphenyl-acetone (**212t**) and **176**. [d]Reaction between 2-indanone (**212u**) and **213a**. [e]Reaction between β-tetralone (**212v**) and **213a**. [f]Reaction between **212v** and **214d**.

3.3 Attempted *O*-demethylation of schwarzinicine analogue 215a

For the aromatic substituent variation strategy, we wished to replace the aromatic methoxy groups in **142** with hydroxyl groups to investigate the potential role of hydrogen bonding in the vasorelaxant activity. A hydroxyl group can participate in binding interaction as both hydrogen bond donor and acceptor, while a methoxy group can only act as a hydrogen bond acceptor. In addition to analogue **215zm**, which bears an aromatic hydroxyl group, it was desirable to prepare analogues with more aromatic hydroxyl groups. Schwarzinicine A (**142**) and analogue **215a**, which has six and five aromatic methoxy groups, respectively, appeared to be the obvious candidates for *O*-demethylation.

O-Demethylation was first performed on analogue **215a** (Table 3.2). Our first choice of reagent for this purpose was BBr_3, which is one of the most commonly used dealkylating reagents.[215] However, the unavailability of the BBr_3 (prohibited to be brought in by suppliers) at our lab forced us to switch to the less reactive variant BCl_3.[215,216] Using a similar procedure reported by Land *et al.*,[217] compound **215a** was treated with BCl_3 in CH_2Cl_2 (entry 1, Table 3.2). Subsequent workup and chromatographic purification of the reaction mixture gave recovered starting material with no trace of the desired product being detected. The failure to *O*-demethylate analogue **215a** with BCl_3 prompted us to seek an alternative method.

Table 3.2. *O*-Demethylation of analogue **215a**



215a **219**

Entry	Method	Time	Yield (%)
1.	I	72 h	-[a]
2.	II	20 min	22[b]

Methods: I.CH_2Cl_2, BCl_3 (9.7 equiv.) at rt; II. Pyridine hydrochloride (20.6 equiv.), microwave irradiation at 200 °C.
[a]Starting material was recovered. [b]Decomposition was observed on storage.

In the search for an alternative strategy, we were attracted to a report by Kulkarni *et al.*[218] that described *O*-demethylation of methyl aryl ethers using pyridine hydrochloride in solvent-free conditions and under microwave irradiation. The very short reaction times reported attracted our attention the most. Based on the reported procedure, analogue **215a** was mixed with neat pyridine hydrochloride and the mixture was subjected to microwave irradiation at 200 °C for 20 minutes (entry 2,

Table 3.2). Subsequent workup and chromatographic purification of the crude product on silica yielded *O*-demethylated product **219** (based on inspection of its ^{1}H NMR spectrum). Unfortunately, analogue **219** decomposed rapidly and within days its ^{1}H NMR spectrum became unrecognisable when compared to the spectrum of the fresh sample (Figure 3.2). It was previously reported that catecholamines are generally unstable compounds, i.e., they are prone to rapid oxidation especially under neutral and alkaline conditions.[219–221] Since it did not appear to be practical to prepare stable *O*-demethylated analogues for bioactivity assessment, the synthesis of other *O*-demethylated schwarzinicine analogues were not further attempted.

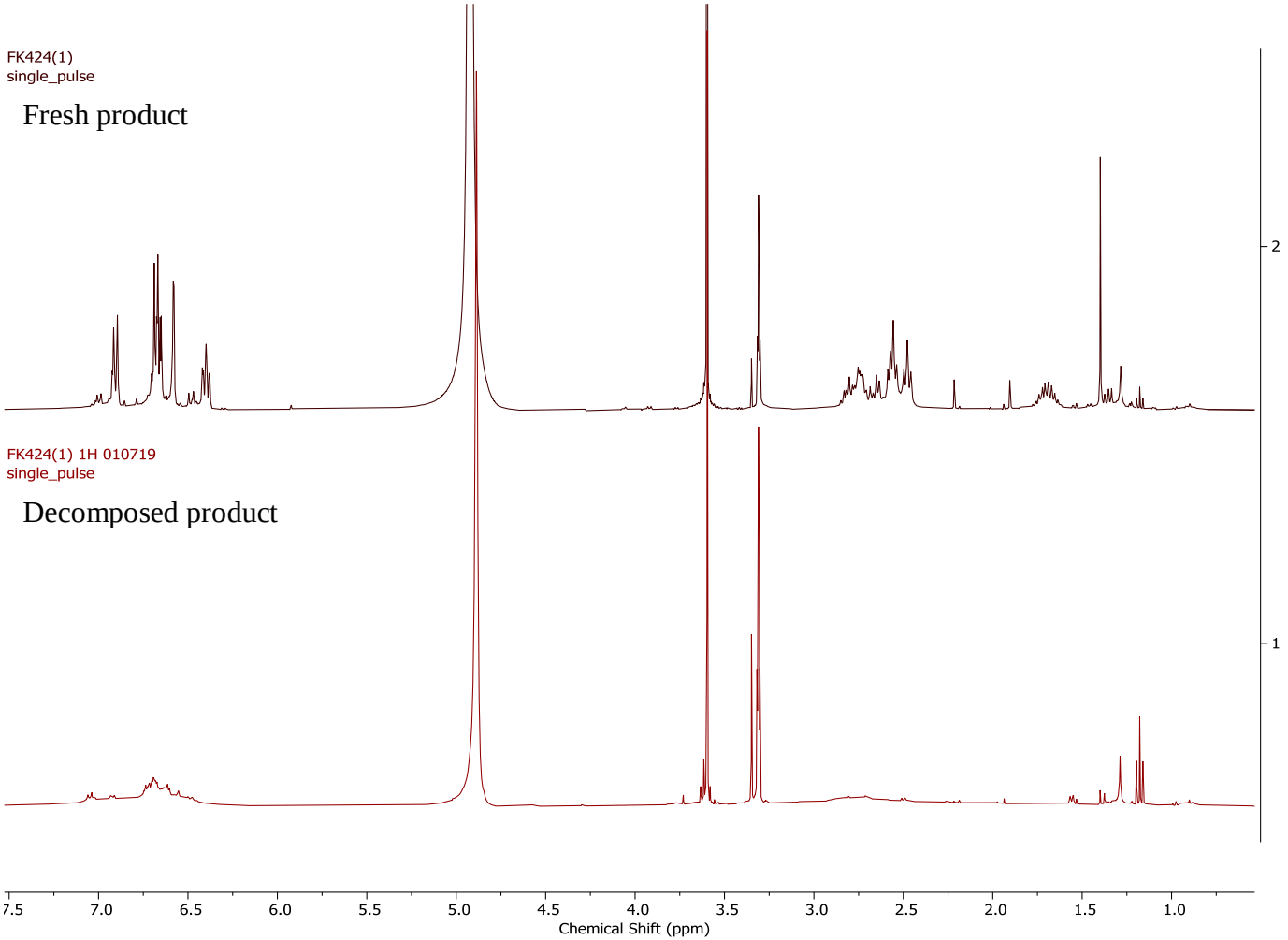
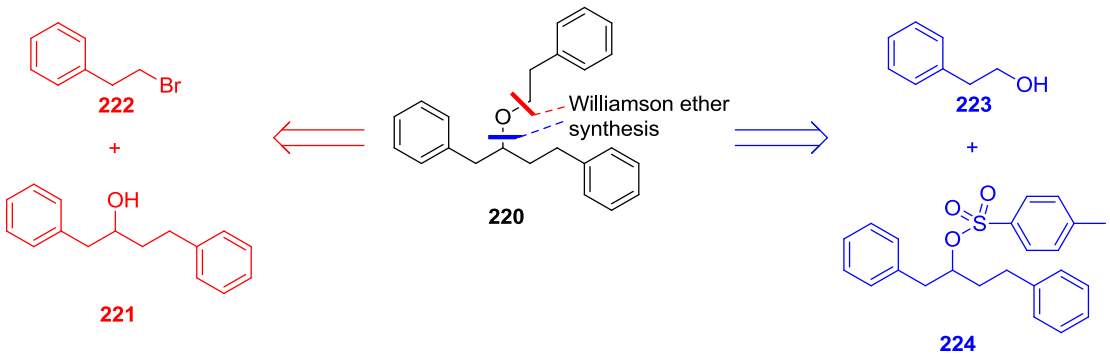


Figure 3.2. ^{1}H NMR spectra of fresh and decomposed **219** (CD_3OD, 400 MHz)

3.4 Attempted preparation of schwarzinicine A isostere (220)

We were interested to find out the effect of substituting the central nitrogen atom in **142** with an oxygen atom on activity. Oxygen is a classical isostere of nitrogen. Thus, we designed and attempted to synthesize the ether isostere analogue **220**. A retrosynthetic analysis of **220** resulted in two possible routes being proposed and they are shown in Scheme 3.3.

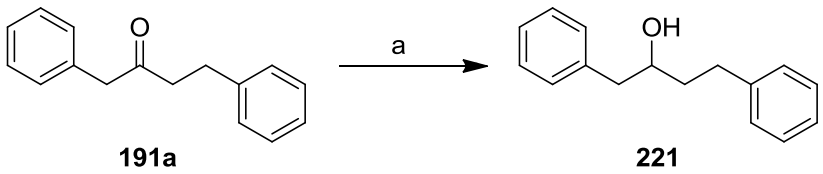
Williamson ether synthesis was applied in both synthetic routes for the final reaction step. In the first route (in red), the secondary alcohol **221** would undergo etherification with (2-bromoethyl)benzene (**222**) to form ether **220**. On the other hand, in the second route (in blue), phenethyl alcohol (**223**) would undergo etherification with compound **224** to form the target molecule. The tosylated derivative **224** was used instead of **222** since hydroxyl is generally a poor leaving group.[222,223]



Scheme 3.3. Retrosynthetic analysis of ether **220**

3.4.1 First attempt

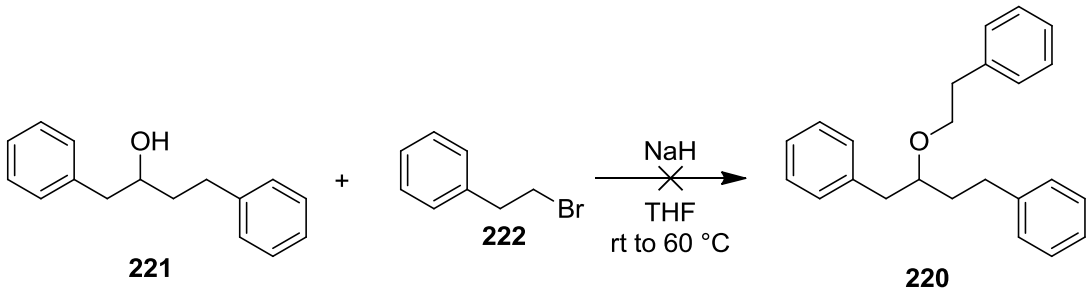
With ketone **191a** in hand (Scheme 3.1), we could prepare alcohol **221** from a ketone reduction step. Thus, ketone **191a** was reduced with $NaBH_4$ in EtOH at 0 °C to give alcohol **221** in 83% yield (Scheme 3.4).[224]



Reagents and conditions: (a) $NaBH_4$, EtOH, 0 °C, 1.5 h, 83%.

Scheme 3.4. Reduction of ketone **191a**

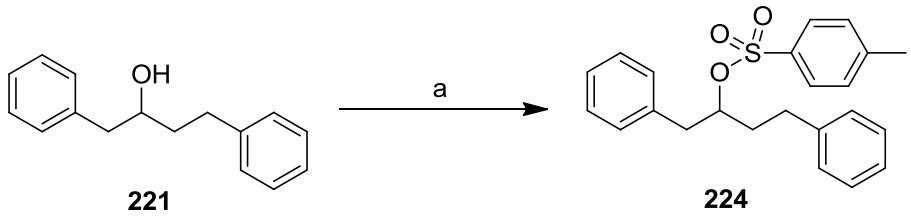
The etherification of alcohol **221** with bromide **222** (Scheme 3.5) was performed based on the procedure adapted from Ouyang *et al.*[225] Excess NaH (12 equiv.) was first used to generate alkoxide ion from alcohol **221**. However, recovery of the starting materials of alcohol **221** and bromide **222** from the reaction mixture following workup and chromatographic purification appeared to suggest that the alkoxide ion was not successfully generated in the reaction due to unknown reasons.



Scheme 3.5. Attempted etherification of alcohol **221**

3.4.2 Second attempt

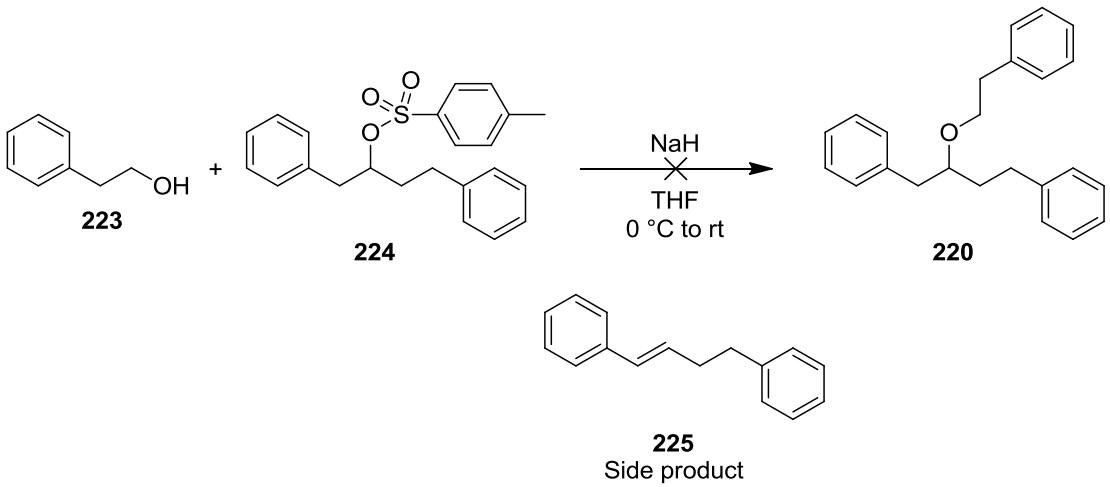
After the unsuccessful first attempt, we turned our attention to the second proposed synthetic pathway (Scheme 3.3, in blue), whereby commercially available primary alcohol **223** would be converted into its alkoxide, which would then react with compound **224** to give the target compound. Thus, alcohol **221** was smoothly converted into tosylate **224** in 78% yield (Scheme 3.6).[226]



Reagents and conditions: (a) *p*-Toluenesulfonyl chloride, Et_3N, DMAP, CH_2Cl_2, rt, 18 h, 79%.

Scheme 3.6. Tosylation of alcohol **221**

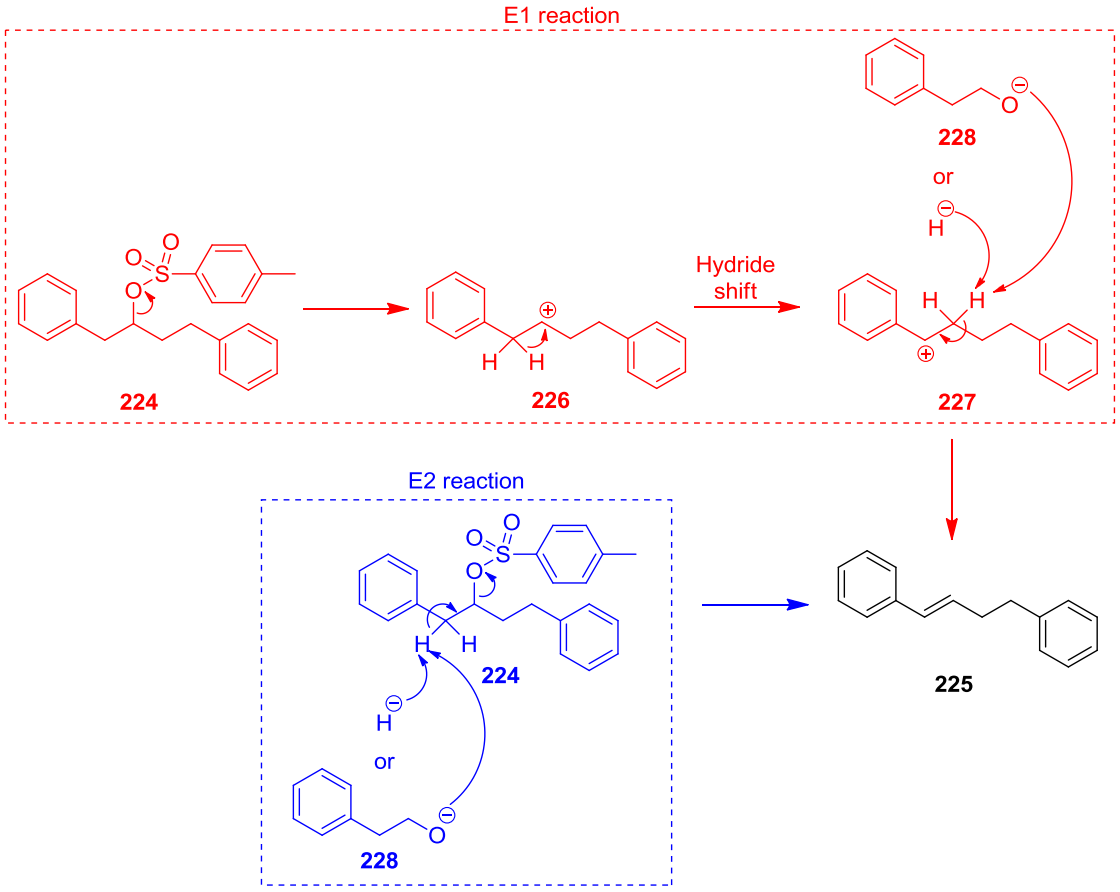
In the next reaction, NaH was used to generate the alkoxide ion of alcohol **223**, which was then allowed to react with **224** (Scheme 3.7) *in situ* based on the procedure reported by Granander *et al.*[227] Disappointingly, the expected product **220** was not detected. Instead, a side product identified as alkene **225** (based on ^{1}H NMR analysis) was isolated from the reaction upon workup and chromatographic purification.



Scheme 3.7. Attempted etherification of alcohol **223**

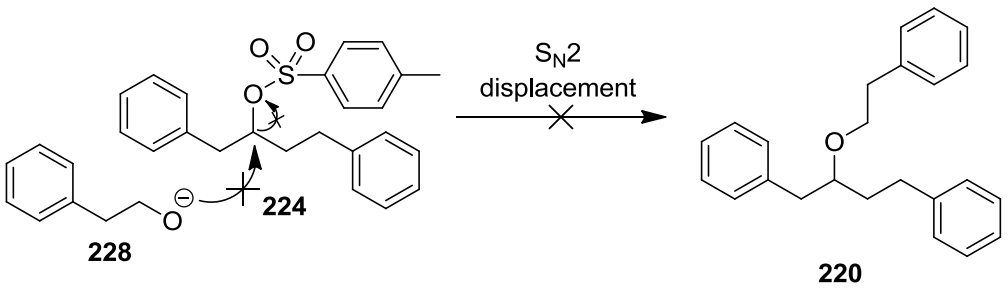
We hypothesized that the formation of alkene **225** could follow the E1 and/or E2 reaction pathways.[228] The postulated mechanisms are presented in Scheme 3.8. In the E1 pathway (in red), the departure of the tosylate group in **224** results in the formation of the secondary carbocation **226**. A hydride shift then ensues to produce the resonance stabilized benzylic carbocation **227**. In the last step, either the hydride

ion from NaH or alkoxide **228** abstracts the proton that is adjacent to the carbocationic centre to afford **225** as the unwanted product. In the E2 pathway (in blue),[229] the hydride ion from NaH or alkoxide **228** abstracts the benzylic proton, which triggers a concurrent elimination of the tosylate group to give **225**.



Scheme 3.8. Proposed mechanisms for the formation of **225**

In any case, the formation of the desired product **220** via an S_N2 displacement reaction between **224** and alkoxide **228** (Scheme 3.9) had been overridden by the elimination reactions.[230] Therefore, optimization of the reaction conditions to favour the S_N2 displacement reaction should be sought in due course.



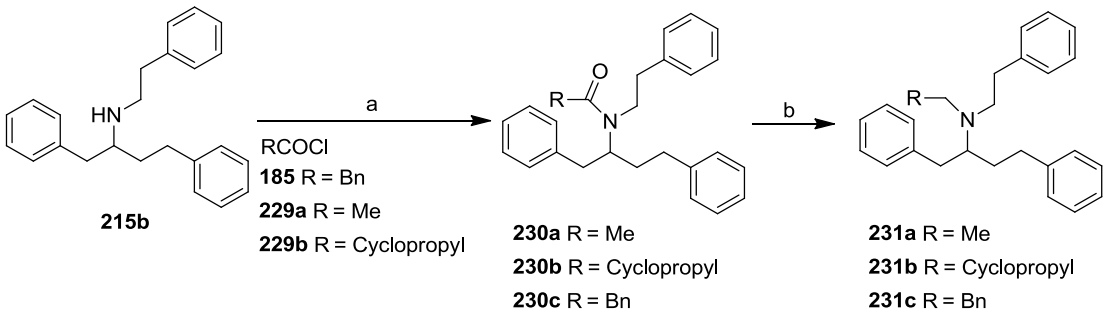
Scheme 3.9. Unsuccessful formation of **220** via S_N2 mechanism

3.5 Preparation of *N*-substituted schwarzinicine analogues

3.5.1 *N*-Alkylation of analogue 215b

Other than preparing analogues containing different chemical groups associated with the three aromatic moieties in **142**, it was also desirable to probe analogues that incorporate additional alkyl chains of various lengths. The secondary amine nitrogen atom in analogue **215b** provides a convenient site for alkylation.

In the first step of the process as shown in Scheme 3.10, the treatment of amine **215b** with acid chlorides **185**, **229a** and **229b** in the presence of Et_3N in CH_2Cl_2 at 0 °C gave the respective amides **230a–c** in high yields.[231] Reduction of amides **230a–c** using $LiAlH_4$ in THF, from 0 °C to reflux, afforded tertiary amines **231a–c**, respectively.[232]

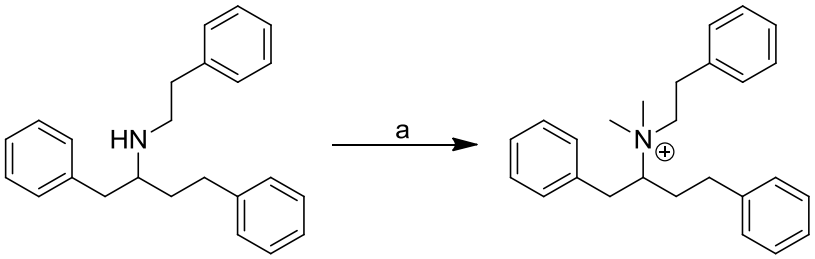


Reagents and conditions: (a) Et_3N, CH_2Cl_2, 0 °C; (b) $LiAlH_4$, THF, 0 °C to reflux.

Scheme 3.10. *N*-Alkylation of analogue **215b**

3.5.2 Quaternization of amines 215b and 217b

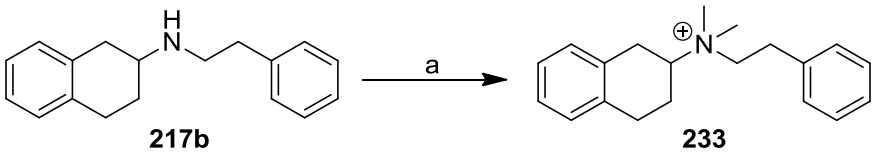
It was desirable to determine the effect of having a permanent positive charge on the nitrogen atom on activity. As a result, quaternization of the selected amines **215b** and **217b** with MeI and K_2CO_3 in EtOH at room temperature led to the formation of quaternary ammonium salts **232** (Scheme 3.11) and **233** (Scheme 3.12), respectively.[233]



215b **232**

Reagents and conditions: (a) MeI, K_2CO_3, EtOH, rt, 24 h, 44%.

Scheme 3.11. Quaternization of amine **215b**



217b **233**

Reagents and conditions: (a) MeI, K_2CO_3, EtOH, rt, 24 h, 83%.

Scheme 3.12. Quaternization of amine **217b**

The structures of both ammonium species **232** and **233** were determined based on ^{1}H and ^{13}C NMR data. However, the HRESIMS data did not show the molecular ion peaks for **232** and **233** (*m/z* 358.54 and 280.43, respectively) (Figures 3.3 and 3.4). It was proposed that the ammonium species **232** and **233** fragmented via several Hofmann elimination pathways, which explains the absence of the expected molecular ion peaks.[234,235]

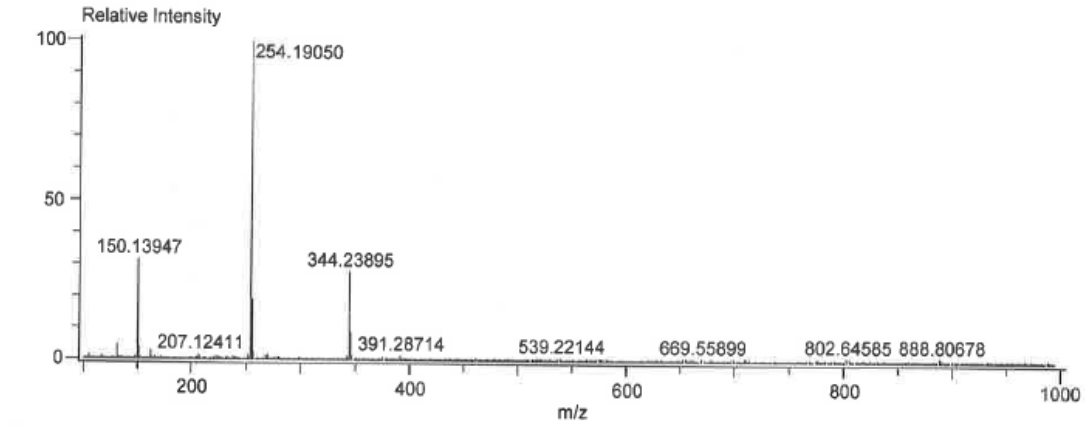


Figure 3.3. HRESIMS spectrum for compound **232**

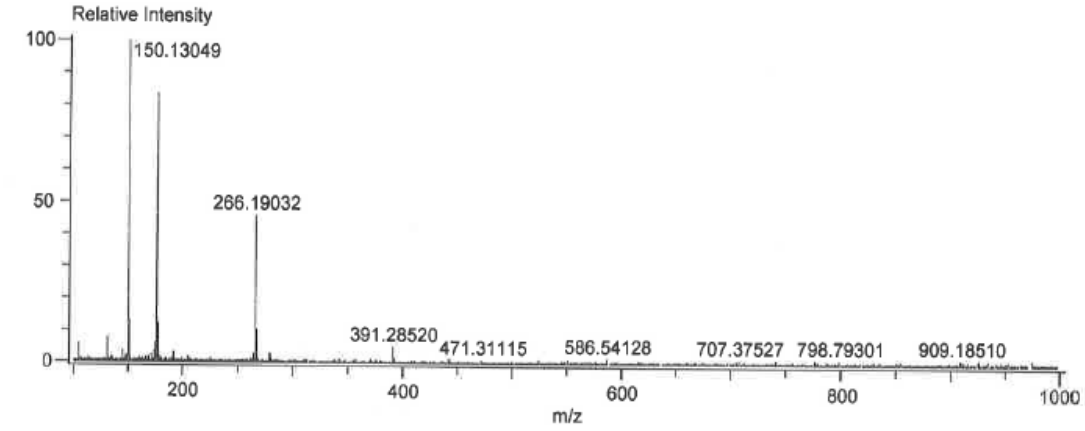
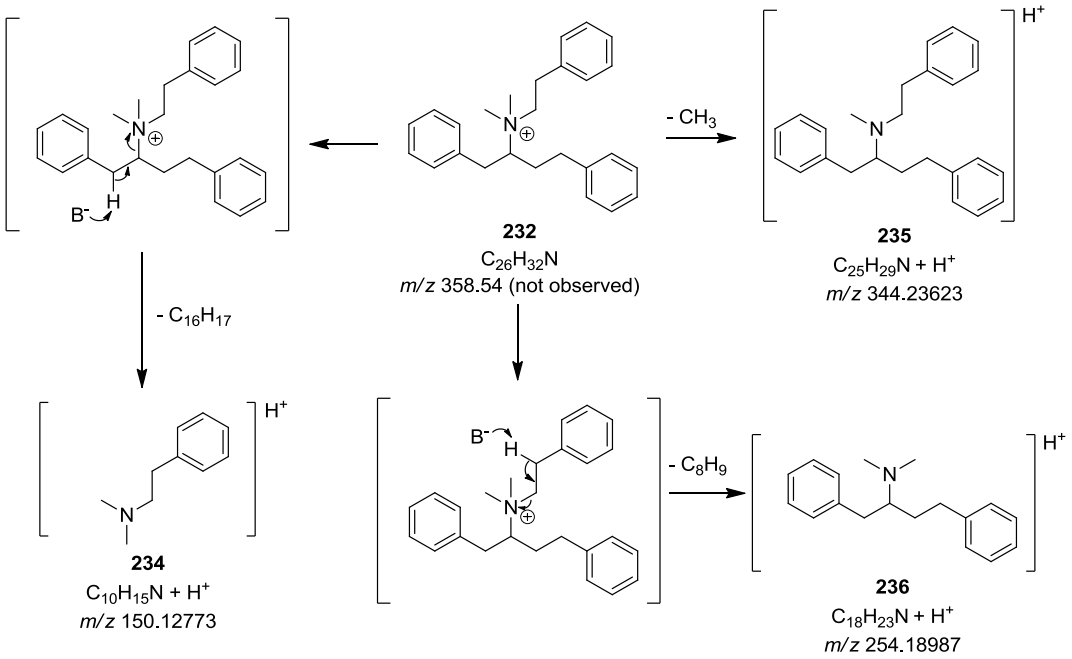


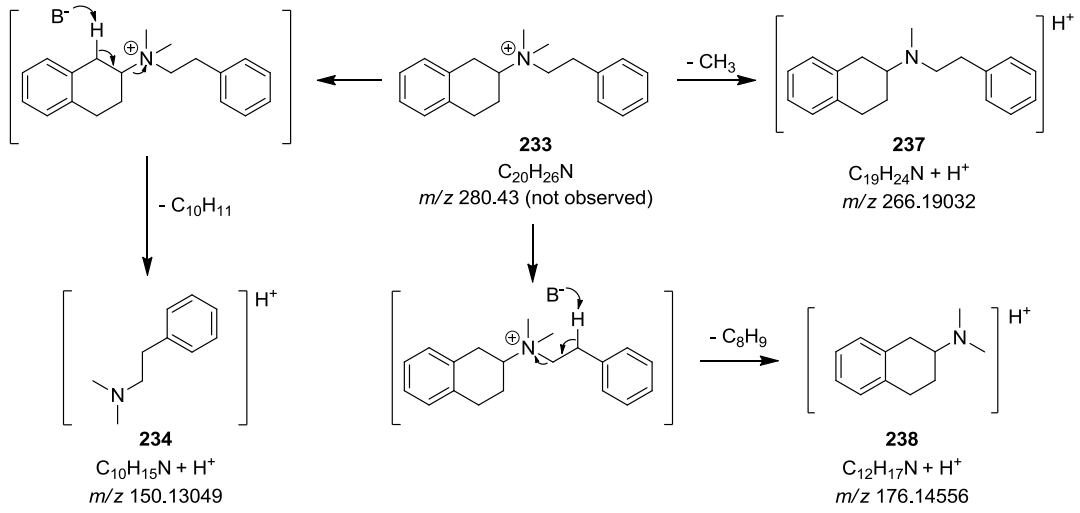
Figure 3.4. HRESIMS spectrum for compound **233**

Fragmentations of the ammonium salt **232** produced three major daughter ion species detected at *m/z* 150, 254 and 344 (Figure 3.3), which were due to the three different Hofmann elimination pathways shown in Scheme 3.13. The fragment ion observed at *m/z* 150 was due to *N*,*N*-dimethyl-2-phenethanamine (**234**), while the fragment ions observed at *m/z* 344 (**235**) and 254 (**236**) were due to the loss of CH_3 and phenethyl (C_8H_9), respectively.



Scheme 3.13. Proposed mass fragmentation pathways of ammonium salt **232**

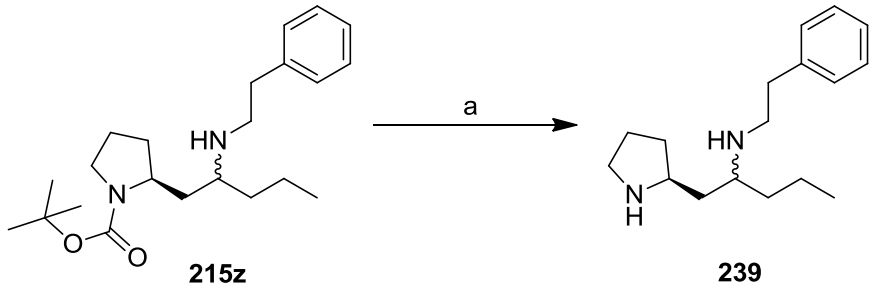
As with the case of **232**, the ammonium salt **233** went through similar fragmentations to give three major daughter ions at *m/z* 150, 176 and 266 in HRESIMS (Figure 3.4 and Scheme 3.14). The fragment ion observed at *m/z* 150 was also due to *N*,*N*-dimethyl-2-phenethanamine (**234**), while the fragment ions observed at *m/z* 266 (**237**) and 176 (**238**) were due to the loss of CH_3 and phenethyl (C_8H_9), respectively.



Scheme 3.14. Proposed mass fragmentation pathways of ammonium salt **233**

3.6 *N*-Boc deprotection of schwarzinicine analogue 215z

With analogue **215z** in hand (Scheme 3.1, Table 3.1), we felt that it would be instructive to consider the effect of the *N*-Boc deprotected pyrrolidine moiety on the vasorelaxant activity. By employing the procedure adapted from Davis *et al.*,[211] the diastereomeric mixture of **215z**, which was inseparable by centrifugal radial TLC from the previous reaction, was treated with TFA in CH_2Cl_2 to afford the diastereomeric mixture **239** (Scheme 3.15).



Reagents and conditions: (a) TFA, CH_2Cl_2, rt, 3 h, 48%.

Scheme 3.15. *N*-Boc deprotection of **215z**

The diastereomeric mixture **239** was successfully separated using centrifugal radial TLC to yield two enantiopure amines with the absolute configurations 1′*S*,2*S* (**239a**) and 1′*S*,2*R* (**239b**) as shown in Figure 3.5. The planar structures of the two diastereomers of **239** were confirmed by HRMS, 1D (^{1}H and ^{13}C) and 2D (COSY, HSQC and HMBC) NMR data.

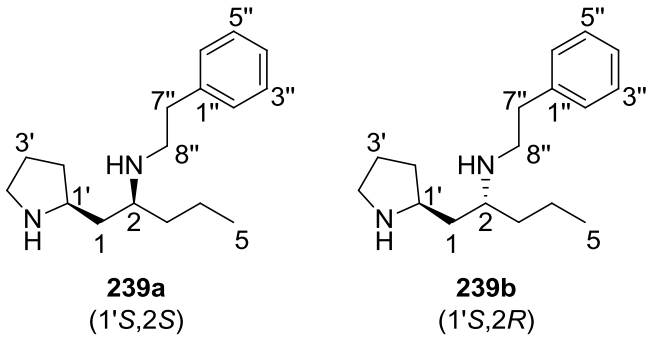


Figure 3.5. The structures of the two diastereomers of **239**

The spectroscopic data of the two diastereomers of **239** were compared and shown in Table 3.3. It is apparent that the ^{1}H and ^{13}C NMR spectra of the two diastereomers of **239** are different as shown in Figures 3.6 and 3.7. Unfortunately, the specific identity of the two isolated diastereomers of **239** could not be assigned with certainty due to insufficient useful NOESY data as well as the unavailability of suitable crystals for X-ray diffraction analysis. Therefore, they are designated as 'diastereomer 1 of **239**' and 'diastereomer 2 of **239**' in this section for ease of reference.

Table 3.3. ^{1}H (700 MHz) and ^{13}C (175 MHz) NMR data of the two diastereomers of **239** in $CDCl_3$

Position	δ_H		δ_C	
	Diastereomer 1	Diastereomer 2	Diastereomer 1	Diastereomer 2
1	1.27 m[a]	1.47 m[a]	34.7	40.3
2	2.84 m[b]	3.02 m	57.6	57.8
3	1.27 m[a]	1.27 m[b]	35.8	32.4
	2.84 m[b]	1.84 m		
4	1.27 m[a]	1.27 m[b]	18.7	18.8
5	0.91 t (7.3)	0.88 t (7.1)	14.1	14.4
1'	3.72 m	2.59 m	59.5	56.9
2'	1.50 dtd (12.7, 7.1, 5.0)	1.27 m[b]	31.2	31.8
	2.06 dq (13.0, 7.4)			
3'	1.82 m	1.69 m	23.7	24.9
4'	2.57 dt (11.6, 7.6)	2.78 m[c]	43.1	46.1
	2.84 m[b]	2.91 m[d]		
1"	-	-	139.2	140.2
2", 6"	7.23 m[c]	7.21 m[e]	128.9[a]	128.8[a]
	7.33 m[c]	7.29 m[e]		
3", 5"	7.23 m[c]	7.21 m[e]	128.7[a]	128.4[a]
	7.33 m[c]	7.29 m[e]		
4"	7.23 m[c]	7.21 m[e]	126.7	126.1
7"	1.61 m	1.47 m[a]	35.7	36.6
	2.84 m[b]	2.78 m[c]		
8"	2.84 m[b]	2.78 m[c]	46.1	48.1
	3.13 dt (11.1, 5.7)	2.91 m[d]		

[a-e]Assignments may be interchanged within each column due to severe or partial overlapped of signals.

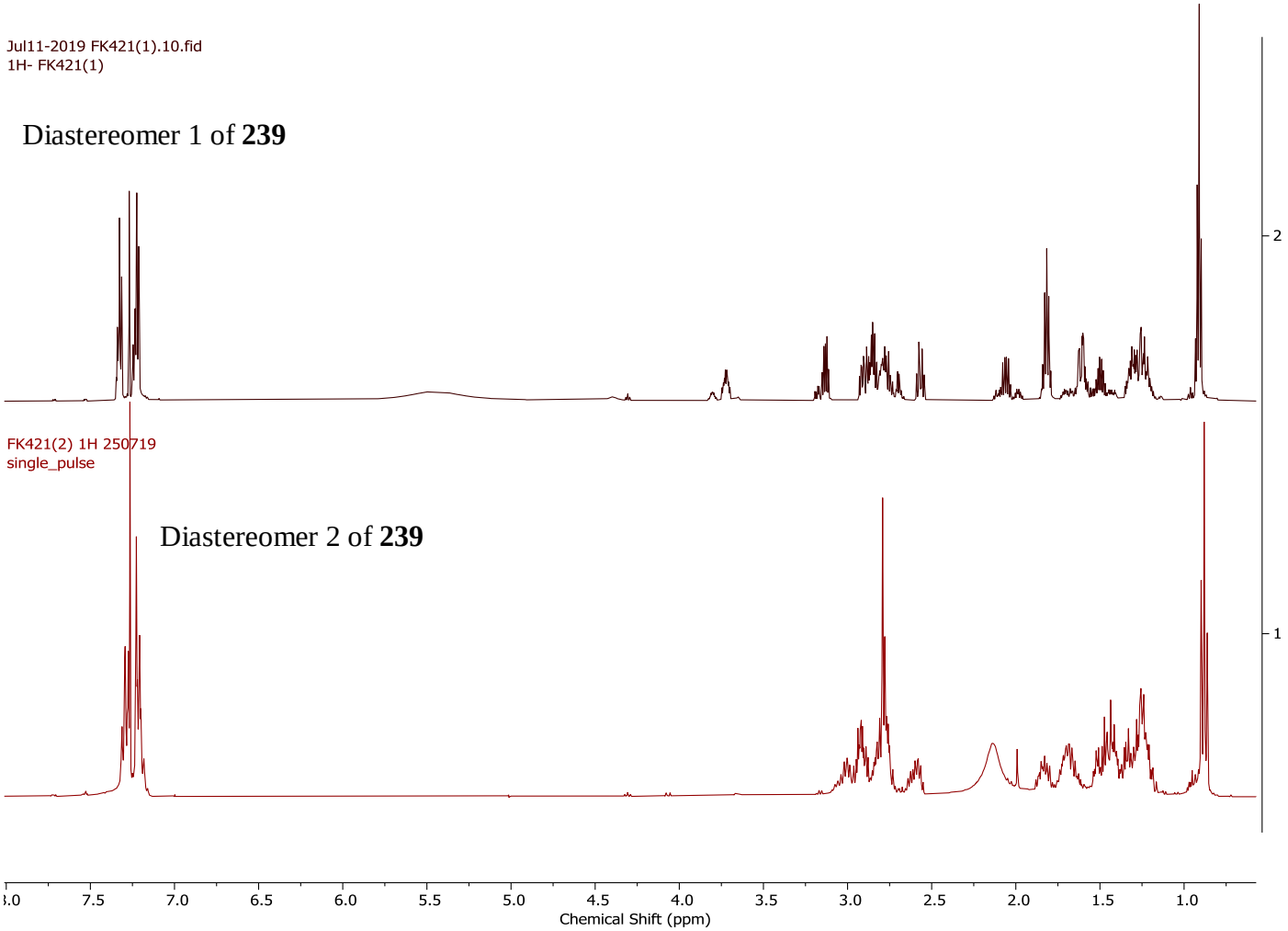


Figure 3.6. ^{1}H NMR spectra of the two diastereomers of **239** ($CDCl_3$, 600 MHz and 400 MHz)

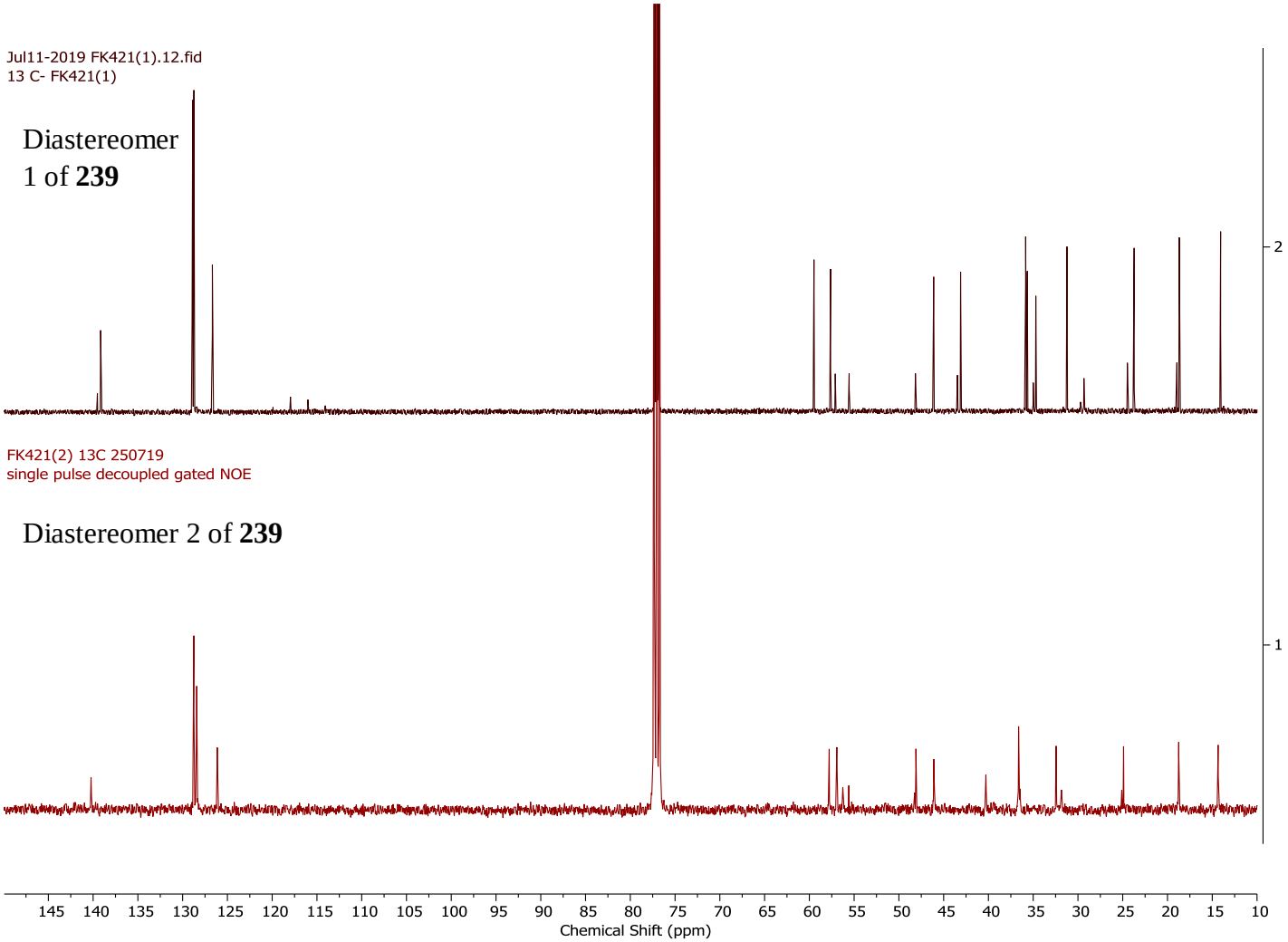


Figure 3.7. ^{13}C NMR spectra of the two diastereomers of **239** ($CDCl_3$, 150 MHz and 100 MHz)

3.7 Summary

A total of 51 schwarzinicine analogues (**215a–z**, **215za–zr**, **216a–d**, **217a**, **217b** and **218**) were successfully synthesized based on the application of Weinreb ketone synthesis and reductive amination as the key synthetic methods. Three *N*-alkyl analogues (**231a–c**) were synthesized based on the formation and subsequent reduction of amides. Analogues **232** and **233** were prepared from quaternization of amines **215b** and **217b**, respectively. Diastereomers **239a** and **239b** were obtained from *N*-Boc deprotection of **215z**. All the synthesized analogues were assessed for their vasorelaxant effects in rat isolated aorta using organ bath assay.

4

Pharmacological evaluations and SAR studies of schwarzinicine alkaloids and synthetic analogues

4.1 Overview

As mentioned in Chapter 1, schwarzinicine A (**142**) was initially found to exhibit promising and selective vasorelaxation in Sprague Dawley (SD) rat isolated aorta. The results have prompted us to investigate the SAR around the structure of schwarzinicine A (**142**) with the aim to further develop it into a useful cardiovascular agent. In this chapter, we report the relaxant responses and ability of schwarzinicines A–D (**142–145**), synthetic schwarzinicine F (**147**) and various other synthetic analogues to inhibit PE-induced contraction on SD rat isolated aorta using organ bath technique. The vasorelaxant activities for a few selected compounds evaluated on spontaneously hypertensive rat (SHR) isolated aorta are also presented.

4.1.1 Organ bath assay

Organ bath assay remains as an important pharmacological method to investigate the effects of applied drugs or compounds on the contraction or relaxation ability of isolated smooth muscle tissues such as vascular, airway, bladder and gastrointestinal tract. A typical organ bath setup is depicted in Figure 4.1.

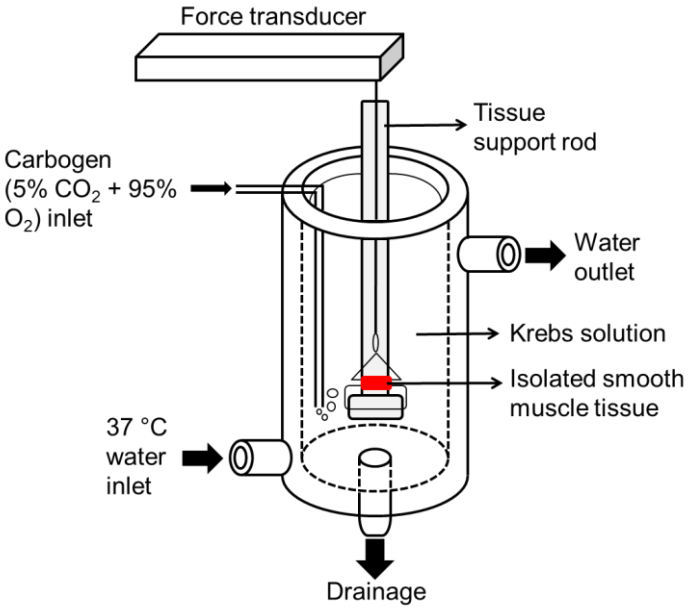


Figure 4.1. Organ bath setup adapted from Jespersen *et al.*[236]

It is useful to construct a concentration-response relationship for a compound using the tissue of interest so that the potency and efficacy of the compound can be assessed and quantified. Since the tissue is functioning as a whole in the organ bath study, this technique delivers a direct measurement of smooth muscle contraction or relaxation in an isolated system. This technique essentially provides a good idea of how the examined compounds would function in the body as a whole.[236] Such results are important in drug development especially during the lead optimization stage as the discovery of a drug with high potency, efficacy and selectivity towards a target tissue is one of the ultimate aims of any drug discovery programme.

4.1.2 Rationale for selecting rat aortic tissue for organ bath assay

The aorta is the main and largest artery in the human body. It comprises of vascular smooth muscle cells that ensure the blood vessels contract and relax in a way that blood circulation is well regulated.[237] It is increasingly recognised that arterial stiffening is closely associated with resistant hypertension.[238]

There are three major advantages that contribute to the wide use of rat aortic tissue in investigating vascular smooth muscle response. Firstly, the aorta is perceived to reflect the blood vessel contraction and relaxation mediated by vascular smooth muscle. Secondly, the aortic tissue from an animal model such as rats is relatively easy to handle and isolate, giving reproducible and dependable responses in *in situ* and *in vitro* assays.[239,240] Lastly, the length of the aorta isolated from a rat is long enough to be divided into many segments, meaning fewer animals are needed to be sacrificed for testing of a large number of compounds.

4.1.3 Laboratory rats

Laboratory rats are domesticated rats of the species *Rattus norvegicus* used for scientific research.[241] With their uses in physiological research dates to as early as 1909, laboratory rats are recognised as a preeminent biomedical research animal model, notably in aging studies, behaviour and neuroscience, toxicology, oncology, and common human diseases such as diabetes and hypertension.[241,242] Compared to other animal models such as rabbits and dogs, laboratory rats are relatively low in cost, high in availability, relatively easy to handle and maintain, making them popular to be used as animal research models.[242]

The two types of rats used in this study are Sprague Dawley (SD) rats and spontaneously hypertensive rats (SHRs). SD rats are an outbred breed first produced by a cross between a hooded male hybrid of unknown origin and an albino Wistar female rat in 1925.[243] They are one of the most widely used and versatile animal models in medical and nutritional research such as aging, neuroscience, metabolic syndrome, toxicology, oncology and hypertension.[239,244–248] In recent hypertension

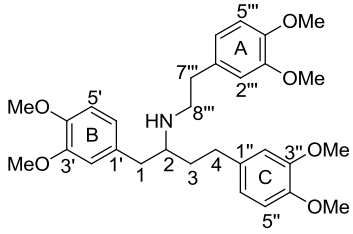
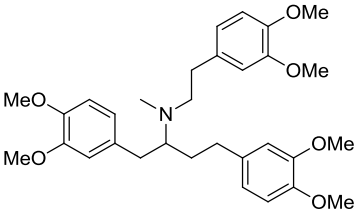
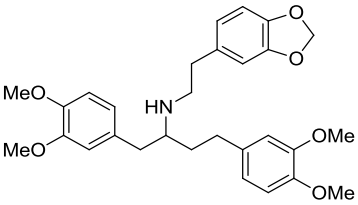
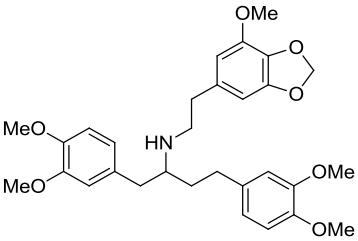
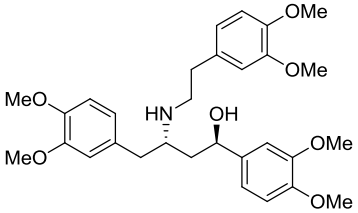
research, SD rats are particularly used as experimental models in investigating the vasorelaxant effects of plant extracts and natural products in rat isolated aorta.[249–253]

In contrast, SHR was reported much later than SD in the 1960s by Okamoto *et al.*, who successfully inbred Wistar rats with high blood pressure.[254] The SBP in SHRs ranges from 180–200 mmHg at 25 weeks of age.[254] At that time, SHRs start to develop characteristics of cardiovascular disease, such as cardiac hypertrophy, cardiac failure and renal dysfunction, making them a suitable model for the study of cardiovascular diseases.[255] SHR is also used as an animal model of established human hypertension such as the study of hypertension-induced changes in signalling mechanisms[256] and testing of new antihypertensive medications.[257,258]

4.2 *In vitro* vasorelaxant activity of schwarzinicines A–D (142–145) and F (147d) on SD rats

Schwarzinicines A–D (**142–145**), synthetic schwarzinicine F (**147d**) and the positive controls, i.e., dobutamine and verapamil (**18**), were assessed for their vasorelaxant activity in aortic rings isolated from adult male SD rats by using the organ bath technique.[170] As shown in Table 4.1, all the compounds tested showed concentration-dependent relaxations. For ease of discussion, compounds promoting 50% relaxation at low concentration (EC_{50} < 5 μM) and with good efficacy (E_{max} > 90%) were regarded as good relaxants.[259] Ethical approval was obtained prior to the commence of the study on SD rats (see Section 6.3.2 and Appendix).

Table 4.1. Vasorelaxant activity of dobutamine, verapamil (**18**), schwarzinicines A–D (**142–145**) and synthetic schwarzinicine F (**147d**) in rat isolated aortic rings pre-contracted with PE (0.1 μM)

Compound	*n*	EC_{50}[a] (μM)	E_{max}[a] (%)
Dobutamine	5	2.50 ± 1.11	92.0 ± 5.0*
Verapamil (**18**)	5	0.21 ± 0.09*	103.5 ± 4.5*
 Schwarzinicine A (**142**)	6[b]	2.01 ± 0.67[b]	119.3 ± 3.6[b]
	6[c]	2.34 ± 0.52[c]	119.0 ± 4.4[c]
 Schwarzinicine B (**143**)	5[d]	0.96 ± 0.25[d]	106.0 ± 1.5[d]*
	6[e]	1.19 ± 0.23[e]	106.3 ± 3.8[e]*
 Schwarzinicine C (**144**)	6	1.88 ± 0.64	120.4 ± 4.2
 Schwarzinicine D (**145**)	6	2.10 ± 0.35	116.1 ± 3.6
 Synthetic schwarzinicine F (**147d**)	5	5.89 ± 3.22	107.1 ± 5.7

[a]Each value represents mean ± standard error of the mean (SEM) of (*n*) determinations. [b]Natural **142**. [c]Synthetic **142**. [d]Natural **143**. [e]Synthetic **143**. *Significantly different from natural **142** ($p < 0.05$).

Due to the lack of material, the vasorelaxant activity of natural schwarzinicines E–G (**146**–**148**) could not be assessed. Since synthetic schwarzinicine F (**147d**) was available, its vasorelaxant activity was determined instead. Broadly, all the schwarzinicine compounds tested were effective at inhibiting PE-induced contraction (E_{max} = 105–120%) with very similar potency (EC_{50} = 0.96–5.89 μM) (Table 4.1 and Figure 4.2a).

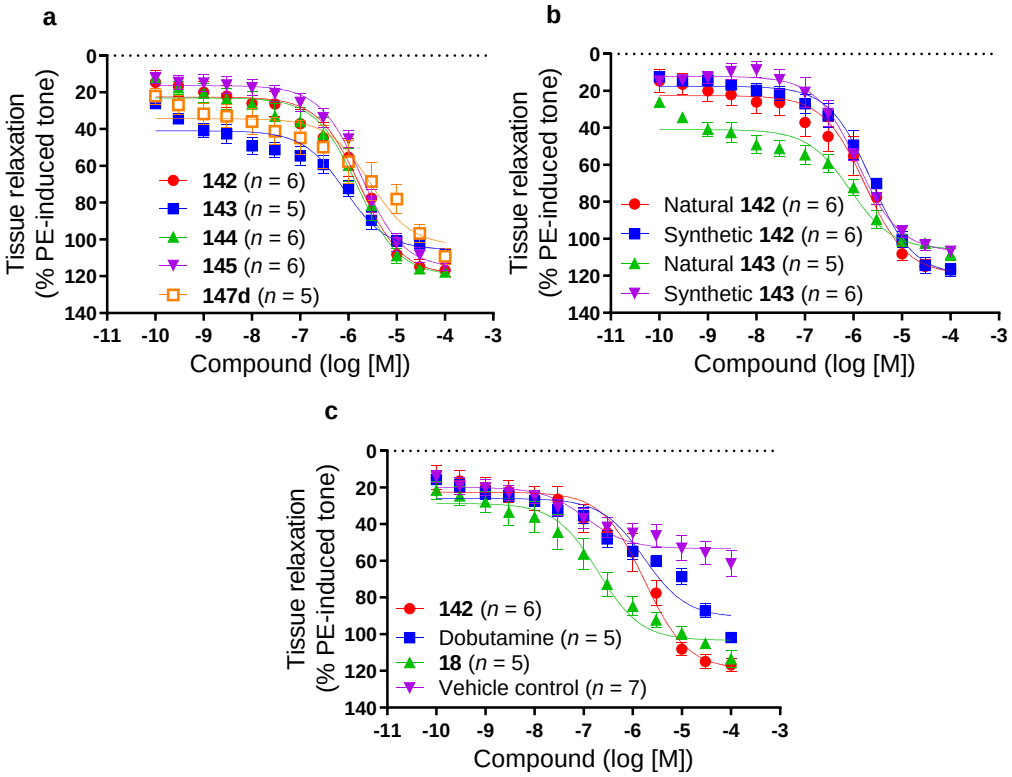


Figure 4.2. Vasorelaxation induced by (**a**) natural schwarzinicines A–D (**142**–**145**) and synthetic schwarzinicine F (**147d**); (**b**) natural and synthetic schwarzinicines A (**142**) and B (**143**); (**c**) schwarzinicine A (**142**), dobutamine and verapamil (**18**), in rat isolated aortic rings pre-contracted with PE (0.1 μM). Each point represents mean ± SEM of (*n*) determinations.

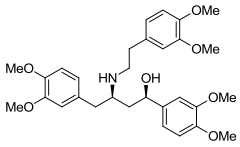
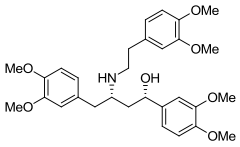
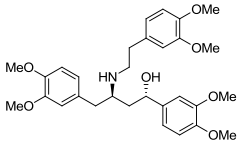
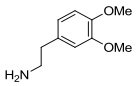
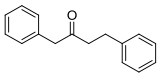
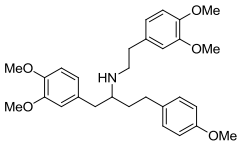
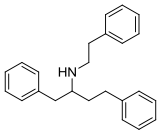
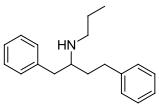
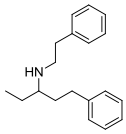
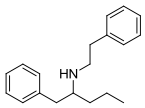
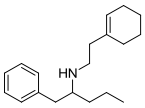
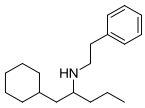
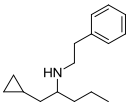
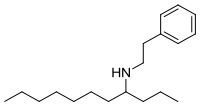
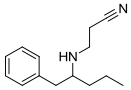
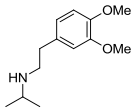
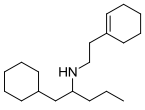
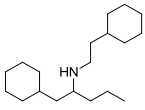
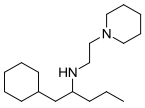
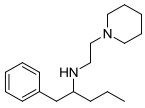
It was worth noting that no significant difference in activity was observed between the natural and synthetic versions of schwarzinicines A (**142**) and B (**143**) (Table 4.1 and Figure 4.2b).

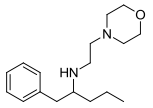
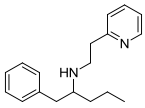
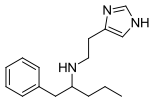
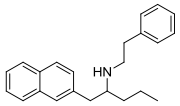
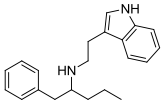
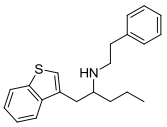
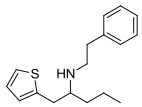
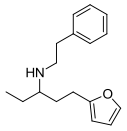
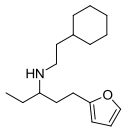
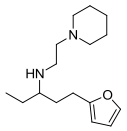
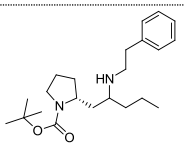
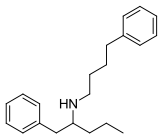
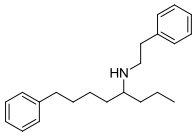
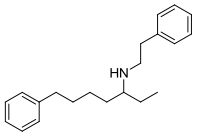
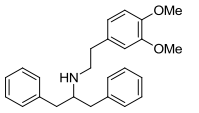
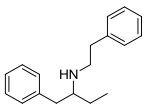
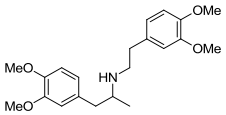
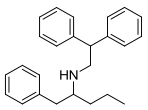
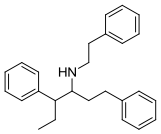
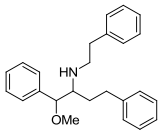
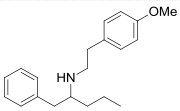
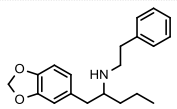
The vasorelaxant activity of natural schwarzinicine A (**142**), which is regarded as the lead compound in the present study, was also compared to those of the positive controls, i.e., dobutamine and verapamil (**18**) (Table 4.1 and Figure 4.2c). As with the schwarzinicine alkaloids, both dobutamine and verapamil are phenylalkylamine vasorelaxant agents. The potency of **142** was comparable to that of dobutamine but was about 10-fold weaker than that of verapamil (**18**). However, **142** produced higher relaxation than both dobutamine and verapamil (**18**) by 27% and 16%, respectively (Table 4.1 and Figure 4.2c).

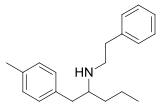
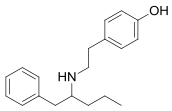
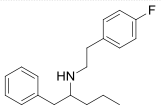
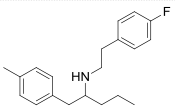
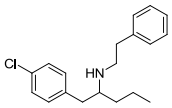
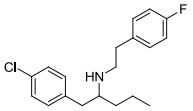
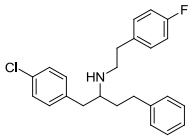
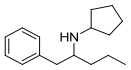
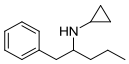
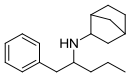
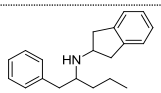
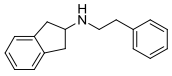
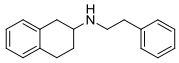
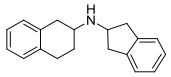
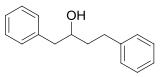
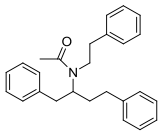
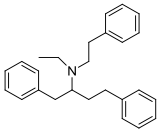
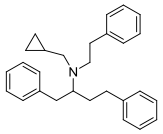
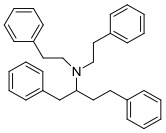
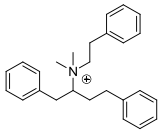
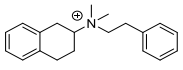
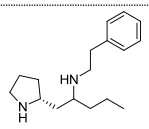
4.3 *In vitro* vasorelaxant activity of synthetic schwarzinicine analogues

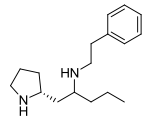
With the confirmation of *in vitro* efficacy of the schwarzinicine alkaloids, we proceeded to evaluate the vasorelaxant activity of several series of synthetic schwarzinicine analogues, prepared based on the analogue design strategies described in Section 3.1.1. The results, including those of 3,4-dimethoxyphenethylamine (DMPEA, **176**), are shown in Table 4.2.

Table 4.2. Vasorelaxant activity of various analogues in rat isolated aortic rings pre-contracted with PE (0.1 μM)

Compound	*n*	EC_{50}[a] (μM)	E_{max}[a] (%)	Compound	*n*	EC_{50}[a] (μM)	E_{max}[a] (%)
 **147a**	5	2.81 ± 2.02	97.0 ± 2.3*	 **147b**	7	0.36 ± 0.10*	96.8 ± 6.4*
 **147c**	6	3.84 ± 0.96	123.0 ± 4.3	 DMPEA (**176**)	6	0.14 ± 0.04*	53.4 ± 4.2*
 **191a**	5	4.56 ± 1.59	75.7 ± 2.5*	 **215a**	6	2.99 ± 0.69	121.8 ± 5.4
 **215b**	5	2.30 ± 0.27	116.0 ± 5.0	 **215c**	5	3.83 ± 0.42	120.6 ± 3.2
 **215d**	7	1.24 ± 0.25	111.5 ± 1.9	 **215e**	5	3.06 ± 0.73	112.6 ± 4.9
 **215f**	6	2.41 ± 0.9	116.6 ± 5.1	 **215g**	7	1.84 ± 0.45	113.7 ± 4.3
 **215h**	6	1.51 ± 0.53	116.1 ± 5.5	 **215i**	5	1.05 ± 0.25	89.7 ± 1.7*
 **215j**	5	1.43 ± 0.40	89.5 ± 3.4*	 **215k**	5	40.4 ± 13.6*	63.9 ± 4.4*
 **215l**	6	1.00 ± 0.38	84.7 ± 2.2*	 **215m**	5	0.32 ± 0.07*	83.6 ± 3.7*
 **215n**	6	0.22 ± 0.08*	88.4 ± 1.8*	 **215o**	6	0.13 ± 0.05*	110.5 ± 7.3

Compound	*n*	EC_{50}[a] (μM)	E_{max}[a] (%)	Compound	*n*	EC_{50}[a] (μM)	E_{max}[a] (%)
 **215p**	6	2.74 ± 0.96	89.8 ± 5.3*	 **215q**	5	1.13 ± 0.38	114.3 ± 5.3
 **215r**	6	1.37 ± 0.46	121.6 ± 8.4	 **215s**	5	1.60 ± 0.45	115.0 ± 3.7
 **215t**	6	0.44 ± 0.09*	114.0 ± 1.2	 **215u**	6	0.37 ± 0.09*	112.5 ± 2.0
 **215v**	6	0.41 ± 0.10*	109.9 ± 2.2	 **215w**	5	0.02 ± 0.005*	99.7 ± 1.8*
 **215x**	5	2.12 ± 0.73	105.6 ± 2.3*	 **215y**	6	0.42 ± 0.15*	97.8 ± 3.7*
 **215z**	6	0.05 ± 0.02*	103.5 ± 3.2*	 **215za**	5	2.74 ± 0.75	127.4 ± 5.3
 **215zb**	5	2.02 ± 0.47	121.1 ± 3.9	 **215zc**	6	3.36 ± 1.08	124.8 ± 6.3
 **215zd**	5	1.86 ± 0.37	114.9 ± 1.8	 **215ze**	6	1.12 ± 0.35	120.0 ± 3.7
 **215zf**	5	2.89 ± 0.82	103.6 ± 8.9	 **215zg**	7	1.68 ± 0.54	96.6 ± 2.1*
 **215zh**	6	2.13 ± 0.77	78.1 ± 3.4*	 **215zi**	5	4.16 ± 1.37	113.7 ± 3.9
 **215zj**	7	1.28 ± 0.04	113.8 ± 1.7	 **215zk**	5	1.06 ± 0.31	113.0 ± 2.5

Compound	*n*	EC_{50}[a] (µM)	E_{max}[a] (%)	Compound	*n*	EC_{50}[a] (µM)	E_{max}[a] (%)
 **215zl**	6	2.64 ± 0.51	120.3 ± 3.0	 **215zm**	5	0.05 ± 0.007*	111.0 ± 2.3
 **215zn**	5	3.83 ± 0.55	119.5 ± 3.3	 **215zo**	6	1.23 ± 0.47	118.3 ± 5.2
 **215zp**	5	1.95 ± 0.86	113.7 ± 2.9	 **215zq**	5	1.09 ± 0.38	99.1 ± 5.3*
 **215zr**	5	0.65 ± 0.33	92.2 ± 4.0*	 **216a**	7	3.09 ± 0.96	116.4 ± 8.3
 **216b**	5	2.25 ± 0.95	114.0 ± 7.1	 **216c**	6	0.48 ± 0.12*	105.7 ± 3.3*
 **216d**	7	0.35 ± 0.06*	113.9 ± 3.1	 **217a**	6	0.20 ± 0.05*	113.1 ± 2.8
 **217b**	7	0.50 ± 0.07*	119.1 ± 3.9	 **218**	5	1.32 ± 0.32	121.6 ± 3.1
 **221**	5	2.96 ± 1.70	84.1 ± 4.8*	 **230a**	6	20.3 ± 0.75*	82.9 ± 7.6*
 **231a**	6	1.21 ± 0.29	85.0 ± 3.0*	 **231b**	7	0.14 ± 0.05*	75.4 ± 5.7*
 **231c**	5	1.39 ± 0.50	68.9 ± 11.3*	 **232**	5	1.97 ± 0.39	136.0 ± 2.9*
 **233**	5	0.18 ± 0.04*	114.1 ± 5.1	 Diastereomer 1 of **239**	6	0.06 ± 0.02*	94.7 ± 3.9*

Compound	*n*	EC_{50}[a] (μM)	E_{max}[a] (%)	Compound	*n*	EC_{50}[a] (μM)	E_{max}[a] (%)
 Diastereomer 2 of **239**	5	0.12 ± 0.05*	100.3 ± 6.4*				

[a]Each value represents mean ± SEM of (*n*) determinations. *Significantly different from natural schwarzinicine A (**142**) ($p < 0.05$).

4.3.1 SAR analysis

4.3.1.1 Aromatic methoxy substituents

It is notable that the structure of schwarzinicine A (**142**) incorporated six aromatic methoxy groups from three units of 3,4-dimethoxyphenyl moieties. In order to investigate the significance of the methoxy groups for vasorelaxant activity, analogues **215a** and **215b** were made and evaluated (Figure 4.3a). Analogue **215a**, which has the highest structural similarity to **142** amongst the analogues synthesized, i.e., lacking one methoxy in ring C, showed similar activity as **142**. Interestingly, analogue **215b**, which is devoid of all the methoxy groups in **142**, also showed similar activity as **142**. This infers that the presence or absence of the aromatic methoxy groups has no effect on the vasorelaxant activity manifested by **142**.

Consistent with the above observation, schwarzinicine C (**144**), which has a 3,4-methylenedioxy-substituted ring A instead of a 3,4-dimethoxy-substitution, exhibited similar activity as schwarzinicine A (**142**) (Figure 4.3b). Additionally, schwarzinicine D (**145**), which has an additional methoxy group at C-5''' in ring A compared to schwarzinicine C (**144**), also exhibited similar activity as **142** (Figure 4.3b). These observations suggest that the differences between these alkyloxy substituents and substitution patterns in the phenyl ring C have little influence on vasorelaxant activity.

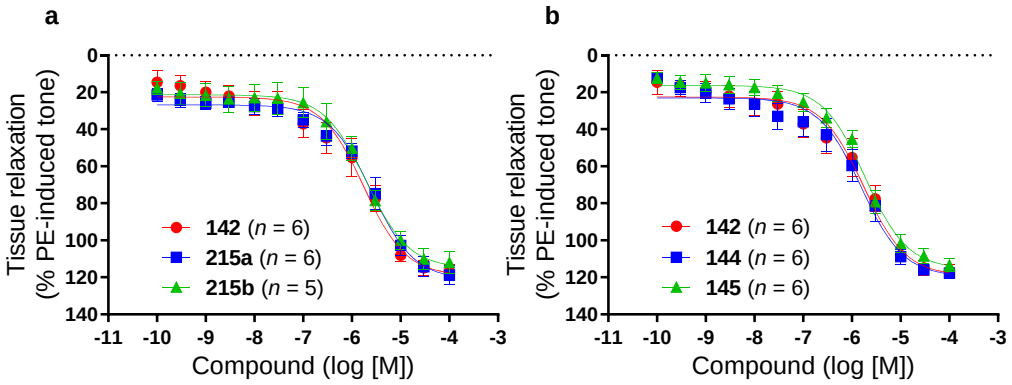


Figure 4.3. Vasorelaxation induced by (**a**) schwarzinicine A (**142**), **215a** and **215b**; (**b**) schwarzinicines A (**142**), C (**144**) and D (**145**), in rat isolated aortic rings pre-contracted with PE (0.1 μM). Each point represents mean ± SEM of (*n*) determinations.

Since the methoxy groups in the template structure of **142** were regarded as nonessential for activity, we can assume that the differences in the methoxy substitution patterns amongst the synthetic analogues, to be discussed from this point onwards, have no or little bearing on how their vasorelaxant activities are compared.

4.3.1.2 Phenyl rings A, B and C

In order to establish the necessity of the phenyl groups for activity, we made various analogues that have one or more of their phenyl groups removed. Analogues **215c**, **215d** and **215e**, which are devoid of rings A, B and C, respectively, showed similar activity as **142** (Figure 4.4a). This suggests that the absence of any one ring in the structure of **142** is tolerable and does not negatively affect activity. Many of the analogues made subsequently were based on modifications of the structures of **215d** and **215e**, which serve as simplified scaffolds for the lead compound **142**.

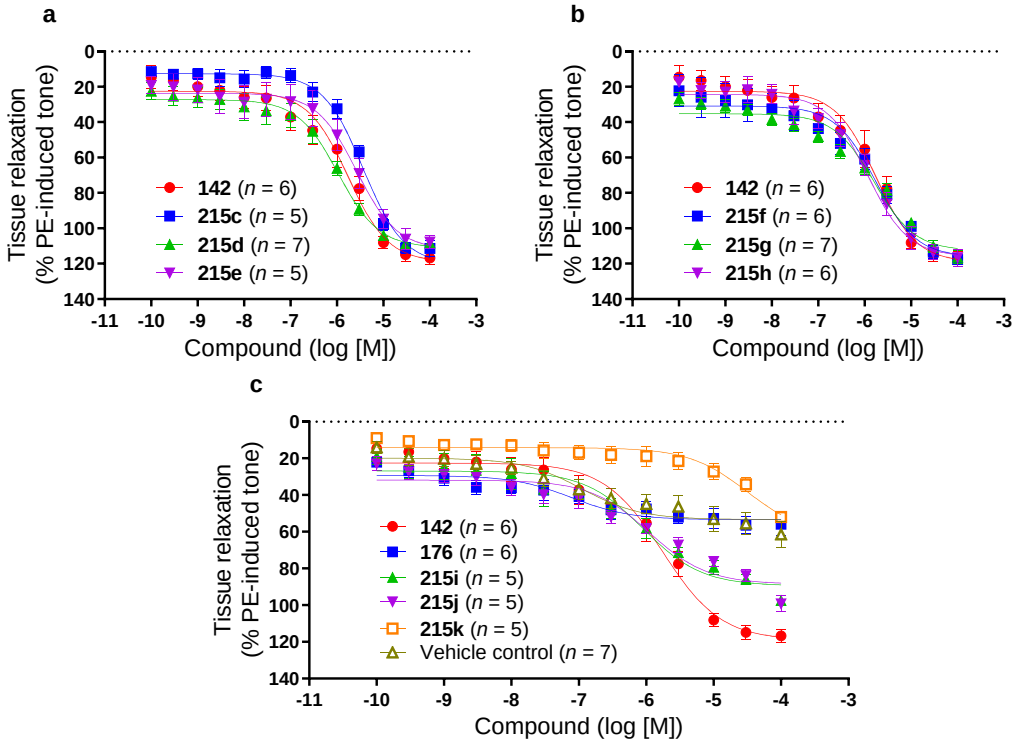


Figure 4.4. Vasorelaxation induced by (**a**) schwarzinicine A (**142**) and **215c–e**; (**b**) schwarzinicine A (**142**) and **215f–h**; (**c**) schwarzinicine A (**142**), DMPEA (**176**) and **215i–k**, in rat isolated aortic rings pre-contracted with PE (0.1 µM). Each point represents mean ± SEM of (*n*) determinations.

To assess the requirement of both the remaining two phenyl rings for activity, one of the two phenyl rings was substituted with a non-aromatic carbocyclic ring as exemplified by 1-cyclohexenyl in **215f**, cyclohexyl in **215g** and cyclopropyl in **215h**. These three analogues showed comparable activity to **142** (Figure 4.4b). This suggests that the absence of up to two of the three phenyl rings in **142** is tolerable for activity.

It would be interesting to find out whether analogues that only have one phenyl ring (without the presence of other rings) will show any activity. We subsequently prepared analogue **215i**, which is the cyclohexyl ring-opened analogue of **215g**. Similarly, analogue **215j**, which has a nitrile group replacing phenyl ring A in **215e**, and analogue **215k**, which lacks both rings B and C, were also prepared. All the three analogues showed reduced relaxation activity compared to **142** (Figure 4.4c).

DMPEA (**176**), which only has one aromatic ring and represents the phenethylamine fragment present in **142**, was also evaluated for vasorelaxant activity. As expected, it showed no relaxation effect (in fact it has no significant difference in activity with vehicle control) (Figure 4.4c). Thus, it appears that a minimum of two rings with at least one of the two being a phenyl ring are required for activity.

4.3.1.3 Ring variation

In order to provide support to the suggestion that at least one phenyl ring is required in analogues that have two rings to show activity, analogues **215l**, **215m** and **215n** were prepared. For these analogues, both the phenyl rings present in **215e** have been replaced with carbocyclic or heterocyclic non-aromatic rings. The three analogues were subsequently tested and found to show poor vasorelaxant activity (Table 4.2 and Figure 4.5a). In contrast, compound **215o**, which is the phenyl analogue of **215n** (phenyl in place of cyclohexyl in **215n**), showed potent vasorelaxant activity (EC_{50} = 0.13 µM, E_{max} = 110.5%) when tested (Table 4.2 and Figure 4.5a). These observations firmly confirm that a minimum of two rings with one of the rings being a phenyl ring are required for good vasorelaxant activity (E_{max} > 90%). As such, all subsequent analogues made and assessed would have two or three rings with at least one being an aromatic group.

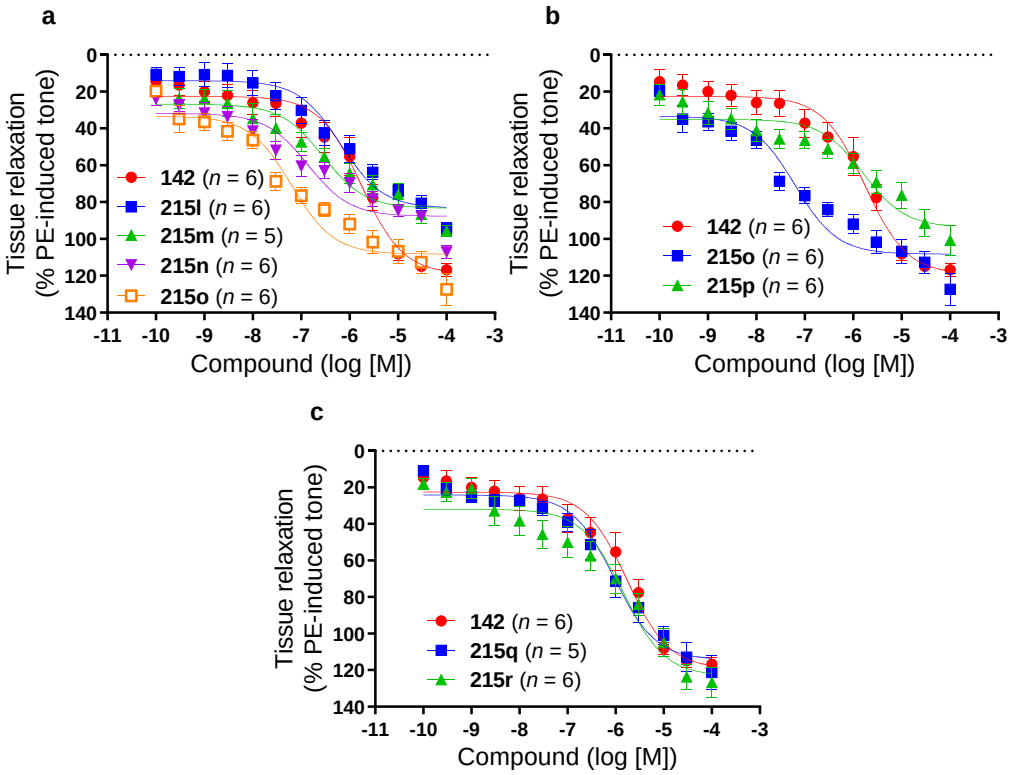


Figure 4.5. Vasorelaxation induced by (**a**) schwarzinicine A (**142**) and **215l–o**; (**b**) schwarzinicine A (**142**), **215o** and **215p**; (**c**) schwarzinicine A (**142**), **215q** and **215r**, in rat isolated aortic rings pre-contracted with PE (0.1 μM). Each point represents mean ± SEM of (*n*) determinations.

It was also worth noting that analogue **215o** showed a 18-fold increase in potency (with comparable efficacy) when compared to **215f**, which has comparable activity as **142** (Table 4.2). In term of structure, analogue **215o** incorporated an *N*-piperidinyl ring in place of the cyclohexenyl ring in **215f**. This suggests that the basic tertiary amine nitrogen in **215o** may play a role in the improved potency observed. Interestingly, when the *N*-piperidinyl ring in **215o** was replaced with an *N*-morpholine in **215p**, the relaxation effect dropped from E_{max} of 110.5% to 89.8% (Table 4.2 and Figure 4.5b). On checking the p*K*a values of piperidine and morpholine, the nitrogen atom of the former appears to be a lot more basic than the latter (piperidine p*K*a = 11.2 *vs* morpholine p*K*a = 8.4).[175] We, therefore, postulate that the significant

difference in activity for **215o** and **215p** may be due to the requirement of a basic nitrogen atom in ring A for enhanced potency.

Analogues **215q** and **215r**, which incorporated a 2-pyridinyl and a 4-imidazolyl substituent, respectively, in place of phenyl ring A in **215e**, showed comparable activity to **142** (Figure 4.5c). This appears to suggest that the nitrogen atoms present in the pyridinyl (**215q**) and imidazolyl (**215r**) moieties do not contribute to any favourable binding interaction with the biological target. Additionally, the nitrogen atoms present in these heteroaromatic moieties are not quite as basic as that in the piperidinyl moiety in **215o** (p*K*a values of piperidine, pyridine and imidazole are 11.2, 5.5 and 7.0, respectively).[175] This may account for the reason why these nitrogen atoms do not impart any potency enhancement effect to **215q** and **215r**.

Replacement of a phenyl ring in **215e** with a larger bicyclic aromatic moiety such as a naphthyl in **215s** did not negatively affect the activity (Figure 4.6a). On the contrary, replacement of a phenyl ring in **215e** with a larger bicyclic heteroaromatic group such as a 3-indolyl in **215t** and a 3-benzothiophenyl group in **215u**, increased potency by 5-fold (Table 4.2 and Figure 4.6a).

On the other hand, replacement of phenyl ring B in **215e** with a smaller heteroaromatic ring such as a 2-thiophenyl in **215v** also increased the potency by 5-fold. Exceptionally, replacement of phenyl ring C in **215d** with a 2-furyl group in **215w** resulted in a remarkable 100-fold potency enhancement with a slight drop in efficacy (EC_{50} = 0.02 μM, E_{max} = 99.7%) when compared to **142** (Table 4.2 and Figure 4.6b).

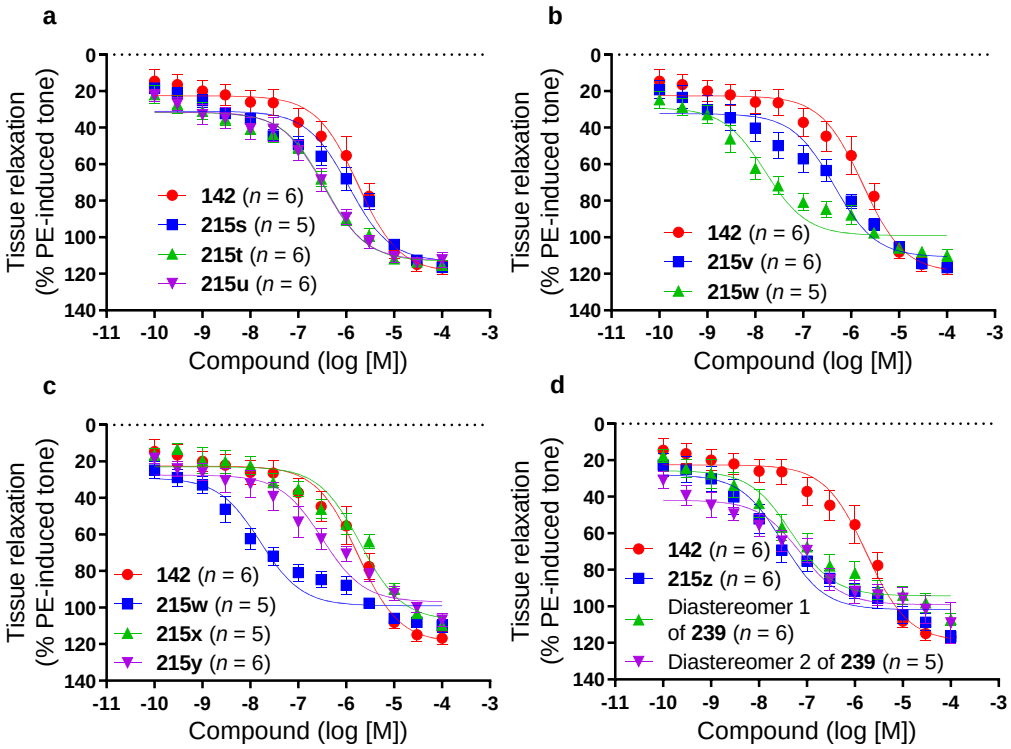


Figure 4.6. Vasorelaxation induced by (**a**) schwarzinicine A (**142**) and **215s–u**; (**b**) schwarzinicine A (**142**), **215v** and **215w**; (**c**) schwarzinicine A (**142**) and **215w–y**; (**d**) schwarzinicine A (**142**), **215z**, diastereomers 1 and 2 of **239**, in rat isolated aortic rings pre-contracted with PE (0.1 μM). Each point represents mean ± SEM of (*n*) determinations.

Unexpectedly, replacement of phenyl ring A in the very potent analogue, **215w**, with a cyclohexyl ring in **215x**, resulted in attenuation of potency. However, **215x** still showed fairly comparable vasorelaxant activity to **142** (Figure 4.6c). On the other hand, analogue **215y**, which possesses an *N*-piperindinyl ring in place of the cyclohexyl ring in **215x**, showed a 5-fold improved potency (albeit with a slight reduction in efficacy) when compared to both **215x** and **142** (Table 4.2 and Figure 4.6c). This observation is somewhat consistent with the vasorelaxation noted above for **215o**, whereby we speculated that the presence of the basic piperidinyl nitrogen atom plays a role in potency enhancement.

It was established earlier that good vasorelaxing compounds need to have two or three rings with at least one being a phenyl ring. Based on the activity observed for both **215x** and **215y**, we could now extend the phenyl ring requirement to aromatic groups in general, which include a heteroaromatic ring.

Replacement of phenyl ring B in **215e** with a 1-Boc-2*R*-pyrrolidinyl group gave a pair of unresolved diastereomeric mixture **215z**, which also showed excellent potency (40-fold enhancement) while retaining a good level of efficacy (EC_{50} = 0.05 μM, E_{max} = 103.5%) when compared to **142** (Table 4.2 and Figure 4.6d). Removal of the *N*-Boc group from **215z** gave a pair of diastereomeric mixture **239**, which following separation by centrifugal radial TLC furnished two pure *N*-Boc deprotected diastereomers of **215z**. Although the two diastereomers were found to be more potent than **142** by 34- and 17-fold, while retaining a good level of efficacy (Figure 4.8d), their vasorelaxant effects were not better than that of **215z**. The absolute stereochemistry of the two diastereomers could not be readily determined.

4.3.1.4 Chain length

Compounds **215za**, **215zb**, **215zc**, **215ze** and **215zf** represent analogues resembling **215d** and **215e** that possess different chain lengths:

i. between the phenyl rings (i.e., six to nine bonds away);
ii. from the central nitrogen atom to the phenyl rings (i.e., three to six bonds away); and
iii. of alkyl side chains (i.e., methyl, ethyl or propyl)

On the other hand, **215zd** is an analogue that resembles **215a** or **215b**, except that rings B and C are four instead of five bonds away. Surprisingly, all these six

analogues (**215za**, **215zb**, **215zc**, **215zd**, **215ze** and **215zf**) showed similar activity as **142** (Figures 4.7a and 4.7b). These observations imply that small variations of length, between the aromatic rings, between the central nitrogen atom and the aromatic rings, and for the alkyl side chains, are well tolerated for vasorelaxant activity.

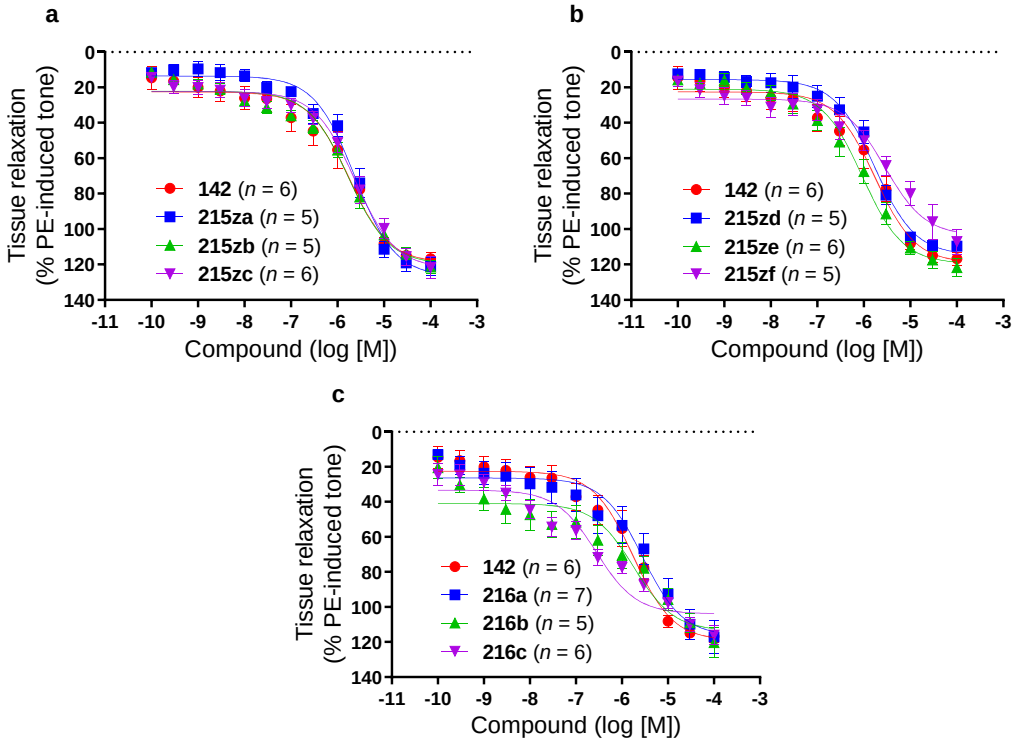


Figure 4.7. Vasorelaxation induced by (**a**) schwarzinicine A (**142**) and **215za–zc**; (**b**) schwarzinicine A (**142**) and **215zd–zf**; (**c**) schwarzinicine A (**142**) and **216a–c**, in rat isolated aortic rings pre-contracted with PE (0.1 μM). Each point represents mean ± SEM of (*n*) determinations.

On a similar note, replacement of the phenethylamine portion in **215e** with a smaller non-aromatic carbocyclic fragment, i.e., cyclopentyl and cyclopropyl in **216a** and **216b**, respectively, did not negatively affect activity (Figure 4.7c). However, substituting the phenethylamine portion with the bigger 2-norbornyl group in **216c** gave rise to a 4-fold increase in potency compared to **142** (Table 4.2 and Figure 4.7c). These results appear to suggest that ring A in **215e** needs not to be linked to the central nitrogen atom via an ethylene fragment for good vasorelaxant activity.

4.3.1.5 Structural extension

Compounds **215zg**, **215zh** and **215zi** represent structural extension analogues based on the structures of **215b** and **215e**. The introduction of a phenyl group at C-7''' in **215e** resulted in a slight decrease in efficacy (E_{max} = 96.6%) as demonstrated by **215zg**, while the introduction of an ethyl side chain at C-1 in **215b** led to a significant decrease in efficacy (E_{max} = 78.1%) as demonstrated by **215zh** (Figure 4.8a). However, the vasorelaxation efficacy was restored when the ethyl side chain in **215zh** was replaced with a methoxy group in **215zi** (Figure 4.8a), which showed comparable activity to **142**.

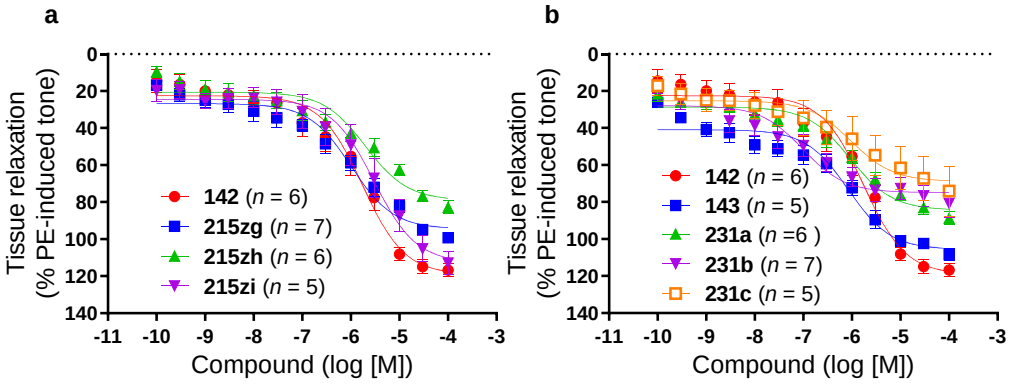


Figure 4.8. Vasorelaxation induced by (**a**) schwarzinicine A (**142**) and **215zg–zi**; (**b**) schwarzinicines A (**142**), B (**143**) and **231a–c**, in rat isolated aortic rings pre-contracted with PE (0.1 µM). Each point represents mean ± SEM of (*n*) determinations.

Structural extension at the central nitrogen atom with alkyl substituents is generally not favourable. It was observed that efficacy decreases with the increase in size of the substituents on the central nitrogen atom, as demonstrated by schwarzinicine B (**143**), **231a**, **231b** and **231c** (Figure 4.8b). Schwarzinicine B (**143**), which is the *N*-methyl derivative of **142**, showed a slight decrease in efficacy (E_{max} = 106.0%) compared to **142** (Table 4.2 and Figure 4.8b). Analogues **231a**, **231b** and

231c, which are the *N*-ethyl, *N*-cyclopropylmethyl and *N*-phenethyl derivatives of **215b**, respectively, showed a gradual and significant decrease in efficacy as their *N*-alkyl substituents increase in size (Table 4.2 and Figure 4.8b).

4.3.1.6 Rigidification

Compound **216d** represents a rigidified analogue of **215e**, where the phenethyl group in **215e** is substituted with a 2-indanyl moiety in **216d**. The C-7‴–C-8‴ and C-7‴–C-1‴ bonds in **216d** are much more inflexible compared to those in **215e**. Due to the availability of commercial building blocks, analogues **217a** (2-indanyl) and **217b** (2-tetrahydronaphthalenyl), which lack the propyl side chain in **216d**, were also readily prepared. The three rigidified analogues **216d**, **217a** and **217b** were found to be more potent than **142** by 5.7-, 10- and 4-fold, respectively (Table 4.2 and Figure 4.9). It would be interesting to also impart rigidification to the other phenethyl fragment in **217a** and **217b**, thus analogue **218** (indane-2-aminotetralin) was prepared. However, **218** only showed comparable activity to **142**, i.e., **218** showed inferior potency compared to **216d**, **217a** and **217b** (Figure 4.9). The results may suggest that a certain degree of conformational restriction to one of the phenyl-bearing sidearms in the scaffold does lead to improved potency.

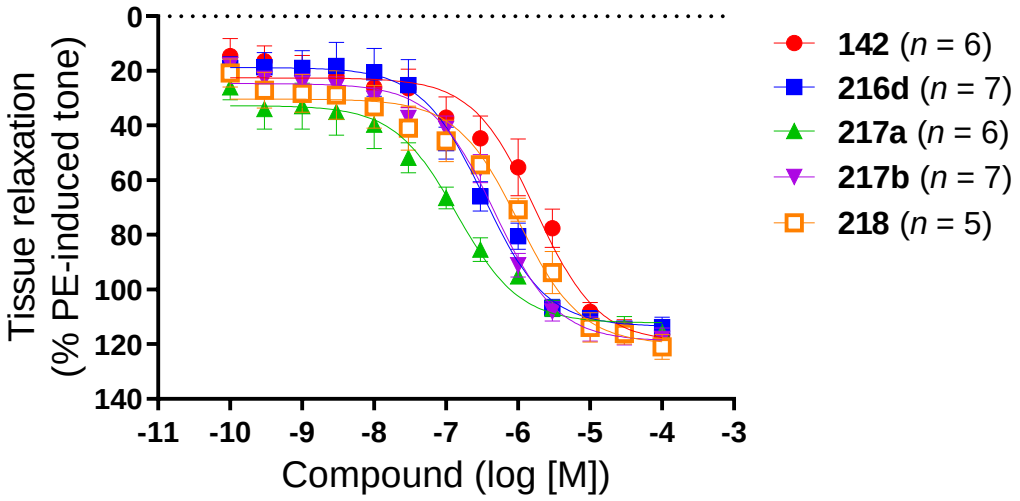


Figure 4.9. Vasorelaxation induced by schwarzinicine A (**142**), **216d**, **217a**, **217b** and **218** in rat isolated aortic rings pre-contracted with PE (0.1 µM). Each point represents mean ± SEM of (*n*) determinations.

4.3.1.7 Ionization state of central nitrogen atom

Compounds **232** and **233** are the *N*,*N*-dimethyl ammonium salts of **215b** and **217b**, respectively. When compared to **215b**, compound **232** showed a significantly higher efficacy (by 17%) with comparable potency (Table 4.2 and Figure 4.10a). However, comparing to **217b**, compound **233** showed a significantly higher potency (by 2.8-fold) with comparable efficacy (Table 4.2 and Figure 4.10a). In any case, the results may suggest that a charged nitrogen atom is important for activity. This notion was further supported by the observation that analogue **230a**, which possesses a non-basic central nitrogen atom due to its amide functionality, showed very poor activity when compared to **215b** (Figure 4.10a). For **142** and all other *N*-containing analogues (except **230a**), the basic nitrogen atoms are expected to be in the protonated state under the organ bath conditions (buffer solution pH 7.0–7.6). The lack of activity shown by **191a** and **221** (Figure 4.10b) is therefore not surprising since the non-basic ketone and hydroxyl groups are not charged during interaction with the biological

target. Taken together, the above results infer that the central nitrogen atom is essential for activity and is required to be in the ionized state when binding to its biological target.

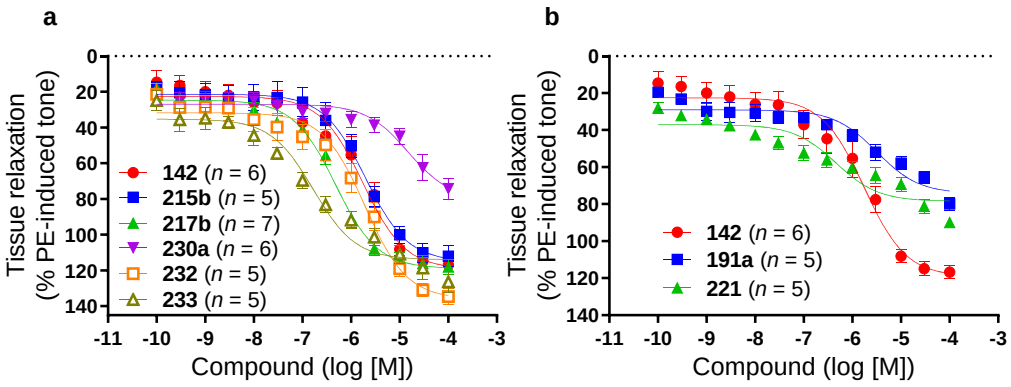


Figure 4.10. Vasorelaxation induced by (**a**) schwarzinicine A (**142**), **215b**, **217b**, **230a**, **232** and **233**; (**b**) schwarzinicine A (**142**), **191a** and **221**, in rat isolated aortic rings pre-contracted with PE (0.1 μM). Each point represents mean ± SEM of (*n*) determinations.

4.3.1.8 Electron withdrawing and donating substituents on phenyl rings

Although the phenyl rings in schwarzinicine A (**142**) are substituted with two methoxy groups each, it would be interesting to explore the effects of substituting the phenyl rings in **215b** with other electron donating groups, as well as electron withdrawing groups. Analogues **215zj**, **215zk** and **215zl**, which have one of their phenyl rings substituted with an electron donating group, i.e., a *p*-methoxy, a 3,4-methylenedioxy and a *p*-methyl group, respectively, showed comparable activity to **142** (Figure 4.11a). Interestingly, when the *p*-methoxy group in ring A of **215zj** was replaced with a *p*-hydroxy group as in **215zm**, the relaxation potency increased by 40-fold as compared to **142** (Table 4.2 and Figure 4.11a). Taken together, the results of **215zj**, **215zk**, **215zl** and **215zm** suggest that while simple electron donating groups

have no influence on activity, the *p*-hydroxyl group has potency enhancement effect, possibly due to its interaction with the biological target as a H-bond donor. It was imperative that we should also assess the *O*-demethylated analogue of **142**, i.e., a catechol congener. However, the preparation of the catechol congener of **142** proved to be more challenging than expected as it rapidly decomposed on storage (see Section 3.3).

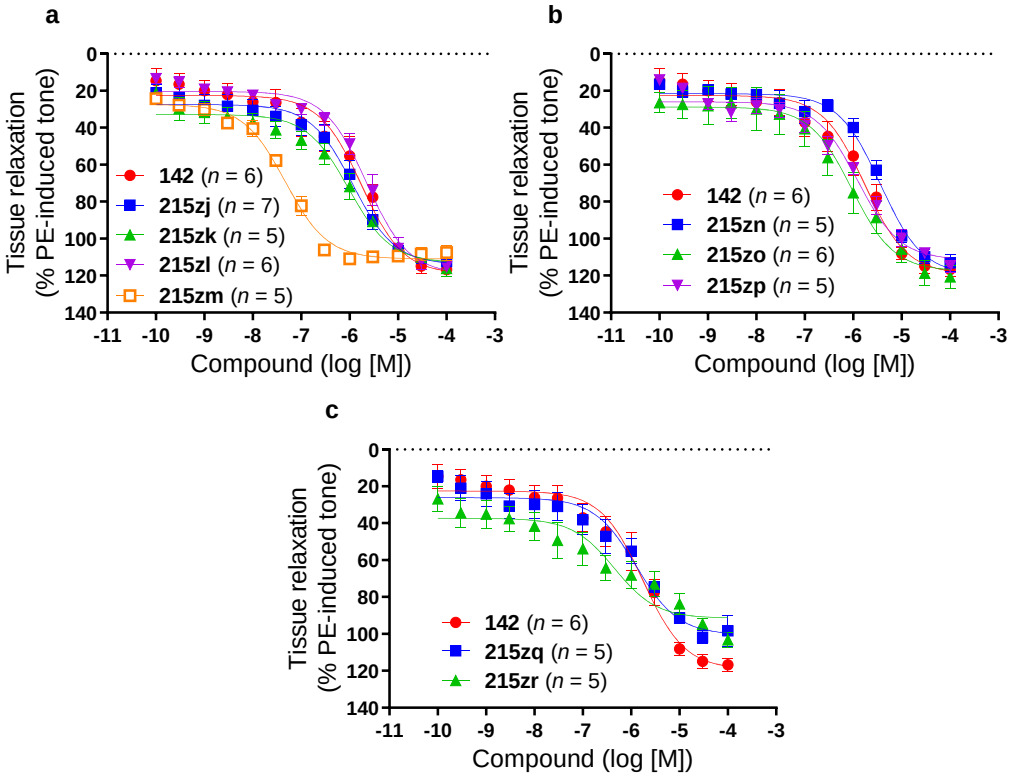


Figure 4.11. Vasorelaxation induced by (**a**) schwarzinicine A (**142**) and **215zj–zm**; (**b**) schwarzinicine A (**142**) and **215zn–zp**; (**c**) schwarzinicine A (**142**), **215zq** and **215zr**, in rat isolated aortic rings pre-contracted with PE (0.1 μM). Each point represents mean ± SEM of (*n*) determinations.

Several compounds possessing electron withdrawing substituents such as chloride and fluoride, as reflected by analogues **215zn**, **215zo**, **215zp**, **215zq** and **215zr**, were prepared and assessed. The results suggest that incorporation of either a *p*-chloro or *p*-fluoro in one of the phenyl rings, as demonstrated by **215zn**, **215zo** and

215zp, is well tolerated (Figure 4.11b). However, incorporation of both *p*-chloro and *p*-fluorophenyl rings, as exemplified by **215zq** and **215zr**, has a detrimental effect on efficacy (Figure 4.11c). Comparing the results between **215zq** and **215zr**, it appears that the presence of a third phenyl ring enhanced potency (by 1.7-fold) at the expense of efficacy (Figure 4.11c).

4.3.1.9 Stereochemistry

It was previously noted that while natural schwarzinicine A (**142**) is a scalemic mixture, natural schwarzinicine B (**143**) is enantiopure. Since both the natural and synthetic analogues of **142** and **143** showed comparable vasorelaxation (Figure 4.2b), this may suggest that the stereochemistry of the lone chiral centre at C-2 has no effect on vasorelaxant activity. As for natural schwarzinicine F (**147**), which possesses another chiral centre at C-4 compared to **142**, it was isolated as an enantiopure compound. In our efforts to synthesize schwarzinicine F (**147d**), we also afforded **147a**, **147b** and **147c**, which are the other three stereoisomers of schwarzinicine F (**147d**). As such, we were presented with the opportunity to examine the influence of the different configurations at C-2 (NHR) and C-4 (OH) on activity. Both **147a** and **147b** showed a slight reduction in efficacy compared to **142**. While **147a** displayed a similar potency as **142**, **147b** showed a 5.6-fold improved potency over **142** (Figure 4.12). Interestingly, both synthetic schwarzinicine F (**147d**) and its enantiomer (**147c**), exhibited similar activity to **142** (Figure 4.12). The results observed indicated that the introduction of a hydroxyl group at C-4 in **147** in *syn* fashion attenuates efficacy, while the 2*S*,4*S* configuration showed the greatest potency enhancement. On the other hand, the vasorelaxant activity of the 1,3-*anti* isomers (2*R*, 4*S* and 2*S*, 4*R*) appeared to be unaffected.

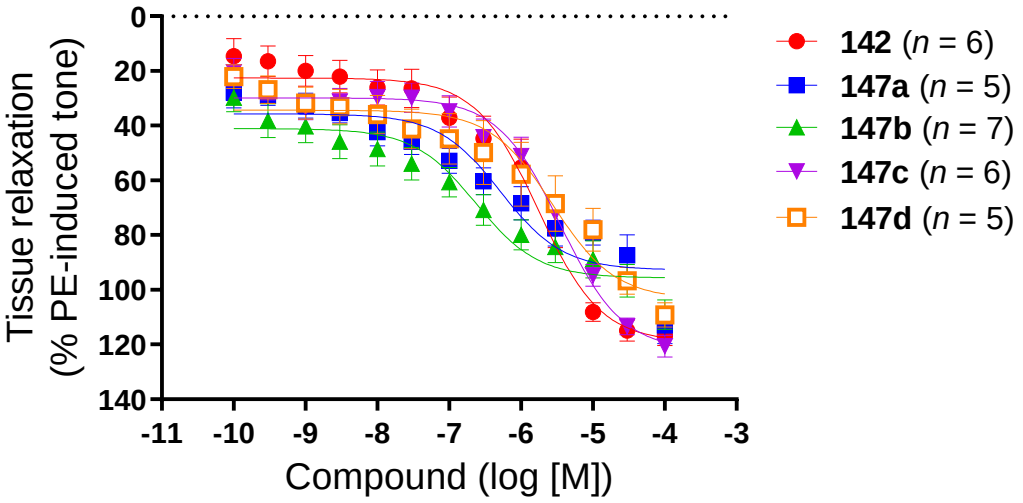
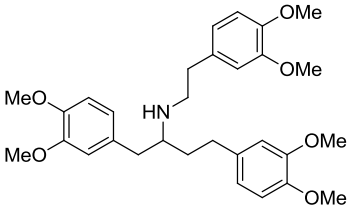
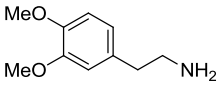
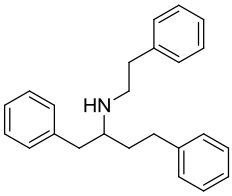
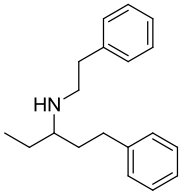
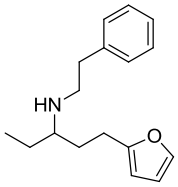
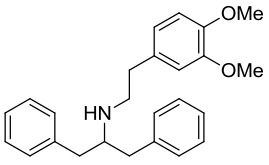
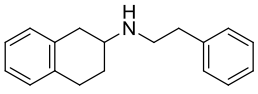


Figure 4.12. Vasorelaxation induced by schwarzinicine A (**142**), **147a–c** and synthetic schwarzinicine F (**147d**) in rat isolated aortic rings pre-contracted with PE (0.1 µM). Each point represents mean ± SEM of (*n*) determinations.

4.4 *In vitro* vasorelaxant activity of selected compounds on spontaneously hypertensive rats (SHRs)

We have carried out extensive investigations and shown unequivocal vasorelaxant effects of various analogues against isolated blood vessels obtained from SD rats. We have subsequently evaluated the efficacy and potency of schwarzinicine A (**142**) as well as a few selected analogues using isolated aorta of spontaneously hypertensive rats (SHRs), which is a well-established model of genetic hypertension and heart failure. We wished to determine whether the activities of these analogues in SD rats could also be observed in SHRs. Dobutamine and verapamil (**18**), which were used as positive controls in the previous study involving SD rats, were also included in this study. The results are shown in Table 4.3. Ethical approval for this study was obtained prior to the commence of the study on SHRs (see Section 6.3.2 and Appendix).

Table 4.3. Vasorelaxant activity of selected compounds in rat isolated aortic rings pre-contracted with PE (0.1 µM)

Compound	*n*	EC_{50}[a] (µM)	E_{max}[a] (%)
Dobutamine	5	4.57 ± 2.04	98.5 ± 10.7
Verapamil (**18**)	5	0.59 ± 0.39	124.3 ± 1.8
 Schwarzinicine A (**142**)	5[b] 7[c]	1.14 ± 0.20[b] 1.21 ± 0.26[c]	123.7 ± 9.3[b] 116.3 ± 4.1[c]
 DMPEA (**176**)	6	0.19 ± 0.08*	69.9 ± 3.3*
 **215b**	5	3.64 ± 1.33	133.6 ± 19.4
 **215d**	5	3.39 ± 1.16	118.6 ± 3.6
 **215w**	6	0.87 ± 0.18	117.5 ± 3.1
 **215zd**	5	1.92 ± 0.63	120.4 ± 4.7
 **217b**	7	0.22 ± 0.08*	116.8 ± 5.0

[a]Each value represents mean ± SEM of (*n*) determinations. [b]Natural schwarzinicine A (**142**). [c]Synthetic **142**. *Significantly different from natural **142** ($p < 0.05$).

As expected, comparable vasorelaxant effects were observed for both natural and synthetic schwarzinicine A (**142**) (Figure 4.13a). There was no statistical difference between the activity of the positive controls (dobutamine and verapamil (**18**)) and natural **142** (Table 4.3, Figure 4.13a). However, dobutamine did appear to show a slightly poorer potency and efficacy, while verapamil (**18**) appeared to show a slightly better potency with comparable efficacy when compared to natural **142** (Figure 4.13a).

In agreement with the results based on SD rats, analogues **215b**, **215d** and **215zd** showed comparable relaxation activity compared to **142**, while DMPEA (**176**) was found to be completely inactive (Figure 4.13b). However, analogue **215w**, which recorded an excellent potency level on SD rats, only showed a slight potency improvement compared to **142** (with no significant difference) (Figure 4.13c). On the other hand, analogue **217b** showed a > 5-fold potency improvement with comparable efficacy when compared to **142** (Figure 4.13c). This is consistent with the results observed based on SD rats.

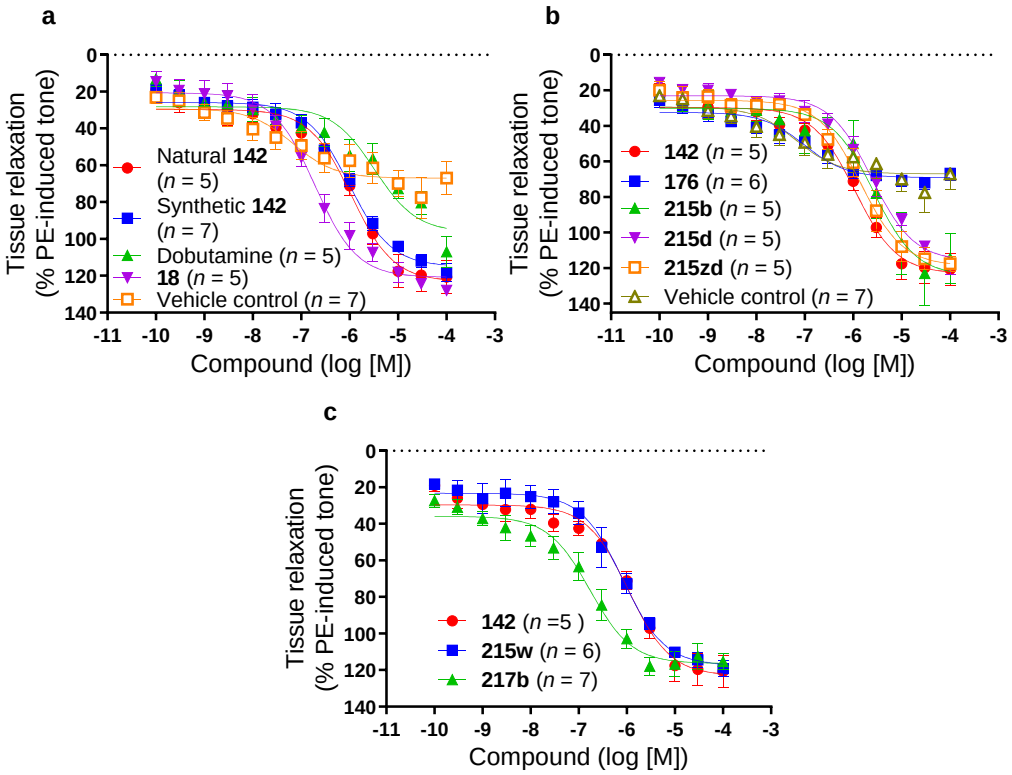


Figure 4.13. Vasorelaxation induced by (**a**) natural and synthetic schwarzinicine A (**142**), dobutamine and verapamil (**18**); (**b**) schwarzinicine A (**142**), DMPEA (**176**), **215b**, **215d** and **215zd**; (**c**) schwarzinicine A (**142**), **215w** and **217b**, in rat isolated aortic rings pre-contracted with PE (0.1 µM). Each point represents mean ± SEM of (*n*) determinations.

4.5 Summary

We have shown unequivocal vasorelaxant effects of schwarzinicines A–D (**142–145**) and F (**147**) in isolated aortic rings of SD rats. Schwarzinicine A (**142**) as the lead compound induced a higher relaxant effect than the positive controls used (i.e., dobutamine and verapamil (**18**)).

Several series of schwarzinicine analogues were also synthesized and evaluated for SAR studies around the structure of schwarzinicine A (**142**). The results of the SAR studies are briefly summarized in this section, while selected results are also illustrated in Figure 4.14.

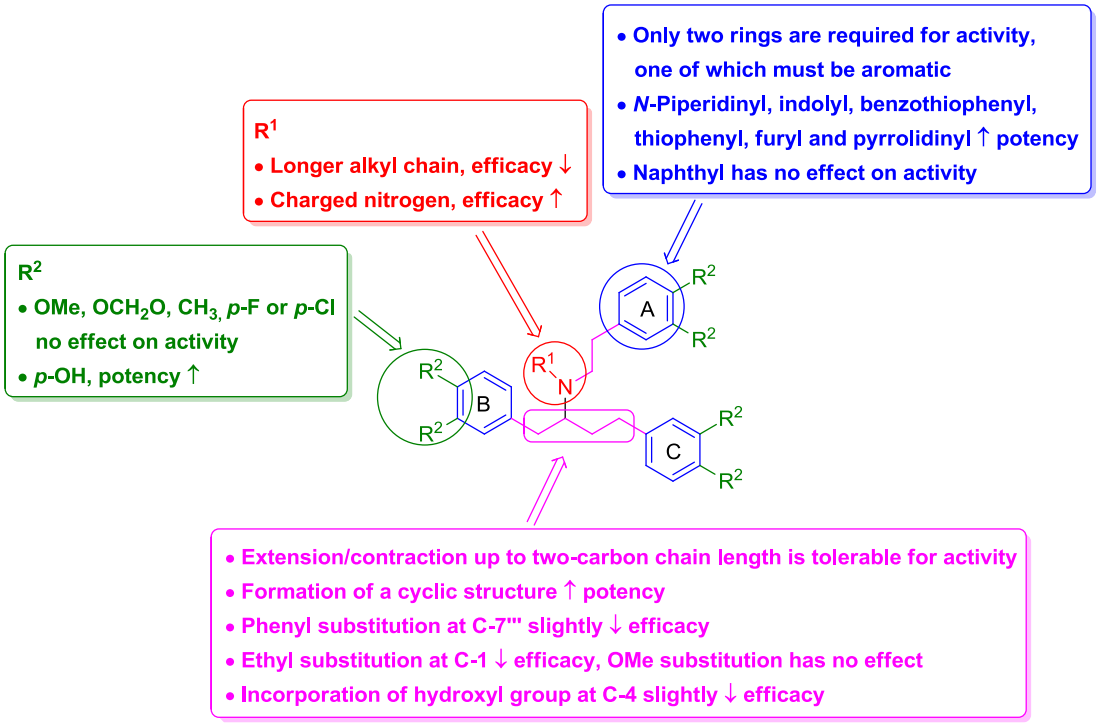


Figure 4.14. Schematic SAR model for the vasorelaxant activity of synthetic schwarzinicine analogues

We have demonstrated that the presence of aromatic methoxy/methylenedioxy groups in the schwarzinicine scaffold has no or little effect on the activity. We have also demonstrated that the minimum structural requirement for the vasorelaxant activity, with reference to the schwarzinicine A (**142**) structure, is the presence of two rings with one being an aromatic ring.

Potency enhancement effects were observed when one of the phenyl rings was replaced with:

i. a non-aromatic ring incorporating a basic nitrogen atom such as an *N*-piperidinyl in **215o** and **215y**

ii. a bicyclic heteroaromatic group such as a 3-indolyl in **215t** and a 3-benzothiophenyl group in **215u**

iii. a monocyclic heteroaromatic group such as a 2-thiophenyl in **215v** and a 2-furyl group in **215w**

iv. a non-aromatic heterocyclic group such as a 2-pyrrolidinyl in **215z** and **239**

v. a *p*-hydroxyphenyl group in **215zm**

As demonstrated by **215za**, **215zb**, **215zc**, **215zd**, **215ze**, **215zf**, **216a**, **216b** and **216c**, we observed that small variations of the alkyl chain lengths are well tolerated for vasorelaxant activity. Furthermore, **216c**, which has a 2-norbornyl group directly attached to its nitrogen atom showed enhanced potency.

The detrimental effect of the *N*-alkyl substituent introduced to the schwarzinicine scaffold increases with the size of the alkyl group as exemplified by schwarzinicine B (**143**), **231a**, **231b** and **231c**.

A certain degree of conformational restriction to one of the phenyl-bearing side arms appears to improve potency as demonstrated by **216d**, **217a** and **217b**.

We determined that the central nitrogen atom is essential for activity and must be in the ionized form when binding to the biological target as demonstrated by **232** and **233**.

Simple electron donating groups such as those in **215zj**, **215zk**, **215zl** have no influence on activity, while the potency enhancement effect due to the *p*-hydroxyl group in **215zm** is possibly due to it being a H-bond donor. Incorporation of an electron withdrawing group such as a *p*-chloro or *p*-fluoro in one of the phenyl rings is well tolerated as exemplified by **215zn**, **215zo** and **215zp**. However, incorporation of both *p*-chloro and *p*-fluorophenyl rings, as exemplified by **215zq** and **215zr**, has a detrimental effect on efficacy.

The stereochemistry of the lone chiral centre at C-2 in schwarzinicine A (**142**) appears to have no effect on vasorelaxant activity. However, the specific configurations at C-2 and C-4 of the schwarzinicine F (**147**) stereoisomers may have potency enhancement effect as exemplified by **147b**.

Further to testing the compounds in isolated aortic rings of SD rats, we also evaluated selected compounds including **142**, **215b**, **215d**, **215w**, **215zd** and **217b** for their vasorelaxant effects using aortic rings isolated from SHRs. The results obtained for these compounds are broadly consistent with the results obtained based on SD rats.

Collectively, the overall results strongly advocate further studies and development of new analogues based on the structure of schwarzinicine A (**142**). In addition to schwarzinicine A (**142**), the compounds that have emerged from the present work as promising candidates for further mechanism of action studies include **215o**, **215t**, **215u**, **215v**, **215w**, **215z**, **215zm**, **216c**, **216d**, **217a**, **217b**, **233** and diastereomer 2 of **239** (all with $EC_{50} < 1$ μM and $E_{max} \geq 100\%$).

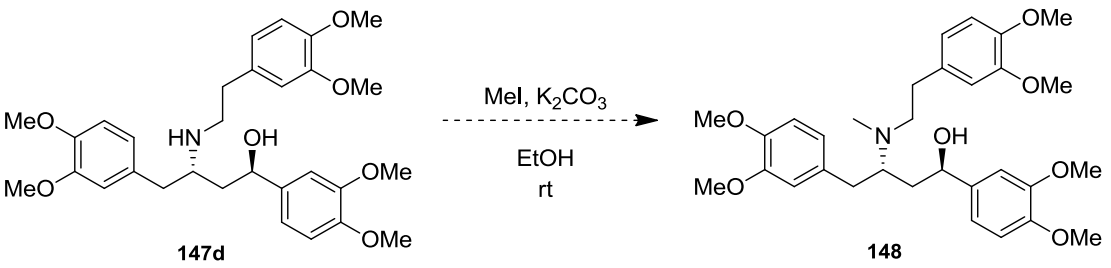
5

Future work

5.1 Future studies

5.1.1 Proposed approach to total synthesis of schwarzinicine G (148)

The stereochemistry of schwarzinicine G (**148**) could not be determined due to a lack of material and decomposition. Hence, it is our aim to synthesize **148** to resolve the stereochemical issue as we did for schwarzinicine F (**147**). We envisage that **148** adopts the same configuration as **147**. Thus, with **147d** in hand, we aim to convert **147d** to **148** via an *N*-methylation reaction with MeI (Scheme 5.1) based on the procedure reported by Yasa *et al.*.[233] Subsequently, the absolute configuration of natural **148** can be confirmed by comparing its NMR data, ECD spectrum and specific optical rotation with those of the synthetic compound.



Scheme 5.1. Proposed *N*-methylation of **147d**

5.1.2 Perpetuation of SAR studies

Based on the outcome obtained from the current SAR studies of schwarzinicine A (**142**), the ring variation design strategy yielded the most intriguing results with six analogues, namely, **215o**, **215t**, **215u**, **215v**, **215w** and **215z**, found to exhibit higher potency than the lead compound **142**. Thus, it is imperative that further exploration utilizing other ring systems for analogue design should be carried out. With consideration of commercial availability of starting materials, structures **240a–c** are representative examples of analogues that can be prepared and tested for their vasorelaxant activity based on this approach (Figure 5.1). It is noteworthy that analogues **240a** and **240b** incorporate a bicyclic heteroaromatic group (1-benzofuryl and 2-benzimidazolyl, respectively), while compound **240c** incorporates a monocyclic heteroaromatic moiety (5-oxazolyl), in place of phenyl ring B or C.

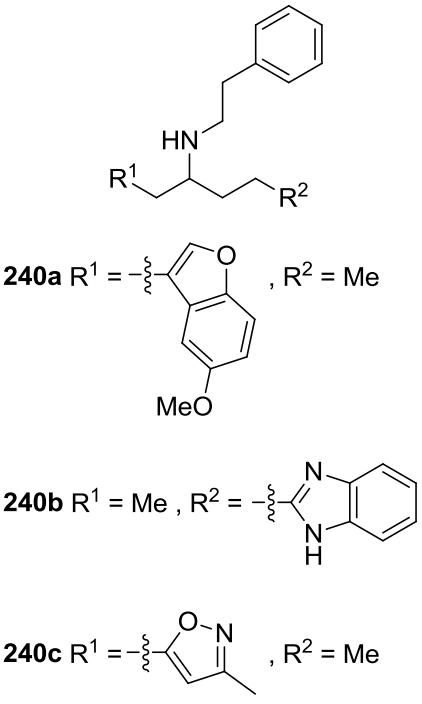
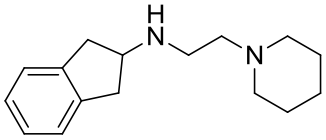
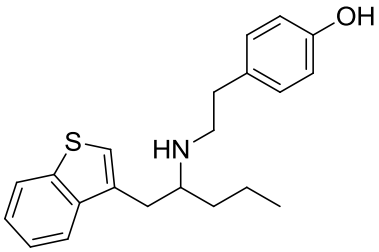
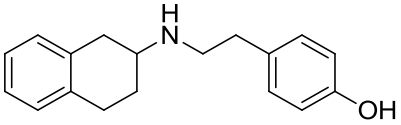
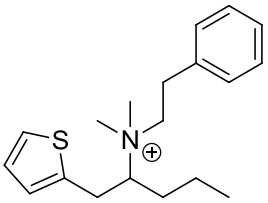


Figure 5.1. Representative examples of ring variation analogues to be made

In theory, different analogue design strategies can be employed in tandem, guided by existing analogues that showed improved activity compared to **142** as the

lead compound. For instance, various hybrid analogues that combine two chemical groups that were previously identified to have activity enhancement effect can be designed and prepared. Representative examples (**241–244**) are shown in Table 5.1.

Table 5.1. Representative analogues designed based on the hybrid approach

Compound	Strategies combined
 **241**	**215o** (ring variation) x **217a** (rigidification)
 **242**	**215u** (ring variation) x **215zm** (aromatic substituent variation)
 **243**	**215zm** (aromatic substituent variation) x **217b** (rigidification)
 **244**	**215v** (ring variation) x **232** (quaternization)

The electron donating (methoxy, 3,4-methylenedioxy, methyl, hydroxy) and electron withdrawing (chloro and fluoro) aromatic substituents explored in the present study for analogue design were rather limited. Based on the commercial availability of the relevant chemical building blocks, analogues incorporating a variety of aromatic substituents can be prepared in future in order to give a more complete

picture of the effects these substituents have on the activity of **142**. Representative examples (**245a**–**e**) suggested to be made are shown in Figure 5.2.

We also wished to test the *O*-demethylated analogue of schwarzinicine A (**142**) in this study since the *p*-hydroxyphenyl substituted compound **215zm** showed superior potency compared to **142**. However, the catechol congener of **142** (compound **219**) prepared was prone to decomposition, thus hindering its biological assessment. With this in mind, analogues devoid of the catechol moiety can be prepared instead. Compounds **246a** and **246b**, which each comprises two and three *p*-hydroxyphenyl groups, respectively (Figure 5.2), represent possible analogues to be made in the future. Compounds **246a** and **246b** may provide clues on the importance of having more H-bond donors in the molecule for activity.

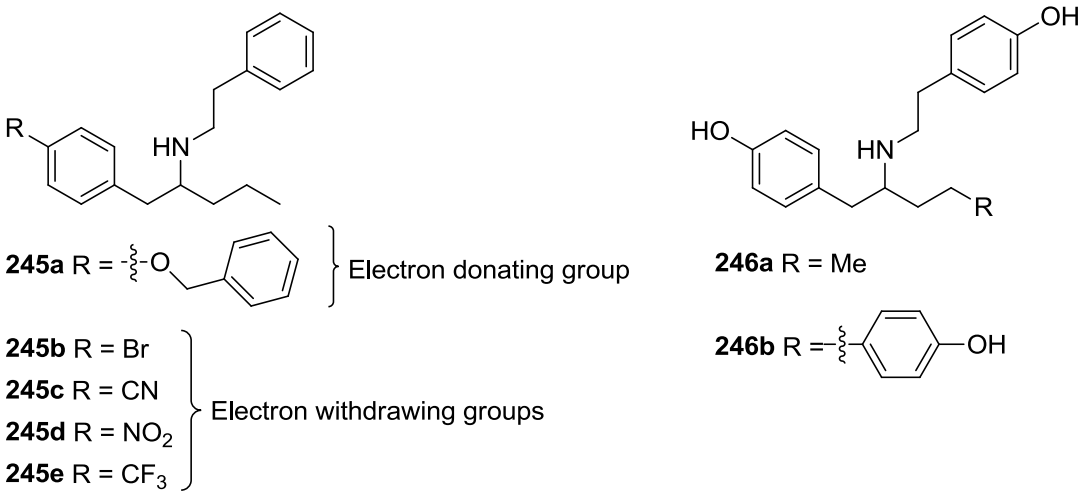


Figure 5.2. Representative examples of analogues designed based on the aromatic substituent variation strategy

5.1.3 Further studies on SHRs

So far, only a few selected schwarzinicine analogues (**215b**, **215d**, **215w**, **215zd** and **217b**) were evaluated for their vasorelaxation effect in SHRs as described in Section 4.4. There are a few more compounds that also exhibited superior vasorelaxant activities in SD rat isolated aorta but have yet to be tested in SHRs due to time constraint. These include the heterocyclic compounds **215o**, **215t**, **215u**, **215v** and **215z**, as well as the quaternary ammonium species **232** and **233**, which will be tested for their vasorelaxant effect in SHRs. In addition, the rigidified analogues **216d**, **217a** and **217b** along with *p*-hydroxyphenyl substituted compound **215zm** will also be added to the evaluation list.

6

Experimental

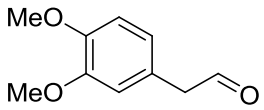
6.1 Chemistry

All reactions were carried out under inert atmosphere of N_2 unless otherwise specified. THF was purified and dried with reference to the procedure reported by Simas *et al.*[260] Acetone, CH_2Cl_2 and $ClCH_2CH_2Cl$ were dried using Sigma-Aldrich 3 Å MS (8–12 mesh) based on the procedure reported by Williams *et al.*[261] HPLC grade solvents were used when chiral HPLC analyses were carried out. All chemicals were purchased from commercial suppliers and used without further purification unless otherwise specified. Reactions were monitored by TLC and this was done on Merck TLC Silica gel 60 F_{254} aluminium backed plates with pre-coated silica. Centrifugal radial TLC was performed on a Harrison 7924T Chromatotron, on glass plates coated with Merck Silica Gel 60 PF254 containing gypsum, 1–2 mm thick. Chiral HPLC was performed on a Waters ACQUITY Arc liquid chromatograph with a Waters 2998 PDA detector. Separation was carried out using a Daicel CHIRALPAK IA analytical column (4.6 X 150 mm) packed with amylose tris-(3,5-dimethylphenylcarbamate) immobilized on 5 µm silica gel at 28 °C and fractions were collected using a Waters Fraction Collector III. ECD spectra were obtained on a JASCO J-815 CD Spectrometer. Optical rotations were determined on a JASCO P-1020 automatic

digital polarimeter. IR spectra were recorded using a PerkinElmer Spectrum RX1 FTIR and a PerkinElmer Frontier FT-IR/FIR spectrometer. HRESIMS results were obtained using a JMS-T100LP DART-TOF mass spectrometer and Agilent 6530 Q-TOF mass spectrometer. NMR spectra were recorded on a Bruker 400, 600 or 700 MHz NMR spectrometer. Chemical shifts (δ) were recorded in parts per million (ppm) and coupling constants (*J*) in Hertz (Hz) and were referenced to internal standard (tetramethylsilane (TMS): δ = 0 ppm for ^{1}H and ^{13}C NMR) and residual solvent peak ($CDCl_3$: δ = 77.2 ppm and CD_3OD: δ = 3.31 ppm for ^{13}C NMR).

6.1.1 Total syntheses of schwarzinicines A (142) and B (143)

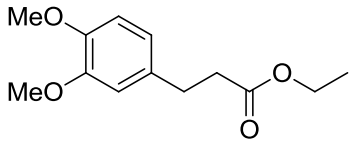
6.1.1.1 Synthesis of 3,4-dimethoxyphenylacetaldehyde (177b)



3,4-Dimethoxyphenylacetaldehyde (177b).[262] Based on the reaction conditions reported by Henrion *et al.*[192] in entry 1 (Table 2.1), to a stirring solution of (3,4-dimethoxyphenyl)acetonitrile (**177a**) (50.3 mg, 0.28 mmol, 1 equiv.) in CH_2Cl_2 (1.5 mL) in an ice bath was added DIBAL-H (1.0 M in cyclohexane) (0.3 mL, 0.3 mmol, 1.1 equiv.). The mixture was stirred in the ice bath for 30 min prior to addition of cold 1 M HCl solution (7 mL). The solution was then left to stir at room temperature for 30 min before it was extracted with CH_2Cl_2 (3 X 7 mL). The combined organic layer was washed with water (2 X 10 mL) prior to drying with $MgSO_4$ and concentrated *in vacuo*. The crude product was purified by centrifugal radial TLC using an eluent system of EtOAc–hexane (1:2) to yield aldehyde **177b** as a colourless oil (2.8 mg, 0.04 mmol, 6%). R_f = 0.51 (EtOAc–hexane, 3:2); IR (neat) ν_{max} 2938, 2839, 1677, 1591, 1514, 1464, 1426, 1268, 1138, 1024 cm^{-1}; ^{1}H NMR ($CDCl_3$, 400 MHz) δ 9.73

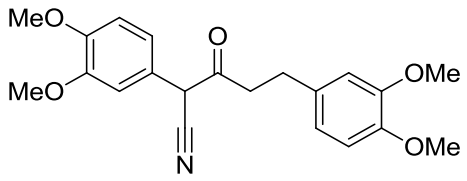
(t, *J* = 2.4 Hz, 1H), 6.87 (d, *J* = 8.2 Hz, 1H), 6.78 (dd, *J* = 8.2, 2.1 Hz, 1H), 6.71 (d, *J* = 2.1 Hz, 1H), 3.88 (s, 6H), 3.63 (d, *J* = 2.4 Hz, 2H); ^{13}C NMR ($CDCl_3$, 100 MHz) δ 199.6, 149.6, 148.4, 124.1, 121.8, 112.6, 111.6, 55.9, 55.9, 50.1; HRESIMS *m/z* 181.08605 $[M + H]^+$ (calcd for $C_{10}H_{13}O_3$, 181.08647). The data is in good agreement with the values reported in the literature.[262]

6.1.1.2 Full synthetic route to 142 and 143

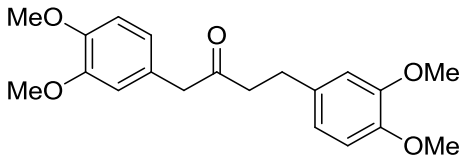


Ethyl 3-(3,4-dimethoxyphenyl)propanoate (193).[263] Based on the procedure reported by Neises *et al.*,[206] to a stirred solution of (3,4-dimethoxyphenyl)propionic acid (**192**) (1.01 g, 4.80 mmol, 1 equiv.) in CH_2Cl_2 (10 mL) was added EtOH (1.1 mL, 18.8 mmol, 3.9 equiv.) and DMAP (61.5 mg, 0.50 mmol, 0.1 equiv.) at room temperature. To the ice-cooled reaction mixture was added EDC (918.4 mg, 4.79 mmol, 1 equiv.) and was allowed to stir at room temperature for 2.5 h. The resulting mixture was diluted with CH_2Cl_2 (10 mL) and washed with 0.5 M HCl solution (2 X 8 mL), followed by saturated $KHCO_3$ solution (2 X 8 mL). The combined organic layer was washed with brine (10 mL), dried with $MgSO_4$ and subsequently concentrated *in vacuo*. The crude product was purified by centrifugal radial TLC using an eluent system of EtOAc–hexane (1:1) to yield ester **193** as a light yellow oil (937.2 mg, 3.93 mmol, 82%). R_f = 0.70 (EtOAc–hexane, 3:1); IR (neat) ν_{max} 2937, 2836, 1729, 1591, 1514, 1452, 1372, 1258, 1235, 1183, 1153, 1137, 1026 cm^{-1}; ^{1}H NMR ($CDCl_3$, 700 MHz) δ 6.79 (d, *J* = 8.1 Hz, 1H), 6.76 – 6.72 (m, 2H), 4.13 (q, *J* = 7.1 Hz, 2H), 3.87 (s, 3H), 3.85 (s, 3H), 2.90 (t, *J* = 7.8 Hz, 2H), 2.60 (t, *J* = 8.0 Hz, 2H), 1.24 (t, *J* = 7.2 Hz, 3H); ^{13}C NMR ($CDCl_3$, 175 MHz) δ 173.0, 148.8, 147.5, 133.2, 120.1, 111.6,

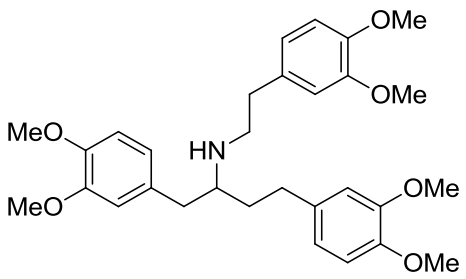
111.3, 60.4, 55.9, 55.8, 36.2, 30.6, 14.2; HRESIMS *m/z* 239.1277 $[M + H]^+$ (calcd for $C_{13}H_{19}O_4$, 239.1283). The spectroscopic data are in good agreement with those reported in the literature.[263]



1-Cyano-1,4-di-(3',4'-dimethoxyphenyl)-butanone-2 (194).[207] To an ice-cooled solution of (3,4-dimethoxyphenyl)acetonitrile (**177a**) (155.0 mg, 0.87 mmol, 2 equiv.) in THF (10 mL) was slowly added *n*-BuLi (1.6 M, 0.55 mL, 0.88 mmol, 2 equiv.). After stirring for 15 min in the ice bath, ester **193** (102.5 mg, 0.43 mmol, 1 equiv.) in THF (0.85 mL) was added into the solution. After stirring for 5 min, water (10 mL) and brine (4 mL) were subsequently added into the reaction mixture. The mixture was extracted with $CHCl_3$ (5 X 10 mL). The combined organic layer was dried with Na_2SO_4 and concentrated *in vacuo*. The crude product was purified by centrifugal radial TLC using an eluent system of Et_2O–hexane (7:1) to yield ketonitrile **194** as a brown oil (37.8 mg, 0.1 mmol, 23%). R_f = 0.12 (Et_2O–hexane, 8:1); IR (neat) ν_{max} 3005, 2921, 2848, 2249, 2205, 1726, 1593, 1513, 1462, 1419, 1259, 1237, 1141, 1023 cm^{-1}; ^1H NMR ($CDCl_3$, 700 MHz) δ 6.87 – 6.82 (m, 2H), 6.74 – 6.70 (m, 2H), 6.60 – 6.56 (m, 2H), 4.55 (s, 1H), 3.89 (s, 3H), 3.85 (s, 3H), 3.84 (s, 3H), 3.82 (s, 3H), 2.94 – 2.78 (m, 4H); ^{13}C NMR ($CDCl_3$, 175 MHz) δ 198.3, 149.8, 149.7, 148.8, 147.5, 132.3, 121.4, 120.6, 120.1, 116.3, 111.6, 111.6, 111.1, 110.4, 56.0, 56.0, 55.9, 55.8, 50.7, 41.2, 29.3; HRESIMS *m/z* 387.1904 $[M + NH_4]^+$ (calcd for $C_{21}H_{27}N_2O_5$, 387.1920).



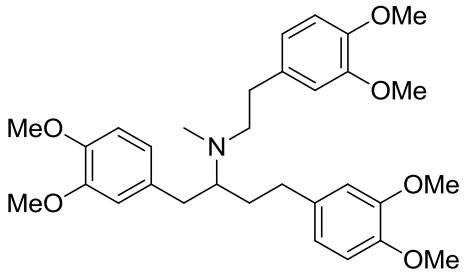
1,4-Di-(3',4'-dimethoxyphenyl)-butanone-2 (175).[158] Adapted from the procedure reported by Carroll *et al.*,[207] to a stirred solution of ketonitrile **194** (68.0 mg, 0.18 mmol, 1 equiv.) in AcOH (6 mL) was added concentrated HCl (6 mL) at room temperature. The mixture was stirred and heated at 60 °C for 2 h. After cooling to room temperature, water (22 mL) was added into the solution, which was then refluxed for 1 h. The solution was subsequently extracted with $CHCl_3$ (3 X 15 mL). The combined organic layer was washed with saturated $KHCO_3$ solution (3 X 10 mL), water (2 X 10 mL) and subsequently brine (10 mL). It was then dried with Na_2SO_4 and concentrated *in vacuo*. The crude product was purified by centrifugal radial TLC using an eluent system of CH_2Cl_2–hexane (2:1) to yield ketone **175** as a yellow oil (36.8 mg, 0.11 mmol, 61%). R_f = 0.61 (2% MeOH–CH_2Cl_2); IR (neat) ν_{max} 2999, 2935, 2835, 1709, 1591, 1511, 1455, 1256, 1234, 1141, 1023 cm^{-1}; ^1H NMR ($CDCl_3$, 400 MHz) δ 6.80 (d, *J* = 8.1 Hz, 1H), 6.75 (d, *J* = 8.7 Hz, 1H), 6.70 (dd, *J* = 8.1, 2.0 Hz, 1H), 6.67 (d, *J* = 2.0 Hz, 1H), 6.65 (d, *J* = 2.0 Hz, 2H), 3.87 (s, 3H), 3.85 (s, 6H), 3.84 (s, 3H), 3.60 (s, 2H), 2.87 – 2.77 (m, 2H), 2.78 – 2.73 (m, 2H); ^{13}C NMR ($CDCl_3$, 100 MHz) δ 208.0, 149.0, 148.8, 148.1, 147.3, 133.5, 126.5, 121.6, 120.1, 112.3, 111.7, 111.3, 111.2, 55.9, 55.9, 55.8, 55.8, 50.0, 43.5, 29.4; HRESIMS *m/z* 345.1698 $[M + H]^+$ (calcd for $C_{20}H_{25}O_5$, 345.1702). The spectroscopic data are in good agreement with those obtained for the natural product.[158]



Schwarzinicine A (142).[170] To a stirring solution of ketone **175** (100.6 mg, 0.29 mmol, 1 equiv.) in $ClCH_2CH_2Cl$ (4 mL) was added DMPEA (**176**) (109.3 mg, 0.60 mmol, 2.1 equiv.), $NaBH(OAc)_3$ (253.4 mg, 1.20 mmol, 4.1 equiv.) and AcOH (0.04 mL, 0.70 mmol, 2.4 equiv.). The solution was stirred at room temperature for 30 h before addition of 1 M NaOH solution (4 mL). The mixture was then extracted with EtOAc (3 X 8 mL). The combined organic layer was washed with brine (4 mL) and subsequently dried with Na_2SO_4 before concentrated *in vacuo*. The crude product was purified by centrifugal radial TLC using an eluent system of EtOAc–hexane (2:1) to yield **142** as a yellow oil (56.7 mg, 0.11 mmol, 38%). R_f = 0.19 (EtOAc–hexane, 6:1); IR (neat) ν_{max} 3313, 2998, 2933, 2834, 1590, 1513, 1462, 1259, 1234, 1139, 1026 cm^{-1}; ^1H NMR ($CDCl_3$, 600 MHz) δ 6.78 (d, *J* = 8.6 Hz, 1H), 6.73 (d, *J* = 8.1 Hz, 1H), 6.72 (d, *J* = 8.0 Hz, 1H), 6.67 (d, *J* = 1.9 Hz, 1H), 6.66 (dd, *J* = 6.7, 2.0 Hz, 2H), 6.63 (d, *J* = 2.1 Hz, 1H), 6.62 – 6.61 (m, 1H), 6.61 – 6.59 (m, 1H), 3.86 (s, 3H), 3.85 (s, 3H), 3.85 (s, 3H), 3.84 (s, 3H), 3.83 (s, 3H), 3.82 (s, 3H), 2.92 – 2.86 (m, 1H), 2.79 – 2.69 (m, 3H), 2.70 – 2.64 (m, 2H), 2.64 – 2.57 (m, 3H), 1.81 – 1.74 (m, 1H), 1.74 – 1.66 (m, 1H); ^{13}C NMR ($CDCl_3$, 150 MHz) δ 148.9, 148.9, 148.8, 147.5, 147.5, 147.2, 134.9, 132.4, 131.7, 121.1, 120.5, 120.1, 112.3, 111.9, 111.7, 111.3, 111.2, 111.1, 58.7, 56.0, 55.9, 55.8, 55.8, 55.8, 55.8, 48.5, 40.3, 36.0, 35.6, 31.6; HRESIMS *m/z* 510.2860 $[M + H]^+$ (calcd for $C_{30}H_{40}N_1O_6$, 510.2856); The spectroscopic data are in good agreement with those obtained for the natural product.[170]

Chiral-phase HPLC analysis of 142

142 (1.5 mg) was dissolved in EtOH (1 mL) prior to injection (10.0 µL). The eluting solvent of hexane–EtOH–Et_2NH (80:20:0.1) was used and the flow rate of the eluting solvent was set at 1.0 mL/min to resolve **142** (t_R = 8.21 and 8.92 min).



Schwarzinicine B (143).[170] To a stirring solution of **142** (19.9 mg, 0.04 mmol, 1 equiv.) in MeOH (4 mL) was added 37% aq. formaldehyde (**174**) (0.1 mL, 1.34 mmol, 34 equiv.) and $NaBH_3CN$ (37.0 mg, 0.59 mmol, 15 equiv.). The mixture was stirred at room temperature for 1 h before addition of AcOH (0.4 mL, 6.99 mmol, 175 equiv.). The solution was stirred further at room temperature for 23 h before addition of 1 M NaOH solution (8 mL). The mixture was then extracted with CH_2Cl_2 (3 X 10 mL). The organic phase was washed with brine (8 mL) and dried with Na_2SO_4 before concentrated *in vacuo*. The crude product was purified by centrifugal radial TLC using an eluent system of Et_2O–hexane (4:1) to yield **143** as a yellow oil (11.1 mg, 0.02 mmol, 50%). R_f = 0.13 (Et_2O–hexane, 9:1); IR (neat) ν_{max} 2997, 2935, 2835, 1590, 1514, 1462, 1261, 1235, 1141, 1029 cm^{-1}; ^1H NMR ($CDCl_3$, 400 MHz) δ 6.81 – 6.78 (m, 1H), 6.76 (d, *J* = 6.8 Hz, 1H), 6.74 (d, *J* = 7.9 Hz, 2H), 6.73 (d, *J* = 8.7 Hz, 1H), 6.65 (dd, *J* = 8.1, 2.0 Hz, 1H), 6.62 (d, *J* = 2.0 Hz, 1H), 6.57 (dd, *J* = 6.2, 1.9 Hz, 2H), 3.88 (s, 3H), 3.85 (s, 6H), 3.84 (s, 3H), 3.83 (s, 3H), 3.80 (s, 3H), 2.89 (dd, *J* = 13.0, 4.0 Hz, 1H), 2.84 – 2.59 (m, 6H), 2.62 – 2.53 (m, 1H), 2.39 (s, 3H), 2.44 – 2.29 (m, 1H), 1.75 – 1.63 (m, 1H), 1.63 – 1.52 (m, 1H); ^{13}C NMR ($CDCl_3$, 100 MHz) δ

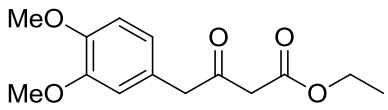
148.8, 148.7, 148.6, 147.3, 147.1, 146.9, 135.3, 133.4, 133.4, 121.1, 120.6, 120.1, 112.3, 112.1, 111.7, 111.1, 111.1, 111.0, 64.5, 55.9, 55.9, 55.8, 55.8, 55.7, 36.9, 34.9, 34.6, 32.5, 32.5; HRESIMS *m/z* 524.3005 $[M + H]^+$ (calcd for $C_{31}H_{42}N_1O_6$, 524.3012); The spectroscopic data are in good agreement with those obtained for the natural product.[170]

Chiral-phase HPLC analysis of 143

143 (1.2 mg) was dissolved in EtOH (1 mL) prior to injection (3.0 µL). The eluting solvent of hexane–EtOH–Et_2NH (90:10:0.1) was used and the flow rate of the eluting solvent was set at 1.0 mL/min to resolve **143** (t_R = 6.90 and 7.35 min).

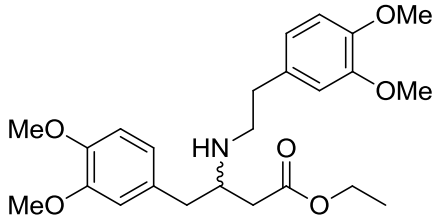
6.1.2 Total synthesis of schwarzinicine F (147)

6.1.2.1 First attempt



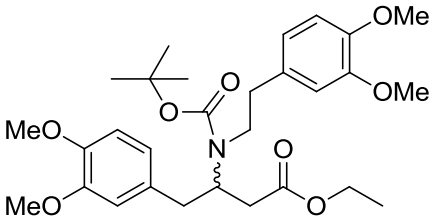
Ethyl 4-(3,4-dimethoxyphenyl)-3-oxobutanoate (197).[264] Based on the procedure reported by Allan *et al.*[209]and Brooks *et al.*,[210] to a mixture of ethyl potassium malonate (**198**) (567.2 mg, 3.33 mmol, 1.3 equiv.) and $MgCl_2$ (251.8 mg, 2.64 mmol, 1 equiv.) was added THF (6 mL). The suspension was refluxed for 3 h. After stirring for 2 h, to a stirring solution of 3,4-dimethoxyphenylacetic acid (**184**) (506.9 mg, 2.58 mmol, 1 equiv.) in THF (5 mL) was added CDI (505.7 mg, 3.12 mmol, 1.2 equiv.). The solution was stirred at room temperature for 45 min before its addition into the magnesium malonate suspension. The resulting mixture was stirred at room temperature for 18 h prior to addition of 1.0 M HCl solution (10 mL). It was then extracted with EtOAc (3 X 20 mL). The combined organic layer was washed with water (40 mL) followed by saturated aq. $KHCO_3$ solution (40 mL) and subsequently

brine (40 mL). It was dried using $MgSO_4$ and concentrated *in vacuo*. The crude product was purified by centrifugal radial TLC using an eluent system of Et_2O–hexane (1:1) to yield **197** as a yellow oil (598.2 mg, 2.25 mmol, 87%). R_f = 0.18 (Et_2O–hexane, 1:1); IR (neat) ν_{max} 2938, 2910, 2838, 1740, 1712, 1514, 1463, 1419, 1315, 1258, 1236, 1141, 1024 cm^{-1}; ^1H NMR ($CDCl_3$, 700 MHz) δ 6.84 (d, *J* = 8.2 Hz, 1H), 6.76 (dd, *J* = 8.1, 2.0 Hz, 1H), 6.72 (d, *J* = 2.1 Hz, 1H), 4.18 (q, *J* = 7.1 Hz, 2H), 3.87 (s, 3H), 3.87 (s, 3H), 3.76 (s, 2H), 3.45 (s, 2H), 1.26 (t, *J* = 7.2 Hz, 3H); ^{13}C NMR ($CDCl_3$, 175 MHz) δ 200.9, 167.2, 149.2, 148.4, 125.6, 121.8, 112.5, 111.4, 61.4, 55.9, 55.9, 49.7, 48.1, 14.1; HRESIMS *m/z* 267.1220 $[M + H]^+$ (calcd for $C_{14}H_{19}O_5$, 267.1233). The spectroscopic data are in good agreement with those reported in the literature.[264]



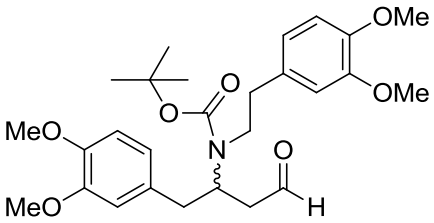
Ethyl 3-((3,4-dimethoxyphenethyl)amino)-4-(3,4-dimethoxyphenyl)butanoate (195). Following the method to prepare schwarzinicine A (**142**), DMPEA (**176**) (451.2 mg, 2.49 mmol, 1.1 equiv.), $NaBH(OAc)_3$ (781.2 mg, 3.69 mmol, 1.6 equiv.) and AcOH (0.13 mL, 2.27 mmol, 1 equiv.) were used to react with β-ketoester **197** (598.2 mg, 2.25 mmol, 1 equiv.) in $ClCH_2CH_2Cl$ (4 mL) for 27 h to afford amine **195** as a yellow oil (441.7 mg, 1.02 mmol, 45%). Eluent system of Et_2O–hexane (1:6) was used in centrifugal radial TLC purification. R_f = 0.15 (Et_2O–hexane, 9:1); IR (neat) ν_{max} 3317, 2935, 2835, 1726, 1590, 1513, 1461, 1259, 1234, 1139, 1025 cm^{-1}; ^1H NMR ($CDCl_3$, 700 MHz) δ 6.74 (d, *J* = 3.1 Hz, 1H), 6.72 (d, *J* = 3.1 Hz, 1H), 6.67 (d, *J* = 2.1 Hz, 1H), 6.66 (d, *J* = 2.0 Hz, 1H), 6.63 (dd, *J* = 16.6, 2.0 Hz, 1H), 6.63 (d, *J* =

2.0 Hz, 1H), 4.11 (q, *J* = 7.1 Hz, 2H), 3.86 (s, 3H), 3.86 (s, 3H), 3.85 (s, 3H), 3.84 (s, 3H), 3.19 (p, *J* = 6.6 Hz, 1H), 2.90 (ddd, *J* = 11.2, 7.6, 6.1 Hz, 1H), 2.81 (dt, *J* = 11.1, 7.3 Hz, 1H), 2.73 – 2.64 (m, 4H), 2.40 (ddd, *J* = 54.4, 15.4, 6.3 Hz, 2H), 1.24 (t, *J* = 7.1 Hz, 3H); ^{13}C NMR ($CDCl_3$, 175 MHz) δ 172.4, 148.8, 147.5, 147.4, 132.2, 130.8, 121.2, 120.4, 112.3, 111.7, 111.1, 111.0, 60.4, 56.4, 55.8, 55.8, 55.8, 55.8, 48.6, 40.3, 38.9, 35.9, 14.2; HRESIMS *m/z* 432.2368 $[M + H]^+$ (calcd for $C_{24}H_{34}N_1O_6$, 432.2386).

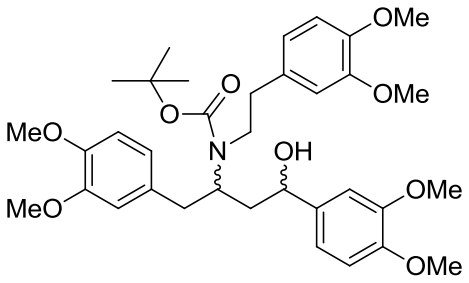


Ethyl 3-((*tert*-butoxycarbonyl)(3,4-dimethoxyphenethyl)amine)-4-(3,4-dimethoxyphenyl)butanoate (199). Based on the procedure reported by Davis *et al.*,[211] to a stirring solution of **195** (94.7 mg, 0.22 mmol, 1 equiv.) in THF (8 mL) was added di-*tert*-butyl dicarbonate (0.18 mL, 0.78 mmol, 3.5 equiv.), Et_3N (0.18 mL, 1.29 mmol, 5.9 equiv.) and DMAP (2.3 mg, 0.02 mmol, 0.1 equiv.). The solution was stirred at room temperature for 6 h prior to addition of water (6 mL). It was extracted with EtOAc (2 X 15 mL). The combined organic layer was washed with brine (6 mL), dried with Na_2SO_4 before concentrated *in vacuo*. The crude product was purified by centrifugal radial TLC using an eluent system of Et_2O–hexane (1:8) to yield **199** as a yellow oil (80.7 mg, 0.15 mmol, 68%). R_f = 0.11 (Et_2O–hexane, 1:1); IR (neat) ν_{max} 2973, 2934, 2832, 1731, 1686, 1514, 1465, 1453, 1418, 1366, 1259, 1235, 1154, 1027 cm^{-1}; ^{1}H NMR ($CDCl_3$, 400 MHz) δ 6.82 – 6.58 (m, 6H), 4.11 (q, *J* = 7.2 Hz, 2H), 3.87 (s, 3H), 3.86 (s, 3H), 3.85 (s, 3H), 3.84 (s, 3H), 3.23 – 2.31 (m, 9H), 1.48 (s, 9H), 1.25 (q, *J* = 6.8 Hz, 3H); ^{13}C NMR ($CDCl_3$, 100 MHz) δ 172.0, 155.1, 155.1, 154.8, 148.9, 147.7, 147.6, 147.5, 147.4, 132.0, 131.3, 121.3, 120.7, 120.6, 112.4, 112.3,

112.0, 111.9, 111.3, 111.2, 111.1, 79.4, 77.4, 77.4, 76.7, 60.7, 60.5, 55.9, 55.9, 55.9, 55.8, 39.2, 39.0, 38.3, 38.1, 35.5, 28.5, 14.2; HRESIMS *m/z* 532.2839 $[M + H]^+$ (calcd for $C_{29}H_{42}N_1O_6$, 532.2910).

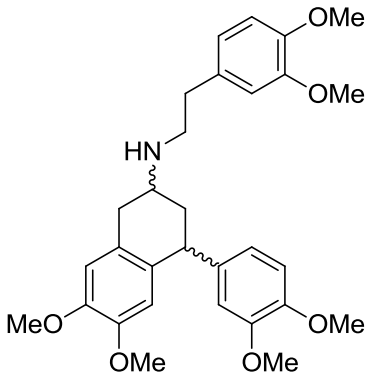


***Tert*-butyl 3,4-dimethoxyphenethyl(1-(3,4-dimethoxyphen)-4-oxobutan-2-yl)carbamate (200).** Based on the procedure reported by Dineen *et al.*,[212] to a stirring solution of **199** (117.9 mg, 0.22 mmol, 1 equiv.) in CH_2Cl_2 (4 mL) at -78 °C was added DIBAL-H (0.3 mL, 0.3 mmol, 1.4 equiv.). The mixture was stirred at -78 °C for 20 min prior to quenching with MeOH (4 mL) followed by addition of 1 M HCl solution (4 mL). It was then extracted with EtOAc (3 X 12 mL). The combined organic layer was dried with Na_2SO_4 before concentrated *in vacuo*. The crude product was purified by centrifugal radial TLC using an eluent system of Et_2O–hexane (1:2) to yield **200** as a yellow oil (92.0 mg, 0.19 mmol, 86%). R_f = 0.05 (Et_2O–hexane, 1:1); IR (neat) ν_{max} 3005, 2973, 2937, 2834, 1721, 1684, 1514, 1465, 1418, 1365, 1260, 1235, 1154, 1027 cm^{-1}; ^1H NMR ($CDCl_3$, 400 MHz) δ 9.64 (d, *J* = 10.4 Hz, 1H), 6.83 – 6.59 (m, 6H), 4.47 – 4.18 (m, 1H), 3.87 (s, 3H), 3.86 (s, 3H), 3.85 (s, 6H), 3.30 – 2.43 (m, 8H), 1.47 (s, 9H); ^{13}C NMR ($CDCl_3$, 100 MHz) δ 200.9, 155.1, 148.9, 147.7, 147.6, 131.8, 130.8, 121.3, 120.6, 112.2, 112.0, 111.9, 111.3, 111.1, 79.8, 55.9, 55.9, 55.3, 47.3, 38.6, 35.6, 34.6, 28.5; HRESIMS *m/z* 488.2646 $[M + H]^+$ (calcd for $C_{27}H_{38}N_1O_7$, 488.2648).



***Tert*-butyl (1,4-bis(3,4-dimethoxyphenyl)-4-hydroxybutan-2-yl)(3,4-dimethoxyphenethyl)carbamate (202).** To a stirring Mg turnings (71.7 mg, 2.95 mmol, 2.5 equiv.) in THF (2 mL) was added a small portion (about 10%) of 4-bromoveratrole (**201**) (0.17 mL, 1.18 mmol, 1 equiv.) in THF (3 mL). The remaining portion of the bromide was added gradually into the stirring reaction mixture over the course of 1 h as the mixture was heated to reflux. It was refluxed further for 1 h before left to cool to room temperature. The resulting mixture was added to **200** (143.2 mg, 0.29 mmol, 0.2 equiv.) in THF (4 mL) in an ice bath. It was warmed and stirred at room temperature for 1.5 h prior to addition of saturated aq. NH_4Cl solution (5 mL). The mixture was extracted with EtOAc (3 X 10 mL). The combined organic layer was washed with brine (5 mL) and dried with Na_2SO_4 before concentrated *in vacuo*. The crude product was purified by centrifugal radial TLC using an eluent system of $CHCl_3$–hexane (1:1) to yield diastereomer pair 1 of **202** as a yellow oil (63.0 mg, 0.10 mmol, 34%) and diastereomer pair 2 of **202** as a yellow oil (62.9 mg, 0.10 mmol, 34%). Diastereomer pair 1: R_f = 0.14 ($CHCl_3$–hexane, 6:1); IR (neat) ν_{max} 3510, 3001, 2935, 2836, 1683, 1514, 1464, 1417, 1365, 1260, 1235, 1155, 1027 cm^{-1}; ^1H NMR ($CDCl_3$, 600 MHz) δ 6.96 – 6.60 (m, 9H), 4.74 – 4.49 (m, 1H), 3.88 (s, 3H), 3.86 (s, 9H), 3.86 (s, 3H), 3.85 (s, 3H), 3.29 – 3.09 (m, 2H), 3.00 – 2.88 (m, 1H), 2.81 (dd, *J* = 14.6, 6.9 Hz, 1H), 2.76 – 2.63 (m, 3H), 1.99 – 1.75 (m, 2H), 1.53 (s, 9H); ^{13}C NMR ($CDCl_3$, 150 MHz) δ 155.5, 149.1, 149.0, 148.6, 148.2, 147.8, 147.6, 136.3, 132.1, 131.8, 120.9, 120.6, 117.7, 112.0, 111.7, 111.5, 111.2, 110.9, 108.8, 80.5, 70.0, 56.0,

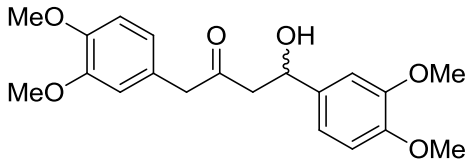
55.9, 55.9, 55.9, 43.1, 39.0, 36.2, 36.2, 28.5; HRESIMS (LC/MS) (t_R = 6.92 min for a 15 min run) *m/z* 648.3140 $[M + Na]^+$ (calcd for $C_{35}H_{47}N_1Na_1O_9$, 648.3140). Diastereomer pair 2: R_f = 0.1 ($CHCl_3$–hexane, 6:1); IR (neat) ν_{max} 3460, 3003, 2936, 2836, 1683, 1513, 1464, 1417, 1259, 1233, 1154, 1139, 1026 cm^{-1}; ^1H NMR ($CDCl_3$, 600 MHz) δ 6.86 – 6.63 (m, 9H), 4.66 – 4.48 (m, 1H), 3.87 (s, 6H), 3.87 (s, 3H), 3.85 (s, 3H), 3.84 (s, 6H), 3.23 – 2.56 (m, 7H), 2.16 – 1.94 (m, 2H), 1.48 (s, 9H); ^{13}C NMR ($CDCl_3$, 150 MHz) δ 156.3, 149.0, 148.8, 148.4, 147.6, 147.5, 136.9, 132.2, 131.3, 121.2, 120.7, 118.7, 112.2, 112.1, 111.4, 111.1, 110.9, 109.1, 79.6, 72.5, 56.0, 55.9, 55.9, 55.8, 55.8, 41.6, 39.0, 36.1, 36.1, 28.5; HRESIMS (LC/MS) (t_R = 6.37 min for a 15 min run) *m/z* 648.3141 $[M + Na]^+$ (calcd for $C_{35}H_{47}N_1$ Na_1O_9, 648.3141).



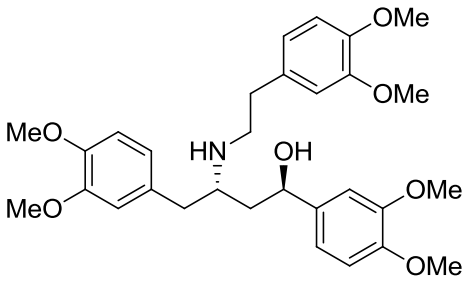
***N*-(3,4-Dimethoxyphenethyl)-4-(3,4-dimethoxyphenyl)-6,7-dimethoxy-1,2,3,4-tetrahydronaphthalen-2-amine (203).** Based on the procedure reported by Alonso *et al.*,[213] to a solution of diastereomer pair 1 of **202** (36.5 mg, 0.06 mmol, 1 equiv.) in an ice bath in CH_2Cl_2 (4 mL) was added TFA (0.02 mL, 0.26 mmol, 4.3 equiv.). The solution was stirred at room temperature for 40 min at room temperature prior to addition of 3M NaOH solution (4 mL). The mixture was extracted with EtOAc (3 X 10 mL). The combined organic layer was dried with Na_2SO_4 and concentrated *in vacuo*. The crude product was purified by centrifugal radial TLC using an eluent system of $CHCl_3$ to yield diastereomer pair 1 of **203** as a yellow oil (1.9 mg, 0.004

mmol, 7%) and diastereomer pair 2 of **203** as a yellow oil (1.3 mg, 0.003 mmol, 5%). Diastereomer pair 1: R_f = 0.46 (5% MeOH–$CHCl_3$); IR (neat) ν_{max} 3383, 3003, 2939, 2837, 1733, 1598, 1515, 1462, 1255, 1147, 1028 cm^{-1}; ^1H NMR ($CDCl_3$, 700 MHz) δ 6.77 (d, *J* = 7.9 Hz, 1H), 6.73 – 6.69 (m, 2H), 6.66 – 6.63 (m, 2H), 6.58 (d, *J* = 2.1 Hz, 1H), 6.50 (s, 1H), 6.21 (s, 1H), 3.96 (dd, *J* = 12.4, 5.7 Hz, 1H), 3.86 (s, 3H), 3.84 (s, 3H), 3.76 (s, 3H), 3.76 (s, 3H), 3.73 (s, 3H), 3.57 (s, 3H), 3.45 – 3.40 (m, 1H), 3.40 – 3.34 (m, 1H), 3.28 – 3.17 (m, 5H), 2.76 (d, *J* = 12.1 Hz, 1H), 2.24 (q, *J* = 12.3 Hz, 1H); ^{13}C NMR ($CDCl_3$, 175 MHz) δ 149.1, 148.9, 148.1, 147.9, 147.8, 147.8, 136.8, 130.1, 128.8, 124.2, 120.7, 120.6, 112.0, 111.9, 111.7, 111.4, 111.3, 111.3, 56.0, 55.9, 55.9, 55.8, 55.8, 55.7, 55.2, 46.8, 45.1, 36.5, 32.7, 32.4; HRESIMS (LC/MS) (t_R = 3.93 min for a 30 min run) *m/z* 508.2707 $[M + H]^+$ (calcd for $C_{30}H_{38}N_1O_6$, 508.2707). Diastereomer pair 2: R_f = 0.36 (5% MeOH–$CHCl_3$); IR (neat) ν_{max} 3393, 3001, 2940, 2836, 1731, 1601, 1515, 1462, 1254, 1143, 1028 cm^{-1}; ^1H NMR ($CDCl_3$, 700 MHz) δ 6.75 (d, *J* = 8.7 Hz, 1H), 6.72 – 6.70 (m, 2H), 6.70 (d, *J* = 8.3 Hz, 1H), 6.54 (d, *J* = 1.5 Hz, 1H), 6.47 (s, 1H), 6.42 (s, 1H), 6.33 (dd, *J* = 8.5, 2.1 Hz, 1H), 4.31 – 4.26 (m, 1H), 3.84 (s, 3H), 3.82 (s, 3H), 3.81 (s, 3H), 3.79 (s, 3H), 3.71 (s, 6H), 3.49 – 3.43 (m, 1H), 3.38 – 3.30 (m, 2H), 3.21 (t, *J* = 8.5 Hz, 2H), 3.18 – 3.10 (m, 1H), 3.09 – 3.01 (m, 1H), 2.53 (td, *J* = 12.0, 5.7 Hz, 1H), 2.45 (d, *J* = 12.1 Hz, 1H); ^{13}C NMR ($CDCl_3$, 175 MHz) δ 149.2, 149.0, 148.2, 148.2, 148.1, 147.7, 137.7, 128.8, 127.9, 124.8, 120.7, 120.5, 112.3, 111.8, 111.5, 111.4, 111.0, 110.9, 56.0, 55.9, 55.9, 55.9, 55.9, 55.7, 51.6, 47.1, 42.7, 34.2, 32.7, 32.2; HRESIMS (LC/MS) (t_R = 3.48 min for a 30 min run) *m/z* 508.2717 $[M + H]^+$ (calcd for $C_{30}H_{38}N_1O_6$, 508.2717).

6.1.2.2 Second approach



1,4-Bis(3,4-dimethoxyphenyl)-4-hydroxybutan-2-one (205). Based on the procedure reported by Bertolini *et al.*,[214] to a stirring solution of 3,4-dimethoxyphenylacetone (**206**) (390.4 mg, 2.01 mmol, 1.6 equiv.) in THF (10 mL) at -78 °C was added LDA (1.5 M in cyclohexane) (1.6 mL, 2.4 mmol, 1.9 equiv.). After stirring for 15 min, 3,4-dimethoxybenzaldehyde (**207**) (207.8 mg, 1.25 mmol, 1 equiv.) in THF (5 mL) was added into the mixture. The solution was stirred at -78 °C for 4.5 h prior to addition of water (10 mL). The mixture was extracted with EtOAc (3 X 15 mL). The combined organic layer was washed with brine (10 mL), dried with Na_2SO_4 and concentrated *in vacuo*. The crude product was purified by centrifugal radial TLC using an eluent system of Et_2O–hexane (2:1) to yield **205** as a yellow oil (208.3 mg, 0.58 mmol, 46%). R_f = 0.08 (Et_2O–hexane, 6:1); IR (neat) ν_{max} 3502, 3003, 2936, 2836, 1708, 1592, 1512, 1462, 1419, 1258, 1233, 1138, 1023 cm^{-1}; ^1H NMR ($CDCl_3$, 400 MHz) δ 6.88 (d, *J* = 1.2 Hz, 1H), 6.84 – 6.79 (m, 3H), 6.71 (dd, *J* = 8.1, 2.0 Hz, 1H), 6.66 (d, *J* = 2.0 Hz, 1H), 5.07 (dd, *J* = 8.9, 3.5 Hz, 1H), 3.87 (s, 6H), 3.86 (s, 3H), 3.85 (s, 3H), 3.65 (s, 2H), 2.95 – 2.78 (m, 2H); ^{13}C NMR ($CDCl_3$, 100 MHz) δ 209.2, 149.2, 149.1, 148.5, 148.3, 135.5, 125.9, 121.8, 117.9, 112.4, 111.4, 111.0, 108.9, 70.0, 56.0, 56.0, 56.0, 55.9, 50.5, 50.3; HRESIMS *m/z* 378.18984 $[M + NH_4]^+$ (calcd for $C_{20}H_{28}N_1O_6$, 378.19166).



Schwarzinicine F (147d).[170] To a stirring solution of ketone **205** (104.2 mg, 0.29 mmol, 1 equiv.) in THF (8 mL) in an ice bath was added DMPEA (**176**) (200.0 mg, 1.10 mmol, 3.8 equiv.), $MgSO_4$ (536.3 mg) and AcOH (0.13 mL, 2.27 mmol, 7.8 equiv.). The mixture was stirred in the ice bath for 15 min before addition of $NaBH_3CN$ (44.6 mg, 0.71 mmol, 2.4 equiv.). The solution was stirred further at room temperature for 23 h before addition of 1 M NaOH solution (8 mL). The mixture was then extracted with EtOAc (3 X 15 mL). The combined organic layer was washed with brine (8 mL) and dried with Na_2SO_4 before concentrated *in vacuo*. The crude product was purified by centrifugal radial TLC using an eluent system of 1% MeOH–EtOAc to yield **147a/147b** as a yellow oil (65.2 mg, 0.12 mmol, 41%) and **147c/147d** as a yellow oil (9.6 mg, 0.02 mmol, 7%). **147a/147b**: R_f = 0.29 (10% MeOH–EtOAc); IR (neat) ν_{max} 3509, 3291, 3000, 2931, 2837, 1590, 1516, 1463, 1262, 1236, 1141, 1028 cm^{-1}; ^1H NMR ($CDCl_3$, 400 MHz) δ 6.92 (s, 1H), 6.85 – 6.78 (m, 3H), 6.75 (d, *J* = 2.0 Hz, 1H), 6.73 (d, *J* = 2.0 Hz, 1H), 6.70 (d, *J* = 8.1 Hz, 1H), 6.55 (d, *J* = 2.0 Hz, 1H), 6.48 (dd, *J* = 8.1, 2.0 Hz, 1H), 4.81 (dd, *J* = 10.6, 2.0 Hz, 1H), 3.89 (s, 3H), 3.88 (s, 3H), 3.88 (s, 3H), 3.86 (s, 3H), 3.85 (s, 3H), 3.81 (s, 3H), 3.19 – 3.06 (m, 2H), 2.94 – 2.82 (m, 2H), 2.79 (dd, *J* = 13.8, 4.8 Hz, 1H), 2.76 – 2.67 (m, 1H), 2.57 (dd, *J* = 13.6, 7.1 Hz, 1H), 1.70 (dt, *J* = 14.3, 2.3 Hz, 1H), 1.47 (dt, *J* = 14.3, 10.9 Hz, 1H); ^{13}C NMR ($CDCl_3$, 100 MHz) δ 149.0, 148.8, 147.9, 147.6, 138.0, 131.9, 130.6, 121.4, 120.6, 117.7, 112.4, 111.9, 111.3, 111.2, 110.8, 108.8, 75.2, 60.4, 55.9, 55.9, 55.8, 55.8, 47.9, 42.3, 40.0, 36.4; HRESIMS *m/z* 526.2793 $[M + H]^+$ (calcd for $C_{30}H_{40}N_1O_7$,

526.2805); **147c/147d**: R_f = 0.22 (10% MeOH–EtOAc); IR (neat) ν_{max} 3509, 3294, 3003, 2936, 2836, 1593, 1514, 1459, 1259, 1237, 1142, 1027 cm^{-1}; ^1H NMR ($CDCl_3$, 400 MHz) δ 6.90 (s, 1H), 6.84 – 6.80 (m, 2H), 6.74 (d, *J* = 8.1 Hz, 1H), 6.70 (d, *J* = 8.1 Hz, 1H), 6.63 (d, *J* = 2.0 Hz, 1H), 6.60 (dd, *J* = 8.1, 2.0 Hz, 1H), 6.56 (d, *J* = 2.0 Hz, 1H), 6.53 (dd, *J* = 8.1, 2.1 Hz, 1H), 5.08 (dd, *J* = 8.4, 2.9 Hz, 1H), 3.88 (s, 6H), 3.87 (s, 3H), 3.87 (s, 3H), 3.85 (s, 3H), 3.81 (s, 3H), 3.06 – 2.93 (m, 3H), 2.82 (dd, *J* = 13.7, 7.8 Hz, 1H), 2.78 – 2.75 (m, 1H), 2.72 (dd, *J* = 13.6, 6.1 Hz, 1H), 2.69 – 2.60 (m, 1H), 1.96 (ddd, *J* = 14.6, 8.5, 3.2 Hz, 1H), 1.68 (ddd, *J* = 14.5, 5.8, 2.9 Hz, 1H); ^{13}C NMR ($CDCl_3$, 100 MHz) δ 148.9, 148.8, 147.7, 147.6, 147.5, 138.0, 131.6, 130.6, 120.9, 120.5, 117.4, 111.9, 111.6, 111.1, 111.1, 110.8, 108.8, 71.7, 57.7, 55.9, 55.8, 55.8, 48.5, 39.3, 38.9, 35.7; HRESIMS *m/z* 526.2801 $[M + H]^+$ (calcd for $C_{30}H_{40}N_1O_7$, 526.2801). The spectroscopic data are in good agreement with those obtained for the natural product.[170]

Separation of enantiomers 147a and 147b by chiral HPLC

147a/147b (12 mg) was dissolved in EtOH (6 mL) and resolved using a chiral column (eluting solvent: hexane–EtOH–Et_2NH, 90:10:0.1; flow rate: 1.0 mL/min; 600 injections, injection volume: 10.0 μL each) to yield two fractions. Fraction 1 (**147a**): t_R = 18.37 min, 4.9 mg. Fraction 2 (**147b**): t_R = 19.73 min, 5.8 mg. **147a** $[\alpha]_D^{25}$ +9 (*c* 0.22, $CHCl_3$); **147b** $[\alpha]_D^{25}$ –10 (*c* 0.28, $CHCl_3$).

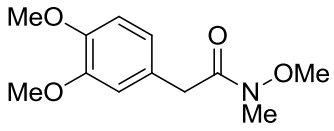
Separation of enantiomers 147c and 147d by chiral HPLC

147c/147d (9.6 mg) was dissolved in EtOH (1.6 mL) and resolved using a chiral column (eluting solvent: hexane–*i*PrOH–Et_2NH, 80:20:0.1; flow rate: 1.0 mL/min; 260 injections, injection volume: 5.0 μL each) to yield two fractions. Fraction 1

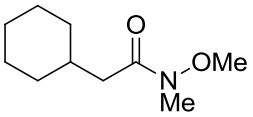
(**147c**): t_R = 11.08 min, 3.8 mg. Fraction 2 (**147d**): t_R = 14.08 min, 3.8 mg. **147c** $[\alpha]_D^{25}$ –38 (*c* 0.19, $CHCl_3$); **147d** $[\alpha]_D^{25}$ +19 (*c* 0.14, $CHCl_3$).

6.1.3 Synthesis of schwarzinicine analogues

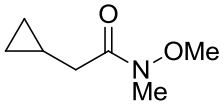
6.1.3.1 Preparation of Weinreb amides from carboxylic acids



***N*-Methoxy-*N*-methyl-(3,4-dimethoxyphenyl)acetamide (177c).** Based on the procedures reported by García-Domínguez *et al.*[196] and Tan *et al.*,[197] in a stirring solution of 3,4-dimethoxyphenylacetic acid (**184**) (508.5 mg, 2.59 mmol, 1 equiv.) in CH_2Cl_2 (15 mL) was added *N*,*O*-dimethylhydroxylamine hydrochloride (402.6 mg, 4.13 mmol, 1.6 equiv.), EDC (738.8 mg, 3.85 mmol, 1.5 equiv.) and DMAP (472.4 mg, 3.87 mmol, 1.5 equiv.). The mixture was stirred at room temperature for 21 h, followed by addition of water (10 mL) and extraction with CH_2Cl_2 (3 X 8 mL). The combined organic layer was washed with 5% HCl solution (10 mL) and brine (10 mL) before drying with Na_2SO_4 and concentrated *in vacuo*. The crude product was purified by centrifugal radial TLC using an eluent system of Et_2O–hexane (8:1) to yield Weinreb amide **177c** as an orange oil (550.8 mg, 2.30 mmol, 89%). R_f = 0.14 (Et_2O–hexane, 8:1); IR (neat) ν_{max} 2999, 2938, 2836, 1660, 1591, 1515, 1464, 1422, 1383, 1262, 1238, 1155, 1142, 1028 cm^{-1}; ^1H NMR ($CDCl_3$, 700 MHz) δ 6.87 – 6.85 (m, 1H), 6.83 – 6.81 (m, 2H), 3.88 (s, 3H), 3.86 (s, 3H), 3.72 (s, 2H), 3.63 (s, 3H), 3.20 (s, 3H); ^{13}C NMR ($CDCl_3$, 175 MHz) δ 172.6, 148.9, 147.9, 127.4, 121.4, 112.4, 111.1, 61.3, 55.9, 55.8, 38.9, 32.2; HRESIMS *m/z* 240.1246 $[M + H]^+$ (calcd for $C_{12}H_{18}N_1O_4$, 240.1236).

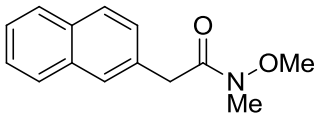


2-Cyclohexyl-*N*-methoxy-*N*-methylacetamide (210a).[265] Following the general procedure described for the synthesis of Weinreb amide **177c**, 2-cyclohexylacetic acid (**208a**) (419.5 mg, 2.95 mmol, 1 equiv.) was reacted with *N*,*O*-dimethylhydroxylamine hydrochloride (445.3 mg, 4.56 mmol, 1.5 equiv.), EDC (854.3 mg, 4.46 mmol, 1.5 equiv.) and DMAP (541.3 mg, 4.43 mmol, 1.5 equiv.) in CH_2Cl_2 (10 mL) for 23 h to yield Weinreb amide **210a** as a yellow oil (503.1 mg, 2.72 mmol, 92%). Eluent system of EtOAc–hexane (1:3) was used in centrifugal radial TLC purification. R_f = 0.30 (EtOAc–hexane, 1:3); IR (neat) ν_{max} 2921, 2850, 1659, 1446, 1382, 1176, 1002 cm^{-1}; ^1H NMR ($CDCl_3$, 700 MHz) δ 3.67 (s, 3H), 3.18 (s, 3H), 2.30 (d, *J* = 7.0 Hz, 2H), 1.85 (ttt, *J* = 10.8, 7.0, 3.5 Hz, 1H), 1.77 – 1.72 (m, 2H), 1.72 – 1.62 (m, 3H), 1.29 (qt, *J* = 12.7, 3.4 Hz, 2H), 1.14 (qt, *J* = 12.8, 3.4 Hz, 1H), 0.97 (qd, *J* = 12.5, 3.5 Hz, 2H); ^{13}C NMR ($CDCl_3$, 175 MHz) δ 174.1, 61.2, 39.3, 34.5, 33.4, 32.0, 26.3, 26.2; HRESIMS *m/z* $[M + H]^+$ 186.1499 (calcd for $C_{10}H_{20}N_1O_2$, 186.1492). The spectroscopic data are in good agreement with those reported in the literature.[265]

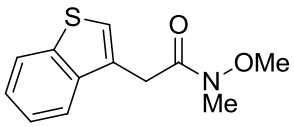


2-Cyclopropyl-*N*-methoxy-*N*-methylacetamide (210b).[266] Following the general procedure described for the synthesis of Weinreb amide **177c**, cyclopropylacetic acid (**208b**) (412.0 mg, 4.12 mmol, 1 equiv.) was reacted with *N*,*O*-dimethylhydroxylamine hydrochloride (596.6 mg, 6.12 mmol, 1.5 equiv.), EDC (1.15 g, 6.00 mmol, 1.5 equiv.) and DMAP (737.0 mg, 6.03 mmol, 1.5 equiv.) in CH_2Cl_2 (6

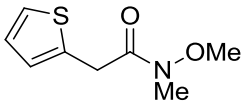
mL) for 24 h to yield Weinreb amide **210b** as a light yellow oil (545.6 mg, 3.81 mmol, 92%). Eluent system of Et_2O–hexane (1:3) was used in centrifugal radial TLC purification. R_f = 0.07 (Et_2O–hexane, 1:3); IR (neat) ν_{max} 3004, 2940, 1653, 1462, 1416, 1368, 1177, 1008 cm^{-1}; ^1H NMR ($CDCl_3$, 700 MHz) δ 3.67 (s, 3H), 3.20 (s, 3H), 2.35 (d, *J* = 7.1 Hz, 2H), 1.15 – 1.05 (m, 1H), 0.62 – 0.50 (m, 2H), 0.17 (q, *J* = 5.1 Hz, 2H); ^{13}C NMR ($CDCl_3$, 175 MHz) δ 174.2, 61.2, 37.3, 32.1, 6.7, 4.4; HRESIMS *m/z* $[M + H]^+$ 144.1022 (calcd for $C_7H_{14}N_1O_2$, 144.1025). The spectroscopic data are in good agreement with those reported in the literature.[266]



***N*-Methoxy-*N*-methyl-2-(naphthalen-2-yl)acetamide (210c).**[267] Following the general procedure described for the synthesis of Weinreb amide **177c**, 2-naphthylacetic acid (**208c**) (407.7 mg, 2.19 mmol, 1 equiv.) was reacted with *N*,*O*-dimethylhydroxylamine hydrochloride (319.8 mg, 3.28 mmol, 1.5 equiv.), EDC (623.9 mg, 3.25 mmol, 1.5 equiv.) and DMAP (401.6 mg, 3.29 mmol, 1.5 equiv.) in CH_2Cl_2 (10 mL) for 17 h to yield Weinreb amide **210c** as a yellow oil (459.5 mg, 2.00 mmol, 92%). Eluent system of Et_2O–hexane (1:1) was used in centrifugal radial TLC purification. R_f = 0.30 (Et_2O–hexane, 3:1); IR (neat) ν_{max} 3053, 2968, 2937, 1653, 1414, 1380, 1171, 1002 cm^{-1}; ^1H NMR ($CDCl_3$, 700 MHz) δ 7.84 – 7.77 (m, 3H), 7.74 (s, 1H), 7.48 – 7.41 (m, 3H), 3.94 (s, 2H), 3.61 (s, 3H), 3.21 (s, 3H); ^{13}C NMR ($CDCl_3$, 175 MHz) δ 172.4, 133.5, 132.5, 132.4, 128.1, 127.8, 127.6, 127.6, 127.6, 126.0, 125.6, 61.4, 39.6, 32.3; HRESIMS *m/z* $[M + H]^+$ 230.1189 (calcd for $C_{14}H_{16}N_1O_2$, 230.1181). The spectroscopic data are in good agreement with those reported in the literature.[267]

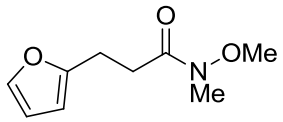


2-(Benzo[*b*]thiophen-3-yl)-*N*-methoxy-*N*-methylacetamide (210d). Following the general procedure described for the synthesis of Weinreb amide **177c**, benzo[*b*]thiophene-3-acetic acid (**208d**) (399.5 mg, 2.08 mmol, 1 equiv.) was reacted with *N*,*O*-dimethylhydroxylamine hydrochloride (304.7 mg, 3.12 mmol, 1.5 equiv.), EDC (600.1 mg, 3.13 mmol, 1.5 equiv.) and DMAP (382.7 mg, 3.13 mmol, 1.5 equiv.) in CH_2Cl_2 (10 mL) for 17 h to yield Weinreb amide **210d** as a yellow oil (359.6 mg, 1.53 mmol, 74%). Eluent system of Et_2O–hexane (1:1) was used in centrifugal radial TLC purification. R_f = 0.36 (Et_2O–hexane, 4:1); IR (neat) ν_{max} 3060, 2965, 2937, 1654, 1426, 1381, 1176 cm^{-1}; ^1H NMR ($CDCl_3$, 400 MHz) δ 7.84 (tdd, *J* = 8.0, 1.3, 0.8 Hz, 2H), 7.42 – 7.34 (m, 2H), 7.32 (s, 1H), 4.00 (s, 2H), 3.62 (s, 3H), 3.22 (s, 3H); ^{13}C NMR ($CDCl_3$, 100 MHz) δ 171.4, 140.1, 138.8, 129.1, 124.3, 124.2, 124.1, 122.8, 121.9, 61.4, 32.5, 32.3; HRESIMS (LC/MS) (t_R = 3.82 min for a 30 min run) *m/z* [M + H]$^+$ 236.0742 (calcd for $C_{12}H_{14}N_1O_2S_1$, 236.0742).

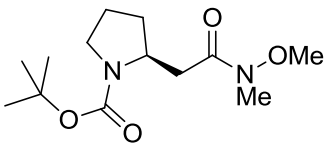


***N*-Methoxy-*N*-methyl-2-(thiophen-2-yl)acetamide (210e).**[268] Following the general procedure described for the synthesis of Weinreb amide **177c**, 2-thiopheneacetic acid (**208e**) (399.9 mg, 2.81 mmol, 1 equiv.) was reacted with *N*,*O*-dimethylhydroxylamine hydrochloride (417.3 mg, 4.28 mmol, 1.5 equiv.), EDC (816.2 mg, 4.26 mmol, 1.5 equiv.) and DMAP (518.0 mg, 4.24 mmol, 1.5 equiv.) in CH_2Cl_2 (10 mL) for 23 h to yield Weinreb amide **210e** as a light yellow oil (430.9 mg, 2.33 mmol, 83%). Eluent system of Et_2O–hexane (4:1) was used in centrifugal radial

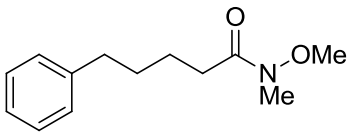
TLC purification. R_f = 0.42 (Et_2O–hexane, 9:1); IR (neat) ν_{max} 3101, 2968, 2938, 1656, 1424, 1384, 1174 cm^{-1}; ^1H NMR ($CDCl_3$, 700 MHz) δ 7.22 – 7.19 (m, 1H), 6.98 – 6.93 (m, 2H), 3.98 (s, 2H), 3.69 (s, 3H), 3.22 (s, 3H); ^{13}C NMR ($CDCl_3$, 175 MHz) δ 171.1, 136.1, 126.7, 126.6, 124.8, 61.4, 33.3, 32.3; HRESIMS *m/z* $[M + H]^+$ 186.0592 (calcd for $C_8H_{12}N_1O_2S_1$, 186.0589). The spectroscopic data are in good agreement with those reported in the literature.[268]



3-(Furan-2-yl)-*N*-methoxy-*N*-methylpropanamide (210f).[269] Following the general procedure described for the synthesis of Weinreb amide **177c**, 3-(2-furyl)propionic acid (**208f**) (402.5 mg, 2.87 mmol, 1 equiv.) was reacted with *N*,*O*-dimethylhydroxylamine hydrochloride (426.9 mg, 4.38 mmol, 1.5 equiv.), EDC (823.8 mg, 4.30 mmol, 1.5 equiv.) and DMAP (534.0 mg, 4.37 mmol, 1.5 equiv.) in CH_2Cl_2 (10 mL) for 23 h to yield Weinreb amide **210f** as a light yellow oil (450.3 mg, 2.46 mmol, 86%). Eluent system of Et_2O–hexane (1:1) was used in centrifugal radial TLC purification. R_f = 0.48 (Et_2O–hexane, 9:1); IR (neat) ν_{max} 2937, 1653, 1423, 1386, 1175 cm^{-1}; ^1H NMR ($CDCl_3$, 700 MHz) δ 7.31 (dd, *J* = 1.8, 1.0 Hz, 1H), 6.28 (dd, *J* = 3.2, 1.9 Hz, 1H), 6.04 (dd, *J* = 2.8, 0.9 Hz, 1H), 3.66 (s, 3H), 3.19 (s, 3H), 2.98 (t, *J* = 8.1 Hz, 2H), 2.78 (t, *J* = 7.8 Hz, 2H); ^{13}C NMR ($CDCl_3$, 175 MHz) δ 173.2, 154.9, 141.0, 110.2, 105.2, 61.3, 32.2, 30.4, 23.1; HRESIMS *m/z* $[M + H]^+$ 184.0981 (calcd for $C_9H_{14}N_1O_3$, 184.0974). The spectroscopic data are in good agreement with those reported in the literature.[269]

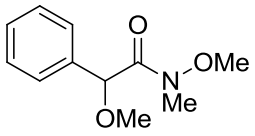


***Tert*-butyl 2-(2-(methoxy(methyl)amino)-2-oxoethyl)pyrrolidine-1-carboxylate (210g).**[270] Following the general procedure described for the synthesis of Weinreb amide **177c**, Boc-L-beta-homoproline (**208g**) (801.9 mg, 3.50 mmol, 1 equiv.) was reacted with *N,O*-dimethylhydroxylamine hydrochloride (510.4 mg, 5.23 mmol, 1.5 equiv.), EDC (1.01 g, 5.27 mmol, 1.5 equiv.) and DMAP (643.7 mg, 5.27 mmol, 1.5 equiv.) in CH_2Cl_2 (10 mL) for 23 h to yield Weinreb amide **210g** as a light yellow oil (763.9 mg, 2.80 mmol, 80%). Eluent system of Et_2O–hexane (3:1) was used in centrifugal radial TLC purification. R_f = 0.19 (Et_2O–hexane, 3:1); IR (neat) ν_{max} 2971, 2883, 1681, 1453, 1388, 1251, 1165, 1109, 1002 cm^{-1}; ^1H NMR ($CDCl_3$, 700 MHz) δ 4.29 – 4.15 (m, 1H), 3.69 (s, 3H), 3.46 – 3.25 (m, 2H), 3.18 (s, 3H), 2.97 (dd, *J* = 94.7, 13.8 Hz, 1H), 2.61 – 2.30 (m, 1H), 2.13 – 2.00 (m, 1H), 1.91 – 1.73 (m, 3H), 1.46 (s, 9H); ^{13}C NMR ($CDCl_3$, 175 MHz) δ 172.4, 154.4, 79.4, 79.0, 61.2, 54.0, 46.6, 46.2, 36.6, 36.2, 32.0, 31.4, 30.7, 28.6, 23.5, 22.8; HRESIMS *m/z* $[M + H]^+$ 273.1805 (calcd for $C_{13}H_{25}N_2O_4$, 273.1814). The spectroscopic data are in good agreement with those reported in the literature.[270]



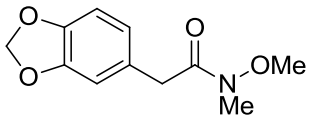
***N*-Methoxy-*N*-methyl-5-phenylpentanamide (210h).**[271] Following the general procedure described for the synthesis of Weinreb amide **177c**, 5-phenylvaleric acid (**208h**) (399.1 mg, 2.24 mmol, 1 equiv.) was reacted with *N,O*-dimethylhydroxylamine hydrochloride (329.4 mg, 3.38 mmol, 1.5 equiv.), EDC

(646.3 mg, 3.37 mmol, 1.5 equiv.) and DMAP (415.0 mg, 3.40 mmol, 1.5 equiv.) in CH_2Cl_2 (10 mL) for 21 h to yield Weinreb amide **210h** as a yellow oil (456.7 mg, 2.06 mmol, 92%). Eluent system of EtOAc–hexane (1:2) was used in centrifugal radial TLC purification. R_f = 0.32 (EtOAc–hexane, 1:2); IR (neat) ν_{max} 3026, 2935, 2860, 1660, 1453, 1415, 1383, 1177 cm^{-1}; ^1H NMR ($CDCl_3$, 700 MHz) δ 7.29 – 7.24 (m, 2H), 7.20 – 7.15 (m, 3H), 3.66 (s, 3H), 3.17 (s, 3H), 2.64 (t, *J* = 7.1 Hz, 2H), 2.44 (t, *J* = 6.7 Hz, 2H), 1.73 – 1.62 (m, 4H); ^{13}C NMR ($CDCl_3$, 175 MHz) δ 174.6, 142.4, 128.4, 128.3, 125.7, 61.2, 35.8, 32.1, 31.7, 31.2, 24.3; HRESIMS *m/z* $[M + H]^+$ 222.1502 (calcd for $C_{13}H_{20}N_1O_2$, 222.1494). The spectroscopic data are in good agreement with those reported in the literature.[271]

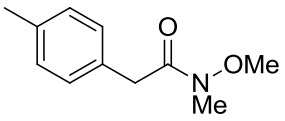


***N*-Methoxy-*N*-methyl-2-methoxy-2-phenylacetamide (210i).**[272] Following the general procedure described for the synthesis of Weinreb amide **177c**, (±)-α-methoxyphenylacetic acid (**208i**) (399.8 mg, 2.41 mmol, 1 equiv.) was reacted with *N*,*O*-dimethylhydroxylamine hydrochloride (356.6 mg, 3.66 mmol, 1.5 equiv.), EDC (701.7 mg, 3.66 mmol, 1.5 equiv.) and DMAP (448.1 mg, 3.67 mmol, 1.5 equiv.) in CH_2Cl_2 (10 mL) for 18 h to yield Weinreb amide **210i** as a light yellow oil (401.2 mg, 1.92 mmol, 80%). Eluent system of Et_2O–hexane (1:1) was used in centrifugal radial TLC purification. R_f = 0.19 (Et_2O–hexane, 1:1); IR (neat) ν_{max} 2930, 1795, 1574, 1528, 1448, 1095 cm^{-1}; ^1H NMR ($CDCl_3$, 700 MHz) δ 7.48 – 7.42 (m, 2H), 7.41 – 7.30 (m, 3H), 5.12 (s, 1H), 3.42 (s, 3H), 3.39 (s, 3H), 3.17 (s, 3H); ^{13}C NMR ($CDCl_3$, 175 MHz) δ 171.2, 136.5, 128.6, 128.6, 128.1, 80.8, 61.0, 57.2, 32.4; HRESIMS *m/z* [M +

H]$^+$ 210.1131 (calcd for $C_{11}H_{16}N_1O_3$, 210.1130). The spectroscopic data are in good agreement with those reported in the literature.[272]



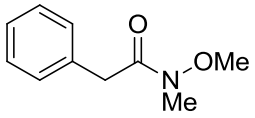
***N*-Methoxy-*N*-methyl-2-(benzo[*d*][1,3]dioxol-5-yl)acetamide (210j).** Following the general procedure described for the synthesis of Weinreb amide **177c**, 3,4-(methylenedioxy)phenylacetic acid (**208j**) (407.3 mg, 2.26 mmol, 1 equiv.) was reacted with *N,O*-dimethylhydroxylamine hydrochloride (328.4 mg, 3.37 mmol, 1.5 equiv.), EDC (641.9 mg, 3.35 mmol, 1.5 equiv.) and DMAP (412.6 mg, 3.38 mmol, 1.5 equiv.) in CH_2Cl_2 (10 mL) for 17.5 h to yield Weinreb amide **210j** as a light yellow oil (413.7 mg, 1.85 mmol, 82%). Eluent system of Et_2O–hexane (4:1) was used in centrifugal radial TLC purification. R_f = 0.24 (Et_2O–hexane, 4:1); IR (neat) ν_{max} 2969, 2938, 2898, 1655, 1489, 1442, 1416, 1243, 1181, 1035, 1002 cm^{-1}; ^{1}H NMR ($CDCl_3$, 700 MHz) δ 6.81 (d, *J* = 1.3 Hz, 1H), 6.77 – 6.72 (m, 2H), 5.93 (s, 2H), 3.68 (s, 2H), 3.64 (s, 3H), 3.19 (s, 3H); ^{13}C NMR ($CDCl_3$, 175 MHz) δ 172.5, 147.7, 146.4, 128.5, 122.4, 109.8, 108.2, 100.9, 61.3, 38.9, 32.2; HRESIMS *m/z* 224.0920 [M + H]$^+$ (calcd for $C_{11}H_{14}N_1O_4$, 224.0923).



***N*-Methoxy-*N*-methyl-2-(*p*-tolyl)acetamide (210k).**[273] Following the general procedure described for the synthesis of Weinreb amide **177c**, *p*-tolylacetic acid (**208k**) (457.4 mg, 3.05 mmol, 1 equiv.) was reacted with *N,O*-dimethylhydroxylamine hydrochloride (442.5 mg, 4.54 mmol, 1.5 equiv.), EDC (867.3 mg, 4.52 mmol, 1.5 equiv.) and DMAP (378.7 mg, 3.10 mmol, 1 equiv.) in CH_2Cl_2 (12 mL) for 19.5 h to

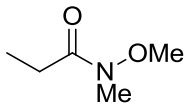
yield Weinreb amide **210k** as a yellow oil (491.9 mg, 2.55 mmol, 84%). Eluent system of Et_2O–hexane (4:1) was used in centrifugal radial TLC purification. R_f = 0.40 (Et_2O–hexane, 4:1); IR (neat) ν_{max} 3003, 2937, 1658, 1515, 1417, 1379, 1173, 1004 cm^{-1}; ^1H NMR ($CDCl_3$, 700 MHz) δ 7.18 (d, *J* = 7.9 Hz, 2H), 7.12 (d, *J* = 7.9 Hz, 2H), 3.73 (s, 2H), 3.61 (s, 3H), 3.19 (s, 3H), 2.32 (s, 3H); ^{13}C NMR ($CDCl_3$, 175 MHz) δ 172.7, 136.3, 131.8, 129.2, 129.1, 61.3, 39.0, 32.2, 21.1; HRESIMS *m/z* 194.1181 $[M + H]^+$ (calcd for $C_{11}H_{16}N_1O_2$, 194.1181). The spectroscopic data are in good agreement with those reported in the literature.[273]

6.1.3.2 Preparation of Weinreb amides from acyl chlorides

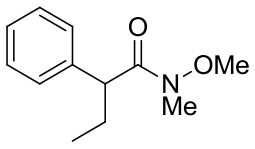


***N*-Methoxy-*N*-methyl-2-phenylacetamide (186).**[269] Based on the procedure reported by Trost *et al.*,[198] phenylacetyl chloride (**185**) (928.0 mg, 6.00 mmol, 1 equiv.) was added dropwise into a mixture of *N,O*-dimethylhydroxylamine hydrochloride (719.2 mg, 7.37 mmol, 1.2 equiv.) and pyridine (1.3 mL, 16.1 mmol, 2.7 equiv.) in CH_2Cl_2 (20 mL) in an ice bath. The reaction mixture was allowed to warm and stir at room temperature for 2 h. It was then diluted with EtOAc (40 mL), washed with 1 M HCl solution (2 X 40 mL), followed with saturated aq. $KHCO_3$ solution (2 X 40 mL) and finally brine (40 mL). The organic layer was dried over $MgSO_4$ and concentrated *in vacuo*. The crude product was purified by centrifugal radial TLC using an eluent system of Et_2O–hexane (1:3) to yield Weinreb amide **186** as a yellow oil (1.05 g, 5.86 mmol, 98%). R_f = 0.39 (Et_2O–hexane, 4:1); IR (neat) ν_{max} 3031, 2939, 1661, 1496, 1456, 1417, 1384, 1174, 1000 cm^{-1}; ^1H NMR ($CDCl_3$, 400 MHz,) δ 7.36 – 7.19 (m,

5H), 3.77 (s, 2H), 3.60 (s, 3H), 3.19 (s, 3H); ^{13}C NMR ($CDCl_3$, 100 MHz) δ 172.6, 135.0, 129.4, 128.6, 126.9, 61.4, 39.5, 32.3; HRESIMS *m/z* 180.1029 $[M + H]^+$ (calcd for $C_{10}H_{14}N_1O_2$, 180.1025). The spectroscopic data are in good agreement with those reported in the literature.[269]

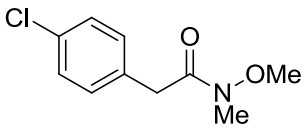


***N*-Methoxy-*N*-methylpropionamide (210l).**[274,275] Following the general procedure described for the synthesis of Weinreb amide **186**, propionyl chloride (**209a**) (2.01 g, 21.7 mmol, 1 equiv.) was reacted with *N,O*-dimethylhydroxylamine hydrochloride (2.32 g, 23.8 mmol, 1.1 equiv.) and pyridine (4.4 mL, 54.4 mmol, 2.5 equiv.) in CH_2Cl_2 (20 mL) for 2.5 h to yield Weinreb amide **210l** as a colourless oil (912.6 mg, 7.79 mmol, 36%). The product was used in the next reaction without further purification. R_f = 0.44 (Et_2O–hexane, 4:1); IR (neat) ν_{max} 2979, 2942, 1664, 1466, 1420, 1380, 1180, 1010 cm^{-1}; ^{1}H NMR ($CDCl_3$, 700 MHz) δ 3.69 (s, 3H), 3.19 (s, 3H), 2.46 (q, *J* = 7.6 Hz, 2H), 1.14 (t, *J* = 7.5 Hz, 3H); ^{13}C NMR ($CDCl_3$, 175 MHz) δ 175.6, 61.2, 32.3, 25.2, 8.8; HRESIMS *m/z* 118.0870 $[M + H]^+$ (calcd for $C_5H_{12}N_1O_2$, 118.0868). The spectroscopic data are in good agreement with those reported in the literature.[274,275]



***N*-Methoxy-*N*-methyl-2-phenylbutanamide (210m).**[276,277] Following the general procedure described for the synthesis of Weinreb amide **186**, 2-phenylbutyryl chloride (**209b**) (0.38 mL, 2.27 mmol, 1 equiv.) was reacted with *N,O*-dimethylhydroxylamine

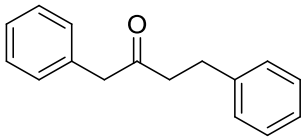
hydrochloride (238.8 mg, 2.45 mmol, 1.1 equiv.) and pyridine (0.45 mL, 5.56 mmol, 2.4 equiv.) in CH_2Cl_2 (13 mL) for 2 h to yield Weinreb amide **210m** as a colourless oil (458.7 mg, 2.21 mmol, 97%). Eluent system of Et_2O–hexane (1:2) was used in centrifugal radial TLC purification. R_f = 0.58 (Et_2O–hexane, 4:1); IR (neat) ν_{max} 2958, 1658, 1450, 1385, 1173 cm^{-1}; ^1H NMR ($CDCl_3$, 700 MHz) δ 7.34 – 7.19 (m, 5H), 3.90 (s, 1H), 3.47 (s, 3H), 3.16 (s, 3H), 2.08 (dq, *J* = 14.9, 7.4 Hz, 1H), 1.75 (dq, *J* = 14.6, 7.4 Hz, 1H), 0.88 (t, *J* = 7.4 Hz, 3H); ^{13}C NMR ($CDCl_3$, 175 MHz) δ 174.8, 140.2, 128.5, 128.2, 126.8, 61.3, 49.3, 32.2, 27.2, 12.3; HRESIMS *m/z* 208.1336 $[M + H]^+$ (calcd for $C_{12}H_{18}N_1O_2$, 208.1338). The spectroscopic data are in good agreement with those reported in the literature.[276,277]



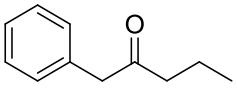
2-(4-Chlorophenyl)-*N*-methoxy-*N*-methylacetamide (210n).[273] Following the general procedure described for the synthesis of Weinreb amide **186**, 4-chlorophenylacetyl chloride (**209c**) (400.5 mg, 2.12 mmol, 1 equiv.) was reacted with *N*,*O*-dimethylhydroxylamine hydrochloride (233.4 mg, 2.39 mmol, 1.1 equiv.) and pyridine (0.45 mL, 5.56 mmol, 2.6 equiv.) in CH_2Cl_2 (5 mL) for 2 h to yield Weinreb amide **210n** as an orange oil (424.6 mg, 1.99 mmol, 94%). Eluent system of Et_2O–hexane (1:1) was used in centrifugal radial TLC purification. R_f = 0.37 (Et_2O–hexane, 3:1); IR (neat) ν_{max} 2970, 2938, 1657, 1491, 1410, 1380, 1172, 1089, 1002 cm^{-1}; ^1H NMR ($CDCl_3$, 700 MHz) δ 7.28 (d, *J* = 8.4 Hz, 2H), 7.22 (d, *J* = 8.4 Hz, 2H), 3.74 (s, 2H), 3.63 (s, 3H), 3.19 (s, 3H); ^{13}C NMR ($CDCl_3$, 175 MHz) δ 171.9, 133.4, 132.7, 130.7, 128.6, 61.3, 38.6, 32.2; HRESIMS *m/z* 214.0641 $[M + H]^+$ (calcd for

$C_{10}H_{13}{}^{35}Cl_1N_1O_2$, 214.0635). The spectroscopic data are in good agreement with those reported in the literature.[273]

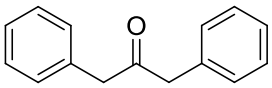
6.1.3.3 Weinreb ketone synthesis



1,4-Diphenylbutan-2-one (191a).[278,279] Based on the procedure reported by Datta *et al.*,[200] to an ice-cold solution of Weinreb amide **186** (799.1 mg, 4.46 mmol, 1 equiv.) in THF (12 mL) was added dropwise into a solution of phenethylmagnesium chloride (**190a**) (0.5 M in THF) (20 mL, 20.0 mmol, 4.5 equiv.). The reaction mixture was stirred in an ice bath for 5 h prior to addition of cold 10% HCl solution (20 mL). After stirring for 5 min, the mixture was extracted with EtOAc (3 X 30 mL). The combined organic layer was washed with water (20 mL) and brine (20 mL) before drying with $MgSO_4$ and concentrated *in vacuo*. The crude product was purified by centrifugal radial TLC using an eluent system of Et_2O–hexane (1:3) to yield ketone **191a** as a yellow oil (591.1 mg, 2.64 mmol, 59%). R_f = 0.69 (Et_2O–hexane, 3:1); IR (neat) ν_{max} 3029, 2929, 1710, 1496, 1454 cm^{-1}; ^1H NMR ($CDCl_3$, 400 MHz) δ 7.34 – 7.22 (m, 5H), 7.20 – 7.10 (m, 5H), 3.65 (s, 2H), 2.89 – 2.83 (m, 2H), 2.79 – 2.73 (m, 2H); ^{13}C NMR ($CDCl_3$, 100 MHz) δ 207.5, 141.0, 134.2, 129.5, 128.9, 128.6, 128.4, 127.1, 126.2, 50.5, 43.6, 29.9; HRESIMS *m/z* 225.1283 $[M + H]^+$ (calcd for $C_{16}H_{17}O_1$, 225.1279). The spectroscopic data are in good agreement with those reported in the literature.[278,279]

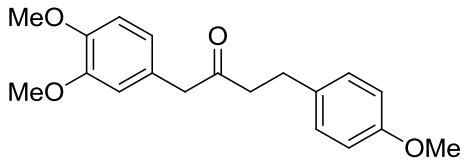


1-Phenylpentan-2-one (191b).[280] Following the method to prepare ketone **191a**, Weinreb amide **186** (738.2 mg, 4.12 mmol, 1 equiv.) was used to react with propylmagnesium chloride (**190b**) (2.0 M in Et_2O) (8 mL, 16.0 mmol, 3.9 equiv.) in THF (10 mL) for 2 h to yield ketone **191b** as a light yellow oil (413.0 mg, 2.55 mmol, 62%). Eluent system of Et_2O–hexane (1:5) was used in centrifugal radial TLC purification. R_f = 0.70 (Et_2O–hexane, 3:1); IR (neat) ν_{max} 3030, 2963, 2875, 1711, 1496, 1454, 1124 cm^{-1}; ^1H NMR ($CDCl_3$, 700 MHz) δ 7.34 – 7.30 (m, 2H), 7.29 – 7.23 (m, 1H), 7.22 – 7.18 (m, 2H), 3.67 (s, 2H), 2.42 (t, *J* = 7.3 Hz, 2H), 1.58 (h, *J* = 7.4 Hz, 2H), 0.86 (t, *J* = 7.4 Hz, 3H); ^{13}C NMR ($CDCl_3$, 175 MHz) δ 208.5, 134.4, 129.4, 128.7, 126.9, 50.2, 43.9, 17.2, 13.6; HRESIMS *m/z* 163.1127 $[M + H]^+$ (calcd for $C_{11}H_{15}O_1$, 163.1123). The spectroscopic data are in good agreement with those reported in the literature.[280]

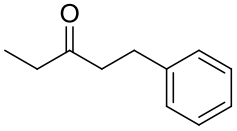


1,3-Diphenylpropan-2-one (191c).[281] Small portion (about 10%) of benzyl bromide (1.29 g, 7.54 mmol, 1 equiv.) in THF (4 mL) was added to Mg turnings (369.0 mg, 15.2 mmol, 2 equiv.) in THF (3 mL). The remaining portion of the bromide was added dropwise into the stirring reaction mixture at room temperature. The resulting mixture was heated and stirred for 5 min before left to cool to room temperature to afford benzylmagnesium bromide (**190c**). Following the general procedure described for the synthesis of ketone **191a**, Weinreb amide **186** (266.5 mg, 1.49 mmol, 0.2 equiv.) was used to react with **190c** prepared earlier in THF (6 mL) for 2 h to yield ketone **191c** as a yellow oil (142.2 mg, 0.68 mmol, 46%). Eluent system of Et_2O–

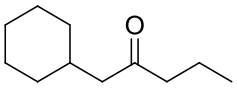
hexane (1:4) was used in centrifugal radial TLC purification. R_f = 0.48 (Et_2O–hexane, 1:2); IR (neat) ν_{max} 3063, 3029, 1718, 1654, 1602, 1496, 1454, 1056 cm^{-1}; ^1H NMR ($CDCl_3$, 700 MHz) δ 7.34 – 7.22 (m, 6H), 7.17 – 7.12 (m, 4H), 3.71 (s, 4H); ^{13}C NMR ($CDCl_3$, 175 MHz) δ 205.7, 134.0, 129.5, 128.7, 127.1, 49.1; HRESIMS *m/z* 211.1124 $[M + H]^+$ (calcd for $C_{15}H_{15}O_1$, 211.1123). The data is in good agreement with the values reported in the literature.[281]



1-(3,4-Dimethoxy-phenyl)-4-(4-methoxy-phenyl)-butan-2-one (191d). Following the general procedure described for the synthesis of ketone **191a**, Weinreb amide **177c** (394.6 mg, 1.65 mmol, 1 equiv.) was used to react with 4-methoxyphenethylmagnesium chloride (**190d**) (0.5 M in THF) (15 mL, 7.50 mmol, 4.5 equiv.) in THF (10 mL) for 2 h to yield ketone **191d** as a yellow oil (362.5 mg, 1.15 mmol, 70%). Eluent system of CH_2Cl_2–hexane (1:3) was used in centrifugal radial TLC purification. R_f = 0.23 (CH_2Cl_2–hexane, 3:1); IR (neat) ν_{max} 3002, 2936, 2836, 1714, 1613, 1590, 1515, 1464, 1029 cm^{-1}; ^1H NMR ($CDCl_3$, 700 MHz) δ 7.06 – 7.02 (m, 2H), 6.83 – 6.77 (m, 3H), 6.70 (dd, *J* = 8.2, 2.1 Hz, 1H), 6.64 (d, *J* = 2.1 Hz, 1H), 3.86 (s, 3H), 3.84 (s, 3H), 3.77 (s, 3H), 3.58 (s, 2H), 2.81 (t, *J* = 7.5 Hz, 2H), 2.73 (t, *J* = 7.2 Hz, 2H); ^{13}C NMR ($CDCl_3$, 175 MHz) δ 208.0, 157.9, 149.0, 148.1, 132.9, 129.2, 126.5, 121.6, 113.8, 112.3, 111.3, 55.9, 55.8, 55.2, 50.0, 43.5, 28.9; HRESIMS *m/z* 315.1586 $[M + H]^+$ (calcd for $C_{19}H_{23}O_4$, 315.1596).

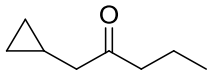


1-Phenylpentan-3-one (212a).[282] Following the method to prepare ketone **191a**, Weinreb amide **210l** (402.8 mg, 3.44 mmol, 1 equiv.) was used to react with phenethylmagnesium chloride (**190a**) (1.0 M in THF) (15 mL, 15.0 mmol, 4.4 equiv.) in THF (15 mL) for 2.5 h to yield ketone **212a** as a colourless oil (420.6 mg, 2.59 mmol, 75%). Eluent system of Et_2O–hexane (1:5) was used in centrifugal radial TLC purification. R_f = 0.68 (Et_2O–hexane, 3:1); IR (neat) ν_{max} 3063, 3028, 2977, 2938, 1717, 1497, 1454, 1113 cm^{-1}; ^1H NMR ($CDCl_3$, 700 MHz) δ 7.32 – 7.14 (m, 5H), 2.90 (t, *J* = 7.7 Hz, 2H), 2.73 (t, *J* = 7.8 Hz, 2H), 2.40 (q, *J* = 7.3 Hz, 2H), 1.04 (t, *J* = 7.4 Hz, 3H); ^{13}C NMR ($CDCl_3$, 175 MHz) δ 210.7, 141.2, 128.5, 128.3, 126.1, 43.9, 36.1, 29.9, 7.8; HRESIMS *m/z* 163.1130 $[M + H]^+$ (calcd for $C_{11}H_{15}O_1$, 163.1123). The spectroscopic data are in good agreement with those reported in the literature.[282]

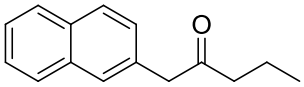


1-Cyclohexylpentan-2-one (212b). Small portion (about 10%) of 1-bromopropane (1 mL, 11.0 mmol, 1 equiv.) in THF (5 mL) was added to Mg turnings (542.0 mg, 22.3 mmol, 2 equiv.) in THF (4 mL). The remaining portion of the bromide was added dropwise into the stirring reaction mixture at room temperature. The resulting mixture was heated and stirred for 5 min before left to cool to room temperature to afford propylmagnesium bromide (**211b**). Following the method to prepare ketone **191a**, Weinreb amide **210a** (511.7 mg, 2.76 mmol, 0.3 equiv.) was used to react with **211b** prepared earlier in THF (5 mL) for 2 h to afford ketone **212b** as a colourless oil (404.9 mg, 2.41 mmol, 87%). Eluent system of EtOAc–hexane (1:6) was used in centrifugal

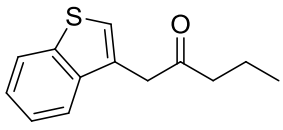
radial TLC purification. R_f = 0.68 (EtOAc–hexane, 1:3); IR (neat) ν_{max} 2922, 2851, 1710, 1449, 1368, 1032 cm^{-1}; ^1H NMR ($CDCl_3$, 700 MHz) δ 2.35 (t, *J* = 7.3 Hz, 2H), 2.26 (d, *J* = 6.9 Hz, 2H), 1.88 – 1.77 (m, 1H), 1.72 – 1.61 (m, 7H), 1.59 (h, *J* = 7.4 Hz, 2H), 1.31 – 1.23 (m, 2H), 1.18 – 1.09 (m, 1H), 0.91 (t, *J* = 7.2 Hz, 3H); ^{13}C NMR ($CDCl_3$, 175 MHz) δ 211.3, 50.6, 45.4, 33.9, 33.3, 26.2, 26.1, 17.2, 13.8; HRESIMS *m/z* 169.1591 $[M + H]^+$ (calcd for $C_{11}H_{21}O_1$, 169.1592).



1-Cyclopropylpentan-2-one (212c). Small portion (about 10%) of 1-bromopropane (0.3 mL, 3.30 mmol, 1 equiv.) in THF (2 mL) was added to Mg turnings (172.8 mg, 7.11 mmol, 2.2 equiv.) in THF (3 mL). The remaining portion of the bromide was added dropwise into the stirring reaction mixture at room temperature. The resulting mixture was heated and stirred for 5 min before left to cool to room temperature to afford propylmagnesium bromide (**211b**). Following the general procedure described for the synthesis of ketone **191a**, Weinreb amide **210b** (117.3 mg, 0.82 mmol, 0.2 equiv.) was used to react with **211b** prepared earlier in THF (4 mL) for 2 h to yield ketone **212c** as a yellow oil (55.1 mg, 0.44 mmol, 53%). Eluent system of Et_2O–hexane (1:5) was used in centrifugal radial TLC purification. R_f = 0.56 (Et_2O–hexane, 1:3); IR (neat) ν_{max} 2957, 2924, 2854, 1722, 1461, 1260, 1019 cm^{-1}; ^1H NMR ($CDCl_3$, 700 MHz) δ 2.44 (t, *J* = 7.3 Hz, 2H), 2.28 (d, *J* = 7.0 Hz, 2H), 1.61 (h, *J* = 7.4 Hz, 2H), 1.03 – 0.95 (m, 1H), 0.92 (t, *J* = 7.4 Hz, 3H), 0.58 – 0.54 (m, 2H), 0.11 (dt, *J* = 6.0, 4.6 Hz, 2H); ^{13}C NMR ($CDCl_3$, 175 MHz) δ 211.3, 48.1, 44.3, 17.2, 13.8, 6.4, 4.5; HRESIMS *m/z* 127.1118 $[M + H]^+$ (calcd for $C_8H_{15}O_1$, 127.1123).

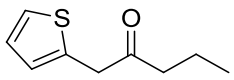


1-(Naphthalen-2-yl)pentan-2-one (212d). Small portion (about 10%) of 1-bromopropane (0.4 mL, 4.40 mmol, 1 equiv.) in THF (2 mL) was added to Mg turnings (217.7 mg, 8.96 mmol, 2 equiv.) in THF (3 mL). The remaining portion of the bromide was added dropwise into the stirring reaction mixture at room temperature. The resulting mixture was heated and stirred for 5 min before left to cool to room temperature to afford propylmagnesium bromide (**211b**). Following the general procedure described for the synthesis of ketone **191a**, Weinreb amide **210c** (202.1 mg, 0.88 mmol, 0.2 equiv.) was used to react with **211b** prepared earlier in THF (6 mL) for 2 h to yield ketone **212d** as an off-white amorphous solid (100.2 mg, 0.47 mmol, 53%). Eluent system of Et_2O–hexane (1:6) was used in centrifugal radial TLC purification. R_f = 0.72 (Et_2O–hexane, 4:1); IR (neat) ν_{max} 2959, 2933, 2874, 1703, 1406, 1366, 1324, 1121, 1037 cm^{-1}; ^1H NMR ($CDCl_3$, 400 MHz) δ 7.80 (dt, *J* = 9.1, 5.0 Hz, 3H), 7.66 (s, 1H), 7.53 – 7.39 (m, 2H), 7.32 (dd, *J* = 8.4, 1.5 Hz, 1H), 3.83 (s, 2H), 2.45 (t, *J* = 7.3 Hz, 2H), 1.59 (dq, *J* = 14.6, 7.4 Hz, 2H), 0.86 (td, *J* = 7.4, 1.3 Hz, 3H); ^{13}C NMR ($CDCl_3$, 100 MHz) δ 208.6, 133.5, 132.4, 131.9, 128.4, 128.1, 127.7, 127.6, 127.5, 126.2, 125.8, 50.3, 44.0, 17.2, 13.6; HRESIMS *m/z* 213.1287 $[M + H]^+$ (calcd for $C_{15}H_{17}O_1$, 213.1279).



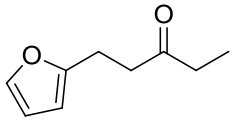
1-(Benzo[*b*]thiophen-3-yl)pentan-2-one (212e). Small portion (about 10%) of 1-bromopropane (0.6 mL, 6.61 mmol, 1 equiv.) in THF (2 mL) was added to Mg turnings (314.0 mg, 12.9 mmol, 2 equiv.) in THF (3 mL). The remaining portion of

the bromide was added dropwise into the stirring reaction mixture at room temperature. The resulting mixture was heated and stirred for 5 min before left to cool to room temperature to afford propylmagnesium bromide (**211b**). Following the method to prepare ketone **191a**, Weinreb amide **210d** (238.0 mg, 1.01 mmol, 0.2 equiv.) was used to react with **211b** prepared earlier in THF (6 mL) for 2 h to afford ketone **212e** as a yellow oil (83.5 mg, 0.38 mmol, 38%). Eluent system of Et_2O–hexane (1:7) was used in centrifugal radial TLC purification. R_f = 0.71 (Et_2O–hexane, 4:1); IR (neat) ν_{max} 2960, 2931, 2874, 1709, 1427, 1363, 1123, 1021 cm^{-1}; ^1H NMR ($CDCl_3$, 700 MHz) δ 7.87 (d, *J* = 8.1 Hz, 1H), 7.68 (d, *J* = 7.6 Hz, 1H), 7.42 – 7.34 (m, 2H), 7.30 (s, 1H), 3.91 (s, 2H), 2.45 (t, *J* = 7.3 Hz, 2H), 1.59 (h, *J* = 7.4 Hz, 2H), 0.86 (t, *J* = 7.4 Hz, 3H); ^{13}C NMR ($CDCl_3$, 175 MHz) δ 207.7, 140.2, 138.6, 128.9, 124.5, 124.5, 124.3, 122.9, 121.7, 43.6, 43.2, 17.2, 13.6; HRESIMS (LC/MS) (t_R = 5.68 min for a 30 min run) *m/z* 219.0842 $[M + H]^+$ (calcd for $C_{13}H_{15}O_1S_1$, 219.0842).

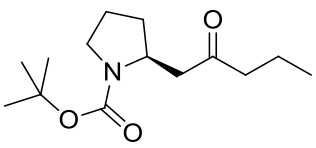


1-(Thiophen-2-yl)pentan-2-one (212f). Following the general procedure described for the synthesis of ketone **191a**, Weinreb amide **210e** (636.0 mg, 3.43 mmol, 1 equiv.) was used to react with propylmagnesium chloride (**190b**) (2.0 M in Et_2O) (7 mL, 14.0 mmol, 4 equiv.) in THF (9 mL) for 2 h to yield ketone **212f** as a light yellow oil (133.0 mg, 0.79 mmol, 23%). Eluent system of Et_2O–hexane (1:5) was used in centrifugal radial TLC purification. R_f = 0.63 (Et_2O–hexane, 7:1); IR (neat) ν_{max} 2963, 2877, 1709, 1413, 1210, 1037 cm^{-1}; ^1H NMR ($CDCl_3$, 400 MHz) δ 7.25 – 7.18 (m, 1H), 6.98 (dd, *J* = 5.1, 3.5 Hz, 1H), 6.92 – 6.86 (m, 1H), 3.88 (s, 2H), 2.48 (t, *J* = 7.3 Hz, 2H), 1.61 (h, *J* = 7.4 Hz, 2H), 0.90 (t, *J* = 7.4 Hz, 3H); ^{13}C NMR ($CDCl_3$, 100

MHz) δ 207.0, 135.4, 127.0, 126.7, 125.0, 43.6, 43.6, 17.2, 13.6; HRESIMS *m/z* 169.0686 $[M + H]^+$ (calcd for $C_9H_{13}O_1S_1$, 169.0687).

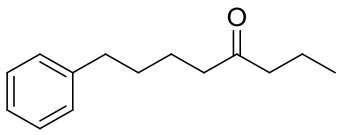


1-(Furan-2-yl)pentan-3-one (212g). Small portion (about 10%) of bromoethane (0.61 mL, 8.2 mmol, 1 equiv.) in THF (5 mL) was added to Mg turnings (408.1 mg, 16.8 mmol, 2 equiv.) in THF (3 mL). The remaining portion of the bromide was added dropwise into the stirring reaction mixture at room temperature. The resulting mixture was heated and stirred for 5 min before left to cool to room temperature to afford ethylmagnesium bromide (**211a**). Following the method to prepare ketone **191a**, Weinreb amide **210f** (307.1 mg, 1.68 mmol, 0.2 equiv.) was used to react with **211a** prepared earlier in THF (10 mL) for 2 h to afford ketone **212g** as a yellow oil (182.2 mg, 1.2 mmol, 71%). Eluent system of Et_2O–hexane (1:6) was used in centrifugal radial TLC purification. R_f = 0.83 (Et_2O–hexane, 7:1); IR (neat) ν_{max} 2925, 2858, 1711, 1369, 1261, 1090, 1020 cm^{-1}; ^1H NMR ($CDCl_3$, 700 MHz) δ 7.29 (dd, *J* = 1.9, 0.8 Hz, 1H), 6.27 (dd, *J* = 3.1, 1.9 Hz, 1H), 5.99 (dd, *J* = 3.2, 1.0 Hz, 1H), 2.92 (t, *J* = 7.5 Hz, 2H), 2.76 (t, *J* = 7.5 Hz, 2H), 2.44 (q, *J* = 7.3 Hz, 2H), 1.06 (t, *J* = 7.3 Hz, 3H); ^{13}C NMR ($CDCl_3$, 175 MHz) δ 210.1, 154.7, 141.1, 110.2, 105.1, 40.4, 36.0, 22.2, 7.8; HRESIMS *m/z* 153.0912 $[M + H]^+$ (calcd for $C_9H_{13}O_2$, 153.0916).



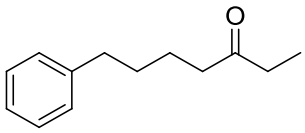
***Tert*-butyl 2-(2-oxopentyl)pyrrolidine-1-carboxylate (212h).** Small portion (about 10%) of 1-bromopropane (0.7 mL, 7.71 mmol, 1 equiv.) in THF (5 mL) was added to

Mg turnings (374.6 mg, 15.4 mmol, 2 equiv.) in THF (3 mL). The remaining portion of the bromide was added dropwise into the stirring reaction mixture at room temperature. The resulting mixture was heated and stirred for 5 min before left to cool to room temperature to afford propylmagnesium bromide (**211b**). Following the method to prepare ketone **191a**, Weinreb amide **210g** (696.4 mg, 2.56 mmol, 0.3 equiv.) was used to react with **211b** prepared earlier in THF (8 mL) for 2 h to afford ketone **212h** as a yellow oil (83.5 mg, 1.48 mmol, 58%). Eluent system of Et_2O–hexane (1:4) was used in centrifugal radial TLC purification. R_f = 0.62 (Et_2O–hexane, 2:1); IR (neat) ν_{max} 2966, 2880, 1688, 1390, 1165, 1107 cm^{-1}; ^1H NMR ($CDCl_3$, 700 MHz) δ 4.23 – 4.08 (m, 1H), 3.44 – 3.22 (m, 2H), 3.13 – 2.84 (m, 1H), 2.51 – 2.31 (m, 3H), 2.06 (dq, *J* = 12.7, 8.2 Hz, 1H), 1.90 – 1.73 (m, 2H), 1.65 – 1.56 (m, 3H), 1.46 (s, 9H), 1.03 – 0.82 (m, 3H); ^{13}C NMR ($CDCl_3$, 175 MHz) δ 209.9, 209.7, 154.4, 154.3, 79.5, 79.2, 53.6, 53.4, 47.7, 46.9, 46.6, 46.1, 45.3, 45.1, 31.5, 30.8, 28.5, 23.6, 22.8, 17.3, 17.1, 13.7; HRESIMS *m/z* 256.1902 $[M + H]^+$ (calcd for $C_{14}H_{26}N_1O_3$, 256.1913).

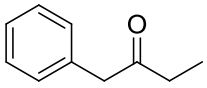


8-Phenyloctan-4-one (212i).[283] Following the general procedure described for the synthesis of ketone **191a**, Weinreb amide **210h** (435.9 mg, 1.97 mmol, 1 equiv.) was used to react with propylmagnesium chloride (**190b**) (2.0 M in Et_2O) (3 mL, 6.0 mmol, 3 equiv.) in THF (6 mL) for 2 h to yield ketone **212i** as a yellow oil (363.3 mg, 1.78 mmol, 90%). Eluent system of EtOAc–hexane (1:6) was used in centrifugal radial TLC purification. R_f = 0.54 (EtOAc–hexane, 1:4); IR (neat) ν_{max} 2934, 2870, 1710, 1455, 1370, 1125, 1026 cm^{-1}; ^1H NMR ($CDCl_3$, 700 MHz) δ 7.30 – 7.24 (m, 2H), 7.20 – 7.14 (m, 3H), 2.66 – 2.60 (m, 2H), 2.44 – 2.39 (m, 2H), 2.36 (t, *J* = 7.3 Hz,

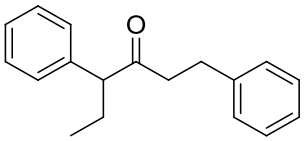
2H), 1.66 – 1.55 (m, 6H), 0.90 (t, J = 7.4 Hz, 3H); ^{13}C NMR ($CDCl_3$, 175 MHz) δ 211.3, 142.2, 128.4, 128.3, 125.7, 44.7, 42.6, 35.8, 31.1, 23.5, 17.3, 13.8; HRESIMS *m/z* 205.1595 $[M + H]^+$ (calcd for $C_{14}H_{21}O_1$, 205.1592). The spectroscopic data are in good agreement with those reported in the literature.[283]



7-Phenylheptan-3-one (212j).[284] Small portion (about 10%) of bromoethane (0.8 mL, 10.7 mmol, 1 equiv.) in THF (5 mL) was added to Mg turnings (502.6 mg, 20.7 mmol, 1.9 equiv.) in THF (5 mL). The remaining portion of the bromide was added dropwise into the stirring reaction mixture at room temperature. The resulting mixture was heated and stirred for 5 min before left to cool to room temperature to afford ethylmagnesium bromide (**211a**). Following the method to prepare ketone **191a**, Weinreb amide **210h** (456.7 mg, 2.06 mmol, 0.2 equiv.) was used to react with **211a** prepared earlier in THF (10 mL) for 2 h to afford ketone **212j** as a yellow oil (346.0 mg, 1.82 mmol, 88%). Eluent system of EtOAc–hexane (1:6) was used in centrifugal radial TLC purification. R_f = 0.64 (EtOAc–hexane, 1:2); IR (neat) ν_{max} 3027, 2973, 2934, 1711, 1455, 1369, 1113, 1025 cm^{-1}; ^{1}H NMR ($CDCl_3$, 700 MHz) δ 7.30 – 7.14 (m, 5H), 2.68 – 2.58 (m, 2H), 2.45 – 2.38 (m, 4H), 1.69 – 1.56 (m, 4H), 1.04 (t, J = 7.3 Hz, 3H); ^{13}C NMR ($CDCl_3$, 175 MHz) δ 211.7, 142.2, 128.4, 128.3, 125.7, 42.2, 35.9, 35.8, 31.1, 23.6, 7.8; HRESIMS *m/z* 191.1442 $[M + H]^+$ (calcd for $C_{13}H_{19}O_1$, 191.1436). The spectroscopic data are in good agreement with those reported in the literature.[284]

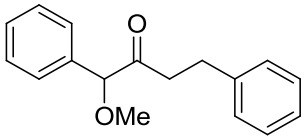


1-Phenylbutan-2-one (212k).[285] Small portion (about 10%) of bromoethane (1 mL, 13.4 mmol, 1 equiv.) in THF (5 mL) was added to Mg turnings (548.5 mg, 22.6 mmol, 1.7 equiv.) in THF (3 mL). The remaining portion of the bromide was added dropwise into the stirring reaction mixture at room temperature. The resulting mixture was heated and stirred for 5 min before left to cool to room temperature to afford ethylmagnesium bromide (**211a**). Following the method to prepare ketone **191a**, Weinreb amide **186** (396.6 mg, 2.21 mmol, 0.2 equiv.) was used to react with **211a** prepared earlier in THF (10 mL) for 2 h to afford ketone **212k** as a yellow oil (113.0 mg, 0.76 mmol, 34%). Eluent system of Et_2O–hexane (1:6) was used in centrifugal radial TLC purification. R_f = 0.72 (Et_2O–hexane, 4:1); IR (neat) ν_{max} 3030, 2978, 2938, 1710, 1454, 1349, 1109, 1036 cm^{-1}; ^1H NMR ($CDCl_3$, 700 MHz) δ 7.35 – 7.19 (m, 5H), 3.69 (s, 2H), 2.48 (q, *J* = 7.3 Hz, 2H), 1.03 (t, *J* = 7.3 Hz, 3H); ^{13}C NMR ($CDCl_3$, 175 MHz) δ 209.1, 134.5, 129.4, 128.7, 126.9, 49.8, 35.2, 7.8; HRESIMS *m/z* 149.0961 $[M + H]^+$ (calcd for $C_{10}H_{13}O_1$, 149.0966). The spectroscopic data are in good agreement with those reported in the literature.[285]

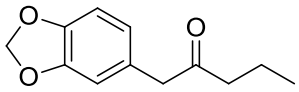


1,4-Diphenylhexan-3-one (212l). Following the method to prepare ketone **191a**, Weinreb amide **210m** (385.8 mg, 1.86 mmol, 1 equiv.) was used to react with phenethylmagnesium chloride (**190a**) (1.0 M in THF) (7 mL, 7.0 mmol, 3.8 equiv.) in THF (6 mL) for 2 h to yield ketone **212l** as a light yellow oil (390.8 mg, 1.55 mmol, 83%). Eluent system of Et_2O–hexane (1:7) was used in centrifugal radial TLC

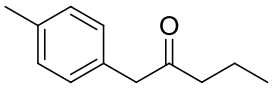
purification. R_f = 0.54 (Et_2O–hexane, 1:4); IR (neat) ν_{max} 3029, 2955, 1708, 1453, 1359, 1071 cm^{-1}; ^1H NMR ($CDCl_3$, 700 MHz) δ 7.32 – 7.03 (m, 10H), 3.48 (t, *J* = 7.4 Hz, 1H), 2.85 (ddd, *J* = 14.8, 9.0, 6.4 Hz, 1H), 2.75 (ddd, *J* = 14.3, 9.3, 6.0 Hz, 1H), 2.72 – 2.62 (m, 2H), 2.05 (dp, *J* = 14.5, 7.3 Hz, 1H), 1.70 (dp, *J* = 15.0, 7.5 Hz, 1H), 0.80 (t, *J* = 7.4 Hz, 3H); ^{13}C NMR ($CDCl_3$, 175 MHz) δ 209.6, 141.0, 138.8, 128.8, 128.4, 128.3, 128.2, 127.2, 126.0, 61.0, 43.4, 29.8, 25.1, 12.1; HRESIMS *m/z* 253.1591 $[M + H]^+$ (calcd for $C_{18}H_{21}O_1$, 253.1592).



1-Methoxy-1,4-diphenylbutan-2-one (212m). Small portion (about 10%) of (2-bromoethyl)benzene (**222**) (1.02 g, 5.51 mmol, 1 equiv.) in THF (5 mL) was added to Mg turnings (288.1 mg, 11.9 mmol, 2.2 equiv.) in THF (5 mL). The remaining portion of the bromide was added dropwise into the stirring reaction mixture at room temperature. The resulting mixture was heated and stirred for 5 min before left to cool to room temperature to afford phenethylmagnesium bromide (**211c**). Following the general procedure described for the synthesis of ketone **191a**, Weinreb amide **210i** (324.9 mg, 1.55 mmol, 0.3 equiv.) was used to react with **211c** prepared earlier in THF (10 mL) for 2 h to yield ketone **212m** as a light yellow oil (334.3 mg, 1.31 mmol, 85%). Eluent system of Et_2O–hexane (1:5) was used in centrifugal radial TLC purification. R_f = 0.61 (Et_2O–hexane, 3:1); IR (neat) ν_{max} 3029, 2924, 1717, 1087 cm^{-1}; ^1H NMR ($CDCl_3$, 400 MHz) δ 7.41 – 7.03 (m, 10H), 4.64 (s, 1H), 3.32 (s, 3H), 2.87 – 2.64 (m, 4H); ^{13}C NMR ($CDCl_3$, 100 MHz) δ 207.6, 140.9, 135.7, 128.8, 128.6, 128.4, 128.3, 127.2, 126.0, 89.2, 57.2, 39.1, 29.3; HRESIMS *m/z* 272.1418 $[M + H_2O]^+$ (calcd for $C_{17}H_{20}O_3$, 272.1412).

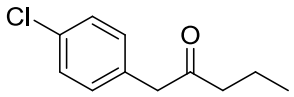


1-(1,3-Benzdioxol-5-yl)pentan-2-one (212n). Small portion (about 10%) of 1-bromopropane (0.65 mL, 7.15 mmol, 1 equiv.) in THF (6 mL) was added to Mg turnings (349.3 mg, 14.4 mmol, 2 equiv.) in THF (2 mL). The remaining portion of the bromide was added dropwise into the stirring reaction mixture at room temperature. The resulting mixture was heated and stirred for 5 min before left to cool to room temperature to afford propylmagnesium bromide (**211b**). Following the method to prepare ketone **191a**, Weinreb amide **210j** (395.2 mg, 1.77 mmol, 0.2 equiv.) was used to react with **211b** prepared earlier in THF (5 mL) for 2 h to afford ketone **212n** as a yellow oil (263.9 mg, 1.28 mmol, 72%). Eluent system of Et_2O–hexane (1:3) was used in centrifugal radial TLC purification. R_f = 0.61 (Et_2O–hexane, 3:1); IR (neat) ν_{max} 2962, 2880, 1709, 1489, 1442, 1243, 1035 cm^{-1}; ^1H NMR ($CDCl_3$, 700 MHz) δ 6.76 (d, *J* = 7.8 Hz, 1H), 6.68 (d, *J* = 1.7 Hz, 1H), 6.64 (dd, *J* = 7.9, 1.7 Hz, 1H), 5.95 (s, 2H), 3.58 (s, 2H), 2.42 (t, *J* = 7.3 Hz, 2H), 1.58 (h, *J* = 7.4 Hz, 2H), 0.88 (t, *J* = 7.4 Hz, 3H); ^{13}C NMR ($CDCl_3$, 175 MHz) δ 208.6, 147.8, 146.6, 127.9, 122.5, 109.8, 108.4, 101.0, 49.7, 43.8, 17.2, 13.7; HRESIMS *m/z* 207.1021 $[M + H]^+$ (calcd for $C_{12}H_{15}O_3$, 207.1021).

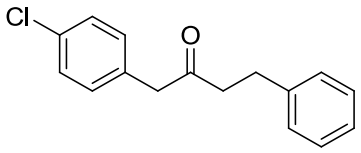


1-(*p*-Tolyl)pentan-2-one (212o).[286] Following the general procedure described for the synthesis of ketone **191a**, Weinreb amide **210k** (402.6 mg, 2.08 mmol, 1 equiv.) was used to react with propylmagnesium chloride (**190b**) (2.0 M in Et_2O) (5 mL, 10.0 mmol, 4.8 equiv.) in THF (6 mL) for 2 h to yield ketone **212o** as a light yellow oil (241.0 mg, 1.37 mmol, 66%). Eluent system of Et_2O–hexane (1:4) was used in

centrifugal radial TLC purification. R_f = 0.63 (Et_2O–hexane, 3:1); IR (neat) ν_{max} 2962, 2932, 1710, 1514, 1457, 1411, 1365, 1187, 1122, 1047 cm^{-1}; ^1H NMR ($CDCl_3$, 700 MHz) δ 7.16 – 7.06 (m, 4H), 3.62 (s, 2H), 2.41 (t, *J* = 7.3 Hz, 2H), 2.33 (s, 3H), 1.57 (h, *J* = 7.4 Hz, 2H), 0.86 (t, *J* = 7.5 Hz, 3H); ^{13}C NMR ($CDCl_3$, 175 MHz) δ 208.8, 136.5, 131.3, 129.4, 129.2, 49.8, 43.8, 21.1, 17.2, 13.7; HRESIMS *m/z* 177.1279 $[M + H]^+$ (calcd for $C_{12}H_{17}O_1$, 177.1279). The spectroscopic data are in good agreement with those reported in the literature.[286]

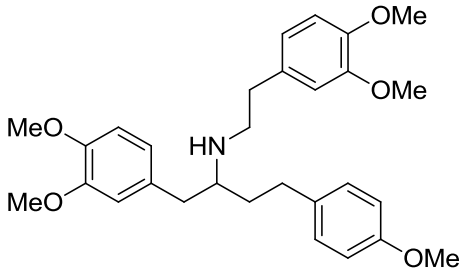


1-(4-Chlorophenyl)pentan-2-one (212p).[287] Small portion (about 10%) of 1-bromopropane (0.9 mL, 9.91 mmol, 1 equiv.) in THF (5 mL) was added to Mg turnings (507.6 mg, 20.9 mmol, 2.1 equiv.) in THF (2 mL). The remaining portion of the bromide was added dropwise into the stirring reaction mixture at room temperature. The resulting mixture was heated and stirred for 5 min before left to cool to room temperature to afford propylmagnesium bromide (**211b**). Following the general procedure described for the synthesis of ketone **191a**, Weinreb amide **210n** (543.7 mg, 2.54 mmol, 0.3 equiv.) was used to react with **211b** prepared earlier in THF (10 mL) for 2 h to yield ketone **212p** as a yellow oil (230.5 mg, 1.17 mmol, 46%). Eluent system of Et_2O–hexane (1:5) was used in centrifugal radial TLC purification. R_f = 0.69 (Et_2O–hexane, 3:1); IR (neat) ν_{max} 2948, 1714, 1334, 1086 cm^{-1}; ^1H NMR ($CDCl_3$, 700 MHz) δ 7.32 – 7.28 (m, 2H), 7.19 – 7.09 (m, 2H), 3.65 (s, 2H), 2.43 (t, *J* = 7.3 Hz, 2H), 1.59 (h, *J* = 7.4 Hz, 2H), 0.88 (t, *J* = 7.4 Hz, 3H); ^{13}C NMR ($CDCl_3$, 175 MHz) δ 207.9, 132.9, 132.7, 130.8, 128.8, 49.2, 44.1, 17.2, 13.6; HRESIMS *m/z* 197.0726 $[M + H]^+$ (calcd for $C_{11}H_{14}{}^{35}Cl_1O_1$, 197.0733). The spectroscopic data are in good agreement with those reported in the literature.[287]



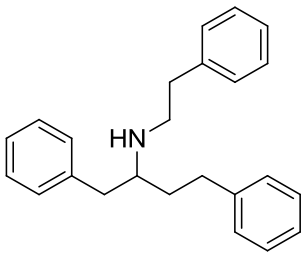
1-(4-Chlorophenyl)-4-phenylbutan-2-one (212q). Following the method to prepare ketone **191a**, Weinreb amide **210n** (382.1 mg, 1.79 mmol, 1 equiv.) was used to react with phenethylmagnesium chloride (**190a**) (1.0 M in THF) (8 mL, 8.0 mmol, 4.5 equiv.) in THF (5 mL) for 2 h to yield ketone **212q** as a yellow amorphous solid (146.5 mg, 0.57 mmol, 32%). Eluent system of Et_2O–hexane (1:4) was used in centrifugal radial TLC purification. R_f = 0.67 (Et_2O–hexane, 3:1); IR (neat) ν_{max} 3028, 2931, 1710, 1490, 1453, 1410, 1358, 1324, 1076, 1014 cm^{-1}; ^1H NMR ($CDCl_3$, 700 MHz) δ 7.34 – 7.03 (m, 9H), 3.63 (s, 2H), 2.87 (t, *J* = 7.5 Hz, 2H), 2.77 (t, *J* = 7.6 Hz, 2H); ^{13}C NMR ($CDCl_3$, 175 MHz) δ 206.8, 140.7, 133.0, 132.4, 130.7, 128.8, 128.5, 128.3, 126.2, 49.5, 43.6, 29.8; HRESIMS *m/z* 259.0894 $[M + H]^+$ (calcd for $C_{16}H_{16}{}^{35}Cl_1O_1$, 259.0890).

6.1.3.4 Reductive amination



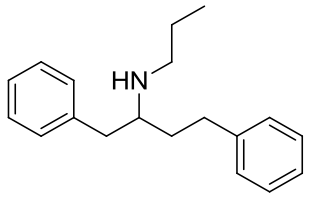
***N*-(3,4-Dimethoxyphenethyl)-1-(3,4-dimethoxy-phenyl)-4-(4-methoxy-phenyl)-butan-2-amine (215a).** To a stirring solution of ketone **191d** (207.3 mg, 0.66 mmol, 1 equiv.) in $ClCH_2CH_2Cl$ (5 mL) was added DMPEA (**176**) (133.6 mg, 0.74 mmol, 1.1 equiv.), $NaBH(OAc)_3$ (224.4 mg, 1.06 mmol, 1.6 equiv.) and AcOH (0.04 mL, 0.70 mmol, 1.1 equiv.). The solution was stirred at room temperature for 22.5 h before addition of 1

M NaOH solution (9 mL). The mixture was then extracted with EtOAc (3 X 10 mL). The combined organic layer was washed with brine (10 mL) and subsequently dried with Na_2SO_4 before concentrated *in vacuo*. The crude product was purified by centrifugal radial TLC using an eluent system of Et_2O–hexane (1:3) to yield **215a** as an orange oil (151.1 mg, 0.32 mmol, 48%). R_f = 0.07 (Et_2O–hexane, 9:1); IR (neat) ν_{max} 3310, 3002, 2936, 2836, 1732, 1610, 1590, 1520, 1456, 1259, 1156, 1141, 1030 cm^{-1}; ^1H NMR ($CDCl_3$, 600 MHz) δ 7.08 – 7.03 (m, 2H), 6.83 – 6.77 (m, 2H), 6.72 (dd, *J* = 8.1, 1.7 Hz, 2H), 6.66 – 6.58 (m, 4H), 3.86 (s, 3H), 3.85 (s, 3H), 3.82 (s, 3H), 3.82 (s, 3H), 3.77 (s, 3H), 3.03 – 2.53 (m, 9H), 1.82 (d, *J* = 42.0 Hz, 2H); ^{13}C NMR ($CDCl_3$, 150 MHz) δ 157.8, 149.0, 148.9, 147.6, 147.6, 133.7, 131.4, 130.9, 129.2, 121.1, 120.5, 113.8, 112.2, 111.8, 111.2, 111.2, 58.9, 55.9, 55.8, 55.3, 48.1, 39.5, 34.9, 34.79, 30.9; HRESIMS *m/z* 480.2753 $[M + H]^+$ (calcd for $C_{29}H_{38}N_1O_5$, 480.2750).

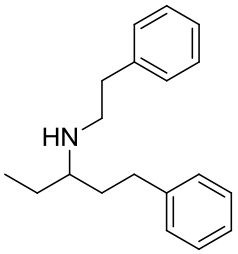


***N*-Phenethyl-1,4-diphenyl-butan-2-amine (215b).** Following the method to prepare amine **215a**, PEA (**213a**) (0.32 mL, 2.60 mmol, 1.1 equiv.), $NaBH(OAc)_3$ (815.9 mg, 3.85 mmol, 1.6 equiv.) and AcOH (0.14 mL, 2.45 mmol, 1 equiv.) were used to react with ketone **191a** (537.0 mg, 2.39 mmol, 1 equiv.) in $ClCH_2CH_2Cl$ (15 mL) for 23.5 h to afford amine **215b** as a light yellow oil (654.1 mg, 1.99 mmol, 83%). Eluent system of Et_2O–hexane (1:3) was used in centrifugal radial TLC purification. R_f = 0.64 (Et_2O–hexane, 7:1); IR (neat) ν_{max} 3314, 3062, 3026, 2925, 2855, 1602, 1495, 1454, 1121, 1030 cm^{-1}; ^1H NMR ($CDCl_3$, 600 MHz) δ 7.29 – 7.20 (m, 6H), 7.20 – 7.14 (m, 3H), 7.14 – 7.05 (m, 6H), 2.93 – 2.58 (m, 9H), 1.77 – 1.68 (m, 2H); ^{13}C NMR ($CDCl_3$,

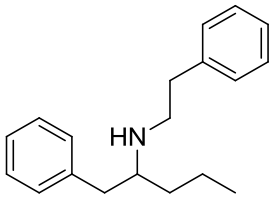
150 MHz) δ 142.3, 139.9, 139.2, 129.2, 128.6, 128.4, 128.4, 128.3, 126.1, 125.7, 58.5, 48.2, 40.5, 36.4, 35.3, 32.0; HRESIMS *m/z* 330.2240 $[M + H]^+$ (calcd for $C_{24}H_{28}N_1$, 330.2222).



1,4-Diphenyl-*N*-propylbutan-2-amine (215c). Following the method to prepare amine **215a**, propylamine (**213b**) (0.09 mL, 1.09 mmol, 1.2 equiv.), $NaBH(OAc)_3$ (304.5 mg, 1.44 mmol, 1.6 equiv.) and AcOH (0.06 mL, 1.05 mmol, 1.2 equiv.) were used to react with ketone **191a** (197.4 mg, 0.88 mmol, 1 equiv.) in $ClCH_2CH_2Cl$ (5 mL) for 23.5 h to afford amine **215c** as a light yellow oil (114.9 mg, 0.43 mmol, 49%). Eluent system of Et_2O-–hexane (1:4) was used in centrifugal radial TLC purification. R_f = 0.5 (Et_2O–hexane, 9:1); IR (neat) ν_{max} 3319, 3026, 2930, 1602, 1495, 1453, 1122, 1030 cm^{-1}; ^1H NMR ($CDCl_3$, 600 MHz) δ 7.31 – 7.14 (m, 10H), 2.85 – 2.75 (m, 2H), 2.75 – 2.65 (m, 3H), 2.58 (ddd, *J* = 11.1, 8.0, 6.4 Hz, 1H), 2.50 (ddd, *J* = 11.1, 7.8, 6.4 Hz, 1H), 1.79 – 1.68 (m, 2H), 1.46 – 1.34 (m, 2H), 0.84 (t, *J* = 7.4 Hz, 3H); ^{13}C NMR ($CDCl_3$, 150 MHz) δ 142.5, 139.5, 129.3, 128.4, 128.3, 128.3, 126.1, 125.7, 58.6, 48.9, 40.7, 35.5, 32.1, 23.4, 11.8; HRESIMS *m/z* 268.2062 $[M + H]^+$ (calcd for $C_{19}H_{26}N_1$, 268.2065).

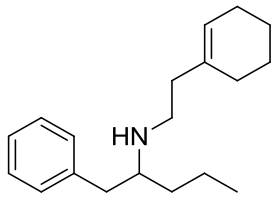


***N*-Phenethyl-1-phenylpentan-3-amine (215d).** Following the method to prepare amine **215a**, PEA (**213a**) (0.17 mL, 1.38 mmol, 1.1 equiv.), $NaBH(OAc)_3$ (431.8 mg, 2.04 mmol, 1.6 equiv.) and AcOH (0.075 mL, 1.31 mmol, 1 equiv.) were used to react with ketone **212a** (206.3 mg, 1.27 mmol, 1 equiv.) in $ClCH_2CH_2Cl$ (5 mL) for 22 h to afford amine **215d** as a yellow oil (245.6 mg, 0.92 mmol, 72%). Eluent system of Et_2O–hexane (1:5) was used in centrifugal radial TLC purification. R_f = 0.58 (Et_2O–hexane, 9:1); IR (neat) ν_{max} 3326, 3026, 2930, 1603, 1495, 1454, 1139, 1030 cm^{-1}; ^1H NMR ($CDCl_3$, 600 MHz) δ 7.33 – 7.09 (m, 10H), 2.90 – 2.79 (m, 2H), 2.79 – 2.72 (m, 2H), 2.60 – 2.50 (m, 2H), 2.50 – 2.42 (m, 1H), 1.72 – 1.63 (m, 2H), 1.49 – 1.41 (m, 2H), 0.86 – 0.81 (m, 3H); ^{13}C NMR ($CDCl_3$, 150 MHz) δ 142.6, 140.2, 128.7, 128.4, 128.3, 126.1, 125.7, 58.2, 48.2, 36.7, 35.2, 32.0, 26.3, 9.8; HRESIMS *m/z* 268.2057 $[M + H]^+$ (calcd for $C_{19}H_{26}N_1$, 268.2065).

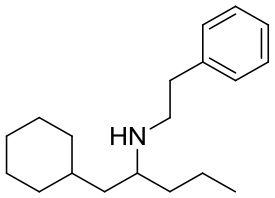


***N*-Phenethyl-1-phenylpentan-2-amine (215e).** Following the method to prepare amine **215a**, PEA (**213a**) (0.11 mL, 0.89 mmol, 1.1 equiv.), $NaBH(OAc)_3$ (272.1 mg, 1.28 mmol, 1.6 equiv.) and AcOH (0.05 mL, 0.87 mmol, 1.1 equiv.) were used to react with ketone **191b** (130.1 mg, 0.80 mmol, 1 equiv.) in $ClCH_2CH_2Cl$ (4 mL) for 18 h to afford amine **215e** as a yellow oil (56.2 mg, 0.21 mmol, 26%). Eluent system

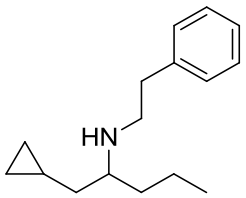
of Et_2O–hexane (1:4) was used in centrifugal radial TLC purification. R_f = 0.59 (Et_2O–hexane, 9:1); IR (neat) ν_{max} 3326, 3026, 2956, 2930, 1603, 1496, 1454, 1139, 1030 cm^{-1}; ^1H NMR ($CDCl_3$, 600 MHz) δ 7.27 – 7.21 (m, 4H), 7.20 – 7.15 (m, 2H), 7.13 – 7.08 (m, 4H), 2.95 – 2.86 (m, 1H), 2.86 – 2.79 (m, 1H), 2.79 – 2.60 (m, 5H), 1.46 – 1.39 (m, 1H), 1.39 – 1.27 (m, 3H), 0.88 (t, *J* = 6.8 Hz, 3H); ^{13}C NMR ($CDCl_3$, 150 MHz) δ 139.8, 139.4, 129.2, 128.6, 128.4, 128.4, 126.1, 126.1, 59.0, 48.2, 40.5, 36.2, 35.9, 19.0, 14.3; HRESIMS *m/z* 268.2048 $[M + H]^+$ (calcd for $C_{19}H_{26}N_1$, 268.2065).



***N*-(2-(Cyclohex-1-en-1-yl)ethyl)-1-phenylpentan-2-amine (215f).** Following the method to prepare amine **215a**, 2-(1-cyclohexenyl)ethylamine (**213c**) (132.3 mg, 1.06 mmol, 1.3 equiv.), $NaBH(OAc)_3$ (271.0 mg, 1.28 mmol, 1.6 equiv.) and AcOH (0.05 mL, 0.87 mmol, 1.1 equiv.) were used to react with ketone **191b** (127.8 mg, 0.79 mmol, 1 equiv.) in $ClCH_2CH_2Cl$ (6 mL) for 22.5 h to afford amine **215f** as a yellow oil (52.4 mg, 0.19 mmol, 24%). Eluent system of Et_2O–hexane (1:4) was used in centrifugal radial TLC purification. R_f = 0.5 (Et_2O–hexane, 3:1); IR (neat) ν_{max} 3315, 2923, 1454, 1136 cm^{-1}; ^1H NMR ($CDCl_3$, 700 MHz) δ 7.31 – 7.16 (m, 5H), 5.33 (tt, *J* = 3.6, 1.6 Hz, 1H), 2.81 – 2.61 (m, 5H), 2.57 (dt, *J* = 11.2, 7.0 Hz, 1H), 2.08 (t, *J* = 6.8 Hz, 2H), 1.90 – 1.85 (m, 2H), 1.83 – 1.72 (m, 2H), 1.58 – 1.30 (m, 7H), 0.92 (t, *J* = 7.1 Hz, 3H); ^{13}C NMR ($CDCl_3$, 175 MHz) δ 139.6, 134.9, 129.3, 128.4, 126.2, 123.2, 59.4, 44.5, 40.8, 37.9, 36.0, 27.8, 25.2, 22.8, 22.3, 19.1, 14.3; HRESIMS *m/z* 272.2390 $[M + H]^+$ (calcd for $C_{19}H_{30}N_1$, 272.2378).

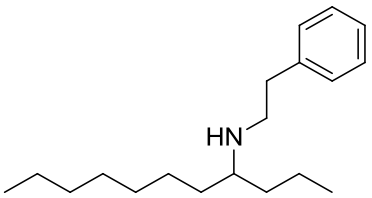


1-Cyclohexyl-*N*-phenethylpentan-2-amine (215g). Following the method to prepare amine **215a**, PEA (**213a**) (0.16 mL, 1.30 mmol, 1.1 equiv.), $NaBH(OAc)_3$ (411.0 mg, 1.94 mmol, 1.6 equiv.) and AcOH (0.07 mL, 1.22 mmol, 1 equiv.) were used to react with ketone **212b** (201.9 mg, 1.20 mmol, 1 equiv.) in $ClCH_2CH_2Cl$ (10 mL) for 23 h to afford amine **215g** as a yellow oil (193.9 mg, 0.71 mmol, 59%). Eluent system of Et_2O–hexane (1:9) was used in centrifugal radial TLC purification. R_f = 0.48 (Et_2O–hexane, 1:3); IR (neat) ν_{max} 3341, 2918, 2848, 1450, 1105 cm^{-1}; ^1H NMR ($CDCl_3$, 400 MHz) δ 7.33 – 7.13 (m, 5H), 2.93 – 2.72 (m, 4H), 2.53 (p, *J* = 5.8 Hz, 1H), 1.70 – 1.56 (m, 5H), 1.44 – 1.06 (m, 10H), 0.88 (t, *J* = 7.1 Hz, 3H), 0.84 – 0.75 (m, 2H); ^{13}C NMR ($CDCl_3$, 175 MHz) δ 140.1, 128.7, 128.4, 126.2, 54.6, 48.3, 42.4, 36.7, 36.4, 34.4, 33.9, 33.5, 26.6, 26.3, 26.3, 18.8, 14.4; HRESIMS *m/z* 274.2526 $[M + H]^+$ (calcd for $C_{19}H_{32}N_1$, 274.2535).

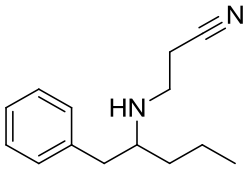


1-Cyclopropyl-*N*-phenethylpentan-2-amine (215h). Following the method to prepare amine **215a**, PEA (**213a**) (0.12 mL, 0.98 mmol, 1.2 equiv.), $NaBH(OAc)_3$ (273.6 mg, 1.29 mmol, 1.6 equiv.) and AcOH (0.05 mL, 0.87 mmol, 1 equiv.) were used to react with ketone **212c** (105.0 mg, 0.83 mmol, 1 equiv.) in $ClCH_2CH_2Cl$ (10 mL) for 24 h to afford amine **215h** as a yellow oil (132.6 mg, 0.57 mmol, 69%).

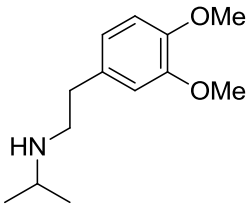
Eluent system of Et_2O–hexane (1:3) was used in centrifugal radial TLC purification. R_f = 0.27 (Et_2O–hexane, 1:3); IR (neat) ν_{max} 3339, 2956, 2920, 2870, 1455, 1105, 1015 cm^{-1}; ^1H NMR ($CDCl_3$, 400 MHz) δ 7.34 – 7.15 (m, 5H), 2.93 – 2.72 (m, 3H), 2.57 (p, *J* = 6.0 Hz, 1H), 1.59 – 1.12 (m, 6H), 0.89 (t, *J* = 7.2 Hz, 3H), 0.64 – 0.49 (m, 1H), 0.40 – 0.31 (m, 2H), 0.03 – -0.06 (m, 3H); ^{13}C NMR ($CDCl_3$, 100 MHz) δ 140.2, 128.7, 128.4, 126.1, 58.2, 48.6, 39.1, 36.6, 36.5, 19.0, 14.4, 7.8, 4.7, 4.0; HRESIMS *m/z* 232.2069 $[M + H]^+$ (calcd for $C_{16}H_{26}N_1$, 232.2065).



***N*-Phenethylundecan-4-amine (215i).** Following the method to prepare amine **215a**, PEA (**213a**) (0.08 mL, 0.65 mmol, 1.1 equiv.), $NaBH(OAc)_3$ (209.2 mg, 0.99 mmol, 1.6 equiv.) and AcOH (0.04 mL, 0.70 mmol, 1.1 equiv.) were used to react with 4-undecanone (**212r**) (104.6 mg, 0.61 mmol, 1 equiv.) in $ClCH_2CH_2Cl$ (8 mL) for 22 h to afford amine **215i** as a yellow oil (121.3 mg, 0.44 mmol, 72%). Eluent system of Et_2O–hexane (1:1) was used in centrifugal radial TLC purification. R_f = 0.57 (Et_2O–hexane, 4:1); IR (neat) ν_{max} 3328, 2922, 1462, 1358, 1116 cm^{-1}; ^1H NMR ($CDCl_3$, 400 MHz) δ 7.34 – 7.14 (m, 5H), 2.93 – 2.73 (m, 4H), 2.46 (p, *J* = 5.9 Hz, 1H), 1.49 – 1.09 (m, 16H), 0.94 – 0.82 (m, 6H); ^{13}C NMR ($CDCl_3$, 100 MHz) δ 140.2, 128.7, 128.4, 126.1, 57.3, 48.5, 36.6, 36.4, 34.0, 31.9, 29.9, 29.3, 25.7, 22.7, 18.9, 14.4, 14.1; HRESIMS *m/z* 276.2697 $[M + H]^+$ (calcd for $C_{19}H_{34}N_1$, 276.2691).

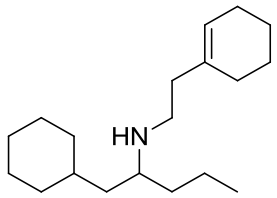


3-((1-Phenylpentan-2-yl)amino)propanenitrile (215j). Following the method to prepare amine **215a**, 3-amino-propionitrile (**213d**) (63.5 mg, 0.91 mmol, 1.2 equiv.), $NaBH(OAc)_3$ (253.4 mg, 1.20 mmol, 1.6 equiv.) and AcOH (0.05 mL, 0.87 mmol, 1.2 equiv.) were used to react with ketone **191b** (120.5 mg, 0.74 mmol, 1 equiv.) in $ClCH_2CH_2Cl$ (5 mL) for 23 h to afford amine **215j** as a yellow oil (92.8 mg, 0.43 mmol, 58%). Eluent system of Et_2O–hexane (1:5) was used in centrifugal radial TLC purification. R_f = 0.43 (Et_2O–hexane, 3:1); IR (neat) ν_{max} 3333, 2955, 2927, 2865, 2248, 1602, 1456, 1134 cm^{-1}; ^1H NMR ($CDCl_3$, 600 MHz) δ 7.33 – 7.15 (m, 5H), 2.92 – 2.81 (m, 2H), 2.78 (dq, *J* = 7.2, 5.5 Hz, 1H), 2.73 (dd, *J* = 13.4, 5.6 Hz, 1H), 2.62 (dd, *J* = 13.4, 7.3 Hz, 1H), 2.44 – 2.30 (m, 2H), 1.53 – 1.29 (m, 4H), 0.91 (t, *J* = 7.0 Hz, 3H); ^{13}C NMR ($CDCl_3$, 150 MHz) δ 139.2, 129.2, 128.5, 126.3, 118.7, 58.5, 42.6, 41.0, 36.4, 19.2, 19.0, 14.2; HRESIMS *m/z* 217.17107 $[M + H]^+$ (calcd for $C_{14}H_{21}N_2$, 217.17047).

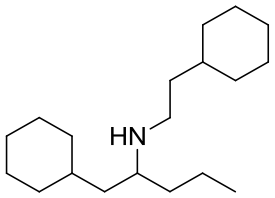


2-(3,4-Dimethoxyphenyl)-1-(isopropylamino)ethane (215k).[288] Following the method to prepare amine **215a**, DMPEA (**176**) (401.8 mg, 2.22 mmol, 1 equiv.), $NaBH(OAc)_3$ (751.8 mg, 3.55 mmol, 1.6 equiv.) and AcOH (0.14 mL, 2.45 mmol, 1.1 equiv.) were used to react with acetone (**212s**) (0.25 mL, 3.40 mmol, 1.5 equiv.) in $ClCH_2CH_2Cl$ (5 mL) for 24 h to afford amine **215k** as an amorphous white solid (21.5

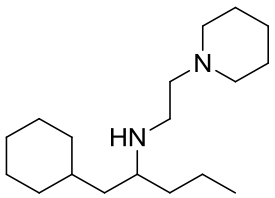
mg, 0.10 mmol, 5%). Eluent system of 5% MeOH–EtOAc was used in centrifugal radial TLC purification. R_f = 0.09 (20% MeOH–EtOAc); IR (neat) ν_{max} 3302, 2962, 2836, 1591, 1514, 1450, 1260, 1236, 1141, 1027 cm^{-1}; ^1H NMR ($CDCl_3$, 600 MHz) δ 6.83 – 6.73 (m, 3H), 3.86 (s, 3H), 3.85 (s, 3H), 3.00 (s, 5H), 1.28 (dd, *J* = 5.5, 2.8 Hz, 6H); ^{13}C NMR ($CDCl_3$, 150 MHz) δ 149.1, 147.8, 130.8, 120.6, 112.0, 111.4, 55.9, 55.9, 49.7, 47.6, 33.9, 20.9; HRESIMS *m/z* 224.1661 $[M + H]^+$ (calcd for $C_{13}H_{22}N_1O_2$, 224.1651). The spectroscopic data are in good agreement with those reported in the literature.[288]



***N*-(2-(Cyclohex-1-en-1-yl)ethyl)-1-cyclohexylpentan-2-amine (215l).** Following the method to prepare amine **215a**, 2-(1-cyclohexenyl)ethylamine (**213c**) (89.8 mg, 0.72 mmol, 1.2 equiv.), $NaBH(OAc)_3$ (205.0 mg, 0.97 mmol, 1.6 equiv.) and AcOH (0.03 mL, 0.53 mmol, 0.9 equiv.) were used to react with ketone **212b** (102.9 mg, 0.61 mmol, 1 equiv.) in $ClCH_2CH_2Cl$ (8 mL) for 22 h to afford amine **215l** as a yellow oil (38.3 mg, 0.14 mmol, 23%). Eluent system of EtOAc–hexane (1:2) was used in centrifugal radial TLC purification. R_f = 0.39 (EtOAc–hexane, 1:1); IR (neat) ν_{max} 3320, 2910, 1456, 1120 cm^{-1}; ^1H NMR ($CDCl_3$, 400 MHz) δ 5.49 (tt, *J* = 3.5, 1.7 Hz, 1H), 2.79 – 2.44 (m, 3H), 2.12 (t, *J* = 6.8 Hz, 2H), 2.04 – 1.88 (m, 5H), 1.75 – 1.49 (m, 10H), 1.45 – 1.08 (m, 10H), 0.91 (t, *J* = 7.0 Hz, 3H); ^{13}C NMR ($CDCl_3$, 100 MHz) δ 135.5, 123.1, 54.7, 44.5, 42.6, 38.4, 36.9, 34.5, 34.0, 33.5, 28.0, 26.7, 26.4, 26.4, 25.3, 23.0, 22.5, 18.9, 14.4; HRESIMS *m/z* 278.2838 $[M + H]^+$ (calcd for $C_{19}H_{36}N_1$, 278.2848).

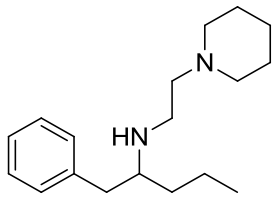


1-Cyclohexyl-*N*-(2-cyclohexylethyl)pentan-2-amine (215m). Following the method to prepare amine **215a**, 2-cyclohexyl-ethylamine (**213e**) (94.8 mg, 0.75 mmol, 2 equiv.), $NaBH(OAc)_3$ (311.4 mg, 1.47 mmol, 4 equiv.) and AcOH (0.04 mL, 0.70 mmol, 1.9 equiv.) were used to react with ketone **212b** (61.7 mg, 0.37 mmol, 1 equiv.) in $ClCH_2CH_2Cl$ (5 mL) for 47 h to afford amine **215m** as a light yellow oil (14.3 mg, 0.05 mmol, 14%). Eluent system of EtOAc–hexane (1:6) was used in centrifugal radial TLC purification. R_f = 0.30 (EtOAc–hexane, 5:1); IR (neat) ν_{max} 3333, 2919, 2850, 1448, 1108 cm^{-1}; ^1H NMR ($CDCl_3$, 400 MHz) δ 2.70 – 2.49 (m, 3H), 1.75 – 1.61 (m, 9H), 1.50 – 1.07 (m, 17H), 1.00 – 0.79 (m, 7H); ^{13}C NMR ($CDCl_3$, 100 MHz) δ 54.6, 44.5, 42.4, 37.8, 36.7, 35.8, 34.6, 33.9, 33.7, 33.5, 33.4, 26.7, 26.6, 26.4, 26.4, 18.9, 14.4; HRESIMS *m/z* 280.2994 $[M + H]^+$ (calcd for $C_{19}H_{38}N_1$, 280.3004).

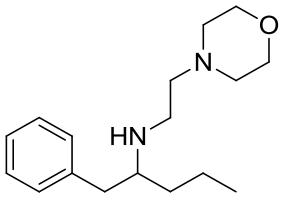


1-Cyclohexyl-*N*-(2-(piperidin-1-yl)ethyl)pentan-2-amine (215n). Following the method to prepare amine **215a**, 1-(2-aminoethyl)piperidine (**213f**) (98.9 mg, 0.77 mmol, 1.1 equiv.), $NaBH(OAc)_3$ (247.5 mg, 1.17 mmol, 1.6 equiv.) and AcOH (0.04 mL, 0.70 mmol, 1 equiv.) were used to react with ketone **212b** (120.0 mg, 0.71 mmol, 1 equiv.) in $ClCH_2CH_2Cl$ (8 mL) for 24 h to afford amine **215n** as a yellow oil (128.3 mg, 0.46 mmol, 65%). Eluent system of Et_2O–hexane (1:3) was used in centrifugal

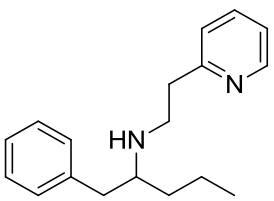
radial TLC purification. R_f = 0.17 (Et_2O–hexane, 1:3); IR (neat) ν_{max} 3326, 2920, 2850, 2803, 1447, 1120, 1042 cm^{-1}; ^1H NMR ($CDCl_3$, 400 MHz) δ 2.72 – 2.56 (m, 2H), 2.56 – 2.44 (m, 1H), 2.41 (td, *J* = 6.2, 3.4 Hz, 2H), 2.38 – 2.30 (m, 4H), 1.78 – 1.60 (m, 5H), 1.56 (p, *J* = 5.6 Hz, 4H), 1.48 – 1.08 (m, 11H), 0.98 – 0.78 (m, 6H); ^{13}C NMR ($CDCl_3$, 100 MHz) δ 58.6, 54.8, 54.6, 43.9, 42.7, 37.1, 34.5, 34.1, 33.4, 26.7, 26.5, 26.4, 26.2, 24.6, 18.9, 14.4; HRESIMS *m/z* 281.2948 $[M + H]^+$ (calcd for $C_{18}H_{37}N_2$, 281.2957).



1-Phenyl-*N*-(2-(piperidin-1-yl)ethyl)pentan-2-amine (215o). Following the method to prepare amine **215a**, 1-(2-aminoethyl)piperidine (**213f**) (143.8 mg, 1.12 mmol, 1.1 equiv.), $NaBH(OAc)_3$ (336.7 mg, 1.59 mmol, 1.6 equiv.) and AcOH (0.07 mL, 1.22 mmol, 1.2 equiv.) were used to react with ketone **191b** (160.0 mg, 0.99 mmol, 1 equiv.) in $ClCH_2CH_2Cl$ (5 mL) for 24 h to afford amine **215o** as a light yellow oil (82.2 mg, 0.30 mmol, 30%). Eluent system of Et_2O–hexane (4:1) was used in centrifugal radial TLC purification. R_f = 0.23 (Et_2O–hexane, 9:1); IR (neat) ν_{max} 3301, 2931, 2854, 2802, 1453, 1154, 1118, 1041 cm^{-1}; ^1H NMR ($CDCl_3$, 700 MHz) δ 7.31 – 7.27 (m, 2H), 7.23 – 7.17 (m, 3H), 2.79 – 2.66 (m, 4H), 2.61 (dt, *J* = 11.5, 6.4 Hz, 1H), 2.44 – 2.18 (m, 8H), 1.52 – 1.31 (m, 8H), 0.91 (t, *J* = 7.0 Hz, 3H); ^{13}C NMR ($CDCl_3$, 175 MHz) δ 139.6, 129.3, 128.4, 126.1, 59.7, 58.0, 54.4, 43.9, 40.8, 36.0, 25.9, 24.4, 19.1, 14.3; HRESIMS *m/z* 275.2486 $[M + H]^+$ (calcd for $C_{18}H_{31}N_2$, 275.2487).

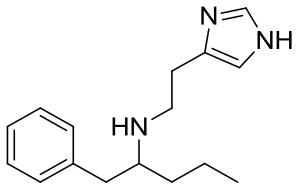


***N*-(2-Morpholinoethyl)-1-phenylpentan-2-amine (215p).** Following the method to prepare amine **215a**, 4-(2-aminoethyl)morpholine (**213g**) (138.9 mg, 1.07 mmol, 1.1 equiv.), $NaBH(OAc)_3$ (325.8 mg, 1.54 mmol, 1.6 equiv.) and AcOH (0.06 mL, 1.05 mmol, 1.1 equiv.) were used to react with ketone **191b** (155.3 mg, 0.96 mmol, 1 equiv.) in $ClCH_2CH_2Cl$ (5 mL) for 25.5 h to afford amine **215p** as a light yellow oil (89.2 mg, 0.32 mmol, 33%). Eluent system of Et_2O–hexane (5:1) was used in centrifugal radial TLC purification. R_f = 0.18 (Et_2O–hexane, 9:1); IR (neat) ν_{max} 3305, 2955, 2930, 2855, 2807, 1454, 1296, 1272, 1116, 1022 cm^{-1}; ^1H NMR ($CDCl_3$, 700 MHz) δ 7.31 – 7.28 (m, 2H), 7.24 – 7.19 (m, 3H), 3.56 – 3.41 (m, 4H), 2.80 (dd, *J* = 13.5, 5.1 Hz, 1H), 2.76 – 2.69 (m, 2H), 2.63 (dd, *J* = 13.4, 8.3 Hz, 1H), 2.55 (ddd, *J* = 11.7, 7.8, 5.0 Hz, 1H), 2.46 (ddd, *J* = 12.7, 7.8, 5.1 Hz, 1H), 2.37 (dt, *J* = 12.4, 5.3 Hz, 1H), 2.33 – 2.20 (m, 4H), 1.55 – 1.46 (m, 1H), 1.46 – 1.36 (m, 3H), 0.93 (t, *J* = 7.1 Hz, 3H); ^{13}C NMR ($CDCl_3$, 175 MHz) δ 139.6, 129.3, 128.5, 126.2, 66.9, 59.8, 57.6, 53.3, 43.5, 40.9, 36.3, 19.1, 14.3; HRESIMS *m/z* 277.2273 $[M + H]^+$ (calcd for $C_{17}H_{29}N_2O_1$, 277.2280).



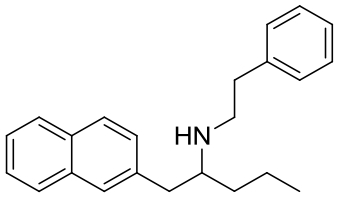
1-Phenyl-*N*-(2-(pyridine-2-yl)ethyl)pentan-2-amine (215q). Following the method to prepare amine **215a**, 2-(2-pyridyl)ethylamine (**213h**) (122.5 mg, 1.00 mmol, 1.1

equiv.), $NaBH(OAc)_3$ (315.1 mg, 1.48 mmol, 1.6 equiv.) and AcOH (0.06 mL, 1.05 mmol, 1.1 equiv.) were used to react with ketone **191b** (148.1 mg, 0.91 mmol, 1 equiv.) in $ClCH_2CH_2Cl$ (5 mL) for 25.5 h to afford amine **215q** as an orange oil (87.9 mg, 0.33 mmol, 36%). Eluent system of Et_2O–hexane (4:1) was used in centrifugal radial TLC purification. R_f = 0.2 (Et_2O–hexane, 9:1); IR (neat) ν_{max} 3314, 2955, 2927, 1591, 1435, 1140 cm^{-1}; ^1H NMR ($CDCl_3$, 700 MHz) δ 8.39 (d, *J* = 5.2 Hz, 1H), 7.53 (td, *J* = 7.6, 1.8 Hz, 1H), 7.26 – 7.23 (m, 2H), 7.22 – 7.17 (m, 1H), 7.16 – 7.12 (m, 2H), 7.11 – 7.04 (m, 2H), 3.08 (dt, *J* = 11.3, 6.7 Hz, 1H), 3.02 – 2.95 (m, 1H), 2.93 (t, *J* = 6.8 Hz, 2H), 2.81 (dq, *J* = 7.9, 5.8 Hz, 1H), 2.75 (dd, *J* = 13.6, 5.6 Hz, 1H), 2.69 (dd, *J* = 13.6, 7.6 Hz, 1H), 1.51 – 1.44 (m, 1H), 1.44 – 1.33 (m, 3H), 0.89 (t, *J* = 7.1 Hz, 3H); ^{13}C NMR ($CDCl_3$, 175 MHz) δ 160.0, 149.1, 139.3, 136.4, 129.3, 128.4, 126.1, 123.2, 121.2, 59.1, 46.4, 40.4, 37.9, 35.7, 19.0, 14.2; HRESIMS *m/z* 269.2010 $[M + H]^+$ (calcd for $C_{18}H_{25}N_2$, 269.2018).

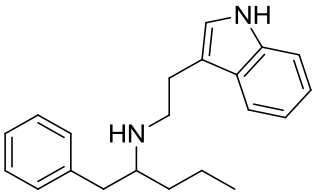


***N*-(2-(1*H*-Imidazol-4-yl)ethyl)-1-phenylpentan-2-amine (215r).** Following the method to prepare amine **215a**, histamine (**213i**) (82.3 mg, 0.74 mmol, 1.2 equiv.), $NaBH(OAc)_3$ (213.6 mg, 1.01 mmol, 1.6 equiv.) and AcOH (0.04 mL, 0.70 mmol, 1.1 equiv.) were used to react with ketone **191b** (103.5 mg, 0.64 mmol, 1 equiv.) in $ClCH_2CH_2Cl$ (10 mL) for 26 h to afford amine **215r** as an orange oil (24.3 mg, 0.09 mmol, 14%). Eluent system of 10% MeOH–EtOAc was used in centrifugal radial TLC purification. R_f = 0.10 (10% MeOH–EtOAc); IR (neat) ν_{max} 3084, 2956, 2927, 2869, 1455, 1088 cm^{-1}; ^1H NMR ($CDCl_3$, 400 MHz) δ 7.36 – 7.14 (m, 6H), 6.66 (s,

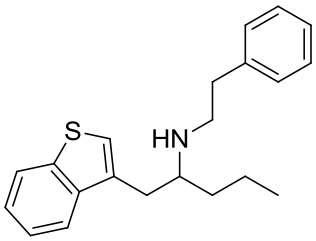
1H), 3.05 – 2.95 (m, 1H), 2.89 – 2.76 (m, 2H), 2.76 – 2.50 (m, 4H), 1.62 – 1.49 (m, 1H), 1.49 – 1.34 (m, 3H), 0.94 (t, J = 7.0 Hz, 3H); ^{13}C NMR ($CDCl_3$, 100 MHz) δ 139.9, 134.1, 134.1, 129.3, 128.6, 126.2, 120.6, 59.2, 46.2, 40.9, 36.0, 30.3, 18.9, 14.3; HRESIMS *m/z* 258.1960 $[M + H]^+$ (calcd for $C_{16}H_{24}N_3$, 258.1970).



1-(Naphthalen-2-yl)-*N*-phenethylpentan-2-amine (215s). Following the method to prepare amine **215a**, PEA (**213a**) (0.07 mL, 0.57 mmol, 1.2 equiv.), $NaBH(OAc)_3$ (173.4 mg, 0.82 mmol, 1.7 equiv.) and AcOH (0.03 mL, 0.52 mmol, 1.1 equiv.) were used to react with ketone **212d** (104.5 mg, 0.49 mmol, 1 equiv.) in $ClCH_2CH_2Cl$ (4 mL) for 23 h to afford amine **215s** as a yellow oil (108.8 mg, 0.34 mmol, 69%). Eluent system of Et_2O–hexane (1:3) was used in centrifugal radial TLC purification. R_f = 0.57 (Et_2O–hexane, 1:4); IR (neat) ν_{max} 3315, 3055, 3025, 2955, 2926, 2869, 1601, 1495, 1454, 1366, 1137 cm^{-1}; ^{1}H NMR ($CDCl_3$, 600 MHz) δ 7.79 (d, J = 7.8 Hz, 1H), 7.74 (d, J = 7.8 Hz, 1H), 7.72 (d, J = 8.3 Hz, 1H), 7.55 (s, 1H), 7.48 – 7.40 (m, 2H), 7.25 (d, J = 8.3 Hz, 1H), 7.13 – 7.00 (m, 5H), 2.96 – 2.74 (m, 5H), 2.74 – 2.63 (m, 2H), 1.54 – 1.43 (m, 1H), 1.43 – 1.26 (m, 3H), 0.89 (t, J = 6.9 Hz, 3H); ^{13}C NMR ($CDCl_3$, 150 MHz) δ 139.8, 137.1, 133.5, 132.1, 128.5, 128.3, 127.9, 127.6, 127.6, 127.6, 127.5, 126.0, 125.9, 125.2, 58.9, 48.5, 41.1, 36.4, 36.3, 19.0, 14.3; HRESIMS *m/z* 318.2218 $[M + H]^+$ (calcd for $C_{23}H_{28}N_1$, 318.2222).

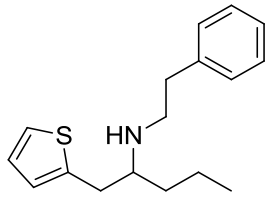


***N*-(2-(1*H*-Indol-3-yl)ethyl)-1-phenylpentan-2-amine (215t).** Following the method to prepare amine **215a**, tryptamine (**213j**) (121.0 mg, 0.76 mmol, 1.1 equiv.), $NaBH(OAc)_3$ (228.1 mg, 1.08 mmol, 1.6 equiv.) and AcOH (0.04 mL, 0.70 mmol, 1 equiv.) were used to react with ketone **191b** (108.0 mg, 0.67 mmol, 1 equiv.) in $ClCH_2CH_2Cl$ (4 mL) for 23 h to afford amine **215t** as a brown oil (34.0 mg, 0.11 mmol, 17%). Eluent system of Et_2O–hexane (4:1) was used in centrifugal radial TLC purification. R_f = 0.2 (Et_2O–hexane, 4:1); IR (neat) ν_{max} 3416, 3058, 3027, 2956, 2926, 2869, 1672, 1454, 1094 cm^{-1}; ^1H NMR ($CDCl_3$, 700 MHz) δ 8.02 (s, 1H), 7.57 (dd, *J* = 7.8, 1.1 Hz, 1H), 7.33 (dt, *J* = 8.1, 0.9 Hz, 1H), 7.21 – 7.12 (m, 3H), 7.10 (ddd, *J* = 7.9, 6.9, 1.0 Hz, 1H), 7.07 – 7.04 (m, 2H), 6.85 (d, *J* = 2.2 Hz, 1H), 3.05 – 2.98 (m, 1H), 2.98 – 2.90 (m, 3H), 2.84 – 2.78 (m, 1H), 2.74 (dd, *J* = 13.6, 5.8 Hz, 1H), 2.68 (dd, *J* = 13.6, 7.6 Hz, 1H), 1.52 – 1.44 (m, 1H), 1.44 – 1.29 (m, 3H), 0.86 (t, *J* = 7.2 Hz, 3H); ^{13}C NMR ($CDCl_3$, 175 MHz) δ 139.1, 136.3, 129.2, 128.3, 127.3, 126.1, 122.1, 122.0, 119.3, 118.8, 113.3, 111.1, 59.1, 46.7, 40.2, 35.7, 25.3, 19.0, 14.2; HRESIMS *m/z* 307.2169 $[M + H]^+$ (calcd for $C_{21}H_{27}N_2$, 307.2174).



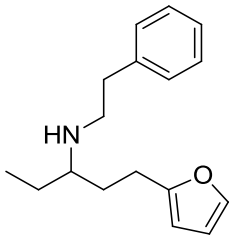
1-(Benzo[*b*]thiophen-3-yl)-*N*-phenethylpentan-2-amine (215u). Following the method to prepare amine **215a**, PEA (**213a**) (0.05 mL, 0.41 mmol, 1.5 equiv.),

$NaBH(OAc)_3$ (118.8 mg, 0.56 mmol, 2 equiv.) and AcOH (0.02 mL, 0.35 mmol, 1.3 equiv.) were used to react with ketone **212e** (61.2 mg, 0.28 mmol, 1 equiv.) in $ClCH_2CH_2Cl$ (5 mL) for 24 h to afford amine **215u** as a yellow oil (60.9 mg, 0.19 mmol, 68%). Eluent system of Et_2O–hexane (1:4) was used in centrifugal radial TLC purification. R_f = 0.41 (Et_2O–hexane, 4:1); IR (neat) ν_{max} 3314, 3063, 3026, 2955, 2926, 2868, 1455, 1427, 1138, 1080, 1020 cm^{-1}; ^1H NMR ($CDCl_3$, 400 MHz) δ 7.87 – 7.82 (m, 1H), 7.77 – 7.70 (m, 1H), 7.41 – 7.30 (m, 2H), 7.24 – 7.12 (m, 3H), 7.11 – 7.04 (m, 2H), 6.99 (s, 1H), 3.01 – 2.63 (m, 7H), 1.58 – 1.44 (m, 1H), 1.44 – 1.31 (m, 3H), 0.90 (t, *J* = 7.0 Hz, 3H); ^{13}C NMR ($CDCl_3$, 100 MHz) δ 140.5, 139.8, 139.1, 134.0, 128.6, 128.4, 126.1, 124.1, 123.8, 122.9, 122.7, 121.7, 57.0, 48.4, 36.5, 36.3, 33.8, 19.1, 14.3; HRESIMS (LC/MS) (t_R = 2.87 min for a 15 min run) *m/z* 324.1790 $[M + H]^+$ (calcd for $C_{21}H_{26}NS$, 324.1790).

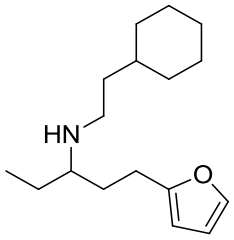


***N*-Phenethyl-1-(thiophen-2-yl)pentan-2-amine (215v).** Following the method to prepare amine **215a**, PEA (**213a**) (0.09 mL, 0.73 mmol, 1.2 equiv.), $NaBH(OAc)_3$ (214.2 mg, 1.01 mmol, 1.6 equiv.) and AcOH (0.04 mL, 0.70 mmol, 1.1 equiv.) were used to react with ketone **212f** (105.9 mg, 0.63 mmol, 1 equiv.) in $ClCH_2CH_2Cl$ (5 mL) for 23 h to afford amine **215v** as a yellow oil (78.1 mg, 0.29 mmol, 45%). Eluent system of Et_2O–hexane (3:1) was used in centrifugal radial TLC purification. R_f = 0.49 (Et_2O–hexane, 1:1); IR (neat) ν_{max} 3317, 2925, 1454, 1143 cm^{-1}; ^1H NMR ($CDCl_3$, 400 MHz) δ 7.31 – 7.13 (m, 5H), 7.11 (dd, *J* = 5.1, 1.2 Hz, 1H), 6.88 (dd, *J* = 5.2, 3.4 Hz, 1H), 6.72 (dd, *J* = 3.5, 1.2 Hz, 1H), 2.97 – 2.80 (m, 4H), 2.75 (dd, *J* = 7.3,

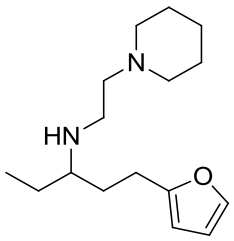
5.2 Hz, 3H), 1.64 – 1.43 (m, 1H), 1.46 – 1.23 (m, 3H), 0.89 (t, *J* = 6.9 Hz, 3H); ^{13}C NMR ($CDCl_3$, 100 MHz) δ 141.7, 140.0, 128.7, 128.4, 126.7, 126.1, 125.6, 123.7, 58.8, 48.5, 36.6, 36.2, 34.4, 19.1, 14.2; HRESIMS *m/z* 274.1642 $[M + H]^+$ (calcd for $C_{17}H_{24}N_1S_1$, 274.1629).



1-(Furan-2-yl)-*N*-phenethylpentan-3-amine (215w). Following the method to prepare amine **215a**, PEA (**213a**) (0.21 mL, 1.71 mmol, 1.1 equiv.), $NaBH(OAc)_3$ (529.1 mg, 2.50 mmol, 1.6 equiv.) and AcOH (0.09 mL, 1.57 mmol, 1 equiv.) were used to react with ketone **212g** (231.9 mg, 1.52 mmol, 1 equiv.) in $ClCH_2CH_2Cl$ (8 mL) for 24 h to afford amine **215w** as a colourless oil (182.8 mg, 0.71 mmol, 47%). Eluent system of Et_2O–hexane (1:2) was used in centrifugal radial TLC purification. R_f = 0.57 (Et_2O–hexane, 9:1); IR (neat) ν_{max} 3331, 2928, 2867, 1454, 1143, 1007 cm^{-1}; ^{1}H NMR ($CDCl_3$, 400 MHz) δ 7.34 – 7.16 (m, 6H), 6.26 (dd, *J* = 3.2, 1.9 Hz, 1H), 5.93 (dd, *J* = 3.2, 1.0 Hz, 1H), 2.90 – 2.73 (m, 4H), 2.60 (t, *J* = 7.9 Hz, 2H), 2.47 (p, *J* = 6.0 Hz, 1H), 1.79 – 1.62 (m, 2H), 1.43 (qd, *J* = 7.5, 5.9 Hz, 2H), 0.83 (t, *J* = 7.4 Hz, 3H); ^{13}C NMR ($CDCl_3$, 100 MHz) δ 156.3, 140.8, 140.2, 128.7, 128.4, 126.1, 110.1, 104.6, 58.1, 48.2, 36.7, 31.7, 26.3, 24.3, 9.8; HRESIMS *m/z* 258.1864 $[M + H]^+$ (calcd for $C_{17}H_{24}N_1O_1$, 258.1858).

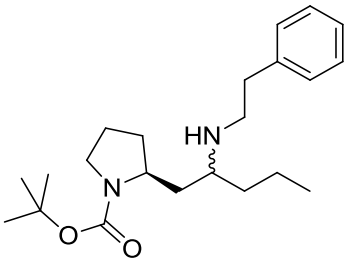


***N*-(2-Cyclohexylethyl)-1-(furan-2-yl)pentan-3-amine (215x).** Following the method to prepare amine **215a**, 2-cyclohexyl-ethylamine (**213e**) (98.8 mg, 0.78 mmol, 1.2 equiv.), $NaBH(OAc)_3$ (230.6 mg, 1.09 mmol, 1.7 equiv.) and AcOH (0.04 mL, 0.70 mmol, 1.1 equiv.) were used to react with ketone **212g** (100.8 mg, 0.66 mmol, 1 equiv.) in $ClCH_2CH_2Cl$ (8 mL) for 20.5 h to afford amine **215x** as a brown oil (46.3 mg, 0.18 mmol, 27%). Eluent system of EtOAc–hexane (4:1) was used in centrifugal radial TLC purification. R_f = 0.38 (EtOAc–hexane, 6:1); IR (neat) ν_{max} 3318, 2915, 1454, 1128, 1006 cm^{-1}; ^1H NMR ($CDCl_3$, 400 MHz) δ 7.32 – 7.28 (m, 1H), 6.32 – 6.24 (m, 1H), 6.06 – 5.93 (m, 1H), 2.66 (t, *J* = 8.0 Hz, 2H), 2.57 (t, *J* = 7.4 Hz, 2H), 2.46 (p, *J* = 6.2 Hz, 1H), 1.80 – 1.58 (m, 9H), 1.46 (p, *J* = 7.0 Hz, 2H), 1.41 – 1.01 (m, 6H), 0.89 (t, *J* = 7.1 Hz, 3H); ^{13}C NMR ($CDCl_3$, 100 MHz) δ 156.4, 140.7, 110.1, 104.6, 58.3, 44.6, 38.2, 35.8, 33.5, 31.7, 26.6, 26.3, 26.3, 24.4, 9.9; HRESIMS *m/z* 264.2320 $[M + H]^+$ (calcd for $C_{17}H_{30}N_1O_1$, 264.2327).



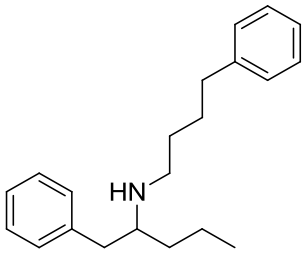
1-(Furan-2-yl)-*N*-(2-(piperidin-1-yl)ethyl)pentan-3-amine (215y). Following the method to prepare amine **215a**, 1-(2-aminoethyl)piperidine (**213f**) (80.9 mg, 0.63 mmol, 1.1 equiv.), $NaBH(OAc)_3$ (202.5 mg, 0.96 mmol, 1.7 equiv.) and AcOH (0.04

mL, 0.70 mmol, 1.2 equiv.) were used to react with ketone **212g** (88.2 mg, 0.58 mmol, 1 equiv.) in $ClCH_2CH_2Cl$ (8 mL) for 23.5 h to afford amine **215y** as a brown oil (44.8 mg, 0.17 mmol, 29%). Eluent system of EtOAc–hexane (9:1) was used in centrifugal radial TLC purification. R_f = 0.22 (EtOAc–hexane, 9:1); IR (neat) ν_{max} 3320, 2927, 1467, 1127, 1019 cm^{-1}; ^1H NMR ($CDCl_3$, 400 MHz) δ 7.30 (dd, *J* = 1.9, 0.9 Hz, 1H), 6.28 (dd, *J* = 3.2, 1.9 Hz, 1H), 5.99 (dd, *J* = 3.2, 0.9 Hz, 1H), 2.72 – 2.61 (m, 4H), 2.50 – 2.32 (m, 7H), 1.79 – 1.69 (m, 2H), 1.56 (p, *J* = 5.6 Hz, 4H), 1.52 – 1.37 (m, 4H), 0.90 (t, *J* = 7.5 Hz, 3H); ^{13}C NMR ($CDCl_3$, 100 MHz) δ 156.4, 140.7, 110.1, 104.6, 58.6, 58.6, 54.6, 43.7, 31.8, 26.4, 26.1, 24.5, 24.3, 10.0; HRESIMS *m/z* 265.2278 $[M + H]^+$ (calcd for $C_{16}H_{29}N_2O_1$, 265.2280).

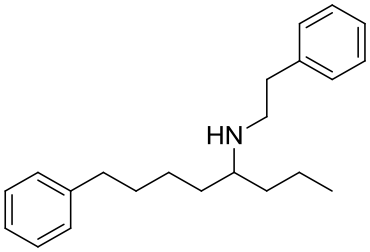


(2*S*)-*Tert*-butyl 2-(2-(phenethylamino)pentyl)pyrrolidine-1-carboxylate (215z). Following the method to prepare amine **215a**, PEA (**213a**) (0.22 mL, 1.79 mmol, 1.1 equiv.), $NaBH(OAc)_3$ (645.7 mg, 3.05 mmol, 1.6 equiv.) and AcOH (0.1 mL, 1.75 mmol, 1 equiv.) were used to react with ketone **212h** (309.6 mg, 1.21 mmol, 1 equiv.) in $ClCH_2CH_2Cl$ (10 mL) for 24 h to afford amine **215z** as a yellow oil (318.9 mg, 0.88 mmol, 73%). Eluent system of Et_2O–hexane (9:1) was used in centrifugal radial TLC purification. R_f = 0.43 (Et_2O–hexane, 9:1); IR (neat) ν_{max} 3328, 2926, 2870, 1688, 1392, 1250, 1166, 1104 cm^{-1}; ^1H NMR ($CDCl_3$, 700 MHz) δ 7.35 – 7.13 (m, 5H), 4.00 – 3.67 (m, 1H), 3.43 – 3.24 (m, 1H), 3.04 – 2.72 (m, 4H), 2.71 – 2.37 (m, 1H), 1.94 – 1.56 (m, 6H), 1.45 (s, 9H), 1.33 – 1.17 (m, 5H), 0.88 (t, *J* = 7.3 Hz, 3H); ^{13}C

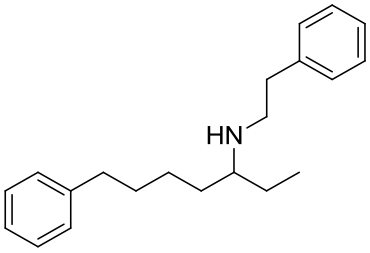
NMR ($CDCl_3$, 175 MHz) δ 154.7, 139.7, 128.7, 128.4, 126.2, 79.3, 55.0, 48.1, 46.4, 45.9, 39.5, 37.2, 36.7, 31.0, 28.6, 22.9, 19.0, 14.2; HRESIMS *m/z* 361.2854 $[M + H]^+$ (calcd for $C_{22}H_{37}N_2O_2$, 361.2855).



1-Phenyl-*N*-(4-phenylbutyl)pentan-2-amine (215za). Following the method to prepare amine **215a**, 4-phenylbutylamine (**213k**) (75.5 mg, 0.51 mmol, 1.2 equiv.), $NaBH(OAc)_3$ (155.7 mg, 0.73 mmol, 1.7 equiv.) and AcOH (0.03 mL, 0.52 mmol, 1.2 equiv.) were used to react with ketone **191b** (70.7 mg, 0.44 mmol, 1 equiv.) in $ClCH_2CH_2Cl$ (4 mL) for 22 h to afford amine **215za** as a yellow oil (65.2 mg, 0.22 mmol, 51%). Eluent system of Et_2O–hexane (1:1) was used in centrifugal radial TLC purification. R_f = 0.58 (Et_2O–hexane, 5:1); IR (neat) ν_{max} 3322, 3027, 2926, 2858, 1494, 1454, 1134 cm^{-1}; ^1H NMR ($CDCl_3$, 700 MHz) δ 7.31 – 7.10 (m, 10H), 2.77 – 2.51 (m, 8H), 1.62 – 1.52 (m, 2H), 1.51 – 1.31 (m, 5H), 0.90 (t, *J* = 6.9 Hz, 3H); ^{13}C NMR ($CDCl_3$, 175 MHz) δ 142.4, 139.7, 129.3, 128.4, 128.4, 128.2, 126.1, 125.7, 59.0, 46.9, 40.7, 36.1, 35.8, 29.7, 29.1, 19.0, 14.3; HRESIMS *m/z* 296.2379 $[M + H]^+$ (calcd for $C_{21}H_{30}N_1$, 296.2378).

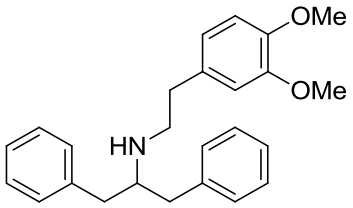


***N*-Phenethyl-8-phenyloctan-4-amine (215zb).** Following the method to prepare amine **215a**, PEA (**213a**) (0.17 mL, 1.38 mmol, 1.1 equiv.), $NaBH(OAc)_3$ (437.8 mg, 2.07 mmol, 1.7 equiv.) and AcOH (0.08 mL, 1.40 mmol, 1.1 equiv.) were used to react with ketone **212i** (254.9 mg, 1.25 mmol, 1 equiv.) in $ClCH_2CH_2Cl$ (10 mL) for 21 h to afford amine **215zb** as a yellow oil (310.4 mg, 1.00 mmol, 80%). Eluent system of EtOAc–hexane (1:6) was used in centrifugal radial TLC purification. R_f = 0.22 (EtOAc–hexane, 1:4); IR (neat) ν_{max} 3339, 3027, 2926, 2857, 1494, 1455, 1104 cm^{-1}; ^1H NMR ($CDCl_3$, 400 MHz) δ 7.33 – 7.12 (m, 10H), 2.83 (dd, *J* = 7.9, 5.1 Hz, 2H), 2.77 (dd, *J* = 7.9, 5.1 Hz, 2H), 2.58 (t, *J* = 7.7 Hz, 2H), 2.46 (p, *J* = 5.8 Hz, 1H), 1.58 (p, *J* = 7.5 Hz, 2H), 1.45 – 1.17 (m, 8H), 0.87 (t, *J* = 7.0 Hz, 3H); ^{13}C NMR ($CDCl_3$, 175 MHz) δ 142.7, 140.1, 128.7, 128.4, 128.4, 128.2, 126.2, 125.6, 57.2, 48.3, 36.5, 36.2, 35.9, 33.7, 31.7, 25.3, 18.9, 14.3; HRESIMS *m/z* 310.2546 $[M + H]^+$ (calcd for $C_{22}H_{32}N_1$, 310.2535).



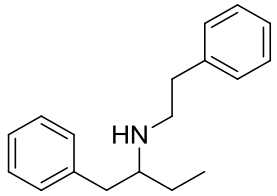
***N*-Phenethyl-7-phenylheptan-3-amine (215zc).** Following the method to prepare amine **215a**, PEA (**213a**) (0.14 mL, 1.14 mmol, 1.1 equiv.), $NaBH(OAc)_3$ (357.3 mg, 1.69 mmol, 1.6 equiv.) and AcOH (0.06 mL, 1.05 mmol, 1 equiv.) were used to react

with ketone **212j** (200.8 mg, 1.06 mmol, 1 equiv.) in $ClCH_2CH_2Cl$ (10 mL) for 23 h to afford amine **215zc** as a yellow oil (241.4 mg, 0.82 mmol, 77%). Eluent system of Et_2O–hexane (1:1) was used in centrifugal radial TLC purification. R_f = 0.45 (Et_2O–hexane, 5:1); IR (neat) ν_{max} 3329, 3027, 2925, 2858, 1456, 1361, 1096 cm^{-1}; ^1H NMR ($CDCl_3$, 400 MHz) δ 7.33 – 7.12 (m, 10H), 2.91 – 2.71 (m, 4H), 2.58 (t, *J* = 7.6 Hz, 2H), 2.40 (p, *J* = 5.9 Hz, 1H), 1.58 (p, *J* = 7.6 Hz, 2H), 1.46 – 1.33 (m, 4H), 1.33 – 1.21 (m, 2H), 0.81 (t, *J* = 7.4 Hz, 3H); ^{13}C NMR ($CDCl_3$, 175 MHz) δ 142.7, 140.1, 128.7, 128.4, 128.4, 128.2, 126.1, 125.6, 58.7, 48.3, 36.5, 35.9, 33.2, 31.7, 26.2, 25.4, 9.8; HRESIMS *m/z* 296.2386 $[M + H]^+$ (calcd for $C_{21}H_{30}N_1$, 296.2378).

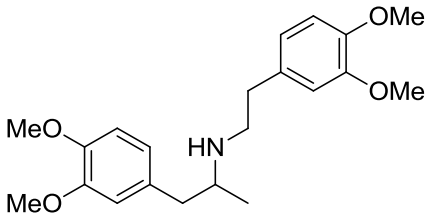


***N*-(3,4-Dimethoxyphenethyl)-1,3-diphenylpropan-2-amine (215zd).** Following the method to prepare amine **215a**, DMPEA (**176**) (171.4 mg, 0.95 mmol, 2.1 equiv.), $NaBH(OAc)_3$ (400.7 mg, 1.89 mmol, 4.1 equiv.) and AcOH (0.05 mL, 0.87 mmol, 1.9 equiv.) were used to react with ketone **191c** (96.9 mg, 0.46 mmol, 1 equiv.) in $ClCH_2CH_2Cl$ (4 mL) for 30 h to afford amine **215zd** as a yellow oil (74.3 mg, 0.20 mmol, 43%). Eluent system of Et_2O–hexane (1:3) was used in centrifugal radial TLC purification. R_f = 0.33 (Et_2O–hexane, 9:1); IR (neat) ν_{max} 3310, 3026, 2934, 2834, 1591, 1515, 1455, 1262, 1238, 1156, 1141, 1030 cm^{-1}; ^1H NMR ($CDCl_3$, 600 MHz) δ 7.25 – 7.21 (m, 4H), 7.20 – 7.16 (m, 2H), 7.10 (d, *J* = 7.3 Hz, 4H), 6.67 (d, *J* = 7.9 Hz, 1H), 6.59 – 6.53 (m, 2H), 3.85 (s, 3H), 3.80 (s, 3H), 2.99 (p, *J* = 6.7 Hz, 1H), 2.83 (t, *J* = 6.9 Hz, 2H), 2.75 – 2.64 (m, 4H), 2.62 (t, *J* = 6.9 Hz, 2H); ^{13}C NMR ($CDCl_3$, 150 MHz) δ 148.8, 147.3, 139.3, 132.2, 129.2, 128.4, 126.1, 120.4, 111.7, 111.2, 61.2,

55.9, 55.7, 48.8, 40.7, 35.8; HRESIMS *m/z* 376.2294 $[M + H]^+$ (calcd for $C_{25}H_{30}N_1O_2$, 376.2277).

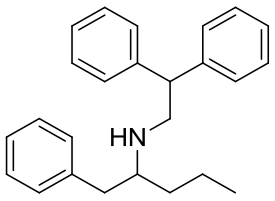


***N*-Phenethyl-1-phenylbutan-2-amine (215ze).** Following the method to prepare amine **215a**, PEA (**213a**) (0.1 mL, 0.81 mmol, 1.1 equiv.), $NaBH(OAc)_3$ (260.7 mg, 1.23 mmol, 1.7 equiv.) and AcOH (0.05 mL, 0.87 mmol, 1.2 equiv.) were used to react with ketone **212k** (109.3 mg, 0.74 mmol, 1 equiv.) in $ClCH_2CH_2Cl$ (5 mL) for 24 h to afford amine **215ze** as a yellow oil (112.9 mg, 0.45 mmol, 61%). Eluent system of EtOAc–hexane (1:4) was used in centrifugal radial TLC purification. R_f = 0.37 (EtOAc–hexane, 1:2); IR (neat) ν_{max} 3320, 3027, 2926, 1493, 1454, 1351, 1134, 1084 cm^{-1}; ^1H NMR ($CDCl_3$, 400 MHz) δ 7.29 – 7.08 (m, 10H), 2.94 – 2.54 (m, 7H), 1.57 – 1.29 (m, 2H), 0.89 (t, *J* = 7.4 Hz, 3H); ^{13}C NMR ($CDCl_3$, 175 MHz) δ 139.9, 139.5, 129.2, 128.6, 128.4, 128.4, 126.1, 126.1, 60.50, 48.4, 40.1, 36.2, 26.1, 9.9; HRESIMS *m/z* 254.1911 $[M + H]^+$ (calcd for $C_{18}H_{24}N_1$, 254.1909).



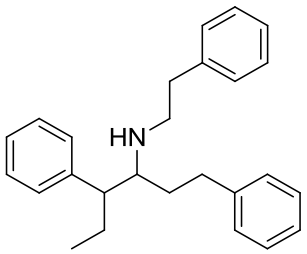
***N*-(3,4-dimethoxyphenethyl)-1-(3,4-dimethoxy-phenyl)-propan-2-amine (215zf)**. Following the method to prepare amine **215a**, DMPEA (**176**) (207.8 mg, 1.15 mmol, 1.1 equiv.), $NaBH(OAc)_3$ (350.3 mg, 1.65 mmol, 1.6 equiv.) and AcOH (0.06 mL, 1.05 mmol, 1 equiv.) were used to react with 3,4-dimethoxyphenylacetone (**212t**)

(0.18 mL, 1.03 mmol, 1 equiv.) in $ClCH_2CH_2Cl$ (5 mL) for 22 h to afford amine **215zf** as a yellow oil (184.2 mg, 0.51 mmol, 50%). Eluent system of EtOAc–hexane (1:2) was used in centrifugal radial TLC purification. R_f = 0.10 (EtOAc–hexane, 6:1); IR (neat) ν_{max} 3306, 2935, 2835, 1607, 1591, 1520, 1455, 1264, 1238, 1142, 1030 cm^{-1}; ^1H NMR ($CDCl_3$, 700 MHz) δ 6.73 (d, *J* = 6.6 Hz, 1H), 6.72 (d, *J* = 6.6 Hz, 1H), 6.67 (d, *J* = 2.0 Hz, 1H), 6.65 (d, *J* = 2.0 Hz, 1H), 6.64 (t, *J* = 2.1 Hz, 1H), 6.62 (t, *J* = 2.2 Hz, 1H), 3.86 (s, 3H), 3.85 (s, 3H), 3.83 (s, 6H), 3.00 – 2.92 (m, 1H), 2.89 – 2.82 (m, 1H), 2.79 – 2.56 (m, 5H), 1.10 (d, *J* = 6.2 Hz, 3H); ^{13}C NMR ($CDCl_3$, 175 MHz) δ 148.9, 148.8, 147.5, 147.4, 132.1, 131.6, 121.1, 120.4, 112.3, 111.8, 111.2, 111.1, 55.8, 55.8, 55.8, 55.8, 54.8, 48.6, 43.1, 35.6, 20.0; HRESIMS *m/z* 360.2167 $[M + H]^+$ (calcd for $C_{21}H_{30}N_1O_4$, 360.2175).

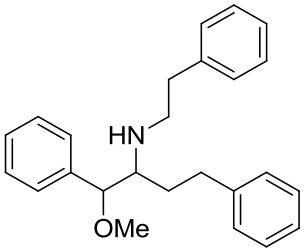


***N*-(2,2-Diphenylethyl)-1-phenylpentan-2-amine (215zg).** Following the method to prepare amine **215a**, 2,2-diphenylethylamine (**213l**) (109.9 mg, 0.56 mmol, 1.1 equiv.), $NaBH(OAc)_3$ (168.8 mg, 0.80 mmol, 1.6 equiv.) and AcOH (0.03 mL, 0.52 mmol, 1 equiv.) were used to react with ketone **191b** (82.4 mg, 0.51 mmol, 1 equiv.) in $ClCH_2CH_2Cl$ (4 mL) for 21 h to afford amine **215zg** as a yellow oil (64.1 mg, 0.19 mmol, 37%). Eluent system of EtOAc–hexane (1:4) was used in centrifugal radial TLC purification. R_f = 0.43 (EtOAc–hexane, 1:4); IR (neat) ν_{max} 3320, 3026, 2954, 2924, 2868, 1492, 1452, 1132, 1030 cm^{-1}; ^1H NMR ($CDCl_3$, 700 MHz) δ 7.27 – 7.10 (m, 13H), 7.06 – 7.02 (m, 2H), 4.13 (t, *J* = 7.7 Hz, 1H), 3.25 (dd, *J* = 11.6, 7.2 Hz, 1H), 3.15 (dd, *J* = 11.6, 8.2 Hz, 1H), 2.76 (dq, *J* = 7.6, 5.9 Hz, 1H), 2.70 (dd, *J* = 13.6,

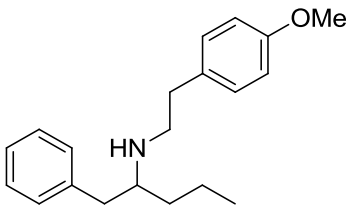
5.7 Hz, 1H), 2.60 (dd, *J* = 13.6, 7.7 Hz, 1H), 1.47 – 1.40 (m, 1H), 1.40 – 1.33 (m, 1H), 1.31 – 1.24 (m, 2H), 0.86 (t, *J* = 7.3 Hz, 3H); ^{13}C NMR ($CDCl_3$, 175 MHz) δ 142.8, 142.4, 139.2, 129.1, 128.6, 128.6, 128.4, 127.9, 127.9, 126.5, 126.1, 59.4, 51.9, 51.0, 40.6, 36.0, 19.0, 14.2; HRESIMS *m/z* 344.2392 $[M + H]^+$ (calcd for $C_{25}H_{30}N_1$, 344.2378).



***N*-Phenethyl-1,4-diphenylhexan-3-amine (215zh).** Following the method to prepare amine **215a**, PEA (**213a**) (0.08 mL, 0.65 mmol, 1.2 equiv.), $NaBH(OAc)_3$ (188.4 mg, 0.89 mmol, 1.7 equiv.) and AcOH (0.03 mL, 0.52 mmol, 1 equiv.) were used to react with ketone **212l** (134.2 mg, 0.53 mmol, 1 equiv.) in $ClCH_2CH_2Cl$ (6 mL) for 24 h to afford amine **215zh** as a yellow oil (12.6 mg, 0.04 mmol, 8%). Eluent system of Et_2O–hexane (1:6) was used in centrifugal radial TLC purification. R_f = 0.24 (Et_2O–hexane, 1:4); IR (neat) ν_{max} 3332, 3026, 2929, 1457, 1120 cm^{-1}; ^{1}H NMR ($CDCl_3$, 700 MHz) δ 7.28 – 7.11 (m, 13H), 7.09 – 7.04 (m, 2H), 2.88 (dt, *J* = 11.1, 6.9 Hz, 1H), 2.76 – 2.58 (m, 7H), 1.86 – 1.76 (m, 2H), 1.76 – 1.68 (m, 1H), 1.58 (ddq, *J* = 14.4, 10.7, 7.2 Hz, 1H), 0.71 (t, *J* = 7.4 Hz, 3H); ^{13}C NMR ($CDCl_3$, 175 MHz) δ 142.7, 142.2, 140.0, 128.6, 128.6, 128.4, 128.3, 128.3, 128.3, 126.4, 126.0, 125.7, 61.7, 51.0, 48.8, 33.0, 32.2, 31.8, 24.5, 12.4; HRESIMS *m/z* 358.2522 $[M + H]^+$ (calcd for $C_{26}H_{32}N_1$, 358.2535).

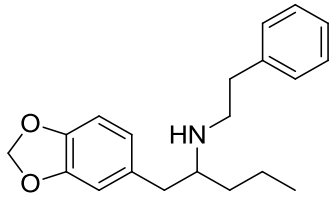


1-Methoxy-*N*-phenethyl-1,4-diphenylbutan-2-amine (215zi). Following the method to prepare amine **215a**, PEA (**213a**) (0.06 mL, 0.49 mmol, 1.2 equiv.), $NaBH(OAc)_3$ (139.9 mg, 0.66 mmol, 1.6 equiv.) and AcOH (0.03 mL, 0.52 mmol, 1.2 equiv.) were used to react with ketone **212m** (107.0 mg, 0.42 mmol, 1 equiv.) in $ClCH_2CH_2Cl$ (10 mL) for 21.5 h to afford amine **215zi** as a yellow oil (77.1 mg, 0.21 mmol, 50%). Eluent system of Et_2O–hexane (1:6) was used in centrifugal radial TLC purification. R_f = 0.6 (Et_2O–hexane, 3:1); IR (neat) ν_{max} 3334, 3032, 2913, 1555, 1467, 1337, 1095 cm^{-1}; ^1H NMR ($CDCl_3$, 400 MHz) δ 7.37 – 7.10 (m, 13H), 7.09 – 7.03 (m, 2H), 4.20 (d, *J* = 5.3 Hz, 1H), 3.19 (s, 3H), 2.89 – 2.77 (m, 2H), 2.68 (ddt, *J* = 12.6, 9.0, 4.4 Hz, 4H), 2.50 (ddd, *J* = 13.7, 10.4, 6.2 Hz, 1H), 1.81 (dddd, *J* = 14.3, 10.3, 6.2, 3.9 Hz, 1H), 1.66 (dddd, *J* = 14.0, 10.4, 7.7, 5.4 Hz, 1H); ^{13}C NMR ($CDCl_3$, 100 MHz) δ 142.7, 140.2, 139.7, 128.7, 128.4, 128.3, 128.2, 127.5, 127.2, 126.0, 125.5, 85.1, 62.4, 57.2, 48.9, 36.7, 32.3, 31.3; HRESIMS *m/z* 360.2327 $[M + H]^+$ (calcd for $C_{25}H_{30}N_1O_1$, 360.23274).



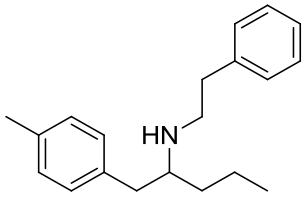
***N*-(4-Methoxyphenethyl)-1-phenylpentan-2-amine (215zj).** Following the method to prepare amine **215a**, 4-methoxyphenethylamine (**213m**) (76.3 mg, 0.50 mmol, 1.3 equiv.), $NaBH(OAc)_3$ (140.1 mg, 0.66 mmol, 1.7 equiv.) and AcOH (0.02 mL, 0.35

mmol, 0.9 equiv.) were used to react with ketone **191b** (61.7 mg, 0.38 mmol, 1 equiv.) in $ClCH_2CH_2Cl$ (4 mL) for 25 h to afford amine **215zj** as a yellow oil (29.7 mg, 0.10 mmol, 26%). Eluent system of Et_2O–hexane (1:5) was used in centrifugal radial TLC purification. R_f = 0.47 (Et_2O–hexane, 6:1); IR (neat) ν_{max} 3317, 2955, 2930, 2868, 2834, 1613, 1512, 1244, 1176, 1036 cm^{-1}; ^1H NMR ($CDCl_3$, 400 MHz) δ 7.28 – 7.15 (m, 3H), 7.12 – 7.07 (m, 2H), 7.05 – 7.00 (m, 2H), 6.81 – 6.74 (m, 2H), 3.78 (s, 3H), 2.92 – 2.81 (m, 1H), 2.81 – 2.55 (m, 6H), 1.49 – 1.28 (m, 4H), 0.88 (t, *J* = 7.0 Hz, 3H); ^{13}C NMR ($CDCl_3$, 100 MHz) δ 157.9, 139.6, 131.9, 129.5, 129.2, 128.3, 126.0, 113.8, 59.0, 55.2, 48.6, 40.7, 36.1, 35.4, 19.0, 14.3; HRESIMS *m/z* 298.2157 $[M + H]^+$ (calcd for $C_{20}H_{28}N_1O_1$, 298.2171).

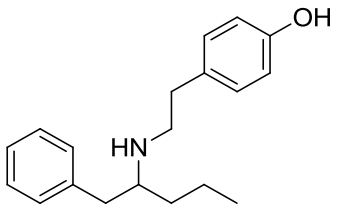


1-(Benzo[*d*][1,3]dioxol-5-yl)-*N*-phenethylpentan-2-amine (215zk). Following the method to prepare amine **215a**, PEA (**213a**) (0.05 mL, 0.41 mmol, 1.1 equiv.), $NaBH(OAc)_3$ (127.3 mg, 0.60 mmol, 1.7 equiv.) and AcOH (0.02 mL, 0.35 mmol, 1 equiv.) were used to react with ketone **212n** (74.5 mg, 0.36 mmol, 1 equiv.) in $ClCH_2CH_2Cl$ (4 mL) for 21 h to afford amine **215zk** as a yellow oil (73.3 mg, 0.24 mmol, 67%). Eluent system of Et_2O–hexane (2:1) was used in centrifugal radial TLC purification. R_f = 0.58 (Et_2O–hexane, 7:1); IR (neat) ν_{max} 3316, 3026, 2925, 2871, 1488, 1442, 1243, 1037 cm^{-1}; ^1H NMR ($CDCl_3$, 700 MHz) δ 7.25 – 7.21 (m, 2H), 7.20 – 7.15 (m, 1H), 7.14 – 7.10 (m, 2H), 6.67 (d, *J* = 7.8 Hz, 1H), 6.60 (d, *J* = 1.7 Hz, 1H), 6.54 (dd, *J* = 7.9, 1.7 Hz, 1H), 5.92 (s, 2H), 2.96 – 2.87 (m, 1H), 2.83 – 2.66 (m, 4H), 2.64 (dd, *J* = 13.6, 5.6 Hz, 1H), 2.54 (dd, *J* = 13.6, 7.5 Hz, 1H), 1.48 – 1.38 (m,

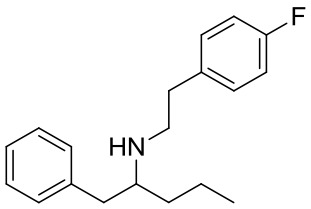
1H), 1.38 – 1.27 (m, 3H), 0.88 (t, *J* = 7.1 Hz, 3H); ^{13}C NMR ($CDCl_3$, 175 MHz) δ 147.6, 145.8, 139.8, 133.1, 128.6, 128.4, 126.1, 122.1, 109.4, 108.1, 100.8, 59.2, 48.4, 40.3, 36.2, 35.9, 19.0, 14.3; HRESIMS *m/z* 312.1970 $[M + H]^+$ (calcd for $C_{20}H_{26}N_1O_2$, 312.1964).



***N*-Phenethyl-1-(*p*-tolyl)pentan-2-amine (215zl).** Following the method to prepare amine **215a**, PEA (**213a**) (0.1 mL, 0.81 mmol, 1.1 equiv.), $NaBH(OAc)_3$ (252.2 mg, 1.19 mmol, 1.6 equiv.) and AcOH (0.05 mL, 0.87 mmol, 1.2 equiv.) were used to react with ketone **212o** (131.0 mg, 0.74 mmol, 1 equiv.) in $ClCH_2CH_2Cl$ (4 mL) for 23 h to afford amine **215zl** as a yellow oil (82.3 mg, 0.29 mmol, 39%). Eluent systems of Et_2O–hexane (1:1) and EtOAc–hexane (1:1) were used in centrifugal radial TLC purification. R_f = 0.58 (EtOAc–hexane, 6:1); IR (neat) ν_{max} 3317, 3025, 2955, 2924, 2869, 1514, 1454, 1120 cm^{-1}; ^{1}H NMR ($CDCl_3$, 700 MHz) δ 7.23 (t, *J* = 7.5 Hz, 2H), 7.19 – 7.15 (m, 1H), 7.12 – 7.09 (m, 2H), 7.04 (d, *J* = 7.8 Hz, 2H), 6.99 (d, *J* = 7.9 Hz, 2H), 2.90 (ddd, *J* = 11.2, 8.1, 6.2 Hz, 1H), 2.84 – 2.77 (m, 1H), 2.77 – 2.70 (m, 3H), 2.68 (dd, *J* = 13.6, 5.8 Hz, 1H), 2.60 (dd, *J* = 13.6, 7.4 Hz, 1H), 2.31 (s, 3H), 1.47 – 1.37 (m, 1H), 1.38 – 1.28 (m, 3H), 0.88 (t, *J* = 7.0 Hz, 3H); ^{13}C NMR ($CDCl_3$, 175 MHz) δ 139.9, 136.3, 135.5, 129.1, 128.6, 128.4, 126.0, 59.1, 48.4, 40.1, 36.3, 36.0, 21.1, 19.0, 14.3; HRESIMS *m/z* 282.2208 $[M + H]^+$ (calcd for $C_{20}H_{28}N_1$, 282.2222).

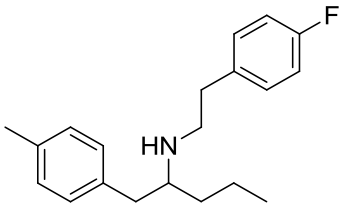


4-(2-((1-Phenylpentan-2-yl)amino)ethyl)phenol (215zm). Following the method to prepare amine **215a**, tyramine (**213n**) (69.8 mg, 0.51 mmol, 1.1 equiv.), $NaBH(OAc)_3$ (170.0 mg, 0.80 mmol, 1.7 equiv.) and AcOH (0.03 mL, 0.52 mmol, 1.1 equiv.) were used to react with ketone **191b** (73.9 mg, 0.46 mmol, 1 equiv.) in THF (8 mL) for 23.5 h to afford amine **215zm** as a yellow oil (15.8 mg, 0.06 mmol, 13%). Eluent system of EtOAc–hexane (1:6) was used in centrifugal radial TLC purification. R_f = 0.37 (EtOAc–hexane, 3:1); IR (neat) ν_{max} 3275, 3026, 2957, 2929, 2872, 1613, 1594, 1515, 1454, 1370, 1248, 1171, 1105 cm^{-1}; ^1H NMR ($CDCl_3$, 400 MHz) δ 7.28 – 7.15 (m, 3H), 7.11 – 7.03 (m, 2H), 6.92 – 6.85 (m, 2H), 6.68 – 6.61 (m, 2H), 2.92 (dt, *J* = 11.4, 6.8 Hz, 1H), 2.87 – 2.71 (m, 3H), 2.71 – 2.57 (m, 3H), 1.58 – 1.45 (m, 1H), 1.45 – 1.21 (m, 3H), 0.87 (t, *J* = 7.1 Hz, 3H); ^{13}C NMR ($CDCl_3$, 100 MHz) δ 155.2, 139.0, 130.0, 129.6, 129.1, 128.5, 126.2, 115.8, 59.2, 48.0, 40.2, 35.5, 34.6, 19.1, 14.2; HRESIMS *m/z* 284.2006 $[M + H]^+$ (calcd for $C_{19}H_{26}N_1O_1$, 284.2014).



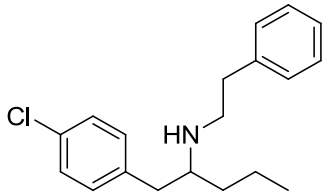
***N*-(4-Fluorophenethyl)-1-phenylpentan-2-amine (215zn).** Following the method to prepare amine **215a**, 4-fluorophenethylamine (**213o**) (106.1 mg, 0.76 mmol, 1.2 equiv.), $NaBH(OAc)_3$ (213.6 mg, 1.01 mmol, 1.6 equiv.) and AcOH (0.04 mL, 0.70 mmol, 1.1 equiv.) were used to react with ketone **191b** (100.8 mg, 0.62 mmol, 1

equiv.) in $ClCH_2CH_2Cl$ (4 mL) for 19 h to afford amine **215zn** as a dark green oil (76.9 mg, 0.27 mmol, 44%). Eluent system of Et_2O–hexane (1:1) was used in centrifugal radial TLC purification. R_f = 0.56 (Et_2O–hexane, 9:1); IR (neat) ν_{max} 3317, 3028, 2956, 2928, 2870, 1602, 1509, 1455, 1221, 1156, 1097 cm^{-1}; ^1H NMR ($CDCl_3$, 700 MHz) δ 7.25 – 7.22 (m, 2H), 7.21 – 7.17 (m, 1H), 7.12 – 7.08 (m, 2H), 7.07 – 7.02 (m, 2H), 6.93 – 6.87 (m, 2H), 2.88 (ddd, *J* = 10.8, 7.7, 6.0 Hz, 1H), 2.79 – 2.59 (m, 6H), 1.50 – 1.41 (m, 1H), 1.41 – 1.31 (m, 3H), 0.89 (t, *J* = 7.0 Hz, 3H); ^{13}C NMR ($CDCl_3$, 175 MHz) δ 162.1, 160.7, 139.3, 135.4, 135.4, 130.0, 129.9, 129.2, 128.4, 126.1, 115.2, 115.1, 59.1, 48.3, 40.6, 36.0, 35.3, 19.0, 14.3; HRESIMS *m/z* 286.1977 $[M + H]^+$ (calcd for $C_{19}H_{25}F_1N_1$, 286.1971).

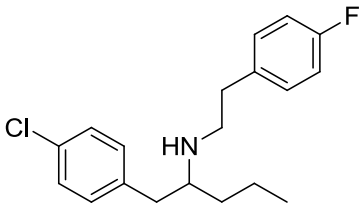


***N*-(4-Fluorophenethyl)-1-(*p*-tolyl)pentan-2-amine (215zo).** Following the method to prepare amine **215a**, 4-fluorophenethylamine (**213o**) (74.3 mg, 0.53 mmol, 1.1 equiv.), $NaBH(OAc)_3$ (164.8 mg, 0.78 mmol, 1.6 equiv.) and AcOH (0.03 mL, 0.52 mmol, 1.1 equiv.) were used to react with ketone **212o** (85.0 mg, 0.48 mmol, 1 equiv.) in $ClCH_2CH_2Cl$ (5 mL) for 26 h to afford amine **215zo** as a yellow oil (66.6 mg, 0.22 mmol, 46%). Eluent system of EtOAc–hexane (1:9) was used in centrifugal radial TLC purification. R_f = 0.46 (EtOAc–hexane, 1:1); IR (neat) ν_{max} 3317, 2956, 2925, 2871, 1601, 1509, 1221, 1157, 1097 cm^{-1}; ^1H NMR ($CDCl_3$, 400 MHz) δ 7.07 – 7.00 (m, 4H), 6.99 – 6.94 (m, 2H), 6.93 – 6.85 (m, 2H), 2.92 – 2.83 (m, 1H), 2.77 – 2.60 (m, 5H), 2.58 – 2.47 (m, 1H), 2.32 (s, 3H), 1.48 – 1.27 (m, 4H), 0.89 (t, *J* = 6.9 Hz, 3H); ^{13}C NMR ($CDCl_3$, 100 MHz) δ 162.6, 160.1, 136.3, 135.5, 130.0, 129.9, 129.0,

129.0, 115.2, 115.0, 59.1, 48.4, 40.2, 36.2, 35.5, 21.0, 19.0, 14.3; HRESIMS *m/z* 300.2115 $[M + H]^+$ (calcd for $C_{20}H_{27}F_1N_1$, 300.2128).

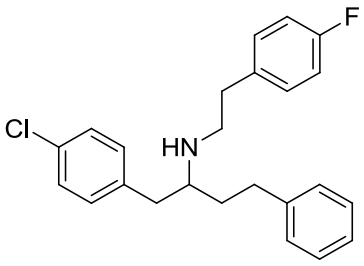


1-(4-Chlorophenyl)-*N*-phenethylpentan-2-amine (215zp). Following the method to prepare amine **215a**, PEA (**213a**) (0.07 mL, 0.57 mmol, 1.1 equiv.), $NaBH(OAc)_3$ (182.9 mg, 0.86 mmol, 1.7 equiv.) and AcOH (0.03 mL, 0.52 mmol, 1 equiv.) were used to react with ketone **212p** (100.2 mg, 0.51 mmol, 1 equiv.) in $ClCH_2CH_2Cl$ (8 mL) for 21.5 h to afford amine **215zp** as a yellow oil (107.1 mg, 0.35 mmol, 70%). Eluent system of EtOAc–hexane (1:4) was used in centrifugal radial TLC purification. R_f = 0.47 (EtOAc–hexane, 1:1); IR (neat) ν_{max} 3323, 2926, 1652, 1478, 1099 cm^{-1}; ^1H NMR ($CDCl_3$, 400 MHz) δ 7.28 – 7.15 (m, 5H), 7.13 – 7.08 (m, 2H), 7.03 – 6.96 (m, 2H), 2.94 – 2.85 (m, 1H), 2.82 – 2.62 (m, 5H), 2.61 – 2.51 (m, 1H), 1.49 – 1.23 (m, 4H), 0.88 (t, *J* = 7.0 Hz, 3H); ^{13}C NMR ($CDCl_3$, 100 MHz) δ 139.8, 138.0, 131.8, 130.5, 128.6, 128.4, 128.4, 126.1, 58.9, 48.4, 40.0, 36.3, 36.1, 19.0, 14.3; HRESIMS *m/z* 302.1674 $[M + H]^+$ (calcd for $C_{19}H_{25}{}^{35}Cl_1N_1$, 302.1676).



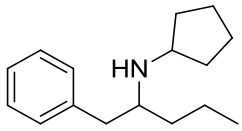
1-(4-Chlorophenyl)-*N*-(4-fluorophenethyl)pentan-2-amine (215zq). Following the method to prepare amine **215a**, 4-fluorophenethylamine (**213o**) (74.3 mg, 0.53 mmol, 1.1 equiv.), $NaBH(OAc)_3$ (179.0 mg, 0.84 mmol, 1.7 equiv.) and AcOH (0.03 mL,

0.52 mmol, 1 equiv.) were used to react with ketone **212p** (98.9 mg, 0.50 mmol, 1 equiv.) in $ClCH_2CH_2Cl$ (8 mL) for 19.5 h to afford amine **215zq** as a yellow oil (116.5 mg, 0.36 mmol, 72%). Eluent system of EtOAc–hexane (1:5) was used in centrifugal radial TLC purification. R_f = 0.32 (EtOAc–hexane, 1:2); IR (neat) ν_{max} 3326, 2928, 1498, 1217, 1104 cm^{-1}; ^1H NMR ($CDCl_3$, 400 MHz) δ 7.23 – 7.16 (m, 2H), 7.09 – 6.98 (m, 4H), 6.97 – 6.88 (m, 2H), 2.91 – 2.82 (m, 1H), 2.79 – 2.60 (m, 5H), 2.60 – 2.50 (m, 1H), 1.47 – 1.23 (m, 4H), 0.88 (t, *J* = 6.8 Hz, 3H); ^{13}C NMR ($CDCl_3$, 100 MHz) δ 162.6, 160.2, 138.0, 135.4, 135.4, 131.8, 130.5, 130.0, 129.9, 128.4, 115.3, 115.0, 59.0, 48.4, 40.1, 36.1, 35.5, 19.0, 14.3; HRESIMS *m/z* 320.1596 $[M + H]^+$ (calcd for $C_{19}H_{24}{}^{35}Cl_1F_1N_1$, 320.1581).

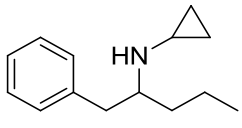


1-(4-Chlorophenyl)-*N*-(4-fluorophenethyl)-4-phenylbutan-2-amine(215zr). Following the method to prepare amine **215a**, 4-fluorophenethylamine (**213o**) (84.9 mg, 0.61 mmol, 1.1 equiv.), $NaBH(OAc)_3$ (187.5 mg, 0.88 mmol, 1.6 equiv.) and AcOH (0.04 mL, 0.70 mmol, 1.3 equiv.) were used to react with ketone **212q** (139.1 mg, 0.54 mmol, 1 equiv.) in $ClCH_2CH_2Cl$ (4 mL) for 23 h to afford amine **215zr** as a yellow oil (125.9 mg, 0.33 mmol, 61%). Eluent system of Et_2O–hexane (1:2) was used in centrifugal radial TLC purification. R_f = 0.44 (Et_2O–hexane, 3:1); IR (neat) ν_{max} 3321, 3027, 2924, 2855, 1601, 1509, 1492, 1220, 1090 cm^{-1}; ^1H NMR ($CDCl_3$, 400 MHz) δ 7.31 – 7.24 (m, 2H), 7.22 – 7.15 (m, 3H), 7.15 – 7.09 (m, 2H), 7.07 – 6.96 (m, 4H), 6.96 – 6.90 (m, 2H), 2.85 (ddd, *J* = 10.7, 7.2, 6.2 Hz, 1H), 2.78 – 2.57

(m, 8H), 1.81 – 1.60 (m, 2H); ^{13}C NMR ($CDCl_3$, 100 MHz) δ 162.7, 160.2, 142.1, 137.6, 135.4, 135.4, 131.9, 130.5, 130.0, 129.9, 128.5, 128.4, 128.3, 125.8, 115.3, 115.1, 58.4, 48.2, 39.9, 35.5, 35.4, 32.0; HRESIMS *m/z* 382.1730 $[M + H]^+$ (calcd for $C_{24}H_{26}{}^{35}Cl_1F_1N_1$, 382.1738).

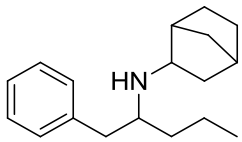


***N*-(1-Phenylpentan-2-yl)cyclopentanamine (216a).** Following the method to prepare amine **215a**, cyclopentylamine (**214a**) (61.8 mg, 0.73 mmol, 1.5 equiv.), $NaBH(OAc)_3$ (171.2 mg, 0.81 mmol, 1.6 equiv.) and AcOH (0.03 mL, 0.52 mmol, 1 equiv.) were used to react with ketone **191b** (80.7 mg, 0.50 mmol, 1 equiv.) in $ClCH_2CH_2Cl$ (4 mL) for 23 h to afford amine **216a** as a yellow oil (25.5 mg, 0.11 mmol, 22%). Eluent system of Et_2O–hexane (1:4) was used in centrifugal radial TLC purification. R_f = 0.34 (Et_2O–hexane, 3:1); IR (neat) ν_{max} 3318, 2954, 2868, 1494, 1454, 1350, 1136, 1031 cm^{-1}; ^{1}H NMR ($CDCl_3$, 400 MHz) δ 7.32 – 7.15 (m, 5H), 3.16 (p, *J* = 6.9 Hz, 1H), 2.83 – 2.58 (m, 3H), 1.92 – 1.70 (m, 2H), 1.67 – 1.29 (m, 8H), 1.28 – 1.15 (m, 1H), 1.15 – 1.00 (m, 1H), 0.94 – 0.86 (m, 3H); ^{13}C NMR ($CDCl_3$, 100 MHz) δ 139.8, 129.3, 128.3, 126.0, 57.3, 57.0, 41.1, 36.6, 33.6, 33.2, 23.6, 23.6, 19.1, 14.3; HRESIMS *m/z* 232.2066 $[M + H]^+$ (calcd for $C_{16}H_{26}N_1$, 232.2065).

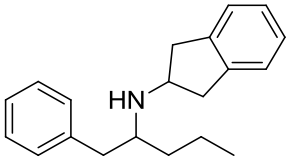


***N*-(1-Phenylpentan-2-yl)cyclopropanamine (216b).** Following the method to prepare amine **215a**, cyclopropylamine (**214b**) (33.0 mg, 0.58 mmol, 1.4 equiv.), $NaBH(OAc)_3$ (144.8 mg, 0.68 mmol, 1.6 equiv.) and AcOH (0.03 mL, 0.52 mmol, 1.2 equiv.) were used to react with ketone **191b** (68.2 mg, 0.42 mmol, 1 equiv.) in $ClCH_2CH_2Cl$ (4 mL) for 25 h to afford amine **216b** as a light yellow oil (50.9 mg,

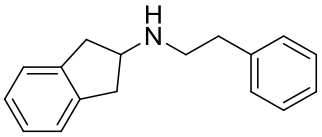
0.25 mmol, 60%). Eluent system of Et_2O–hexane (1:7) was used in centrifugal radial TLC purification. R_f = 0.38 (Et_2O–hexane, 1:3); IR (neat) ν_{max} 3325, 2957, 2930, 2872, 1496, 1454, 1372, 1347, 1014 cm^{-1}; ^1H NMR ($CDCl_3$, 400 MHz) δ 7.32 – 7.17 (m, 5H), 2.98 – 2.84 (m, 1H), 2.82 – 2.64 (m, 2H), 2.06 (tt, *J* = 6.9, 3.7 Hz, 1H), 1.53 – 1.29 (m, 4H), 0.90 (t, *J* = 7.0 Hz, 3H), 0.51 – 0.34 (m, 2H), 0.34 – 0.21 (m, 2H); ^{13}C NMR ($CDCl_3$, 100 MHz) δ 139.9, 129.3, 128.3, 126.0, 59.7, 40.9, 36.2, 28.7, 19.0, 14.3, 7.00, 6.3; HRESIMS *m/z* 204.1759 $[M + H]^+$ (calcd for $C_{14}H_{22}N_1$, 204.1752).



***N*-(1-Phenylpentan-2-yl)bicyclo[2.2.1]heptan-2-amine (216c).** Following the method to prepare amine **215a**, *exo*-2-aminonorbornane (**214c**) (97.8 mg, 0.88 mmol, 1.1 equiv.), $NaBH(OAc)_3$ (282.7 mg, 1.33 mmol, 1.7 equiv.) and AcOH (0.05 mL, 0.87 mmol, 1.1 equiv.) were used to react with ketone **191b** (126.5 mg, 0.78 mmol, 1 equiv.) in $ClCH_2CH_2Cl$ (5 mL) for 24 h to afford amine **216c** as a yellow oil (44.6 mg, 0.17 mmol, 22%). Eluent system of Et_2O–hexane (1:5) was used in centrifugal radial TLC purification. R_f = 0.65 (Et_2O–hexane, 3:1); IR (neat) ν_{max} 3327, 2946, 2866, 1454, 1354, 1122, 1032 cm^{-1}; ^1H NMR ($CDCl_3$, 400 MHz) δ 7.34 – 7.12 (m, 5H), 2.88 – 2.48 (m, 5H), 2.16 – 1.91 (m, 2H), 1.63 – 1.19 (m, 6H), 1.11 – 0.82 (m, 8H); ^{13}C NMR ($CDCl_3$, 100 MHz) δ 139.9, 129.4, 129.3, 128.3, 128.2, 126.0, 125.9, 58.6, 58.5, 56.5, 56.3, 41.3, 41.2, 41.1, 40.8, 40.6, 40.1, 36.8, 35.5, 35.4, 34.8, 34.4, 28.6, 28.6, 27.0, 27.0, 19.3, 19.2, 14.4, 14.2; HRESIMS *m/z* 258.2224 $[M + H]^+$ (calcd for $C_{18}H_{28}N_1$, 258.2222).

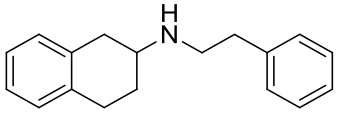


***N*-(1-Phenylpentan-2-yl)-2,3-dihydro-1*H*-inden-2-amine (216d).** Following the method to prepare amine **215a**, 2-aminoindan (**214d**) (102.4 mg, 0.77 mmol, 1.1 equiv.), $NaBH(OAc)_3$ (242.2 mg, 1.14 mmol, 1.6 equiv.) and AcOH (0.04 mL, 0.70 mmol, 1 equiv.) were used to react with ketone **191b** (114.4 mg, 0.71 mmol, 1 equiv.) in $ClCH_2CH_2Cl$ (5 mL) for 21.5 h to afford amine **216d** as a grey oil (37.8 mg, 0.14 mmol, 20%). Eluent system of EtOAc–hexane (1:8) was used in centrifugal radial TLC purification. R_f = 0.58 (EtOAc–hexane, 1:1); IR (neat) ν_{max} 3320, 3034, 2924, 1464, 1347, 1120 cm^{-1}; ^1H NMR ($CDCl_3$, 400 MHz) δ 7.32 – 7.26 (m, 2H), 7.23 – 7.08 (m, 7H), 3.72 (p, *J* = 7.4 Hz, 1H), 3.12 (ddd, *J* = 19.4, 15.5, 7.1 Hz, 2H), 2.94 – 2.84 (m, 1H), 2.77 (dd, *J* = 13.5, 5.9 Hz, 1H), 2.70 – 2.59 (m, 2H), 2.45 (dd, *J* = 15.4, 7.5 Hz, 1H), 1.57 – 1.31 (m, 4H), 1.01 – 0.83 (m, 3H); ^{13}C NMR ($CDCl_3$, 100 MHz) δ 141.6, 139.6, 129.3, 128.4, 126.3, 126.3, 126.1, 124.6, 124.5, 57.2, 41.1, 40.5, 40.2, 36.6, 19.1, 14.3; HRESIMS *m/z* 280.2070 $[M + H]^+$ (calcd for $C_{20}H_{26}N_1$, 280.2065).

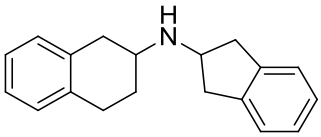


***N*-Phenethyl-2,3-dihydro-1*H*-inden-2-amine (217a).** Following the method to prepare amine **215a**, PEA (**213a**) (0.11 mL, 0.89 mmol, 1.1 equiv.), $NaBH(OAc)_3$ (287.0 mg, 1.35 mmol, 1.6 equiv.) and AcOH (0.05 mL, 0.87 mmol, 1.1 equiv.) were used to react with 2-indanone (**212u**) (108.0 mg, 0.82 mmol, 1 equiv.) in $ClCH_2CH_2Cl$ (8 mL) for 21.5 h to afford amine **217a** as a grey oil (20.4 mg, 0.09 mmol, 11%). Eluent system of EtOAc–hexane (1:6) was used in centrifugal radial

TLC purification. R_f = 0.27 (EtOAc–hexane, 1:1); IR (neat) ν_{max} 3300, 3024, 2933, 2897, 2836, 1454, 1129, 1026 cm^{-1}; ^1H NMR ($CDCl_3$, 400 MHz) δ 7.34 – 7.20 (m, 5H), 7.20 – 7.10 (m, 4H), 3.65 (p, *J* = 6.8 Hz, 1H), 3.15 (dd, *J* = 15.6, 7.1 Hz, 2H), 2.95 (t, *J* = 7.2 Hz, 2H), 2.83 (t, *J* = 7.2 Hz, 2H), 2.73 (dd, *J* = 15.6, 6.7 Hz, 2H); ^{13}C NMR ($CDCl_3$, 100 MHz) δ 141.6, 139.9, 128.7, 128.5, 126.4, 126.2, 124.6, 59.5, 49.6, 39.9, 36.5; HRESIMS *m/z* 238.1589 $[M + H]^+$ (calcd for $C_{17}H_{20}N_1$, 238.1596).

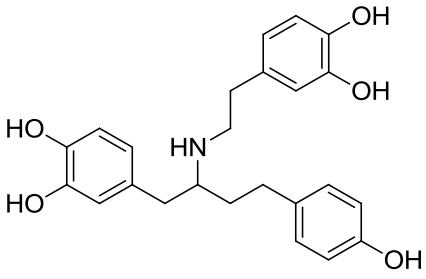


***N*-Phenethyl-1,2,3,4-tetrahydronaphthalen-2-amine (217b).**[289] Following the method to prepare amine **215a**, PEA (**213a**) (0.38 mL, 3.09 mmol, 1.1 equiv.), $NaBH(OAc)_3$ (935.7 mg, 4.41 mmol, 1.6 equiv.) and AcOH (0.16 mL, 2.8 mmol, 1 equiv.) were used to react with β-tetralone (**212v**) (397.2 mg, 2.72 mmol, 1 equiv.) in $ClCH_2CH_2Cl$ (10 mL) for 25 h to afford amine **217b** as a brown oil (529.9 mg, 2.11 mmol, 78%). Eluent system of Et_2O–hexane (1:2) was used in centrifugal radial TLC purification. R_f = 0.28 (Et_2O–hexane, 3:1); IR (neat) ν_{max} 3306, 3023, 2920, 2838, 1492, 1452, 1124 cm^{-1}; ^1H NMR ($CDCl_3$, 700 MHz) δ 7.30 (t, *J* = 7.6 Hz, 2H), 7.24 – 7.19 (m, 3H), 7.12 – 7.03 (m, 4H), 3.01 (t, *J* = 7.3 Hz, 2H), 3.05 – 2.98 (m, 1H), 2.98 – 2.94 (m, 1H), 2.90 – 2.84 (m, 1H), 2.86 (t, *J* = 7.3 Hz, 2H), 2.81 (ddd, *J* = 16.8, 10.9, 5.7 Hz, 1H), 2.61 (dd, *J* = 15.6, 9.4 Hz, 1H), 2.10 – 2.03 (m, 1H), 1.60 (dtd, *J* = 12.6, 10.5, 5.7 Hz, 1H); ^{13}C NMR ($CDCl_3$, 175 MHz) δ 139.8, 136.2, 135.1, 129.3, 128.7, 128.6, 128.5, 126.2, 125.8, 125.7, 53.6, 48.3, 36.5, 36.4, 29.5, 28.1; HRESIMS *m/z* 252.1750 $[M + H]^+$ (calcd for $C_{18}H_{22}N_1$, 252.1752).



***N*-(2,3-Dihydro-1*H*-inden-2-yl)-1,2,3,4-tetrahydronaphthalen-2-amine (218).** Following the method to prepare amine **215a**, 2-aminoindan (**214d**) (112.6 mg, 0.85 mmol, 1.1 equiv.), $NaBH(OAc)_3$ (266.9 mg, 1.26 mmol, 1.7 equiv.) and AcOH (0.04 mL, 0.70 mmol, 0.9 equiv.) were used to react with β-tetralone (**212v**) (110.0 mg, 0.75 mmol, 1 equiv.) in $ClCH_2CH_2Cl$ (5 mL) for 22 h to afford amine **218** as a grey oil (22.0 mg, 0.08 mmol, 11%). Eluent system of EtOAc–hexane (1:9) was used in centrifugal radial TLC purification. R_f = 0.34 (EtOAc–hexane, 1:1); IR (neat) ν_{max} 3300, 3018, 2924, 2837, 1454, 1128 cm^{-1}; ^1H NMR ($CDCl_3$, 400 MHz) δ 7.23 – 7.05 (m, 8H), 3.89 (p, *J* = 7.0 Hz, 1H), 3.28 – 3.16 (m, 2H), 3.16 – 3.01 (m, 2H), 2.97 – 2.73 (m, 4H), 2.64 (dd, *J* = 15.4, 9.1 Hz, 1H), 2.17 – 2.00 (m, 1H), 1.64 (dtd, *J* = 12.7, 10.2, 6.2 Hz, 1H); ^{13}C NMR ($CDCl_3$, 100 MHz) δ 141.7, 136.2, 135.3, 129.4, 128.7, 126.4, 125.8, 125.7, 124.7, 56.6, 51.7, 40.5, 40.3, 37.0, 30.0, 28.2; HRESIMS *m/z* 264.1753 $[M + H]^+$ (calcd for $C_{19}H_{22}N_1$, 264.1752).

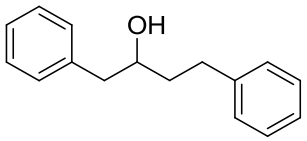
6.1.3.5 *O*-Demethylation of schwarzinicine analogue 215a



4-(2-((3,4-Dihydroxyphenethyl)amino)-4-(4-hydroxyphenyl)butyl)benzene-1,2-diol (219). Based on the procedure reported by Kulkarni *et al.*,[218] neat pyridine hydrochloride (200.0 mg, 1.73 mmol, 21.6 equiv.) was added into compound **215a**

(40.5 mg, 0.08 mmol, 1 equiv.) and the mixture was subjected to microwave irradiation at 200 °C for 20 min. 5% HCl solution (5 mL) and saturated aq. Na_2CO_3 (6 mL) were subsequently added into the mixture. It was extracted with EtOAc (3 X 10 mL) and the combined organic layer was dried with Na_2SO_4 and concentrated *in vacuo*. The crude product was purified by centrifugal radial TLC using an eluent system of Et_2O to yield **219** as a brown oil (7.6 mg, 0.02 mmol, 22%). R_f = 0.16 (5% MeOH–Et_2O, 3:1); ^{1}H NMR (CD_3OD, 400 MHz) δ 6.96 – 6.88 (m, 2H), 6.74 – 6.63 (m, 4H), 6.58 (d, *J* = 2.0 Hz, 2H), 6.40 (ddd, *J* = 8.5, 6.8, 2.1 Hz, 2H), 2.87 – 2.52 (m, 7H), 2.48 (t, *J* = 7.8 Hz, 2H), 1.80 – 1.60 (m, 2H); HRESIMS (LC/MS) (t_R = 1.92 min for a 15 min run) *m/z* 410.1958 $[M + H]^+$ (calcd for $C_{24}H_{28}NO_5$, 409.1958).

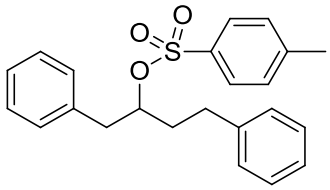
6.1.3.6 Reduction of ketone 191a



1,4-Diphenylbutan-2-ol (221).[290,291] Based on the procedure reported by Lloyd *et al.*,[224] to an ice-cooled solution of ketone **191a** (331.8 mg, 1.48 mmol, 1 equiv.) in EtOH (8 mL) was added $NaBH_4$ (300.2 mg, 7.94 mmol, 5.4 equiv.). The solution was stirred in an ice bath for 1.5 h prior to addition of 1 M NaOH solution (4 mL). It was diluted with CH_2Cl_2 (10 mL) followed by extraction with CH_2Cl_2 (3 X 8 mL). The combined organic layer was washed with water (8 mL) and brine (8 mL). It was then dried with $MgSO_4$ and concentrated *in vacuo*. The crude product was purified by centrifugal radial TLC using an eluent system of Et_2O–hexane (1:3) to yield **221** as a yellow oil (285.7 mg, 1.26 mmol, 85%). R_f = 0.33 (Et_2O–hexane, 1:2); IR (neat) ν_{max} 3382, 3026, 2918, 1602, 1494, 1453, 1079, 1048, 1030 cm^{-1}; ^{1}H NMR ($CDCl_3$, 700 MHz) δ 7.37 – 7.14 (m, 10H), 3.83 (tt, *J* = 8.4, 4.2 Hz, 1H), 2.88 – 2.79 (m, 2H), 2.74

– 2.62 (m, 2H), 1.94 – 1.74 (m, 2H), 1.62 (s, 1H); ^{13}C NMR ($CDCl_3$, 175 MHz) δ 142.0, 138.3, 129.4, 128.6, 128.4, 128.4, 126.5, 125.8, 71.9, 44.1, 38.4, 32.1; HRESIMS *m/z* 244.1697 $[M + NH_4]^+$ (calcd for $C_{16}H_{22}N_1O_1$, 244.1701). The spectroscopic data are in good agreement with those reported in the literature.[290,291]

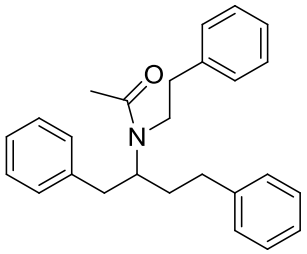
6.1.3.7 Tosylation of alcohol 221



1,4-Diphenylbutan-2-yl 4-methylbenzenesulfonate (224).[290] Based on the procedure reported by Williams *et al.*,[226] to a solution of alcohol **221** (347.8 mg, 1.54 mmol, 1 equiv.) in CH_2Cl_2 (10 mL) was added *p*-toluenesulfonyl chloride (776.5 mg, 4.07 mmol, 2.6 equiv.), Et_3N (1.1 mL, 7.89 mmol, 5.1 equiv) and DMAP (209.7 mg, 1.72 mmol, 1.1 equiv.). The solution was stirred at room temperature for 18 h prior to dilution of EtOAc (10 mL). The solution was washed with saturated aq. NH_4Cl solution (10 mL) and saturated aq. $KHCO_3$ solution (10 mL). The organic phase was dried with $MgSO_4$ and concentrated *in vacuo*. The crude product was purified by centrifugal radial TLC using an eluent system of Et_2O–hexane (1:7) to yield **224** as a yellow oil (458.7 mg, 1.21 mmol, 79%). R_f = 0.22 (Et_2O–hexane, 1:4); IR (neat) ν_{max} 3028, 2924, 2864, 1599, 1496, 1455, 1355, 1172, 1096 cm^{-1}; ^{1}H NMR ($CDCl_3$, 400 MHz) δ 7.72 – 7.63 (m, 2H), 7.31 – 7.10 (m, 8H), 7.11 – 6.97 (m, 4H), 4.78 – 4.68 (m, 1H), 2.94 (qd, *J* = 13.9, 6.4 Hz, 2H), 2.65 (ddd, *J* = 13.9, 9.4, 7.0 Hz, 1H), 2.49 (ddd, *J* = 13.9, 9.1, 6.9 Hz, 1H), 2.42 (s, 3H), 2.00 – 1.79 (m, 2H); ^{13}C NMR ($CDCl_3$, 100 MHz) δ 144.5, 140.8, 136.1, 134.0, 129.7, 129.5, 128.5, 128.4, 128.3, 127.7, 126.7, 126.0, 83.6, 40.8, 35.2, 31.1, 21.6; HRESIMS (LC/MS) (t_R = 11.95 min for a 15 min

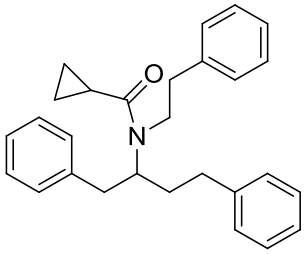
run) *m/z* 403.1340 $[M + Na]^+$ (calcd for $C_{23}H_{24}NaO_3S_1$, 403.1340). The spectroscopic data are in good agreement with those reported in the literature.[290]

6.1.3.8 Formation of amides 230a–c

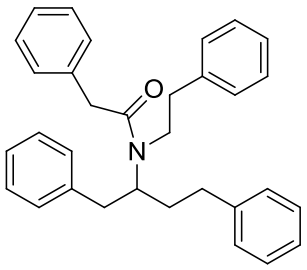


***N*-(1,4-Diphenylbutan-2-yl)-*N*-phenethylacetamide (230a).** Based on the procedure reported by Taniguchi *et al.*,[231] to an ice-cooled solution of amine **215b** (408.6 mg, 1.24 mmol, 1 equiv.) in CH_2Cl_2 (8 mL) was added acetyl chloride (**229a**) (0.14 mL, 1.97 mmol, 1.6 equiv.) and Et_3N (0.31 mL, 2.22 mmol, 1.8 equiv.). The solution was stirred in an ice bath for 45 min prior to addition of water (8 mL). The mixture was extracted with $CHCl_3$ (3 X 10 mL). The combined organic layer was washed with brine (8 mL) before drying with Na_2SO_4 and concentrated *in vacuo*. The crude product was purified by centrifugal radial TLC using an eluent system of Et_2O–hexane (1:1) to yield **230a** as a yellow oil (400.8 mg, 1.08 mmol, 87%). R_f = 0.45 (Et_2O–hexane, 7:1) ; IR (neat) ν_{max} 3026, 2930, 2860, 1634, 1452, 1414, 1030 cm^{-1}; ^1H NMR ($CDCl_3$, 700 MHz) δ 7.37 – 7.05 (m, 15H), 3.88 – 3.77 (m, 1H), 3.61 (td, *J* = 12.3, 4.8 Hz, 1H), 3.33 (ddd, *J* = 13.3, 11.5, 5.3 Hz, 1H), 3.14 (td, *J* = 12.0, 4.7 Hz, 1H), 2.93 – 2.70 (m, 3H), 2.69 – 2.55 (m, 2H), 2.05 (s, 1H), 2.02 – 1.94 (m, 2H), 1.67 (s, 2H); ^{13}C NMR ($CDCl_3$, 175 MHz) δ 171.3, 171.1, 141.6, 140.6, 139.8, 138.2, 138.1, 129.1, 129.0, 128.9, 128.8, 128.7, 128.6, 128.6, 128.4, 128.4, 128.4, 128.3, 128.2, 126.8, 126.7, 126.4, 126.3, 126.3, 125.9, 60.2, 44.0, 40.2, 35.4, 34.6, 34.4, 33.2,

32.6, 22.5, 21.8; HRESIMS *m/z* 394.2159 $[M + Na]^+$ (calcd for $C_{26}H_{29}N_1Na_1O_1$, 394.2147).

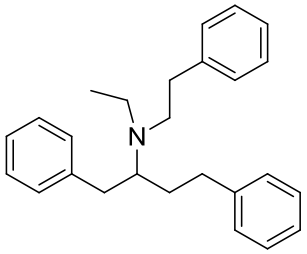


***N*-(1,4-Diphenylbutan-2-yl)-*N*-phenethylcyclopropanecarboxamide (230b).** Following the method to prepare amide **230a**, cyclopropanecarbonyl chloride (**229b**) (80.6 mg, 0.77 mmol, 1.7 equiv.) and Et_3N (0.12 mL, 0.86 mmol, 1.9 equiv.) were used to react with amine **215b** (152.9 mg, 0.46 mmol, 1 equiv.) in CH_2Cl_2 (4 mL) for 45 min to afford amide **230b** as a light yellow oil (165.2 mg, 0.42 mmol, 91%). Eluent system of Et_2O–hexane (1:4) was used in centrifugal radial TLC purification. R_f = 0.46 (Et_2O–hexane, 1:1); IR (neat) ν_{max} 3025, 2928, 1631, 1452, 1423, 1180, 1030 cm^{-1}; ^1H NMR ($CDCl_3$, 700 MHz) δ 7.34 – 7.07 (m, 15H), 4.40 – 4.30 (m, 1H), 3.60 (td, *J* = 12.5, 4.2 Hz, 1H), 3.37 (td, *J* = 13.1, 12.7, 5.2 Hz, 1H), 3.10 (td, *J* = 12.4, 4.2 Hz, 1H), 2.90 – 2.55 (m, 4H), 2.09 – 1.92 (m, 1H), 1.71 – 1.63 (m, 1H), 1.32 – 1.26 (m, 1H), 1.10 – 1.01 (m, 1H), 0.93 – 0.86 (m, 1H), 0.83 – 0.65 (m, 1H), 0.61 – 0.48 (m, 1H), 0.44 – 0.35 (m, 1H); ^{13}C NMR ($CDCl_3$, 175 MHz) δ 173.8, 141.8, 140.9, 139.9, 138.5, 138.2, 129.1, 129.1, 128.9, 128.8, 128.6, 128.6, 128.5, 128.4, 128.4, 128.3, 126.7, 126.6, 126.3, 126.3, 126.2, 125.9, 58.8, 44.5, 40.4, 35.5, 34.7, 34.4, 33.2, 32.8, 12.2, 11.7, 7.7, 7.4, 7.2; HRESIMS *m/z* 398.2480 $[M + H]^+$ (calcd for $C_{28}H_{32}N_1O_1$, 398.2484).

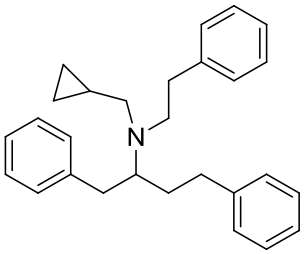


***N*-(1,4-Diphenylbutan-2-yl)-*N*-phenethyl-2-phenylacetamide (230c).** Following the method to prepare amide **230a**, phenylacetyl chloride (**185**) (116.9 mg, 0.76 mmol, 1.6 equiv.) and Et_3N (0.11 mL, 0.79 mmol, 1.7 equiv.) were used to react with amine **215b** (150.6 mg, 0.46 mmol, 1 equiv.) in CH_2Cl_2 (5 mL) for 30 min to afford amide **230c** as a yellow oil (163.6 mg, 0.37 mmol, 80%). Eluent system of Et_2O–hexane (1:6) was used in centrifugal radial TLC purification. R_f = 0.47 (Et_2O–hexane, 1:1); IR (neat) ν_{max} 3061, 3028, 2930, 1731, 1631, 1494, 1453, 1093, 1075 cm^{-1}; ^1H NMR ($CDCl_3$, 700 MHz) δ 7.35 – 7.12 (m, 14H), 7.06 – 7.02 (m, 2H), 7.02 – 6.98 (m, 2H), 6.96 – 6.92 (m, 2H), 3.91 (ddd, *J* = 14.3, 8.3, 5.7 Hz, 1H), 3.67 – 3.56 (m, 2H), 3.39 (ddd, *J* = 13.3, 11.4, 5.3 Hz, 1H), 3.18 – 3.11 (m, 2H), 2.98 – 2.87 (m, 1H), 2.73 (dd, *J* = 13.5, 6.3 Hz, 1H), 2.68 (dd, *J* = 13.5, 8.0 Hz, 1H), 2.60 (dddd, *J* = 49.2, 13.9, 10.2, 6.1 Hz, 1H), 2.51 (ddd, *J* = 14.7, 9.8, 5.3 Hz, 1H), 2.34 (ddd, *J* = 14.2, 9.8, 6.8 Hz, 1H), 1.96 – 1.75 (m, 1H); ^{13}C NMR ($CDCl_3$, 175 MHz) δ 171.7, 141.6, 140.7, 139.7, 138.2, 138.1, 135.3, 135.2, 129.5, 129.2, 129.1, 128.9, 128.9, 128.9, 128.8, 128.7, 128.6, 128.6, 128.6, 128.5, 128.5, 128.4, 128.4, 128.3, 128.2, 127.1, 126.8, 126.7, 126.7, 126.3, 126.3, 126.2, 125.9, 59.5, 49.1, 44.4, 41.2, 40.2, 35.2, 34.5, 34.1, 33.2, 32.4; HRESIMS *m/z* 448.2623 $[M + H]^+$ (calcd for $C_{32}H_{34}N_1O_1$, 448.2640).

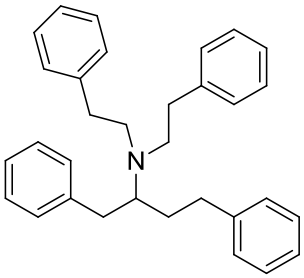
6.1.3.9 Reduction of amides 230a–c



***N*-Ethyl-*N*-phenethyl-1,4-diphenylbutan-2-amine (231a).** Based on the procedure reported by Mu *et al.*,[232] to an ice-cooled solution of amide **230a** (30.0 mg, 0.08 mmol, 1 equiv.) in THF (5 mL) was added $LiAlH_4$ (40.0 mg, 1.05 mmol, 13 equiv.). The suspension was brought to room temperature before refluxed for 35 min. The mixture was cooled in an ice bath and quenched with saturated NH_4Cl solution (5 mL). It was extracted with EtOAc (3 X 5 mL). The combined organic layer was dried with Na_2SO_4 and concentrated *in vacuo*. The crude product was purified by centrifugal radial TLC using an eluent system of Et_2O–hexane (1:3) to yield **231a** as a yellow oil (21.6 mg, 0.06 mmol, 76%). R_f = 0.72 (Et_2O–hexane, 3:1) ; IR (neat) ν_{max} 3026, 2927, 2856, 2808, 1602, 1495, 1453, 1378, 1094, 1030 cm^{-1}; ^1H NMR ($CDCl_3$, 600 MHz) δ 7.33 – 7.08 (m, 13H), 7.05 – 7.01 (m, 2H), 2.90 (dd, *J* = 13.2, 4.5 Hz, 1H), 2.87 – 2.76 (m, 2H), 2.76 – 2.62 (m, 4H), 2.60 – 2.49 (m, 1H), 2.42 – 2.32 (m, 2H), 1.69 – 1.60 (m, 3H), 1.04 (t, *J* = 7.1 Hz, 3H); ^{13}C NMR ($CDCl_3$, 150 MHz) δ 141.9, 140.1, 140.0, 128.2, 127.8, 127.3, 127.2, 127.2, 127.1, 124.8, 124.6, 124.4, 61.0, 51.2, 42.9, 35.5, 35.1, 32.2, 31.7, 13.7; HRESIMS *m/z* 358.2522 $[M + H]^+$ (calcd for $C_{26}H_{32}N_1$, 358.2535).



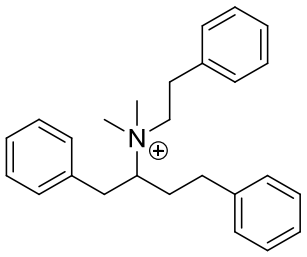
***N*-(Cyclopropylmethyl)-*N*-phenethyl-1,4-diphenylbutan-2-amine (231b).** Following the method to prepare amine **231a**, $LiAlH_4$ (80.0 mg, 2.11 mmol, 6.6 equiv.) was used to react with amide **230b** (126.8 mg, 0.32 mmol, 1 equiv.) in THF (10 mL) for 15 min to afford amine **231b** as a yellow oil (92.4 mg, 0.24 mmol, 75%). Eluent system of Et_2O–hexane (1:9) was used in centrifugal radial TLC purification process. R_f = 0.57 (Et_2O–hexane, 1:5); IR (neat) ν_{max} 3064, 3024, 2932, 2855, 2807, 1601, 1494, 1453, 1116, 1018 cm^{-1}; ^1H NMR ($CDCl_3$, 700 MHz) δ 7.32 – 7.07 (m, 13H), 7.03 (d, *J* = 7.5 Hz, 2H), 2.99 (tt, *J* = 9.2, 4.5 Hz, 1H), 2.93 – 2.86 (m, 2H), 2.80 – 2.66 (m, 5H), 2.57 (dd, *J* = 13.2, 6.1 Hz, 1H), 2.44 – 2.32 (m, 3H), 1.71 – 1.57 (m, 2H), 0.86 – 0.78 (m, 1H), 0.54 – 0.41 (m, 2H), 0.13 (ddt, *J* = 19.6, 9.0, 4.6 Hz, 1H); ^{13}C NMR ($CDCl_3$, 175 MHz) δ 143.7, 143.0, 141.1, 129.2, 128.9, 128.4, 128.3, 128.2, 128.1, 125.8, 125.6, 125.4, 62.2, 55.3, 52.3, 36.4, 36.0, 33.2, 32.7, 10.8, 5.0, 3.5; HRESIMS *m/z* 384.2675 $[M + H]^+$ (calcd for $C_{28}H_{34}N_1$, 384.2691).



***N*,*N*-Diphenethyl-1,4-diphenylbutan-2-amine (231c).** Following the method to prepare amine **231a**, $LiAlH_4$ (73.3 mg, 1.93 mmol, 5.7 equiv.) was used to react with amide **230c** (152.8 mg, 0.34 mmol, 1 equiv.) in THF (15 mL) for 15 min to afford

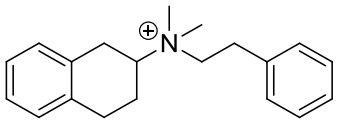
amine **231c** as a yellow oil (70.1 mg, 0.16 mmol, 47%). Eluent system of Et_2O–hexane (1:5) was used in centrifugal radial TLC purification process. R_f = 0.71 (Et_2O–hexane, 1:1); IR (neat) ν_{max} 3025, 2926, 2853, 1494, 1452, 1116, 1028 cm^{-1}; ^1H NMR ($CDCl_3$, 700 MHz) δ 7.32 – 7.11 (m, 16H), 7.10 – 7.06 (m, 2H), 7.02 – 6.98 (m, 2H), 2.90 (dd, *J* = 13.0, 4.8 Hz, 1H), 2.88 – 2.82 (m, 3H), 2.78 – 2.61 (m, 7H), 2.40 (dd, *J* = 13.1, 8.5 Hz, 1H), 2.36 (ddd, *J* = 14.0, 9.8, 6.4 Hz, 1H), 1.71 – 1.57 (m, 2H); ^{13}C NMR ($CDCl_3$, 175 MHz) δ 142.8, 141.0, 140.9, 129.2, 128.9, 128.4, 128.3, 128.3, 128.2, 125.9, 125.7, 125.5, 62.5, 52.6, 36.4, 36.3, 33.2, 32.7; HRESIMS *m/z* 434.2837 $[M + H]^+$ (calcd for $C_{32}H_{36}N_1$, 434.2848).

6.1.3.10 Quaternization of amines 215b and 217b



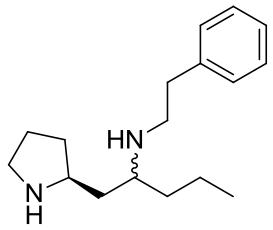
***N*,*N*-Dimethyl-*N*-phenethyl-1,4-diphenylbutan-2-aminium iodide (232).** Based on the procedure reported by Yasa *et al.*,[233] in a stirring solution of amine **215b** (95.7 mg, 0.29 mmol, 1 equiv.) in EtOH (4 mL) was added MeI (4.56 g, 32.1 mmol, 111 equiv.) and K_2CO_3 (131.4 mg, 0.95 mmol, 3.3 equiv.). The mixture was stirred at room temperature for 24 h before concentrated *in vacuo*. The crude product was purified by centrifugal radial TLC using an eluent system of 1% MeOH–EtOAc to yield ammonium salt **232** as an amorphous yellow solid (61.3 mg, 0.13 mmol, 45%). R_f = 0.44 (10% MeOH–EtOAc); IR (neat) ν_{max} 3423, 3018, 2933, 1459 cm^{-1}; ^1H NMR ($CDCl_3$, 400 MHz) δ 7.43 – 7.13 (m, 13H), 7.00 (d, *J* = 7.3 Hz, 2H), 3.89 – 3.67 (m, 3H), 3.53 (dd, *J* = 14.0, 4.8 Hz, 1H), 3.34 (s, 6H), 3.12 – 2.87 (m, 3H), 2.50 – 2.36 (m,

1H), 2.36 – 2.15 (m, 2H), 2.09 – 1.95 (m, 1H); ^{13}C NMR ($CDCl_3$, 175 MHz) δ 139.2, 135.4, 134.6, 129.4, 129.4, 129.3, 129.1, 128.9, 128.6, 127.8, 127.6, 126.8, 72.9, 63.6, 50.0, 49.9, 35.9, 33.5, 31.9, 29.2; HRESIMS *m/z* 150.1277, 254.1899, 344.2362 $[M + H]^+$ (calcd for $C_{10}H_{16}N_1$, $C_{18}H_{24}N_1$, $C_{25}H_{30}N_1$: 150.1283, 254.1909, 344.2378).



***N*,*N*-Dimethyl-*N*-phenethyl-1,2,3,4-tetrahydronaphthalen-2-aminiumiodide (233).** Following the method to prepare ammonium salt **232**, MeI (4.56 g, 32.1 mmol, 51.8 equiv.) and K_2CO_3 (272.7 mg, 1.97 mmol, 3.2 equiv.) were used to react with amine **217b** (155.0 mg, 0.62 mmol, 1 equiv.) in EtOH (5 mL) for 24 h to afford ammonium salt **233** as an amorphous yellow solid (208.9 mg, 0.51 mmol, 82%). Eluent system of 10% MeOH–EtOAc was used in centrifugal radial TLC purification. R_f = 0.38 (10% MeOH–EtOAc); IR (neat) ν_{max} 3421, 3015, 2927, 1450 cm^{-1}; ^{1}H NMR ($CDCl_3$, 400 MHz) δ 7.45 – 7.39 (m, 2H), 7.34 – 7.15 (m, 4H), 7.16 – 7.11 (m, 2H), 7.09 – 7.03 (m, 1H), 4.00 (tdd, *J* = 11.5, 5.5, 2.8 Hz, 1H), 3.93 – 3.75 (m, 2H), 3.44 (s, 3H), 3.39 (s, 3H), 3.28 (ddd, *J* = 15.5, 5.6, 2.1 Hz, 1H), 3.24 – 3.10 (m, 3H), 3.03 – 2.91 (m, 2H), 2.54 – 2.43 (m, 1H), 1.89 – 1.76 (m, 1H); ^{13}C NMR ($CDCl_3$, 100 MHz) δ 134.9, 134.2, 131.3, 129.5, 129.4, 129.2, 128.5, 127.6, 127.1, 126.7, 69.8, 63.4, 49.6, 49.3, 29.7, 29.3, 28.7, 23.9; HRESIMS *m/z* 150.1305, 176.1456, 266.1903 $[M + H]^+$ (calcd for $C_{10}H_{16}N_1$, $C_{12}H_{18}N_1$, $C_{19}H_{24}N_1$: 150.1283, 176.1439, 266.1909).

6.1.3.11 *N*-Boc deprotection of schwarzinicine analogue 215z



***N*-Phenethyl-1-((*S*)-pyrrolidin-2-yl)pentan-2-amine (239).** Based on the procedure reported by Davis *et al.*,[211] to a solution of *N*-Boc protected **215z** (61.7 mg, 0.17 mmol, 1 equiv.) in CH_2Cl_2 (4 mL) was added TFA (0.5 mL, 6.53 mmol, 38.4 equiv.). The solution was stirred at room temperature for 3 h prior to the addition of 3M NaOH solution (6 mL). The mixture was extracted with EtOAc (3 X 10 mL). The combined organic layer was washed with brine (5 mL), dried with Na_2SO_4 and concentrated *in vacuo*. The crude product was purified by centrifugal radial TLC using an eluent system of 5% MeOH–EtOAc (NH_3) to yield diastereomer 1 of **239** as a yellow oil (11.4 mg, 0.04 mmol, 24%) and diastereomer 2 of **239** as a yellow oil (9.8 mg, 0.04 mmol, 24%). Diastereomer 1: R_f = 0.12 (5% MeOH–EtOAc (NH_3)); IR (neat) ν_{max} 3420, 3265, 2960, 2933, 2874, 1673, 1455, 1424, 1199, 1172, 1126 cm^{-1}; ^1H NMR ($CDCl_3$, 600 MHz) δ 7.36 – 7.30 (m, 2H), 7.27 – 7.18 (m, 3H), 3.75 – 3.69 (m, 1H), 3.13 (dt, *J* = 11.1, 5.7 Hz, 1H), 2.94 – 2.71 (m, 5H), 2.57 (dt, *J* = 11.6, 7.6 Hz, 1H), 2.06 (dq, *J* = 13.0, 7.4 Hz, 1H), 1.87 – 1.77 (m, 2H), 1.65 – 1.58 (m, 1H), 1.50 (dtd, *J* = 12.7, 7.1, 5.0 Hz, 1H), 1.37 – 1.16 (m, 5H), 0.91 (t, *J* = 7.3 Hz, 3H); ^{13}C NMR ($CDCl_3$, 150 MHz) δ 139.2, 128.9, 128.7, 126.7, 59.5, 57.6, 46.1, 43.1, 35.8, 35.7, 34.7, 31.2, 23.7, 18.7, 14.1; HRESIMS (LC/MS) (t_R = 2.46 min for a 15 min run) *m/z* 261.2335 $[M + H]^+$ (calcd for $C_{17}H_{29}N_2$, 261.2335). Diastereomer 2: R_f = 0.07 (5% MeOH–EtOAc (NH_3)); IR (neat) ν_{max} 3385, 3289, 2955, 2929, 2870, 1540, 1454,

1401, 1143, 1101, 1031 cm^{-1}; ^{1}H NMR ($CDCl_3$, 400 MHz) δ 7.33 – 7.27 (m, 2H), 7.25 – 7.14 (m, 3H), 3.09 – 2.98 (m, 1H), 2.98 – 2.87 (m, 2H), 2.87 – 2.74 (m, 3H), 2.65 – 2.54 (m, 1H), 1.91 – 1.78 (m, 1H), 1.76 – 1.61 (m, 2H), 1.58 – 1.39 (m, 3H), 1.39 – 1.15 (m, 5H), 0.88 (t, *J* = 7.1 Hz, 3H); ^{13}C NMR ($CDCl_3$, 100 MHz) δ 140.2, 128.8, 128.4, 126.1, 57.8, 56.9, 48.1, 46.1, 40.3, 36.6, 32.4, 31.8, 24.9, 18.8, 14.4; HRESIMS (LC/MS) (t_R = 2.25 min for a 15 min run) *m/z* 261.2335 $[M + H]^+$ (calcd for $C_{17}H_{29}N_2$, 261.2335).

6.2 Computational analysis

Low-energy conformations of four stereoisomers of **147** ((2*R*,4*R*), (2*S*,4*S*), (2*R*,4*S*) and (2*S*,4*R*)) were generated using Confab as implemented in OpenBabel 2.4.1.[292,293] Geometry optimization using DFT at the B3LYP/6-31G* level was then performed using ORCA 4.1.[294,295] The lowest energy geometry-optimized conformers within an 5 kcal/mol cut-off were then subjected to TDDFT ECD calculations at the CAM-B3LYP/def2-TZVP level using a CPCM solvation model for acetonitrile.[296] The final ECD curve was calculated using SpecDis 1.71 following Boltzmann weighting of the individual ECD curves and UV correction.[297] The calculated ECD curve was then compared to the experimental ECD curves for the assignment of the absolute stereochemistry.

6.3 Pharmacological testing

6.3.1 Chemicals and reagents

(*R*)-(–)-Phenylephrine (PE) hydrochloride (Sigma Aldrich, United States), dobutamine hydrochloride (Tocris Bioscience, United States), (±)-verapamil hydrochloride (Acros Organics, United States), 3,4-dimethoxyphenethylamine

(DMPEA, **176**) (Acros Organics, United States) and DMSO (Sigma Aldrich, United States) were used in the testing. PE was dissolved in purified water (purified by ELGA PURELAB® flex water purification system) to prepare 0.1 M stock solution and subsequently diluted down into lower concentrations (10 mM, 1 mM, 0.1 mM, 10 μM, 1 μM and 0.1 μM) in purified water. The two positive controls (dobutamine and verapamil (**18**)), DMPEA (**176**), schwarzinicines A–D (**142–145**), F (**147d**) and all synthesized analogues were first dissolved in DMSO to make up 0.1 M stock solutions before further diluted down into lower concentrations in purified water. The stock solutions that were prepared from a 10-fold serial dilution of 0.1 M compounds included: 10 mM (75% DMSO (v/v)), 1 mM (50% DMSO (v/v)), 0.1 mM (25% DMSO (v/v)), 10 μM (~100% purified water), 1 μM (~100% purified water) and 0.1 μM (~100% purified water). The Krebs-Ringer bicarbonate solution was prepared based on the composition reported by Loong *et al.*[298]

6.3.2 Tissue preparation

Adult male Sprague Dawley (SD) rats (2–3 months old, 300–420 g, purchased from the animal house at Universiti Putra Malaysia) and spontaneously hypertensive rats (SHRs) (4–5 months, 300–470 g, SBP 170–310 mmHg, DBP 130–300 mmHg, purchased from the animal house at Monash University Malaysia) were euthanized with CO_2. Ethical approvals were obtained from the University of Nottingham's Animal Welfare and Ethical Review Body (AWERB REF: UNMC12 and UNMC18). The entire thoracic aorta was immediately excised, cut into segments of 4 mm in length and transferred into Krebs-Ringer bicarbonate solution. Each segment was suspended by a glass rod in a glass organ bath chamber containing 10 mL Krebs-Ringer bicarbonate solution at 37 °C and aerated with 5% CO_2 in 95% O_2. Changes in muscle tension due to tissue contraction and relaxation were recorded by a force

transducer (MLTF050/ST, ADInstruments, US) and a PowerLab data acquisition system (LabChart v7.3.4). The raw data were stored on a laptop (EliteBook 8470p, Hewlett-Packard, US). The tissue was allowed to equilibrate for 15 min in the solution before tension (2 g) was applied. The tissue with loaded tension was allowed to equilibrate for 30 min prior to stimulation with 60 mM KCl solution twice to test the tissue viability. After equilibration, each aortic ring was pre-contracted with PE (0.1 µM). This was then followed by the subsequent individual experimental protocols. When the PE-induced contraction reached a plateau, each compound was added in cumulative concentration from 0.1 nM to 0.1 mM in the organ bath chamber to obtain a cumulative concentration-response curve.

6.3.3 Effects of compounds against phenylephrine (PE)-induced contraction in aorta

To determine the vasorelaxant effect of each compound, each aortic ring was first precontracted with PE (0.1 µM). When the PE-induced contractile response plateaued, cumulative concentration-response curves for each compound (from 0.1 nM to 0.1 mM) were constructed. The relaxation responses were calculated as percentage inhibition of PE-induced contraction. E_{max} and EC_{50} values were obtained, where EC_{50} is the concentration of the compound that produces 50% of its maximum response (E_{max}). DMSO was used as vehicle control in the experiment.

6.3.4 Data analysis and statistics

The raw data were analysed by using Microsoft Excel 2016 and GraphPad Prism 7.05. The data were expressed as mean ± standard error of the mean (SEM) of *n*, which represents the number of animals for each data set. The maximum percentage of relaxation (E_{max}) and the concentration of a compound that produced half-maximal

relaxation (EC_{50}) were obtained from non-linear curves fitting using GraphPad Prism 7.05. Comparison between experimental groups was analysed using unpaired Student's *t*-test. Results were considered to be statistically significant if $p < 0.05$.

References

(1) Chobanian, A. V.; Bakris, G. L.; Black, H. R.; Cushman, W. C.; Green, L. A.; Izzo, J. L.; Jones, D. W.; Materson, B. J.; Oparil, S.; Wright, J. T.; Roccella, E. J. *JAMA* **2003**, *289* (19), 2560–2572.

(2) Kearney, P. M.; Whelton, M.; Reynolds, K.; Muntner, P.; Whelton, P. K.; He, J. *Lancet* **2005**, *365* (9455), 217–223.

(3) Lim, S. S.; Vos, T.; Flaxman, A. D.; Danaei, G.; Shibuya, K.; Adair-Rohani, H.; AlMazroa, M. A.; Amann, M.; Anderson, H. R.; Andrews, K. G.; Aryee, M.; Atkinson, C.; Bacchus, L. J.; Bahalim, A. N.; Balakrishnan, K.; Balmes, J.; Barker-Collo, S.; Baxter, A.; Bell, M. L.; Blore, J. D.; Blyth, F.; Bonner, C.; Borges, G.; Bourne, R.; Boussinesq, M.; Brauer, M.; Brooks, P.; Bruce, N. G.; Brunekreef, B.; Bryan-Hancock, C.; Bucello, C.; Buchbinder, R.; Bull, F.; Burnett, R. T.; Byers, T. E.; Calabria, B.; Carapetis, J.; Carnahan, E.; Chafe, Z.; Charlson, F.; Chen, H.; Chen, J. S.; Cheng, A. T. A.; Child, J. C.; Cohen, A.; Colson, K. E.; Cowie, B. C.; Darby, S.; Darling, S.; Davis, A.; Degenhardt, L.; Dentener, F.; Des Jarlais, D. C.; Devries, K.; Dherani, M.; Ding, E. L.; Dorsey, E. R.; Driscoll, T.; Edmond, K.; Ali, S. E.; Engell, R. E.; Erwin, P. J.; Fahimi, S.; Falder, G.; Farzadfar, F.; Ferrari, A.; Finucane, M. M.; Flaxman, S.; Fowkes, F. G. R.; Freedman, G.; Freeman, M. K.; Gakidou, E.; Ghosh, S.; Giovannucci, E.; Gmel, G.; Graham, K.; Grainger, R.; Grant, B.; Gunnell, D.; Gutierrez, H. R.; Hall, W.; Hoek, H. W.; Hogan, A.; Hosgood, H. D.; Hoy, D.; Hu, H.; Hubbell, B. J.; Hutchings, S. J.; Ibeanusi, S. E.; Jacklyn, G. L.; Jasrasaria, R.; Jonas, J. B.; Kan, H.; Kanis, J. A.; Kassebaum, N.; Kawakami, N.; Khang, Y. H.; Khatibzadeh, S.; Khoo, J.-P.; Kok, C.; Laden, F.; Lalloo, R.; Lan, Q.;

Lathlean, T.; Leasher, J. L.; Leigh, J.; Li, Y.; Lin, J. K.; Lipshultz, S. E.; London, S.; Lozano, R.; Lu, Y.; Mak, J.; Malekzadeh, R.; Mallinger, L.; Marcenes, W.; March, L.; Marks, R.; Martin, R.; McGale, P.; McGrath, J.; Mehta, S.; Memish, Z. A.; Mensah, G. A.; Merriman, T. R.; Micha, R.; Michaud, C.; Mishra, V.; Hanafiah, K. M.; Mokdad, A. A.; Morawska, L.; Mozaffarian, D.; Murphy, T.; Naghavi, M.; Neal, B.; Nelson, P. K.; Nolla, J. M.; Norman, R.; Olives, C.; Omer, S. B.; Orchard, J.; Osborne, R.; Ostro, B.; Page, A.; Pandey, K. D.; Parry, C. D. H.; Passmore, E.; Patra, J.; Pearce, N.; Pelizzari, P. M.; Petzold, M.; Phillips, M. R.; Pope, D.; Pope, C. A.; Powles, J.; Rao, M.; Razavi, H.; Rehfuess, E. A.; Rehm, J. T.; Ritz, B.; Rivara, F. P.; Roberts, T.; Robinson, C.; Rodriguez-Portales, J. A.; Romieu, I.; Room, R.; Rosenfeld, L. C.; Roy, A.; Rushton, L.; Salomon, J. A.; Sampson, U.; Sanchez-Riera, L.; Sanman, E.; Sapkota, A.; Seedat, S.; Shi, P.; Shield, K.; Shivakoti, R.; Singh, G. M.; Sleet, D. A.; Smith, E.; Smith, K. R.; Stapelberg, N. J. C.; Steenland, K.; Stöckl, H.; Stovner, L. J.; Straif, K.; Straney, L.; Thurston, G. D.; Tran, J. H.; Van Dingenen, R.; Van Donkelaar, A.; Veerman, J. L.; Vijayakumar, L.; Weintraub, R.; Weissman, M. M.; White, R. A.; Whiteford, H.; Wiersma, S. T.; Wilkinson, J. D.; Williams, H. C.; Williams, W.; Wilson, N.; Woolf, A. D.; Yip, P.; Zielinski, J. M.; Lopez, A. D.; Murray, C. J. L.; Ezzati, M. *Lancet* **2012**, *380* (9859), 2224–2260.

(4) Messerli, F. H.; Williams, B.; Ritz, E. *Lancet (London, England)* **2007**, *370* (9587), 591–603.

(5) Whelton, P. K.; Carey, R. M.; Aronow, W. S.; Casey, D. E.; Collins, K. J.; Dennison Himmelfarb, C.; DePalma, S. M.; Gidding, S.; Jamerson, K. A.; Jones, D. W.; MacLaughlin, E. J.; Muntner, P.; Ovbiagele, B.; Smith, S. C.;

Spencer, C. C.; Stafford, R. S.; Taler, S. J.; Thomas, R. J.; Williams, K. A.; Williamson, J. D.; Wright, J. T. *Hypertension* **2018**, *71* (6), e13–e115.

(6) Ettehad, D.; Emdin, C. A.; Kiran, A.; Anderson, S. G.; Callender, T.; Emberson, J.; Chalmers, J.; Rodgers, A.; Rahimi, K. *Lancet* **2016**, *387* (10022), 957–967.

(7) Hansson, L.; Lindholm, L. H.; Ekbom, T.; Dahlöf, B.; Lanke, J.; Scherstén, B.; Wester, P.-O.; Hedner, T.; de Faire, U. *Lancet* **1999**, *354* (9192), 1751–1756.

(8) Neal, B.; MacMahon, S.; Chapman, N.; Cutler, J.; Fagard, R.; Whelton, P.; Yusuf, S.; Agodoa, L.; Baigent, C.; Black, H.; Boissel, J. P.; Brenner, B.; Brown, M.; Bulpitt, C.; Byington, R.; Chalmers, J.; Collins, R.; Dahlof, B.; Davis, B.; Estacio, R.; Fox, K.; Hansson, L.; Holman, R.; Hunsicker, L.; Kostis, J.; Kuramoto, K.; Kusek, J.; Lees, R.; Lewis, E.; Lindholm, L. H.; Liu, L.; Lubsen, J.; Malacco, E.; Mancia, G.; Martin, I.; Pepine, C.; Pfeffer, M.; Pitt, B.; Poole-Wilson, P.; Remuzzi, G.; Rodgers, A.; Ruggenenti, P.; Schrier, R.; Sever, P.; Sleight, P.; Staessen, J.; Teo, K.; Turner, R.; Wing, L.; Zanchetti, A.; Algert, C.; Woodward, M. *Lancet* **2000**, *356* (9246), 1955–1964.

(9) Wong, J.; Patel, R. A.; Kowey, P. R. *Prog. Cardiovasc. Dis.* **2004**, *47* (2), 116–130.

(10) Brown, N. J.; Vaughan, D. E. *Circulation* **1998**, *97* (14), 1411–1420.

(11) Ferrario, C. M. *JRAAS* **2006**, *7* (1), 3–14.

(12) Patrick, G. L. *An Introduction to Medicinal Chemistry*, 5th ed.; Oxford Univerisity Press, 2013.

(13) Cushman, D. W.; Ondetti, M. A. *Hypertension* **1991**, *17* (4), 589–592.

(14) Panderi, I. E. *J. Pharm. Biomed. Anal.* **1999**, *21* (2), 257–265.

(15) Patchett, A. A.; Harris, E.; Tristram, E. W.; Wyvratt, M. J.; Wu, M. T.; Taub, D.; Peterson, E. R.; Ikeler, T. J.; Ten Broeke, J.; Payne, L. G.; Ondeyka, D. L.; Thorsett, E. D.; Greenlee, W. J.; Lohr, N. S.; Hoffsommer, R. D.; Joshua, H.; Ruyle, W. V.; Rothrock, J. W.; Aster, S. D.; Maycock, A. L.; Robinson, F. M.; Hirschmann, R.; Sweet, C. S.; Ulm, E. H.; Gross, D. M.; Vassil, T. C.; Stone, C. A. *Nature* **1980**, *288*, 280–283.

(16) Brown, B.; Hall, A. S. *Am. J. Hypertens.* **2005**, *18* (S5), 127S-133S.

(17) Magri', A. L.; Balestrieri, F.; Magri', A. D.; Marini, D. *Talanta* **1995**, *42* (11), 1719–1723.

(18) Vleeming, W.; Van Amsterdam, J. G. C.; Stricker, B. H. C.; De Wildt, D. J. *Drug Saf.* **1998**, *18* (3), 171–188.

(19) Carey, R. M.; Siragy, H. M. *Endocr. Rev.* **2003**, *24* (3), 261–271.

(20) Bhuiyan, M. A.; Ishiguro, M.; Hossain, M.; Nakamura, T.; Ozaki, M.; Miura, S.; Nagatomo, T. *Life Sci.* **2009**, *85* (3–4), 136–140.

(21) Bauer, M.; Harris, R. K.; Rao, R. C.; Apperley, D. C.; Rodger, C. A. *J. Chem. Soc. Perkin Trans. 2* **1998**, No. 3, 475–482.

(22) Ohno, K.; Amano, Y.; Kakuta, H.; Niimi, T.; Takakura, S.; Orita, M.; Miyata, K.; Sakashita, H.; Takeuchi, M.; Komuro, I.; Higaki, J.; Horiuchi, M.; Kim-Mitsuyama, S.; Mori, Y.; Morishita, R.; Yamagishi, S. *Biochem. Biophys. Res. Commun.* **2011**, *404* (1), 434–437.

(23) Burnier, M.; Brunner, H. R. *Lancet* **2000**, *355* (9204), 637–645.

(24) Hedner, T.; Oparil, S.; Rasmussen, K.; Rapelli, A.; Gatlin, M.; Kobi, P.; Sullivan, J.; Oddou-Stock, P. *Am. J. Hypertens.* **1999**, *12* (4), 414–417.

(25) Burnier, M. *Circulation* **2001**, *103* (6), 904–912.

(26) Yusuf, S.; Teo, K.; Anderson, C.; Pogue, J.; Dyal, L.; Copland, I.; Schumacher, H.; Dagenais, G.; Sleight, P. *Lancet* **2016**, *372* (9644), 1174–1183.

(27) Benz, J.; Oshrain, C.; Henry, D.; Avery, C.; Chiang, Y.-T.; Gatlin, M. *J. Clin. Pharmacol.* **1997**, *37* (2), 101–107.

(28) Matchar, D. B.; McCrory, D. C.; Orlando, L. A.; Patel, M. R.; Patel, U. D.; Patwardhan, M. B.; Powers, B.; Samsa, G. P.; Gray, R. N. *Ann. Intern. Med.* **2008**, *148* (1), 16–29.

(29) Freemantle, N.; Cleland, J.; Young, P.; Mason, J.; Harrison, J. *BMJ* **1999**, *318*, 1730–1737.

(30) *Current Cardiovascular Drugs*, 3rd ed.; Frishman, W. H., Cheng-Lai, A., Chen, J., Eds.; Current Medicine Group: London, 2000.

(31) López-Sendón, J.; Swedberg, K.; McMurray, J.; Tamargo, J.; Maggioni, A. P.; Dargie, H.; Tendera, M.; Waagstein, F.; Kjekshus, J.; Lechat, P.; Torp-pedersen, C. *Eur. Heart J.* **2004**, *25* (15), 1341–1362.

(32) Bristow, M. R. *Circulation* **2000**, *101* (5), 558–569.

(33) Gagyi, L.; Gyéresi, Á.; Kilár, F. *J. Biochem. Biophys. Methods* **2008**, *70* (6), 1268–1275.

(34) Hjalmarson, A.; Goldstein, S.; Fagerberg, B.; Wedel, H.; Waagstein, F.; Kjekshus, J.; Wikstrand, J.; Westergren, G.; Thimell, M.; El Allaf, D.; Vítovec,

J.; Aldershvile, J.; Halinen, M.; Dietz, R.; Neuhaus, K. L.; Jánosi, A.; Thorgeirsson, G.; Dunselman, P.; Gullestad, L.; Kuch, J.; Herlitz, J.; Rickenbacher, P.; Ball, S.; Gottlieb, S.; Deedwania, P.; Vandenhoven, G.; Nováková, I.; Danker, S.; Lundström, M.; Meyer-Sabellek, W.; Balla, I.; Sveinsdottir, M.; Dorhout, B.; Hildebrandt, A.; Szczurko, I.; Larsson, C.; Bucher, E.; Scott, E.; Dwyer, D.; Julian, D. G.; DeMets, D. L.; Chatterjee, K.; Feyzi, J.; Lehto, S.; Kárpáti, P.; Motz, W.; Samuelsson, O.; Viersma, J. W.; Andersson, B.; Berthe, C.; Boutefeu, J. M.; Boxho, G.; Decroly, P.; Derbaudrenghien, J. P.; Pirlet, J.; Henry, P.; Heyndrickx, G.; Missault, L.; Nannan, M.; Timmermans, P.; Vachiery, J. L.; Van Mieghem, W.; Vandenbossche, J. L.; Dvorák, K.; Herold, M.; Hradec, J.; Kána, A.; Petr, P.; Rybka, J.; Smíd, J.; Svítil, P.; Toman, J.; Agner, E.; Amtorp, O.; Egstrup, K.; Eliasen, P.; Gotzsche, C. O.; Hildebrandt, P.; Johannesen, A.; Kaiser-Nielsen, P.; Nielsen, H.; Nielsen, P. E.; Pedersen, F.; Rokkedal Nielsen, J.; Skagen, K.; Halinen, M.; Honkanen, T.; Hussi, E.; Juvonen, J.; Jääskeläinen, H.; Rinne, J.; Salonen, T.; Andresen, D.; Berwing, H.; Bethge; Beythien; Bischoff; Bundschu; Daniel; Darius; Delius; Drude; Dietz, R.; Dingerkus; Dück; Eichler; Fach; Förster, A.; Girth; Goss; Hahn; Hambrecht; Hauf, G. F.; Heinemann; Hepp; Janka; Klocke; Konz; Krosse, B.; Kühlkamp; Lewek; Lüderitz, B.; Löbe; Maier; Melchior; Müller; Mäurer; Nast; Neuhaus; Obst; Odemar; Von Olshausen, K. E.; Pomykaj; Schmailzl, K. J. G.; Schrader; Schröder; Schwimmbeck, P. L.; Sigmund, M.; Simon; Strasser; Thilo; Vöhringer; Völler, H.; Weisbrodt; Wirtz; Wunderlich; Czuriga, I.; Hetey, M.; Jánosi, A.; Katona, A.; Lengyel, M.; Nyárádi, A.; Rednik, A.; Sándori, K.; Szabó, P.; Tarján, J.; Tenczer, J.; Timár, S.; Vályi, P.; Veress, G.; Zámolyi, K.; Öze, B.; Thorgeirsson, G.; Thorgeirsson,

G.; Bernink, P. J. L. M.; Bredero, A. C.; Breedveld, R. W.; Breuls, P. N. W. M.; Bucx, J. J. J.; Cornel, J. H.; De Milliano, P. A. R.; Dunselman, P. H. J. M.; Hamer, B. J. B.; Holwerda, N. L.; Hoogsteen, J.; Hoorntje, J. C. A.; Kragten, J. A.; Liem, A. H.; Linssen, G. C. M.; Michels, H. R.; Ramdat Misier, A. R.; Schaafsma, H. J.; Sijbring, P.; Taverne, R. J. T.; Van Kempen, L. H. J.; Van Stralen, R.; Van Veldhuisen, P. J.; Veerhoek, M. J.; Werter, C. J. P. J.; Wesdorp, J. C. L.; Willems, A. R.; Withagen, A. J. A. M.; Zwart, P. A. G.; Bjornerheim, R.; Dahle, M.; Dickstein, K.; Froland, G. S.; Gundersen, T.; Hofsoy, K.; Hole, T. L.; Johansen, T.; Mannsverk, J.; Nesje, P.; Omland, T. M.; Sjödin, C.; Smith, P.; Tjonndal, H. A.; Vikesdal, O.; Waage, K.; Adamus; Jaworska, K.; Kolodziej, P.; Kornacewicz-Jach, Z.; Krzemiñska-Pakula, M.; Piotrowski, J. W.; Piwowarska, W.; Stogowski, A.; Wodniecki, J.; Wrabec, K.; Ahlström, P.; Ekdahl, S.; Hemmingson, L. O.; Holmberg, L.; Lernfelt, B.; Nilsson B Widgren, H.; Ångman, K.; Erne, P.; Mohacsi, P.; Polikar, R.; Schläpfer, H.; Batin, P.; Berkin, K. E.; Callaghan, T. S.; Forfar, J.; Frenneaux, M.; Greenbaum, R. A.; Maltz, M.; Murdoch, D.; Reynolds, G.; Stephens, J.; Struthers, A.; Swan, J.; Tildesley, G.; Abbasi, A.; Alagona, P.; Alderman, J.; Alipour, M.; Anderson, J. L.; Ansari, Z.; Ashraf, M.; Beanblossom, B. T.; Bennett, S.; Benvenuti, D.; Berk, M. R.; Bhalla, R.; Bilazarian, S. D.; Browne, K. F.; Buchter, M. C.; Carlson, R.; Carlson, C. J.; Danisa, K.; Dauber, I.; DeWood, M. A.; Dennish, G.; Denny, D. M.; DiBianco, R.; Diller, P. M.; Dunlap, M.; Dowd, K.; Edmiston, A.; El Shahawy, M.; Elkayam, U.; Farnham, J.; Fenster, P.; Friedman, S.; Heywood, T.; Galichia, J. P.; Geller, M.; Ghali, J. K.; Gheorghiade, M.; Giles, T.; Gillespe, R.; Goldberg, G.; Goldberg, M. C.; Goldscher, D. A.; Gooden, G. P.; Goodman, M.; Goodman, L.; Gorwit, J.;

Gottlieb, S. S.; Gradman, A.; Grech, D.; Hack, T.; Hall, J. H.; Hattenhauer, M. T.; Higginbotham, M. B.; Hutchins, S.; Imburgia, M.; Iteld, B. J.; Jackson, B.; Jafri, S.; Jauch, W.; Jennison, S.; Kahn, B. H.; Kao, W.; Kaplan, K.; Karlsberg, R.; Kennedy, H. L.; Kennedy, J. J.; Kirkegaard, L.; Kraus, D. H.; LaBresh, K.; Lalonde, L.; Lesser, M. F.; Levites, R.; Levy, M.; Lewis, R. K.; Loh, I. K.; Madyoon, H.; Maislos, F.; Mann, D.; Maurice, G. L.; Nisar, A.; Old, W.; Pappas, J. D.; Phadke, K.; Promisloff, S.; Rashkow, A. M.; Reeves, B.; Rosen, J. H.; Rotman, M.; Saleem, T.; Savran, S. V.; Shah, R.; Shalev, Y.; Shanes, J. G.; O'Shaughnessy, M.; Silverman, B.; Steingart, R. M.; Swenson, L.; Syed, K.; Thadani, U.; Thorsen, R. D.; Tonkon, M. J.; Touchon, R.; Uhl, G.; Vaska, K. J.; Wagner, S. G.; Weaver, C. J.; Weiss, R. J.; Wickemeyer, W. J.; Willens, H. J.; Wilson, J. R.; Wright, R.; Yellen, L. *Lancet* **1999**, *353* (9169), 2001–2007.

(35) Dargie, H. J.; Lechat, P. *Lancet* **1999**, *353* (9146), 9–13.

(36) Ruffolo, R. R.; Gellai, M.; Hieble, J. P.; Willette, R. N.; Nichols, A. J. *Eur. J. Clin. Pharmacol.* **1990**, *38* (S2), S82–S88.

(37) Metra, M.; Nodari, S.; D'Aloia, A.; Bontempi, L.; Boldi, E.; Cas, L. D. *Am. Heart J.* **2000**, *139* (3), 511–521.

(38) Frishman, W. H. *Hypertension* **1988**, *11* (3_pt_2), 21–29.

(39) Ellison, D. H.; Velázquez, H.; Wright, F. S. *Am. J. Physiol. Physiol.* **1987**, *253* (3), F546–F554.

(40) Velázquez, H.; Náray-Fejes-Tóth, A.; Silva, T.; Andújar, E.; Reilly, R. F.; Desir, G. V.; Ellison, D. H. *Kidney Int.* **1998**, *54* (2), 464–472.

(41) Obermüller, N.; Bernstein, P.; Velázquez, H.; Reilly, R.; Moser, D.; Ellison, D.

H.; Bachmann, S. *Am. J. Physiol. Physiol.* **1995**, *269* (6), F900–F910.

(42) Duarte, J. D.; Cooper-DeHoff, R. M. *Expert Rev. Cardiovasc. Ther.* **2010**, *8* (6), 793–802.

(43) Conway, J.; Lauwers, P. *Circulation* **1960**, *21* (1), 21–27.

(44) Van Brummelen, P.; Man in 't Veld, A. J.; Schalekamp, M. A. D. H. *Clin. Pharmacol. Ther.* **1980**, *27* (3), 328–336.

(45) Freis, E. D. *Hypertension* **2001**, *38* (1), 1–5.

(46) Hughes, A. D. *J. Renin-Angiotensin-Aldosterone Syst.* **2004**, *5* (4), 155–160.

(47) Sica, D. A. *Hypertension* **2006**, *47* (3), 321–322.

(48) Herráez-Hernández, R.; Campíns-Falcó, P. *J. Chromatogr. B Biomed. Sci. Appl.* **2000**, *740* (2), 169–177.

(49) Ernst, M. E.; Carter, B. L.; Goerdt, C. J.; Steffensmeier, J. J. G.; Phillips, B. B.; Zimmerman, M. B.; Bergus, G. R. *Hypertension* **2006**, *47* (3), 352–358.

(50) Sica, D. A.; Carter, B.; Cushman, W.; Hamm, L. *J. Clin. Hypertens.* **2011**, *13* (9), 639–643.

(51) Scholz, H. *Cardiovasc. Drugs Ther.* **1997**, *10* (SUPPL. 3), 869–872.

(52) Felizola, S. J. A.; Maekawa, T.; Nakamura, Y.; Satoh, F.; Ono, Y.; Kikuchi, K.; Aritomi, S.; Ikeda, K.; Yoshimura, M.; Tojo, K.; Sasano, H. *J. Steroid Biochem. Mol. Biol.* **2014**, *144*, 410–416.

(53) Schiffrin, E. L. *Hypertension* **2006**, *47* (3), 312–318.

(54) Sica, D. A. *J. Clin. Hypertens.* **2006**, *8* (1), 53–56.

(55) Godfraind, T. *Cardiovasc. Drugs Ther.* **1994**, *8* (S2), 353–364.

(56) Henry, P. D. *Am. J. Cardiol.* **1980**, *46* (6), 1047–1058.

(57) Kawai, C.; Konishi, T.; Matsuyama, E.; Okazaki, H. *Circulation* **1981**, *63* (5), 1035–1042.

(58) Sarafidis, P. A.; Bakris, G. L. *J. Am. Coll. Cardiol.* **2008**, *52* (22), 1749–1757.

(59) Myat, A.; Redwood, S. R.; Qureshi, A. C.; Spertus, J. A.; Williams, B. *BMJ* **2012**, *345*, e7473.

(60) Acelajado, M. C.; Hughes, Z. H.; Oparil, S.; Calhoun, D. A. *Circ. Res.* **2019**, *124* (7), 1061–1070.

(61) Carey, R. M.; Calhoun, D. A.; Bakris, G. L.; Brook, R. D.; Daugherty, S. L.; Dennison-Himmelfarb, C. R.; Egan, B. M.; Flack, J. M.; Gidding, S. S.; Judd, E.; Lackland, D. T.; Laffer, C. L.; Newton-Cheh, C.; Smith, S. M.; Taler, S. J.; Textor, S. C.; Turan, T. N.; White, W. B. *Hypertension* **2018**, *72* (5), e53–e90.

(62) Pimenta, E.; Calhoun, D. A. *Curr. Hypertens. Rep.* **2016**, *18* (4), 25.

(63) Gradman, A. H.; Basile, J. N.; Carter, B. L.; Bakris, G. L. *J. Am. Soc. Hypertens.* **2010**, *4* (2), 90–98.

(64) Patridge, E.; Gareiss, P.; Kinch, M. S.; Hoyer, D. *Drug Discov. Today* **2016**, *21* (2), 204–207.

(65) G. de la Torre, B.; Albericio, F. *Molecules* **2019**, *24* (4), 809.

(66) Newman, D. J.; Cragg, G. M. *J. Nat. Prod.* **2016**, *79* (3), 629–661.

(67) Koehn, F. E.; Carter, G. T. *Nat. Rev. Drug Discov.* **2005**, *4* (3), 206–220.

(68) Clardy, J.; Walsh, C. *Nature* **2004**, *432* (7019), 829–837.

(69) Gupta, A. K.; Paquet, M. *J. Cutan. Med. Surg.* **2013**, *17* (3), 173–179.

(70) Lebwohl, M.; Swanson, N.; Anderson, L. L.; Melgaard, A.; Xu, Z.; Berman, B. *N. Engl. J. Med.* **2012**, *366* (11), 1010–1019.

(71) Kantarjian, H. M.; Talpaz, M.; Santini, V.; Murgo, A.; Cheson, B.; O'Brien, S. M. *Cancer* **2001**, *92* (6), 1591–1605.

(72) Kantarjian, H. M.; O'Brien, S.; Cortes, J. *Clin. Lymphoma Myeloma Leuk.* **2013**, *13* (5), 530–533.

(73) Mullard, A. *Nat. Rev. Drug Discov.* **2019**, *18* (2), 85–89.

(74) Venugopal, A. A.; Johnson, S. *Clin. Infect. Dis.* **2012**, *54* (4), 568–574.

(75) D'Incalci, M.; Galmarini, C. M. *Mol. Cancer Ther.* **2010**, *9* (8), 2157–2163.

(76) ElSohly, M. A.; Radwan, M. M.; Gul, W.; Chandra, S.; Galal, A. In *Phytocannabinoids*; Kinghorn, A. D., Falk, H., Gibbons, S., Kobayashi, J., Eds.; Progress in the Chemistry of Organic Natural Products; Springer International Publishing: Cham, 2017; Vol. 103, pp 1–36.

(77) Rinehart, K. L. *Med. Res. Rev.* **2000**, *20* (1), 1–27.

(78) Jampilek, J. *Curr. Med. Chem.* **2019**, *25* (38), 4972–5006.

(79) Nelson, M. L.; Levy, S. B. *Ann. N. Y. Acad. Sci.* **2011**, *1241* (1), 17–32.

(80) O'Brien, M.; Eckardt, J.; Ramlau, R. *Oncologist* **2007**, *12* (10), 1194–1204.

(81) Ulukan, H.; Swaan, P. W. *Drugs* **2002**, *62* (14), 2039–2057.

(82) Strader, C. R.; Pearce, C. J.; Oberlies, N. H. *J. Nat. Prod.* **2011**, *74* (4), 900–907.

(83) Farnsworth, N. R.; Akerele, O.; Bingel, A. S.; Soejarto, D. D.; Guo, Z. *Bull. World Health Organ.* **1985**, *63* (6), 965–981.

(84) Verma, R.; Hanif, K.; Sasmal, D.; Raghubir, R. *Curr. Hypertens. Rev.* **2010**, *6* (3), 190–198.

(85) Tabassum, N.; Ahmad, F. *Pharmacogn. Rev.* **2011**, *5* (9), 30–40.

(86) Al Disi, S. S.; Anwar, M. A.; Eid, A. H. *Front. Pharmacol.* **2016**, *6* (MAR), 1–24.

(87) Teixeira, K.; dos Santos, P.; Citadini Zanette, V.; DalBó, S.; Aguiar Amaral, P. de. *Am. J. Ethnomedicine* **2017**, *04* (01), 1–8.

(88) Horie, S.; Yano, S.; Aimi, N.; Sakai, S.; Watanabe, K. *Life Sci.* **1992**, *50* (7), 491–498.

(89) Zhang, J.; Yu, B.; Zhang, X.-Q.; Sheng, Z.-F.; Li, S.-J.; Wang, Z.-J.; Cui, X.-Y.; Cui, S.-Y.; Zhang, Y.-H. *J. Ethnopharmacol.* **2014**, *151* (1), 729–732.

(90) Ojeda, D.; Jiménez-Ferrer, E.; Zamilpa, A.; Herrera-Arellano, A.; Tortoriello, J.; Alvarez, L. *J. Ethnopharmacol.* **2010**, *127* (1), 7–10.

(91) Oh, H.; Kang, D.-G.; Kwon, J.-W.; Kwon, T.-O.; Lee, S.-Y.; Lee, D.-B.; Lee, H.-S. *Biol. Pharm. Bull.* **2004**, *27* (12), 2035–2037.

(92) Liu, J.-C.; Hsu, F.-L.; Tsai, J.-C.; Chan, P.; Liu, J. Y.-H.; Thomas, G. N.; Tomlinson, B.; Lo, M.-Y.; Lin, J.-Y. *Life Sci.* **2003**, *73* (12), 1543–1555.

(93) Lin, T.-C.; Hsu, F.-L.; Cheng, J.-T. *J. Nat. Prod.* **1993**, *56* (4), 629–632.

(94) Yoopan, N.; Thisoda, P.; Rangkadilok, N.; Sahasitiwat, S.; Pholphana, N.; Ruchirawat, S.; Satayavivad, J. *Planta Med.* **2007**, *73* (6), 503–511.

(95) Alfieri, A.; Maione, F.; Bisio, A.; Romussi, G.; Mascolo, N.; Cicala, C. *Phyther. Res.* **2007**, *21* (7), 690–692.

(96) Achor, R. W. P.; Hanson, N. O.; Gifford Jr., R. W. *J. Am. Med. Assoc.* **1955**, *159* (9), 841–845.

(97) Shamon, S. D.; Perez, M. I. *Cochrane Database Syst. Rev.* **2016**, No. 12, 1–39.

(98) Silverman, R. B.; Holladay, M. W. *The Organic Chemistry of Drug Design and Drug Action*, 3rd Ed.; Academic Press Inc: Massachusetts, 2014.

(99) Polanski, J.; Bogocz, J.; Tkocz, A. *J. Comput. Aided. Mol. Des.* **2016**, *30* (5), 381–389.

(100) Wang, S.; Dong, G.; Sheng, C. *Chem. Rev.* **2019**, *119* (6), 4180–4220.

(101) Liu, G. T. *Med. Chem. (Los. Angeles).* **2009**, *5* (1), 29–43.

(102) Yuan, H.; Ma, Q.; Ye, L.; Piao, G. *Molecules* **2016**, *21* (5), 559.

(103) Yoshida, M.; Horinouchi, S.; Beppu, T. *BioEssays* **1995**, *17* (5), 423–430.

(104) Li, Y.; Seto, E. *Cold Spring Harb. Perspect. Med.* **2016**, *6* (10), a026831.

(105) Mann, B. S.; Johnson, J. R.; Cohen, M. H.; Justice, R.; Pazdur, R. *Oncologist* **2007**, *12* (10), 1247–1252.

(106) Hirata, Y.; Uemura, D. *Pure Appl. Chem.* **1986**, *58* (5), 701–710.

(107) Donoghue, M.; Lemery, S. J.; Yuan, W.; He, K.; Sridhara, R.; Shord, S.; Zhao, H.; Marathe, A.; Kotch, L.; Jee, J.; Wang, Y.; Zhou, L.; Adams, W. M.; Jarral, V.; Pilaro, A.; Lostritto, R.; Gootenberg, J. E.; Keegan, P.; Pazdur, R. *Clin. Cancer Res.* **2012**, *18* (6), 1496–1505.

(108) Taylor, R. D.; MacCoss, M.; Lawson, A. D. G. *J. Med. Chem.* **2014**, *57* (14), 5845–5859.

(109) Dalvie, D.; Nair, S.; Kang, P.; Loi, C.-M. In *Metabolism, Pharmacokinetics and Toxicity of Functional Groups: Impact of Chemical Building Blocks on ADMET*; Smith, D. A., Ed.; Drug Discovery; Royal Society of Chemistry: Cambridge, 2010; pp 275–327.

(110) Ritchie, T. J.; Macdonald, S. J. F.; Peace, S.; Pickett, S. D.; Luscombe, C. N. *Medchemcomm* **2012**, *3* (9), 1062–1069.

(111) Richardson, K. *Contemp. Org. Synth.* **1996**, *3* (2), 125–132.

(112) Jevons, S.; Gymer, G. E.; Brammer, K. W.; Cox, D. A.; Leeming, M. R. G. *Antimicrob. Agents Chemother.* **1979**, *15* (4), 597–602.

(113) Macrae, P. V.; Kirrs, M.; Pullen, F. S.; Tarbit, M. H. *Drug Metab. Dispos.* **1990**, *18* (6), 1100–1102.

(114) Slavin, M. A.; Osborne, B.; Adams, R.; Levenstein, M. J.; Schoch, H. G.; Feldman, A. R.; Meyers, J. D.; Bowden, R. A. *J. Infect. Dis.* **1995**, *171* (6), 1545–1552.

(115) Todd, P. A.; Heel, R. C. *Drugs* **1986**, *31* (3), 198–248.

(116) Hunter, T. *J. Clin. Invest.* **2007**, *117* (8), 2036–2043.

(117) Buchdunger, E.; Zimmermann, J.; Mett, H.; Meyer, T.; Muller, M.; Druker, B. J.; Lydon, N. B. *Cancer Res.* **1996**, *56* (1), 100–104.

(118) Zimmermann, J.; Caravatti, G.; Mett, H.; Meyer, T.; Müller, M.; Lydon, N. B.; Fabbro, D. *Arch. Pharm. (Weinheim).* **1996**, *329* (7), 371–376.

(119) Buchdunger, E.; Zimmermann, J.; Mett, H.; Meyer, T.; Muller, M.; Regenass, U.; Lydon, N. B. *Proc. Natl. Acad. Sci.* **1995**, *92* (7), 2558–2562.

(120) Freire, E. *Drug Discov. Today* **2008**, *13* (19/20), 869–874.

(121) Chang, C. A.; Chen, W.; Gilson, M. K. *Proc. Natl. Acad. Sci.* **2007**, *104* (5), 1534–1539.

(122) Fang, Z.; Song, Y.; Zhan, P.; Zhang, Q.; Liu, X. *Future Med. Chem.* **2014**, *6* (8), 885–901.

(123) Kandel, C. E.; Walmsley, S. L. *Drug Des. Devel. Ther.* **2015**, *9*, 3547–3555.

(124) Kawasuji, T.; Johns, B. A.; Yoshida, H.; Weatherhead, J. G.; Akiyama, T.; Taishi, T.; Taoda, Y.; Mikamiyama-Iwata, M.; Murai, H.; Kiyama, R.; Fuji, M.; Tanimoto, N.; Yoshinaga, T.; Seki, T.; Kobayashi, M.; Sato, A.; Garvey, E. P.; Fujiwara, T. *J. Med. Chem.* **2013**, *56* (3), 1124–1135.

(125) Bohn, L. M.; Lefkowitz, R. J.; Gainetdinov, R. R.; Pepper, K.; Caron, M. G.; Lin, F.-T. *Science (80-.).* **1999**, *286* (5449), 2495–2498.

(126) Blane, G. F.; Boura, A. L. A.; Fitzgerald, A. E.; Lister, R. E. *Br. J. Pharmacol. Chemother.* **1967**, *30* (1), 11–22.

(127) Bentley, K. W.; Hardy, D. G. *J. Am. Chem. Soc.* **1967**, *89* (13), 3281–3292.

(128) Thornber, C. W. *Chem. Soc. Rev.* **1979**, *8* (4), 563–580.

(129) Lima, L. M.; Barreiro, E. J. *Curr. Med. Chem.* **2005**, *12* (1), 23–49.

(130) Ballatore, C.; Huryn, D. M.; Smith, A. B. *ChemMedChem* **2013**, *8* (3), 385–395.

(131) Conlin, A.; Fornier, M.; Hudis, C.; Kar, S.; Kirkpatrick, P. *Nat. Rev. Drug Discov.* **2007**, *6* (12), 953–954.

(132) Höfle, G.; Bedorf, N.; Steinmetz, H.; Schomburg, D.; Gerth, K.; Reichenbach, H. *Angew. Chemie Int. Ed. English* **1996**, *35* (13/14), 1567–1569.

(133) Lee, F. Y. F.; Borzilleri, R.; Fairchild, C. R.; Kim, S.-H.; Long, B. H.; Reventos-Suarez, C.; Vite, G. D.; Rose, W. C.; Kramer, R. A. *Clin. Cancer Res.* **2001**, *7* (5), 1429–1437.

(134) Lee, F. Y. F.; Borzilleri, R.; Fairchild, C. R.; Kamath, A.; Smykla, R.; Kramer, R.; Vite, G. *Cancer Chemother. Pharmacol.* **2008**, *63* (1), 157–166.

(135) Bhardwaj, G. *Expert Opin. Drug Discov.* **2006**, *1* (6), 609–618.

(136) Konzett, H. *Trends Pharmacol. Sci.* **1981**, *2*, 47–49.

(137) Sears, M. R.; Lötvall, J. *Respir. Med.* **2005**, *99* (2), 152–170.

(138) Clement, W. L.; Weiblen, G. D. *Syst. Bot.* **2009**, *34* (3), 530–552.

(139) Berg, C. C.; Corner, E. J. H. *Flora Malesiana, Series I – Seed Plants. Volume 17, Part 2: Moraceae - Ficus*; Nooteboom, H. P., Ed.; Nationaal Herbarium Nederland: Leiden, Netherlands, 2005; Vol. 17/2.

(140) Berg, C. C. *Experientia* **1989**, *45* (7), 605–611.

(141) Cook, J. M.; Rasplus, J.-Y. *Trends Ecol. Evol.* **2003**, *18* (5), 241–248.

(142) Lansky, E. P.; Paavilainen, H. M.; Pawlus, A. D.; Newman, R. A. *J. Ethnopharmacol.* **2008**, *119* (2), 195–213.

(143) Bunawan, H.; Amin, N. M.; Bunawan, S. N.; Baharum, S. N.; Mohd Noor, N. *Evidence-Based Complement. Altern. Med.* **2014**, *2014*, 1–8.

(144) Choo, C.-Y.; Yati Sulong, N. *Curr. Tradit. Med.* **2016**, *2* (1), 3–17.

(145) Burkill, I. H.; Haniff, M. *Gard. Bull. Straits Settlements* **1930**, *6*, 165–321.

(146) Chaudhary, N.; Ali, M. *Pharmacogn. Rev.* **2011**, *5* (9), 96–102.

(147) Hesse, M. *Alkaloids: Nature's Cure or Blessing?*; Wiley-VCH: Weinheim, Germany, 2002.

(148) Pelletier, S. W. In *Alkaloids: Chemical and Biological Perspectives, Volume 1*; Wiley-Interscience: New York, 1983; p 398.

(149) Subramaniam, G.; Ang, K. K. H.; Ng, S.; Buss, A. D.; Butler, M. S. *Phytochem. Lett.* **2009**, *2* (2), 88–90.

(150) Yap, V. A.; Qazzaz, M. E.; Raja, V. J.; Bradshaw, T. D.; Loh, H.-S.; Sim, K.-S.; Yong, K.-T.; Low, Y.-Y.; Lim, K.-H. *Phytochem. Lett.* **2016**, *15*, 136–141.

(151) Zhang, H.-J.; Tamez, P. A.; Aydogmus, Z.; Tan, G. T.; Saikawa, Y.; Hashimoto, K.; Nakata, M.; Hung, N. Van; Xuan, L. T.; Cuong, N. M.; Soejarto, D. D.; Pezzuto, J. M.; Fong, H. H. S. *Planta Med.* **2002**, *68* (12), 1088–1091.

(152) Al-Khdhairawi, A. A. Q.; Krishnan, P.; Mai, C.-W.; Chung, F. F.-L.; Leong,

C.-O.; Yong, K.-T.; Chong, K.-W.; Low, Y.-Y.; Kam, T.-S.; Lim, K.-H. *J. Nat. Prod.* **2017**, *80* (10), 2734–2740.

(153) Wan, C.; Chen, C.; Li, M.; Yang, Y.; Chen, M.; Chen, J. *Plants* **2017**, *6* (4), 44.

(154) Yap, V. A.; Loong, B.-J.; Ting, K.-N.; Loh, S. H.-S.; Yong, K.-T.; Low, Y.-Y.; Kam, T.-S.; Lim, K.-H. *Phytochemistry* **2015**, *109*, 96–102.

(155) Venkatachalam, S. R.; Mulchandani, N. B. *Naturwissenschaften* **1982**, *69* (6), 287–288.

(156) Peraza-Sánchez, S. R.; Chai, H.-B.; Shin, Y. G.; Santisuk, T.; Reutrakul, V.; Farnsworth, N. R.; Cordell, G. A.; Pezzuto, J. M.; Kinghorn, A. D. *Planta Med.* **2002**, *68* (2), 186–188.

(157) Shi, Z.-F.; Lei, C.; Yu, B.-W.; Wang, H.-Y.; Hou, A.-J. *Chem. Biodivers.* **2016**, *13* (4), 445–450.

(158) Latayada, F. S.; Uy, M. M.; Akihara, Y.; Ohta, E.; Nehira, T.; Ômura, H.; Ohta, S. *Phytochemistry* **2017**, *141*, 98–104.

(159) Khan, I.; Rali, T.; Sticher, O. *Planta Med.* **1993**, *59* (3), 286.

(160) Johns, S. R.; Russel, J. H.; Heffernan, M. L. *Tetrahedron Lett.* **1965**, *6* (24), 1987–1991.

(161) Kubo, M.; Yatsuzuka, W.; Matsushima, S.; Harada, K.; Inoue, Y.; Miyamoto, H.; Matsumoto, M.; Fukuyama, Y. *Chem. Pharm. Bull. (Tokyo).* **2016**, *64* (7), 957–960.

(162) Ueda, J.; Takagi, M.; Shin-ya, K. *J. Nat. Prod.* **2009**, *72* (12), 2181–2183.

(163) Wu, P.-L.; Rao, K. V.; Su, C.-H.; Kuoh, C.-S.; Wu, T.-S. *Heterocycles* **2002**, *57* (12), 2401–2408.

(164) Damu, A. G.; Kuo, P.-C.; Shi, L.-S.; Li, C.-Y.; Kuoh, C.-S.; Wu, P.-L.; Wu, T.-S. *J. Nat. Prod.* **2005**, *68* (7), 1071–1075.

(165) Damu, A. G.; Kuo, P.-C.; Shi, L.-S.; Li, C.-Y.; Su, C.-R.; Wu, T.-S. *Planta Med.* **2009**, *75* (10), 1152–1156.

(166) Chemler, S. R. *Curr. Bioact. Compd.* **2009**, *5* (1), 2–19.

(167) Mandhare, A. A.; Dhulap, S. A.; Dhulap, A. S.; Biradar, S. C. *Chem. informatics* **2015**, *1* (1:5), 1–15.

(168) Burtoloso, A. C. B.; Bertonha, A. F.; Rosset, I. G. *Curr. Top. Med. Chem.* **2014**, *14* (2), 191–199.

(169) Cordell, G. A.; Quinn-Beattie, M. Lou; Farnsworth, N. R. *Phyther. Res.* **2001**, *15* (3), 183–205.

(170) Krishnan, P.; Lee, F.-K.; Yap, V. A.; Low, Y.-Y.; Kam, T.-S.; Yong, K.-T.; Ting, K.-N.; Lim, K.-H. *J. Nat. Prod.* **2020**, *83* (1), 152–158.

(171) Seyferth, D. *Organometallics* **2009**, *28* (6), 1598–1605.

(172) Roughley, S. D.; Jordan, A. M. *J. Med. Chem.* **2011**, *54* (10), 3451–3479.

(173) Garst, J. F.; Soriaga, M. P. *Coord. Chem. Rev.* **2004**, *248* (7–8), 623–652.

(174) Rakita, P. E. In *Kirk-Othmer Encyclopedia of Chemical Technology*; John Wiley & Sons, Inc.: Hoboken, NJ, USA, 2005; Vol. 12, pp 818–838.

(175) Clayden, J.; Greeves, N.; Warren, S. *Organic Chemistry*, Second edi.; Oxford

University Press: Oxford, United Kingdom, 2012.

(176) Ashby, E. C.; Laemmle, J.; Neumann, H. M. *Acc. Chem. Res.* **1974**, *7* (8), 272–280.

(177) Maruyama, K.; Katagiri, T. *J. Phys. Org. Chem.* **1989**, *2* (3), 205–213.

(178) Nahm, S.; Weinreb, S. M. *Tetrahedron Lett.* **1981**, *22* (39), 3815–3818.

(179) Balasubramaniam, S.; Aidhen, I. *Synthesis (Stuttg).* **2008**, No. 23, 3707–3738.

(180) Nowak, M. *Synlett* **2015**, *26* (04), 561–562.

(181) Mentzel, M.; Hoffmann, H. M. R. *J. für Prakt. Chemie/Chemiker-Zeitung* **1997**, *339* (1), 517–524.

(182) Qu, B.; Collum, D. B. *J. Org. Chem.* **2006**, *71* (18), 7117–7119.

(183) Abdel-Magid, A. F.; Carson, K. G.; Harris, B. D.; Maryanoff, C. A.; Shah, R. D. *J. Org. Chem.* **1996**, *61* (11), 3849–3862.

(184) Abdel-Magid, A. F.; Maryanoff, C. A.; Carson, K. G. *Tetrahedron Lett.* **1990**, *31* (39), 5595–5598.

(185) Borch, R. F.; Bernstein, M. D.; Durst, H. D. *J. Am. Chem. Soc.* **1971**, *93* (12), 2897–2904.

(186) Abdel-Magid, A. F.; Mehrman, S. J. *Org. Process Res. Dev.* **2006**, *10* (5), 971–1031.

(187) Haddad, M.; Dorbais, J.; Larchevêque, M. *Tetrahedron Lett.* **1997**, *38* (34), 5981–5984.

(188) Menche, D.; Arikan, F.; Li, J.; Rudolph, S. *Org. Lett.* **2007**, *9* (2), 267–270.

(189) Zhang, J.; Labaree, D. C.; Hochberg, R. B. *J. Med. Chem.* **2005**, *48* (5), 1428–1447.

(190) Fürstner, A.; Thiel, O. R.; Kindler, N.; Bartkowska, B. *J. Org. Chem.* **2000**, *65* (23), 7990–7995.

(191) Weiberth, F. J.; Hall, S. S. *J. Org. Chem.* **1987**, *52* (17), 3901–3904.

(192) Henrion, G.; Chavas, T. E. J.; Le Goff, X.; Gagosz, F. *Angew. Chemie Int. Ed.* **2013**, *52* (24), 6277–6282.

(193) Griffith, W. P.; Ley, S. V.; Whitcombe, G. P.; White, A. D. *J. Chem. Soc. Chem. Commun.* **1987**, No. 21, 1625–1627.

(194) Kraus, G. A.; Melekhov, A. *J. Org. Chem.* **1999**, *64* (5), 1720–1722.

(195) Meyer, S. D.; Schreiber, S. L. *J. Org. Chem* **1994**, *59* (5), 7549–7552.

(196) García-Domínguez, P.; Weiss, M.; Lepore, I.; Álvarez, R.; Altucci, L.; Gronemeyer, H.; de Lera, Á. R. *ChemMedChem* **2012**, *7* (12), 2101–2112.

(197) Tan, Y.; Yuan, W.; Gong, L.; Meggers, E. *Angew. Chemie Int. Ed.* **2015**, *54* (44), 13045–13048.

(198) Trost, B. M.; Lehr, K.; Michaelis, D. J.; Xu, J.; Buckl, A. K. *J. Am. Chem. Soc.* **2010**, *132* (26), 8915–8917.

(199) Chuang, K. V.; Navarro, R.; Reisman, S. E. *Angew. Chemie - Int. Ed.* **2011**, *50* (40), 9447–9451.

(200) Datta, A.; Kumar, J. S. R.; Roy, S. *Tetrahedron* **2001**, *57* (7), 1169–1173.

(201) Jiménez-Osés, G.; Brockway, A. J.; Shaw, J. T.; Houk, K. N. *J. Am. Chem. Soc.*

2013, *135* (17), 6633–6642.

(202) Lee, V. J. In *Comprehensive Organic Synthesis*; Elsevier, 1991; pp 69–137.

(203) Penthala, N. R.; Ponugoti, P. R.; Nickell, J. R.; Deaciuc, A. G.; Dwoskin, L. P.; Crooks, P. A. *Bioorg. Med. Chem. Lett.* **2013**, *23* (11), 3342–3345.

(204) Sirvent, J. A.; Foubelo, F.; Yus, M. *Heterocycles* **2014**, *88* (2), 1163–1174.

(205) Yamato, M.; Hashigaki, K.; Qais, N.; Ishikawa, S. *Tetrahedron* **1990**, *46* (17), 5909–5920.

(206) Neises, B.; Steglich, W. *Angew. Chemie Int. Ed. English* **1978**, *17* (7), 522–524.

(207) Carroll, R.; Spoerri, P. E. *J. Am. Chem. Soc.* **1938**, *60* (11), 2656–2658.

(208) Yoon, J. A.; Ahn, S.; Han, Y. T. *Nat. Prod. Commun.* **2018**, *13* (3), 351–353.

(209) Allan, K. M.; Hong, B. D.; Stoltz, B. M. *Org. Biomol. Chem.* **2009**, *7* (23), 4960–4964.

(210) Brooks, D. W.; Lu, L. D.-L.; Masamune, S. *Angew. Chemie Int. Ed. English* **1979**, *18* (1), 72–74.

(211) Davis, F. A.; Yang, B.; Deng, J. *J. Org. Chem.* **2003**, *68* (13), 5147–5152.

(212) Dineen, T. A.; Roush, W. R. *Org. Lett.* **2004**, *6* (12), 2043–2046.

(213) Alonso, D. A.; Alonso, E.; Nájera, C.; Ramón, D. J.; Yus, M. *Tetrahedron* **1997**, *53* (13), 4835–4856.

(214) Bertolini, G.; Vecchietti, V.; Mabilia, M.; Norcini, G.; Restelli, A.; Santangelo, F.; Villa, A.; Casagrande, C. *Eur. J. Med. Chem.* **1992**, *27* (7), 663–672.

(215) Weissman, S. A.; Zewge, D. *Tetrahedron* **2005**, *61* (33), 7833–7863.

(216) Carvalho, C. F.; Sargent, M. V. *J. Chem. Soc. Chem. Commun.* **1984**, *7* (4), 227–229.

(217) Land, E. J.; Perona, A.; Ramsden, C. A.; Riley, P. A. *Org. Biomol. Chem.* **2009**, *7* (5), 944–950.

(218) Kulkarni, P. P.; Kadam, A. J.; Mane, R. B.; Desai, U. V.; Wadgaonkar, P. P. *J. Chem. Res.* **1999**, No. 6, 394–395.

(219) Muñoz, P.; Huenchuguala, S.; Paris, I.; Segura-Aguilar, J. *Parkinsons. Dis.* **2012**, *2012*, 1–13.

(220) Pillar, E. A.; Guzman, M. I. *Environ. Sci. Technol.* **2017**, *51* (9), 4951–4959.

(221) Yang, J.; Saggiomo, V.; Velders, A. H.; Cohen Stuart, M. A.; Kamperman, M. *PLoS One* **2016**, *11* (12), e0166490.

(222) Hamlin, T. A.; Swart, M.; Bickelhaupt, F. M. *ChemPhysChem* **2018**, *19* (11), 1315–1330.

(223) Trader, D. J.; Carlson, E. E. *Mol. Biosyst.* **2012**, *8* (10), 2484–2493.

(224) Lloyd, M. G.; Taylor, R. J. K.; Unsworth, W. P. *Org. Lett.* **2014**, *16* (10), 2772–2775.

(225) Ouyang, H.; Morris-Natschke, S. L.; Ishaq, K. S.; Ward, P.; Liu, D.; Leonard, S.; Thakker, D. R. *J. Med. Chem.* **2002**, *45* (13), 2857–2866.

(226) Williams, D. R.; Plummer, S. V.; Patnaik, S. *Tetrahedron* **2011**, *67* (27–28), 5083–5097.

(227) Granander, J.; Sott, R.; Hilmersson, G. *Tetrahedron* **2002**, *58* (23), 4717–4725.

(228) Feit, I. N.; Saunders, W. H. *J. Am. Chem. Soc.* **1970**, *92* (6), 1630–1634.

(229) Ouellette, R. J.; Rawn, J. D. In *Organic Chemistry*; Elsevier, 2018; pp 299–319.

(230) Ouellette, R. J.; Rawn, J. D. In *Organic Chemistry*; Elsevier, 2018; pp 463–505.

(231) Taniguchi, T.; Ishita, A.; Uchiyama, M.; Tamura, O.; Muraoka, O.; Tanabe, G.; Ishibashi, H. *J. Org. Chem.* **2005**, *70* (5), 1922–1925.

(232) Mu, W.; Zhou, L.; Zou, Y.; Wang, Q.; Goeke, A. *European J. Org. Chem.* **2014**, *2014* (11), 2379–2385.

(233) Yasa, S. R.; Kaki, S. S.; Poornachandra, Y.; Kumar, C. G.; Penumarthy, V. *Bioorg. Med. Chem. Lett.* **2016**, *26* (8), 1978–1982.

(234) Yang, R.-S.; Sheng, H.; Lexa, K. W.; Sherer, E. C.; Zhang, L.-K.; Xiang, B.; Helmy, R.; Mao, B. *J. Am. Soc. Mass Spectrom.* **2017**, *28* (3), 452–460.

(235) Bąchor, R.; Kluczyk, A.; Stefanowicz, P.; Szewczuk, Z. *J. Pept. Sci.* **2015**, *21* (12), 879–886.

(236) Jespersen, B.; Tykocki, N. R.; Watts, S. W.; Cobbett, P. J. *J. Vis. Exp.* **2015**, No. 95, e52324.

(237) Bacakova, L.; Travnickova, M.; Filova, E.; Matějka, R.; Stepanovska, J.; Musilkova, J.; Zarubova, J.; Molitor, M. In *Muscle Cell and Tissue - Current Status of Research Field*; InTech, 2018; pp 229–257.

(238) Williams, B. *J. Am. Coll. Cardiol.* **2009**, *53* (5), 452–454.

(239) Leong, X.-F.; Ng, C.-Y.; Jaarin, K. *Biomed Res. Int.* **2015**, *2015*, 1–11.

(240) Robbins, N.; Thompson, A.; Mann, A.; Blomkalns, A. L. *J. Vis. Exp.* **2014**, No. 93, e52172.

(241) Sharp, P.; Villano, J. *The Laboratory Rat*, Second.; CRC Press, 2012.

(242) Franco, N. H. *Animals* **2013**, *3* (1), 238–273.

(243) Gileta, A. F.; Fitzpatrick, C. J.; Chitre, A. S.; St. Pierre, C. L.; Joyce, E. V.; Maguire, R. J.; McLeod, A. M.; Gonzales, N. M.; Williams, A. E.; Morrow, J. D.; Robinson, T. E.; Flagel, S. B.; Palmer, A. A. *bioRxiv* **2018**, 412924.

(244) Berman, R. F.; Goldman, H.; Altman, H. J. *Neurobiol. Aging* **1988**, *9*, 691–696.

(245) Ellenbroek, B.; Youn, J. *Dis. Model. Mech.* **2016**, *9* (10), 1079–1087.

(246) Wong, S. K.; Chin, K.-Y.; Suhaimi, F. H.; Fairus, A.; Ima-Nirwana, S. *Nutr. Metab. (Lond).* **2016**, *13*, 65.

(247) Kim, Y. S.; Kim, J. S.; Cho, H. S.; Rha, D. S.; Kim, J. M.; Park, J. D.; Choi, B. S.; Lim, R.; Chang, H. K.; Chung, Y. H.; Kwon, I. H.; Jeong, J.; Han, B. S.; Yu, I. J. *Inhal. Toxicol.* **2008**, *20* (6), 575–583.

(248) Maltoni, C.; Ciliberti, A.; Cotti, G.; Conti, B.; Belpoggi, F. *Environ. Health Perspect.* **1989**, *82* (2), 109–124.

(249) Tan, C. S.; Loh, Y. C.; Ch'ng, Y. S.; Ng, C. H.; Yeap, Z. Q.; Ahmad, M.; Asmawi, M. Z.; Yam, M. F. *J. Ethnopharmacol.* **2019**, *232*, 135–144.

(250) Kim, B.; Kim, K.; Lee, S.; Jo, C.; Lee, K.; Ham, I.; Choi, H. *Nutrients* **2019**, *11* (8), 1816.

(251) Zheoat, A. M.; Gray, A. I.; Igoli, J. O.; Ferro, V. A.; Drummond, R. M.

Fitoterapia **2019**, *134*, 5–13.

(252) Liu, W.; Lu, Y.; Chu, S.; Jiang, M.; Bai, G. *J. Funct. Foods* **2019**, *60*, 103432.

(253) Romero, F.; Palacios, J.; Jofré, I.; Paz, C.; Nwokocha, C. R.; Paredes, A.; Cifuentes, F. *Molecules* **2019**, *24* (15), 2748.

(254) Okamoto, K.; Aoki, K. *Jpn. Circ. J.* **1963**, *27* (3), 282–293.

(255) Pinto, Y. M.; Paul, M.; Ganten, D. *Cardiovasc. Res.* **1998**, *39* (1), 77–88.

(256) Takata, Y.; Kato, H. *Life Sci.* **1995**, *58* (2), 91–106.

(257) Lund-Johansen, P. *Journal of Cardiovascular Pharmacology*. 1990, pp S34–S39.

(258) Gómez-Roso, M.; Montero, M. J.; Carrón, R.; Sevilla, M. A. *Br. J. Pharmacol.* **2009**, *158* (8), 1911–1921.

(259) Dong, X.; Wang, Y.; Liu, T.; Wu, P.; Gao, J.; Xu, J.; Yang, B.; Hu, Y. *Molecules* **2011**, *16* (10), 8257–8272.

(260) Simas, A. B. C.; Pereira, V. L. P.; Barreto Jr., C. B.; Sales, D. L. de; Carvalho, L. L. de. *Quim. Nova* **2009**, *32* (9), 2473–2475.

(261) Williams, D. B. G.; Lawton, M. *J. Org. Chem.* **2010**, *75* (24), 8351–8354.

(262) Bezagu, M.; Errico, C.; Chaulot-Talmon, V.; Monti, F.; Tanter, M.; Tabeling, P.; Cossy, J.; Arseniyadis, S.; Couture, O. *J. Am. Chem. Soc.* **2014**, *136* (20), 7205–7208.

(263) Lebel, H.; Ladjel, C.; Bréthous, L. *J. Am. Chem. Soc.* **2007**, *129* (43), 13321–13326.

(264) Capozzi, G.; Roelens, S.; Talami, S. *J. Org. Chem.* **1993**, *58* (27), 7932–7936.

(265) Zygalski, L.; Middel, C.; Harms, K.; Koert, U. *Org. Lett.* **2018**, *20* (16), 5071–5074.

(266) Ho, D. K. H.; Calleja, J.; Gaunt, M. J. *Synlett* **2019**, *30* (04), 454–458.

(267) Wang, H.; Denton, J. R.; Davies, H. M. L. *Org. Lett.* **2011**, *13* (16), 4316–4319.

(268) Bouchez, L. C.; Gerbeaux, C.; Rusch, M.; Patoor, M.; Livendahl, M.; Press, N. J. *Synlett* **2017**, *28* (10), 1219–1223.

(269) Rudzinski, D.; Kelly, C. B.; Leadbeater, N. E. *Chem. Commun.* **2012**, *48* (77), 9610–9612.

(270) Hanessian, S.; Chattopadhyay, A. K. *Org. Lett.* **2014**, *16* (1), 232–235.

(271) Kokotos, C. G.; Baskakis, C.; Kokotos, G. *J. Org. Chem.* **2008**, *73* (21), 8623–8626.

(272) Mass, O.; Lindsey, J. S. *J. Org. Chem.* **2011**, *76* (22), 9478–9487.

(273) Boev, V. I.; Moskalenko, A. I.; Belopukhov, S. L.; Nikonova, G. N. *Russ. J. Org. Chem.* **2017**, *53* (2), 169–177.

(274) Kerr, W. J.; Morrison, A. J.; Pazicky, M.; Weber, T. *Org. Lett.* **2012**, *14* (9), 2250–2253.

(275) Schwertz, G.; Witschel, M. C.; Rottmann, M.; Bonnert, R.; Leartsakulpanich, U.; Chitnumsub, P.; Jaruwat, A.; Ittarat, W.; Schäfer, A.; Aponte, R. A.; Charman, S. A.; White, K. L.; Kundu, A.; Sadhukhan, S.; Lloyd, M.; Freiberg, G. M.; Srikumaran, M.; Siggel, M.; Zwyssig, A.; Chaiyen, P.; Diederich, F. *J.*

Med. Chem. **2017**, *60* (12), 4840–4860.

(276) Einhorn, J.; Einhorn, C.; Luche, J.-L. *Synth. Commun.* **1990**, *20* (8), 1105–1112.

(277) Murray, P. R. D.; Browne, D. L.; Pastre, J. C.; Butters, C.; Guthrie, D.; Ley, S. V. *Org. Process Res. Dev.* **2013**, *17* (9), 1192–1208.

(278) Fukuda, S.; Tsuji, K.; Musashi, J.; Nonaka, R.; Kimura, T.; Satoh, T. *Synthesis (Stuttg).* **2011**, No. 22, 3615–3626.

(279) Zhao, C.; Jia, X.; Wang, X.; Gong, H. *J. Am. Chem. Soc.* **2014**, *136* (50), 17645–17651.

(280) Justik, M. W.; Koser, G. F. *Tetrahedron Lett.* **2004**, *45* (32), 6159–6163.

(281) Chandrasekhar, S.; Shrinidhi, A. *Synth. Commun.* **2014**, *44* (13), 1904–1913.

(282) Huang, P.-Q.; Wang, Y.; Xiao, K.-J.; Huang, Y.-H. *Tetrahedron* **2015**, *71* (24), 4248–4254.

(283) Shono, T.; Nishiguchi, I.; Sasaki, M.; Ikeda, H.; Kurita, M. *J. Org. Chem.* **1983**, *48* (15), 2503–2505.

(284) Ollivier, C.; Renaud, P. *Chem. - A Eur. J.* **1999**, *5* (5), 1468–1473.

(285) Pelter, A.; Smith, K.; Elgendy, S. M. A.; Rowlands, M. *Tetrahedron* **1993**, *49* (32), 7104–7118.

(286) Yuan, L.-Z.; Zhao, G.; Hamze, A.; Alami, M.; Provot, O. *Adv. Synth. Catal.* **2017**, *359* (15), 2682–2691.

(287) Gudla, V.; Balamurugan, R. *Tetrahedron Lett.* **2012**, *53* (39), 5243–5247.

(288) Zuurmond, H. M.; Hessling, J.; Blüml, K.; Lohse, M.; Ijzerman, A. P. *Mol.*

Pharmacol. **1999**, *56* (5), 909–916.

(289) Allewelt, A. L.; Day, A. R. *J. Org. Chem.* **1941**, *06* (3), 384–400.

(290) Lambert, J. B.; Mark, H. W.; Magyar, E. S. *J. Am. Chem. Soc.* **1977**, *99* (9), 3059–3067.

(291) Blakemore, P. R.; Marsden, S. P.; Vater, H. D. *Org. Lett.* **2006**, *8* (4), 773–776.

(292) O'Boyle, N. M.; Banck, M.; James, C. A.; Morley, C.; Vandermeersch, T.; Hutchison, G. R. *J. Cheminform.* **2011**, *3*, 33.

(293) O'Boyle, N. M.; Vandermeersch, T.; Flynn, C. J.; Maguire, A. R.; Hutchison, G. R. *J. Cheminform.* **2011**, *3*, 8.

(294) Neese, F. *Wiley Interdiscip. Rev. Comput. Mol. Sci.* **2012**, *2* (1), 73–78.

(295) Neese, F. *Wiley Interdiscip. Rev. Comput. Mol. Sci.* **2018**, *8* (1), e1327.

(296) Takano, Y.; Houk, K. N. *J. Chem. Theory Comput.* **2005**, *1* (1), 70–77.

(297) Bruhn, T.; Schaumlöffel, A.; Hemberger, Y.; Bringmann, G. *Chirality* **2013**, *25* (4), 243–249.

(298) Loong, B. J.; Tan, J. H.; Lim, K. H.; Mbaki, Y.; Ting, K. N. *Naunyn. Schmiedebergs. Arch. Pharmacol.* **2015**, *388* (10), 1061–1067.

Appendix

		Page
Figure S1	^{1}H NMR spectrum of 3,4-dimethoxyphenylacetaldehyde (**177b**) ($CDCl_3$, 400 MHz)	290
Figure S2	^{13}C NMR spectrum of 3,4-dimethoxyphenylacetaldehyde (**177b**) ($CDCl_3$, 100 MHz)	290
Figure S3	^{1}H NMR spectrum of ethyl 3-(3,4-dimethoxyphenyl)propanoate (**193**) ($CDCl_3$, 700 MHz)	291
Figure S4	^{13}C NMR spectrum of ethyl 3-(3,4-dimethoxyphenyl)propanoate (**193**) ($CDCl_3$, 175 MHz)	291
Figure S5	^{1}H NMR spectrum of 1-cyano-1,4-di-(3',4'-dimethoxyphenyl)-butanone-2 (**194**) ($CDCl_3$, 700 MHz)	292
Figure S6	^{13}C NMR spectrum of 1-cyano-1,4-di-(3',4'-dimethoxyphenyl)-butanone-2 (**194**) ($CDCl_3$, 175 MHz)	292
Figure S7	^{1}H NMR spectrum of 1,4-di-(3',4'-dimethoxyphenyl)-butanone-2 (**175**) ($CDCl_3$, 400 MHz)	293
Figure S8	^{13}C NMR spectrum of 1,4-di-(3',4'-dimethoxyphenyl)-butanone-2 (**175**) ($CDCl_3$, 100 MHz)	293
Figure S9	^{1}H NMR spectrum of synthetic schwarzinicine A (**142**) ($CDCl_3$, 600 MHz)	294
Figure S10	^{13}C NMR spectrum of synthetic schwarzinicine A (**142**) ($CDCl_3$, 150 MHz)	294
Figure S11	^{1}H NMR spectrum of synthetic schwarzinicine B (**143**) ($CDCl_3$, 400 MHz)	295
Figure S12	^{13}C NMR spectrum of synthetic schwarzinicine B (**143**) ($CDCl_3$, 100 MHz)	295
Figure S13	Chiral HPLC profile of natural schwarzinicine A (**142**)	296
Figure S14	Chiral HPLC profile of synthetic schwarzinicine A (**142**)	296
Figure S15	Chiral HPLC profile of natural schwarzinicine B (**143**)	297

Figure S16	Chiral HPLC profile of synthetic schwarzinicine B (**143**)	297
Figure S17	^{1}H NMR spectrum of ethyl 4-(3,4-dimethoxyphenyl)-3-oxobutanoate (**197**) ($CDCl_3$, 700 MHz)	298
Figure S18	^{13}C NMR spectrum of ethyl 4-(3,4-dimethoxyphenyl)-3-oxobutanoate (**197**) ($CDCl_3$, 175 MHz)	298
Figure S19	^{1}H NMR spectrum of ethyl 3-((3,4-dimethoxyphenethyl)amino)-4-(3,4-dimethoxyphenyl)butanoate (**195**) ($CDCl_3$, 700 MHz)	299
Figure S20	^{13}C NMR spectrum of ethyl 3-((3,4-dimethoxyphenethyl)amino)-4-(3,4-dimethoxyphenyl)butanoate (**195**) ($CDCl_3$, 175 MHz)	299
Figure S21	^{1}H NMR spectrum of ethyl 3-((*tert*-butoxycarbonyl)(3,4-dimethoxyphenethyl)amine)-4-(3,4-dimethoxyphenyl)butanoate (**199**) ($CDCl_3$, 400 MHz)	300
Figure S22	^{13}C NMR spectrum of ethyl 3-((*tert*-butoxycarbonyl)(3,4-dimethoxyphenethyl)amine)-4-(3,4-dimethoxyphenyl)butanoate (**199**) ($CDCl_3$, 100 MHz)	300
Figure S23	^{1}H NMR spectrum of *tert*-butyl 3,4-dimethoxyphenethyl(1-(3,4-dimethoxyphen)-4-oxobutan-2-yl)carbamate (**200**) ($CDCl_3$, 400 MHz)	301
Figure S24	^{13}C NMR spectrum of *tert*-butyl 3,4-dimethoxyphenethyl(1-(3,4-dimethoxyphen)-4-oxobutan-2-yl)carbamate (**200**) ($CDCl_3$, 100 MHz)	301
Figure S25	^{1}H NMR spectrum of *tert*-butyl (1,4-bis(3,4-dimethoxyphenyl)-4-hydroxybutan-2-yl)(3,4-dimethoxyphenethyl)carbamate (diastereomer pair 1 of **202**) ($CDCl_3$, 600 MHz)	302
Figure S26	^{13}C NMR spectrum of *tert*-butyl (1,4-bis(3,4-dimethoxyphenyl)-4-hydroxybutan-2-yl)(3,4-dimethoxyphenethyl)carbamate (diastereomer pair 1 of **202**) ($CDCl_3$, 150 MHz)	302
Figure S27	HSQC spectrum of *tert*-butyl (1,4-bis(3,4-dimethoxyphenyl)-4-hydroxybutan-2-yl)(3,4-dimethoxyphenethyl)carbamate (diastereomer pair 1 of **202**) ($CDCl_3$, 600 MHz)	303
Figure S28	COSY spectrum of *tert*-butyl (1,4-bis(3,4-dimethoxyphenyl)-4-hydroxybutan-2-yl)(3,4-dimethoxyphenethyl)carbamate (diastereomer pair 1 of **202**) ($CDCl_3$, 600 MHz)	303

Figure S29	HMBC spectrum of *tert*-butyl (1,4-bis(3,4-dimethoxyphenyl)-4-hydroxybutan-2-yl)(3,4-dimethoxyphenethyl)carbamate (diastereomer pair 1 of **202**) ($CDCl_3$, 600 MHz)	304
Figure S30	^{1}H NMR spectrum of *tert*-butyl (1,4-bis(3,4-dimethoxyphenyl)-4-hydroxybutan-2-yl)(3,4-dimethoxyphenethyl)carbamate (diastereomer pair 2 of **202**) ($CDCl_3$, 600 MHz)	305
Figure S31	^{13}C NMR spectrum of *tert*-butyl (1,4-bis(3,4-dimethoxyphenyl)-4-hydroxybutan-2-yl)(3,4-dimethoxyphenethyl)carbamate (diastereomer pair 2 of **202**) ($CDCl_3$, 150 MHz)	305
Figure S32	HSQC spectrum of *tert*-butyl (1,4-bis(3,4-dimethoxyphenyl)-4-hydroxybutan-2-yl)(3,4-dimethoxyphenethyl)carbamate (diastereomer pair 2 of **202**) ($CDCl_3$, 600 MHz)	306
Figure S33	COSY spectrum of *tert*-butyl (1,4-bis(3,4-dimethoxyphenyl)-4-hydroxybutan-2-yl)(3,4-dimethoxyphenethyl)carbamate (diastereomer pair 2 of **202**) ($CDCl_3$, 600 MHz)	306
Figure S34	HMBC spectrum of *tert*-butyl (1,4-bis(3,4-dimethoxyphenyl)-4-hydroxybutan-2-yl)(3,4-dimethoxyphenethyl)carbamate (diastereomer pair 2 of **202**) ($CDCl_3$, 600 MHz)	307
Figure S35	^{1}H NMR spectrum of *N*-(3,4-dimethoxyphenethyl)-4-(3,4-dimethoxyphenyl)-6,7-dimethoxy-1,2,3,4-tetrahydronaphthalen-2-amine (diastereomer pair 1 of **203**) ($CDCl_3$, 700 MHz)	308
Figure S36	^{13}C NMR spectrum of *N*-(3,4-dimethoxyphenethyl)-4-(3,4-dimethoxyphenyl)-6,7-dimethoxy-1,2,3,4-tetrahydronaphthalen-2-amine (diastereomer pair 1 of **203**) ($CDCl_3$, 175 MHz)	308
Figure S37	HSQC spectrum of *N*-(3,4-dimethoxyphenethyl)-4-(3,4-dimethoxyphenyl)-6,7-dimethoxy-1,2,3,4-tetrahydronaphthalen-2-amine (diastereomer pair 1 of **203**) ($CDCl_3$, 700 MHz)	309
Figure S38	COSY spectrum of *N*-(3,4-dimethoxyphenethyl)-4-(3,4-dimethoxyphenyl)-6,7-dimethoxy-1,2,3,4-tetrahydronaphthalen-2-amine (diastereomer pair 1 of **203**) ($CDCl_3$, 700 MHz)	309
Figure S39	HMBC spectrum of *N*-(3,4-dimethoxyphenethyl)-4-(3,4-dimethoxyphenyl)-6,7-dimethoxy-1,2,3,4-tetrahydronaphthalen-2-amine (diastereomer pair 1 of **203**) ($CDCl_3$, 700 MHz)	310

Figure S40	COSY and HMBC correlations of *N*-(3,4-dimethoxyphenethyl)-4-(3,4-dimethoxyphenyl)-6,7-dimethoxy-1,2,3,4-tetrahydronaphthalen-2-amine (diastereomer pair 1 of **203**)	310
Figure S41	^{1}H NMR spectrum of *N*-(3,4-dimethoxyphenethyl)-4-(3,4-dimethoxyphenyl)-6,7-dimethoxy-1,2,3,4-tetrahydronaphthalen-2-amine (diastereomer pair 2 of **203**) ($CDCl_3$, 700 MHz)	311
Figure S42	^{13}C NMR spectrum of *N*-(3,4-dimethoxyphenethyl)-4-(3,4-dimethoxyphenyl)-6,7-dimethoxy-1,2,3,4-tetrahydronaphthalen-2-amine (diastereomer pair 2 of **203**) ($CDCl_3$, 175 MHz)	311
Figure S43	HSQC spectrum of *N*-(3,4-dimethoxyphenethyl)-4-(3,4-dimethoxyphenyl)-6,7-dimethoxy-1,2,3,4-tetrahydronaphthalen-2-amine (diastereomer pair 2 of **203**) ($CDCl_3$, 700 MHz)	312
Figure S44	COSY spectrum of *N*-(3,4-dimethoxyphenethyl)-4-(3,4-dimethoxyphenyl)-6,7-dimethoxy-1,2,3,4-tetrahydronaphthalen-2-amine (diastereomer pair 2 of **203**) ($CDCl_3$, 700 MHz)	312
Figure S45	HMBC spectrum of *N*-(3,4-dimethoxyphenethyl)-4-(3,4-dimethoxyphenyl)-6,7-dimethoxy-1,2,3,4-tetrahydronaphthalen-2-amine (diastereomer pair 2 of **203**) ($CDCl_3$, 700 MHz)	313
Figure S46	COSY and HMBC correlations of *N*-(3,4-dimethoxyphenethyl)-4-(3,4-dimethoxyphenyl)-6,7-dimethoxy-1,2,3,4-tetrahydronaphthalen-2-amine (diastereomer pair 2 of **203**)	313
Figure S47	^{1}H NMR spectrum of 1,4-bis(3,4-dimethoxyphenyl)-4-hydroxybutan-2-one (**205**) ($CDCl_3$, 400 MHz)	314
Figure S48	^{13}C NMR spectrum of 1,4-bis(3,4-dimethoxyphenyl)-4-hydroxybutan-2-one (**205**) ($CDCl_3$, 100 MHz)	314
Figure S49	^{1}H NMR spectrum of stereoisomers of schwarzinicine F (**147a**/**147b**) ($CDCl_3$, 400 MHz)	315
Figure S50	^{13}C NMR spectrum of stereoisomers of schwarzinicine F (**147a**/**147b**) ($CDCl_3$, 100 MHz)	315
Figure S51	HSQC spectrum of stereoisomers of schwarzinicine F (**147a**/**147b**) ($CDCl_3$, 400 MHz)	316

Figure S52	COSY spectrum of stereoisomers of schwarzinicine F (**147a**/**147b**) ($CDCl_3$, 400 MHz)	316
Figure S53	HMBC spectrum of stereoisomers of schwarzinicine F (**147a**/**147b**) ($CDCl_3$, 400 MHz)	317
Figure S54	COSY and HMBC correlations of stereoisomers of schwarzinicine F (**147a**/**147b**)	317
Figure S55	^{1}H NMR spectrum of stereoisomers of schwarzinicine F (**147c**/**147d**) ($CDCl_3$, 400 MHz)	318
Figure S56	^{13}C NMR spectrum of stereoisomers of schwarzinicine F (**147c**/**147d**) ($CDCl_3$, 100 MHz)	318
Figure S57	HPLC profile of natural schwarzinicine F (**147**)	319
Figure S58	HPLC profile of stereoisomers of schwarzinicine F (**147a**/**147b**)	319
Figure S59	Chiral HPLC profile of **147a**	319
Figure S60	Chiral HPLC profile of **147b**	320
Figure S61	Chiral HPLC profile of stereoisomers of schwarzinicine F (**147c**/**147d**)	320
Figure S62	Chiral HPLC profile of **147c**	320
Figure S63	Chiral HPLC profile of **147d**	321
Figure S64	^{1}H NMR spectrum of *N*-methoxy-*N*-methyl-(3,4-dimethoxyphenyl)acetamide (**177c**) ($CDCl_3$, 700 MHz)	322
Figure S65	^{13}C NMR spectrum of *N*-methoxy-*N*-methyl-(3,4-dimethoxyphenyl)acetamide (**177c**) ($CDCl_3$, 175 MHz)	322
Figure S66	^{1}H NMR spectrum of 2-cyclohexyl-*N*-methoxy-*N*-methylacetamide (**210a**) ($CDCl_3$, 700 MHz)	323
Figure S67	^{13}C NMR spectrum of 2-cyclohexyl-*N*-methoxy-*N*-methylacetamide (**210a**) ($CDCl_3$, 175 MHz)	323
Figure S68	^{1}H NMR spectrum of 2-cyclopropyl-*N*-methoxy-*N*-methylacetamide (**210b**) ($CDCl_3$, 700 MHz)	324
Figure S69	^{13}C NMR spectrum of 2-cyclopropyl-*N*-methoxy-*N*-methylacetamide (**210b**) ($CDCl_3$, 175 MHz)	324

Figure S70	^{1}H NMR spectrum of *N*-methoxy-*N*-methyl-2-(naphthalen-2-yl)acetamide (**210c**) ($CDCl_3$, 700 MHz)	325
Figure S71	^{13}C NMR spectrum of *N*-methoxy-*N*-methyl-2-(naphthalen-2-yl)acetamide (**210c**) ($CDCl_3$, 175 MHz)	325
Figure S72	^{1}H NMR spectrum of 2-(benzo[*b*]thiophen-3-yl)-*N*-methoxy-*N*-methylacetamide (**210d**) ($CDCl_3$, 400 MHz)	326
Figure S73	^{13}C NMR spectrum of 2-(benzo[*b*]thiophen-3-yl)-*N*-methoxy-*N*-methylacetamide (**210d**) ($CDCl_3$, 100 MHz)	326
Figure S74	^{1}H NMR spectrum of *N*-methoxy-*N*-methyl-2-(thiophen-2-yl)acetamide (**210e**) ($CDCl_3$, 700 MHz)	327
Figure S75	^{13}C NMR spectrum of *N*-methoxy-*N*-methyl-2-(thiophen-2-yl)acetamide (**210e**) ($CDCl_3$, 175 MHz)	327
Figure S76	^{1}H NMR spectrum of 3-(furan-2-yl)-*N*-methoxy-*N*-methylpropanamide (**210f**) ($CDCl_3$, 700 MHz)	328
Figure S77	^{13}C NMR spectrum of 3-(furan-2-yl)-*N*-methoxy-*N*-methylpropanamide (**210f**) ($CDCl_3$, 175 MHz)	328
Figure S78	^{1}H NMR spectrum of *tert*-butyl 2-(2-(methoxy(methyl)amino)-2-oxoethyl)pyrrolidine-1-carboxylate (**210g**) ($CDCl_3$, 700 MHz)	329
Figure S79	^{13}C NMR spectrum of *tert*-butyl 2-(2-(methoxy(methyl)amino)-2-oxoethyl)pyrrolidine-1-carboxylate (**210g**) ($CDCl_3$, 175 MHz)	329
Figure S80	^{1}H NMR spectrum of *N*-methoxy-*N*-methyl-5-phenylpentanamide (**210h**) ($CDCl_3$, 700 MHz)	330
Figure S81	^{13}C NMR spectrum of *N*-methoxy-*N*-methyl-5-phenylpentanamide (**210h**) ($CDCl_3$, 175 MHz)	330
Figure S82	^{1}H NMR spectrum of *N*-methoxy-*N*-methyl-2-methoxy-2-phenylacetamide (**210i**) ($CDCl_3$, 700 MHz)	331
Figure S83	^{13}C NMR spectrum of *N*-methoxy-*N*-methyl-2-methoxy-2-phenylacetamide (**210i**) ($CDCl_3$, 175 MHz)	331
Figure S84	^{1}H NMR spectrum of *N*-methoxy-*N*-methyl-2-(benzo[*d*][1,3]dioxol-5-yl)acetamide (**210j**) ($CDCl_3$, 700 MHz)	332
Figure S85	^{13}C NMR spectrum of *N*-methoxy-*N*-methyl-2-(benzo[*d*][1,3]dioxol-5-yl)acetamide (**210j**) ($CDCl_3$, 175	332

MHz)

Figure S86 ^{1}H NMR spectrum of *N*-methoxy-*N*-methyl-2-(*p*-tolyl)acetamide (**210k**) ($CDCl_3$, 700 MHz) 333

Figure S87 ^{13}C NMR spectrum of *N*-methoxy-*N*-methyl-2-(*p*-tolyl)acetamide (**210k**) ($CDCl_3$, 175 MHz) 333

Figure S88 ^{1}H NMR spectrum of *N*-methoxy-*N*-methyl-2-phenylacetamide (**186**) ($CDCl_3$, 400 MHz) 334

Figure S89 ^{13}C NMR spectrum of *N*-methoxy-*N*-methyl-2-phenylacetamide (**186**) ($CDCl_3$, 100 MHz) 334

Figure S90 ^{1}H NMR spectrum of *N*-methoxy-*N*-methylpropionamide (**210l**) ($CDCl_3$, 700 MHz) 335

Figure S91 ^{13}C NMR spectrum of *N*-methoxy-*N*-methylpropionamide (**210l**) ($CDCl_3$, 175 MHz) 335

Figure S92 ^{1}H NMR spectrum of *N*-methoxy-*N*-methyl-2-phenylbutanamide (**210m**) ($CDCl_3$, 700 MHz) 336

Figure S93 ^{13}C NMR spectrum of *N*-methoxy-*N*-methyl-2-phenylbutanamide (**210m**) ($CDCl_3$, 175 MHz) 336

Figure S94 ^{1}H NMR spectrum of 2-(4-chlorophenyl)-*N*-methoxy-*N*-methylacetamide (**210n**) ($CDCl_3$, 700 MHz) 337

Figure S95 ^{13}C NMR spectrum of 2-(4-chlorophenyl)-*N*-methoxy-*N*-methylacetamide (**210n**) ($CDCl_3$, 175 MHz) 337

Figure S96 ^{1}H NMR spectrum of 1,4-diphenylbutan-2-one (**191a**) ($CDCl_3$, 400 MHz) 338

Figure S97 ^{13}C NMR spectrum of 1,4-diphenylbutan-2-one (**191a**) ($CDCl_3$, 100 MHz) 338

Figure S98 ^{1}H NMR spectrum of 1-phenylpentan-2-one (**191b**) ($CDCl_3$, 700 MHz) 339

Figure S99 ^{13}C NMR spectrum of 1-phenylpentan-2-one (**191b**) ($CDCl_3$, 175 MHz) 339

Figure S100 ^{1}H NMR spectrum of 1,3-diphenylpropan-2-one (**191c**) ($CDCl_3$, 700 MHz) 340

Figure S101 ^{13}C NMR spectrum of 1,3-diphenylpropan-2-one (**191c**) ($CDCl_3$, 175 MHz) 340

Figure S102	^{1}H NMR spectrum of 1-(3,4-dimethoxy-phenyl)-4-(4-methoxy-phenyl)-butan-2-one (**191d**) ($CDCl_3$, 700 MHz)	341
Figure S103	^{13}C NMR spectrum of 1-(3,4-dimethoxy-phenyl)-4-(4-methoxy-phenyl)-butan-2-one (**191d**) ($CDCl_3$, 175 MHz)	341
Figure S104	^{1}H NMR spectrum of 1-phenylpentan-3-one (**212a**) ($CDCl_3$, 700 MHz)	342
Figure S105	^{13}C NMR spectrum of 1-phenylpentan-3-one (**212a**) ($CDCl_3$, 175 MHz)	342
Figure S106	^{1}H NMR spectrum of 1-cyclohexylpentan-2-one (**212b**) ($CDCl_3$, 700 MHz)	343
Figure S107	^{13}C NMR spectrum of 1-cyclohexylpentan-2-one (**212b**) ($CDCl_3$, 175 MHz)	343
Figure S108	^{1}H NMR spectrum of 1-cyclopropylpentan-2-one (**212c**) ($CDCl_3$, 700 MHz)	344
Figure S109	^{13}C NMR spectrum of 1-cyclopropylpentan-2-one (**212c**) ($CDCl_3$, 175 MHz)	344
Figure S110	^{1}H NMR spectrum of 1-(naphthalen-2-yl)pentan-2-one (**212d**) ($CDCl_3$, 400 MHz)	345
Figure S111	^{13}C NMR spectrum of 1-(naphthalen-2-yl)pentan-2-one (**212d**) ($CDCl_3$, 100 MHz)	345
Figure S112	^{1}H NMR spectrum of 1-(benzo[*b*]thiophen-3-yl)pentan-2-one (**212e**) ($CDCl_3$, 700 MHz)	346
Figure S113	^{13}C NMR spectrum of 1-(benzo[*b*]thiophen-3-yl)pentan-2-one (**212e**) ($CDCl_3$, 175 MHz)	346
Figure S114	^{1}H NMR spectrum of 1-(thiophen-2-yl)pentan-2-one (**212f**) ($CDCl_3$, 400 MHz)	347
Figure S115	^{13}C NMR spectrum of 1-(thiophen-2-yl)pentan-2-one (**212f**) ($CDCl_3$, 100 MHz)	347
Figure S116	^{1}H NMR spectrum of 1-(furan-2-yl)pentan-3-one (**212g**) ($CDCl_3$, 700 MHz)	348
Figure S117	^{13}C NMR spectrum of 1-(furan-2-yl)pentan-3-one (**212g**) ($CDCl_3$, 175 MHz)	348
Figure S118	^{1}H NMR spectrum of *tert*-butyl 2-(2-oxopentyl)pyrrolidine-1-carboxylate (**212h**) ($CDCl_3$, 700 MHz)	349

Figure S119	^{13}C NMR spectrum of *tert*-butyl 2-(2-oxopentyl)pyrrolidine-1-carboxylate (**212h**) ($CDCl_3$, 175 MHz)	349
Figure S120	^{1}H NMR spectrum of 8-phenyloctan-4-one (**212i**) ($CDCl_3$, 700 MHz)	350
Figure S121	^{13}C NMR spectrum of 8-phenyloctan-4-one (**212i**) ($CDCl_3$, 175 MHz)	350
Figure S122	^{1}H NMR spectrum of 7-phenylheptan-3-one (**212j**) ($CDCl_3$, 700 MHz)	351
Figure S123	^{13}C NMR spectrum of 7-phenylheptan-3-one (**212j**) ($CDCl_3$, 175 MHz)	351
Figure S124	^{1}H NMR spectrum of 1-phenylbutan-2-one (**212k**) ($CDCl_3$, 700 MHz)	352
Figure S125	^{13}C NMR spectrum of 1-phenylbutan-2-one (**212k**) ($CDCl_3$, 175 MHz)	352
Figure S126	^{1}H NMR spectrum of 1,4-diphenylhexan-3-one (**212l**) ($CDCl_3$, 700 MHz)	353
Figure S127	^{13}C NMR spectrum of 1,4-diphenylhexan-3-one (**212l**) ($CDCl_3$, 175 MHz)	353
Figure S128	^{1}H NMR spectrum of 1-methoxy-1,4-diphenylbutan-2-one (**212m**) ($CDCl_3$, 400 MHz)	354
Figure S129	^{13}C NMR spectrum of 1-methoxy-1,4-diphenylbutan-2-one (**212m**) ($CDCl_3$, 100 MHz)	354
Figure S130	^{1}H NMR spectrum of 1-(1,3-benzdioxol-5-yl)pentan-2-one (**212n**) ($CDCl_3$, 700 MHz)	355
Figure S131	^{13}C NMR spectrum of 1-(1,3-benzdioxol-5-yl)pentan-2-one (**212n**) ($CDCl_3$, 175 MHz)	355
Figure S132	^{1}H NMR spectrum of 1-(*p*-tolyl)pentan-2-one (**212o**) ($CDCl_3$, 700 MHz)	356
Figure S133	^{13}C NMR spectrum of 1-(*p*-tolyl)pentan-2-one (**212o**) ($CDCl_3$, 175 MHz)	356
Figure S134	^{1}H NMR spectrum of 1-(4-chlorophenyl)pentan-2-one (**212p**) ($CDCl_3$, 700 MHz)	357
Figure S135	^{13}C NMR spectrum of 1-(4-chlorophenyl)pentan-2-one (**212p**)	357

(CDCl$_3$, 175 MHz)

Figure S136 ^{1}H NMR spectrum of 1-(4-chlorophenyl)-4-phenylbutan-2-one (**212q**) (CDCl$_3$, 700 MHz) 358

Figure S137 ^{13}C NMR spectrum of 1-(4-chlorophenyl)-4-phenylbutan-2-one (**212q**) (CDCl$_3$, 175 MHz) 358

Figure S138 ^{1}H NMR spectrum of *N*-(3,4-dimethoxyphenethyl)-1-(3,4-dimethoxy-phenyl)-4-(4-methoxy-phenyl)-butan-2-amine (**215a**) (CDCl$_3$, 600 MHz) 359

Figure S139 ^{13}C NMR spectrum of *N*-(3,4-dimethoxyphenethyl)-1-(3,4-dimethoxy-phenyl)-4-(4-methoxy-phenyl)-butan-2-amine (**215a**) (CDCl$_3$, 150 MHz) 359

Figure S140 ^{1}H NMR spectrum of *N*-phenethyl-1,4-diphenyl-butan-2-amine (**215b**) (CDCl$_3$, 600 MHz) 360

Figure S141 ^{13}C NMR spectrum of *N*-phenethyl-1,4-diphenyl-butan-2-amine (**215b**) (CDCl$_3$, 150 MHz) 360

Figure S142 ^{1}H NMR spectrum of 1,4-diphenyl-*N*-propylbutan-2-amine (**215c**) (CDCl$_3$, 600 MHz) 361

Figure S143 ^{13}C NMR spectrum of 1,4-diphenyl-*N*-propylbutan-2-amine (**215c**) (CDCl$_3$, 150 MHz) 361

Figure S144 ^{1}H NMR spectrum of *N*-phenethyl-1-phenylpentan-3-amine (**215d**) (CDCl$_3$, 600 MHz) 362

Figure S145 ^{13}C NMR spectrum of *N*-phenethyl-1-phenylpentan-3-amine (**215d**) (CDCl$_3$, 150 MHz) 362

Figure S146 ^{1}H NMR spectrum of *N*-phenethyl-1-phenylpentan-2-amine (**215e**) (CDCl$_3$, 600 MHz) 363

Figure S147 ^{13}C NMR spectrum of *N*-phenethyl-1-phenylpentan-2-amine (**215e**) (CDCl$_3$, 150 MHz) 363

Figure S148 ^{1}H NMR spectrum of *N*-(2-(cyclohex-1-en-1-yl)ethyl)-1-phenylpentan-2-amine (**215f**) (CDCl$_3$, 700 MHz) 364

Figure S149 ^{13}C NMR spectrum of *N*-(2-(cyclohex-1-en-1-yl)ethyl)-1-phenylpentan-2-amine (**215f**) (CDCl$_3$, 175 MHz) 364

Figure S150 ^{1}H NMR spectrum of 1-cyclohexyl-*N*-phenethylpentan-2-amine (**215g**) (CDCl$_3$, 400 MHz) 365

Figure S151 ^{13}C NMR spectrum of 1-cyclohexyl-*N*-phenethylpentan-2- 365

amine (**215g**) ($CDCl_3$, 175 MHz)

Figure S152 ^{1}H NMR spectrum of 1-cyclopropyl-*N*-phenethylpentan-2-amine (**215h**) ($CDCl_3$, 400 MHz) 366

Figure S153 ^{13}C NMR spectrum of 1-cyclopropyl-*N*-phenethylpentan-2-amine (**215h**) ($CDCl_3$, 100 MHz) 366

Figure S154 ^{1}H NMR spectrum of *N*-phenethylundecan-4-amine (**215i**) ($CDCl_3$, 400 MHz) 367

Figure S155 ^{13}C NMR spectrum of *N*-phenethylundecan-4-amine (**215i**) ($CDCl_3$, 100 MHz) 367

Figure S156 ^{1}H NMR spectrum of 3-((1-phenylpentan-2-yl)amino)propanenitrile (**215j**) ($CDCl_3$, 600 MHz) 368

Figure S157 ^{13}C NMR spectrum of 3-((1-phenylpentan-2-yl)amino)propanenitrile (**215j**) ($CDCl_3$, 150 MHz) 368

Figure S158 ^{1}H NMR spectrum of 2-(3,4-dimethoxyphenyl)-1-(isopropylamino)ethane (**215k**) ($CDCl_3$, 600 MHz) 369

Figure S159 ^{13}C NMR spectrum of 2-(3,4-dimethoxyphenyl)-1-(isopropylamino)ethane (**215k**) ($CDCl_3$, 150 MHz) 369

Figure S160 ^{1}H NMR spectrum of *N*-(2-(cyclohex-1-en-1-yl)ethyl)-1-cyclohexylpentan-2-amine (**215l**) ($CDCl_3$, 400 MHz) 370

Figure S161 ^{13}C NMR spectrum of *N*-(2-(cyclohex-1-en-1-yl)ethyl)-1-cyclohexylpentan-2-amine (**215l**) ($CDCl_3$, 100 MHz) 370

Figure S162 ^{1}H NMR spectrum of 1-cyclohexyl-*N*-(2-cyclohexylethyl)pentan-2-amine (**215m**) ($CDCl_3$, 400 MHz) 371

Figure S163 ^{13}C NMR spectrum of 1-cyclohexyl-*N*-(2-cyclohexylethyl)pentan-2-amine (**215m**) ($CDCl_3$, 100 MHz) 371

Figure S164 ^{1}H NMR spectrum of 1-cyclohexyl-*N*-(2-(piperidin-1-yl)ethyl)pentan-2-amine (**215n**) ($CDCl_3$, 400 MHz) 372

Figure S165 ^{13}C NMR spectrum of 1-cyclohexyl-*N*-(2-(piperidin-1-yl)ethyl)pentan-2-amine (**215n**) ($CDCl_3$, 100 MHz) 372

Figure S166 ^{1}H NMR spectrum of 1-phenyl-*N*-(2-(piperidin-1-yl)ethyl)pentan-2-amine (**215o**) ($CDCl_3$, 700 MHz) 373

Figure S167 ^{13}C NMR spectrum of 1-phenyl-*N*-(2-(piperidin-1-yl)ethyl)pentan-2-amine (**215o**) ($CDCl_3$, 175 MHz) 373

Figure S168	^{1}H NMR spectrum of *N*-(2-morpholinoethyl)-1-phenylpentan-2-amine (**215p**) ($CDCl_3$, 700 MHz)	374
Figure S169	^{13}C NMR spectrum of *N*-(2-morpholinoethyl)-1-phenylpentan-2-amine (**215p**) ($CDCl_3$, 175 MHz)	374
Figure S170	^{1}H NMR spectrum of 1-phenyl-*N*-(2-(pyridine-2-yl)ethyl)pentan-2-amine (**215q**) ($CDCl_3$, 700 MHz)	375
Figure S171	^{13}C NMR spectrum of 1-phenyl-*N*-(2-(pyridine-2-yl)ethyl)pentan-2-amine (**215q**) ($CDCl_3$, 175 MHz)	375
Figure S172	^{1}H NMR spectrum of *N*-(2-(1*H*-imidazol-4-yl)ethyl)-1-phenylpentan-2-amine (**215r**) ($CDCl_3$, 400 MHz)	376
Figure S173	^{13}C NMR spectrum of *N*-(2-(1*H*-imidazol-4-yl)ethyl)-1-phenylpentan-2-amine (**215r**) ($CDCl_3$, 100 MHz)	376
Figure S174	^{1}H NMR spectrum of 1-(naphthalen-2-yl)-*N*-phenethylpentan-2-amine (**215s**) ($CDCl_3$, 600 MHz)	377
Figure S175	^{13}C NMR spectrum of 1-(naphthalen-2-yl)-*N*-phenethylpentan-2-amine (**215s**) ($CDCl_3$, 150 MHz)	377
Figure S176	^{1}H NMR spectrum of *N*-(2-(1*H*-indol-3-yl)ethyl)-1-phenylpentan-2-amine (**215t**) ($CDCl_3$, 700 MHz)	378
Figure S177	^{13}C NMR spectrum of *N*-(2-(1*H*-indol-3-yl)ethyl)-1-phenylpentan-2-amine (**215t**) ($CDCl_3$, 175 MHz)	378
Figure S178	^{1}H NMR spectrum of 1-(benzo[*b*]thiophen-3-yl)-*N*-phenethylpentan-2-amine (**215u**) ($CDCl_3$, 400 MHz)	379
Figure S179	^{13}C NMR spectrum of 1-(benzo[*b*]thiophen-3-yl)-*N*-phenethylpentan-2-amine (**215u**) ($CDCl_3$, 100 MHz)	379
Figure S180	^{1}H NMR spectrum of *N*-phenethyl-1-(thiophen-2-yl)pentan-2-amine (**215v**) ($CDCl_3$, 400 MHz)	380
Figure S181	^{13}C NMR spectrum of *N*-phenethyl-1-(thiophen-2-yl)pentan-2-amine (**215v**) ($CDCl_3$, 100 MHz)	380
Figure S182	^{1}H NMR spectrum of 1-(furan-2-yl)-*N*-phenethylpentan-3-amine (**215w**) ($CDCl_3$, 400 MHz)	381
Figure S183	^{13}C NMR spectrum of 1-(furan-2-yl)-*N*-phenethylpentan-3-amine (**215w**) ($CDCl_3$, 100 MHz)	381
Figure S184	^{1}H NMR spectrum of *N*-(2-cyclohexylethyl)-1-(furan-2-yl)pentan-3-amine (**215x**) ($CDCl_3$, 400 MHz)	382

Figure S185	^{13}C NMR spectrum of *N*-(2-cyclohexylethyl)-1-(furan-2-yl)pentan-3-amine (**215x**) ($CDCl_3$, 100 MHz)	382
Figure S186	^{1}H NMR spectrum of 1-(furan-2-yl)-*N*-(2-(piperidin-1-yl)ethyl)pentan-3-amine (**215y**) ($CDCl_3$, 400 MHz)	383
Figure S187	^{13}C NMR spectrum of 1-(furan-2-yl)-*N*-(2-(piperidin-1-yl)ethyl)pentan-3-amine (**215y**) ($CDCl_3$, 100 MHz)	383
Figure S188	^{1}H NMR spectrum of (2*S*)-*tert*-butyl 2-(2-(phenethylamino)pentyl)pyrrolidine-1-carboxylate (**215z**) ($CDCl_3$, 700 MHz)	384
Figure S189	^{13}C NMR spectrum of (2*S*)-*tert*-butyl 2-(2-(phenethylamino)pentyl)pyrrolidine-1-carboxylate (**215z**) ($CDCl_3$, 175 MHz)	384
Figure S190	^{1}H NMR spectrum of 1-phenyl-*N*-(4-phenylbutyl)pentan-2-amine (**215za**) ($CDCl_3$, 700 MHz)	385
Figure S191	^{13}C NMR spectrum of 1-phenyl-*N*-(4-phenylbutyl)pentan-2-amine (**215za**) ($CDCl_3$, 175 MHz)	385
Figure S192	^{1}H NMR spectrum of *N*-phenethyl-8-phenyloctan-4-amine (**215zb**) ($CDCl_3$, 400 MHz)	386
Figure S193	^{13}C NMR spectrum of *N*-phenethyl-8-phenyloctan-4-amine (**215zb**) ($CDCl_3$, 175 MHz)	386
Figure S194	^{1}H NMR spectrum of *N*-phenethyl-7-phenylheptan-3-amine (**215zc**) ($CDCl_3$, 400 MHz)	387
Figure S195	^{13}C NMR spectrum of *N*-phenethyl-7-phenylheptan-3-amine (**215zc**) ($CDCl_3$, 175 MHz)	387
Figure S196	^{1}H NMR spectrum of *N*-(3,4-dimethoxyphenethyl)-1,3-diphenylpropan-2-amine (**215zd**) ($CDCl_3$, 600 MHz)	388
Figure S197	^{13}C NMR spectrum of *N*-(3,4-dimethoxyphenethyl)-1,3-diphenylpropan-2-amine (**215zd**) ($CDCl_3$, 150 MHz)	388
Figure S198	^{1}H NMR spectrum of *N*-phenethyl-1-phenylbutan-2-amine (**215ze**) ($CDCl_3$, 400 MHz)	389
Figure S199	^{13}C NMR spectrum of *N*-phenethyl-1-phenylbutan-2-amine (**215ze**) ($CDCl_3$, 175 MHz)	389
Figure S200	^{1}H NMR spectrum of *N*-(3,4-dimethoxyphenethyl)-1-(3,4-dimethoxy-phenyl)-propan-2-amine (**215zf**) ($CDCl_3$, 700	390

MHz)

Figure S201 ^{13}C NMR spectrum of *N*-(3,4-dimethoxyphenethyl)-1-(3,4-dimethoxy-phenyl)-propan-2-amine (**215zf**) ($CDCl_3$, 175 MHz) 390

Figure S202 ^{1}H NMR spectrum of *N*-(2,2-diphenylethyl)-1-phenylpentan-2-amine (**215zg**) ($CDCl_3$, 700 MHz) 391

Figure S203 ^{13}C NMR spectrum of *N*-(2,2-diphenylethyl)-1-phenylpentan-2-amine (**215zg**) ($CDCl_3$, 175 MHz) 391

Figure S204 ^{1}H NMR spectrum of *N*-phenethyl-1,4-diphenylhexan-3-amine (**215zh**) ($CDCl_3$, 700 MHz) 392

Figure S205 ^{13}C NMR spectrum of *N*-phenethyl-1,4-diphenylhexan-3-amine (**215zh**) ($CDCl_3$, 175 MHz) 392

Figure S206 ^{1}H NMR spectrum of 1-methoxy-*N*-phenethyl-1,4-diphenylbutan-2-amine (**215zi**) ($CDCl_3$, 400 MHz) 393

Figure S207 ^{13}C NMR spectrum of 1-methoxy-*N*-phenethyl-1,4-diphenylbutan-2-amine (**215zi**) ($CDCl_3$, 100 MHz) 393

Figure S208 ^{1}H NMR spectrum of *N*-(4-methoxyphenethyl)-1-phenylpentan-2-amine (**215zj**) ($CDCl_3$, 400 MHz) 394

Figure S209 ^{13}C NMR spectrum of *N*-(4-methoxyphenethyl)-1-phenylpentan-2-amine (**215zj**) ($CDCl_3$, 100 MHz) 394

Figure S210 ^{1}H NMR spectrum of 1-(benzo[*d*][1,3]dioxol-5-yl)-*N*-phenethylpentan-2-amine (**215zk**) ($CDCl_3$, 700 MHz) 395

Figure S211 ^{13}C NMR spectrum of 1-(benzo[*d*][1,3]dioxol-5-yl)-*N*-phenethylpentan-2-amine (**215zk**) ($CDCl_3$, 175 MHz) 395

Figure S212 ^{1}H NMR spectrum of *N*-phenethyl-1-(*p*-tolyl)pentan-2-amine (**215zl**) ($CDCl_3$, 700 MHz) 396

Figure S213 ^{13}C NMR spectrum of *N*-phenethyl-1-(*p*-tolyl)pentan-2-amine (**215zl**) ($CDCl_3$, 175 MHz) 396

Figure S214 ^{1}H NMR spectrum of 4-(2-((1-phenylpentan-2-yl)amino)ethyl)phenol (**215zm**) ($CDCl_3$, 400 MHz) 397

Figure S215 ^{13}C NMR spectrum of 4-(2-((1-phenylpentan-2-yl)amino)ethyl)phenol (**215zm**) ($CDCl_3$, 100 MHz) 397

Figure S216 ^{1}H NMR spectrum of *N*-(4-fluorophenethyl)-1-phenylpentan-2-amine (**215zn**) ($CDCl_3$, 700 MHz) 398

Figure S217	^{13}C NMR spectrum of *N*-(4-fluorophenethyl)-1-phenylpentan-2-amine (**215zn**) ($CDCl_3$, 175 MHz)	398
Figure S218	^{1}H NMR spectrum of *N*-(4-fluorophenethyl)-1-(*p*-tolyl)pentan-2-amine (**215zo**) ($CDCl_3$, 400 MHz)	399
Figure S219	^{13}C NMR spectrum of *N*-(4-fluorophenethyl)-1-(*p*-tolyl)pentan-2-amine (**215zo**) ($CDCl_3$, 100 MHz)	399
Figure S220	^{1}H NMR spectrum of 1-(4-chlorophenyl)-*N*-phenethylpentan-2-amine (**215zp**) ($CDCl_3$, 400 MHz)	400
Figure S221	^{13}C NMR spectrum of 1-(4-chlorophenyl)-*N*-phenethylpentan-2-amine (**215zp**) ($CDCl_3$, 100 MHz)	400
Figure S222	^{1}H NMR spectrum of 1-(4-chlorophenyl)-*N*-(4-fluorophenethyl)pentan-2-amine (**215zq**) ($CDCl_3$, 400 MHz)	401
Figure S223	^{13}C NMR spectrum of 1-(4-chlorophenyl)-*N*-(4-fluorophenethyl)pentan-2-amine (**215zq**) ($CDCl_3$, 100 MHz)	401
Figure S224	^{1}H NMR spectrum of 1-(4-chlorophenyl)-*N*-(4-fluorophenethyl)-4-phenylbutan-2-amine (**215zr**) ($CDCl_3$, 400 MHz)	402
Figure S225	^{13}C NMR spectrum of 1-(4-chlorophenyl)-*N*-(4-fluorophenethyl)-4-phenylbutan-2-amine (**215zr**) ($CDCl_3$, 100 MHz)	402
Figure S226	^{1}H NMR spectrum of *N*-(1-phenylpentan-2-yl)cyclopentanamine (**216a**) ($CDCl_3$, 400 MHz)	403
Figure S227	^{13}C NMR spectrum of *N*-(1-phenylpentan-2-yl)cyclopentanamine (**216a**) ($CDCl_3$, 100 MHz)	403
Figure S228	^{1}H NMR spectrum of *N*-(1-phenylpentan-2-yl)cyclopropanamine (**216b**) ($CDCl_3$, 400 MHz)	404
Figure S229	^{13}C NMR spectrum of *N*-(1-phenylpentan-2-yl)cyclopropanamine (**216b**) ($CDCl_3$, 100 MHz)	404
Figure S230	^{1}H NMR spectrum of *N*-(1-phenylpentan-2-yl)bicyclo[2.2.1]heptan-2-amine (**216c**) ($CDCl_3$, 400 MHz)	405
Figure S231	^{13}C NMR spectrum of *N*-(1-phenylpentan-2-yl)bicyclo[2.2.1]heptan-2-amine (**216c**) ($CDCl_3$, 100 MHz)	405
Figure S232	^{1}H NMR spectrum of *N*-(1-phenylpentan-2-yl)-2,3-dihydro-1*H*-inden-2-amine (**216d**) ($CDCl_3$, 400 MHz)	406

Figure S233	^{13}C NMR spectrum of *N*-(1-phenylpentan-2-yl)-2,3-dihydro-1*H*-inden-2-amine (**216d**) ($CDCl_3$, 100 MHz)	406
Figure S234	^{1}H NMR spectrum of *N*-phenethyl-2,3-dihydro-1*H*-inden-2-amine (**217a**) ($CDCl_3$, 400 MHz)	407
Figure S235	^{13}C NMR spectrum of *N*-phenethyl-2,3-dihydro-1*H*-inden-2-amine (**217a**) ($CDCl_3$, 100 MHz)	407
Figure S236	^{1}H NMR spectrum of *N*-phenethyl-1,2,3,4-tetrahydronaphthalen-2-amine (**217b**) ($CDCl_3$, 700 MHz)	408
Figure S237	^{13}C NMR spectrum of *N*-phenethyl-1,2,3,4-tetrahydronaphthalen-2-amine (**217b**) ($CDCl_3$, 175 MHz)	408
Figure S238	HSQC spectrum of *N*-phenethyl-1,2,3,4-tetrahydronaphthalen-2-amine (**217b**) ($CDCl_3$, 700 MHz)	409
Figure S239	COSY spectrum of *N*-phenethyl-1,2,3,4-tetrahydronaphthalen-2-amine (**217b**) ($CDCl_3$, 700 MHz)	409
Figure S240	HMBC spectrum of *N*-phenethyl-1,2,3,4-tetrahydronaphthalen-2-amine (**217b**) ($CDCl_3$, 700 MHz)	410
Figure S241	^{1}H NMR spectrum of *N*-(2,3-dihydro-1*H*-inden-2-yl)-1,2,3,4-tetrahydronaphthalen-2-amine (**218**) ($CDCl_3$, 400 MHz)	411
Figure S242	^{13}C NMR spectrum of *N*-(2,3-dihydro-1*H*-inden-2-yl)-1,2,3,4-tetrahydronaphthalen-2-amine (**218**) ($CDCl_3$, 100 MHz)	411
Figure S243	^{1}H NMR spectrum of 4-(2-((3,4-dihydroxyphenethyl)amino)-4-(4-hydroxyphenyl)butyl)benzene-1,2-diol (**219**) (CD_3OD, 400 MHz)	412
Figure S244	^{1}H NMR spectrum of 1,4-diphenylbutan-2-ol (**221**) ($CDCl_3$, 700 MHz)	413
Figure S245	^{13}C NMR spectrum of 1,4-diphenylbutan-2-ol (**221**) ($CDCl_3$, 175 MHz)	413
Figure S246	^{1}H NMR spectrum of 1,4-diphenylbutan-2-yl 4-methylbenzenesulfonate (**224**) ($CDCl_3$, 400 MHz)	414
Figure S247	^{13}C NMR spectrum of 1,4-diphenylbutan-2-yl 4-methylbenzenesulfonate (**224**) ($CDCl_3$, 100 MHz)	414
Figure S248	^{1}H NMR spectrum of *N*-(1,4-diphenylbutan-2-yl)-*N*-phenethylacetamide (**230a**) ($CDCl_3$, 700 MHz)	415

Figure S249	^{13}C NMR spectrum of *N*-(1,4-diphenylbutan-2-yl)-*N*-phenethylacetamide (**230a**) ($CDCl_3$, 175 MHz)	415
Figure S250	^{1}H NMR spectrum of *N*-(1,4-diphenylbutan-2-yl)-*N*-phenethylcyclopropanecarboxamide (**230b**) ($CDCl_3$, 700 MHz)	416
Figure S251	^{13}C NMR spectrum of *N*-(1,4-diphenylbutan-2-yl)-*N*-phenethylcyclopropanecarboxamide (**230b**) ($CDCl_3$, 175 MHz)	416
Figure S252	^{1}H NMR spectrum of *N*-(1,4-diphenylbutan-2-yl)-*N*-phenethyl-2-phenylacetamide (**230c**) ($CDCl_3$, 700 MHz)	417
Figure S253	^{13}C NMR spectrum of *N*-(1,4-diphenylbutan-2-yl)-*N*-phenethyl-2-phenylacetamide (**230c**) ($CDCl_3$, 175 MHz)	417
Figure S254	^{1}H NMR spectrum of *N*-ethyl-*N*-phenethyl-1,4-diphenylbutan-2-amine (**231a**) ($CDCl_3$, 600 MHz)	418
Figure S255	^{13}C NMR spectrum of *N*-ethyl-*N*-phenethyl-1,4-diphenylbutan-2-amine (**231a**) ($CDCl_3$, 150 MHz)	418
Figure S256	^{1}H NMR spectrum of *N*-(cyclopropylmethyl)-*N*-phenethyl-1,4-diphenylbutan-2-amine (**231b**) ($CDCl_3$, 700 MHz)	419
Figure S257	^{13}C NMR spectrum of *N*-(cyclopropylmethyl)-*N*-phenethyl-1,4-diphenylbutan-2-amine (**231b**) ($CDCl_3$, 175 MHz)	419
Figure S258	^{1}H NMR spectrum of *N*,*N*-diphenethyl-1,4-diphenylbutan-2-amine (**231c**) ($CDCl_3$, 700 MHz)	420
Figure S259	^{13}C NMR spectrum of *N*,*N*-diphenethyl-1,4-diphenylbutan-2-amine (**231c**) ($CDCl_3$, 175 MHz)	420
Figure S260	^{1}H NMR spectrum of *N*,*N*-dimethyl-*N*-phenethyl-1,4-diphenylbutan-2-aminium iodide (**232**) ($CDCl_3$, 400 MHz)	421
Figure S261	^{13}C NMR spectrum of *N*,*N*-dimethyl-*N*-phenethyl-1,4-diphenylbutan-2-aminium iodide (**232**) ($CDCl_3$, 175 MHz)	421
Figure S262	^{1}H NMR spectrum of *N*,*N*-dimethyl-*N*-phenethyl-1,2,3,4-tetrahydronaphthalen-2-aminium iodide (**233**) ($CDCl_3$, 400 MHz)	422
Figure S263	^{13}C NMR spectrum of *N*,*N*-dimethyl-*N*-phenethyl-1,2,3,4-tetrahydronaphthalen-2-aminium iodide (**233**) ($CDCl_3$, 100 MHz)	422
Figure S264	^{1}H NMR spectrum of *N*-phenethyl-1-((*S*)-pyrrolidin-2-	423

	yl)pentan-2-amine (diastereomer 1 of **239**) ($CDCl_3$, 600 MHz)	
Figure S265	^{13}C NMR spectrum of *N*-phenethyl-1-((*S*)-pyrrolidin-2-yl)pentan-2-amine (diastereomer 1 of **239**) ($CDCl_3$, 150 MHz)	423
Figure S266	HSQC spectrum of *N*-phenethyl-1-((*S*)-pyrrolidin-2-yl)pentan-2-amine (diastereomer 1 of **239**) ($CDCl_3$, 600 MHz)	424
Figure S267	COSY spectrum of *N*-phenethyl-1-((*S*)-pyrrolidin-2-yl)pentan-2-amine (diastereomer 1 of **239**) ($CDCl_3$, 600 MHz)	424
Figure S268	HMBC spectrum of *N*-phenethyl-1-((*S*)-pyrrolidin-2-yl)pentan-2-amine (diastereomer 1 of **239**) ($CDCl_3$, 600 MHz)	425
Figure S269	NOESY spectrum of *N*-phenethyl-1-((*S*)-pyrrolidin-2-yl)pentan-2-amine (diastereomer 1 of **239**) ($CDCl_3$, 600 MHz)	425
Figure S270	COSY and HMBC correlations of *N*-phenethyl-1-((*S*)-pyrrolidin-2-yl)pentan-2-amine (diastereomer 1 of **239**)	426
Figure S271	^{1}H NMR spectrum of *N*-phenethyl-1-((*S*)-pyrrolidin-2-yl)pentan-2-amine (diastereomer 2 of **239**) ($CDCl_3$, 400 MHz)	427
Figure S272	^{13}C NMR spectrum of *N*-phenethyl-1-((*S*)-pyrrolidin-2-yl)pentan-2-amine (diastereomer 2 of **239**) ($CDCl_3$, 100 MHz)	427
Figure S273	HSQC spectrum of *N*-phenethyl-1-((*S*)-pyrrolidin-2-yl)pentan-2-amine (diastereomer 2 of **239**) ($CDCl_3$, 400 MHz)	428
Figure S274	COSY spectrum of *N*-phenethyl-1-((*S*)-pyrrolidin-2-yl)pentan-2-amine (diastereomer 2 of **239**) ($CDCl_3$, 400 MHz)	428
Figure S275	HMBC spectrum of *N*-phenethyl-1-((*S*)-pyrrolidin-2-yl)pentan-2-amine (diastereomer 2 of **239**) ($CDCl_3$, 400 MHz)	429
Figure S276	COSY and HMBC correlations of *N*-phenethyl-1-((*S*)-pyrrolidin-2-yl)pentan-2-amine (diastereomer 2 of **239**)	429
	Animal Welfare and Ethical Review Body approval for studies on SD rats (AWERB REF: UNMC12)	430
	Animal Welfare and Ethical Review Body approval for studies on SHRs (AWERB REF: UNMC18)	436

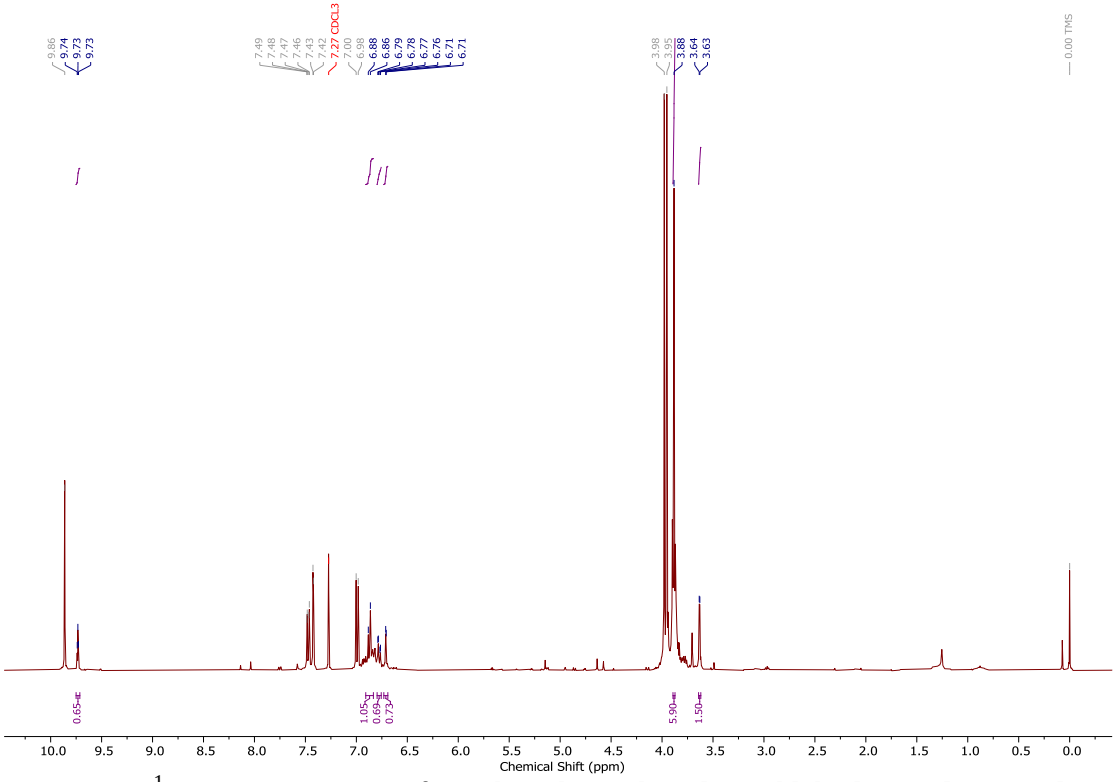


Figure S1. ^{1}H NMR spectrum of 3,4-dimethoxyphenylacetaldehyde (**177b**) ($CDCl_3$, 400 MHz)

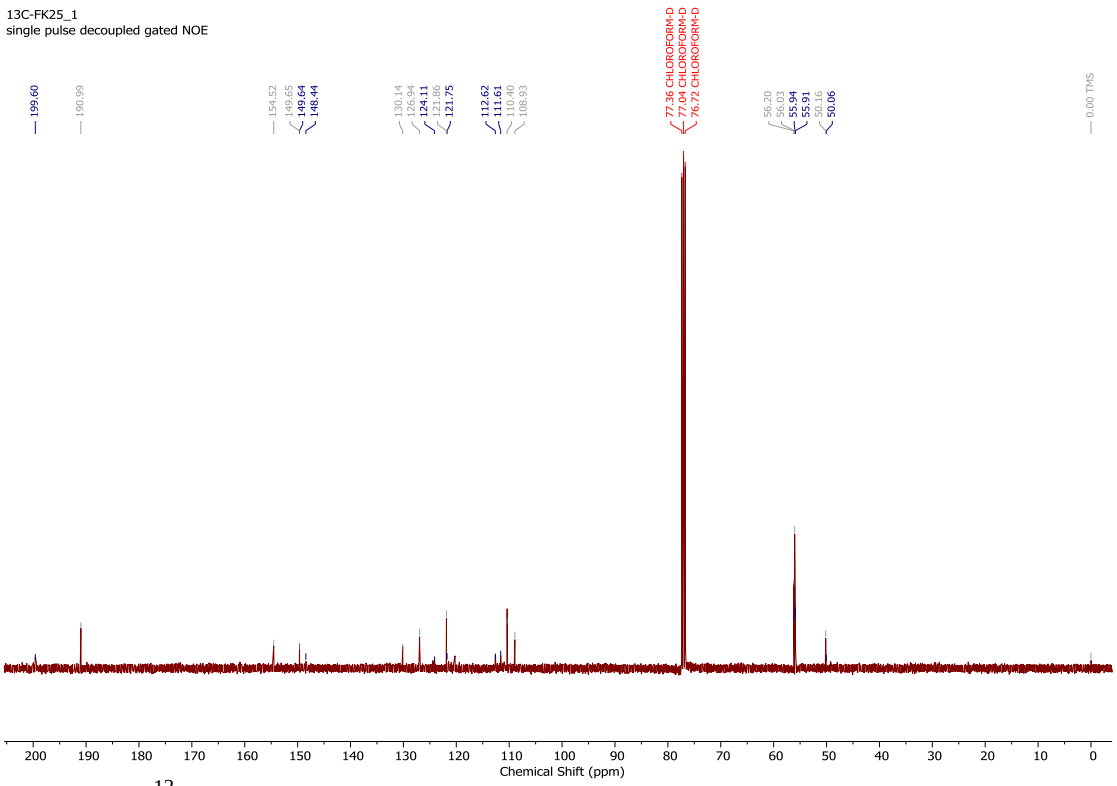


Figure S2. ^{13}C NMR spectrum of 3,4-dimethoxyphenylacetaldehyde (**177b**) ($CDCl_3$, 100 MHz)

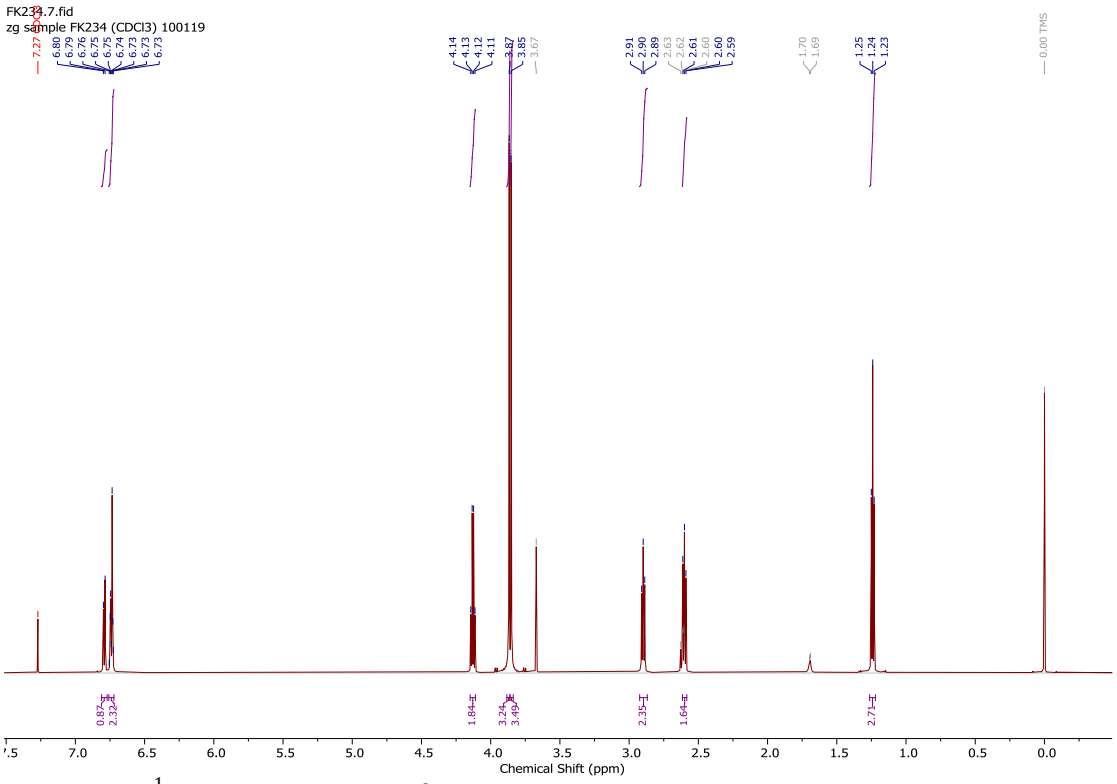


Figure S3. ^{1}H NMR spectrum of ethyl 3-(3,4-dimethoxyphenyl)propanoate (**193**) ($CDCl_3$, 700 MHz)

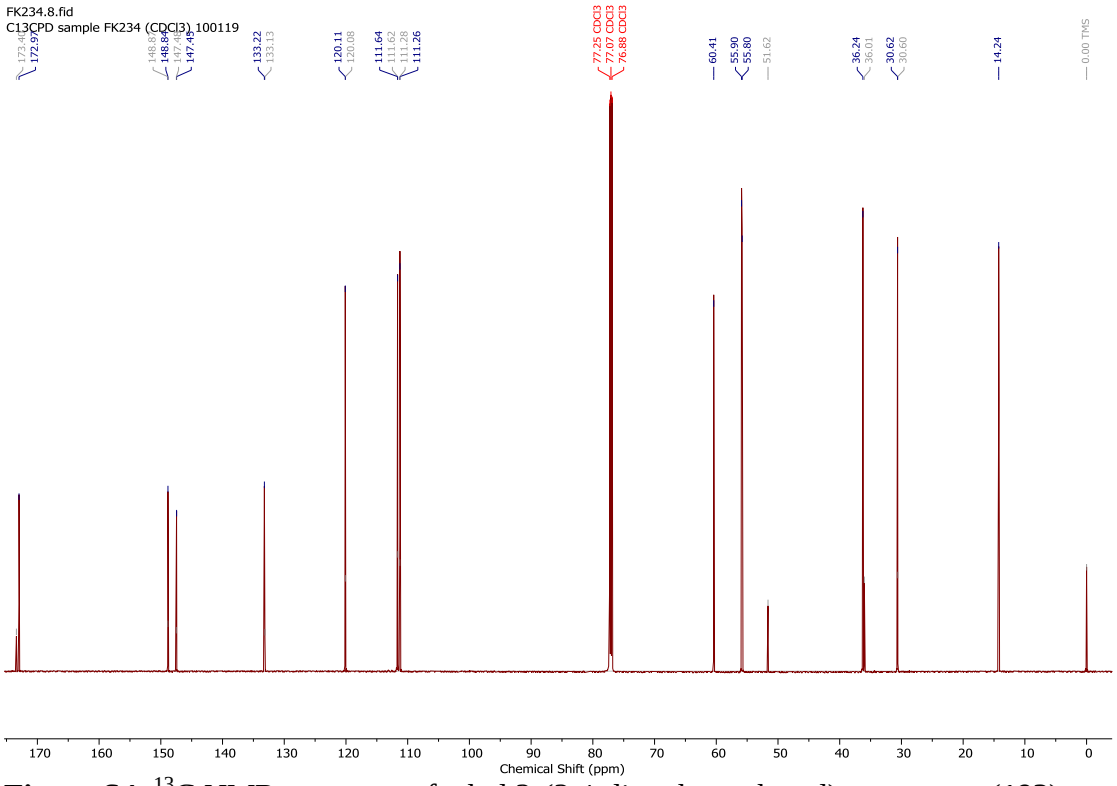


Figure S4. ^{13}C NMR spectrum of ethyl 3-(3,4-dimethoxyphenyl)propanoate (**193**) ($CDCl_3$, 175 MHZ)

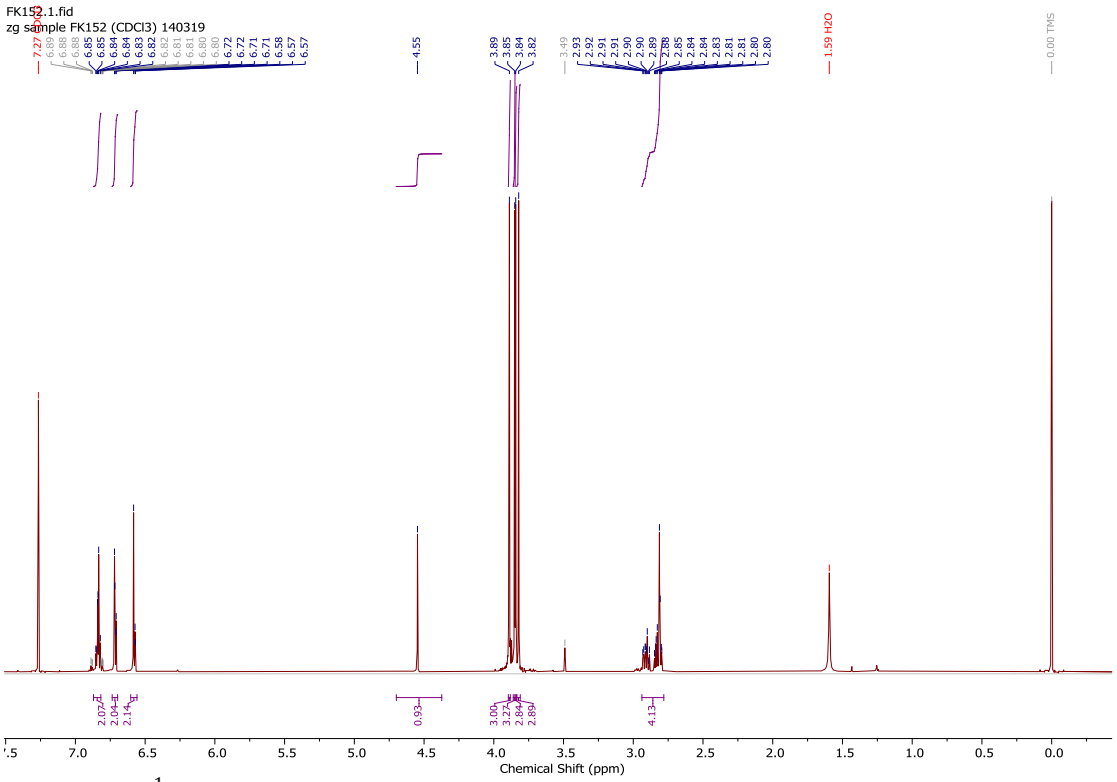


Figure S5. ^{1}H NMR spectrum of 1-cyano-1,4-di-(3',4'-dimethoxyphenyl)-butanone-2 (**194**) ($CDCl_3$, 700 MHz)

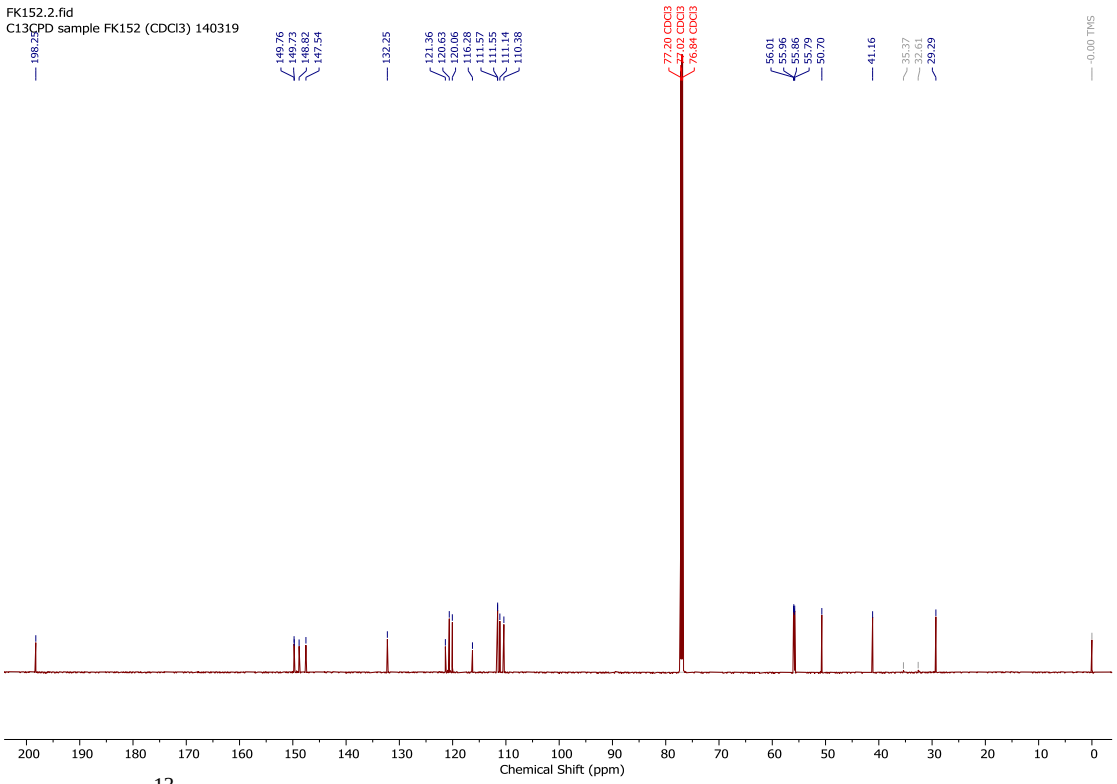


Figure S6. ^{13}C NMR spectrum of 1-cyano-1,4-di-(3',4'-dimethoxyphenyl)-butanone-2 (**194**) ($CDCl_3$, 175 MHz)

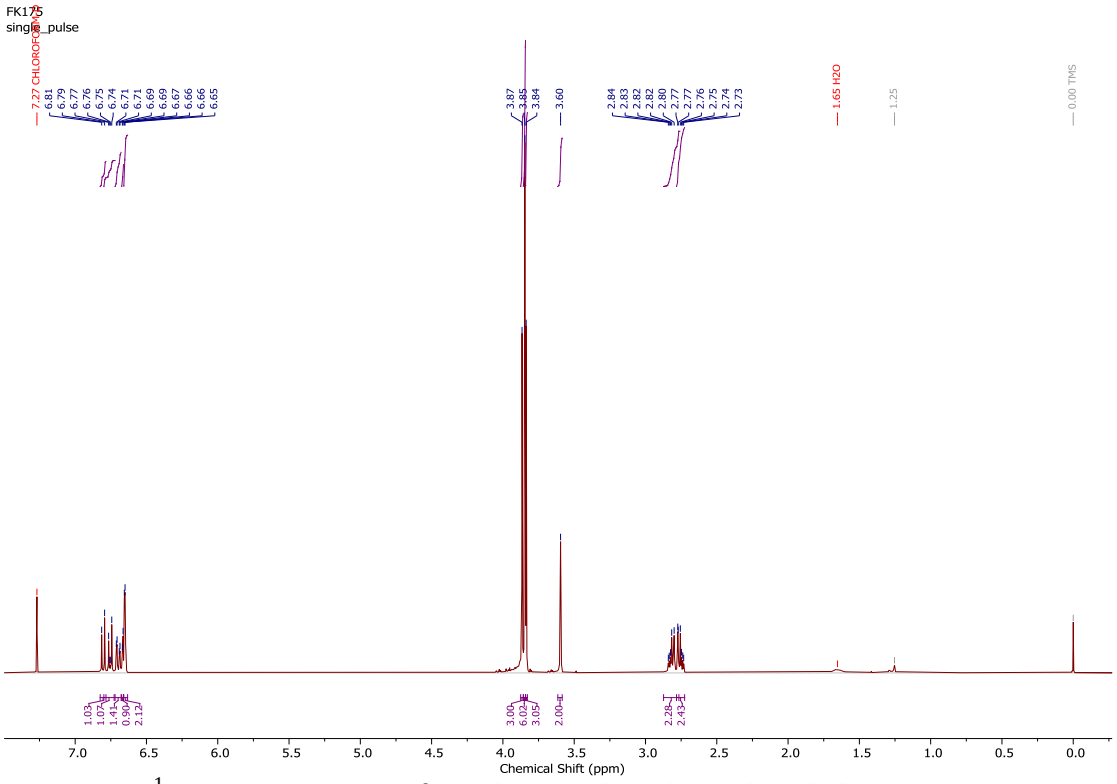


Figure S7. ^{1}H NMR spectrum of 1,4-di-(3',4'-dimethoxyphenyl)-butanone-2 (**175**) ($CDCl_3$, 400 MHz)

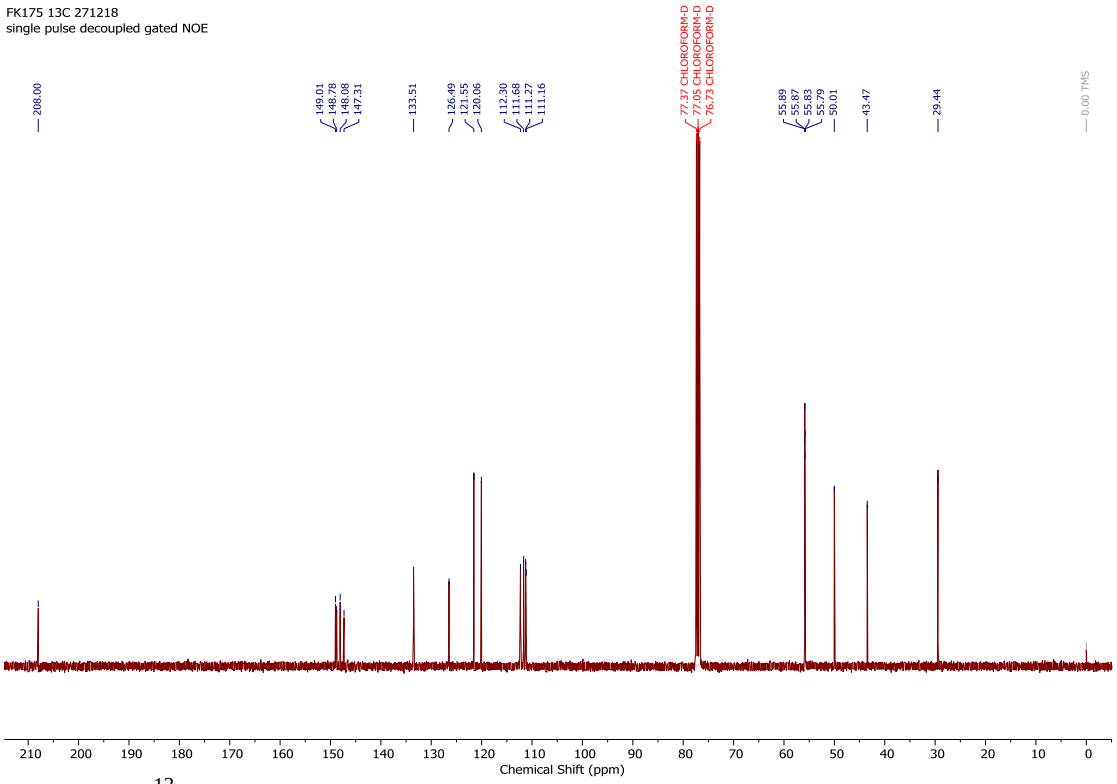


Figure S8. ^{13}C NMR spectrum of 1,4-di-(3',4'-dimethoxyphenyl)-butanone-2 (**175**) ($CDCl_3$, 100 MHz)

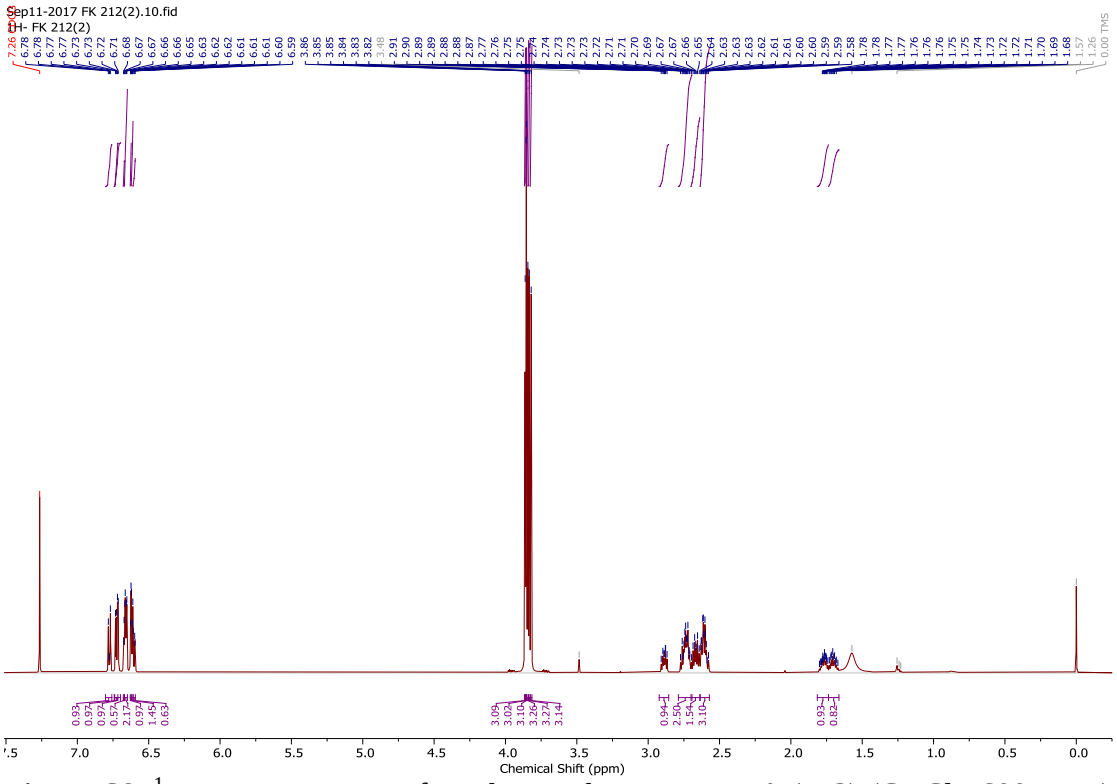


Figure S9. ^{1}H NMR spectrum of synthetic schwarzinicine A (**142**) ($CDCl_3$, 600 MHz)

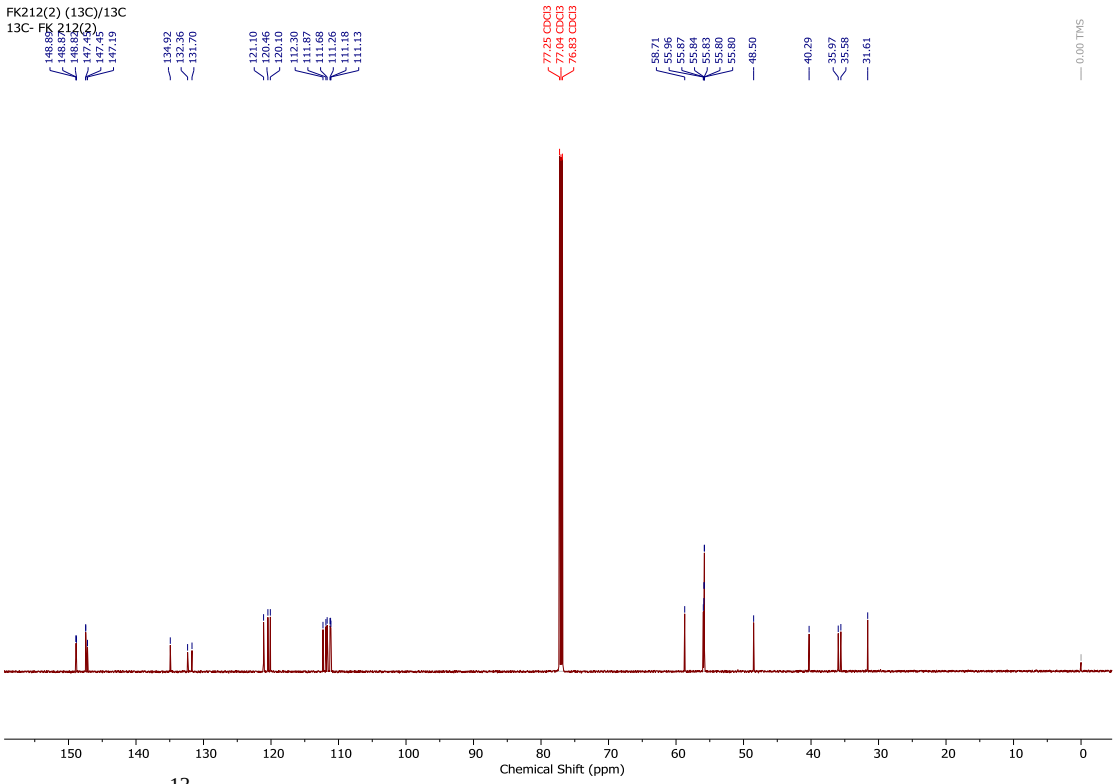


Figure S10. ^{13}C NMR spectrum of synthetic schwarzinicine A (**142**) ($CDCl_3$, 150 MHz)

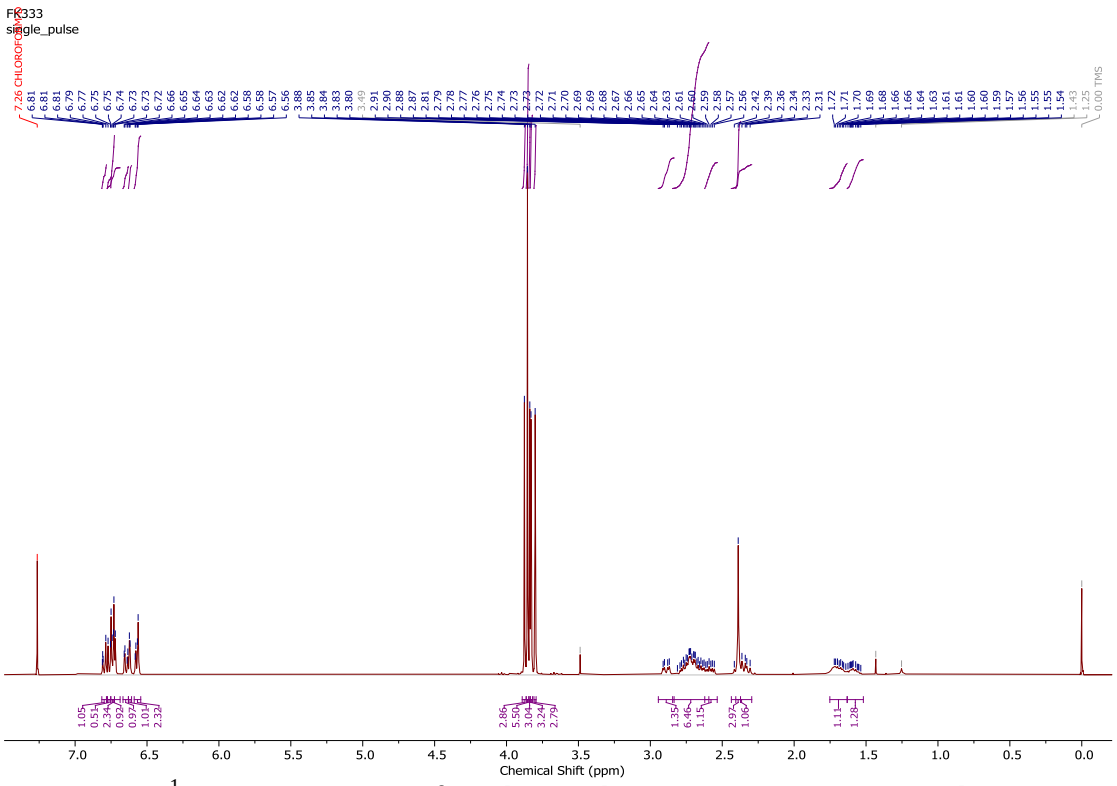


Figure S11. ^{1}H NMR spectrum of synthetic schwarzinicine B (**143**) ($CDCl_3$, 400 MHz)

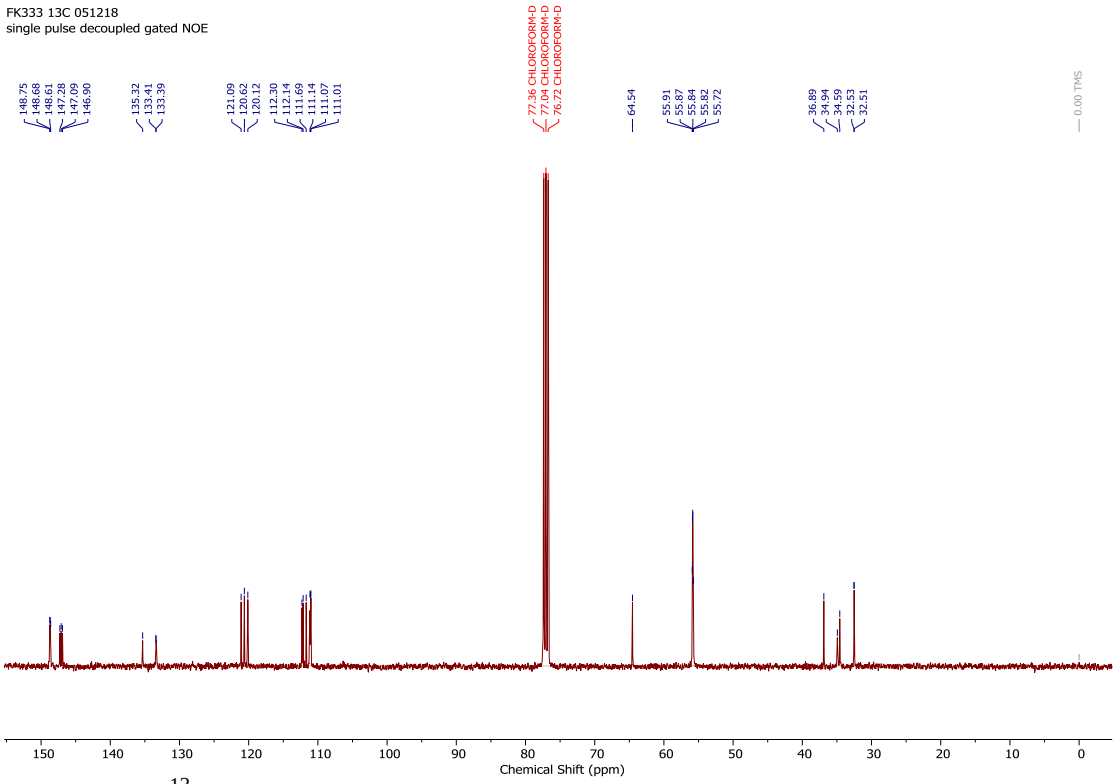
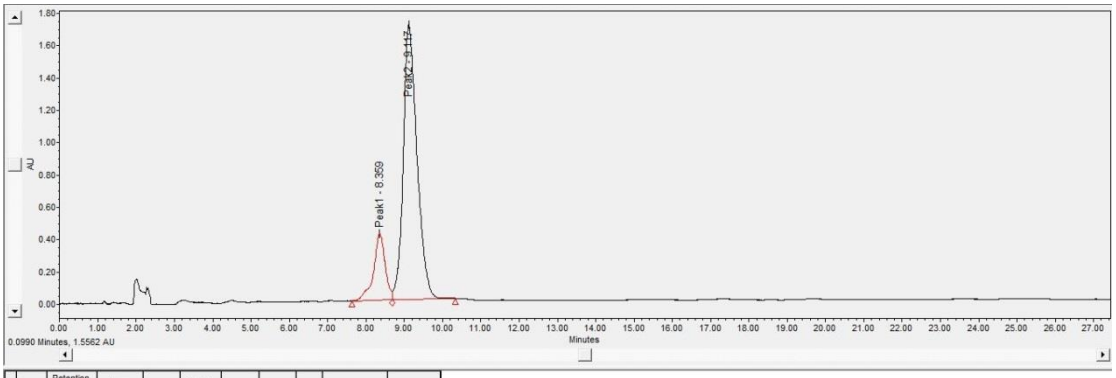
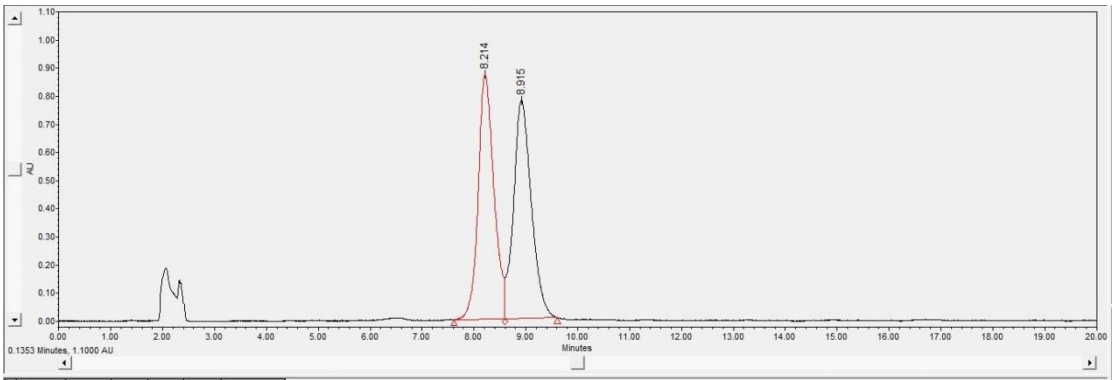


Figure S12. ^{13}C NMR spectrum of synthetic schwarzinicine B (**143**) ($CDCl_3$, 100 MHz)



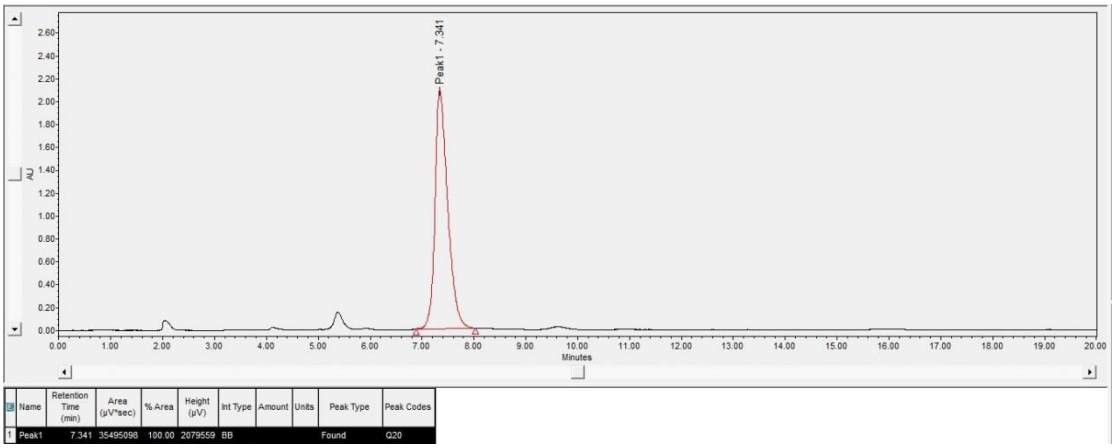
	Name	Retention Time (min)	Area (µV*sec)	% Area	Height (µV)	Int Type	Amount	Units	Peak Type	Peak Codes
1	Peak1	8.359	8654272	16.95	412721	BV			Found	Q20
2	Peak2	9.117	42418020	83.05	1699138	VB			Found	Q20

Figure S13. Chiral HPLC profile of natural schwarzinicine A (**142**)



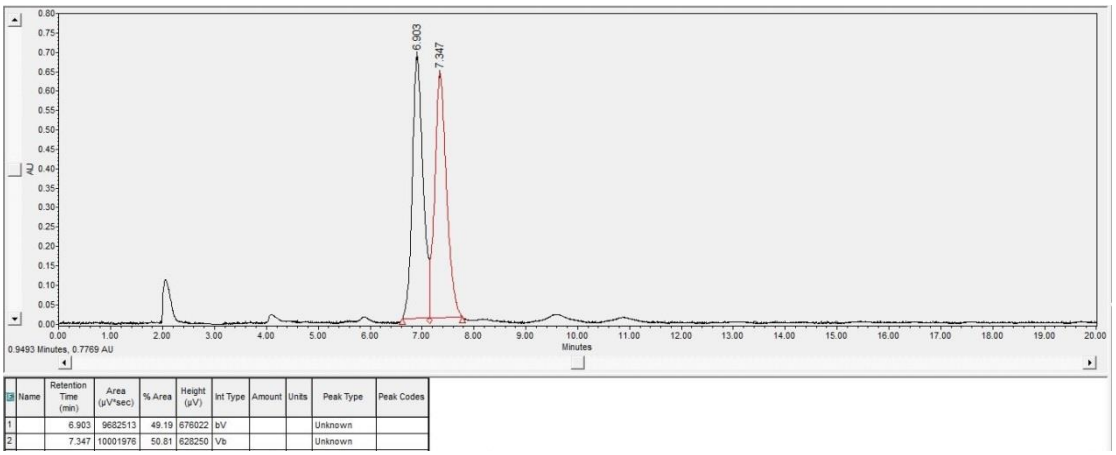
	Retention Time (min)	Area (µV*sec)	% Area	Height (µV)	Int Type	Peak Type
1	8.214	18301497	49.75	870435	BV	Unknown
2	8.915	18488556	50.25	775507	Vb	Unknown

Figure S14. Chiral HPLC profile of synthetic schwarzinicine A (**142**)



	Name	Retention Time (min)	Area (μV*sec)	% Area	Height (μV)	Int Type	Amount	Units	Peak Type	Peak Codes
1	Peak1	7.341	35495098	100.00	2079559	BB			Found	Q20

Figure S15. Chiral HPLC profile of natural schwarzinicine B (**143**)



	Name	Retention Time (min)	Area (μV*sec)	% Area	Height (μV)	Int Type	Amount	Units	Peak Type	Peak Codes
1		6.903	9682513	49.19	676022	bV			Unknown	
2		7.347	10001976	50.81	628250	Vb			Unknown	

Figure S16. Chiral HPLC profile of synthetic schwarzinicine B (**143**)

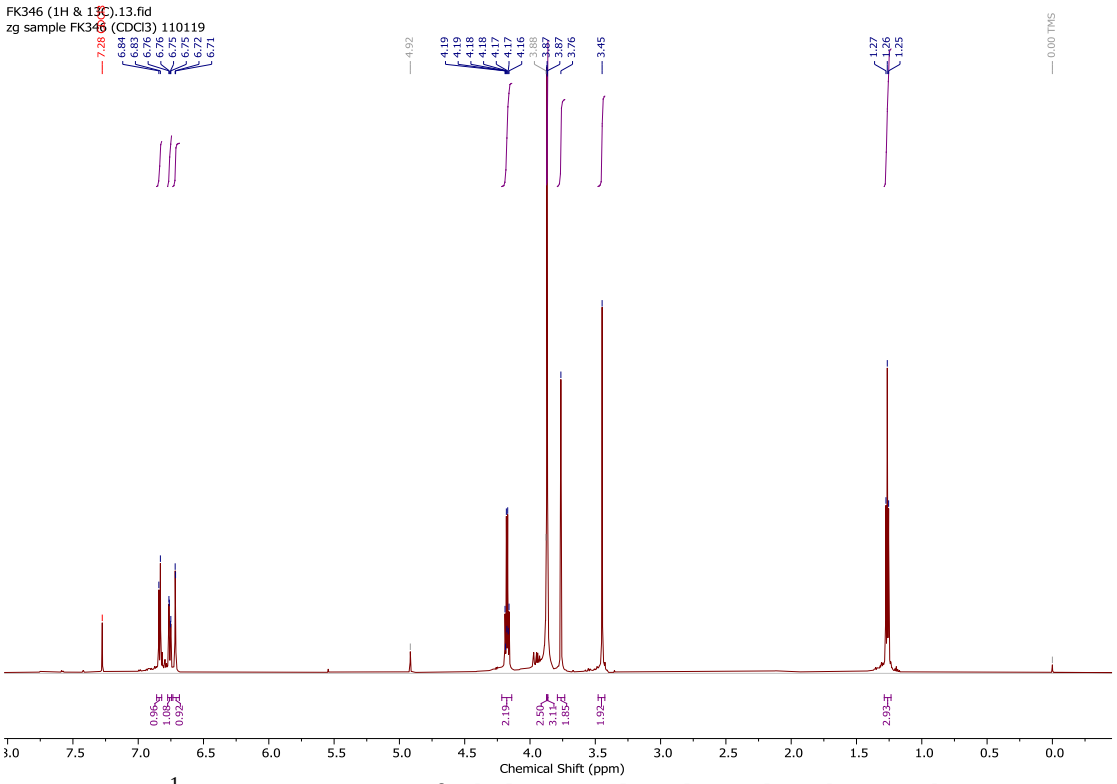


Figure S17. ^{1}H NMR spectrum of ethyl 4-(3,4-dimethoxyphenyl)-3-oxobutanoate (**197**) ($CDCl_3$, 700 MHz)

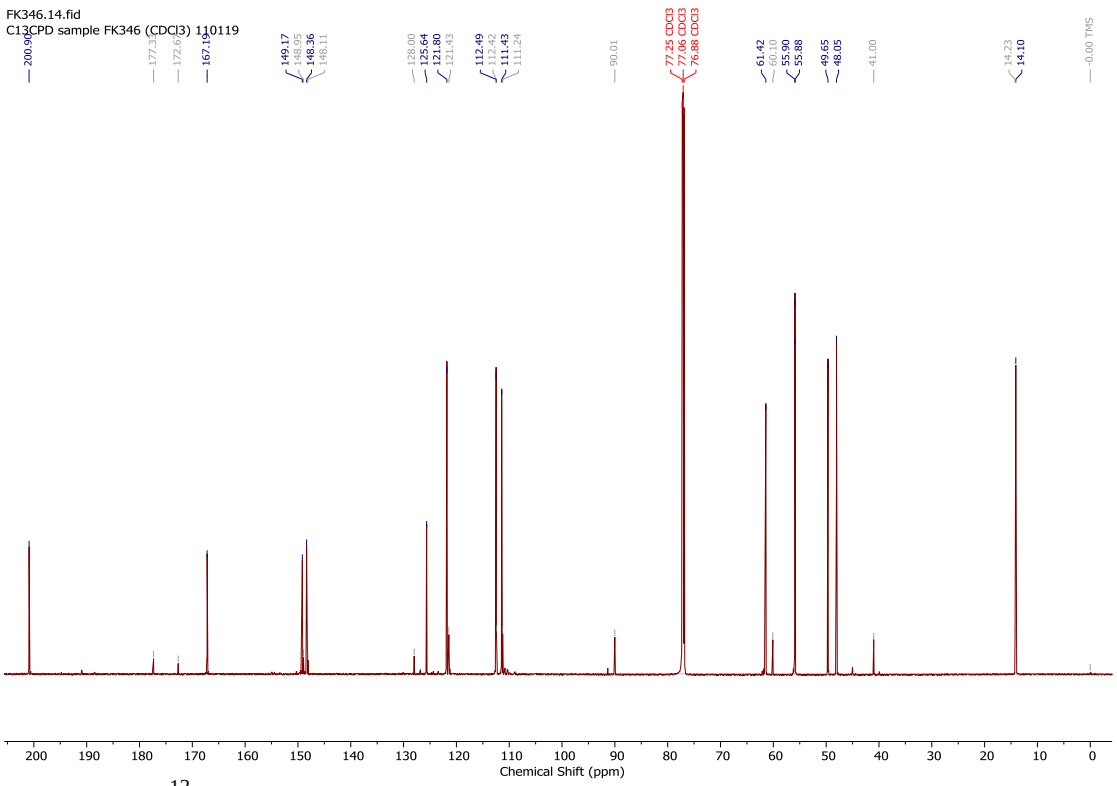


Figure S18. ^{13}C NMR spectrum of ethyl 4-(3,4-dimethoxyphenyl)-3-oxobutanoate (**197**) ($CDCl_3$, 175 MHz)

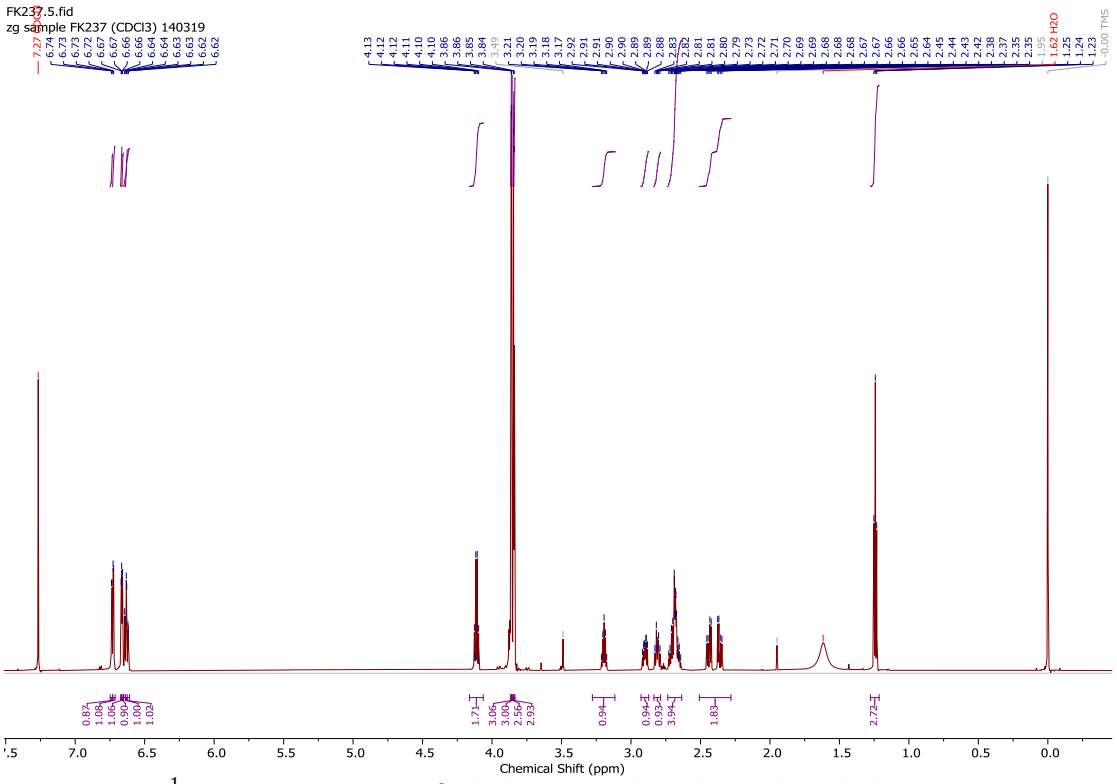


Figure S19. ^{1}H NMR spectrum of ethyl 3-((3,4-dimethoxyphenethyl)amino)-4-(3,4-dimethoxyphenyl)butanoate (**195**) ($CDCl_3$, 700 MHz)

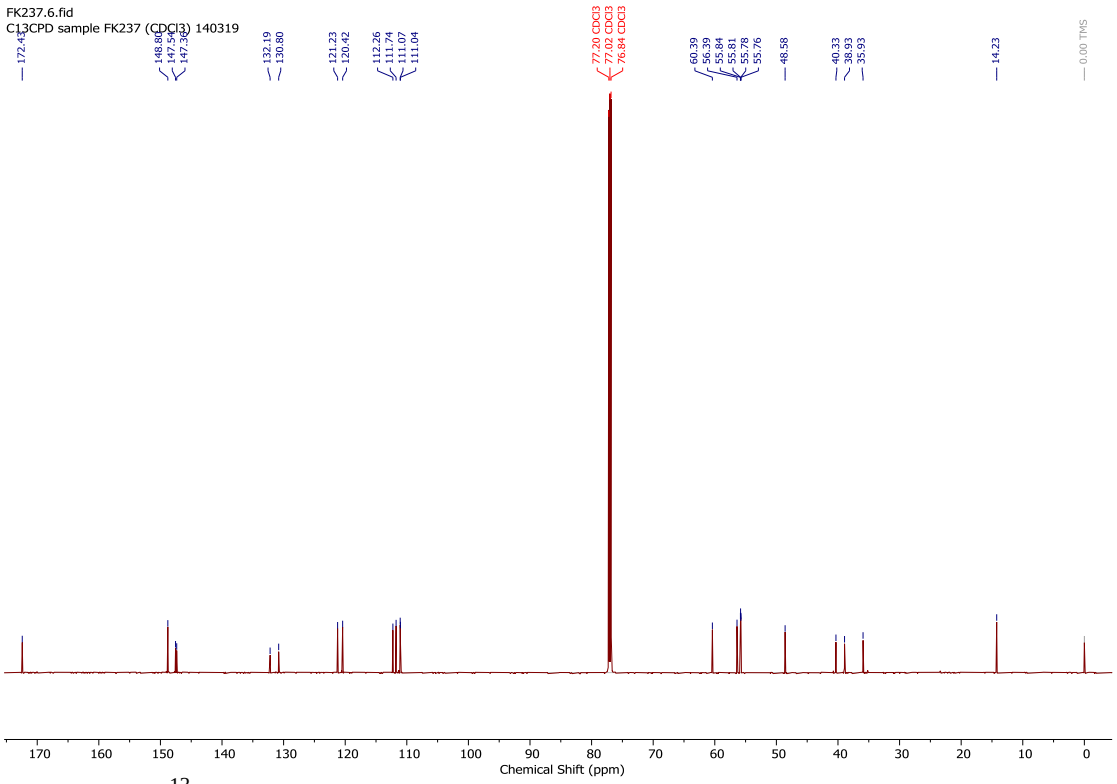


Figure S20. ^{13}C NMR spectrum of ethyl 3-((3,4-dimethoxyphenethyl)amino)-4-(3,4-dimethoxyphenyl)butanoate (**195**) ($CDCl_3$, 175 MHz)

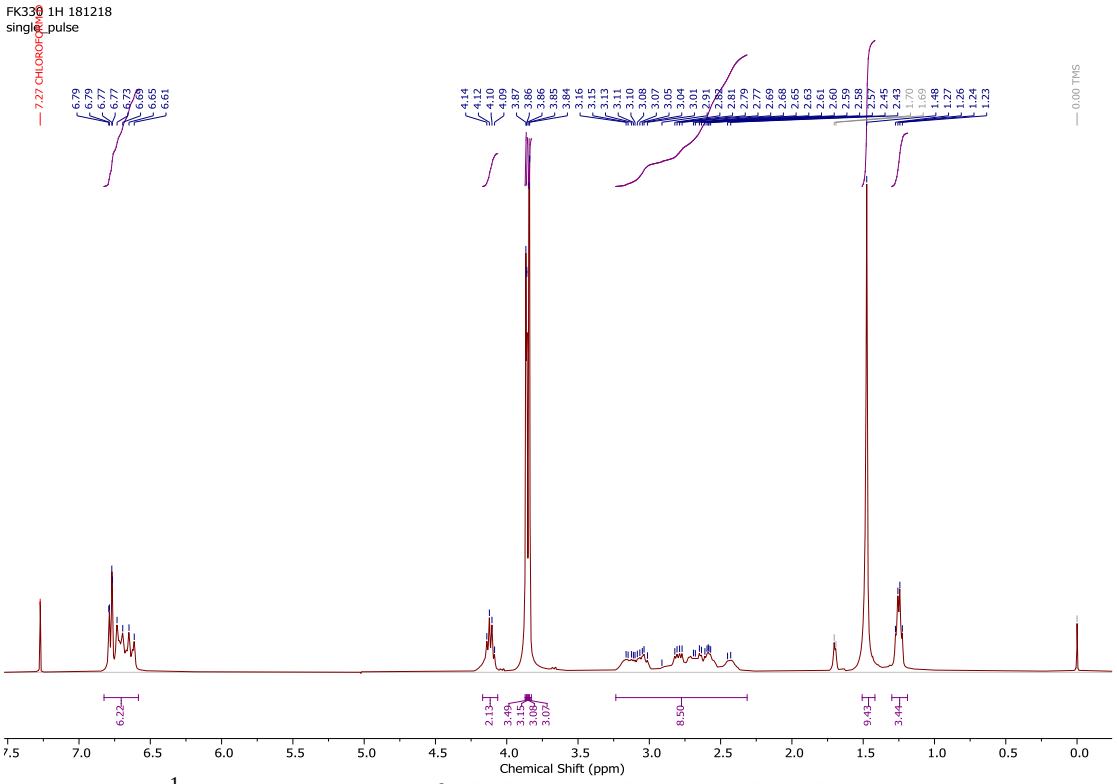


Figure S21. ^{1}H NMR spectrum of ethyl 3-((*tert*-butoxycarbonyl)(3,4-dimethoxyphenethyl)amine)-4-(3,4-dimethoxyphenyl)butanoate (**199**) ($CDCl_3$, 400 MHz)

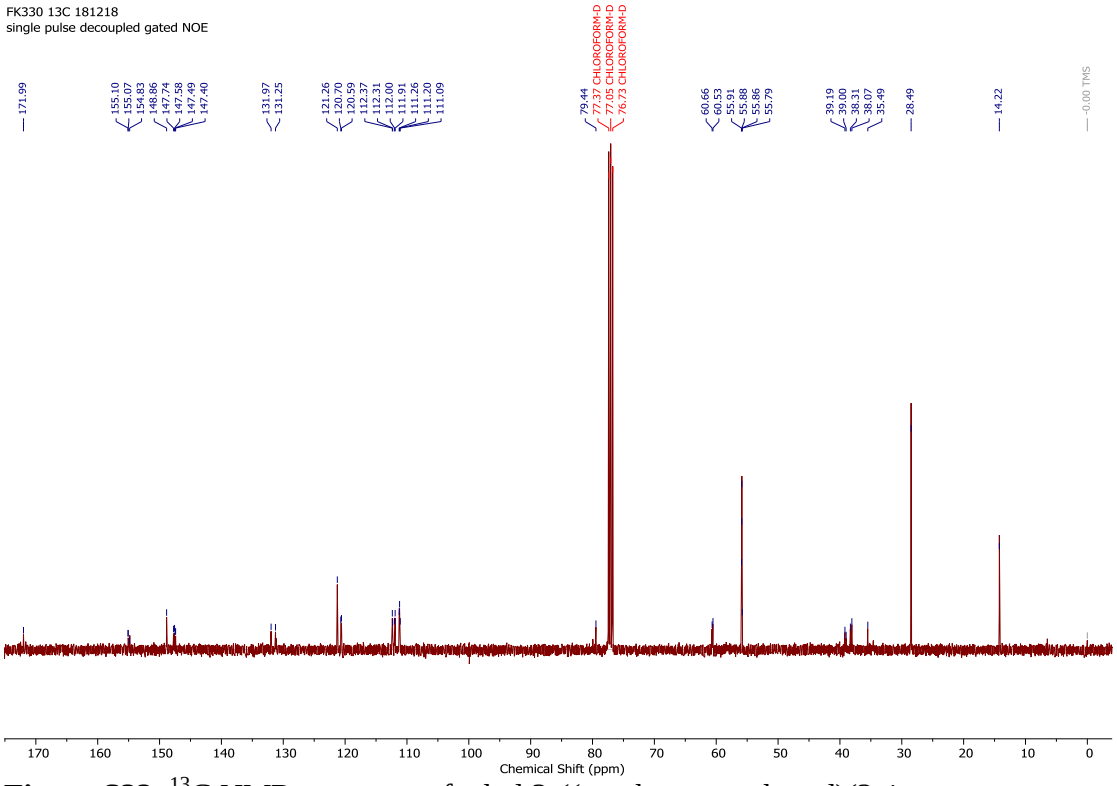


Figure S22. ^{13}C NMR spectrum of ethyl 3-((*tert*-butoxycarbonyl)(3,4-dimethoxyphenethyl)amine)-4-(3,4-dimethoxyphenyl)butanoate (**199**) ($CDCl_3$, 100 MHz)

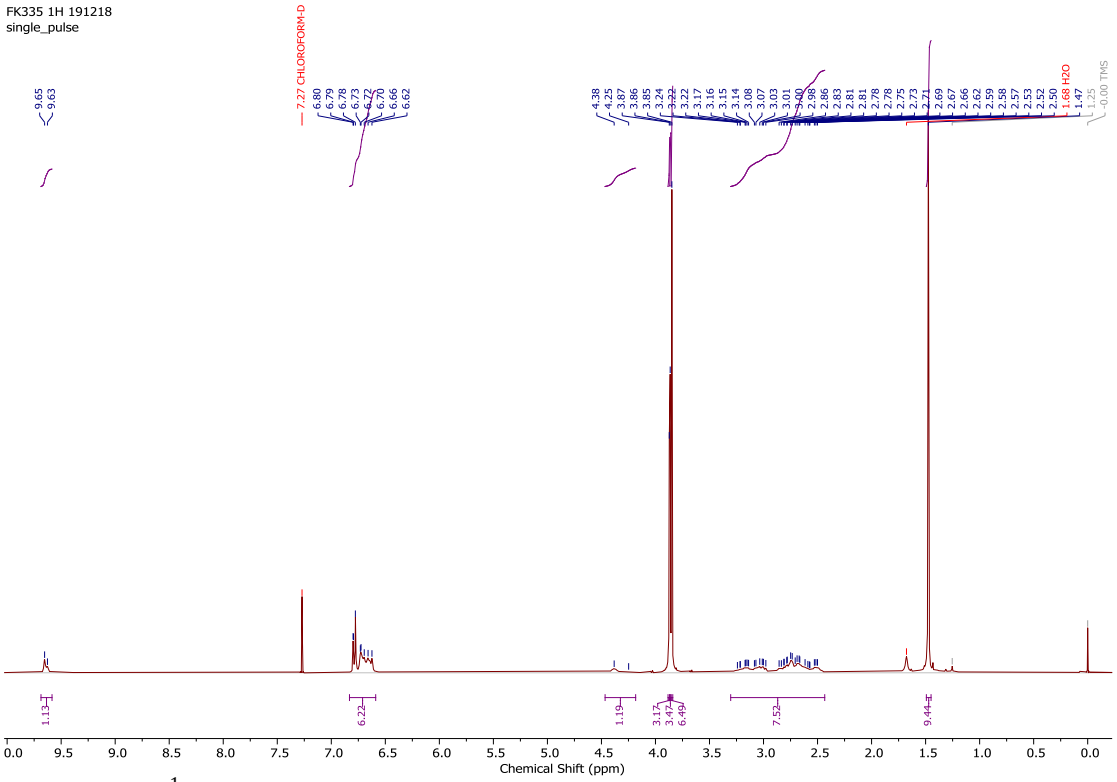


Figure S23. ^{1}H NMR spectrum of *tert*-butyl 3,4-dimethoxyphenethyl(1-(3,4-dimethoxyphen)-4-oxobutan-2-yl)carbamate (**200**) ($CDCl_3$, 400 MHz)

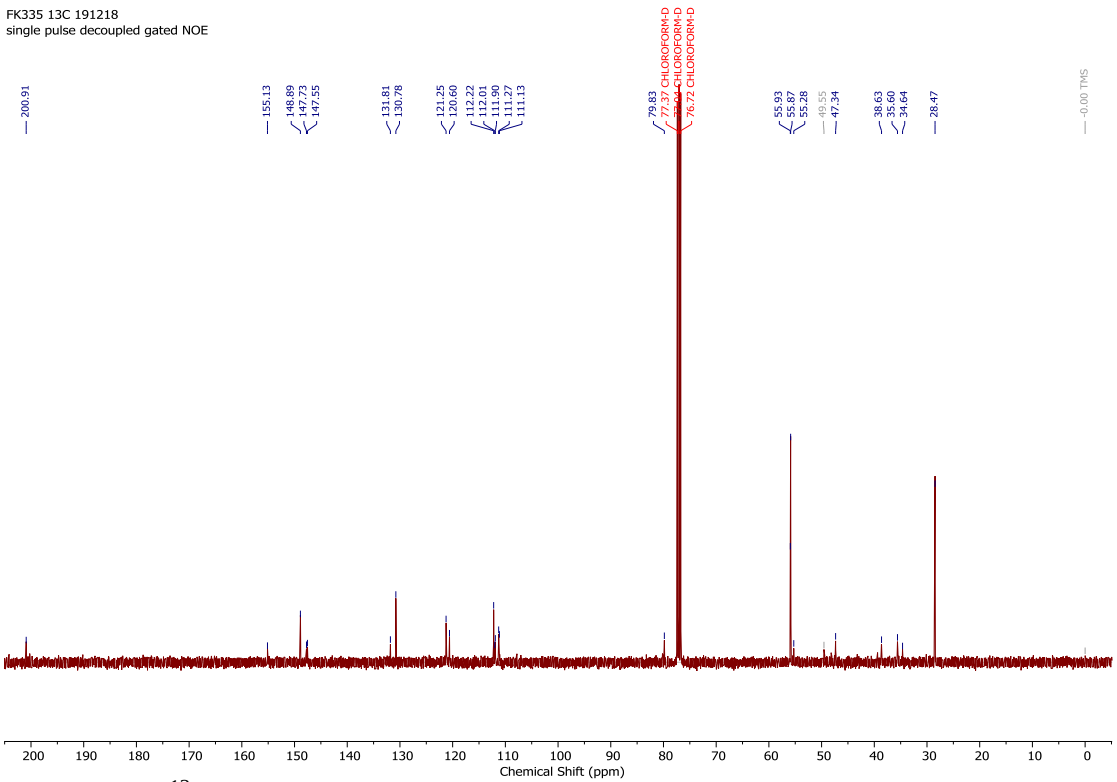


Figure S24. ^{13}C NMR spectrum of *tert*-butyl 3,4-dimethoxyphenethyl(1-(3,4-dimethoxyphen)-4-oxobutan-2-yl)carbamate (**200**) ($CDCl_3$, 100 MHz)

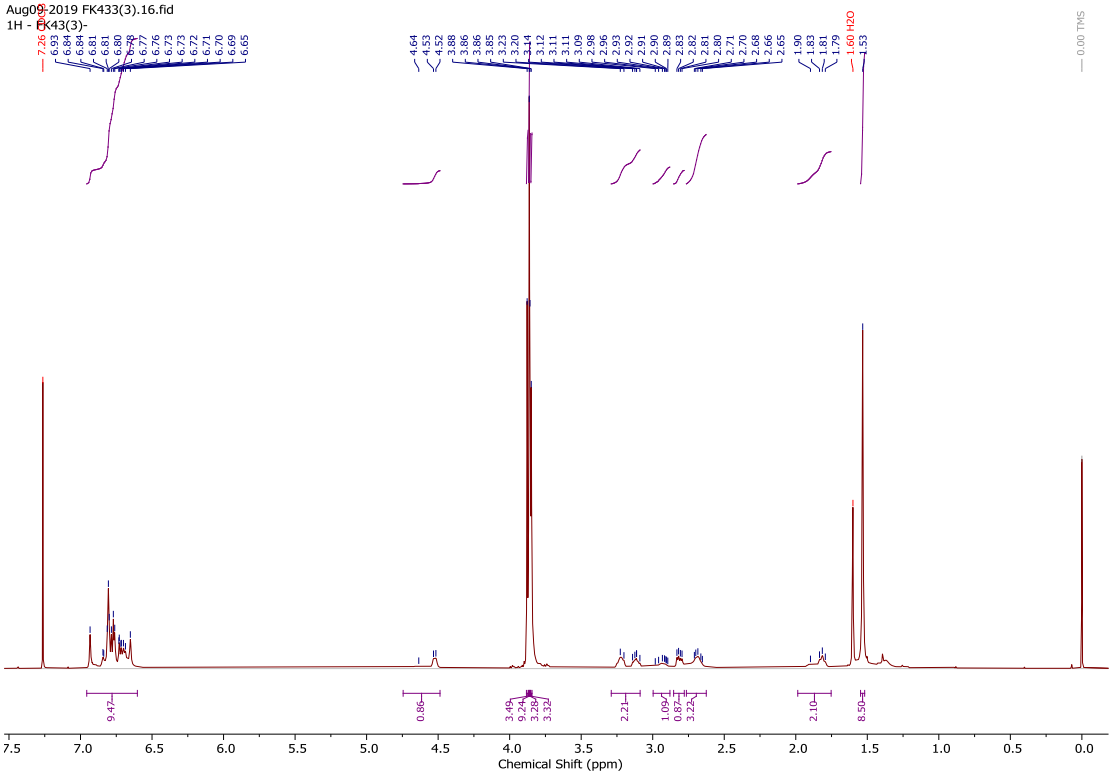


Figure S25. ^{1}H NMR spectrum of *tert*-butyl (1,4-bis(3,4-dimethoxyphenyl)-4-hydroxybutan-2-yl)(3,4-dimethoxyphenethyl)carbamate (diastereomer pair 1 of **202**) ($CDCl_3$, 600 MHz)

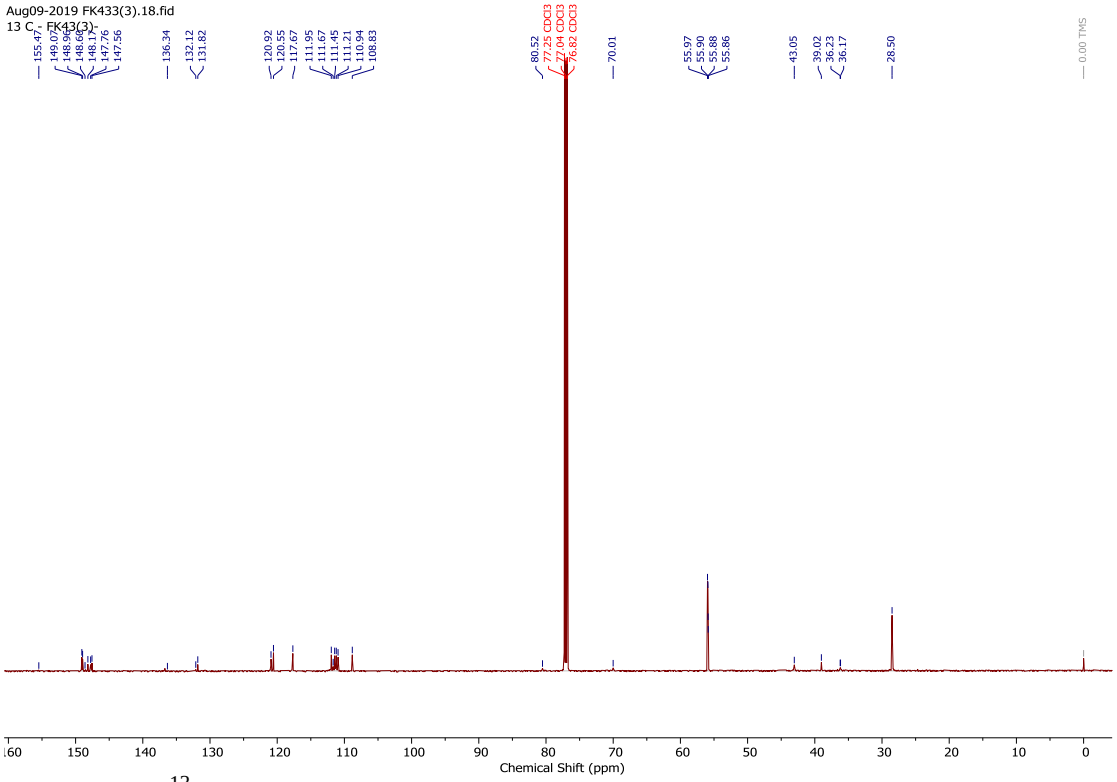


Figure S26. ^{13}C NMR spectrum of *tert*-butyl (1,4-bis(3,4-dimethoxyphenyl)-4-hydroxybutan-2-yl)(3,4-dimethoxyphenethyl)carbamate (diastereomer pair 1 of **202**) ($CDCl_3$, 150 MHz)

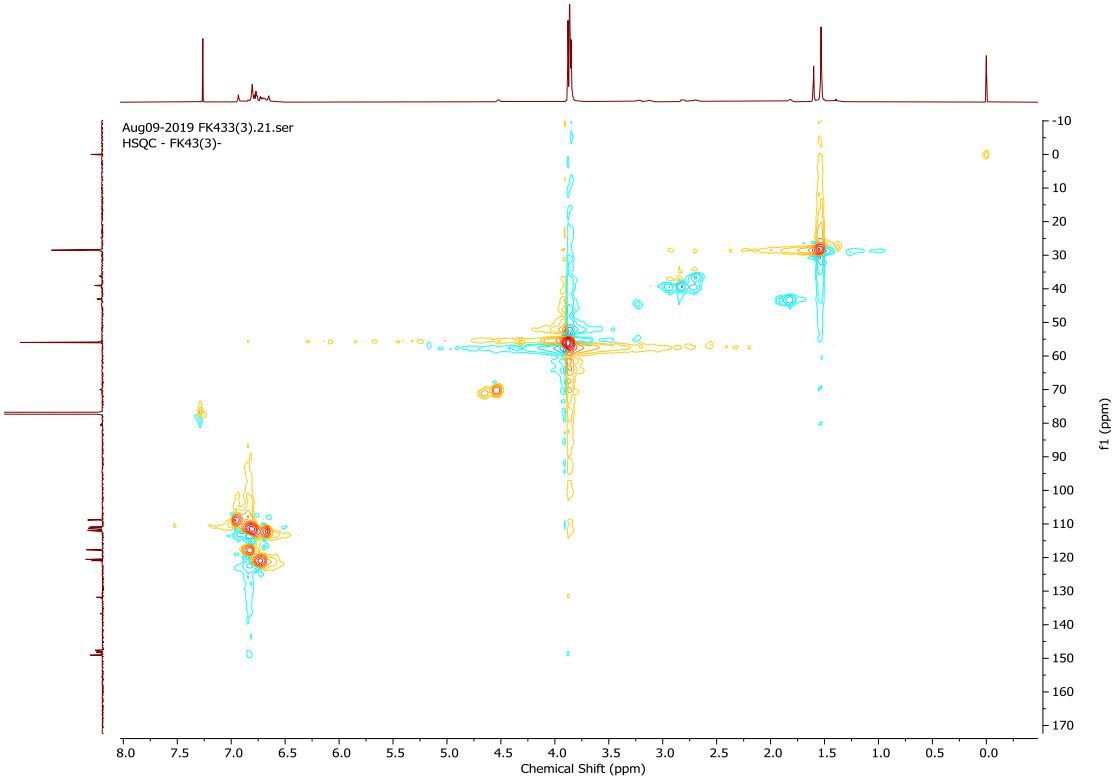


Figure S27. HSQC spectrum of *tert*-butyl (1,4-bis(3,4-dimethoxyphenyl)-4-hydroxybutan-2-yl)(3,4-dimethoxyphenethyl)carbamate (diastereomer pair 1 of **202**) ($CDCl_3$, 600 MHz)

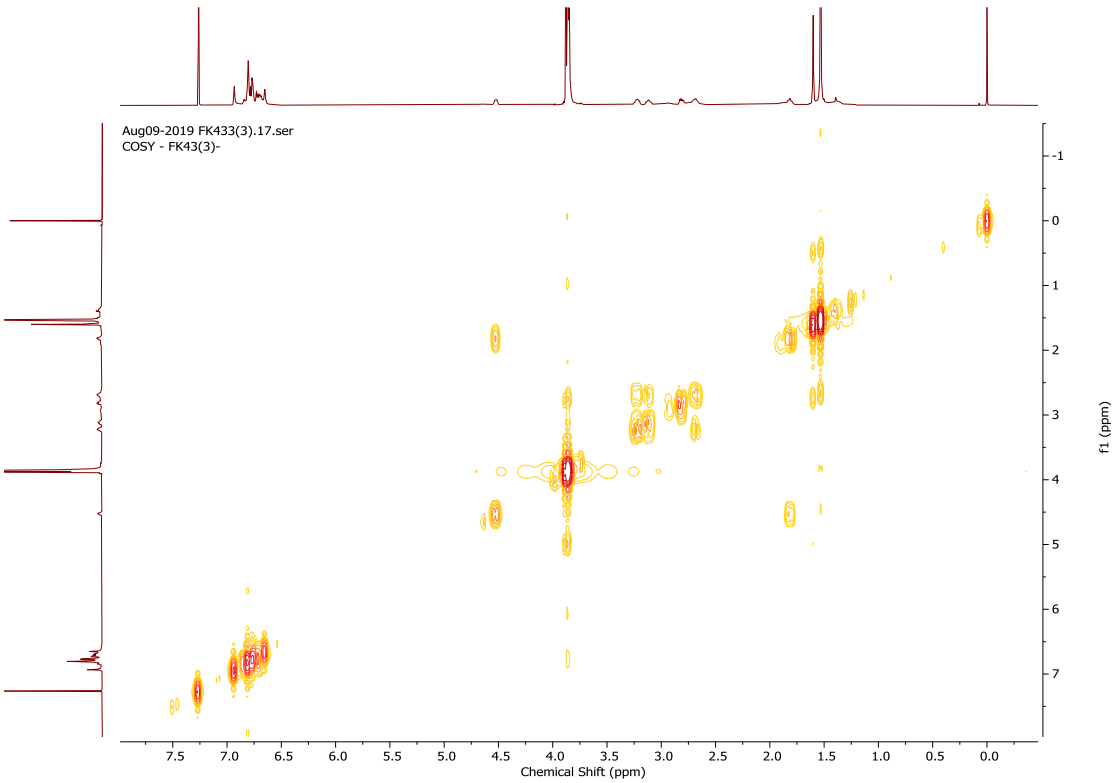


Figure S28. COSY spectrum of *tert*-butyl (1,4-bis(3,4-dimethoxyphenyl)-4-hydroxybutan-2-yl)(3,4-dimethoxyphenethyl)carbamate (diastereomer pair 1 of **202**) ($CDCl_3$, 600 MHz)

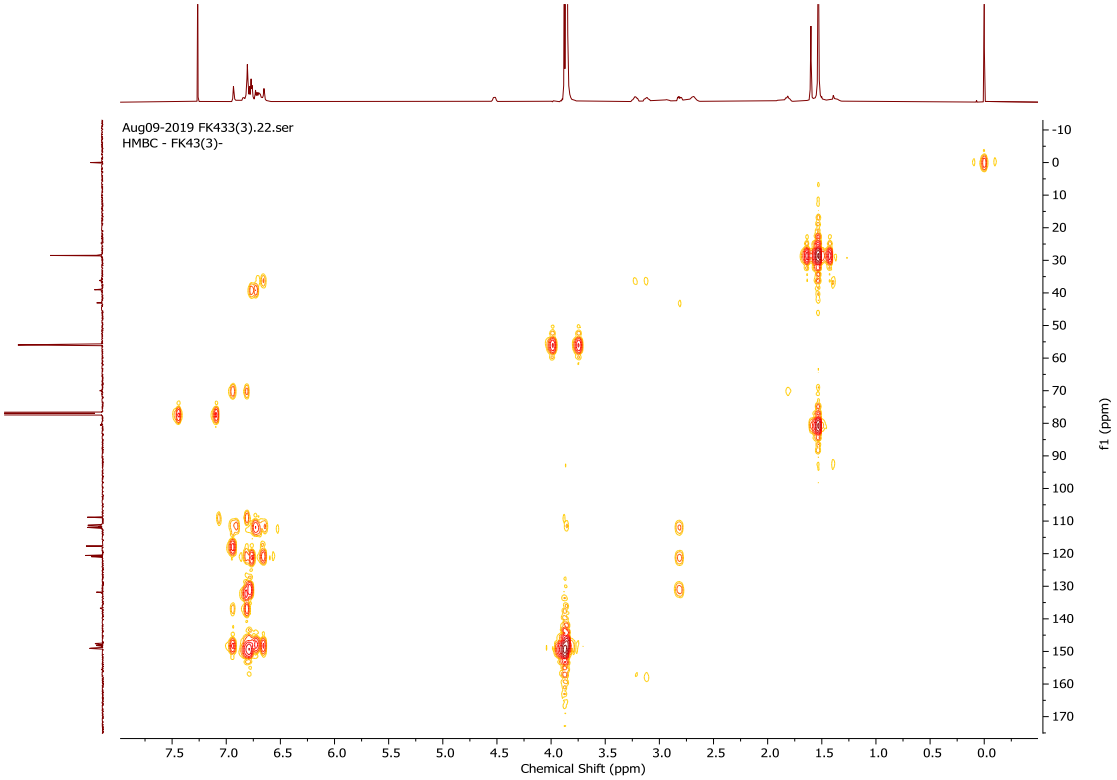


Figure S29. HMBC spectrum of *tert*-butyl (1,4-bis(3,4-dimethoxyphenyl)-4-hydroxybutan-2-yl)(3,4-dimethoxyphenethyl)carbamate (diastereomer pair 1 of **202**) ($CDCl_3$, 600 MHz)

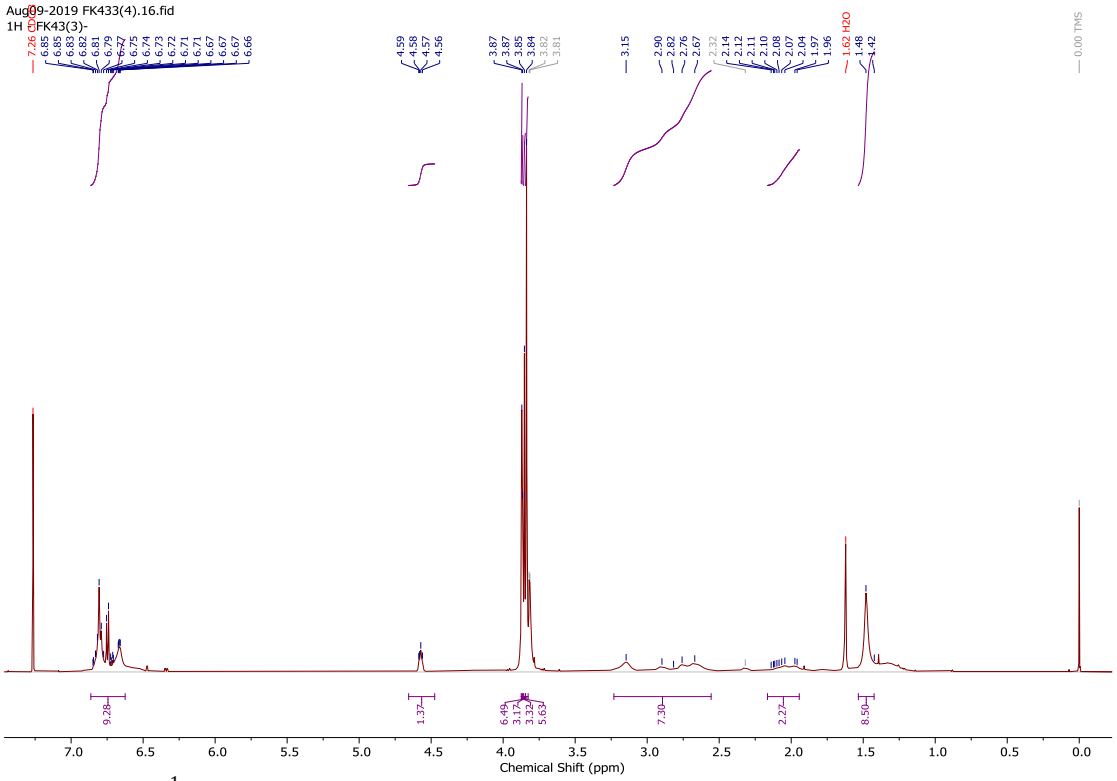


Figure S30. ^{1}H NMR spectrum of *tert*-butyl (1,4-bis(3,4-dimethoxyphenyl)-4-hydroxybutan-2-yl)(3,4-dimethoxyphenethyl)carbamate (diastereomer pair 2 of **202**) ($CDCl_3$, 600 MHz)

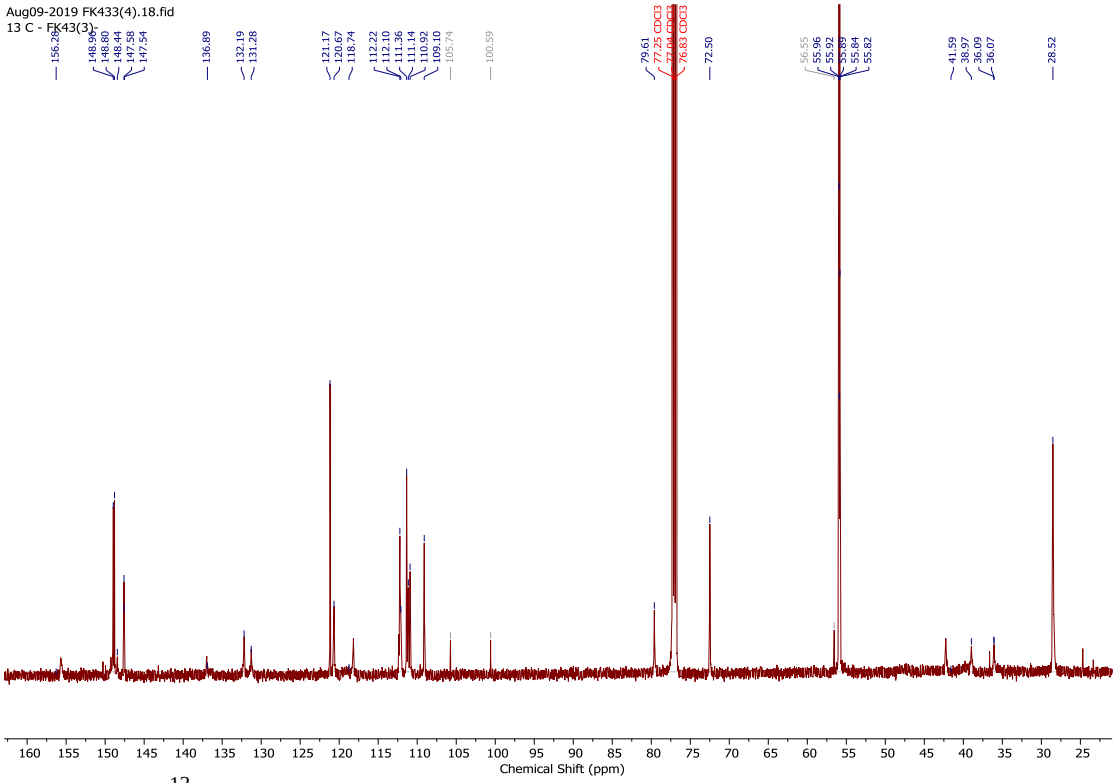


Figure S31. ^{13}C NMR spectrum of *tert*-butyl (1,4-bis(3,4-dimethoxyphenyl)-4-hydroxybutan-2-yl)(3,4-dimethoxyphenethyl)carbamate (diastereomer pair 2 of **202**) ($CDCl_3$, 150 MHz)

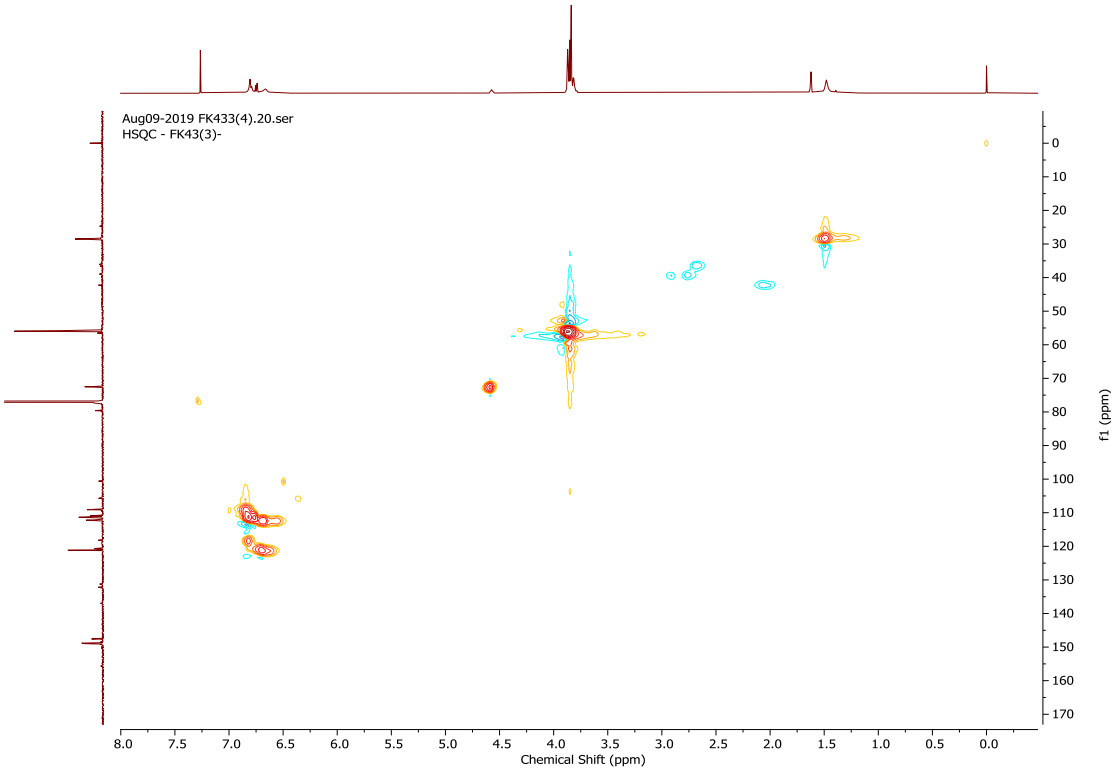


Figure S32. HSQC spectrum of *tert*-butyl (1,4-bis(3,4-dimethoxyphenyl)-4-hydroxybutan-2-yl)(3,4-dimethoxyphenethyl)carbamate (diastereomer pair 2 of **202**) ($CDCl_3$, 600 MHz)

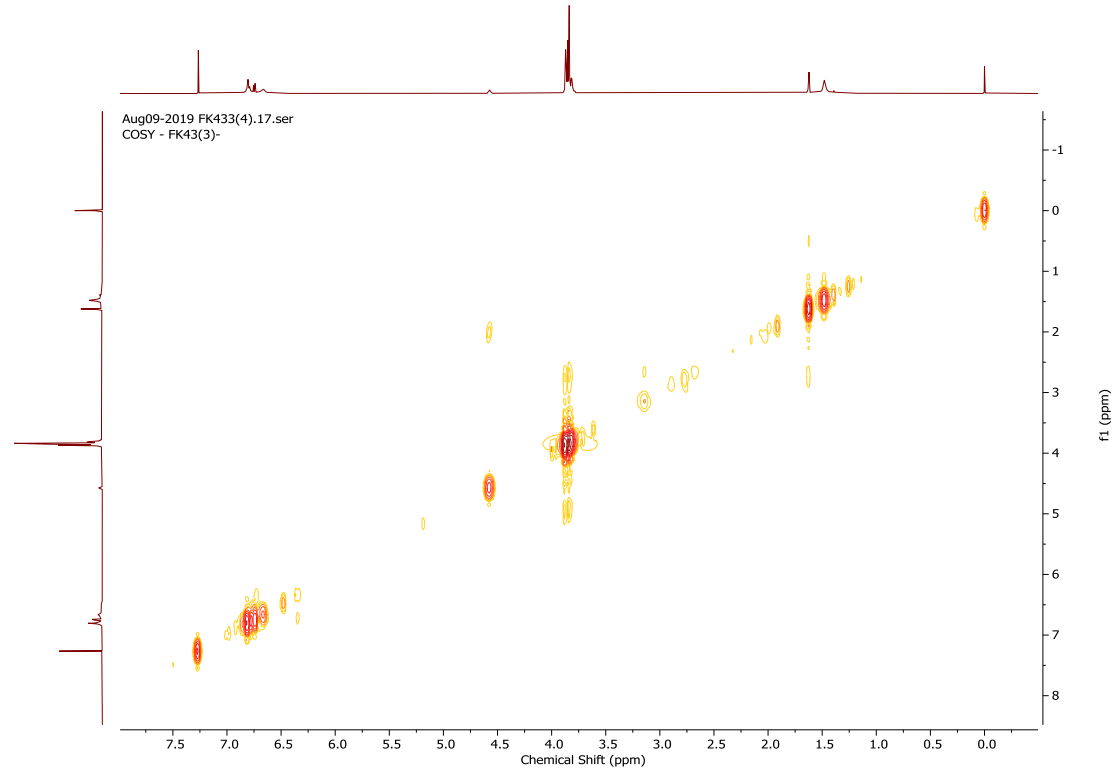


Figure S33. COSY spectrum of *tert*-butyl (1,4-bis(3,4-dimethoxyphenyl)-4-hydroxybutan-2-yl)(3,4-dimethoxyphenethyl)carbamate (diastereomer pair 2 of **202**) ($CDCl_3$, 600 MHz)

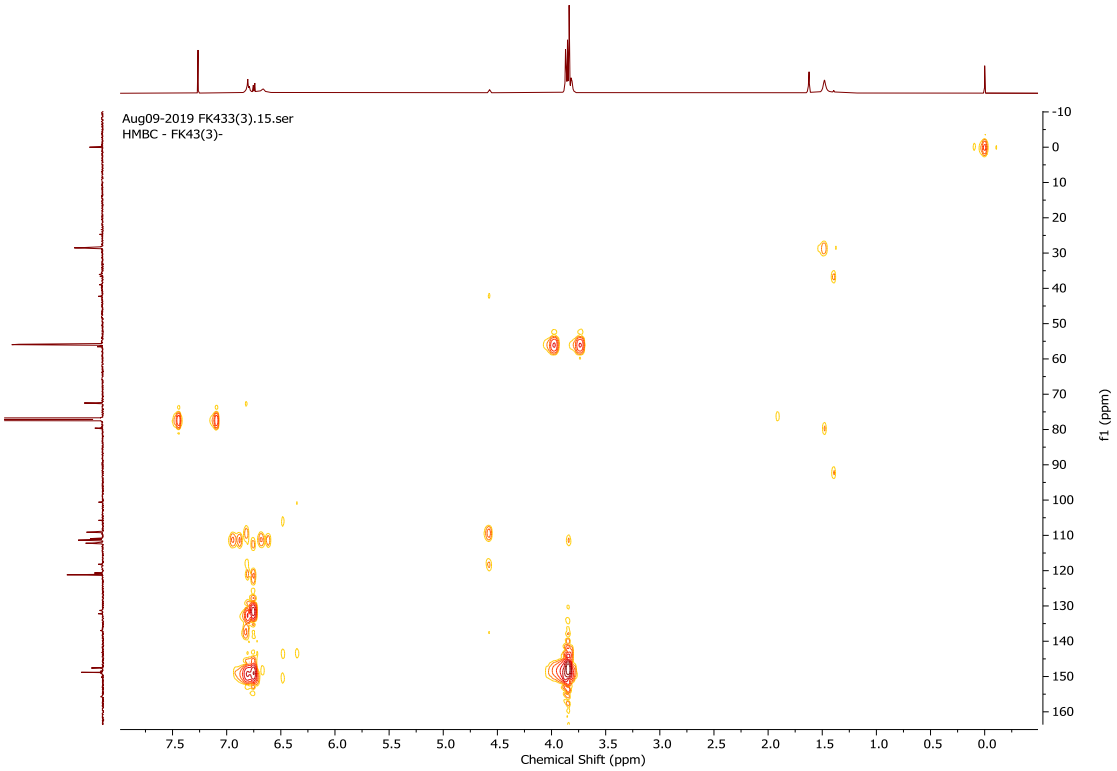


Figure S34. HMBC spectrum of *tert*-butyl (1,4-bis(3,4-dimethoxyphenyl)-4-hydroxybutan-2-yl)(3,4-dimethoxyphenethyl)carbamate (diastereomer pair 2 of **202**) ($CDCl_3$, 600 MHz)

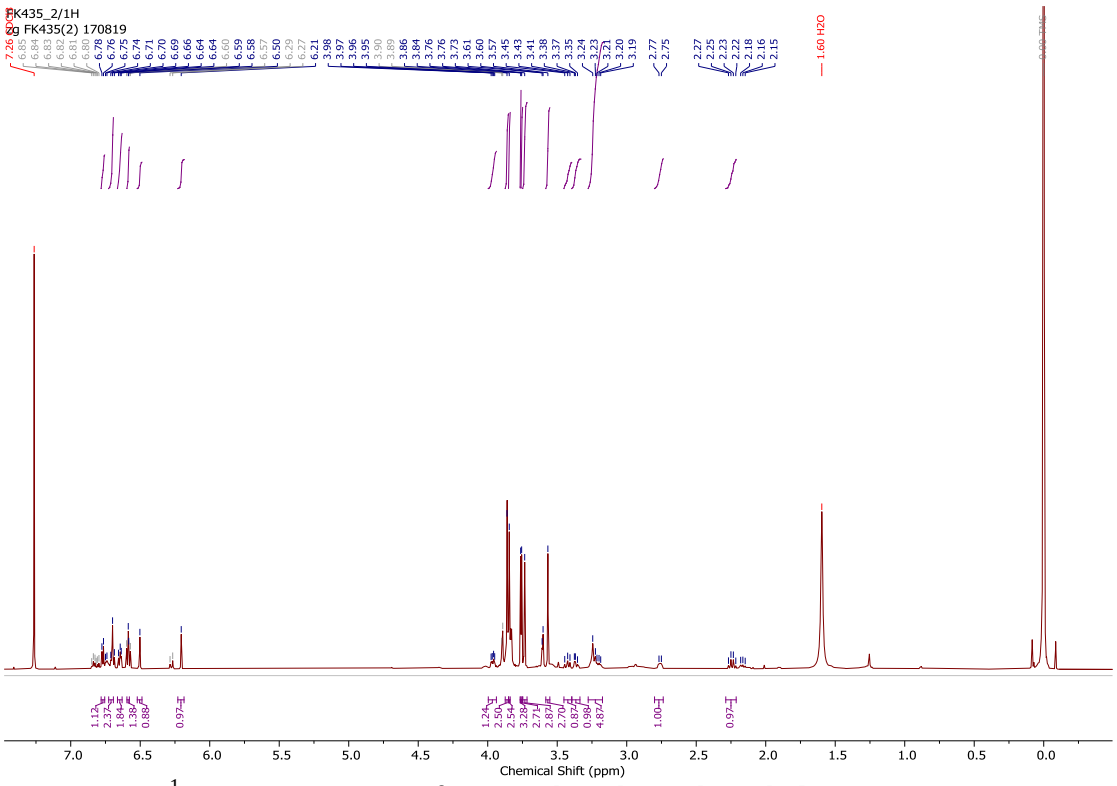


Figure S35. ^{1}H NMR spectrum of *N*-(3,4-dimethoxyphenethyl)-4-(3,4-dimethoxyphenyl)-6,7-dimethoxy-1,2,3,4-tetrahydronaphthalen-2-amine (diastereomer pair 1 of **203**) ($CDCl_3$, 700 MHz)

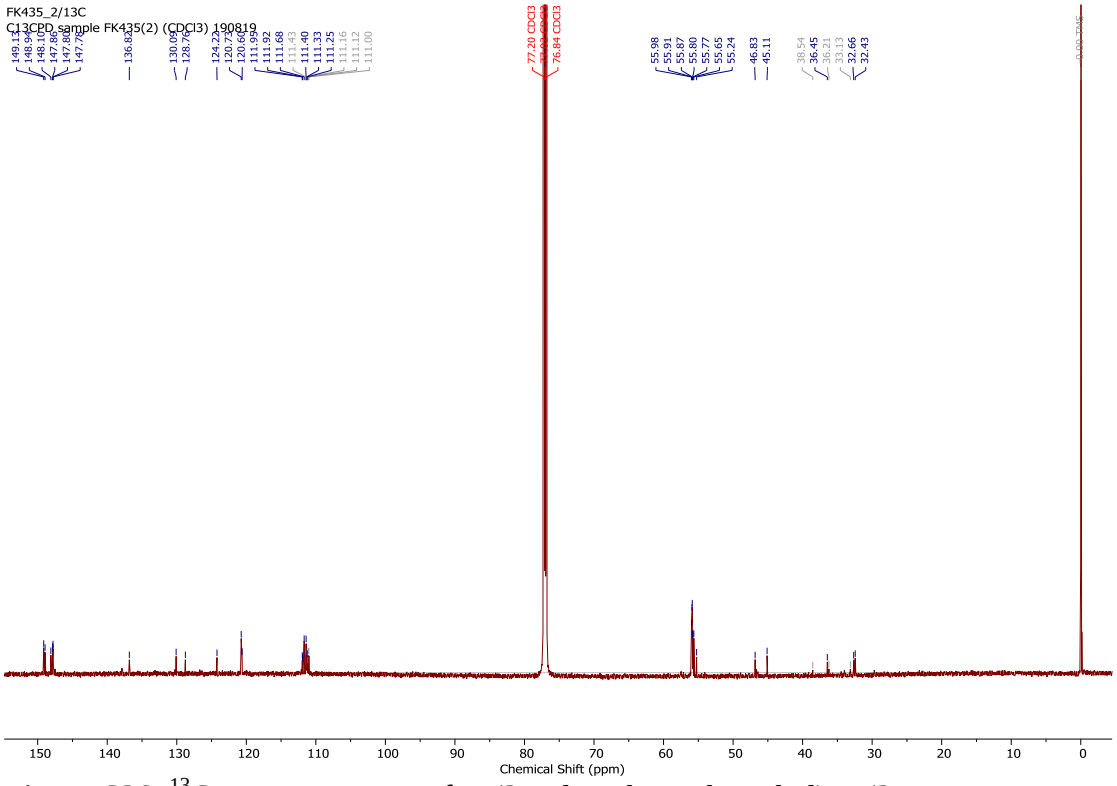


Figure S36. ^{13}C NMR spectrum of *N*-(3,4-dimethoxyphenethyl)-4-(3,4-dimethoxyphenyl)-6,7-dimethoxy-1,2,3,4-tetrahydronaphthalen-2-amine (diastereomer pair 1 of **203**) ($CDCl_3$, 175 MHz)

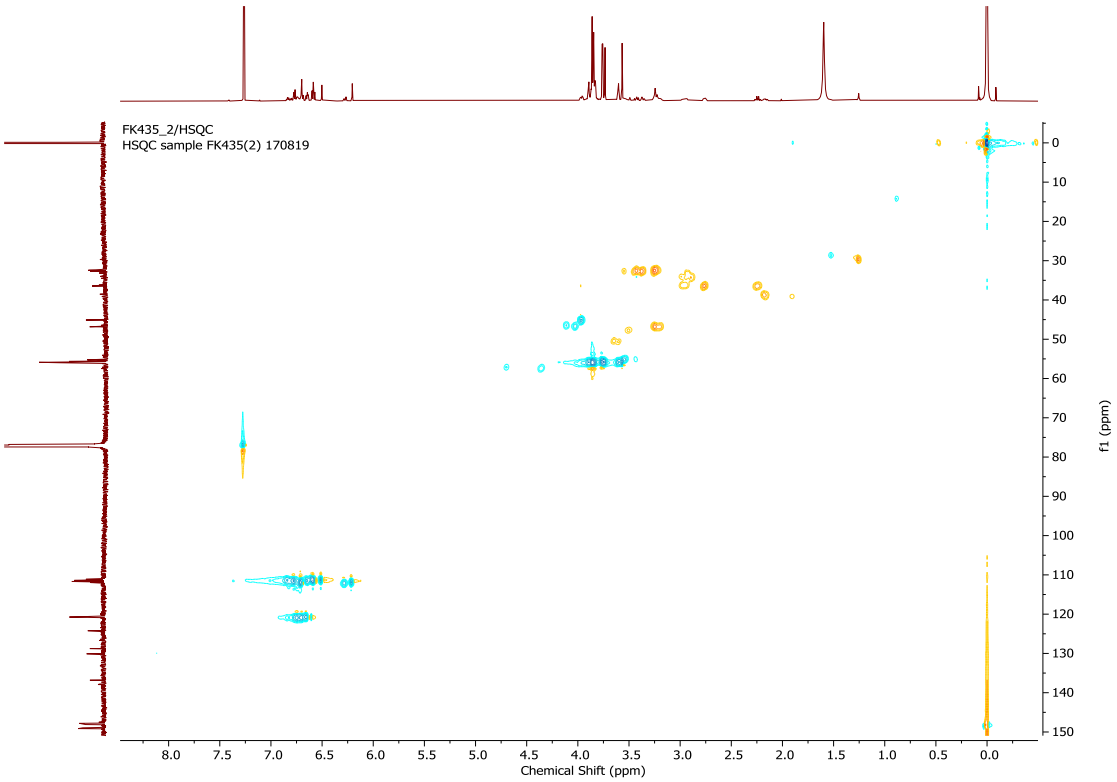


Figure S37. HSQC spectrum of *N*-(3,4-dimethoxyphenethyl)-4-(3,4-dimethoxyphenyl)-6,7-dimethoxy-1,2,3,4-tetrahydronaphthalen-2-amine (diastereomer pair 1 of **203**) ($CDCl_3$, 700 MHz)

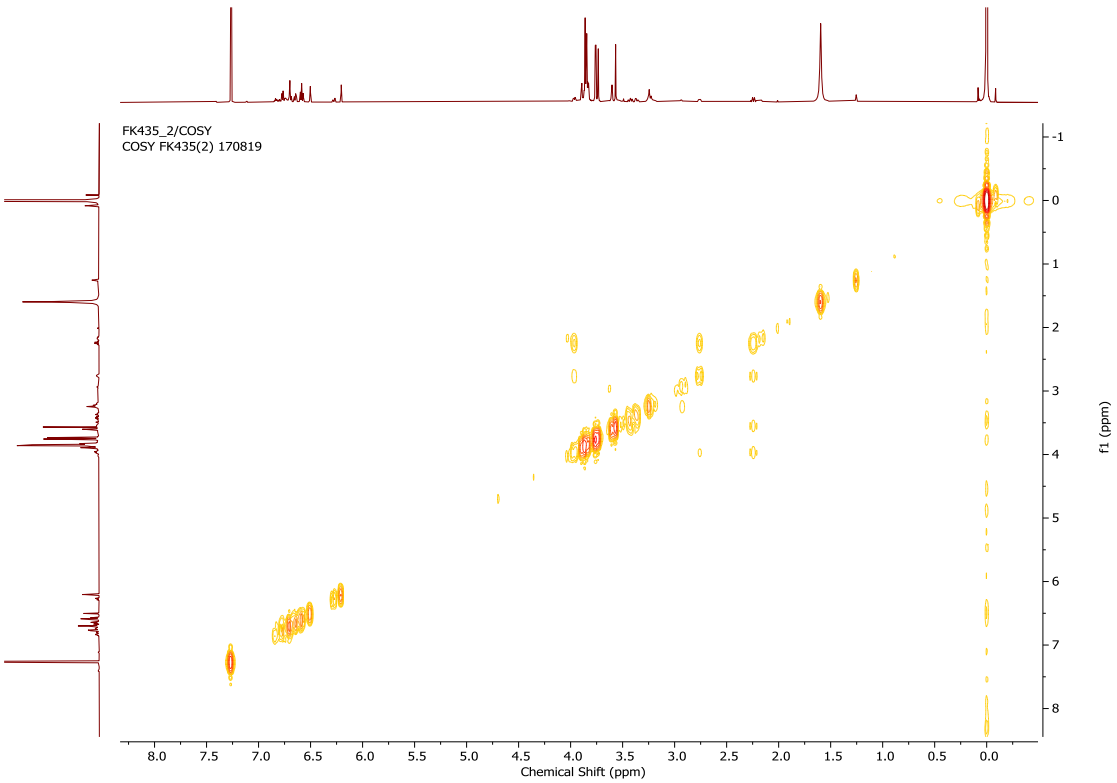


Figure S38. COSY spectrum of *N*-(3,4-dimethoxyphenethyl)-4-(3,4-dimethoxyphenyl)-6,7-dimethoxy-1,2,3,4-tetrahydronaphthalen-2-amine (diastereomer pair 1 of **203**) ($CDCl_3$, 700 MHz)

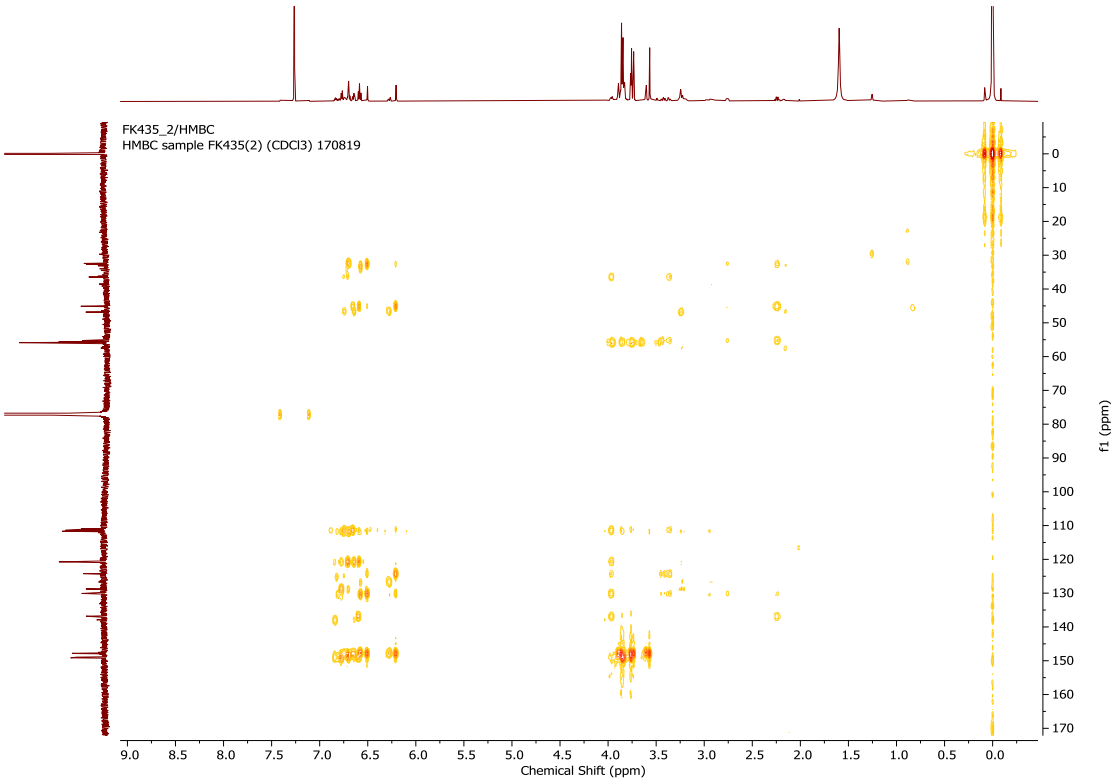


Figure S39. HMBC spectrum of *N*-(3,4-dimethoxyphenethyl)-4-(3,4-dimethoxyphenyl)-6,7-dimethoxy-1,2,3,4-tetrahydronaphthalen-2-amine (diastereomer pair 1 of **203**) ($CDCl_3$, 700 MHz)

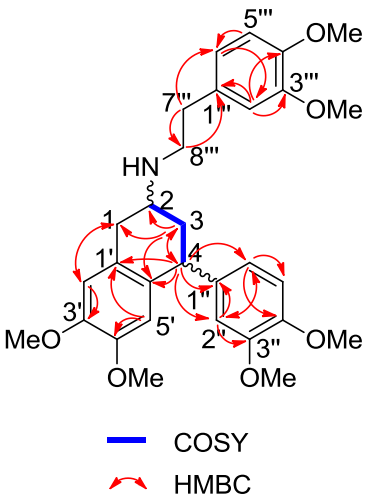


Figure S40. COSY and HMBC correlations of *N*-(3,4-dimethoxyphenethyl)-4-(3,4-dimethoxyphenyl)-6,7-dimethoxy-1,2,3,4-tetrahydronaphthalen-2-amine (diastereomer pair 1 of **203**)

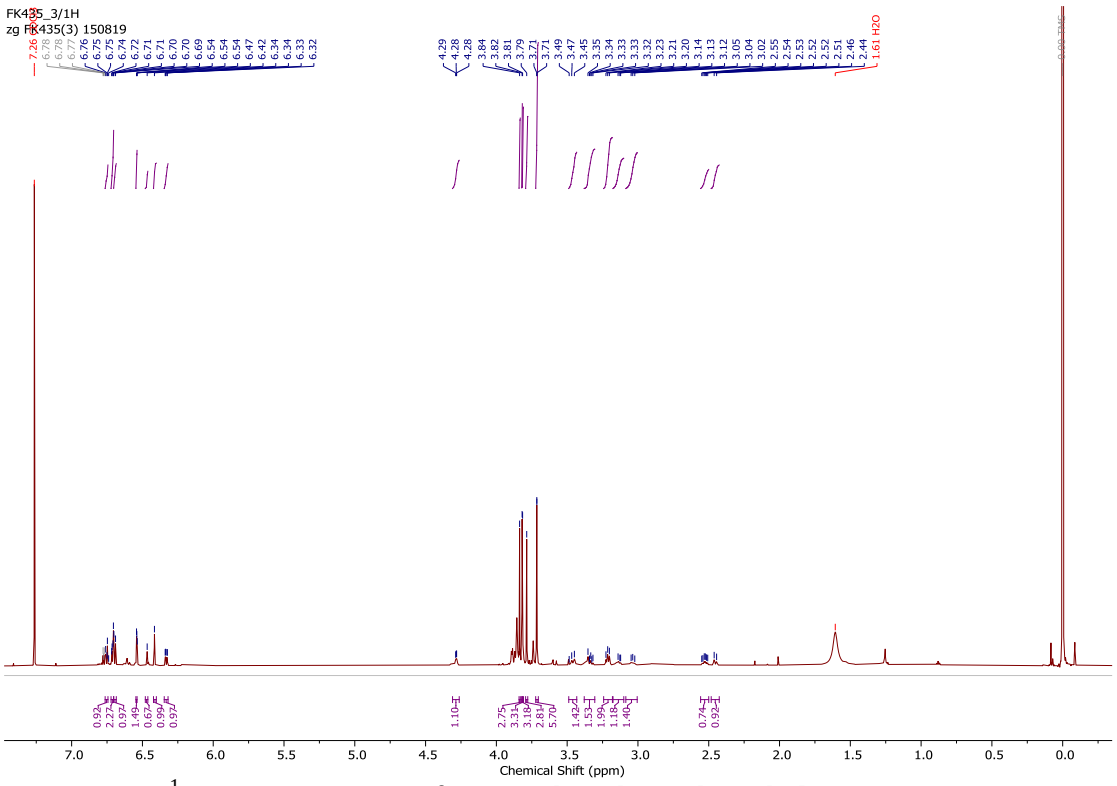


Figure S41. ^{1}H NMR spectrum of *N*-(3,4-dimethoxyphenethyl)-4-(3,4-dimethoxyphenyl)-6,7-dimethoxy-1,2,3,4-tetrahydronaphthalen-2-amine (diastereomer pair 2 of **203**) ($CDCl_3$, 700 MHz)

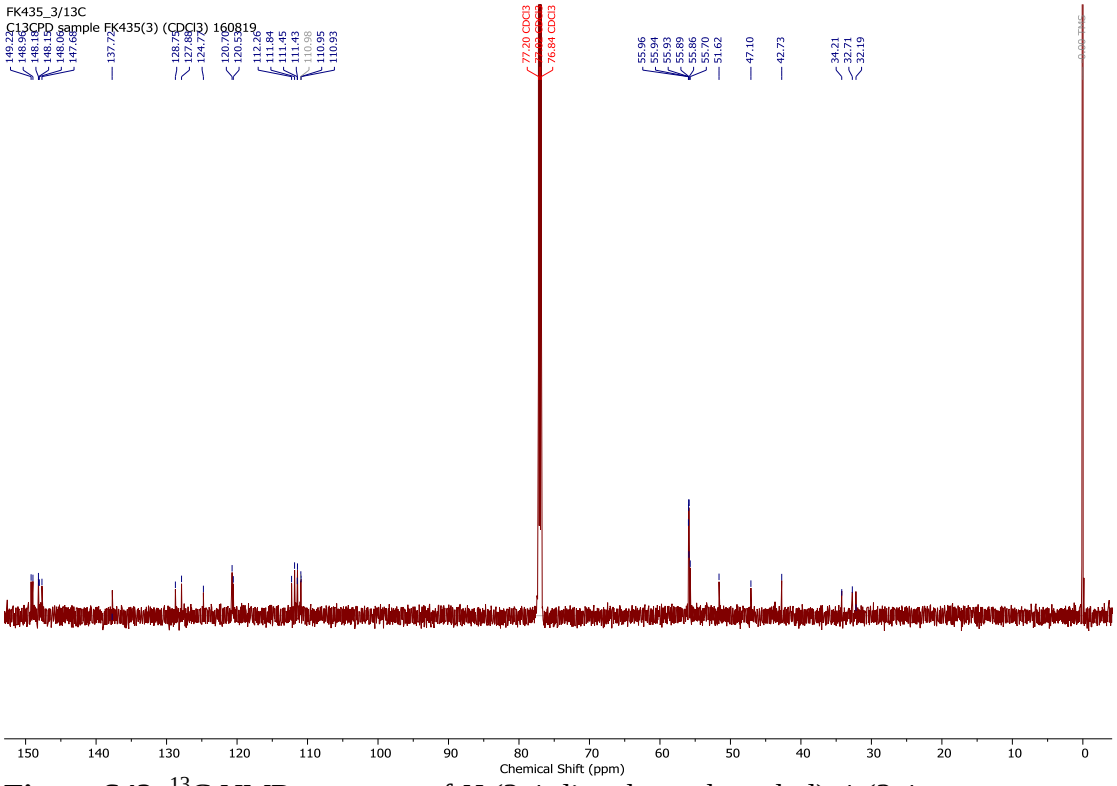


Figure S42. ^{13}C NMR spectrum of *N*-(3,4-dimethoxyphenethyl)-4-(3,4-dimethoxyphenyl)-6,7-dimethoxy-1,2,3,4-tetrahydronaphthalen-2-amine (diastereomer pair 2 of **203**) ($CDCl_3$, 175 MHz)

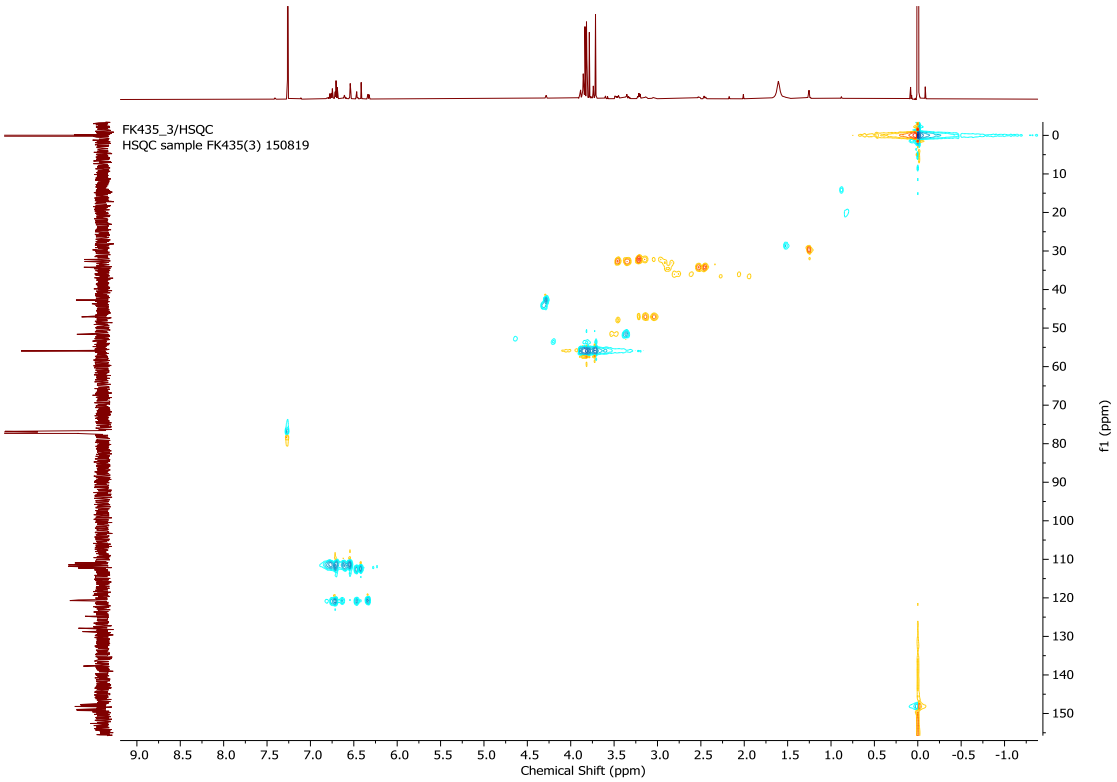


Figure S43. HSQC spectrum of *N*-(3,4-dimethoxyphenethyl)-4-(3,4-dimethoxyphenyl)-6,7-dimethoxy-1,2,3,4-tetrahydronaphthalen-2-amine (diastereomer pair 2 of **203**) ($CDCl_3$, 700 MHz)

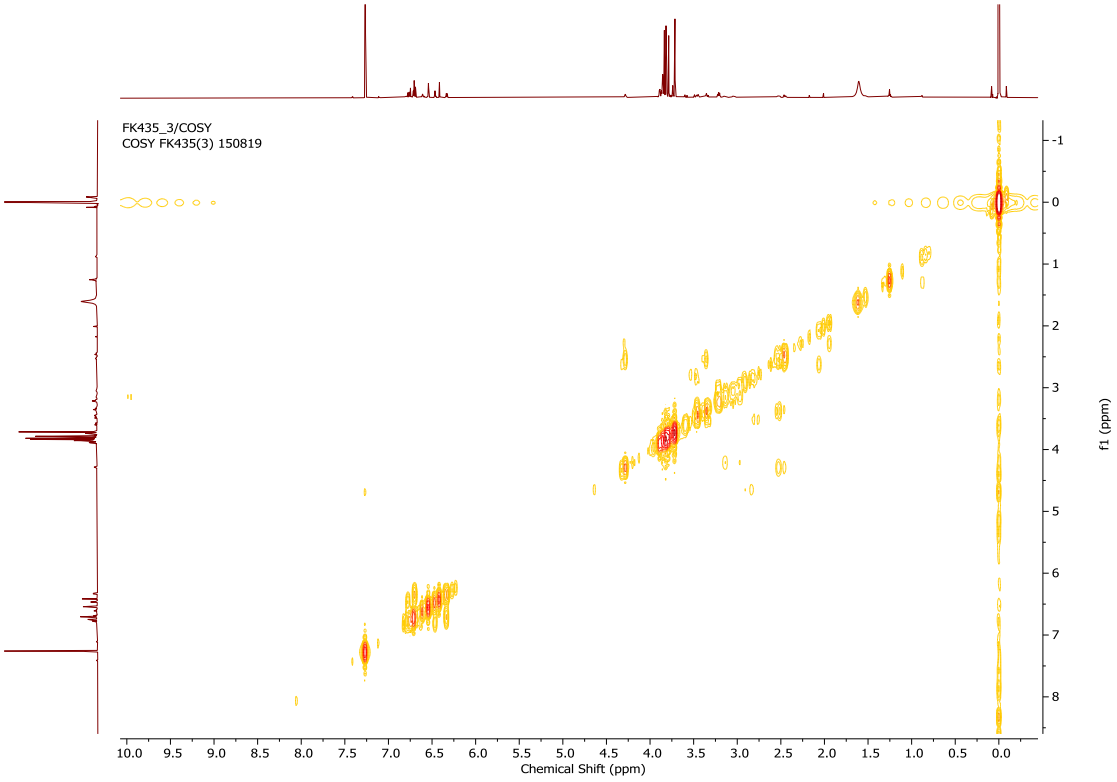


Figure S44. COSY spectrum of *N*-(3,4-dimethoxyphenethyl)-4-(3,4-dimethoxyphenyl)-6,7-dimethoxy-1,2,3,4-tetrahydronaphthalen-2-amine (diastereomer pair 2 of **203**) ($CDCl_3$, 700 MHz)

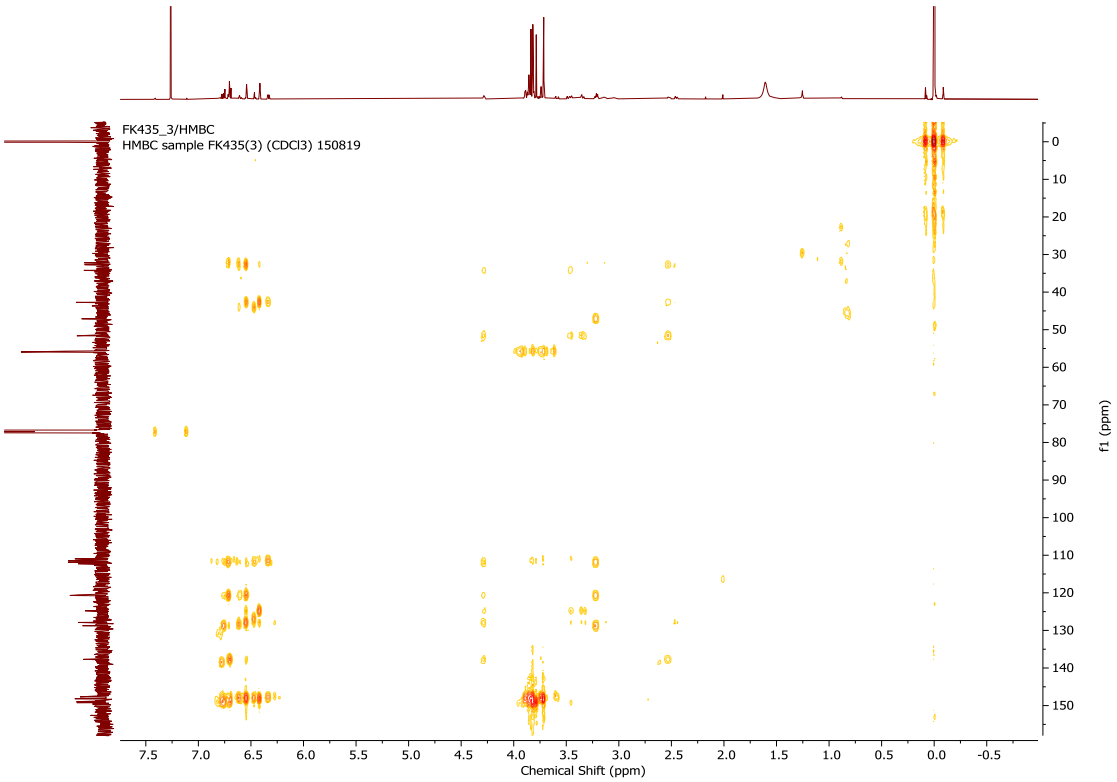


Figure S45. HMBC spectrum of *N*-(3,4-dimethoxyphenethyl)-4-(3,4-dimethoxyphenyl)-6,7-dimethoxy-1,2,3,4-tetrahydronaphthalen-2-amine (diastereomer pair 2 of **203**) ($CDCl_3$, 700 MHz)

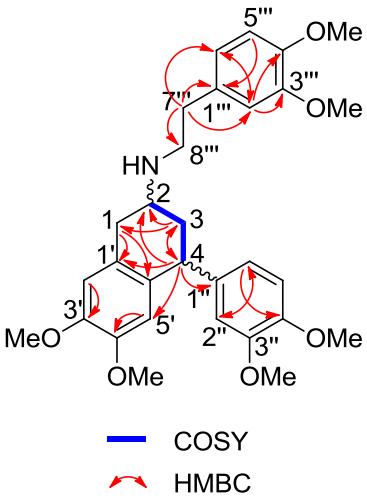


Figure S46. COSY and HMBC correlations of *N*-(3,4-dimethoxyphenethyl)-4-(3,4-dimethoxyphenyl)-6,7-dimethoxy-1,2,3,4-tetrahydronaphthalen-2-amine (diastereomer pair 2 of **203**)

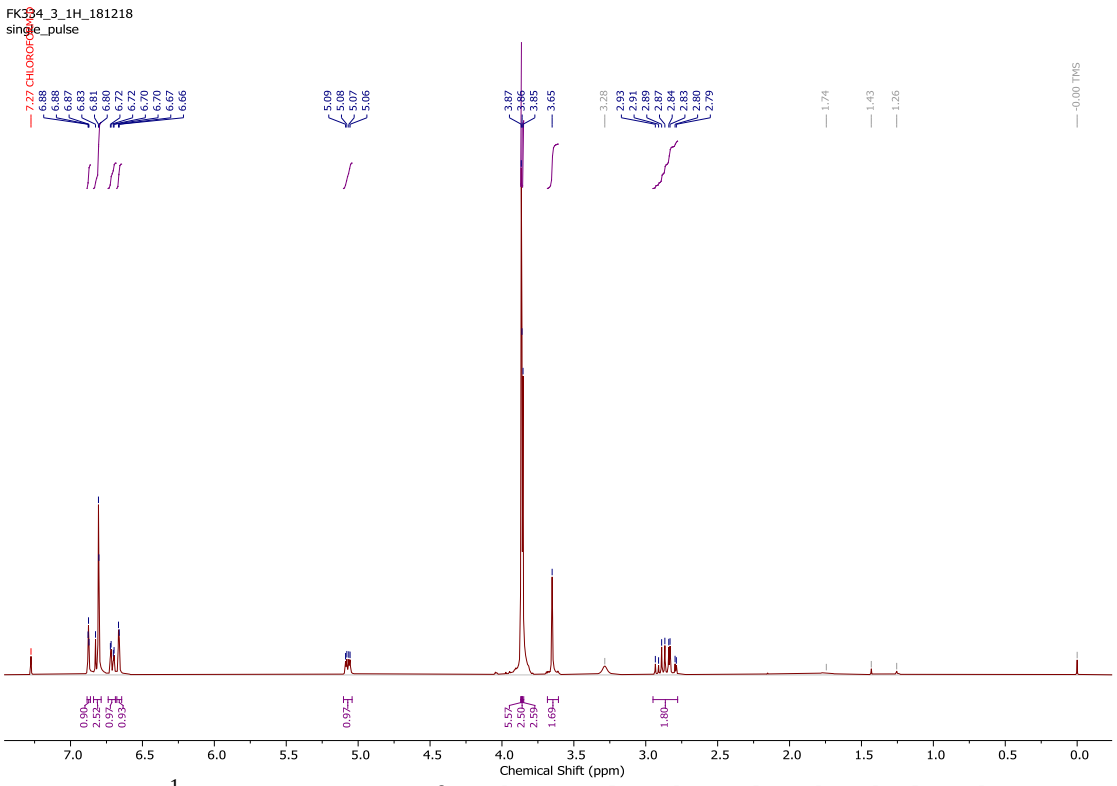


Figure S47. ^{1}H NMR spectrum of 1,4-bis(3,4-dimethoxyphenyl)-4-hydroxybutan-2-one (**205**) ($CDCl_3$, 400 MHz)

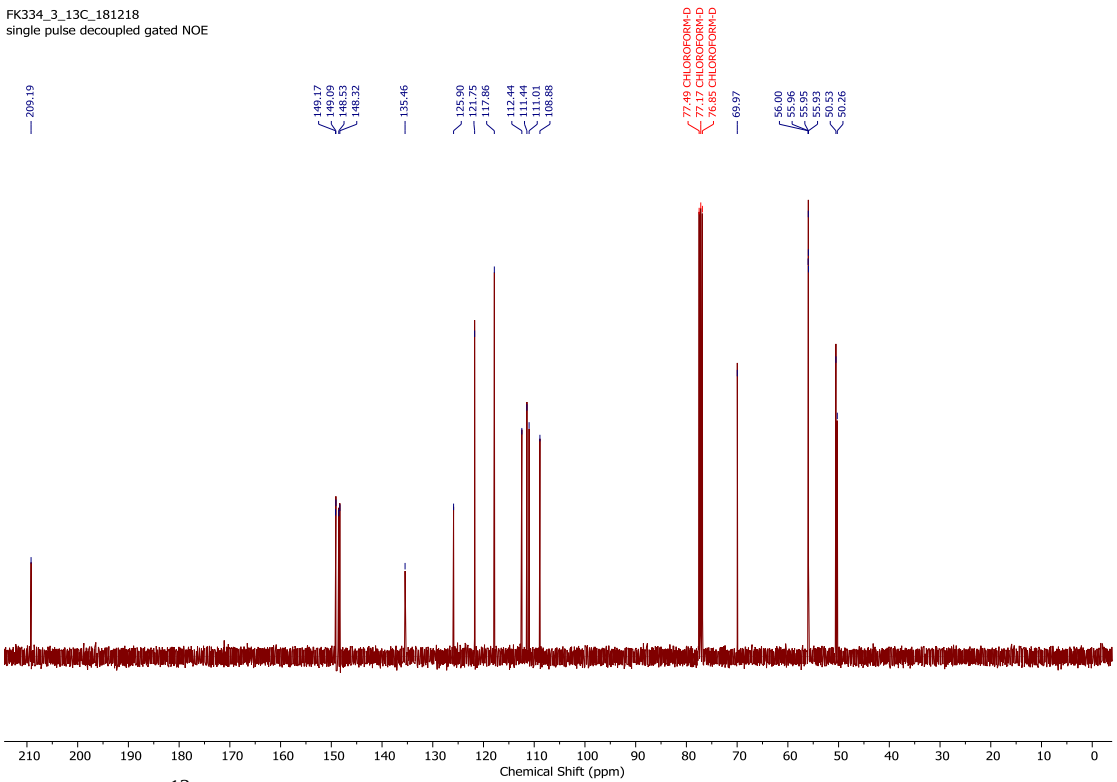


Figure S48. ^{13}C NMR spectrum of 1,4-bis(3,4-dimethoxyphenyl)-4-hydroxybutan-2-one (**205**) ($CDCl_3$, 100 MHz)

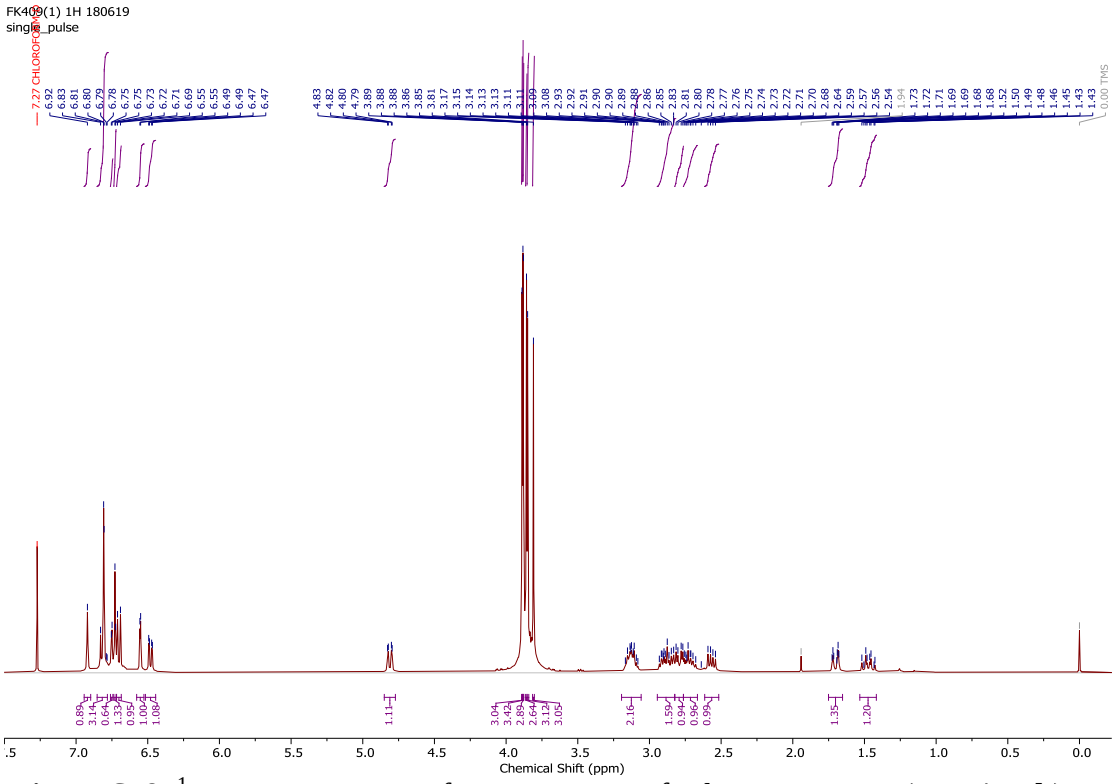


Figure S49. ^{1}H NMR spectrum of stereoisomers of schwarzinicine F (**147a/147b**) ($CDCl_3$, 400 MHz)

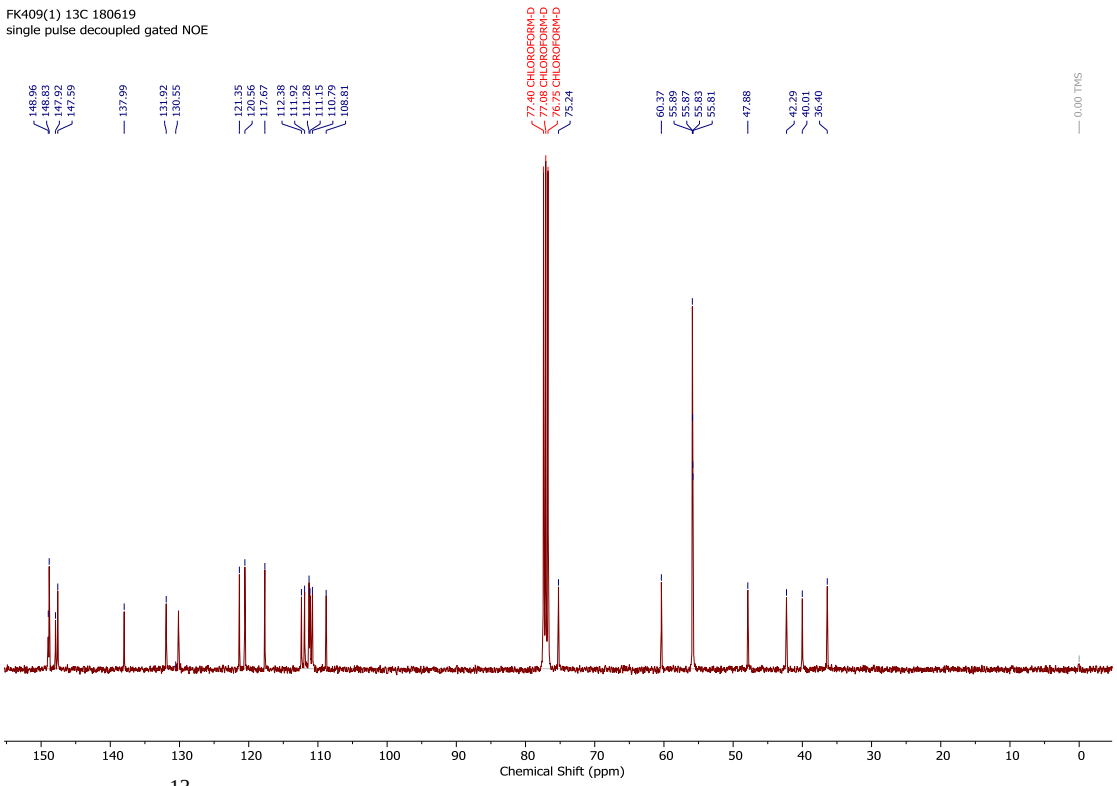


Figure S50. ^{13}C NMR spectrum of stereoisomers of schwarzinicine F (**147a/147b**) ($CDCl_3$, 100 MHz)

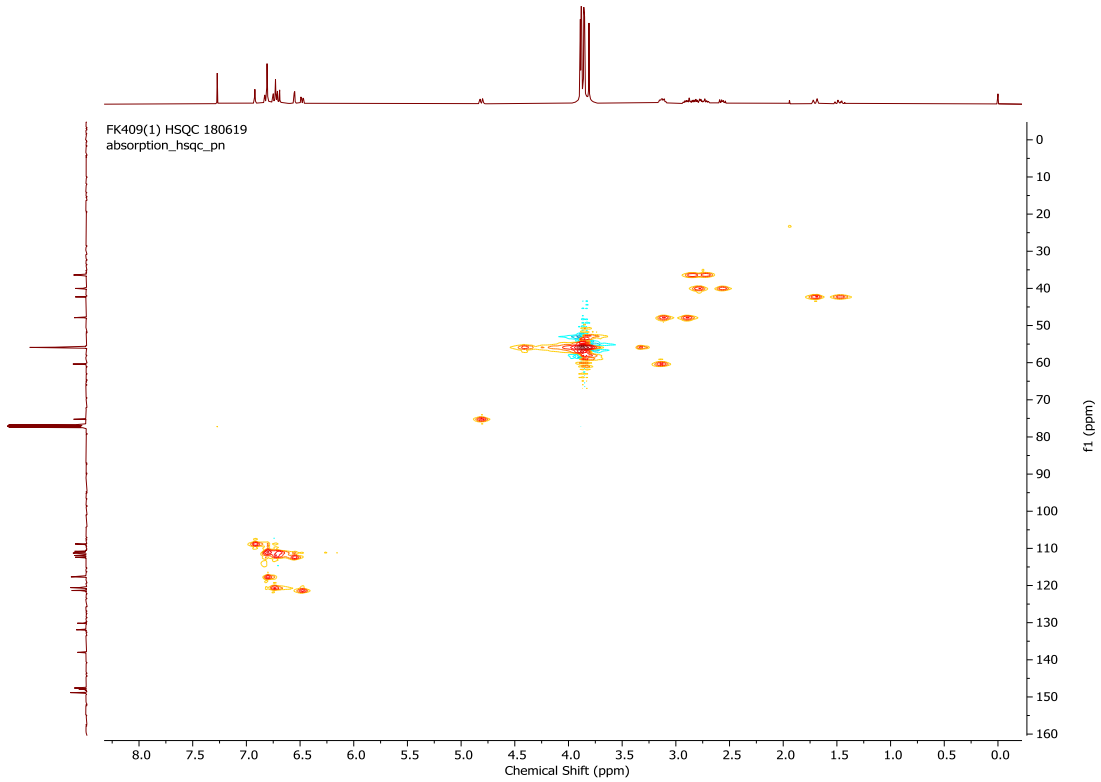


Figure S51. HSQC spectrum of stereoisomers of schwarzinicine F (**147a**/**147b**) ($CDCl_3$, 400 MHz)

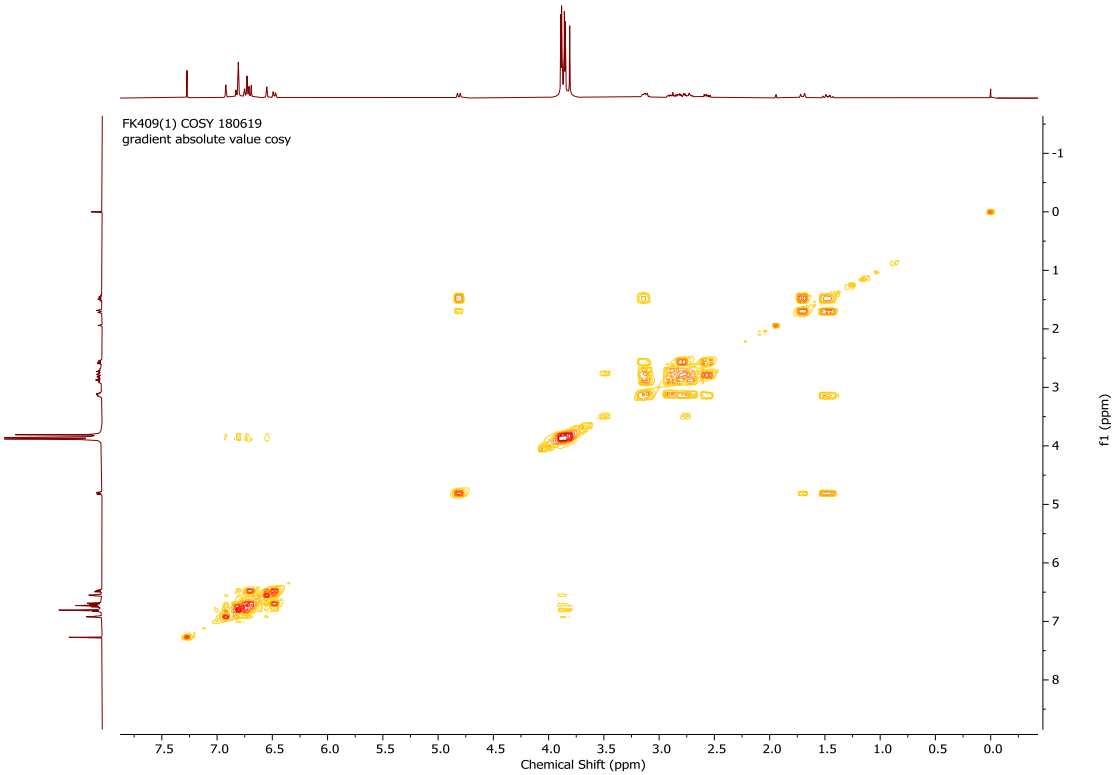


Figure S52. COSY spectrum of stereoisomers of schwarzinicine F (**147a**/**147b**) ($CDCl_3$, 400 MHz)

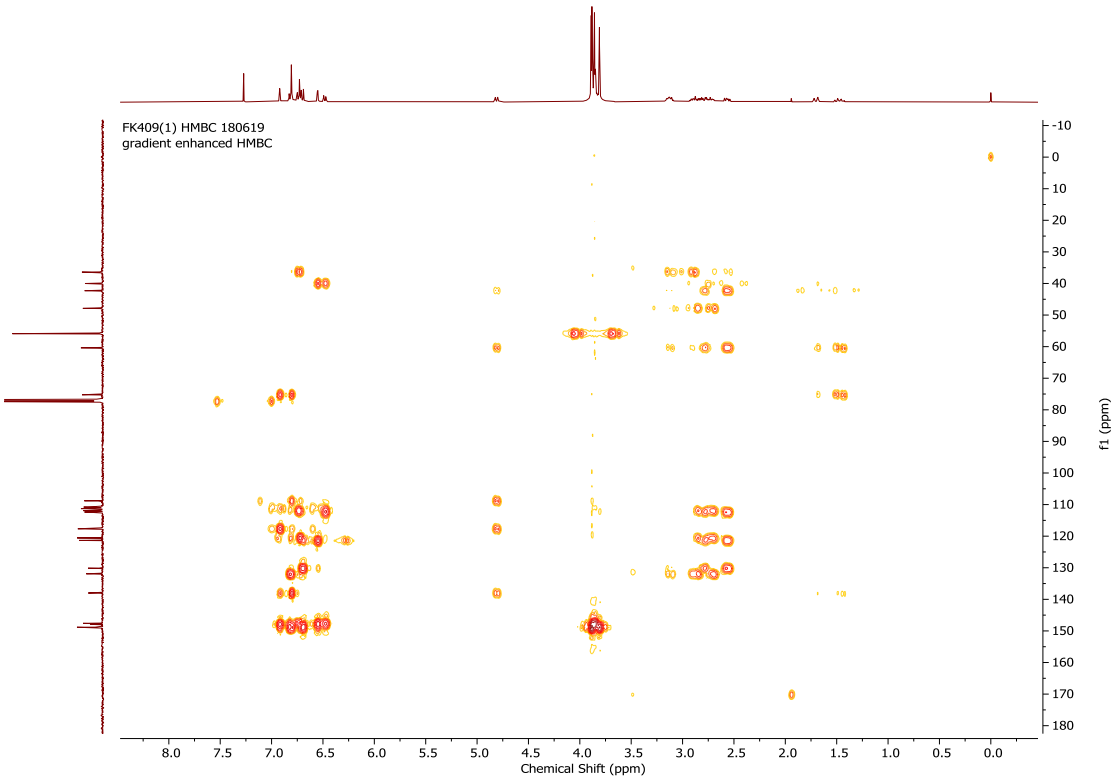


Figure S53. HMBC spectrum of stereoisomers of schwarzinicine F (**147a/147b**) ($CDCl_3$, 400 MHz)

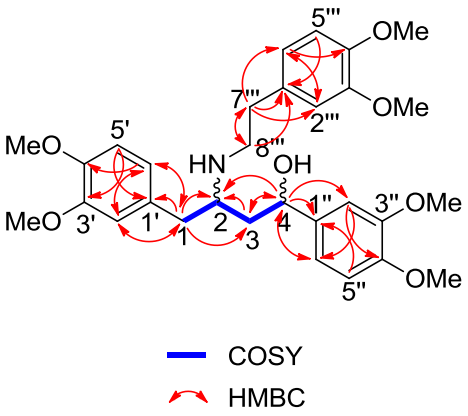


Figure S54. COSY and HMBC correlations of stereoisomers of schwarzinicine F (**147a/147b**)

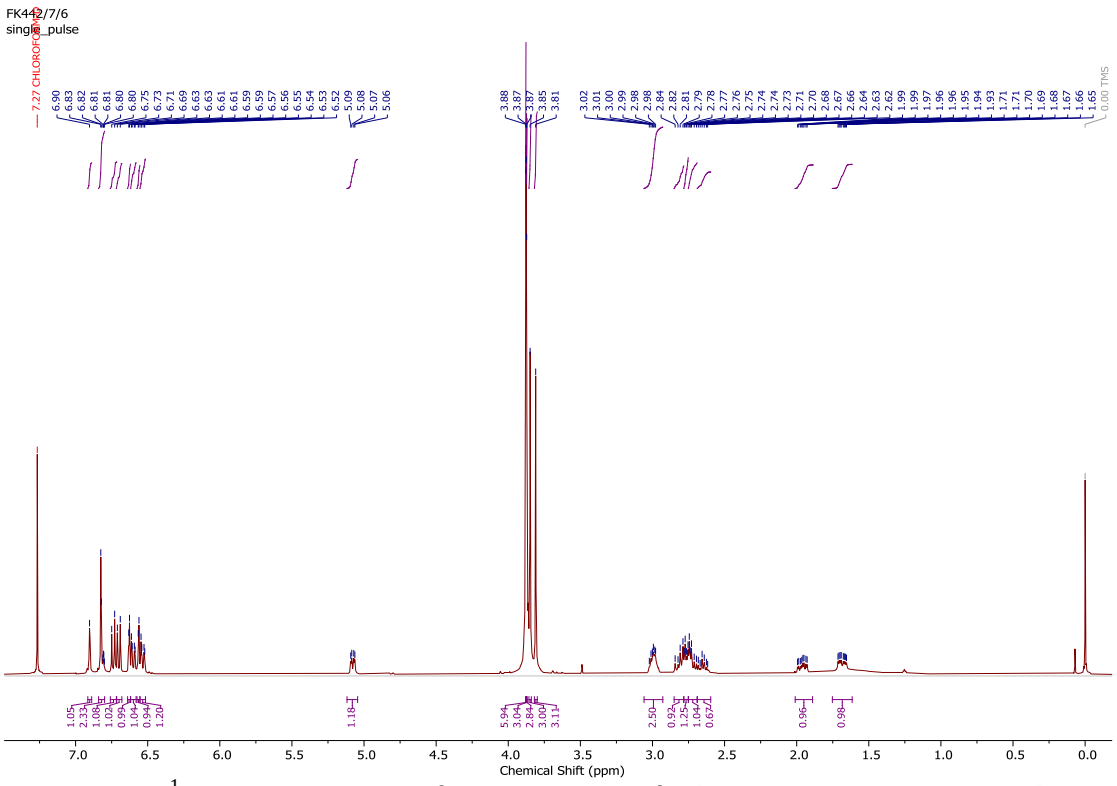


Figure S55. ^{1}H NMR spectrum of stereoisomers of schwarzinicine F (**147c/147d**) ($CDCl_3$, 400 MHz)

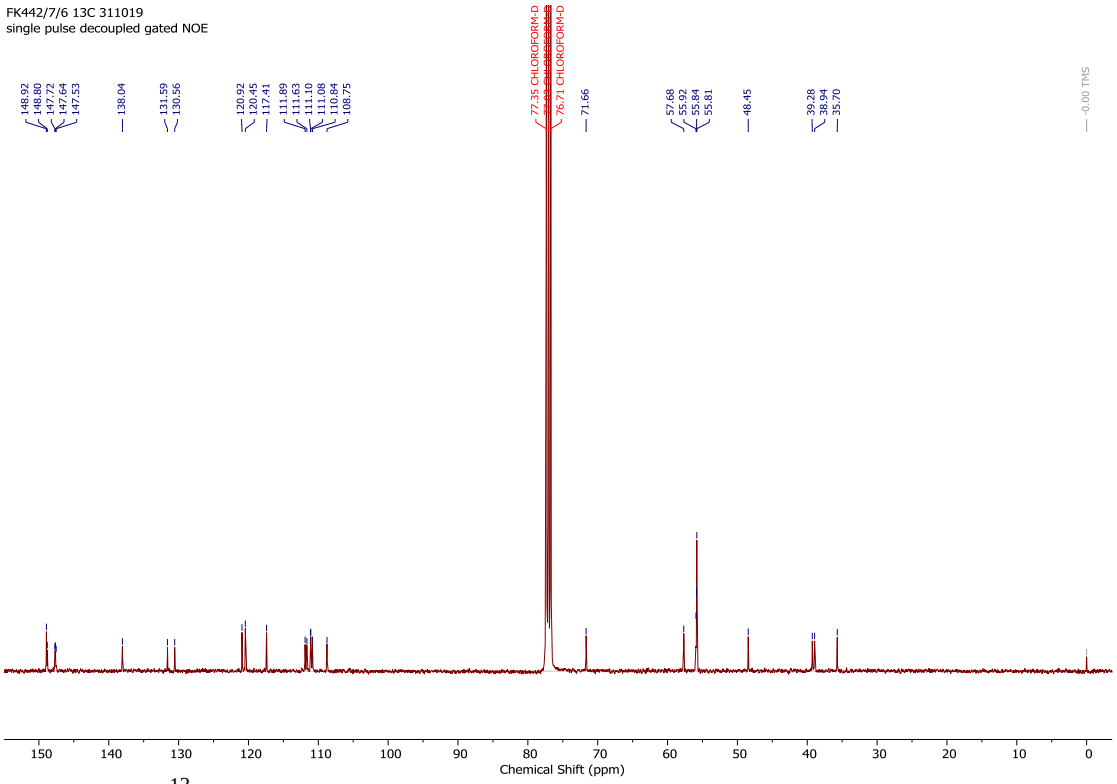
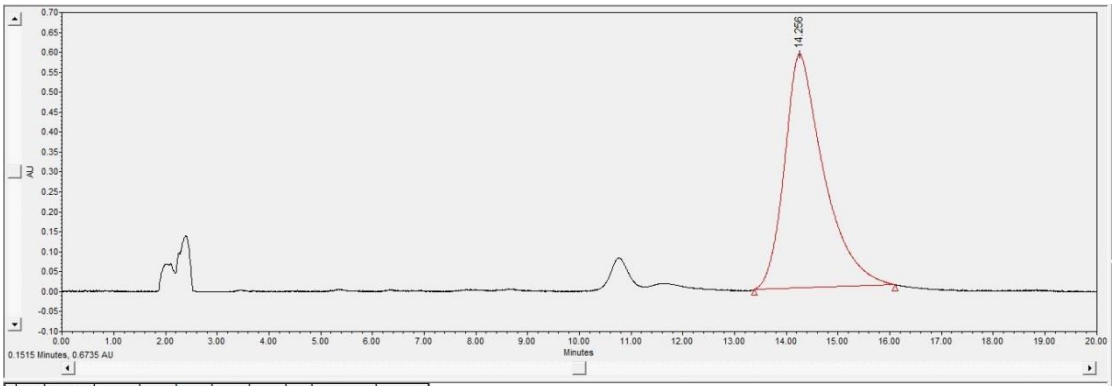
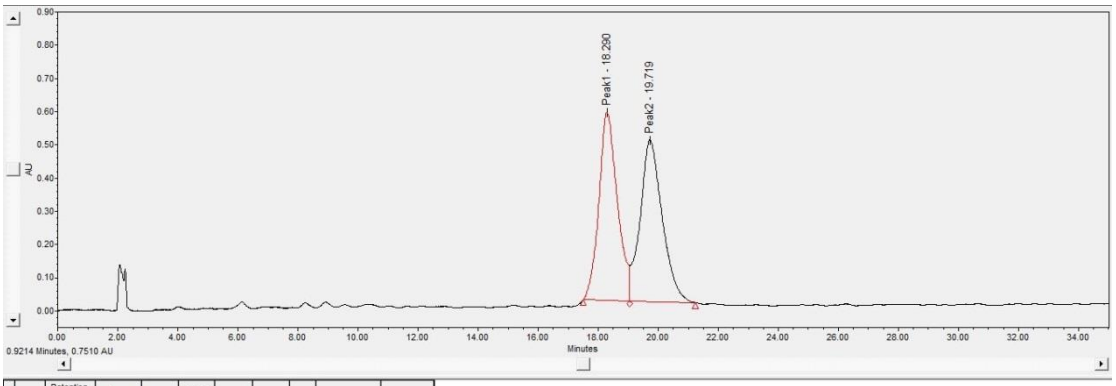


Figure S56. ^{13}C NMR spectrum of stereoisomers of schwarzinicine F (**147c/147d**) ($CDCl_3$, 100 MHz)



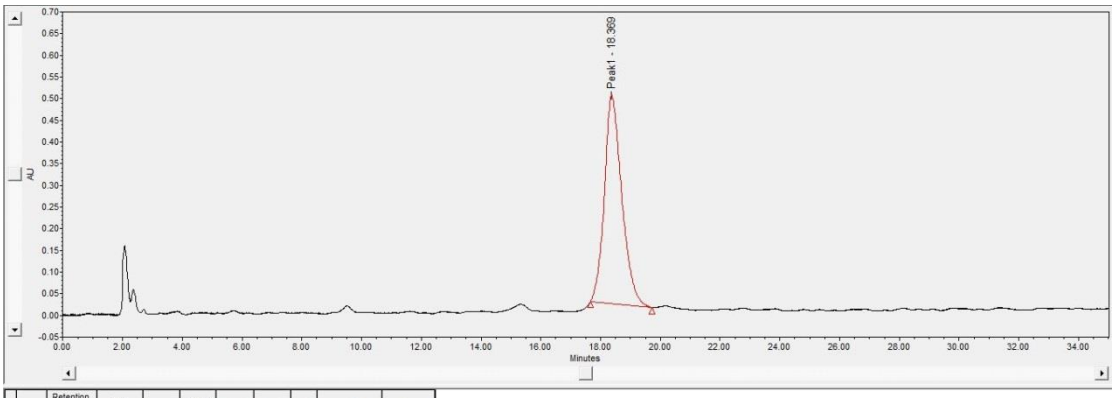
	Name	Retention Time (min)	Area (µV*sec)	% Area	Height (µV)	Int Type	Amount	Units	Peak Type	Peak Codes
1		14.256	31012314	100.00	587271	Bb			Unknown	

Figure S57. Chiral HPLC profile of natural schwarzinicine F (**147**)



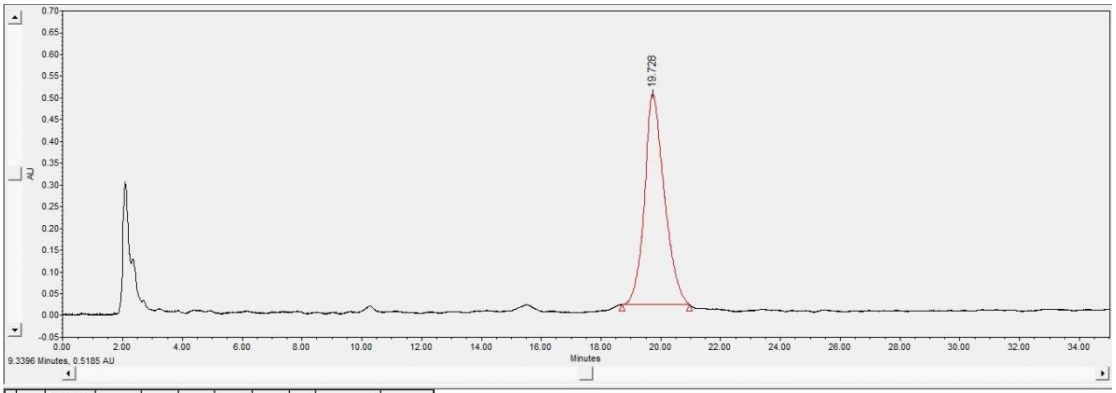
	Name	Retention Time (min)	Area (µV*sec)	% Area	Height (µV)	Int Type	Amount	Units	Peak Type	Peak Codes
1	Peak1	18.290	24143696	49.33	566607	BV			Found	Q20
2	Peak2	19.719	24803651	50.67	486323	VB			Found	Q20

Figure S58. Chiral HPLC profile of stereoisomers of schwarzinicine F (**147a/147b**)



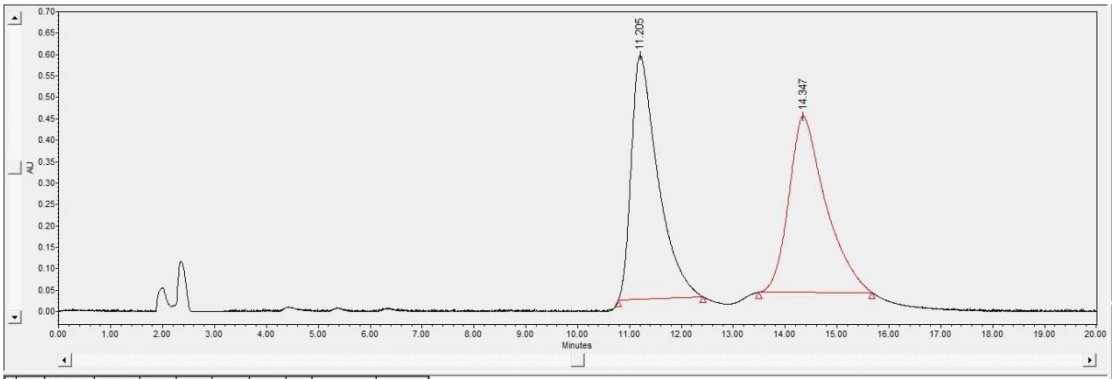
	Name	Retention Time (min)	Area (µV*sec)	% Area	Height (µV)	Int Type	Amount	Units	Peak Type	Peak Codes
1	Peak1	18.369	19620681	100.00	481822	BB			Found	Q20

Figure S59. Chiral HPLC profile of **147a**



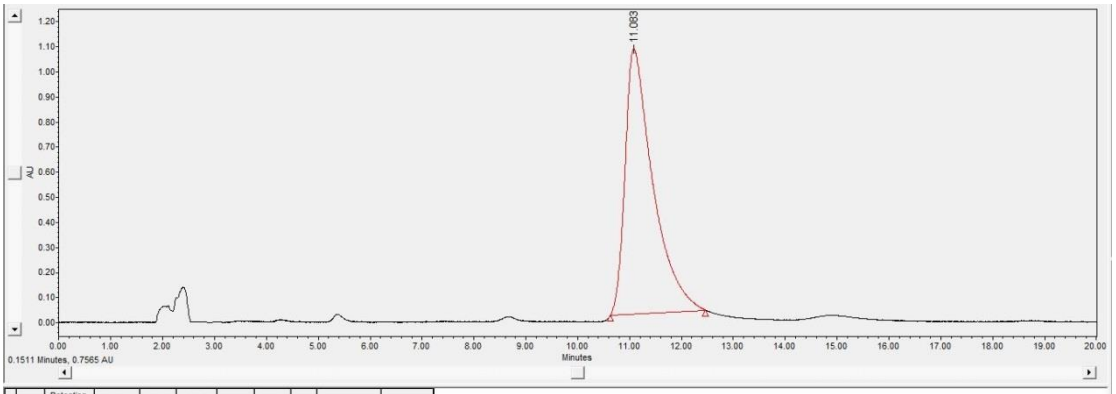
	Name	Retention Time (min)	Area (µV*sec)	% Area	Height (µV)	Int Type	Amount	Units	Peak Type	Peak Codes
1		19.728	22406059	100.00	486005	bb			Unknown	

Figure S60. Chiral HPLC profile of **147b**



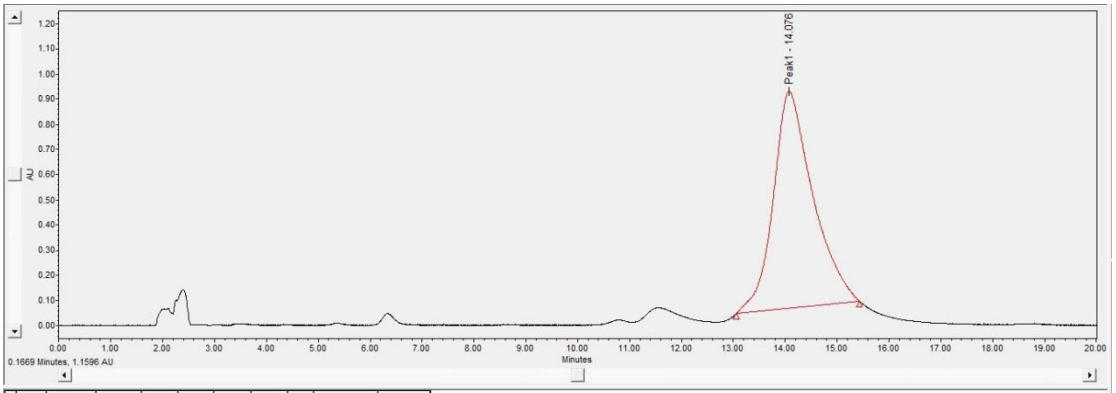
	Name	Retention Time (min)	Area (µV*sec)	% Area	Height (µV)	Int Type	Amount	Units	Peak Type	Peak Codes
1		11.205	20331387	50.04	570174	bb			Unknown	
2		14.347	20301133	49.96	411716	bb			Unknown	

Figure S61. Chiral HPLC profile of stereoisomers of schwarzinicine F (**147c/147d**)



	Name	Retention Time (min)	Area (µV*sec)	% Area	Height (µV)	Int Type	Amount	Units	Peak Type	Peak Codes
1		11.083	39553083	100.00	1058107	bb			Unknown	

Figure S62. Chiral HPLC profile of **147c**



	Name	Retention Time (min)	Area (µV*sec)	% Area	Height (µV)	Int Type	Amount	Units	Peak Type	Peak Codes
1	Peak1	14.076	45647698	100.00	861635	BB			Found	Q20

Figure S63. Chiral HPLC profile of **147d**

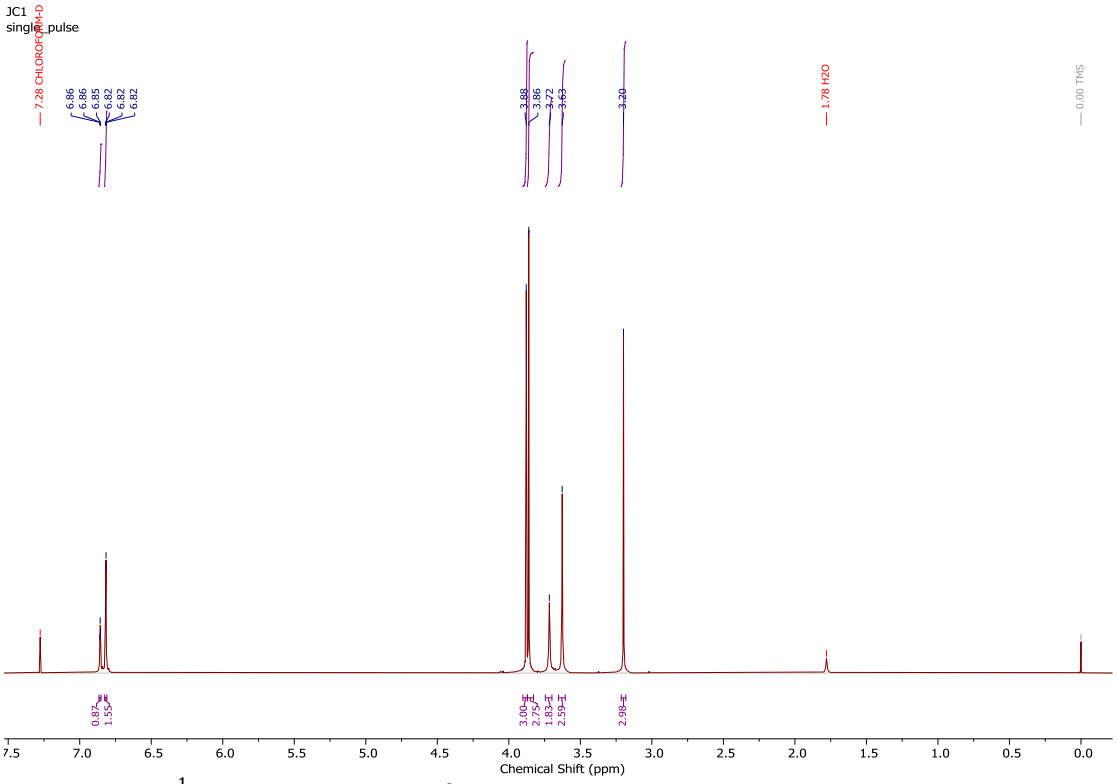


Figure S64. ^{1}H NMR spectrum of *N*-methoxy-*N*-methyl-(3,4-dimethoxyphenyl)acetamide (**177c**) ($CDCl_3$, 700 MHz)

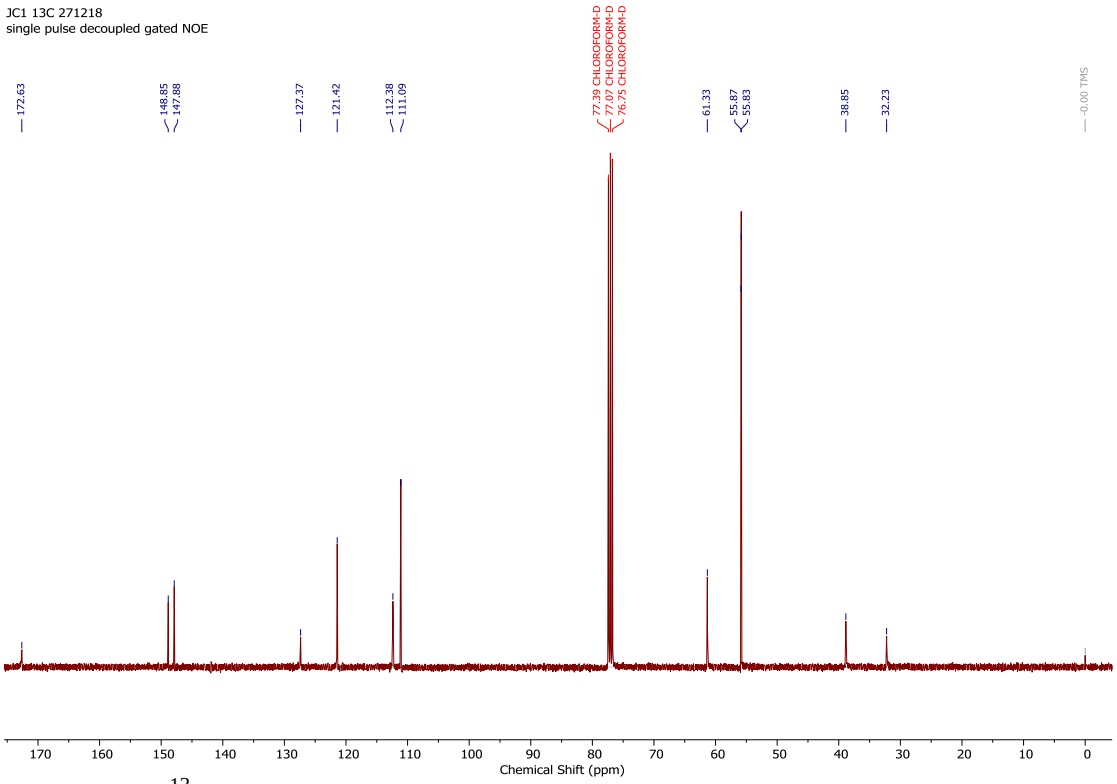


Figure S65. ^{13}C NMR spectrum of *N*-methoxy-*N*-methyl-(3,4-dimethoxyphenyl)acetamide (**177c**) ($CDCl_3$, 175 MHz)

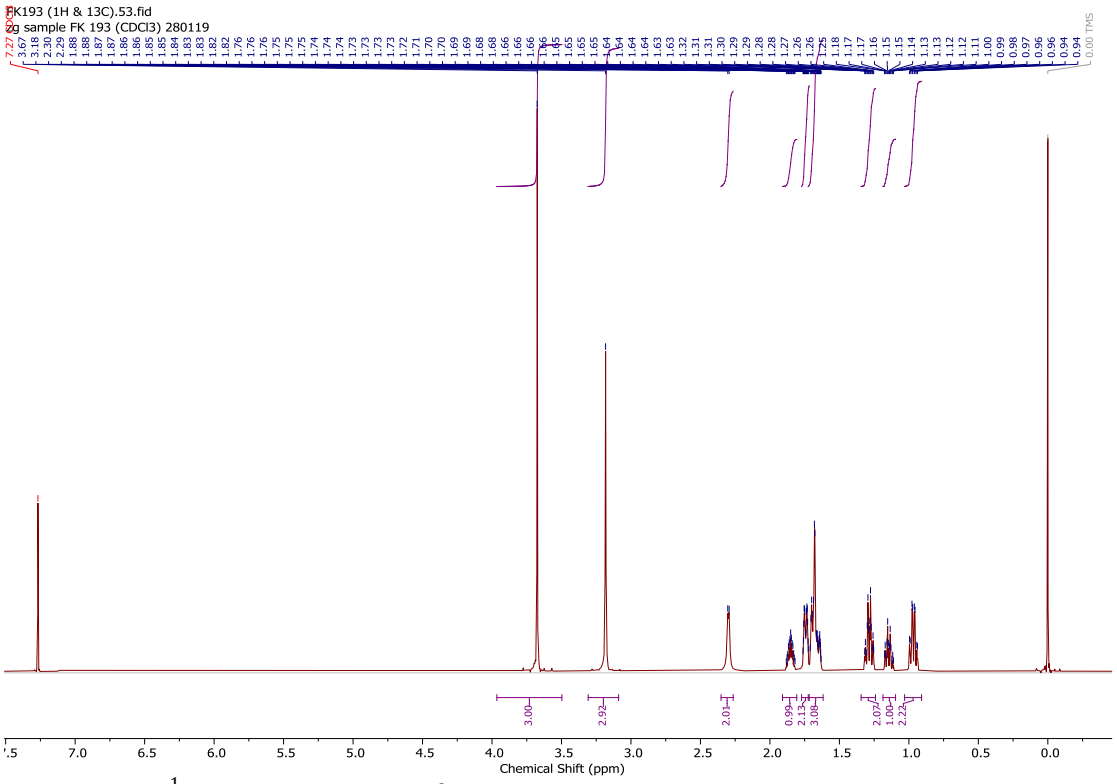


Figure S66. ^{1}H NMR spectrum of 2-cyclohexyl-*N*-methoxy-*N*-methylacetamide (**210a**) ($CDCl_3$, 700 MHz)

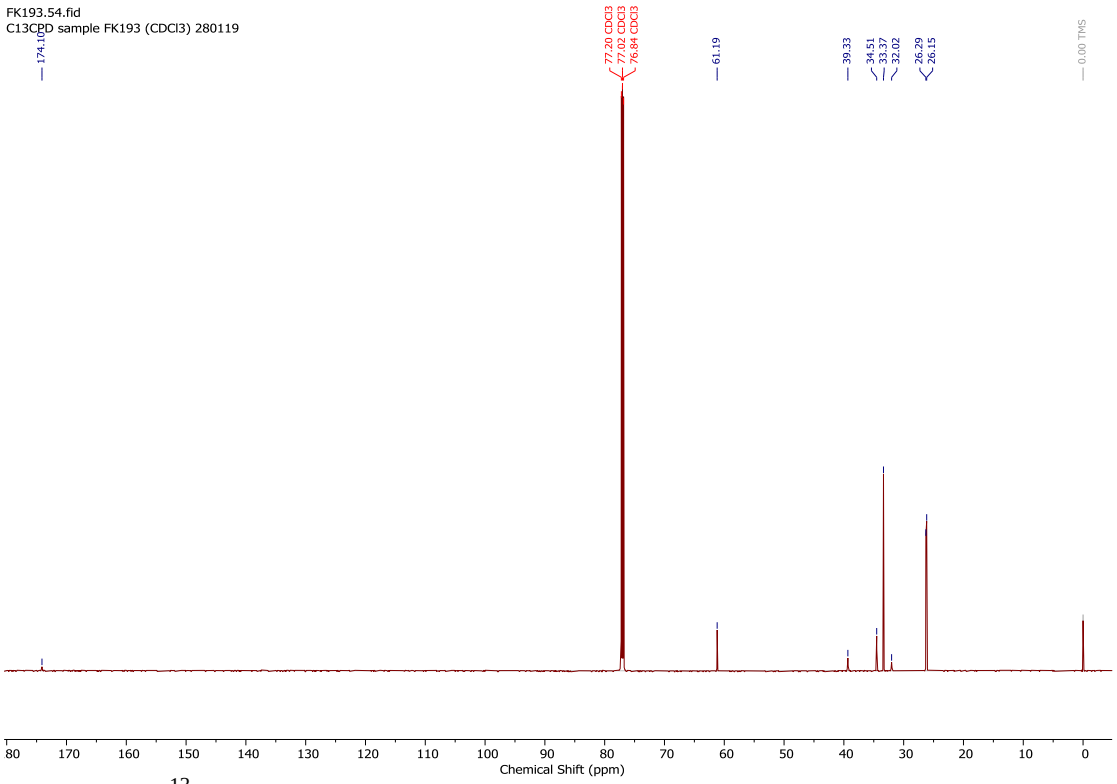


Figure S67. ^{13}C NMR spectrum of 2-cyclohexyl-*N*-methoxy-*N*-methylacetamide (**210a**) ($CDCl_3$, 175 MHz)

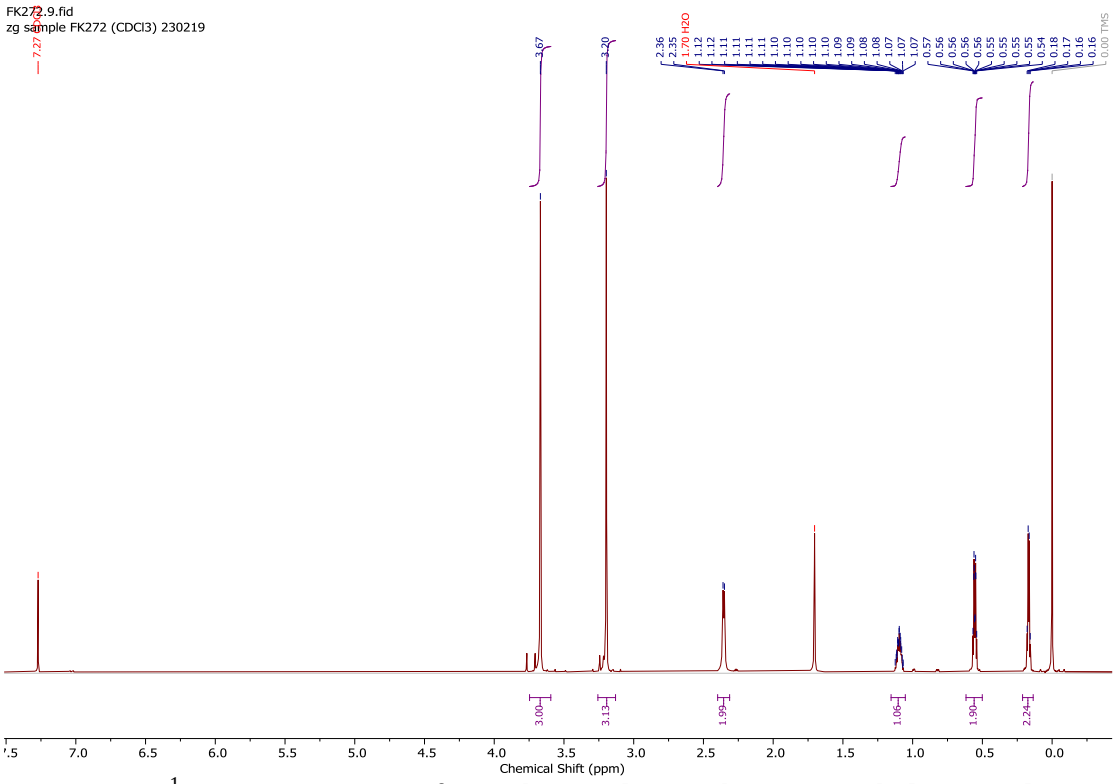


Figure S68. ^{1}H NMR spectrum of 2-cyclopropyl-*N*-methoxy-*N*-methylacetamide (**210b**) ($CDCl_3$, 700 MHz)

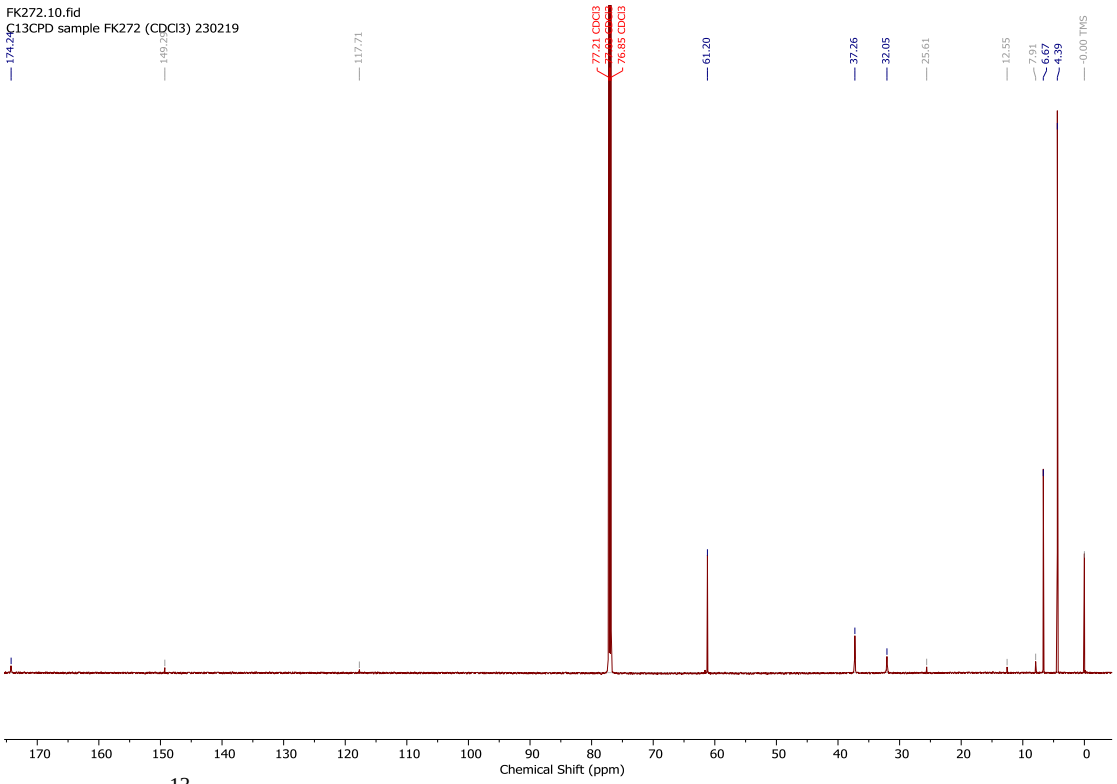


Figure S69. ^{13}C NMR spectrum of 2-cyclopropyl-*N*-methoxy-*N*-methylacetamide (**210b**) ($CDCl_3$, 175 MHz)

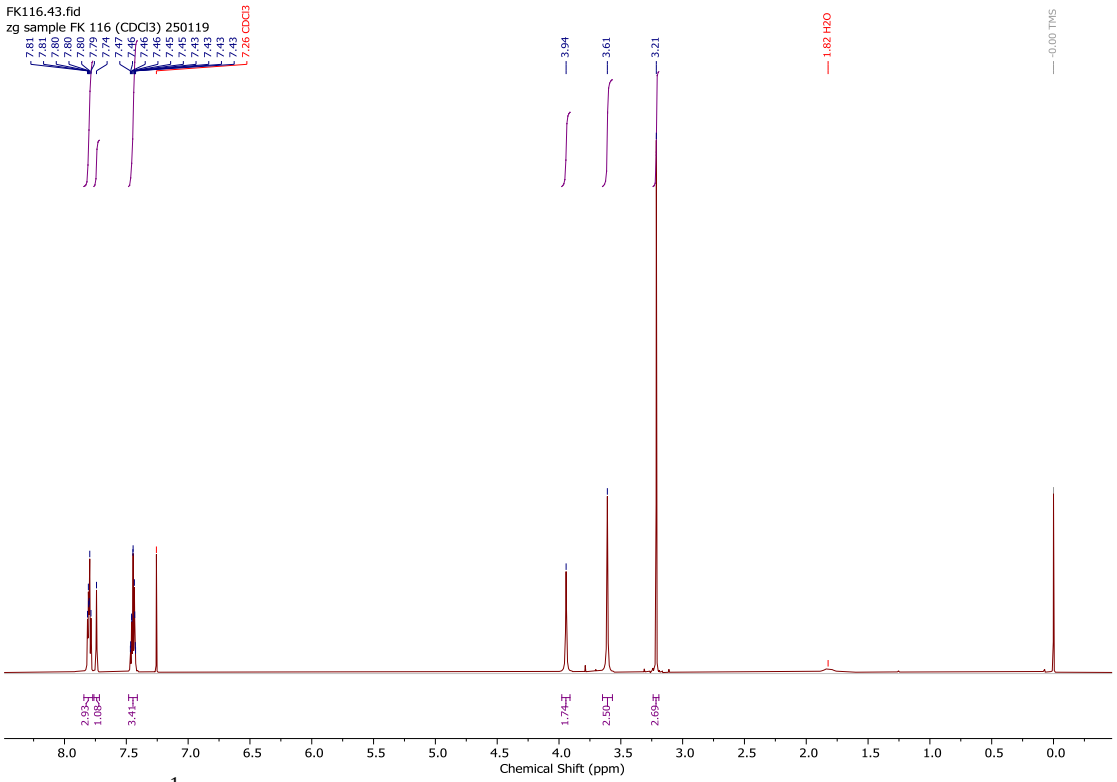


Figure S70. ^{1}H NMR spectrum of *N*-methoxy-*N*-methyl-2-(naphthalen-2-yl)acetamide (**210c**) ($CDCl_3$, 700 MHz)

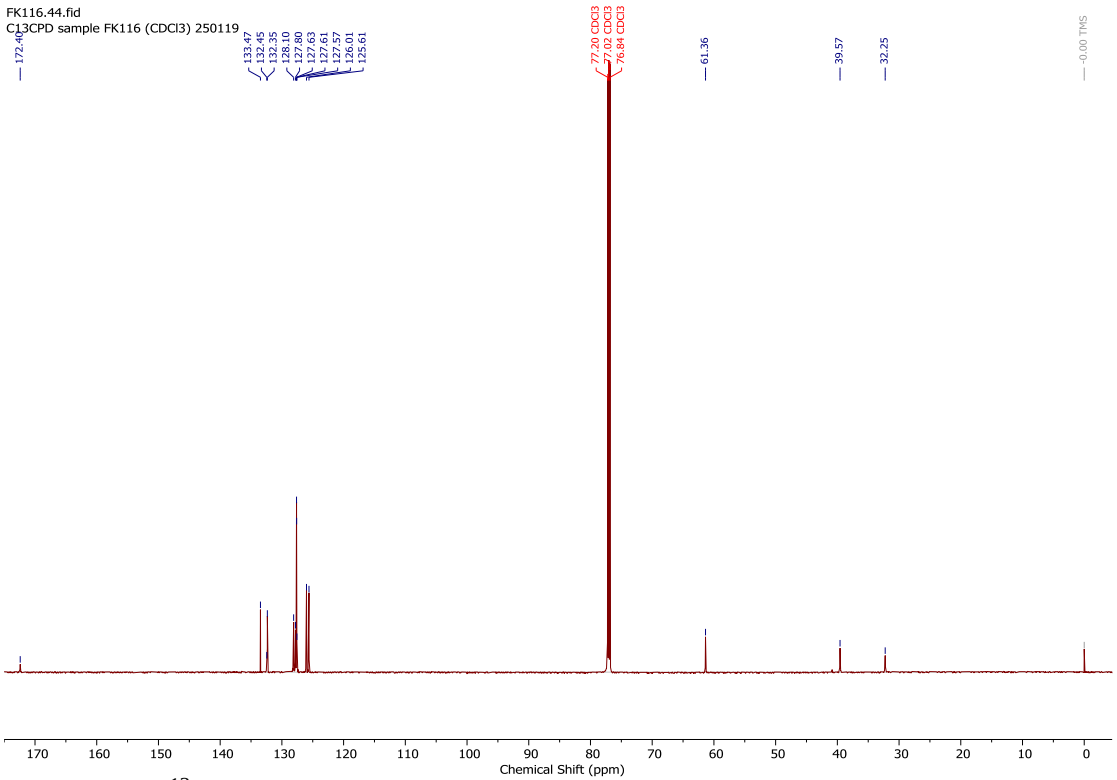


Figure S71. ^{13}C NMR spectrum of *N*-methoxy-*N*-methyl-2-(naphthalen-2-yl)acetamide (**210c**) ($CDCl_3$, 175 MHz)

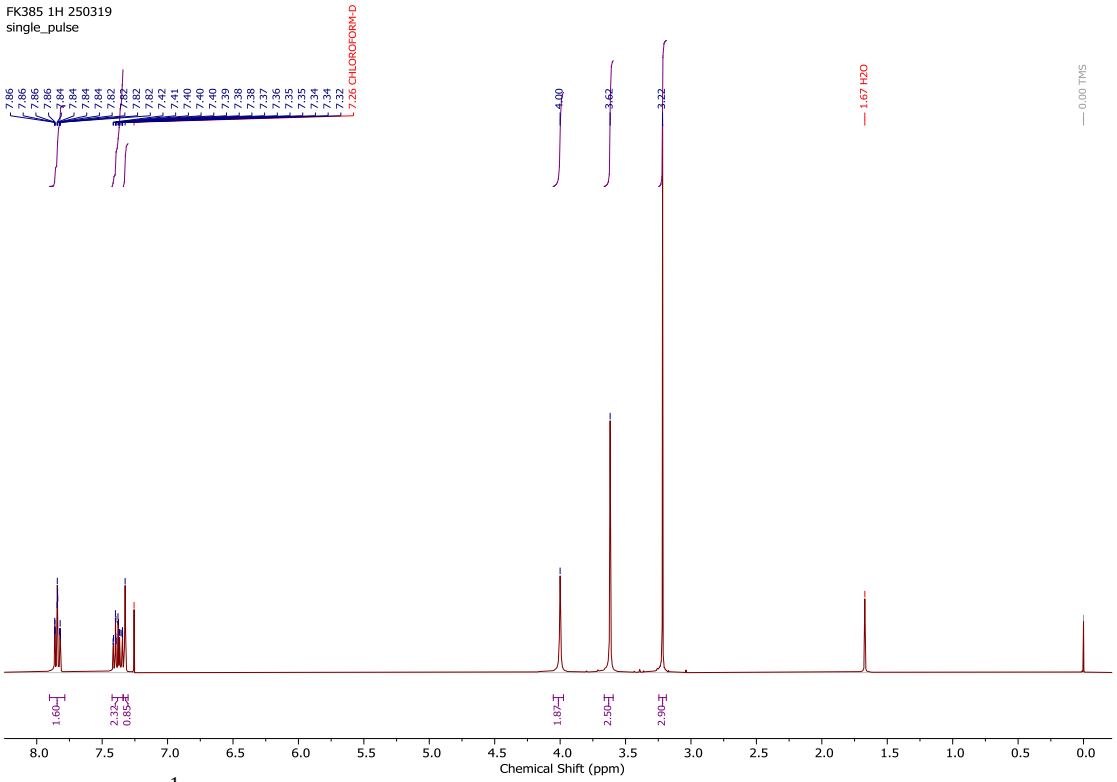


Figure S72. ^{1}H NMR spectrum of 2-(benzo[*b*]thiophen-3-yl)-*N*-methoxy-*N*-methylacetamide (**210d**) ($CDCl_3$, 400 MHz)

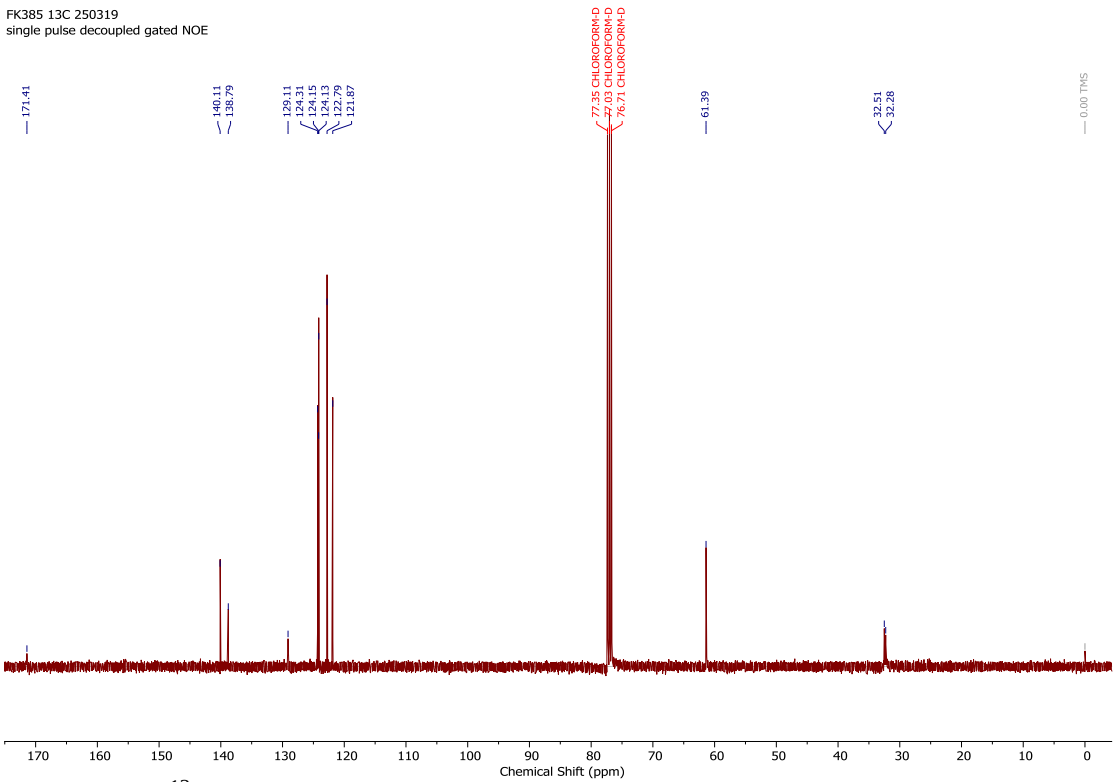


Figure S73. ^{13}C NMR spectrum of 2-(benzo[*b*]thiophen-3-yl)-*N*-methoxy-*N*-methylacetamide (**210d**) ($CDCl_3$, 100 MHz)

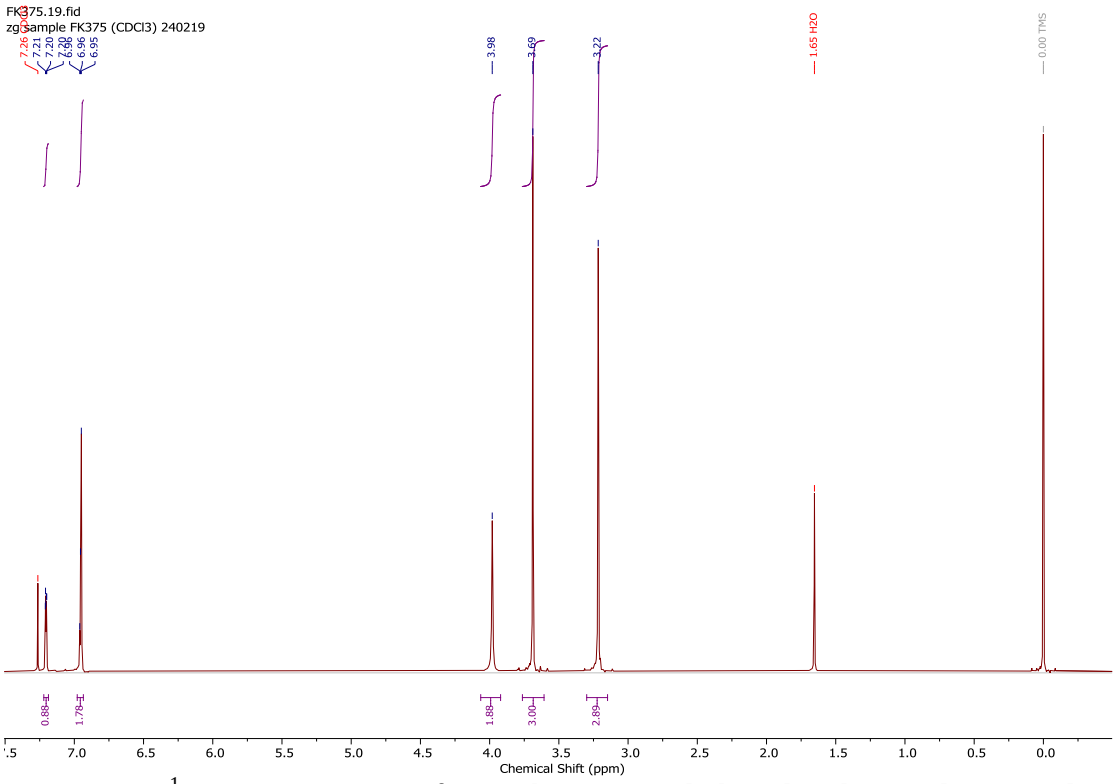


Figure S74. ^{1}H NMR spectrum of *N*-methoxy-*N*-methyl-2-(thiophen-2-yl)acetamide (**210e**) ($CDCl_3$, 700 MHz)

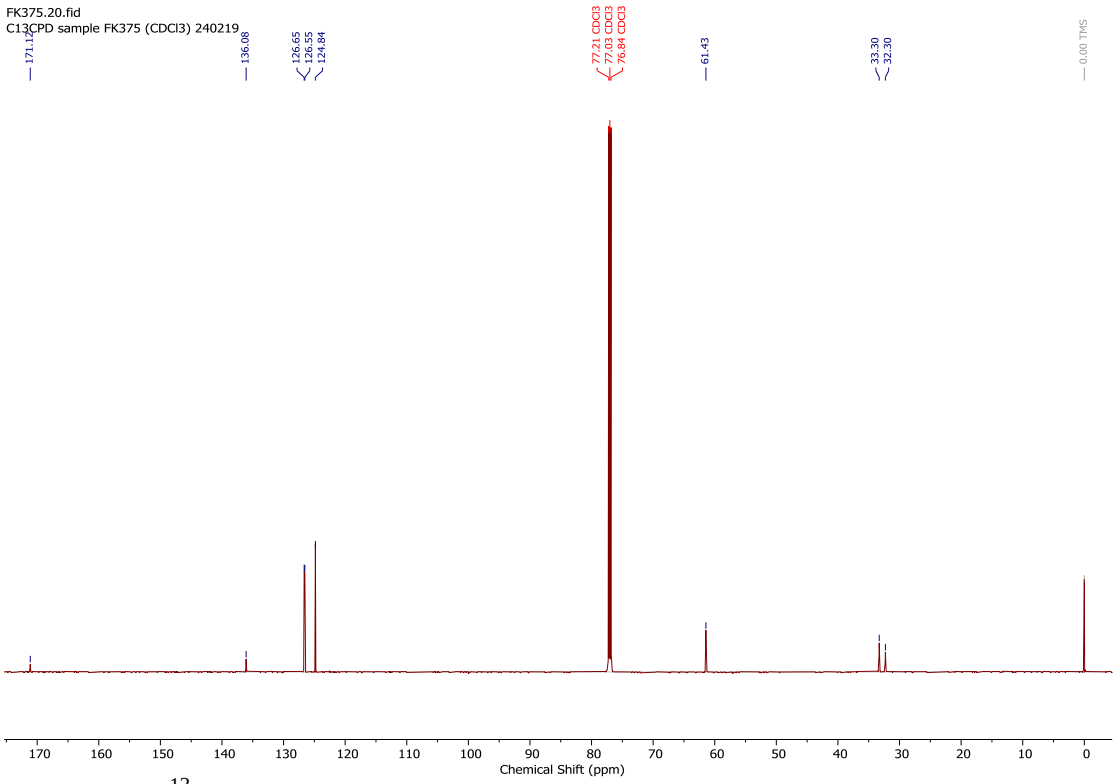


Figure S75. ^{13}C NMR spectrum of *N*-methoxy-*N*-methyl-2-(thiophen-2-yl)acetamide (**210e**) ($CDCl_3$, 175 MHz)

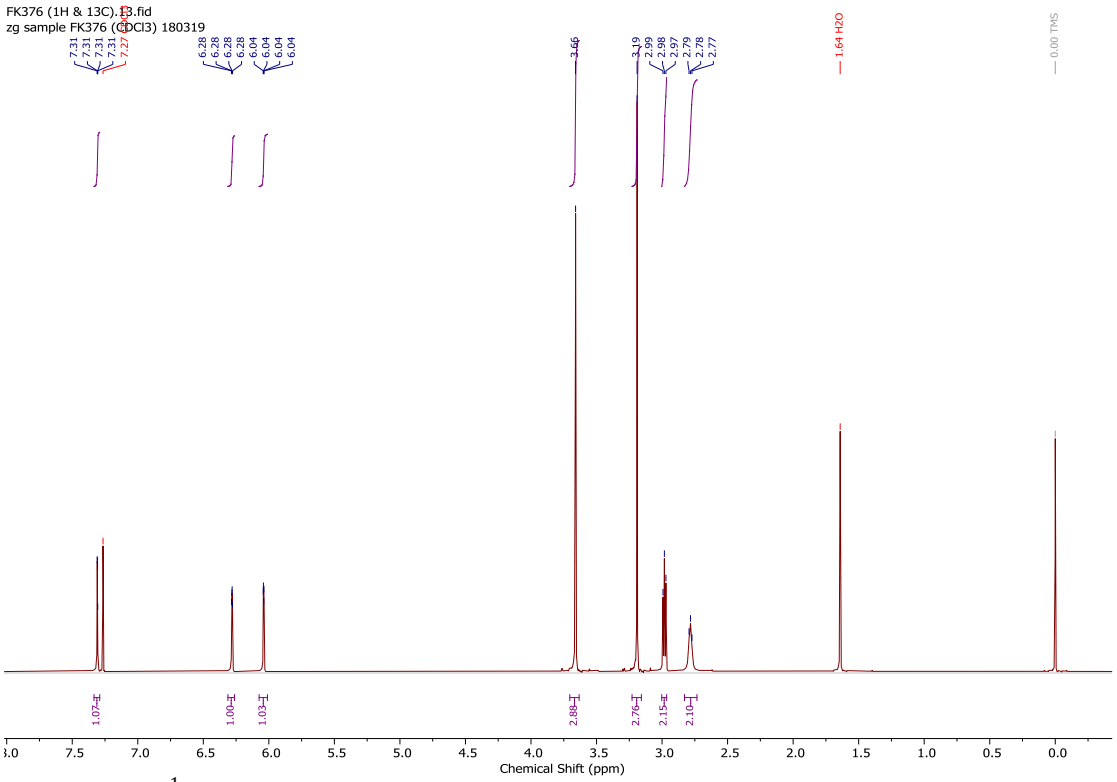


Figure S76. ^{1}H NMR spectrum of 3-(furan-2-yl)-*N*-methoxy-*N*-methylpropanamide (**210f**) ($CDCl_3$, 700 MHz)

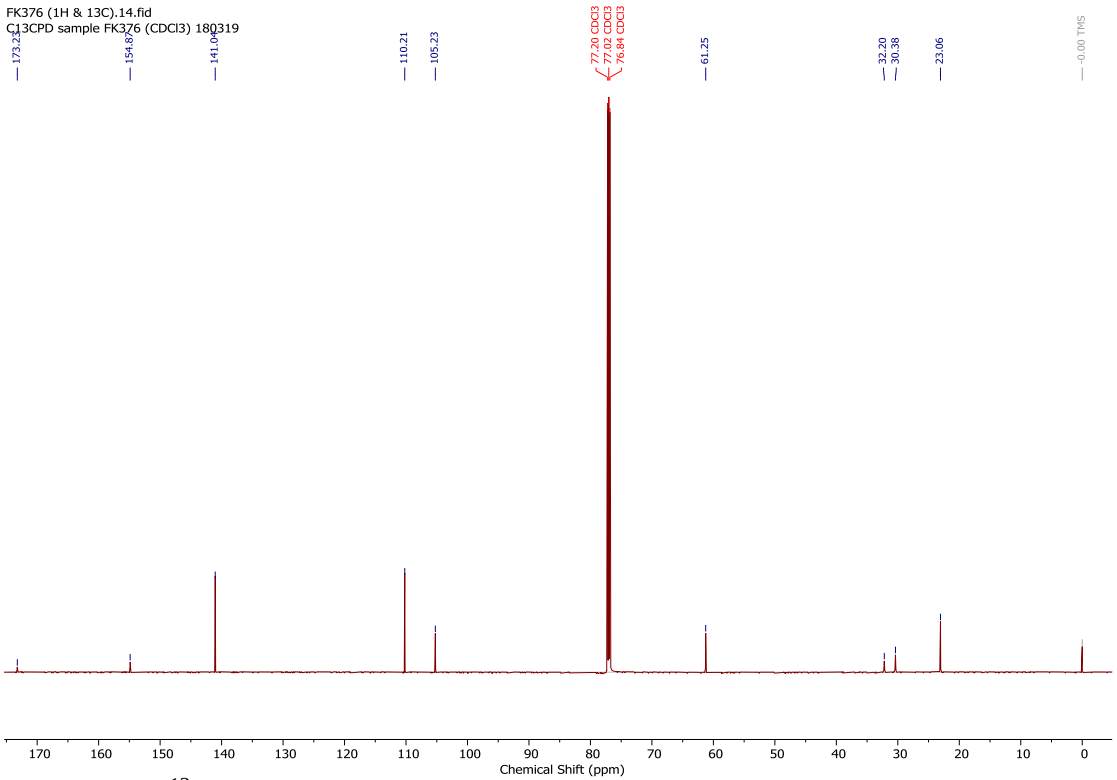


Figure S77. ^{13}C NMR spectrum of 3-(furan-2-yl)-*N*-methoxy-*N*-methylpropanamide (**210f**) ($CDCl_3$, 175 MHz)

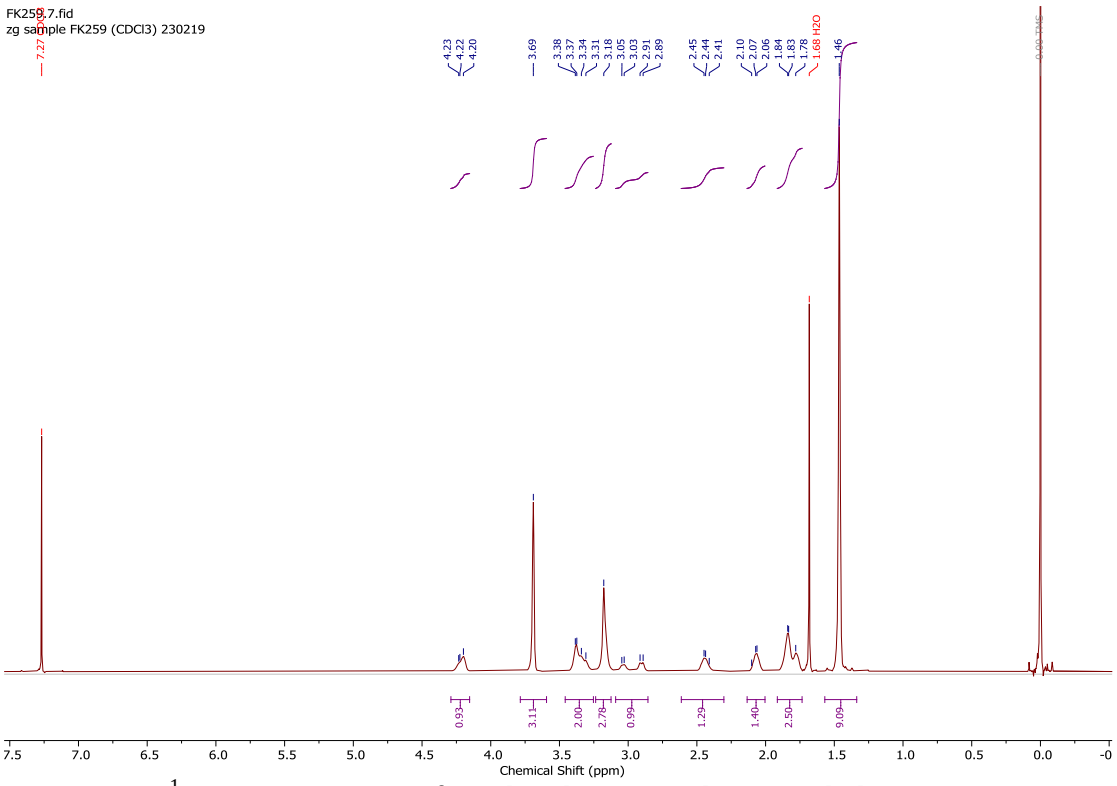


Figure S78. ^{1}H NMR spectrum of *tert*-butyl 2-(2-(methoxy(methyl)amino)-2-oxoethyl)pyrrolidine-1-carboxylate (**210g**) ($CDCl_3$, 700 MHz)

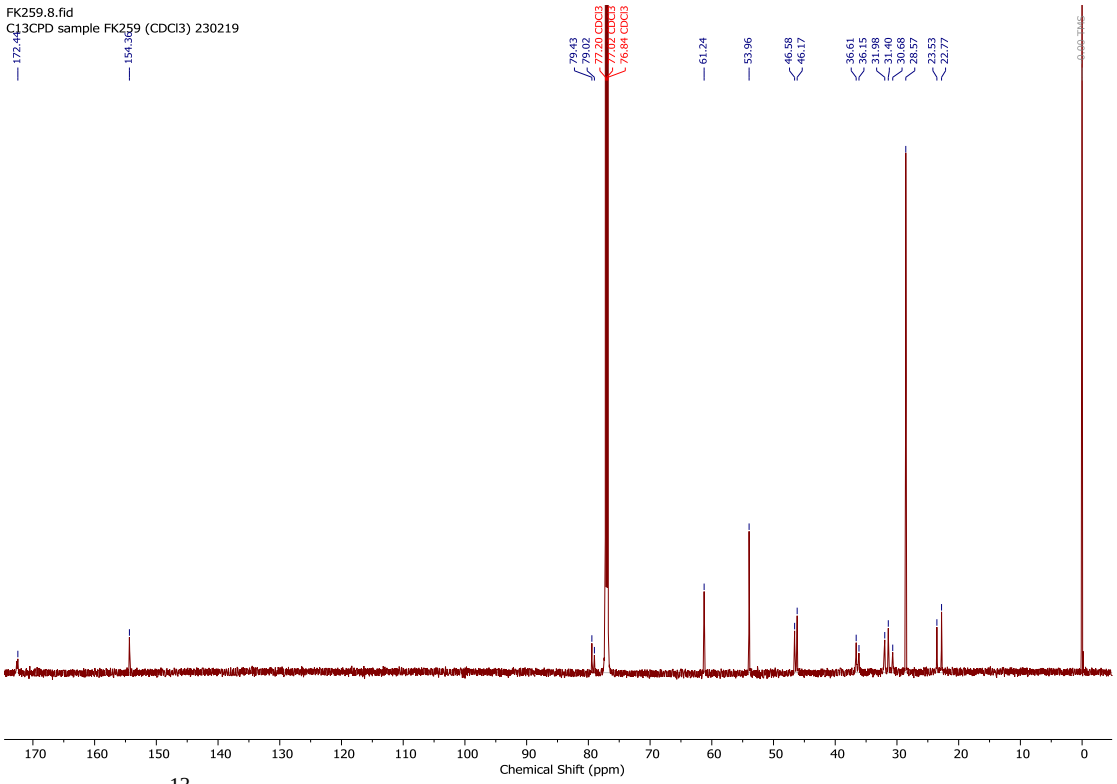


Figure S79. ^{13}C NMR spectrum of *tert*-butyl 2-(2-(methoxy(methyl)amino)-2-oxoethyl)pyrrolidine-1-carboxylate (**210g**) ($CDCl_3$, 175 MHz)

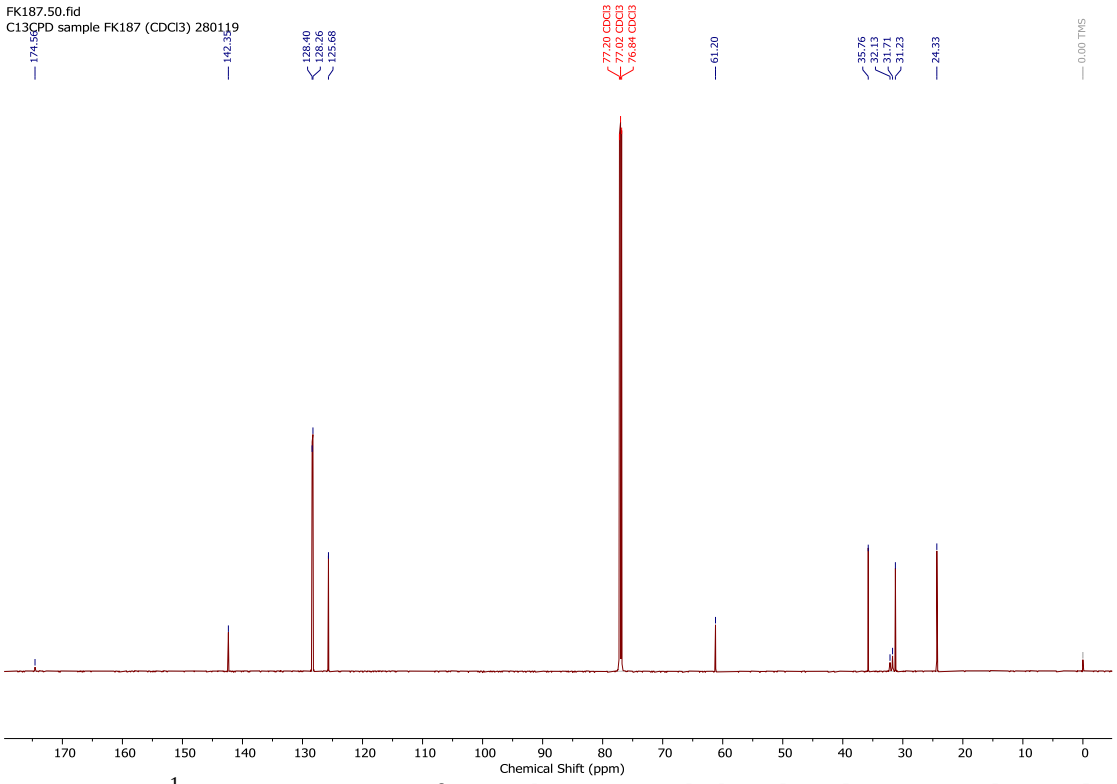


Figure S80. ^{1}H NMR spectrum of *N*-methoxy-*N*-methyl-5-phenylpentanamide (**210h**) ($CDCl_3$, 700 MHz)

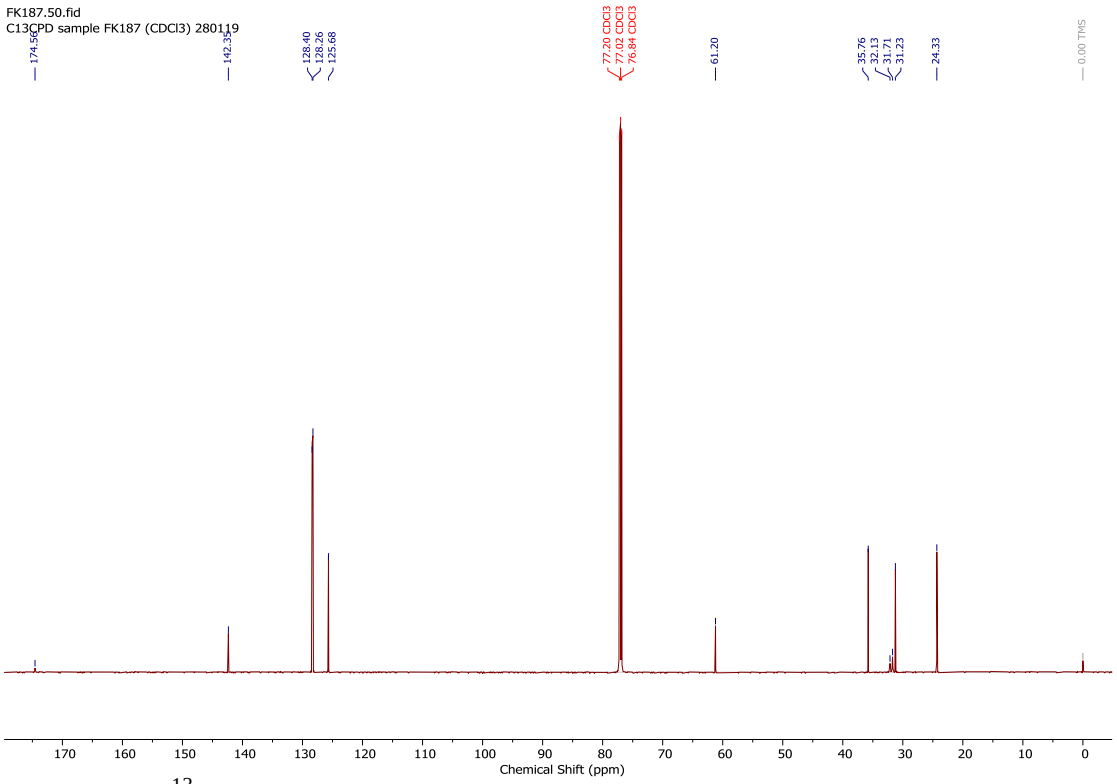


Figure S81. ^{13}C NMR spectrum of *N*-methoxy-*N*-methyl-5-phenylpentanamide (**210h**) ($CDCl_3$, 175 MHz)

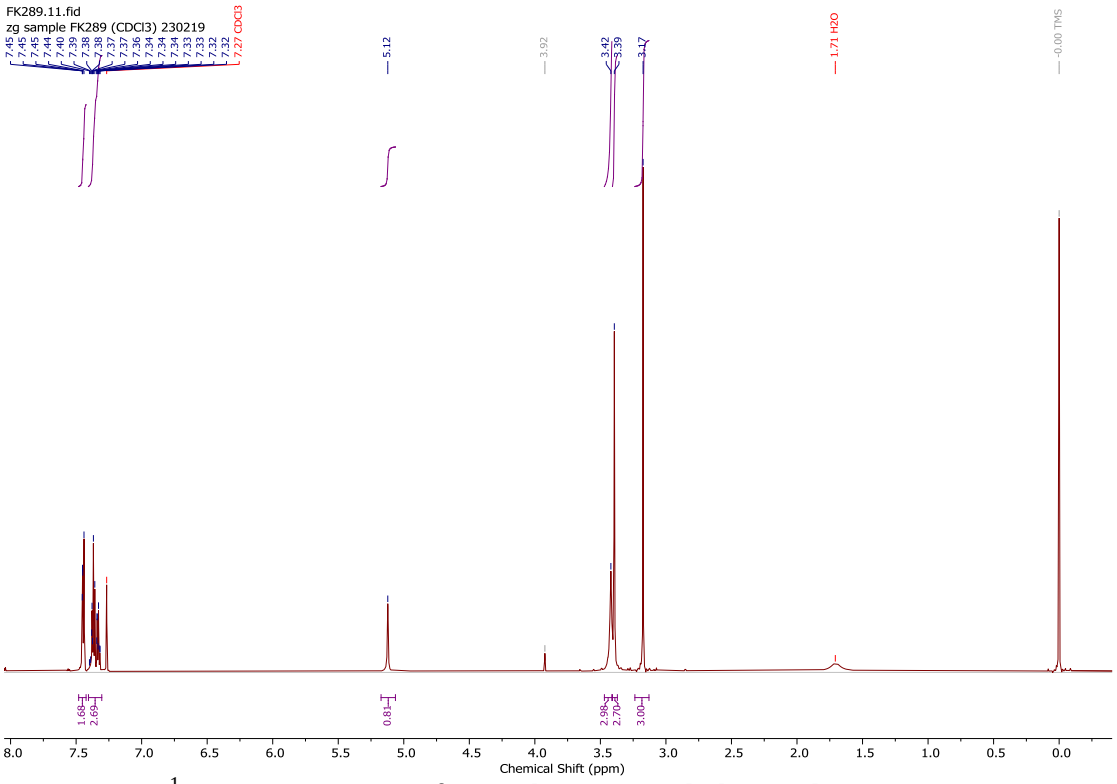


Figure S82. ^{1}H NMR spectrum of *N*-methoxy-*N*-methyl-2-methoxy-2-phenylacetamide (**210i**) ($CDCl_3$, 700 MHz)

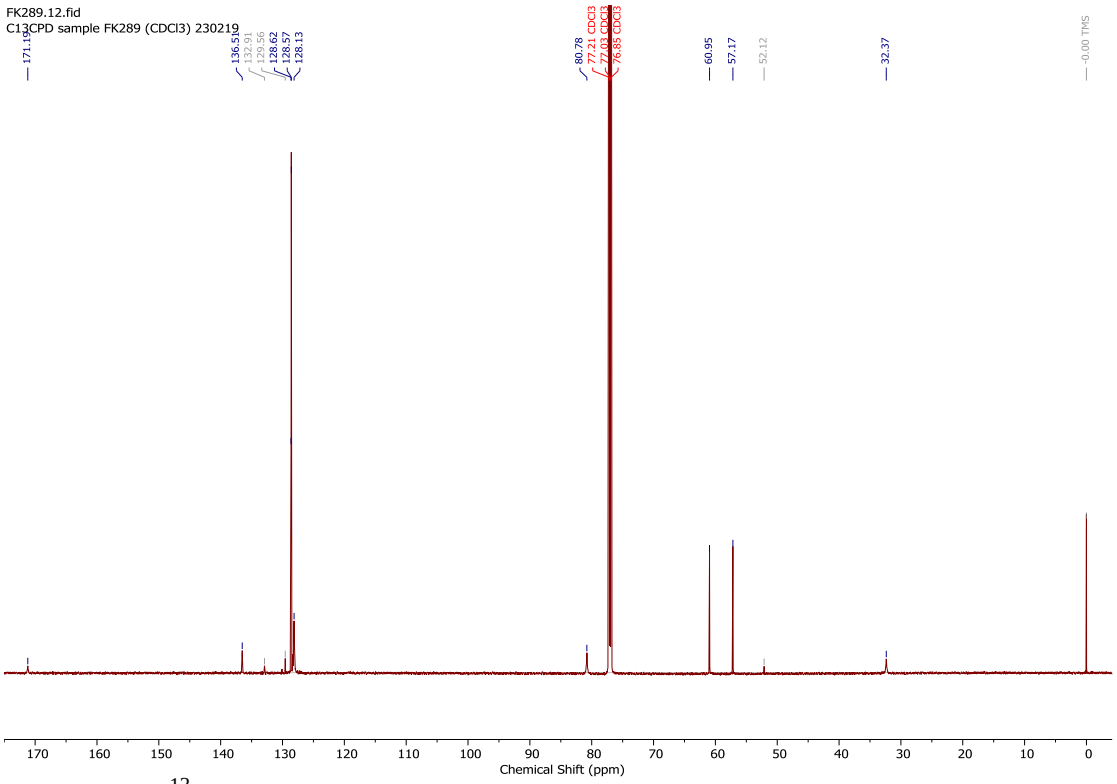


Figure S83. ^{13}C NMR spectrum of *N*-methoxy-*N*-methyl-2-methoxy-2-phenylacetamide (**210i**) ($CDCl_3$, 175 MHz)

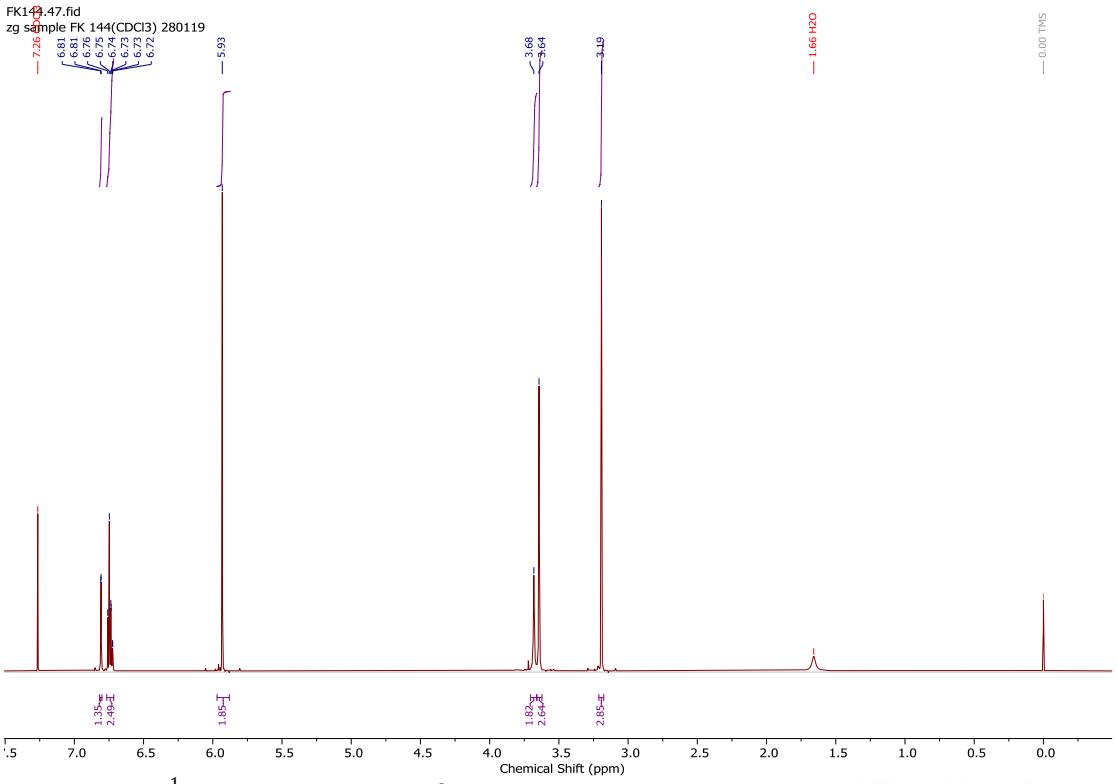


Figure S84. ^{1}H NMR spectrum of *N*-methoxy-*N*-methyl-2-(benzo[*d*][1,3]dioxol-5-yl)acetamide (**210j**) ($CDCl_3$, 700 MHz)

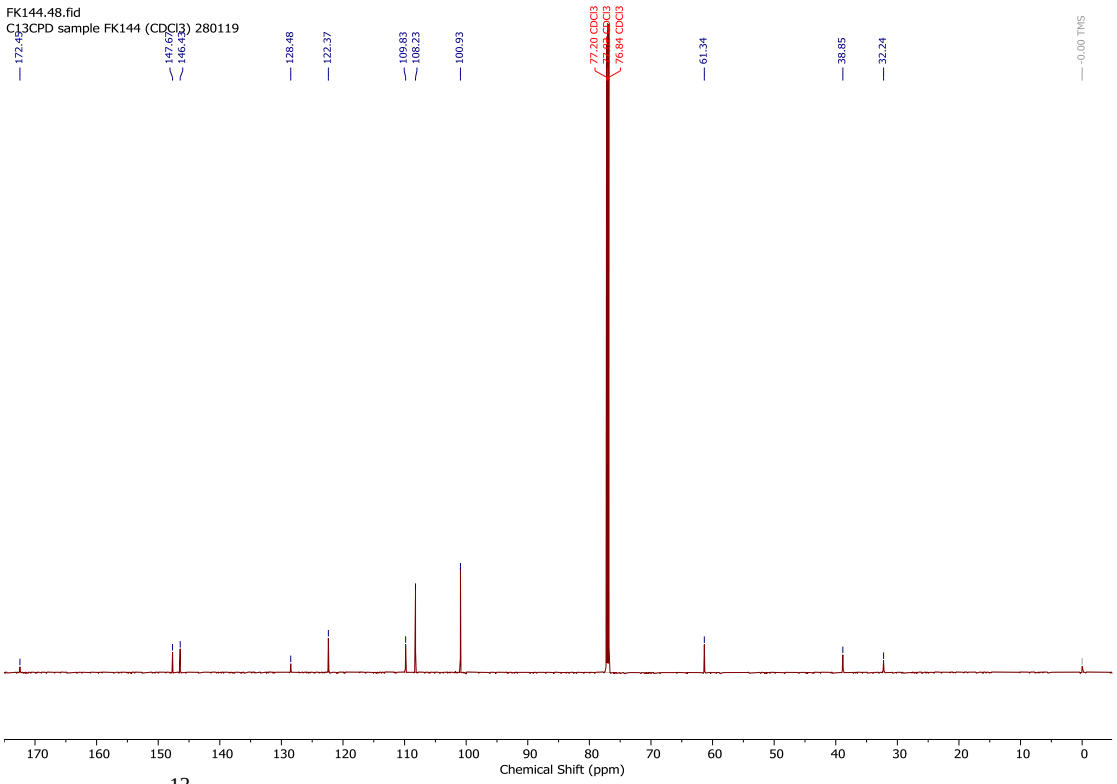


Figure S85. ^{13}C NMR spectrum of *N*-methoxy-*N*-methyl-2-(benzo[*d*][1,3]dioxol-5-yl)acetamide (**210j**) ($CDCl_3$, 175 MHz)

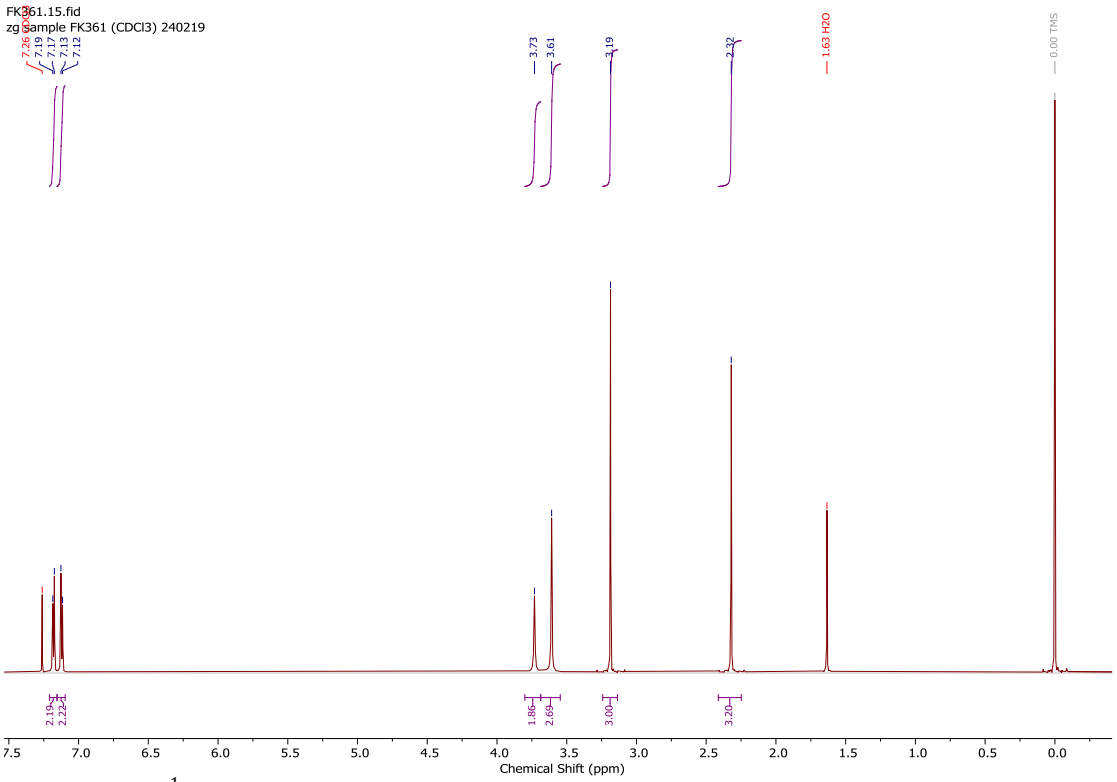


Figure S86. ^{1}H NMR spectrum of *N*-methoxy-*N*-methyl-2-(*p*-tolyl)acetamide (**210k**) ($CDCl_3$, 700 MHz)

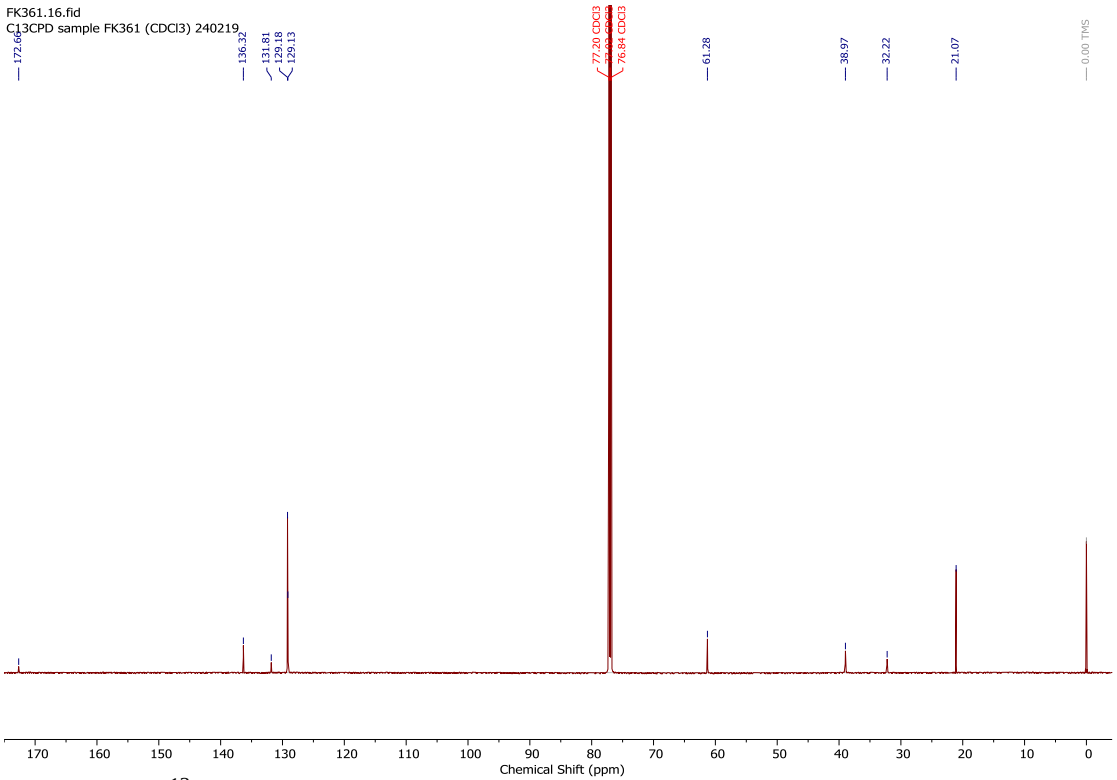


Figure S87. ^{13}C NMR spectrum of *N*-methoxy-*N*-methyl-2-(*p*-tolyl)acetamide (**210k**) ($CDCl_3$, 175 MHz)

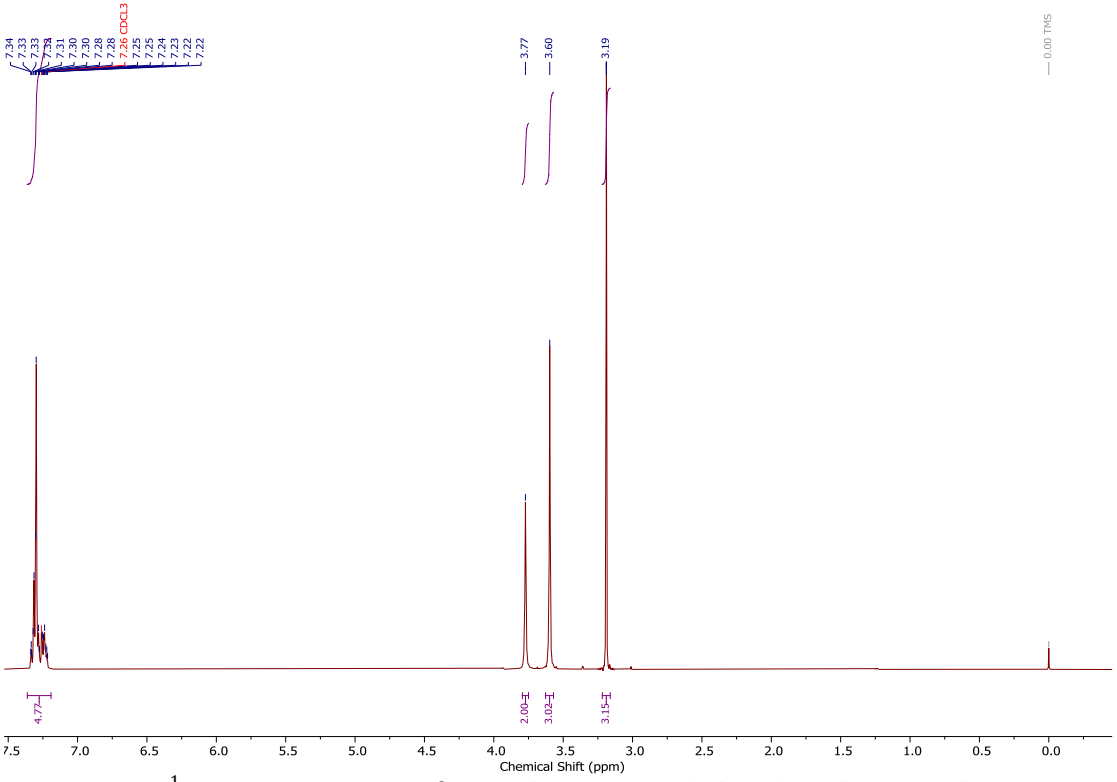


Figure S88. ^{1}H NMR spectrum of *N*-methoxy-*N*-methyl-2-phenylacetamide (**186**) ($CDCl_3$, 400 MHz)

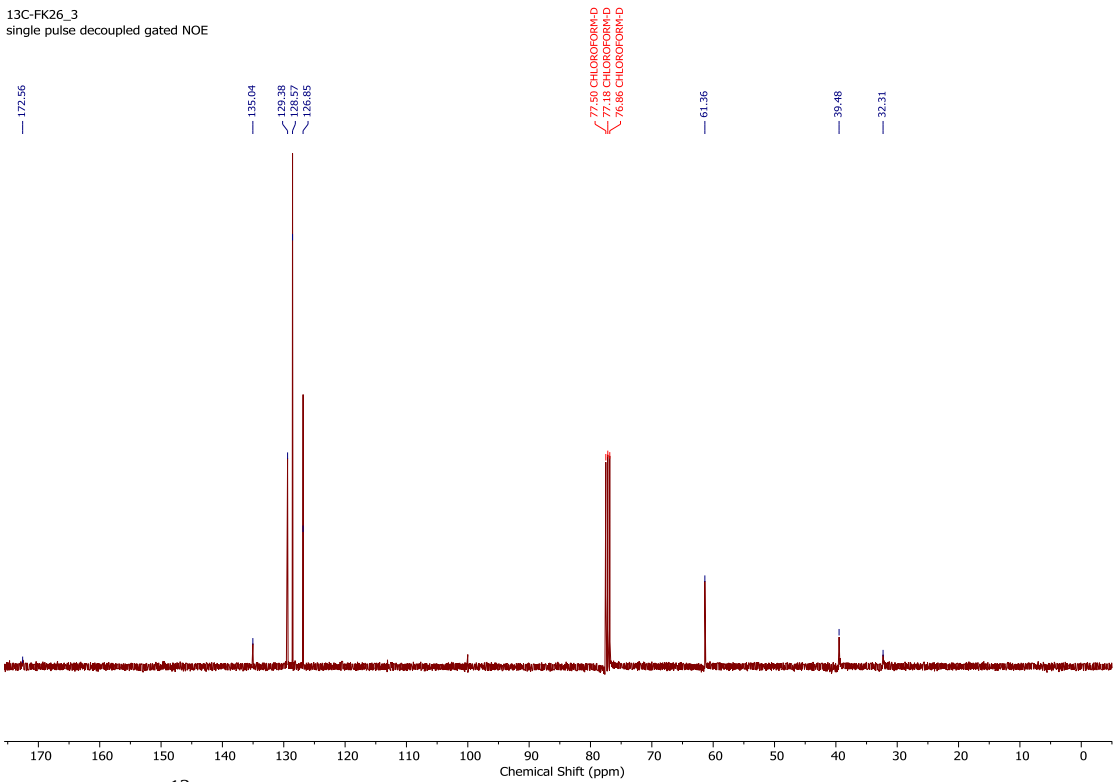


Figure S89. ^{13}C NMR spectrum of *N*-methoxy-*N*-methyl-2-phenylacetamide (**186**) ($CDCl_3$, 100 MHz)

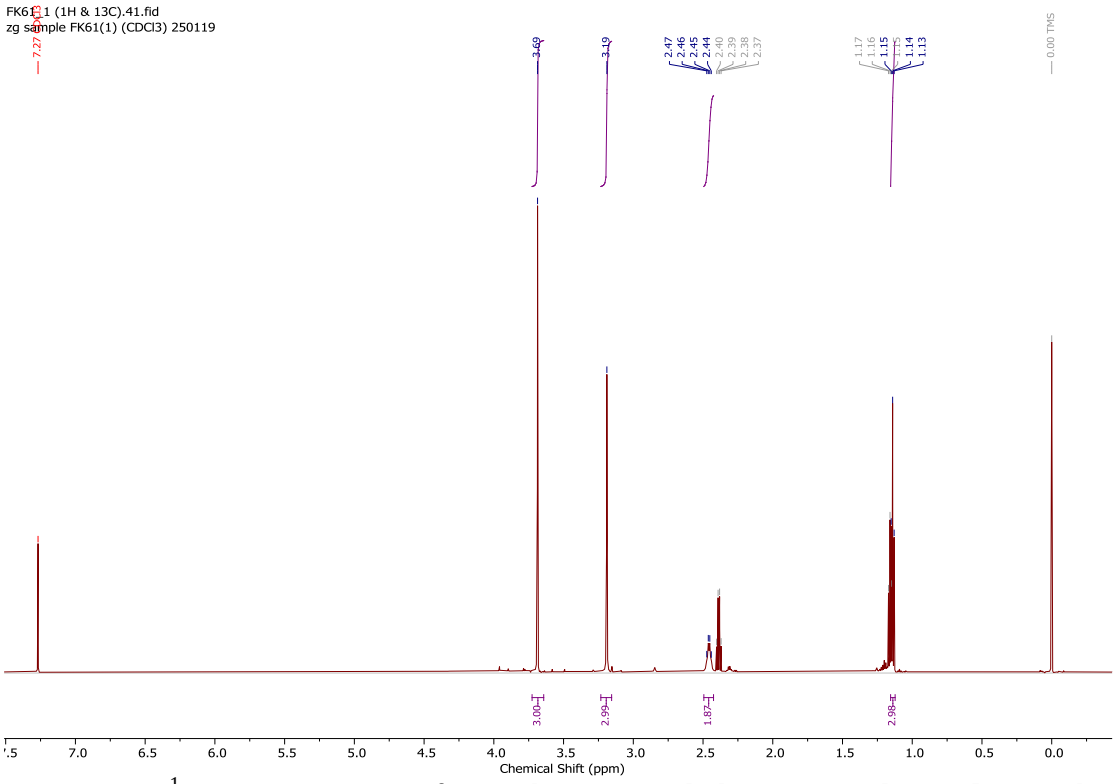


Figure S90. ^{1}H NMR spectrum of *N*-methoxy-*N*-methylpropionamide (**210l**) ($CDCl_3$, 700 MHz)

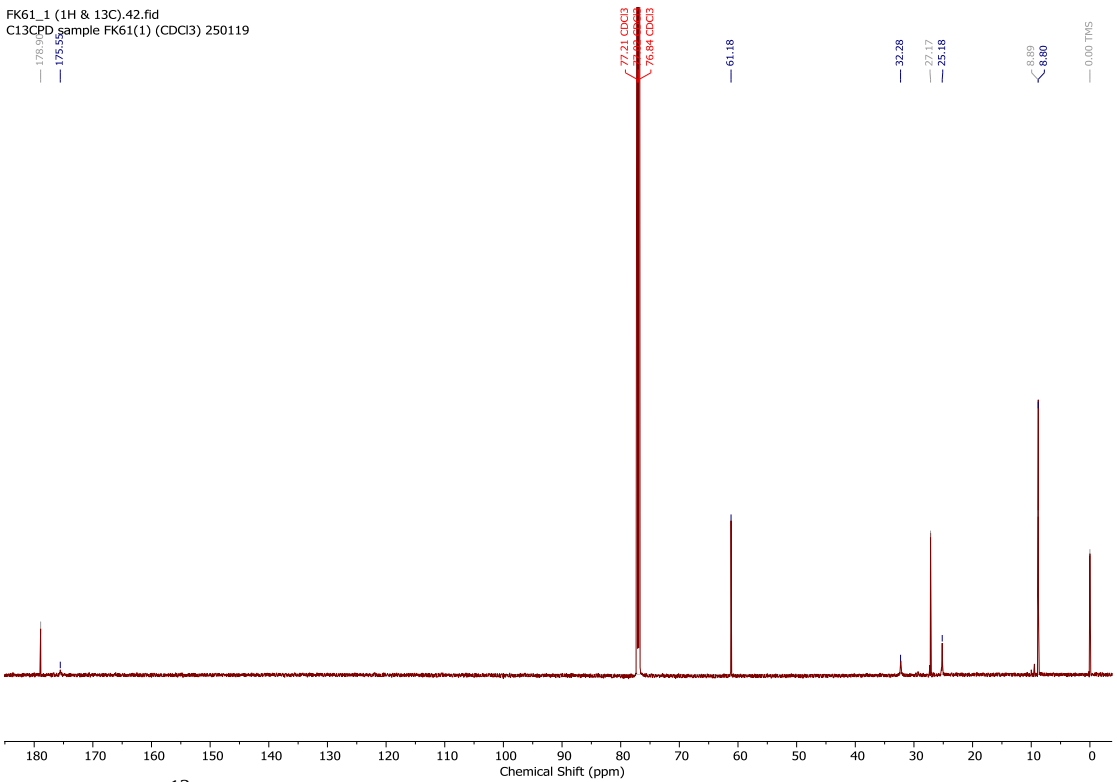


Figure S91. ^{13}C NMR spectrum of *N*-methoxy-*N*-methylpropionamide (**210l**) ($CDCl_3$, 175 MHz)

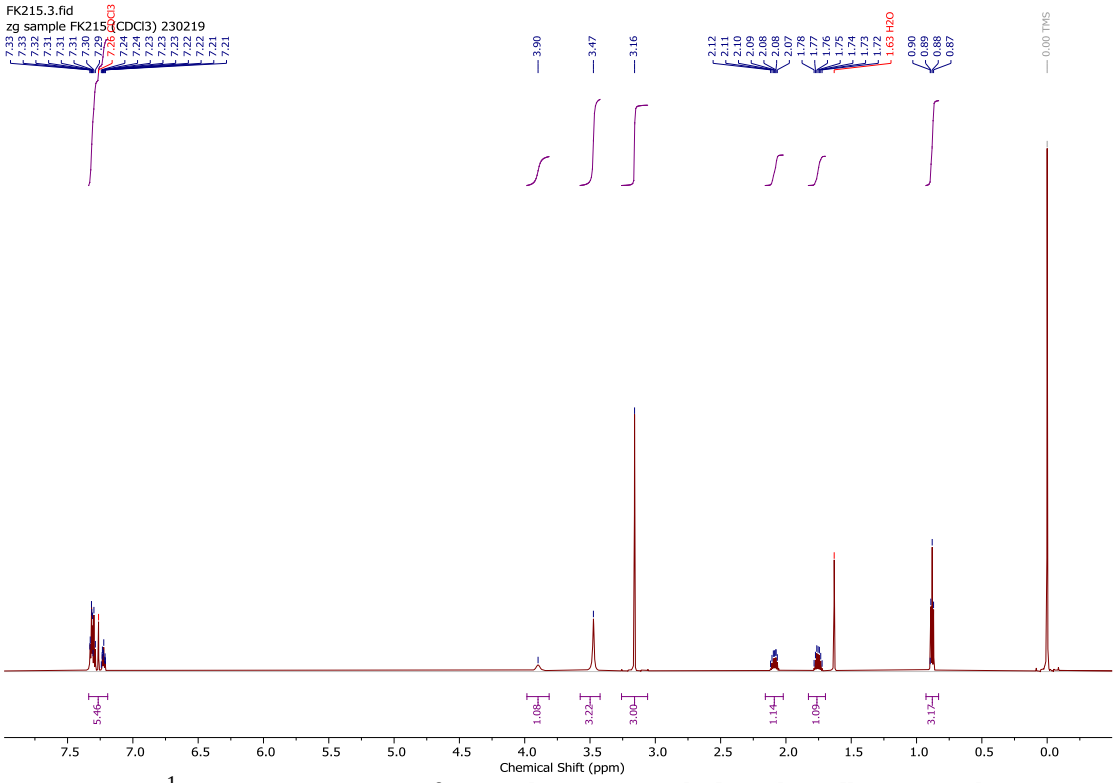


Figure S92. ^{1}H NMR spectrum of *N*-methoxy-*N*-methyl-2-phenylbutanamide (**210m**) ($CDCl_3$, 700 MHz)

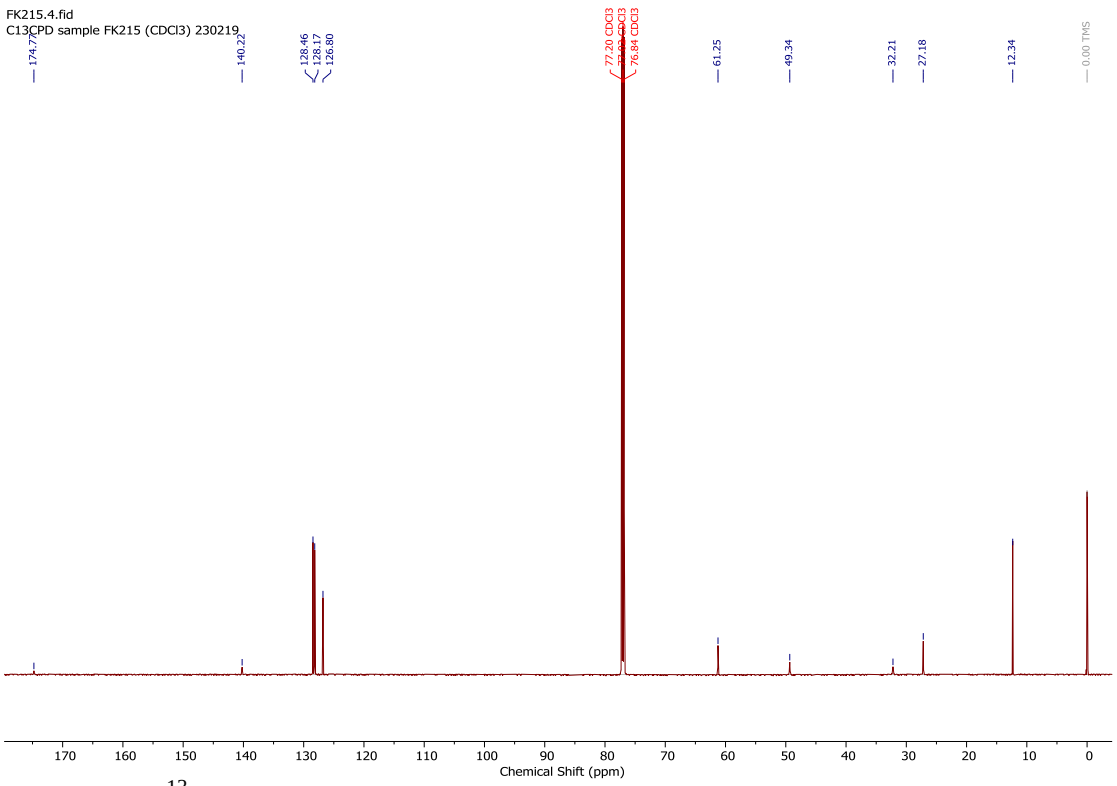


Figure S93. ^{13}C NMR spectrum of *N*-methoxy-*N*-methyl-2-phenylbutanamide (**210m**) ($CDCl_3$, 175 MHz)

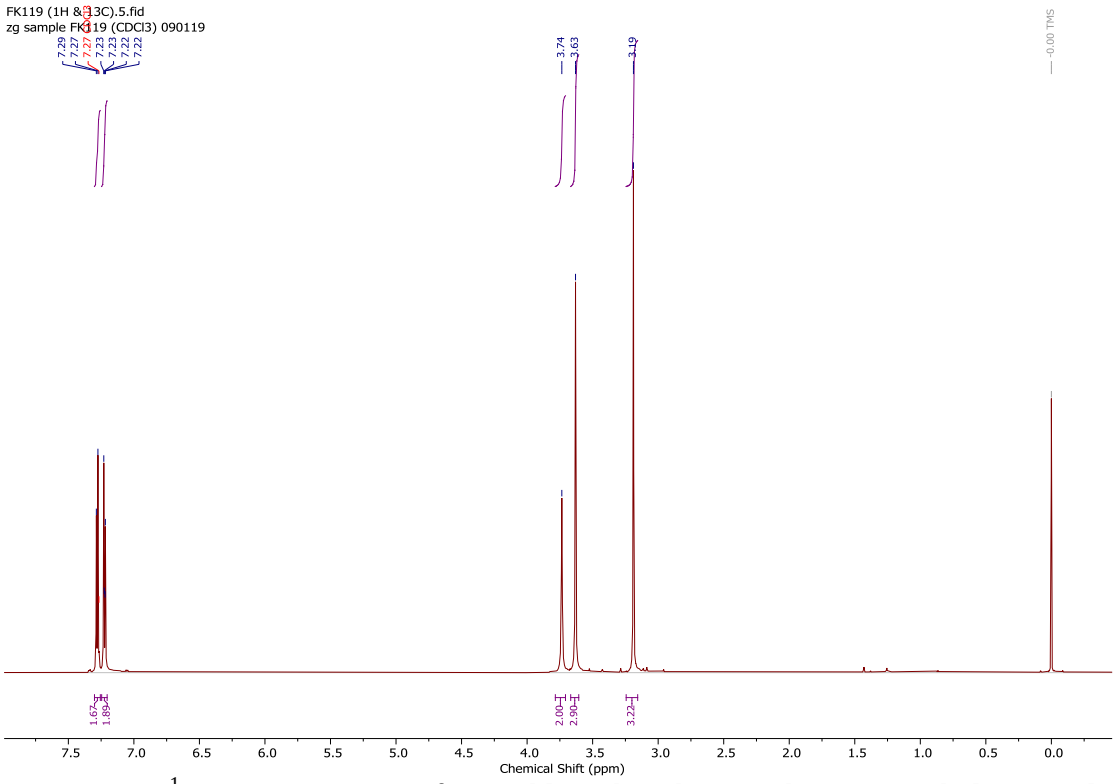


Figure S94. ^{1}H NMR spectrum of 2-(4-chlorophenyl)-*N*-methoxy-*N*-methylacetamide (**210n**) ($CDCl_3$, 700 MHz)

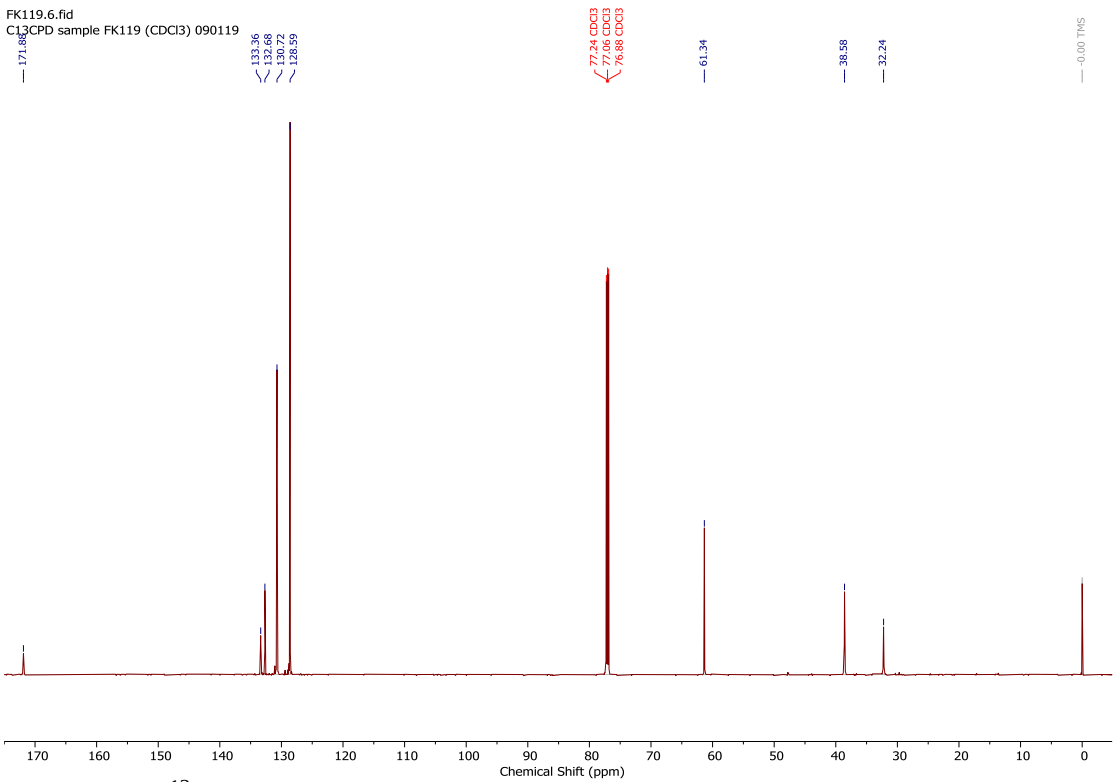


Figure S95. ^{13}C NMR spectrum of 2-(4-chlorophenyl)-*N*-methoxy-*N*-methylacetamide (**210n**) ($CDCl_3$, 175 MHz)

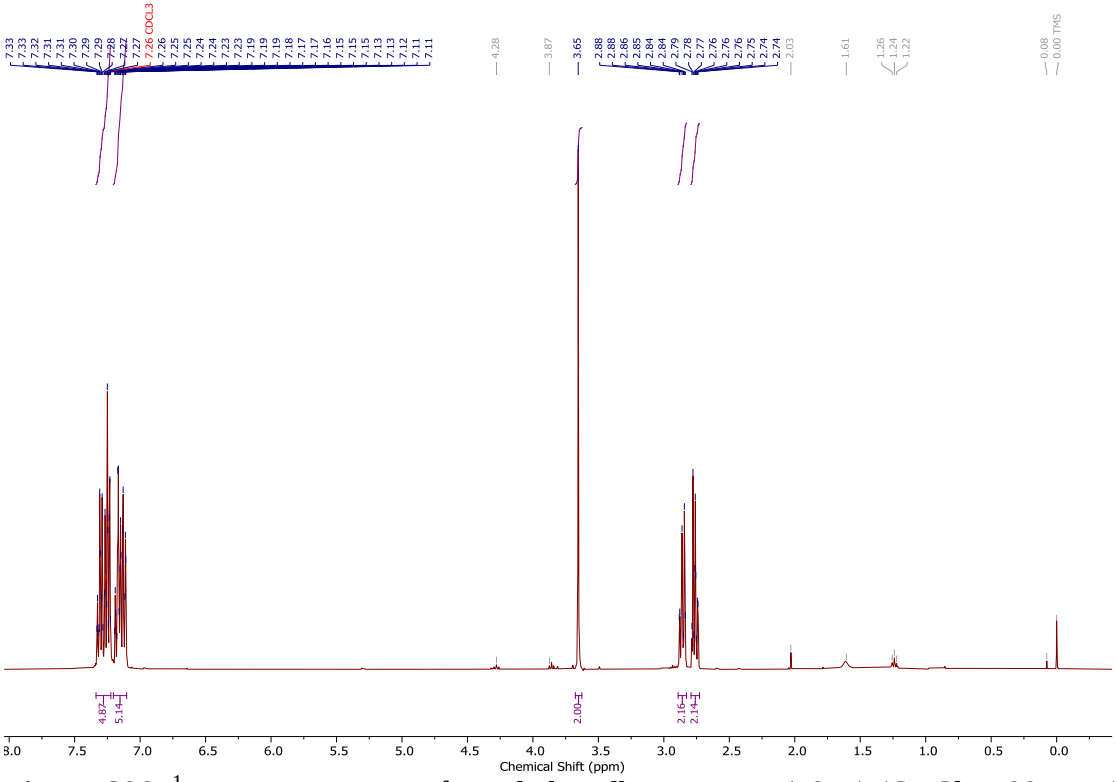


Figure S96. ^{1}H NMR spectrum of 1,4-diphenylbutan-2-one (**191a**) ($CDCl_3$, 400 MHz)

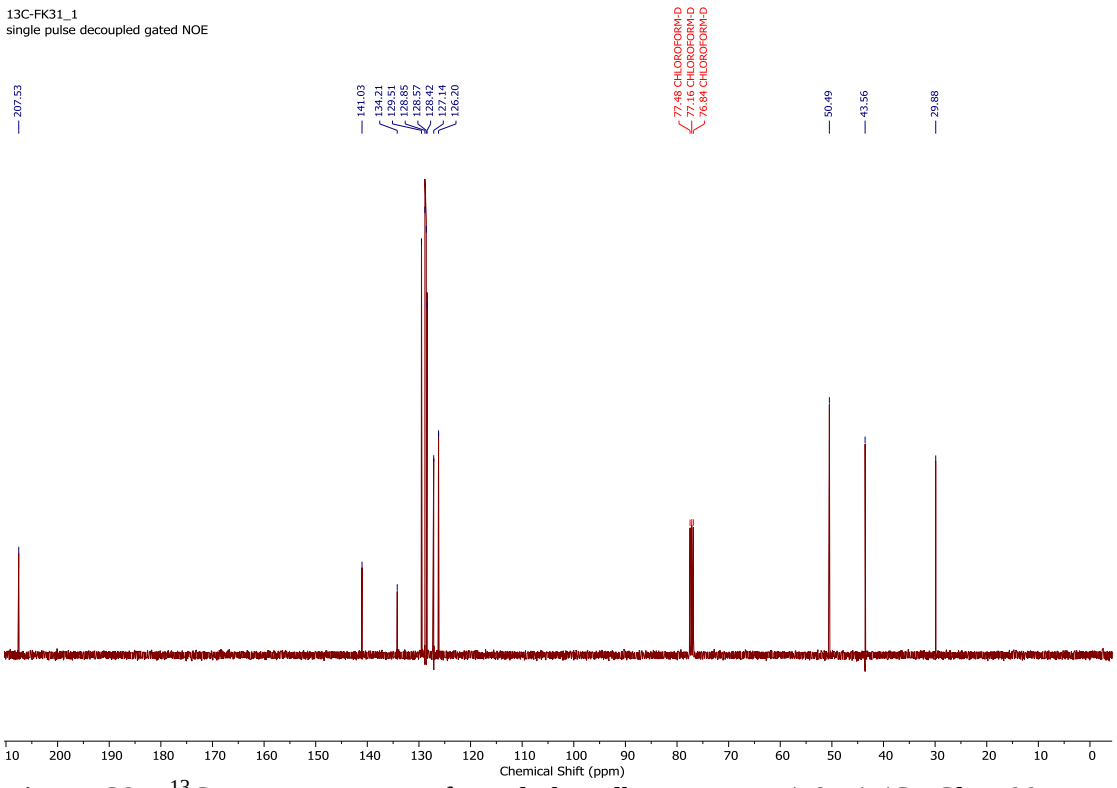


Figure S97. ^{13}C NMR spectrum of 1,4-diphenylbutan-2-one (**191a**) ($CDCl_3$, 100 MHz)

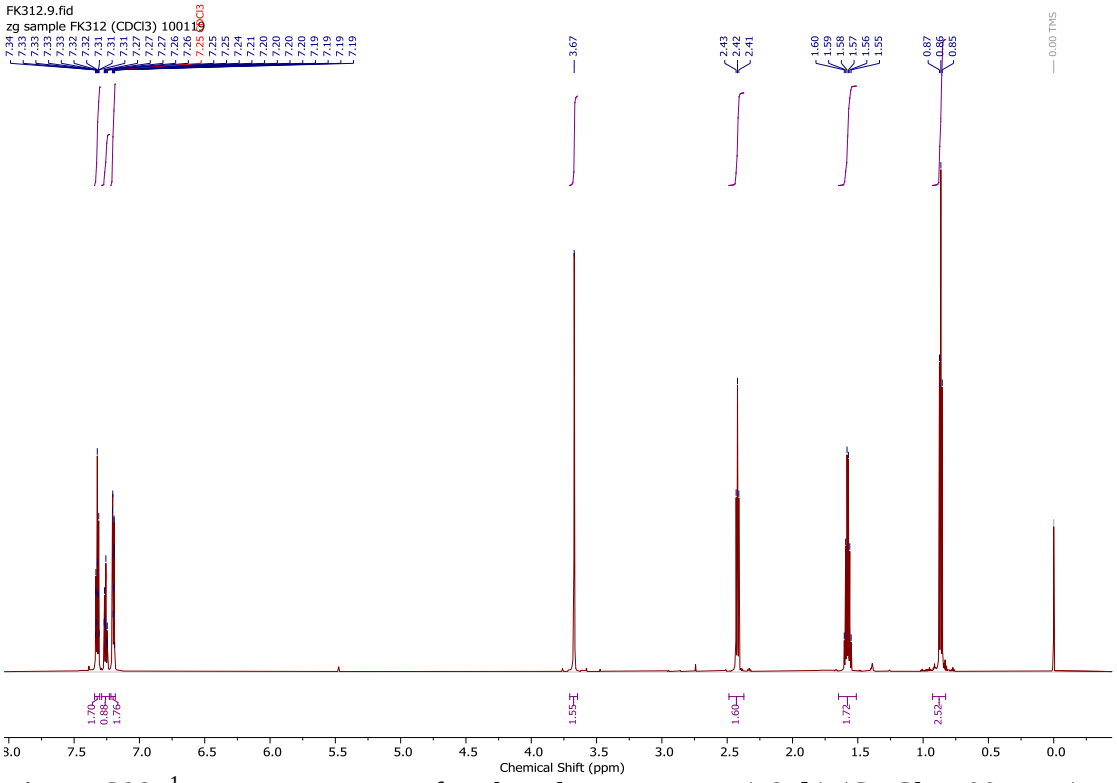


Figure S98. ^{1}H NMR spectrum of 1-phenylpentan-2-one (**191b**) ($CDCl_3$, 700 MHz)

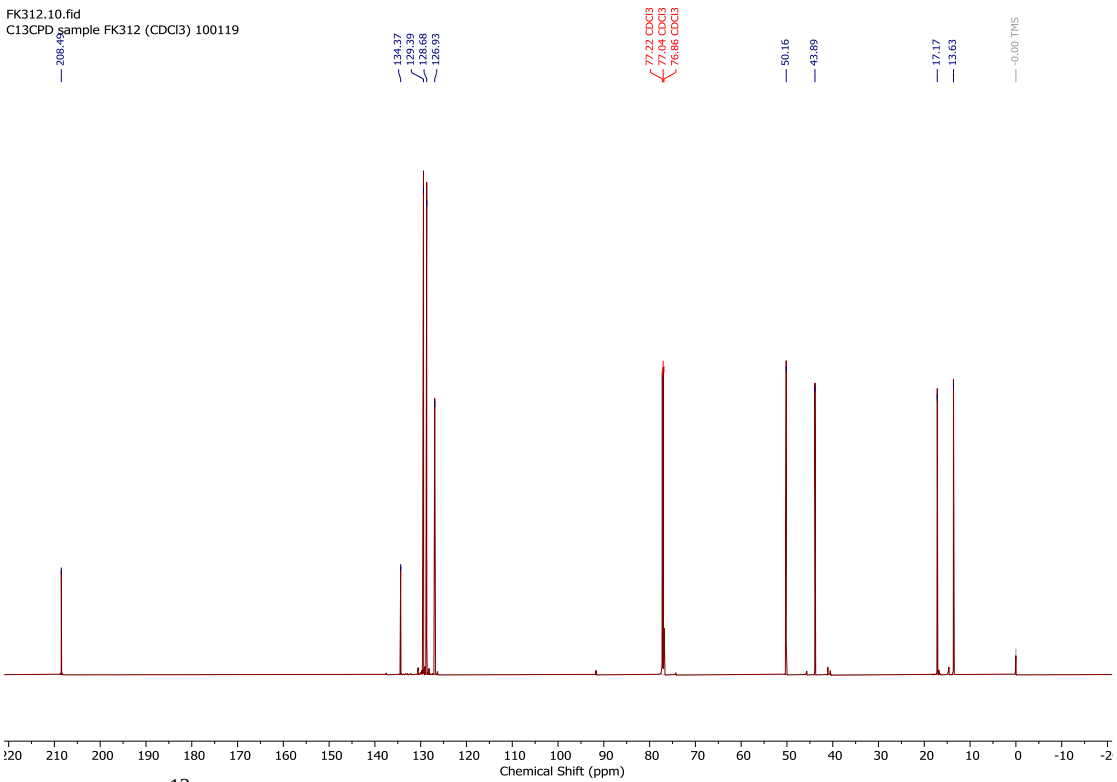


Figure S99. ^{13}C NMR spectrum of 1-phenylpentan-2-one (**191b**) ($CDCl_3$, 175 MHz)

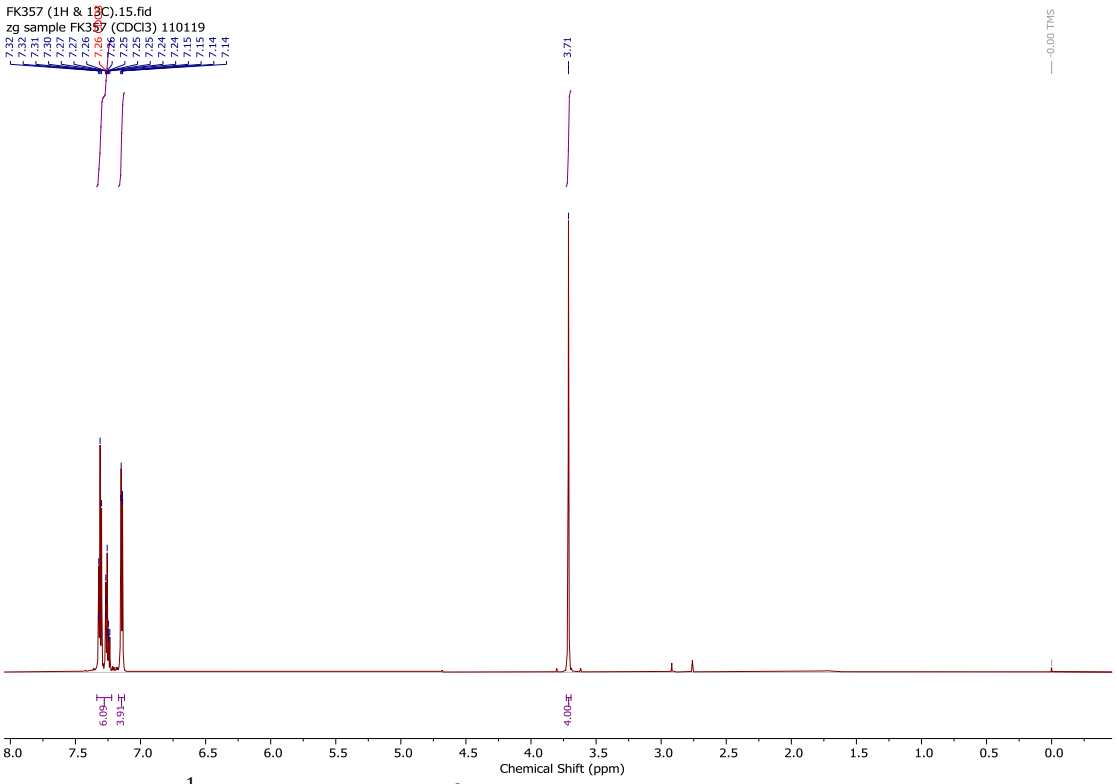


Figure S100. ^{1}H NMR spectrum of 1,3-diphenylpropan-2-one (**191c**) ($CDCl_3$, 700 MHz)

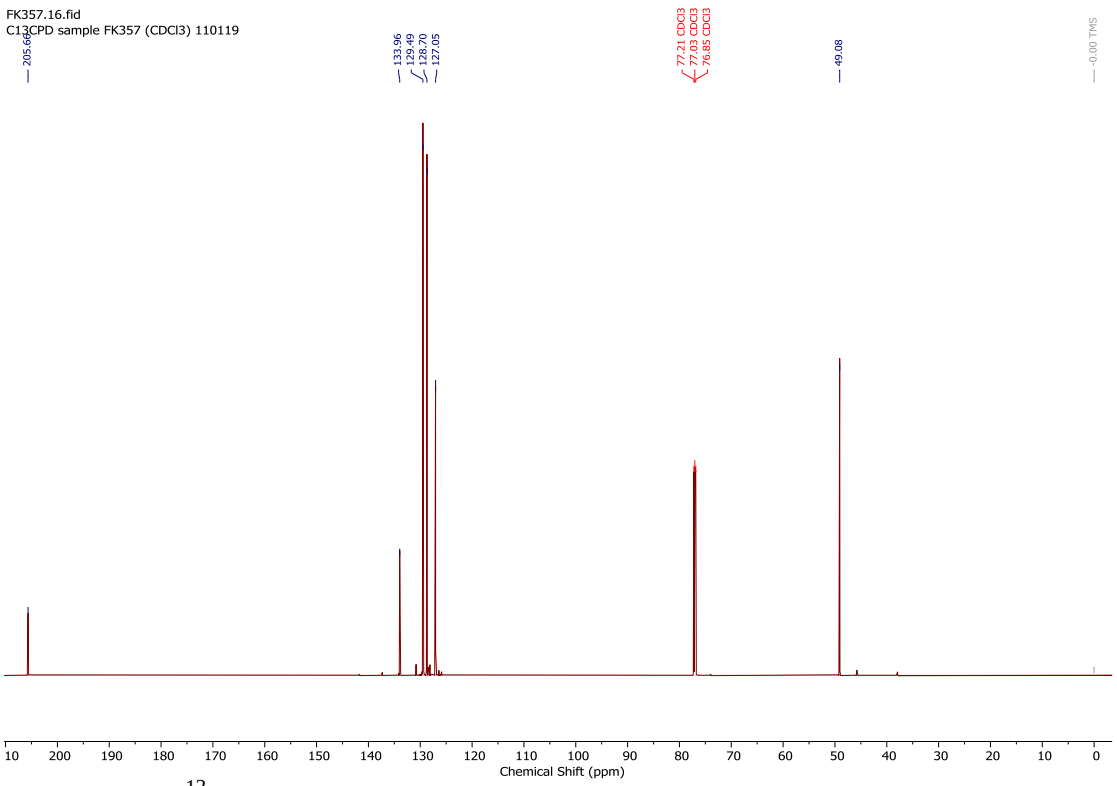


Figure S101. ^{13}C NMR spectrum of 1,3-diphenylpropan-2-one (**191c**) ($CDCl_3$, 175 MHz)

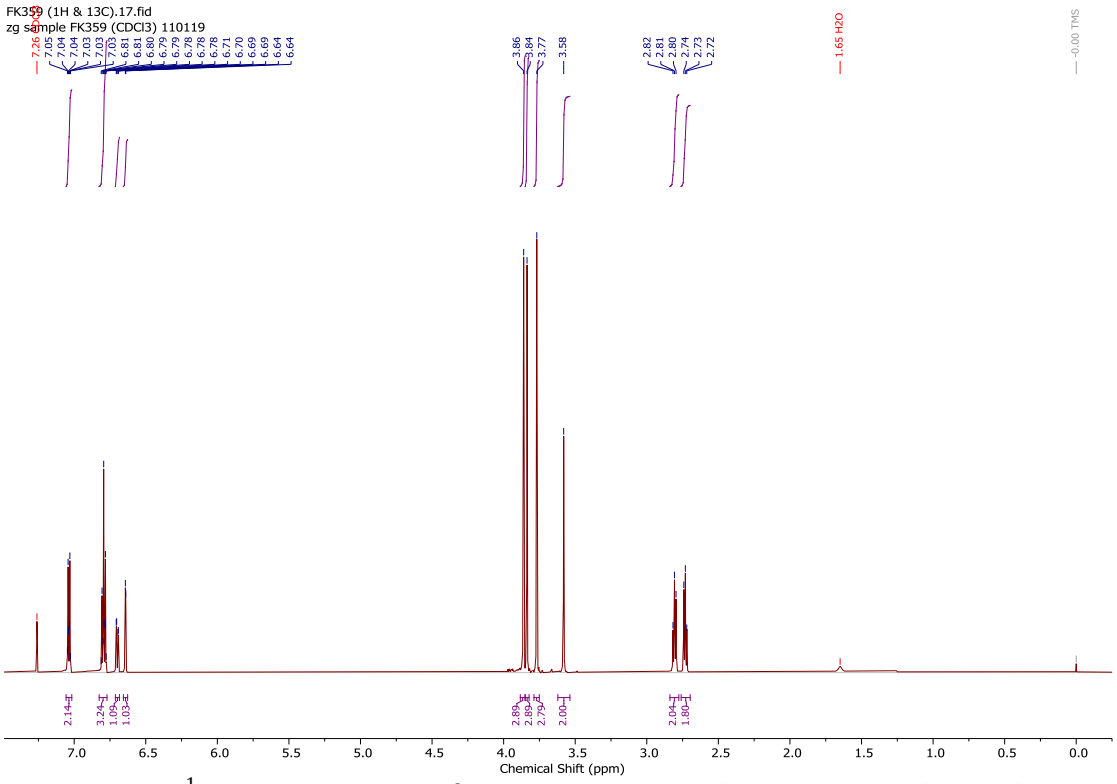


Figure S102. ^{1}H NMR spectrum of 1-(3,4-dimethoxy-phenyl)-4-(4-methoxy-phenyl)-butan-2-one (**191d**) ($CDCl_3$, 700 MHz)

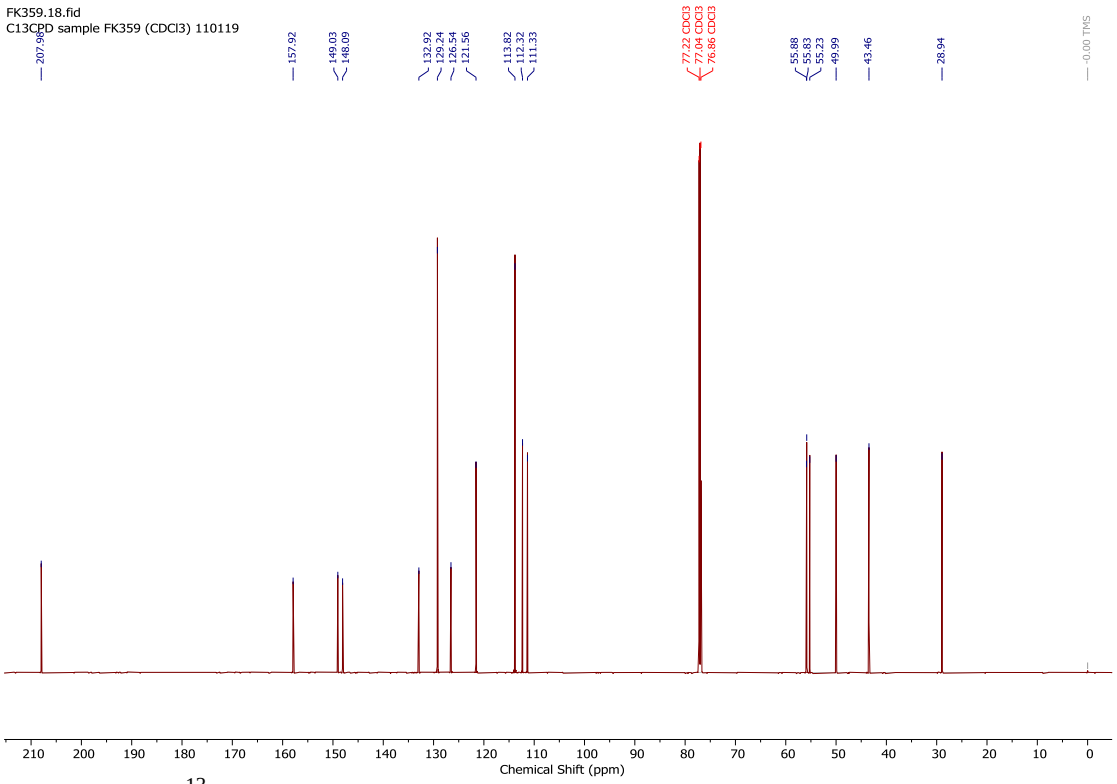


Figure S103. ^{13}C NMR spectrum of 1-(3,4-dimethoxy-phenyl)-4-(4-methoxy-phenyl)-butan-2-one (**191d**) ($CDCl_3$, 175 MHz)

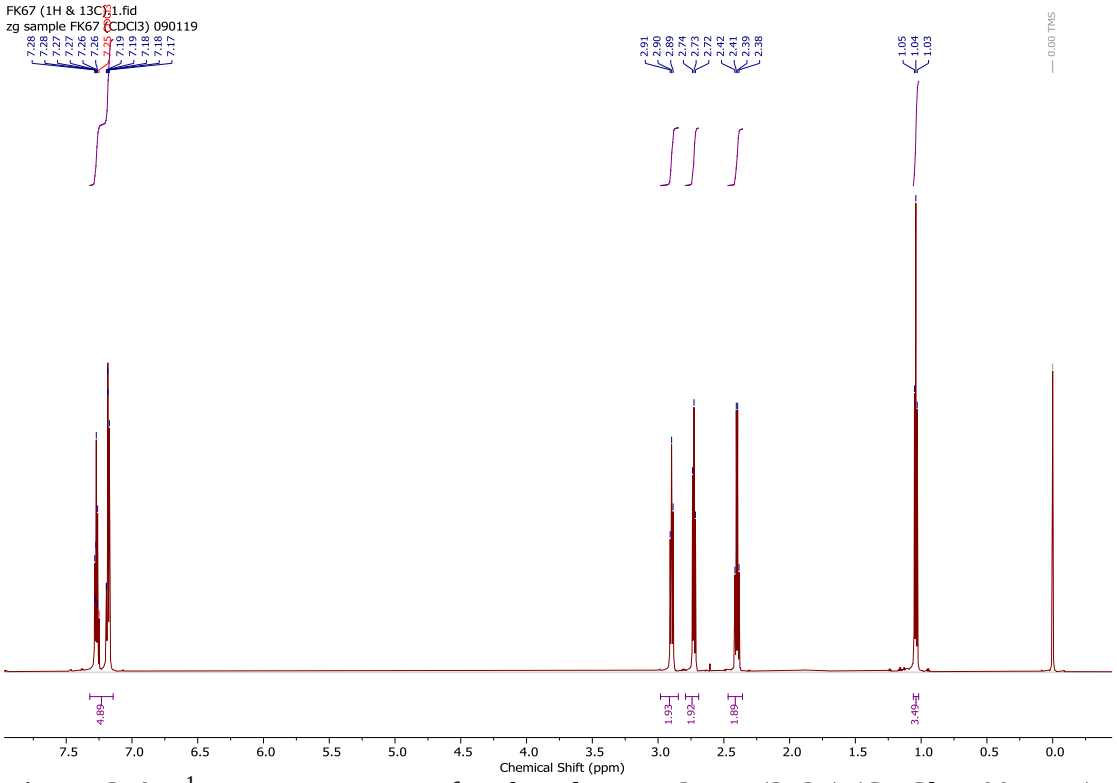


Figure S104. ^{1}H NMR spectrum of 1-phenylpentan-3-one (**212a**) ($CDCl_3$, 700 MHz)

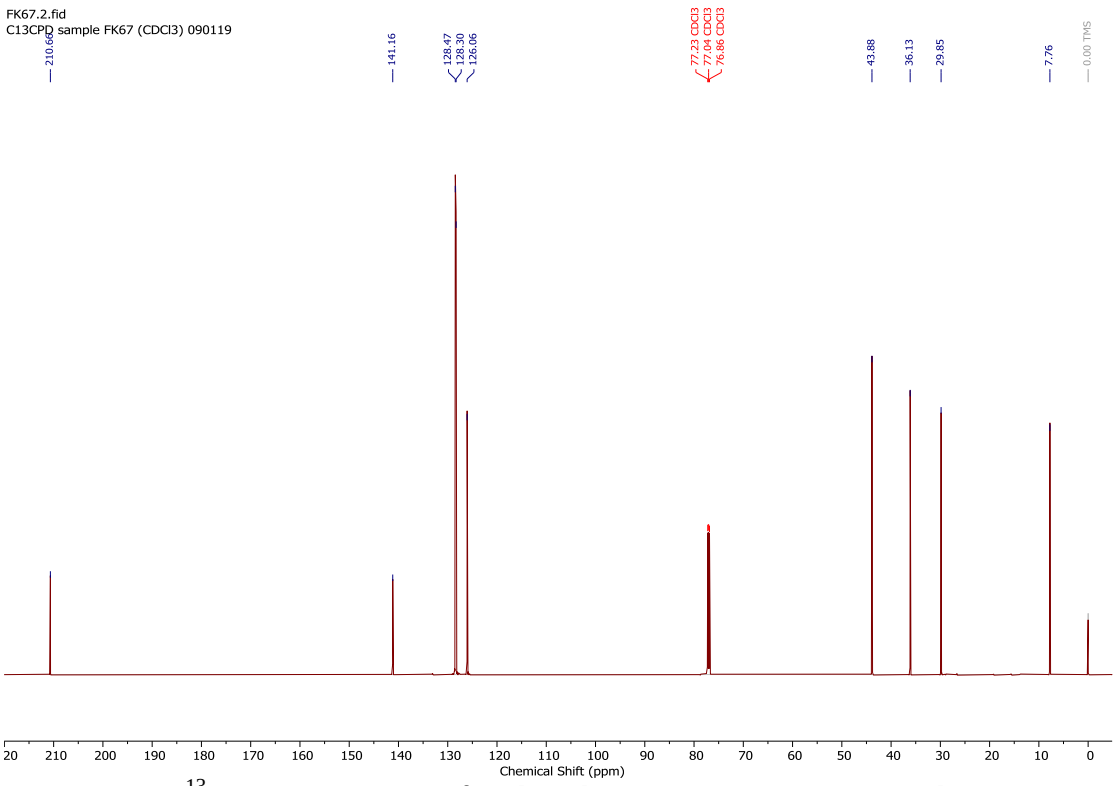


Figure S105. ^{13}C NMR spectrum of 1-phenylpentan-3-one (**212a**) ($CDCl_3$, 175 MHz)

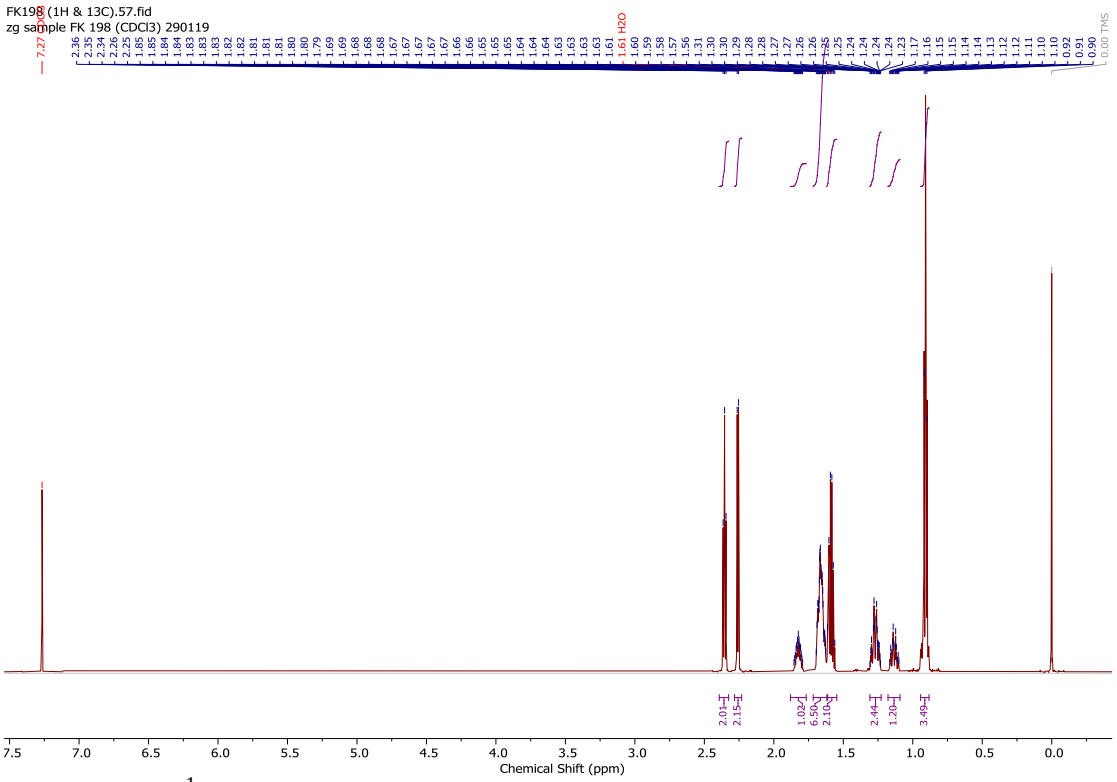


Figure S106. ^{1}H NMR spectrum of 1-cyclohexylpentan-2-one (**212b**) ($CDCl_3$, 700 MHz)

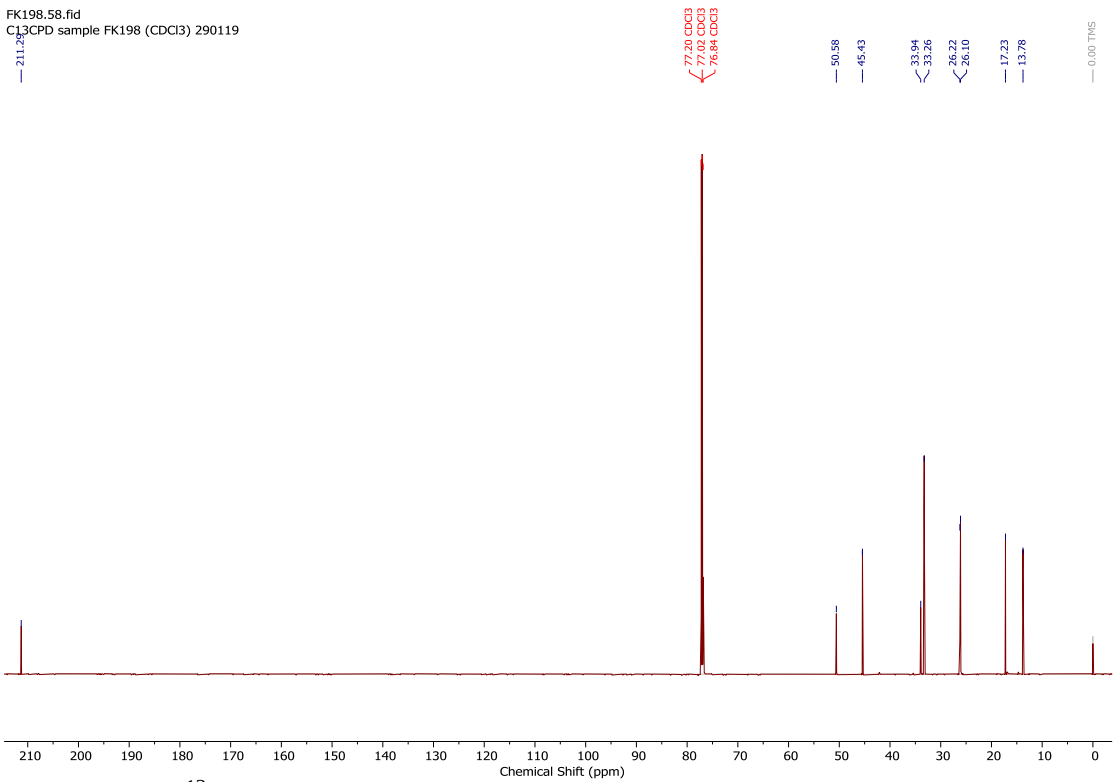


Figure S107. ^{13}C NMR spectrum of 1-cyclohexylpentan-2-one (**212b**) ($CDCl_3$, 175 MHz)

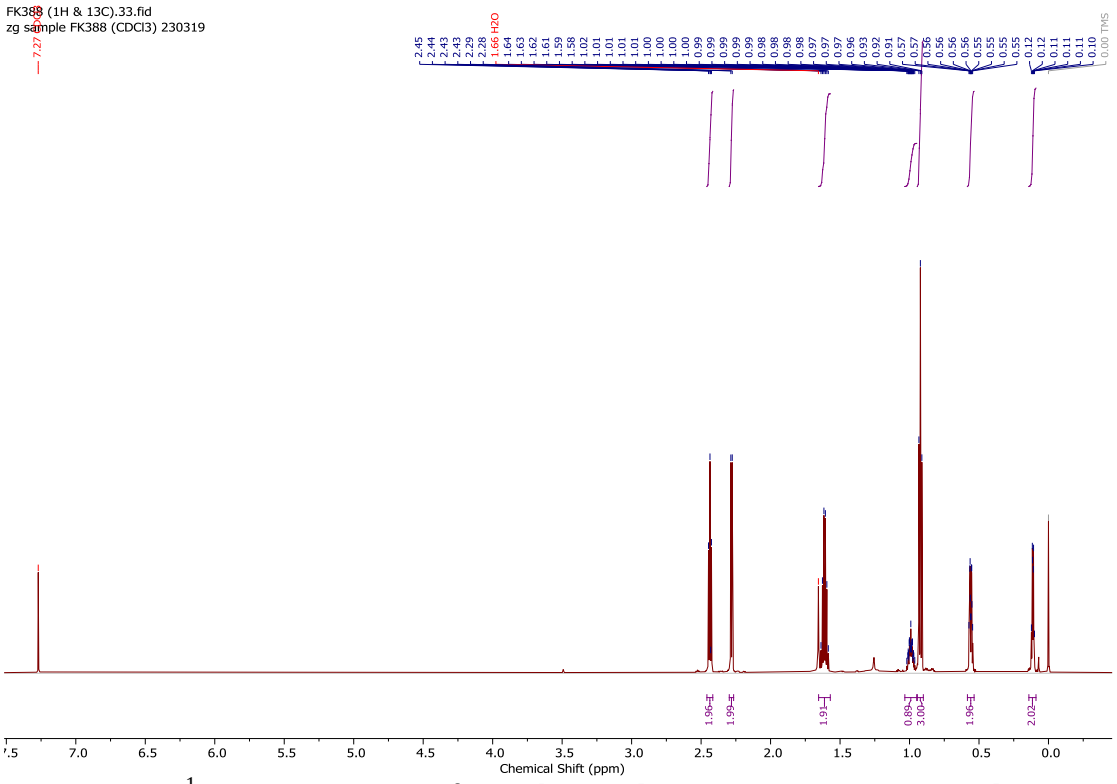


Figure S108. ^{1}H NMR spectrum of 1-cyclopropylpentan-2-one (**212c**) ($CDCl_3$, 700 MHz)

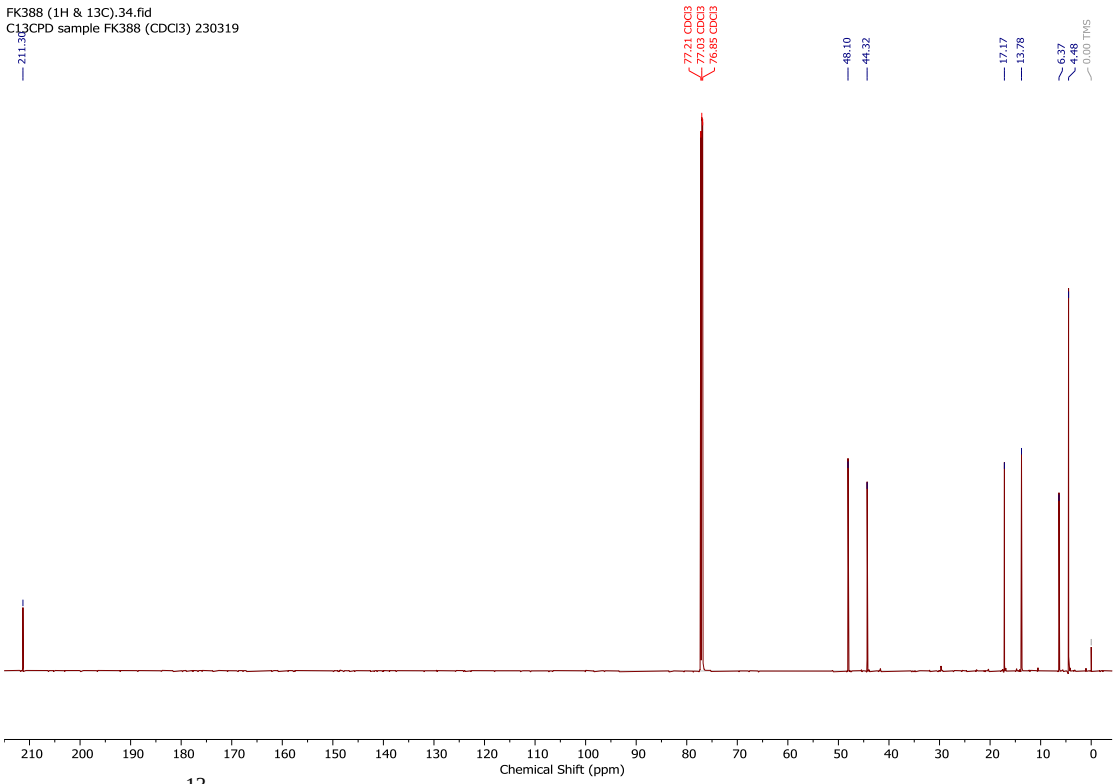


Figure S109. ^{13}C NMR spectrum of 1-cyclopropylpentan-2-one (**212c**) ($CDCl_3$, 175 MHz)

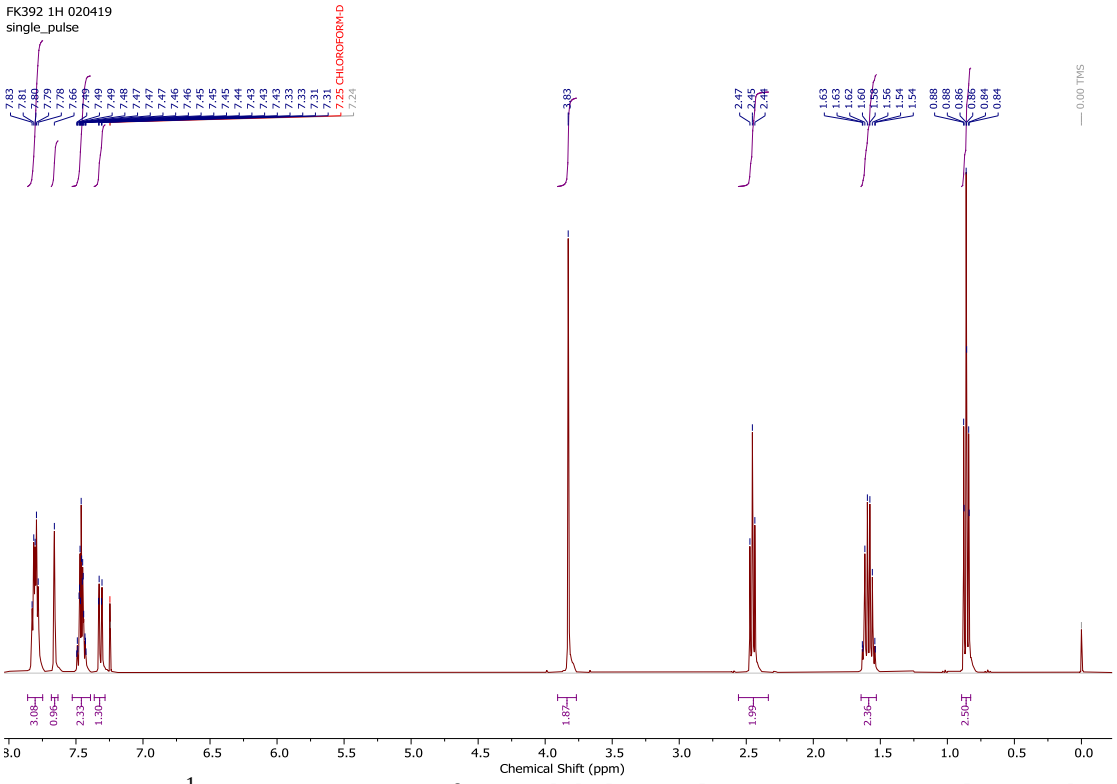


Figure S110. ^{1}H NMR spectrum of 1-(naphthalen-2-yl)pentan-2-one (**212d**) ($CDCl_3$, 400 MHz)

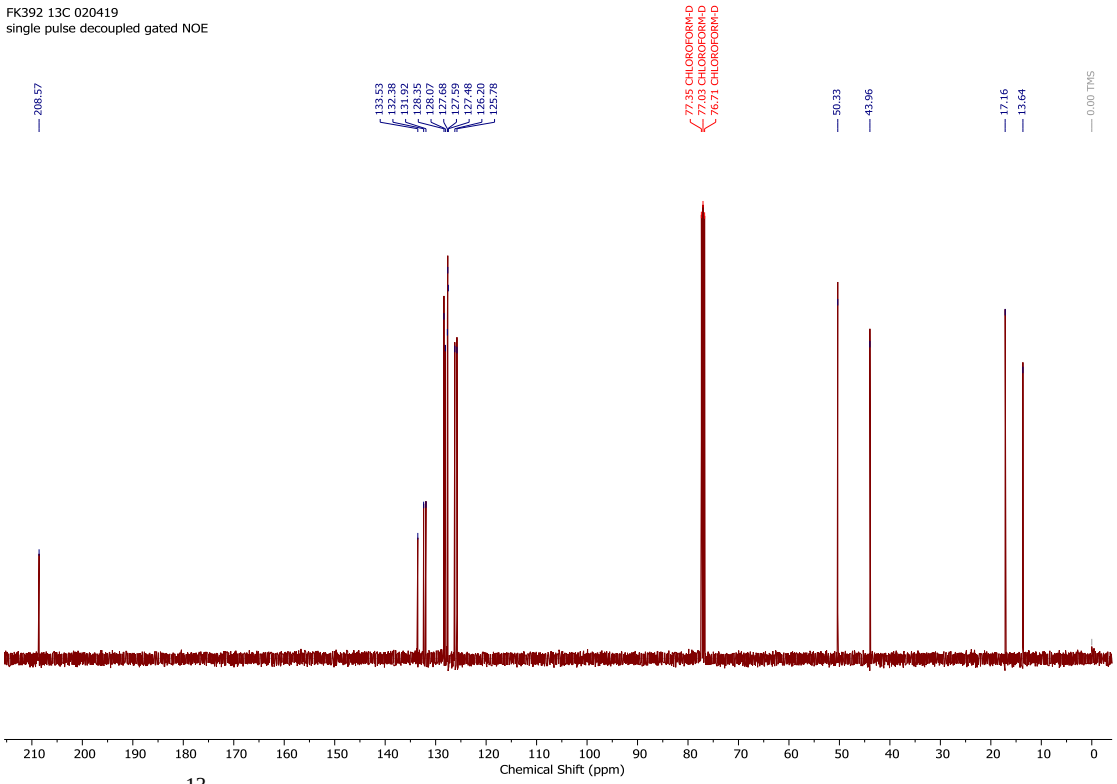


Figure S111. ^{13}C NMR spectrum of 1-(naphthalen-2-yl)pentan-2-one (**212d**) ($CDCl_3$, 100 MHz)

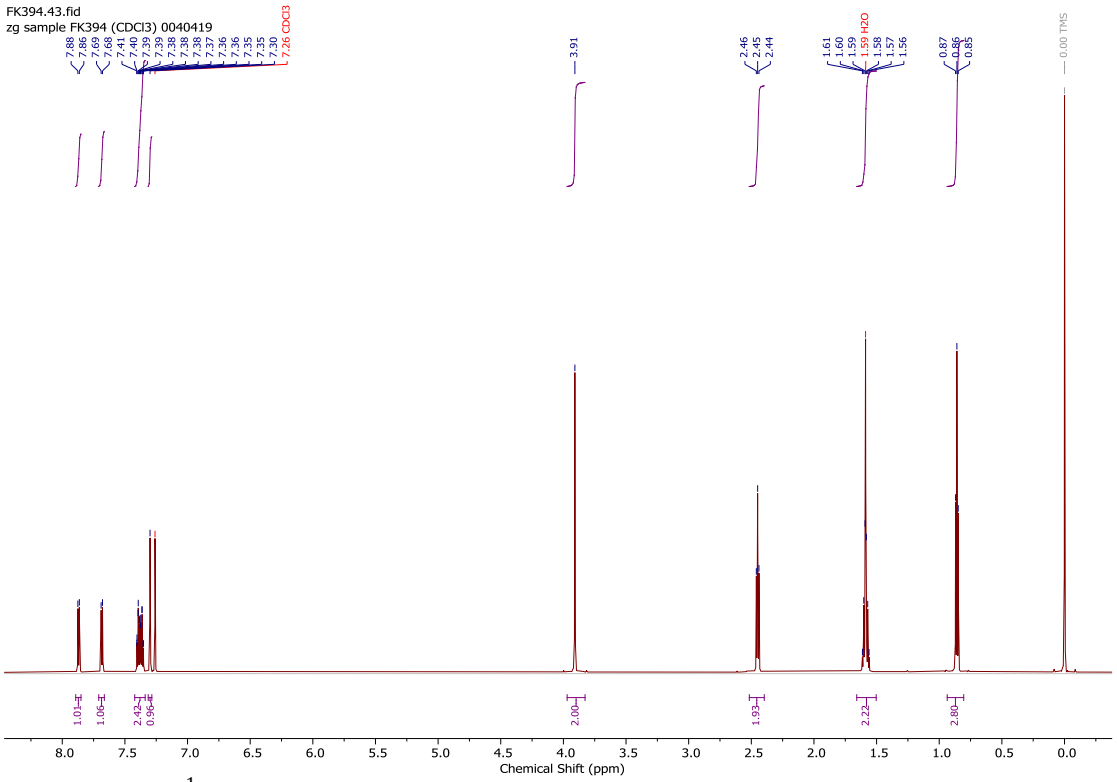


Figure S112. ^{1}H NMR spectrum of 1-(benzo[*b*]thiophen-3-yl)pentan-2-one (**212e**) ($CDCl_3$, 700 MHz)

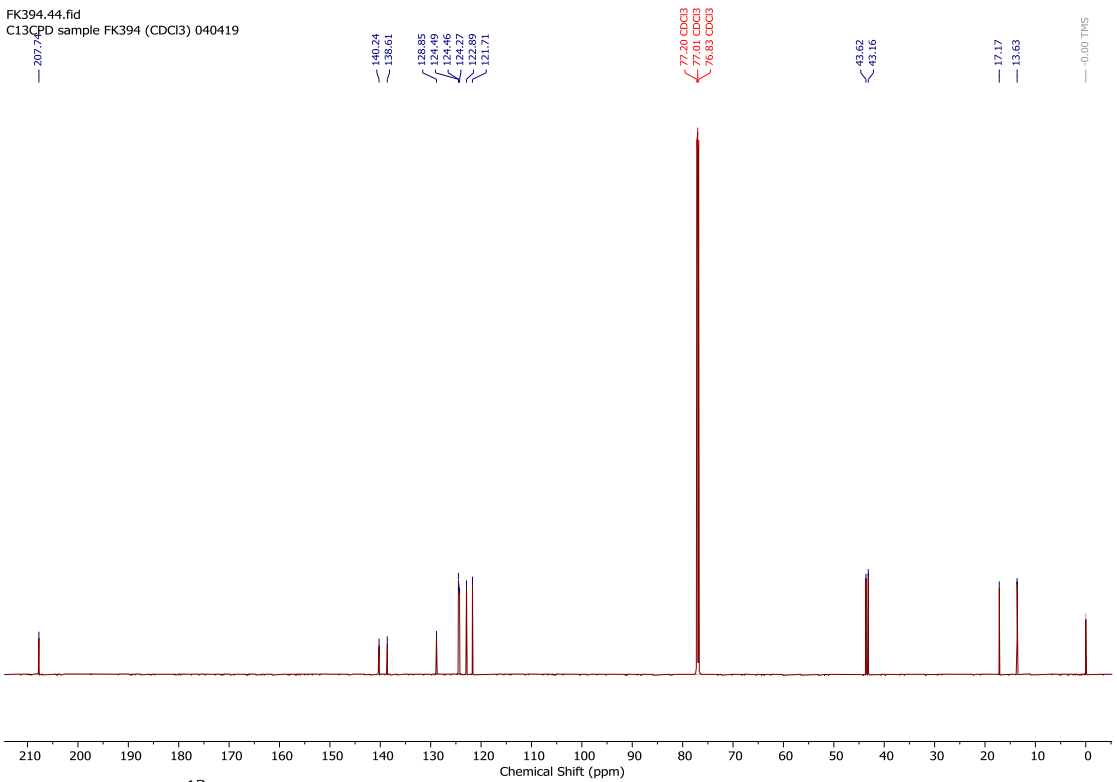


Figure S113. ^{13}C NMR spectrum of 1-(benzo[*b*]thiophen-3-yl)pentan-2-one (**212e**) ($CDCl_3$, 175 MHz)

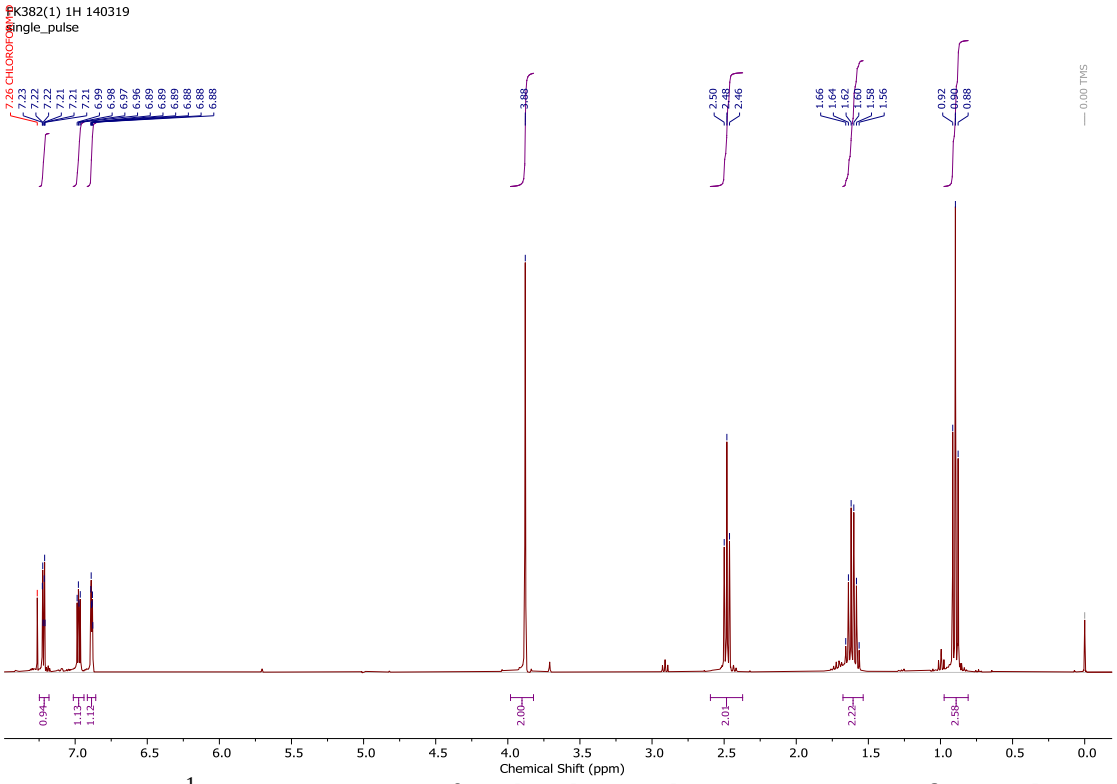


Figure S114. ^{1}H NMR spectrum of 1-(thiophen-2-yl)pentan-2-one (**212f**) ($CDCl_3$, 400 MHz)

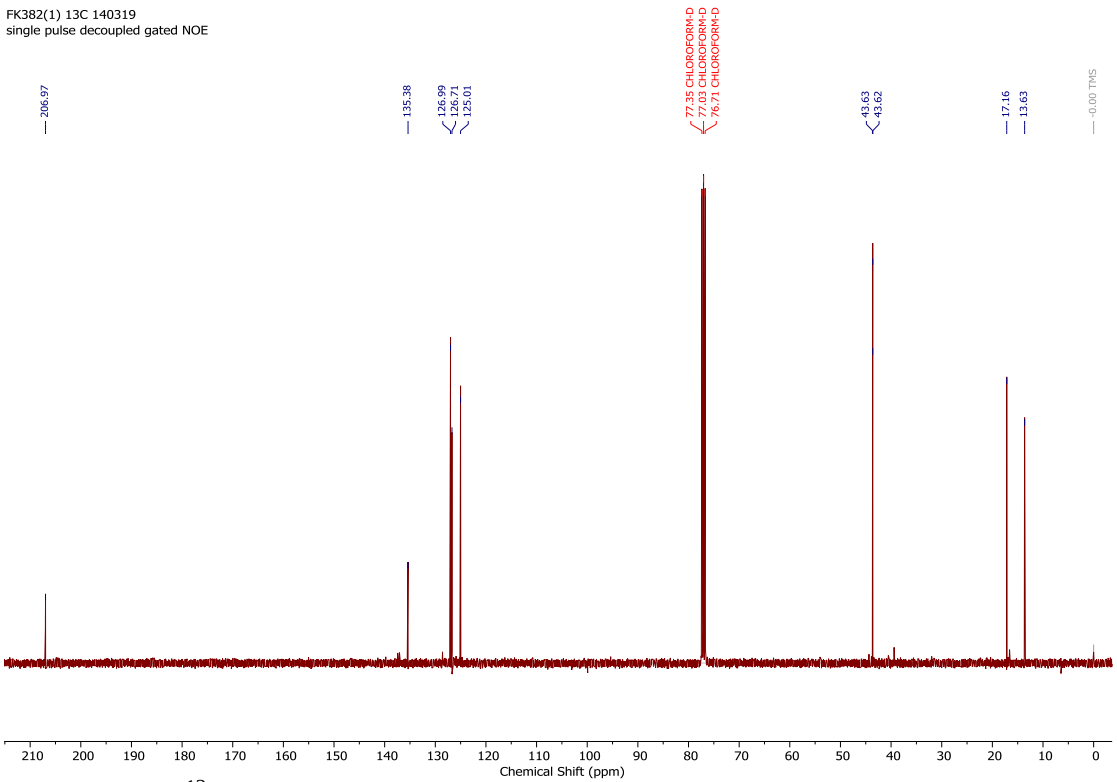


Figure S115. ^{13}C NMR spectrum of 1-(thiophen-2-yl)pentan-2-one (**212f**) ($CDCl_3$, 100 MHz)

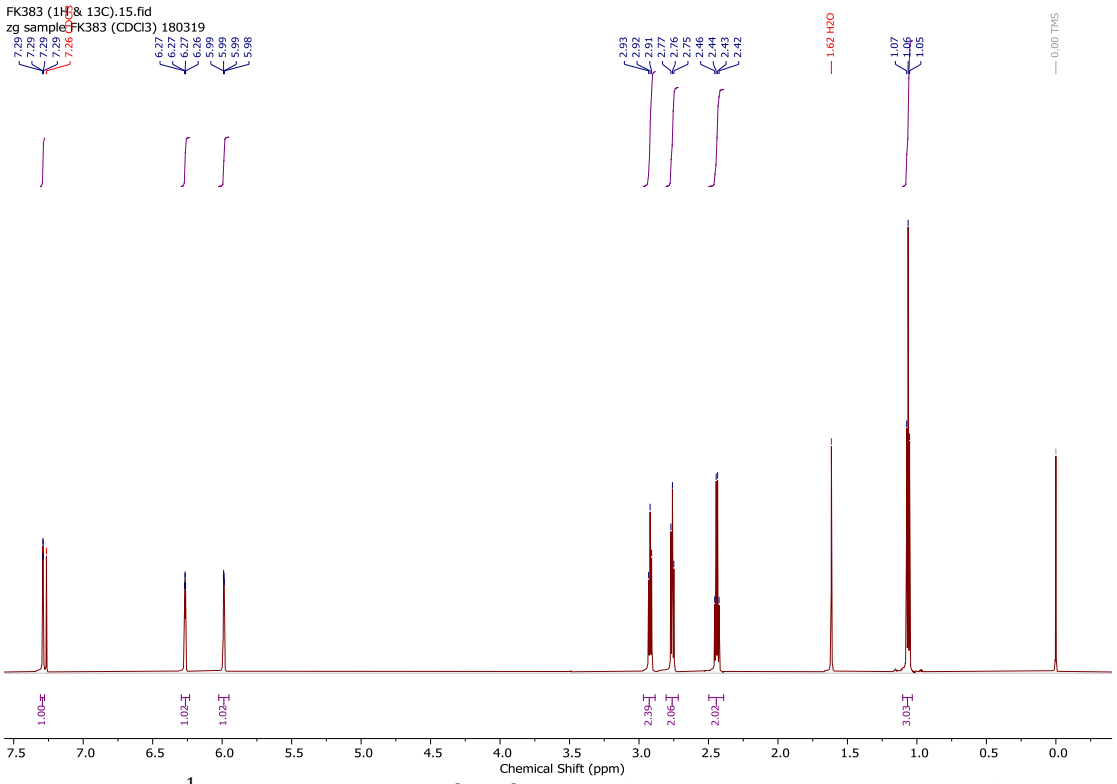


Figure S116. ^{1}H NMR spectrum of 1-(furan-2-yl)pentan-3-one (**212g**) ($CDCl_3$, 700 MHz)

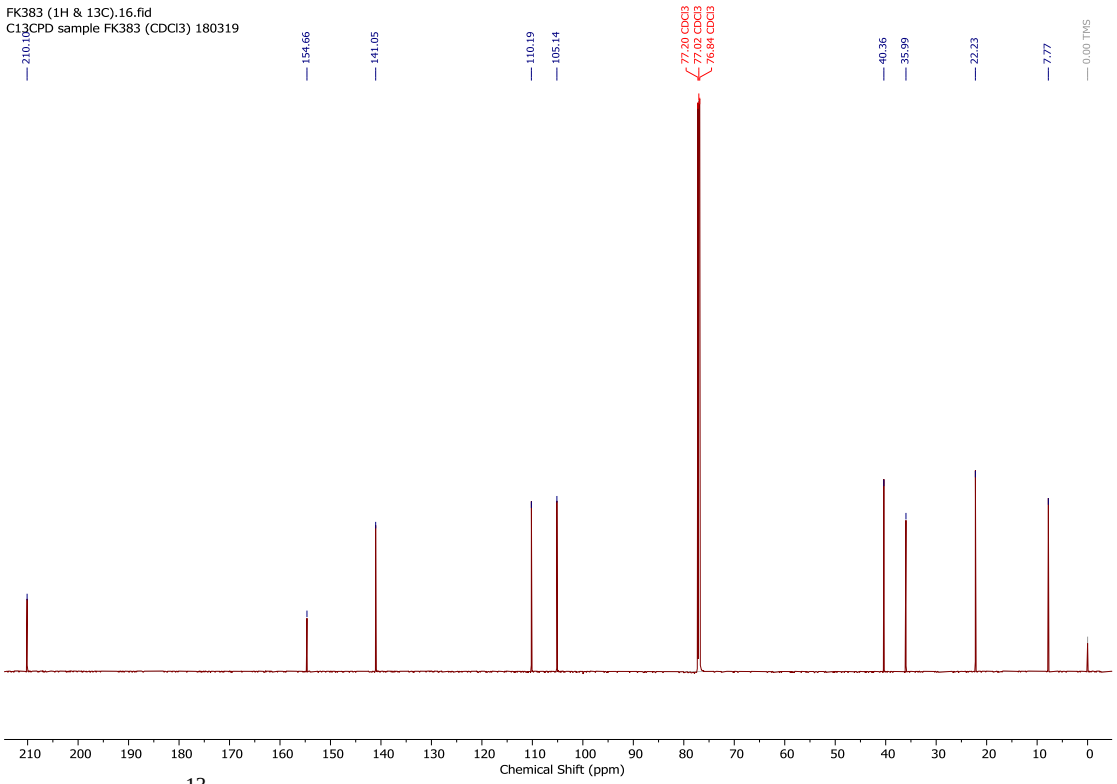


Figure S117. ^{13}C NMR spectrum of 1-(furan-2-yl)pentan-3-one (**212g**) ($CDCl_3$, 175 MHz)

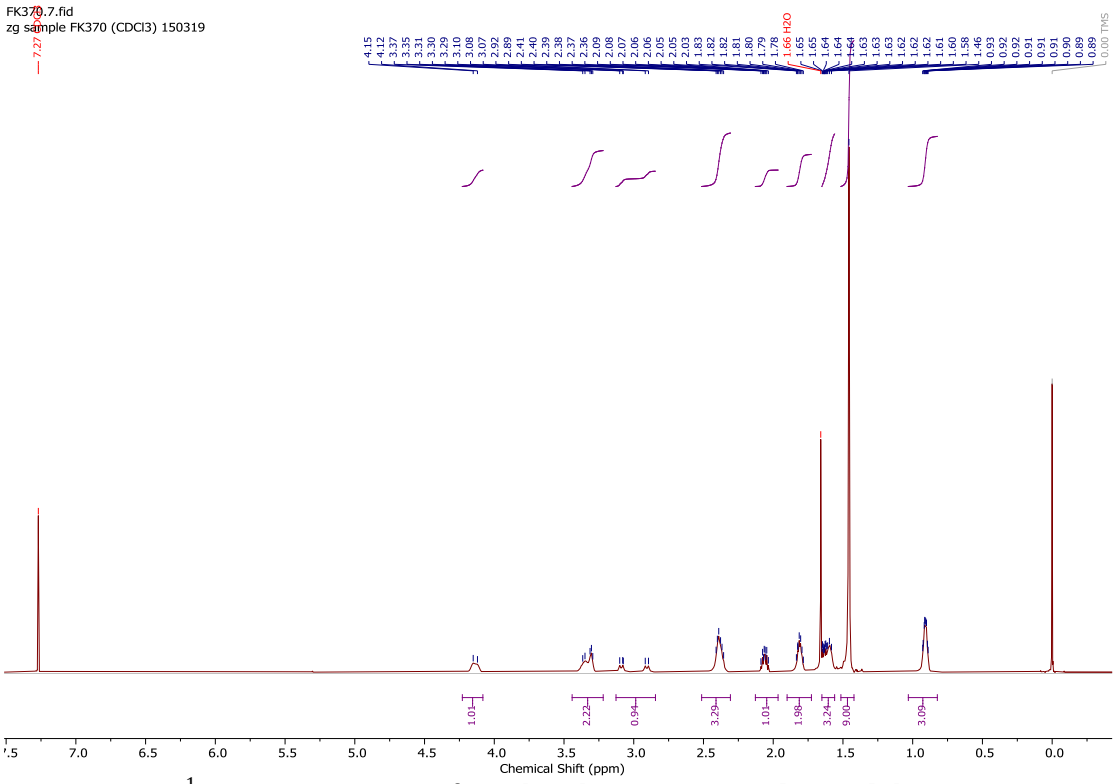


Figure S118. ^{1}H NMR spectrum of *tert*-butyl 2-(2-oxopentyl)pyrrolidine-1-carboxylate (**212h**) ($CDCl_3$, 700 MHz)

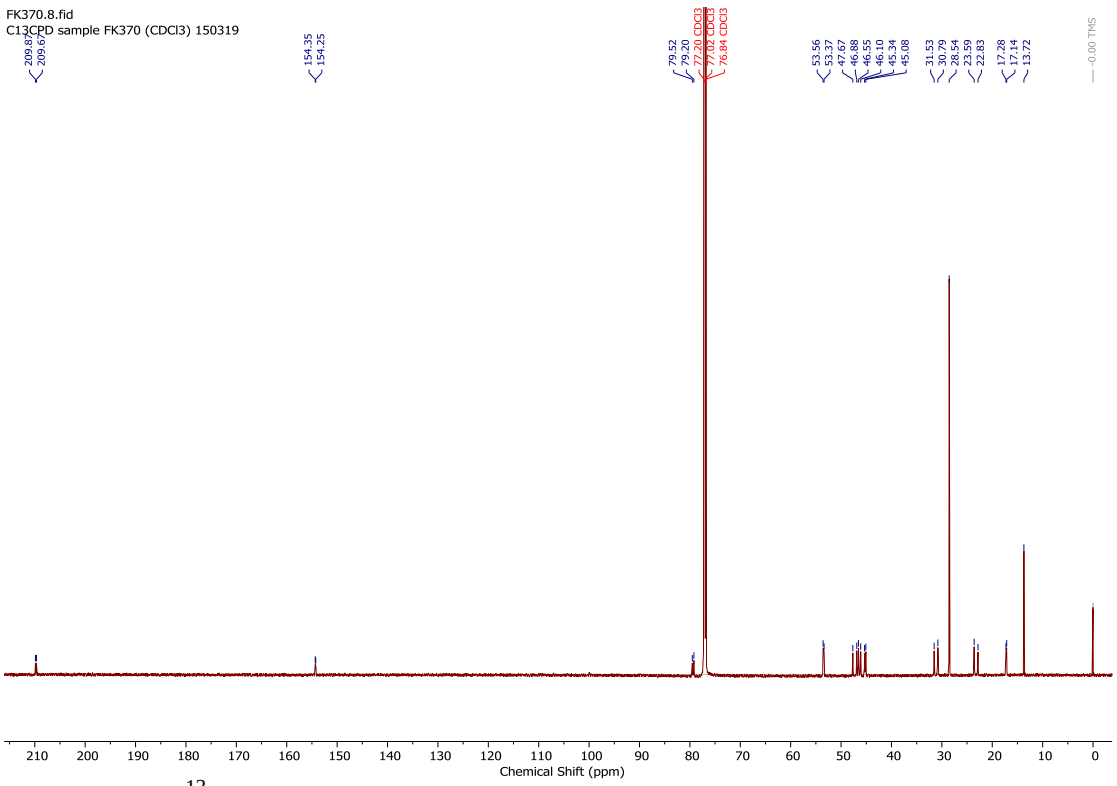


Figure S119. ^{13}C NMR spectrum of *tert*-butyl 2-(2-oxopentyl)pyrrolidine-1-carboxylate (**212h**) ($CDCl_3$, 175 MHz)

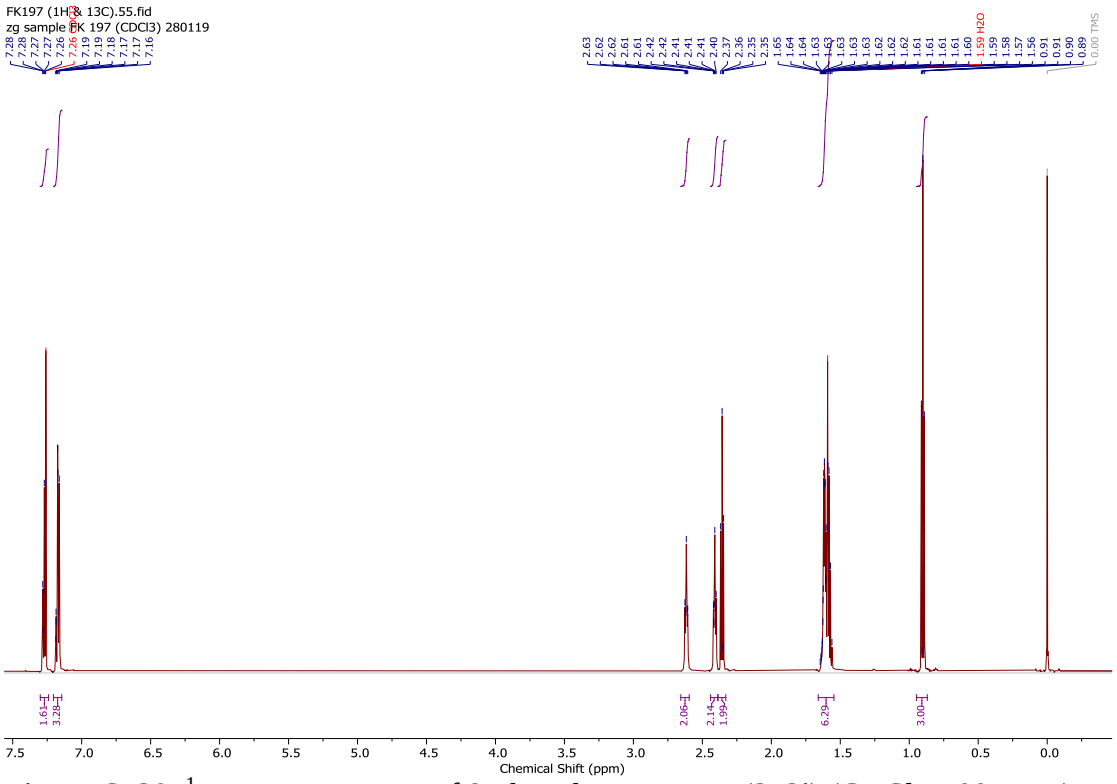


Figure S120. ^{1}H NMR spectrum of 8-phenyloctan-4-one (**212i**) ($CDCl_3$, 700 MHz)

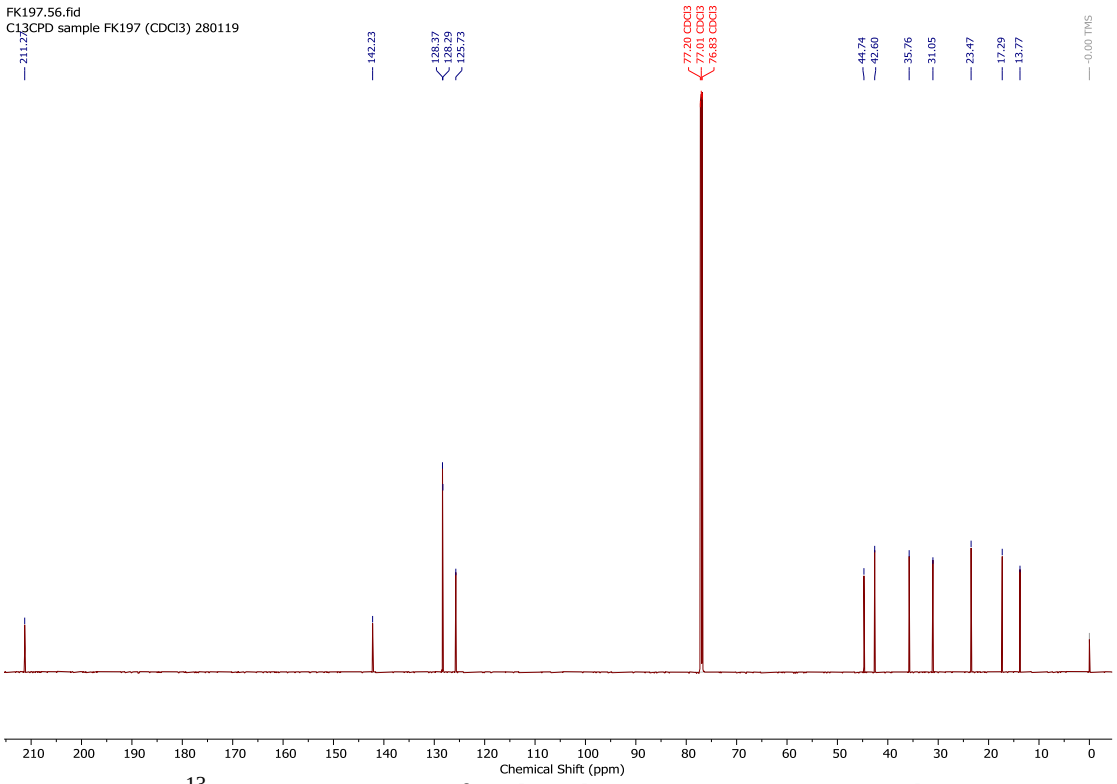


Figure S121. ^{13}C NMR spectrum of 8-phenyloctan-4-one (**212i**) ($CDCl_3$, 175 MHz)

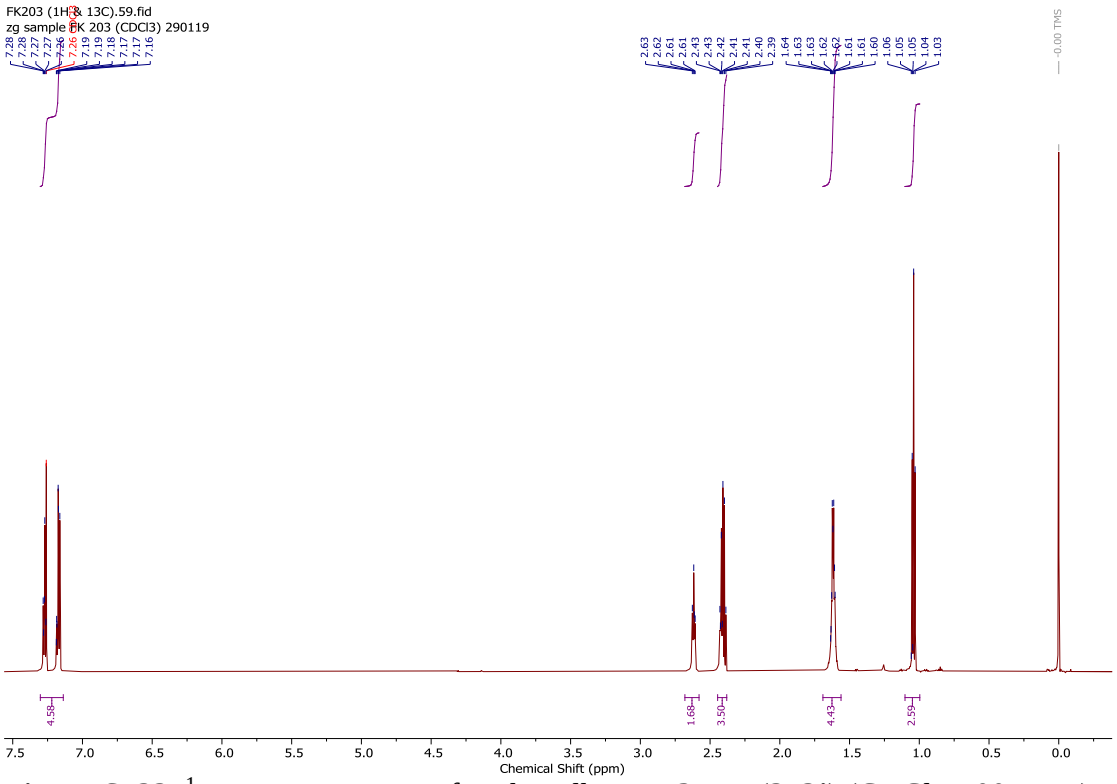


Figure S122. ^{1}H NMR spectrum of 7-phenylheptan-3-one (**212j**) ($CDCl_3$, 700 MHz)

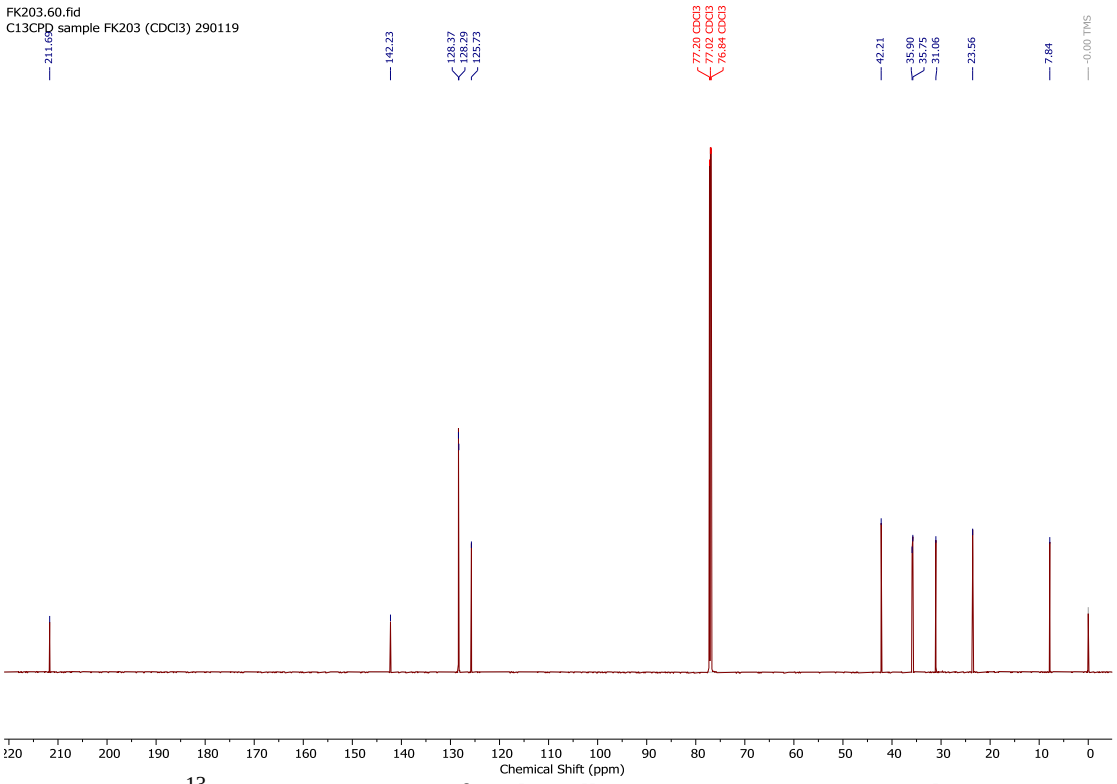


Figure S123. ^{13}C NMR spectrum of 7-phenylheptan-3-one (**212j**) ($CDCl_3$, 175 MHz)

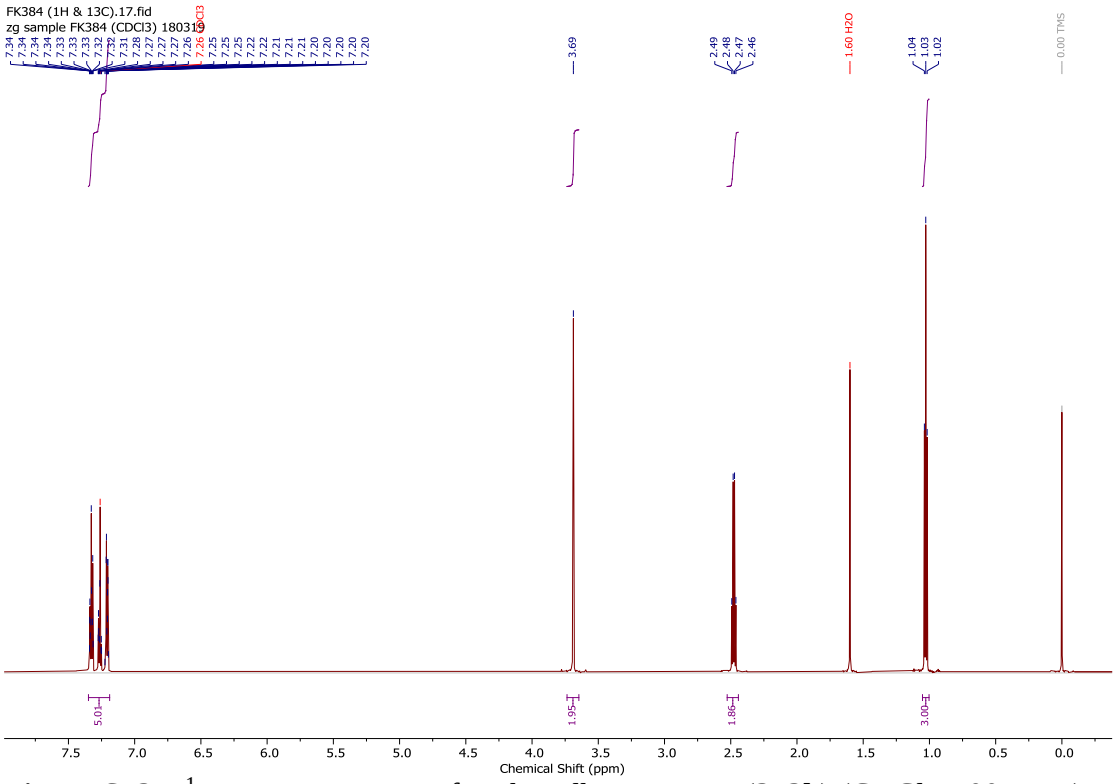


Figure S124. ^{1}H NMR spectrum of 1-phenylbutan-2-one (**212k**) ($CDCl_3$, 700 MHz)

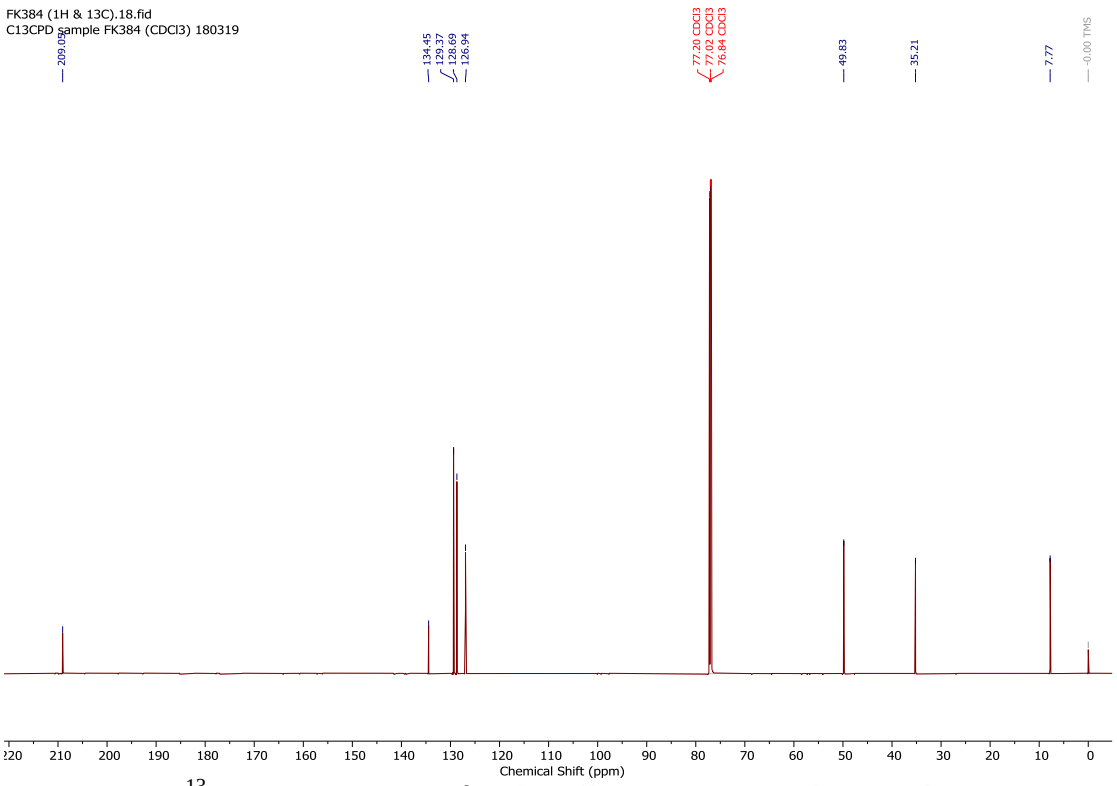


Figure S125. ^{13}C NMR spectrum of 1-phenylbutan-2-one (**212k**) ($CDCl_3$, 175 MHz)

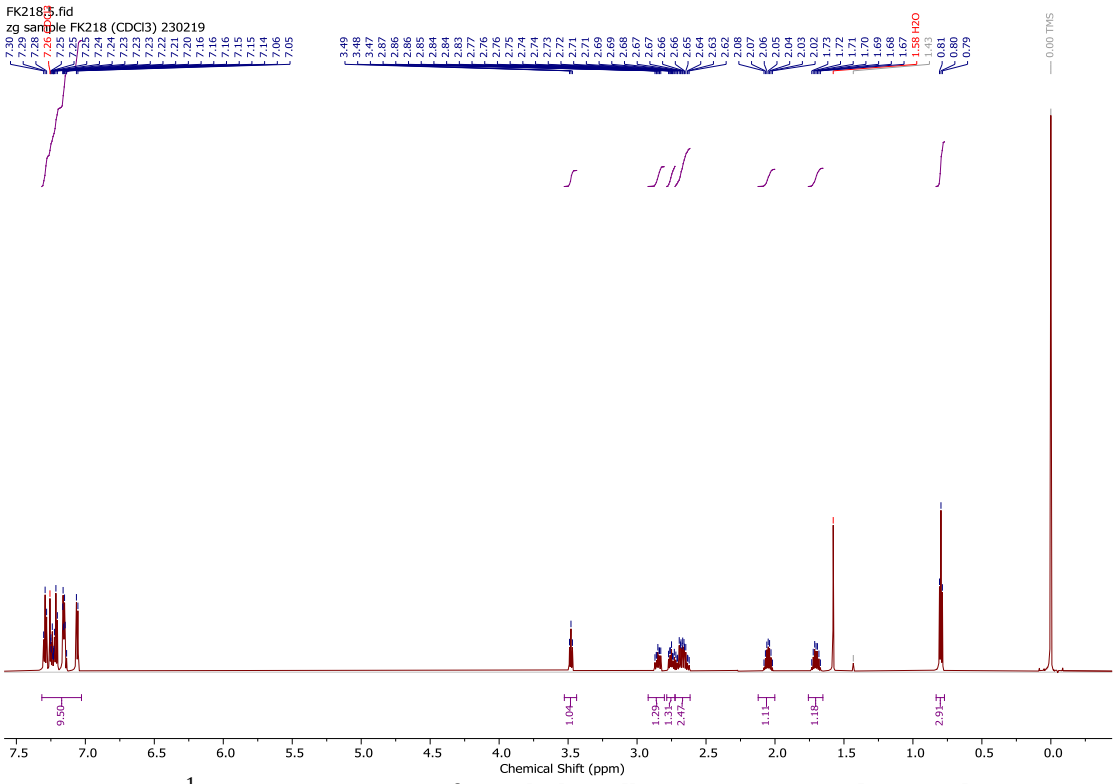


Figure S126. ^{1}H NMR spectrum of 1,4-diphenylhexan-3-one (**212l**) ($CDCl_3$, 700 MHz)

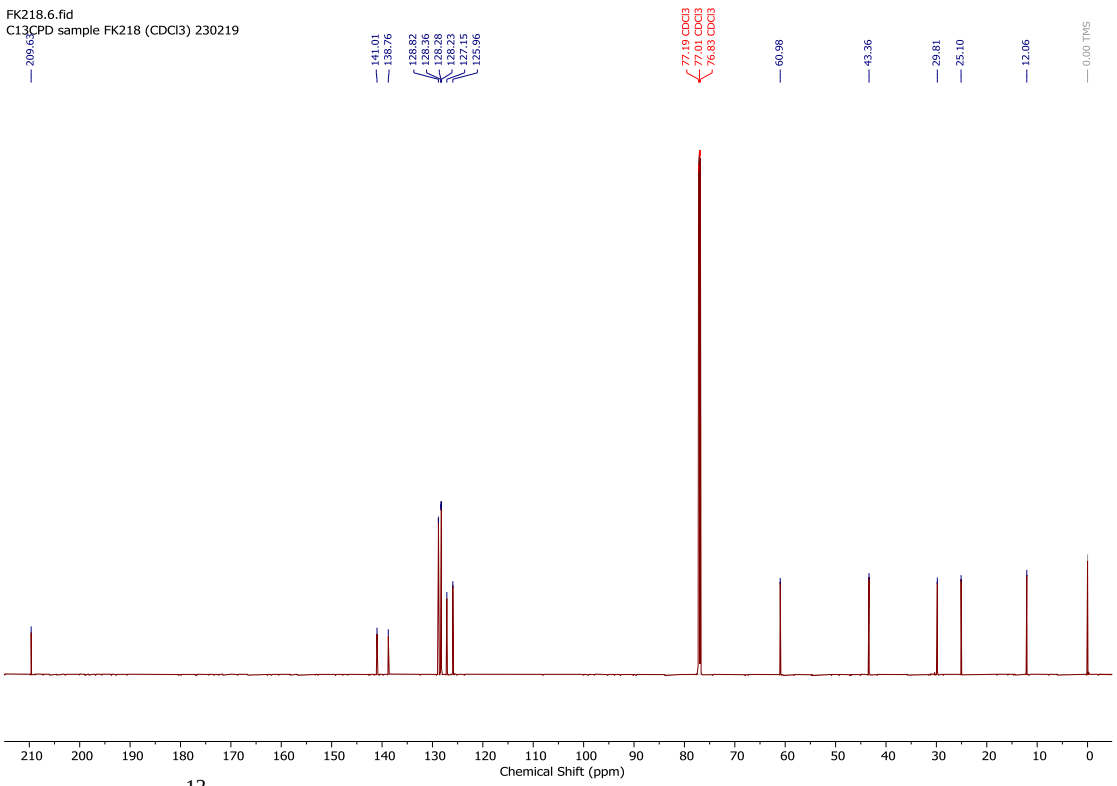


Figure S127. ^{13}C NMR spectrum of 1,4-diphenylhexan-3-one (**212l**) ($CDCl_3$, 175 MHz)

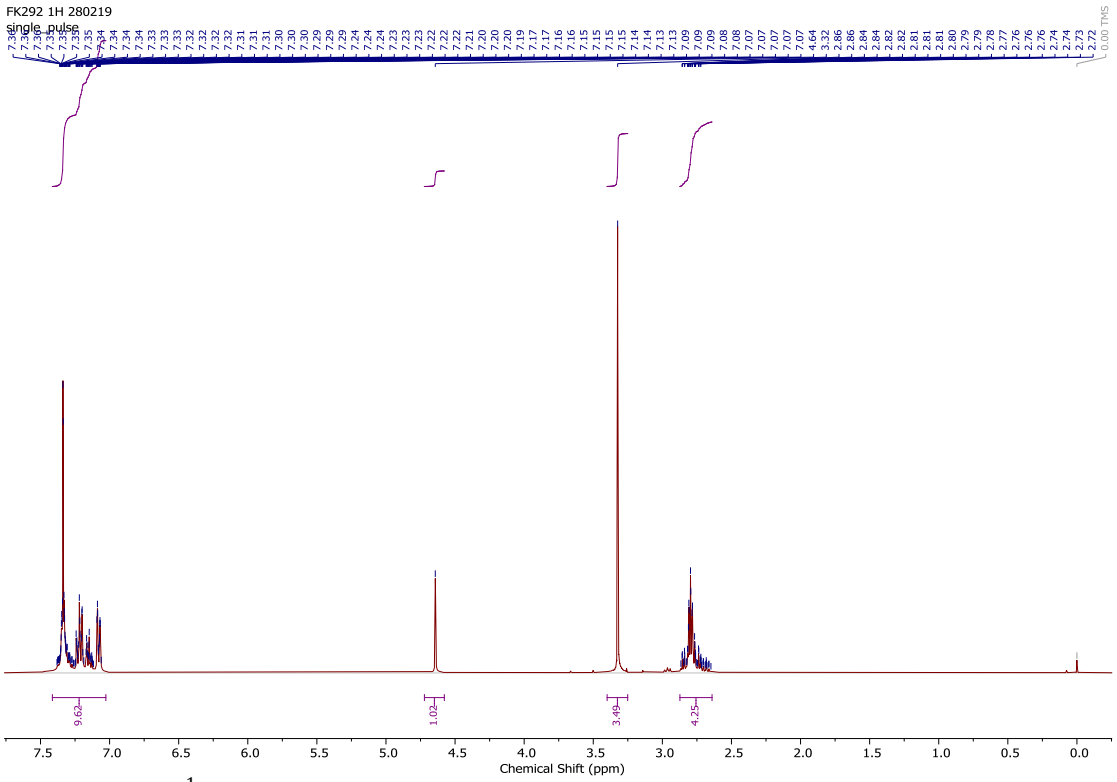


Figure S128. ^{1}H NMR spectrum of 1-methoxy-1,4-diphenylbutan-2-one (**212m**) ($CDCl_3$, 400 MHz)

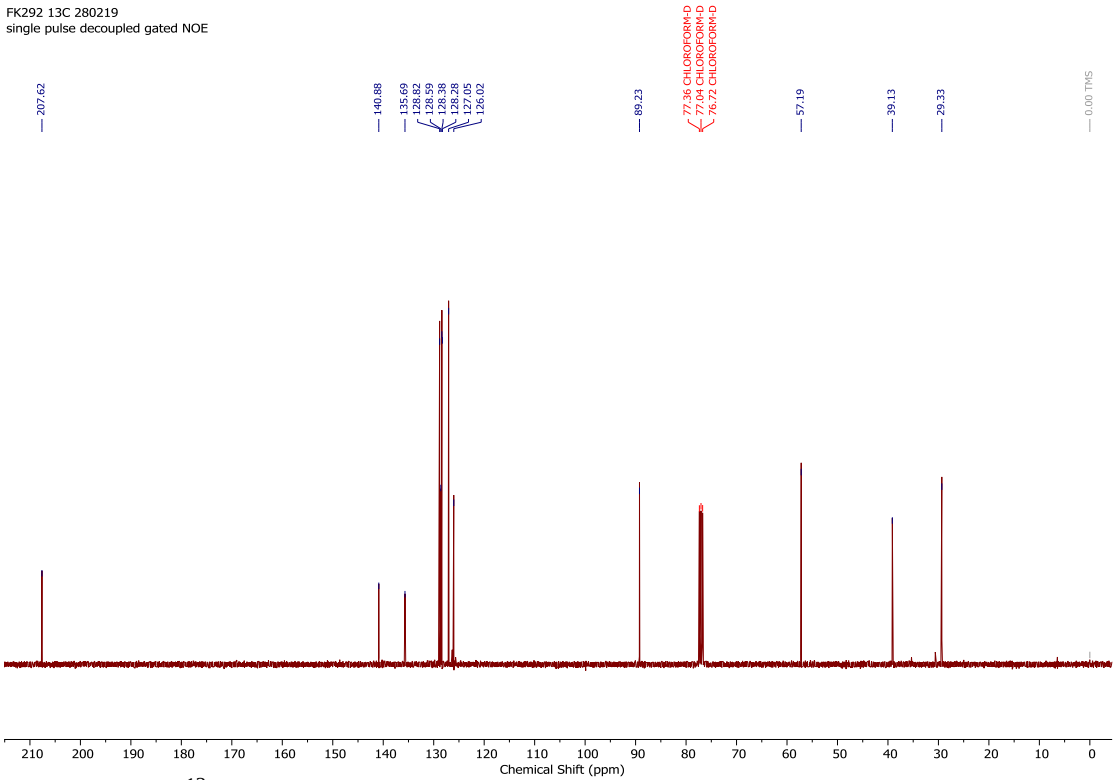


Figure S129. ^{13}C NMR spectrum of 1-methoxy-1,4-diphenylbutan-2-one (**212m**) ($CDCl_3$, 100 MHz)

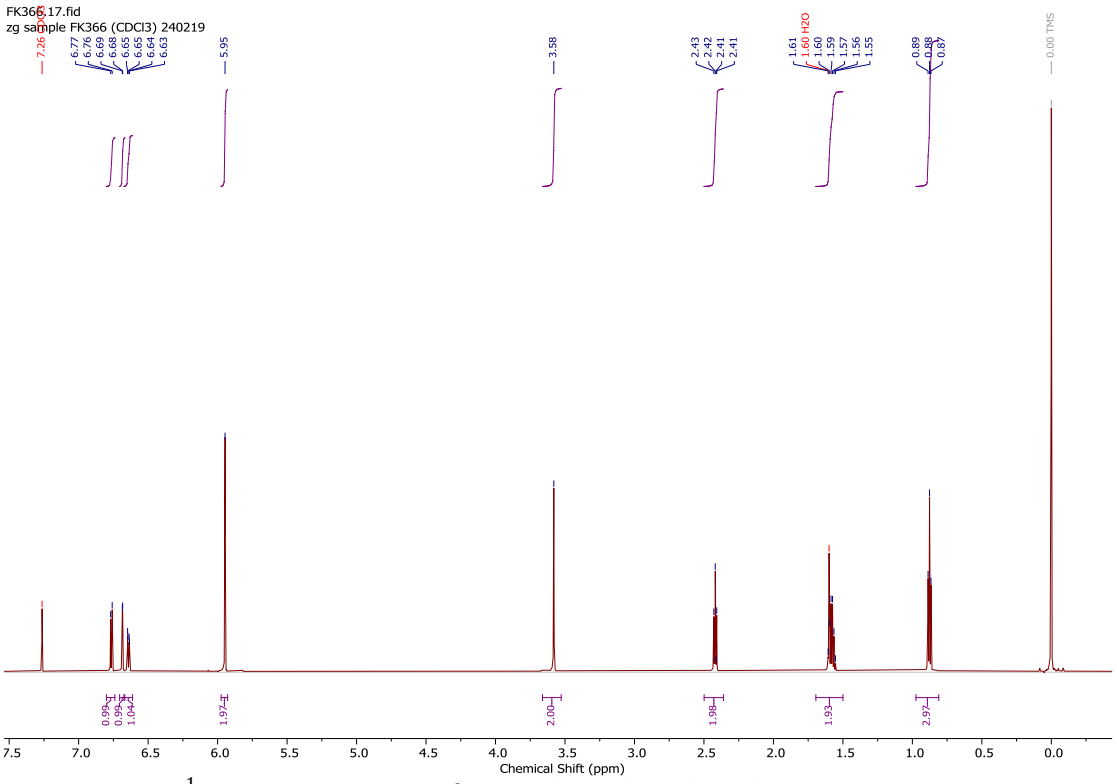


Figure S130. ^{1}H NMR spectrum of 1-(1,3-benzdioxol-5-yl)pentan-2-one (**212n**) ($CDCl_3$, 700 MHz)

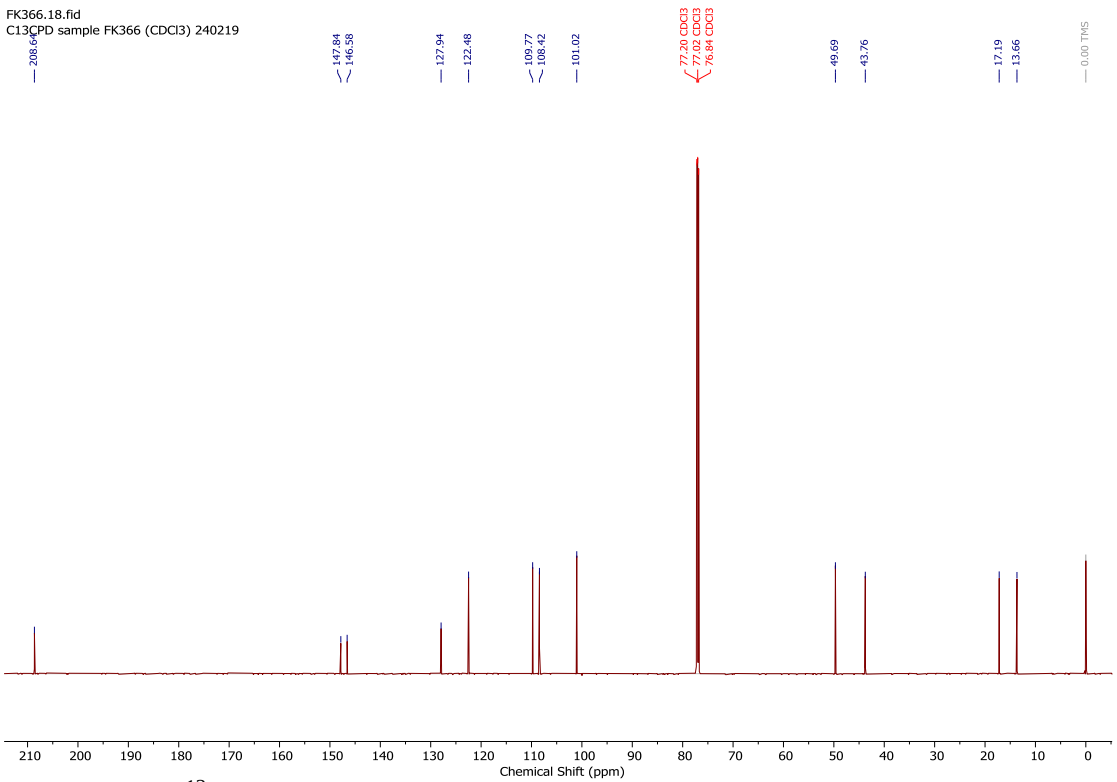


Figure S131. ^{13}C NMR spectrum of 1-(1,3-benzdioxol-5-yl)pentan-2-one (**212n**) ($CDCl_3$, 175 MHz)

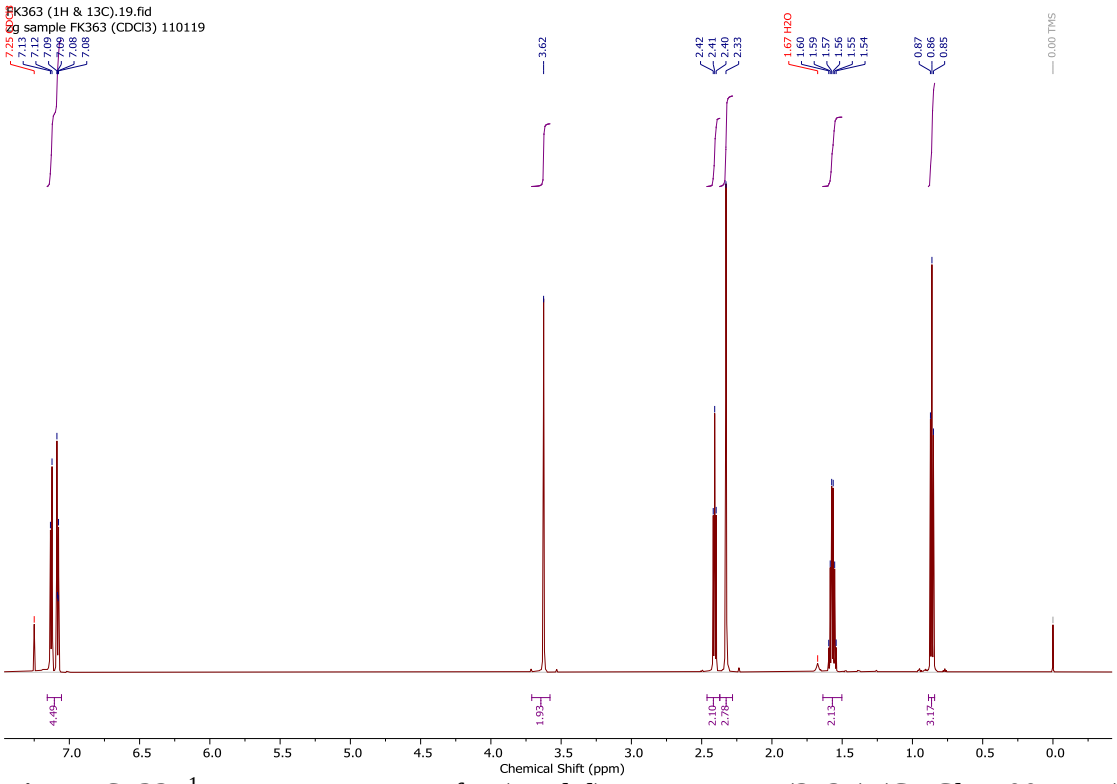


Figure S132. ^{1}H NMR spectrum of 1-(*p*-tolyl)pentan-2-one (**212o**) ($CDCl_3$, 700 MHz)

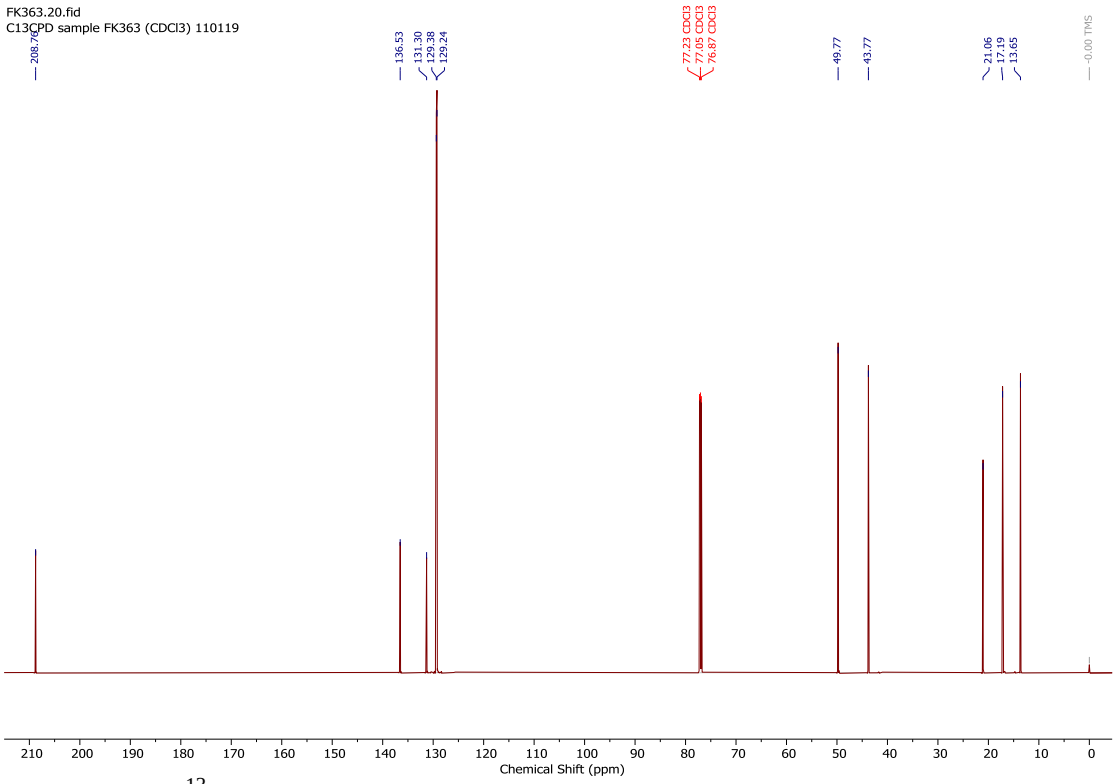


Figure S133. ^{13}C NMR spectrum of 1-(*p*-tolyl)pentan-2-one (**212o**) ($CDCl_3$, 175 MHz)

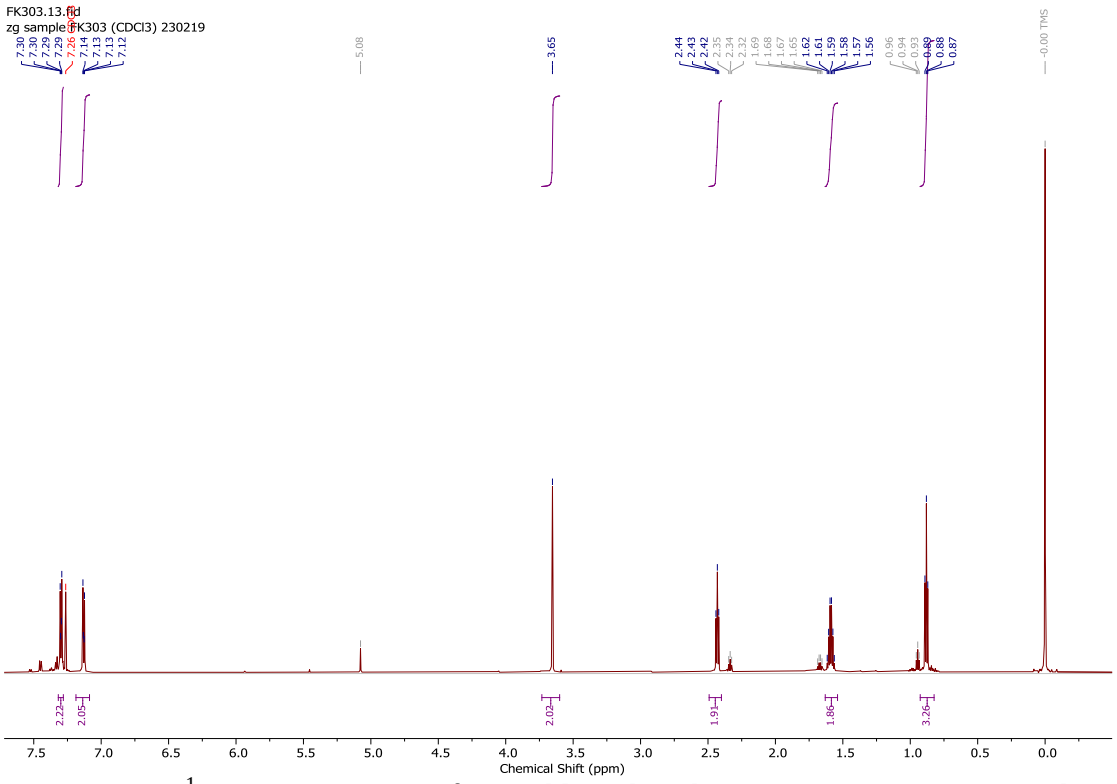


Figure S134. ^{1}H NMR spectrum of 1-(4-chlorophenyl)pentan-2-one (**212p**) ($CDCl_3$, 700 MHz)

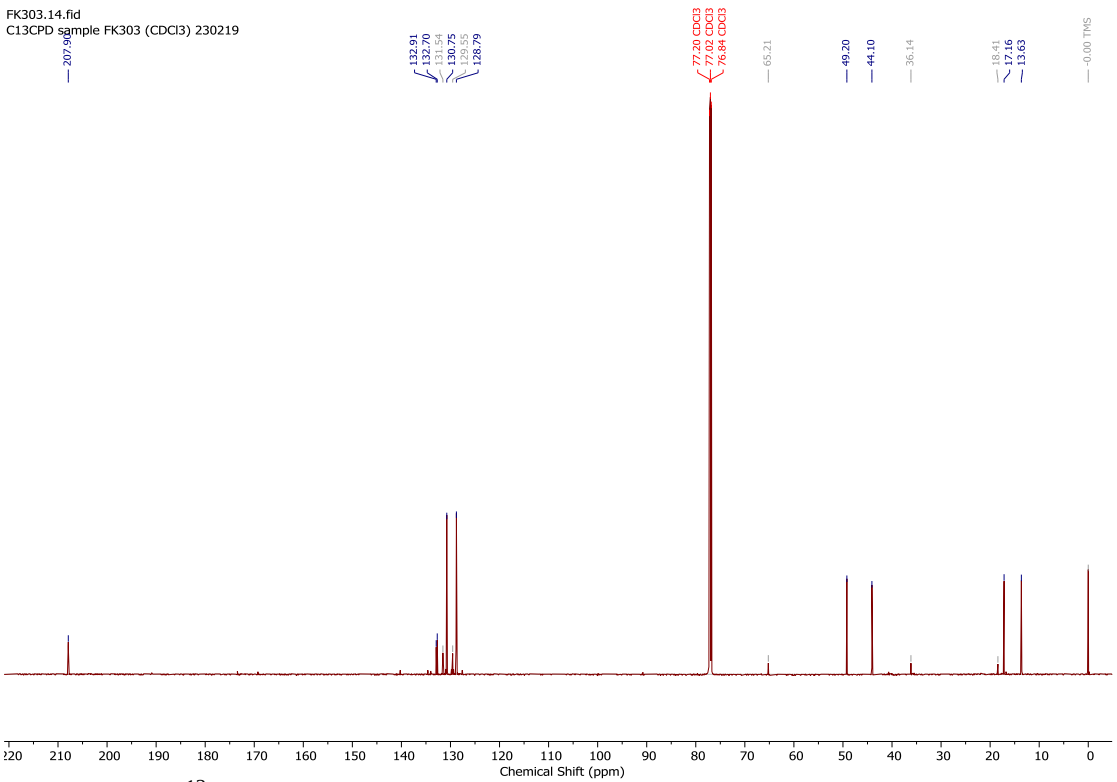


Figure S135. ^{13}C NMR spectrum of 1-(4-chlorophenyl)pentan-2-one (**212p**) ($CDCl_3$, 175 MHz)

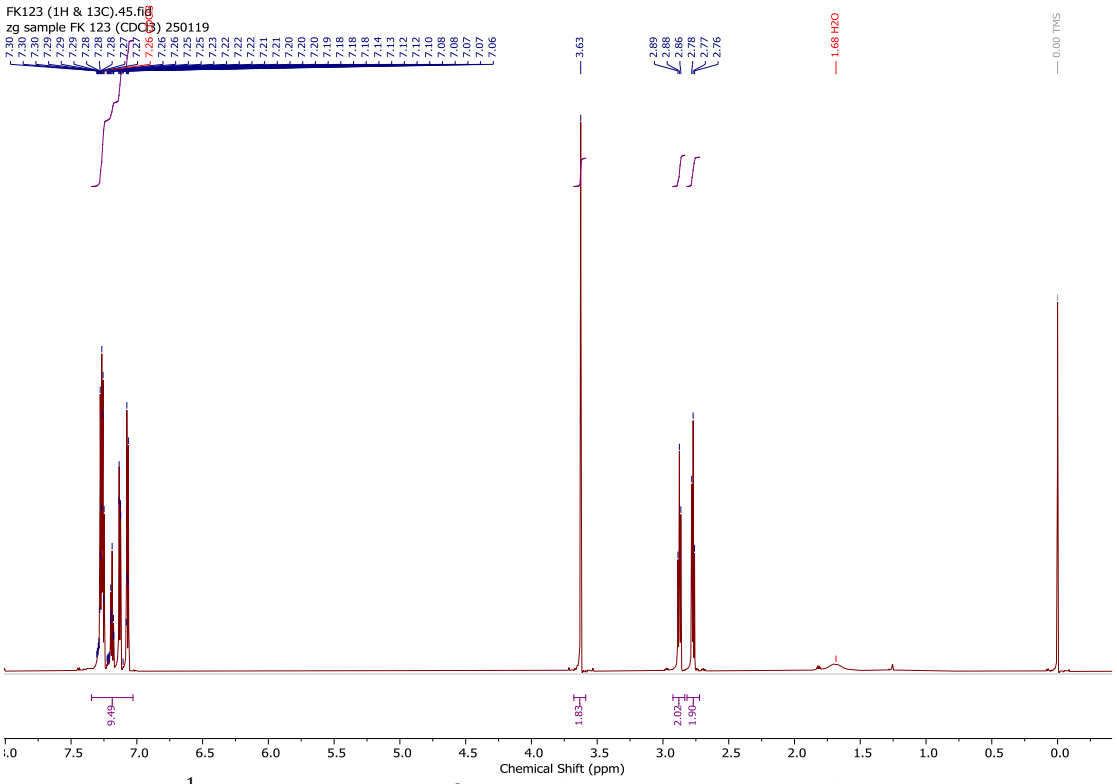


Figure S136. ^{1}H NMR spectrum of 1-(4-chlorophenyl)-4-phenylbutan-2-one (**212q**) ($CDCl_3$, 700 MHz)

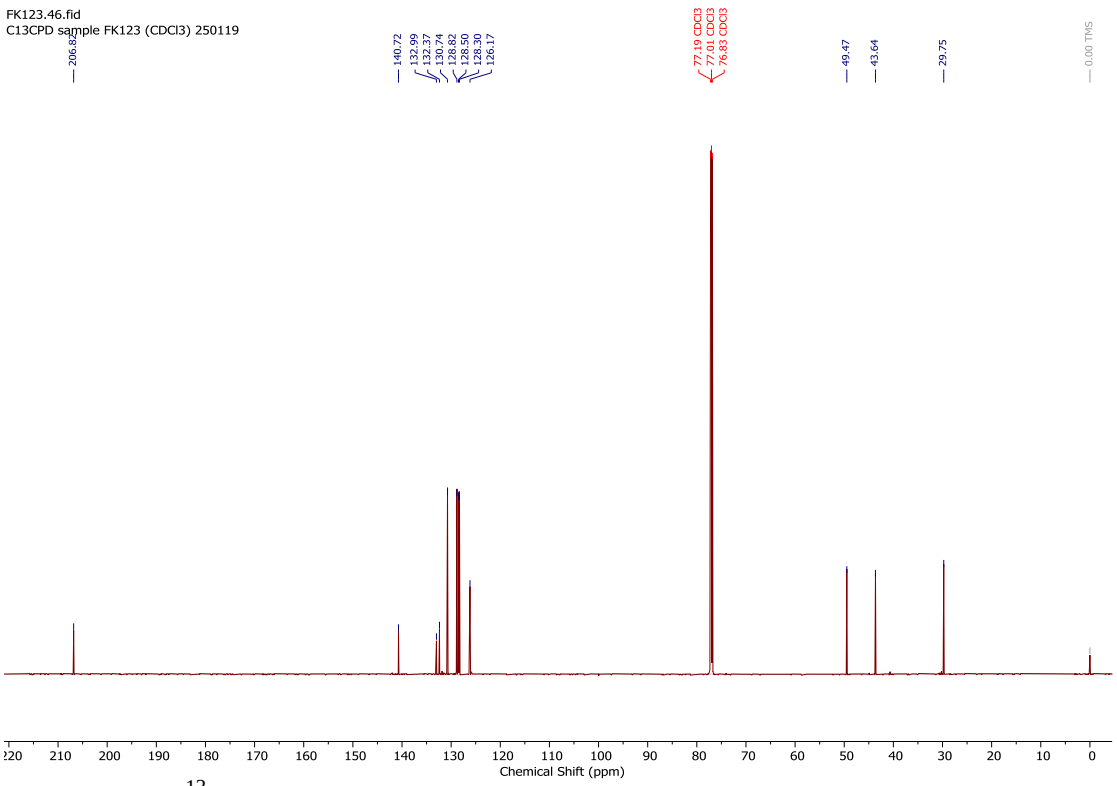


Figure S137. ^{13}C NMR spectrum of 1-(4-chlorophenyl)-4-phenylbutan-2-one (**212q**) ($CDCl_3$, 175 MHz)

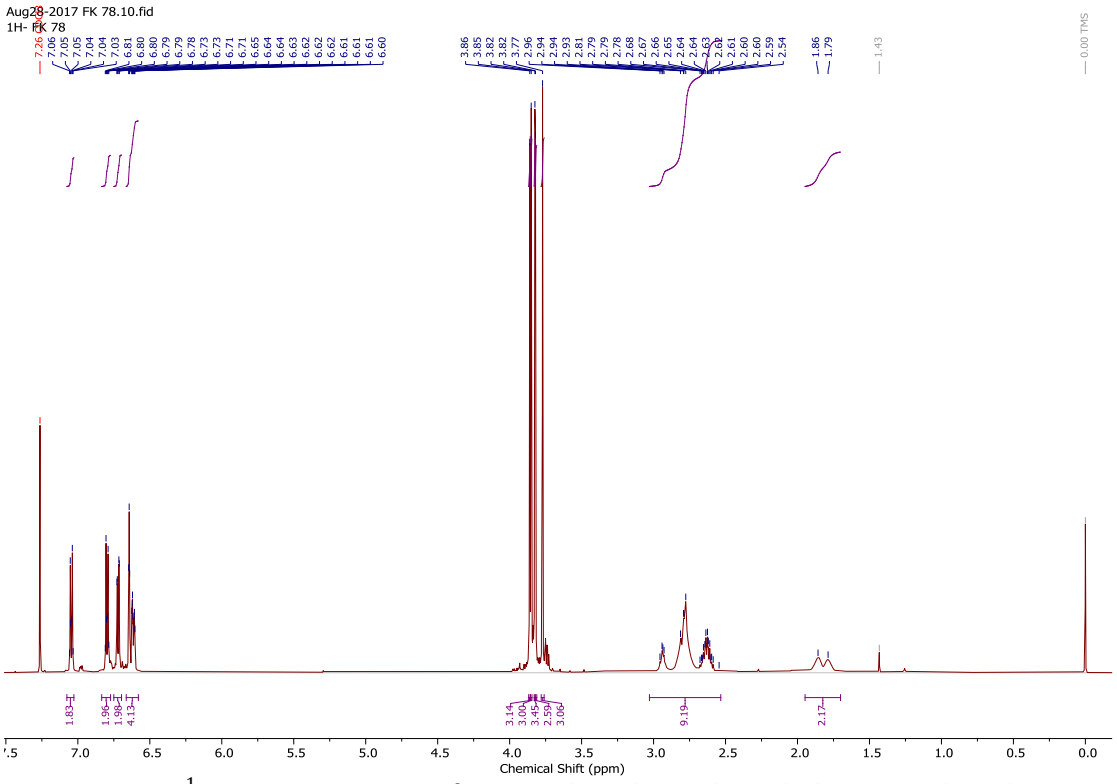


Figure S138. ^{1}H NMR spectrum of *N*-(3,4-dimethoxyphenethyl)-1-(3,4-dimethoxy-phenyl)-4-(4-methoxy-phenyl)-butan-2-amine (**215a**) ($CDCl_3$, 600 MHz)

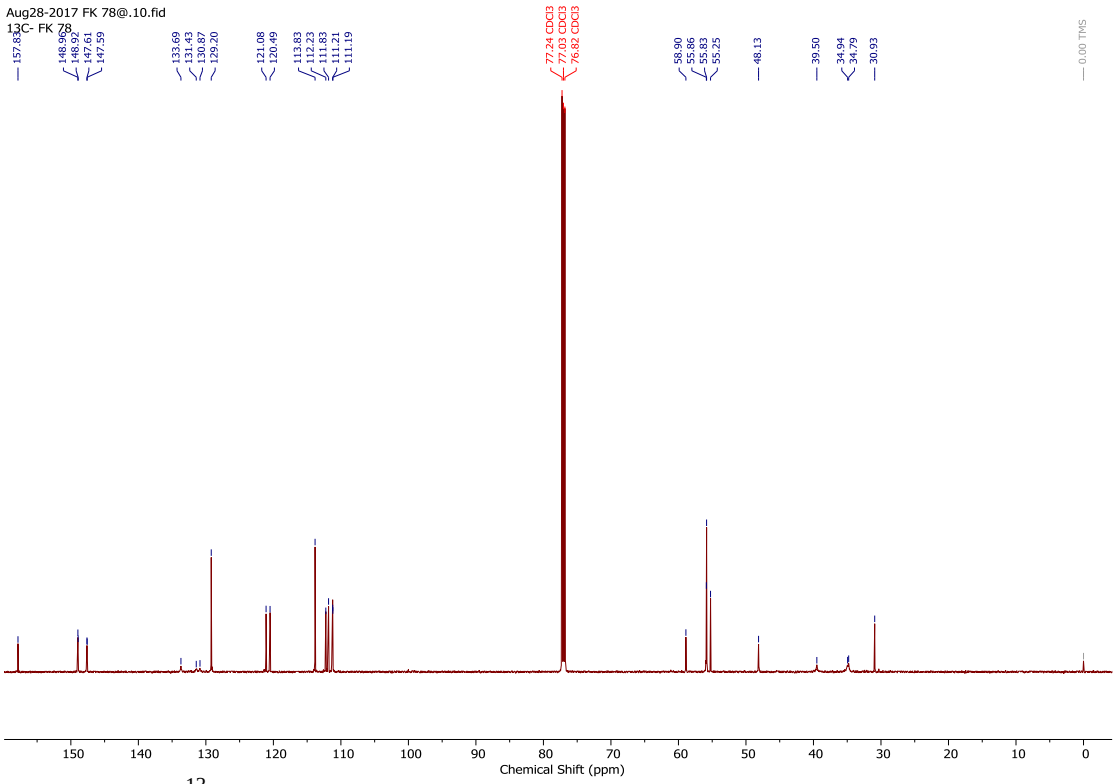


Figure S139. ^{13}C NMR spectrum of *N*-(3,4-dimethoxyphenethyl)-1-(3,4-dimethoxy-phenyl)-4-(4-methoxy-phenyl)-butan-2-amine (**215a**) ($CDCl_3$, 150 MHz)

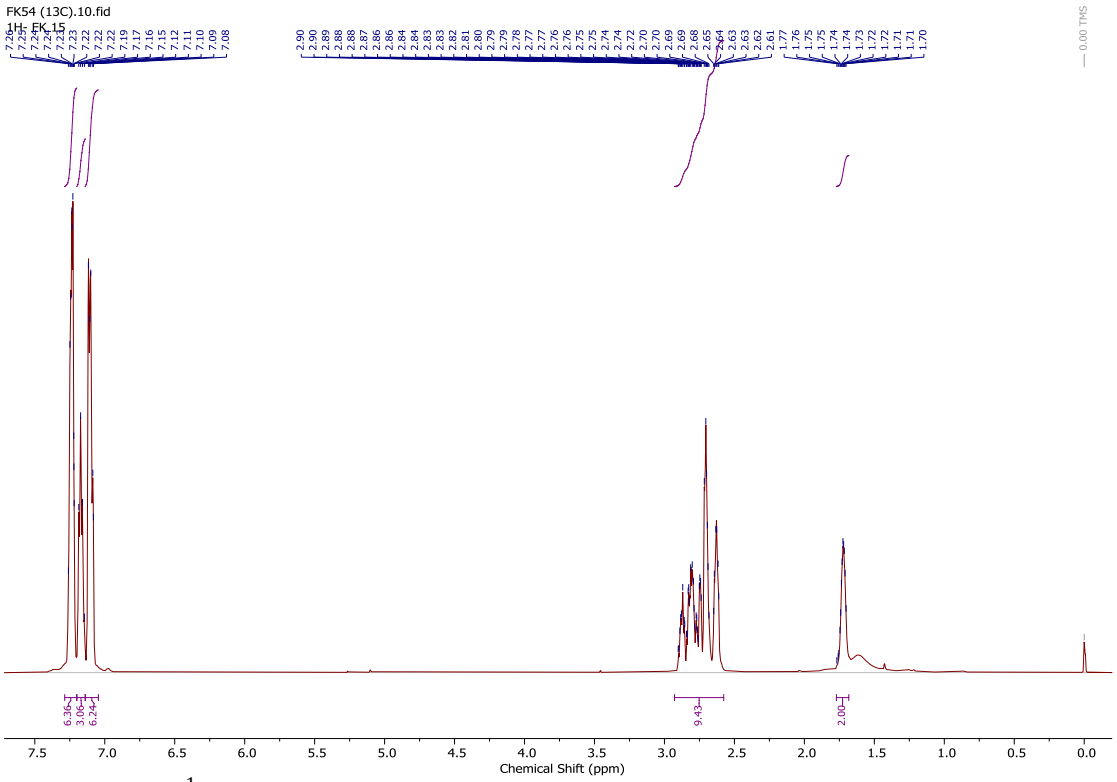


Figure S140. ^{1}H NMR spectrum of *N*-phenethyl-1,4-diphenyl-butan-2-amine (**215b**) ($CDCl_3$, 600 MHz)

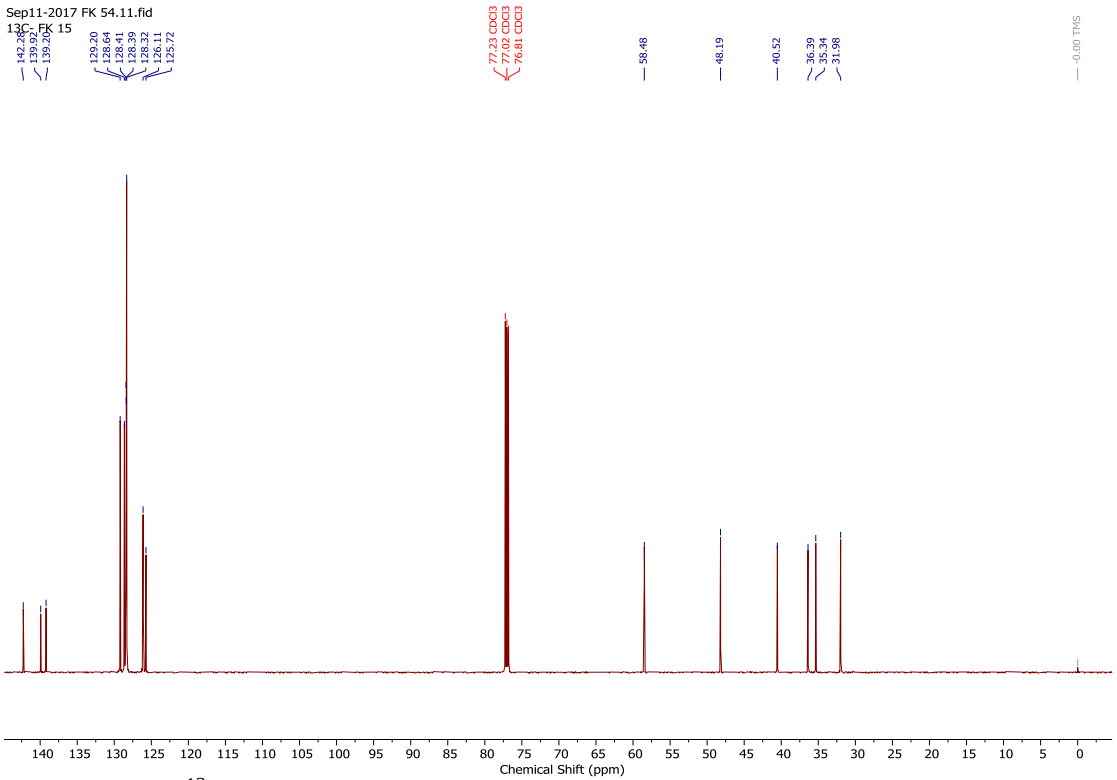


Figure S141. ^{13}C NMR spectrum of *N*-phenethyl-1,4-diphenyl-butan-2-amine (**215b**) ($CDCl_3$, 150 MHz)

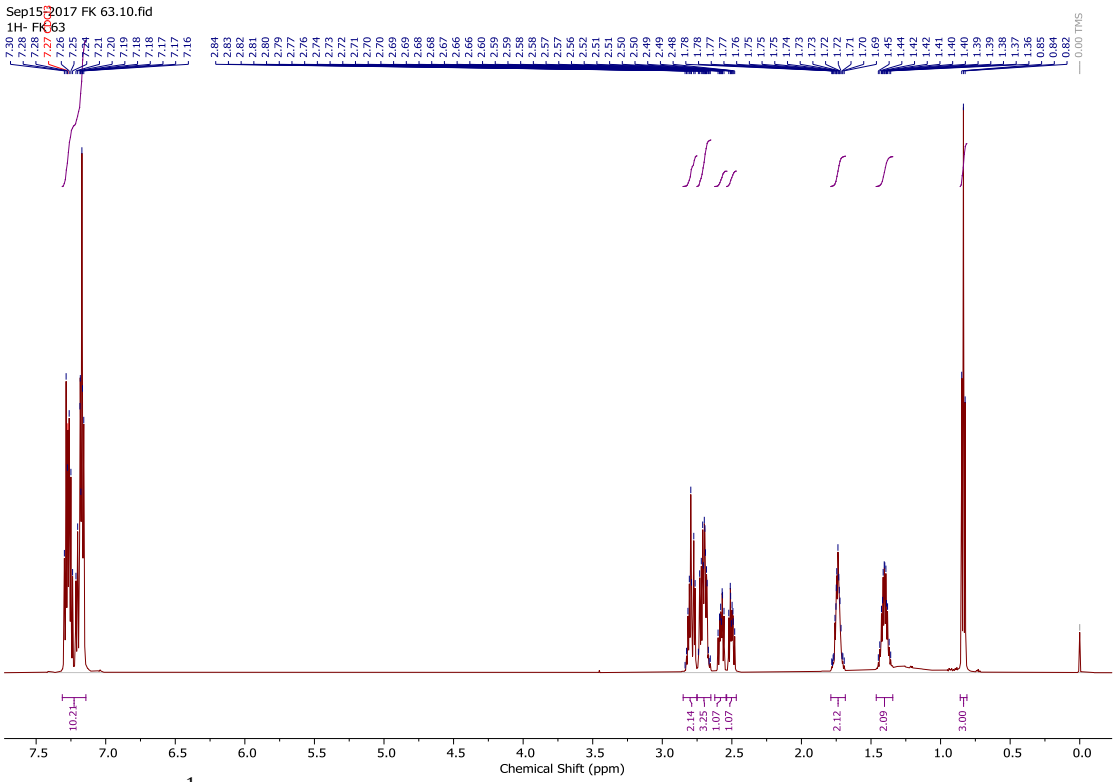


Figure S142. ^{1}H NMR spectrum of 1,4-diphenyl-*N*-propylbutan-2-amine (**215c**) ($CDCl_3$, 600 MHz)

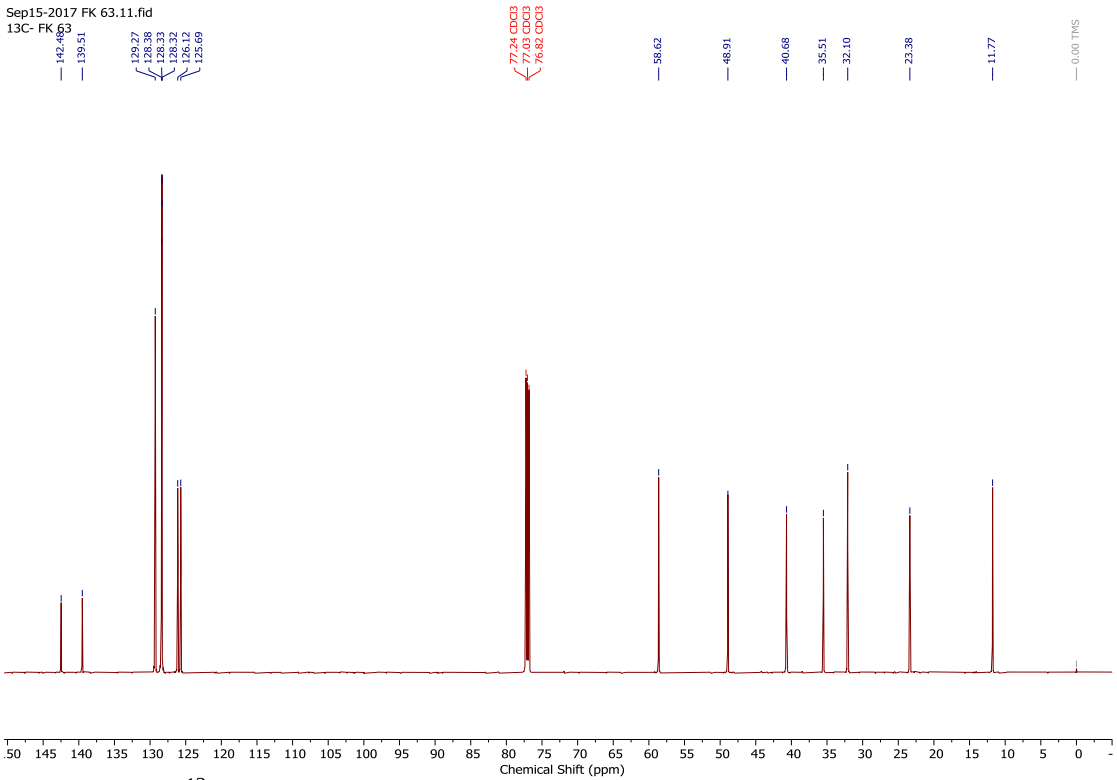


Figure S143. ^{13}C NMR spectrum of 1,4-diphenyl-*N*-propylbutan-2-amine (**215c**) ($CDCl_3$, 150 MHz)

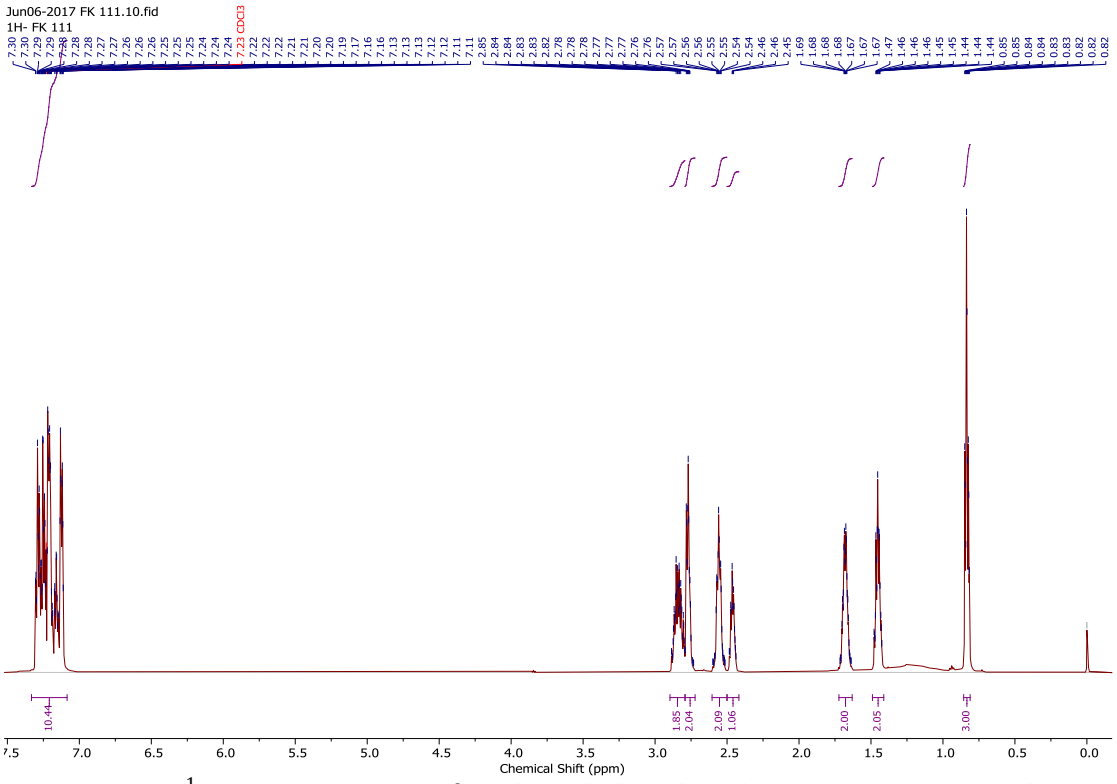


Figure S144. ^{1}H NMR spectrum of *N*-phenethyl-1-phenylpentan-3-amine (**215d**) ($CDCl_3$, 600 MHz)

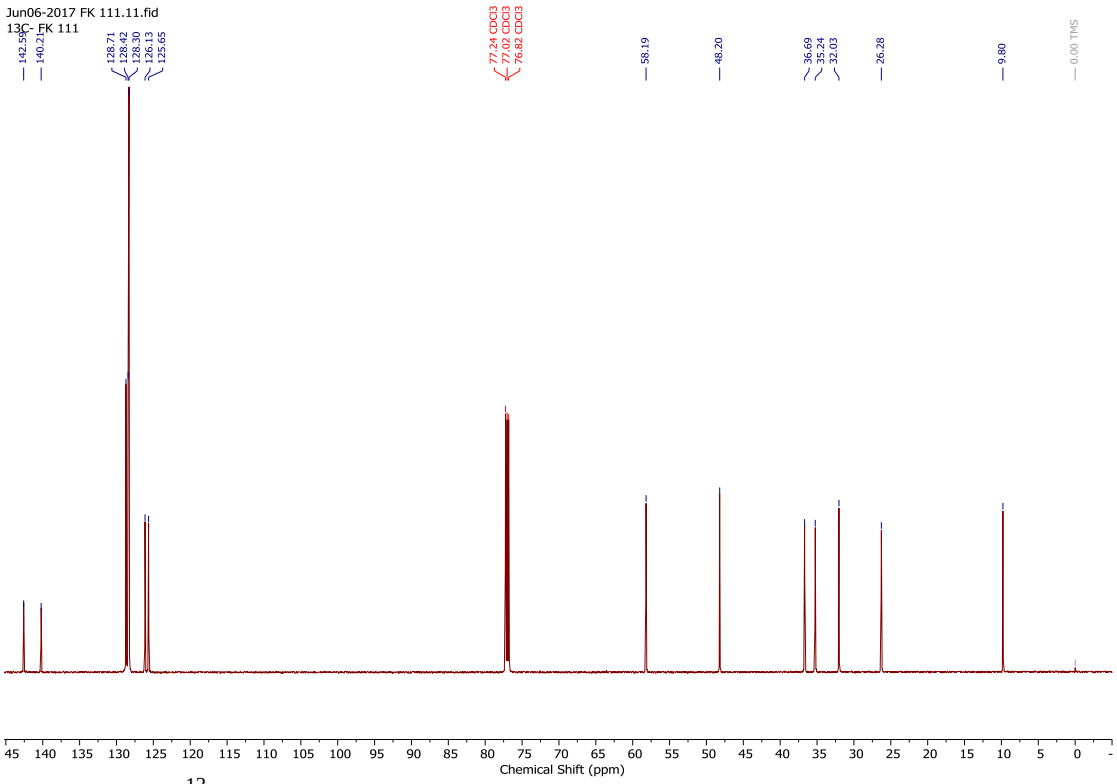


Figure S145. ^{13}C NMR spectrum of *N*-phenethyl-1-phenylpentan-3-amine (**215d**) ($CDCl_3$, 150 MHz)

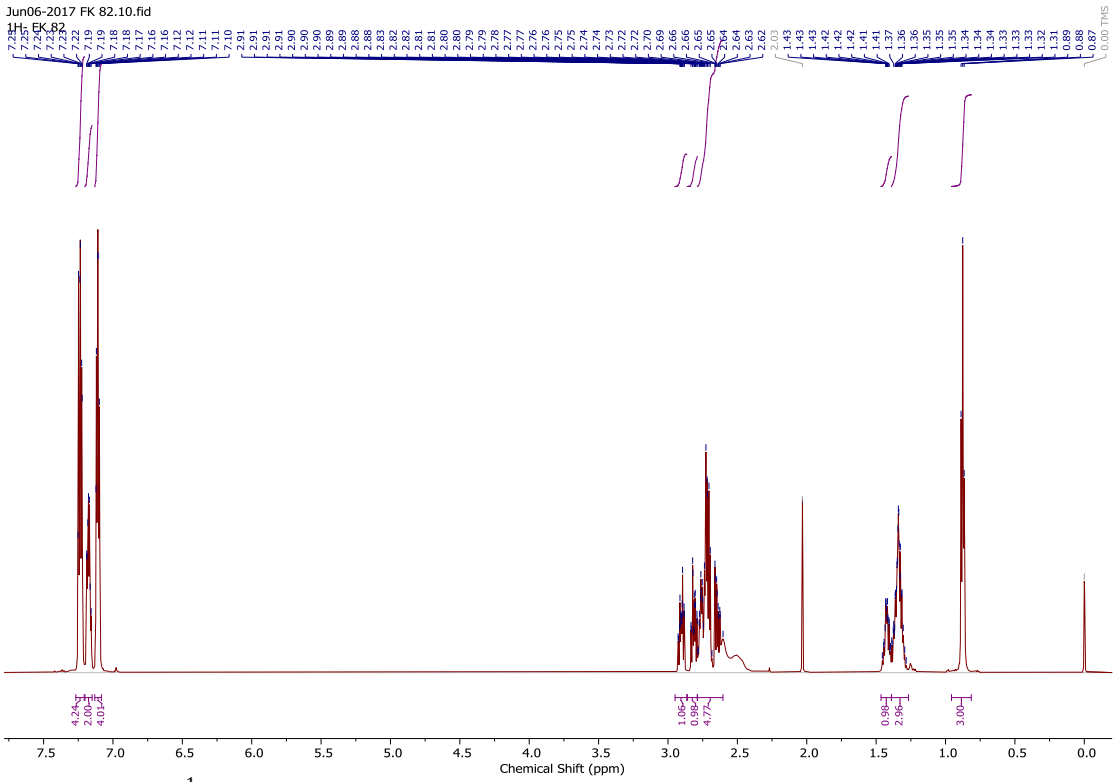


Figure S146. ^{1}H NMR spectrum of *N*-phenethyl-1-phenylpentan-2-amine (**215e**) ($CDCl_3$, 600 MHz)

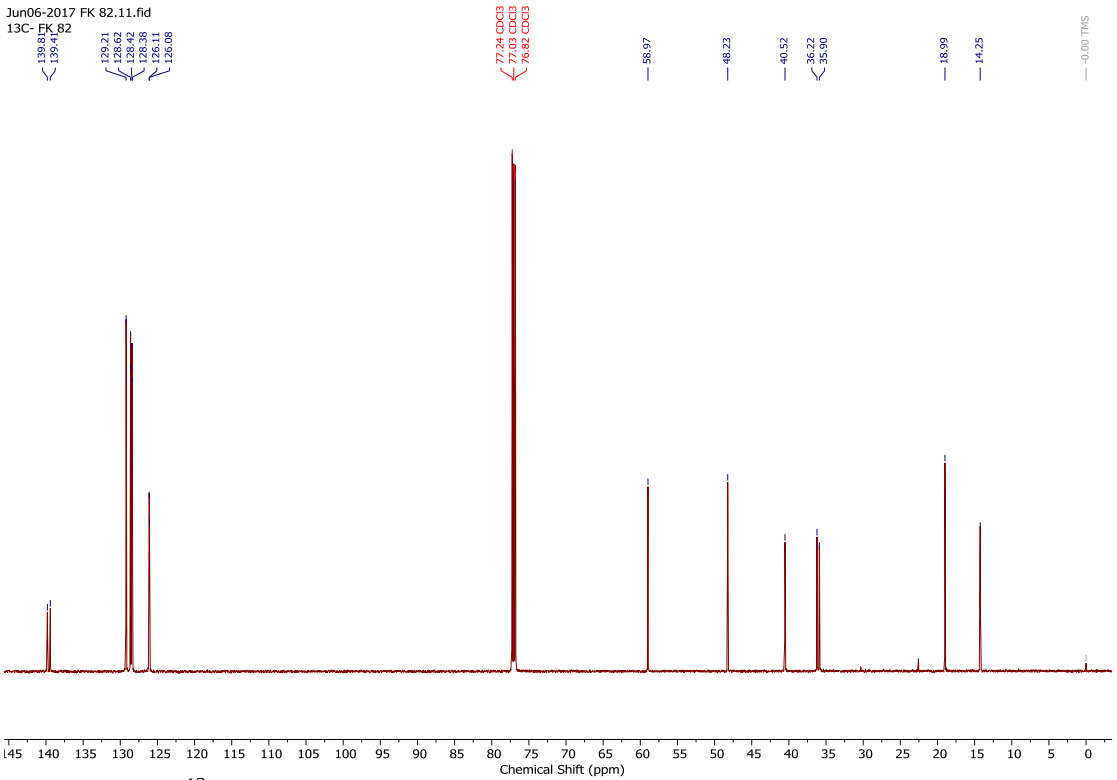


Figure S147. ^{13}C NMR spectrum of *N*-phenethyl-1-phenylpentan-2-amine (**215e**) ($CDCl_3$, 150 MHz)

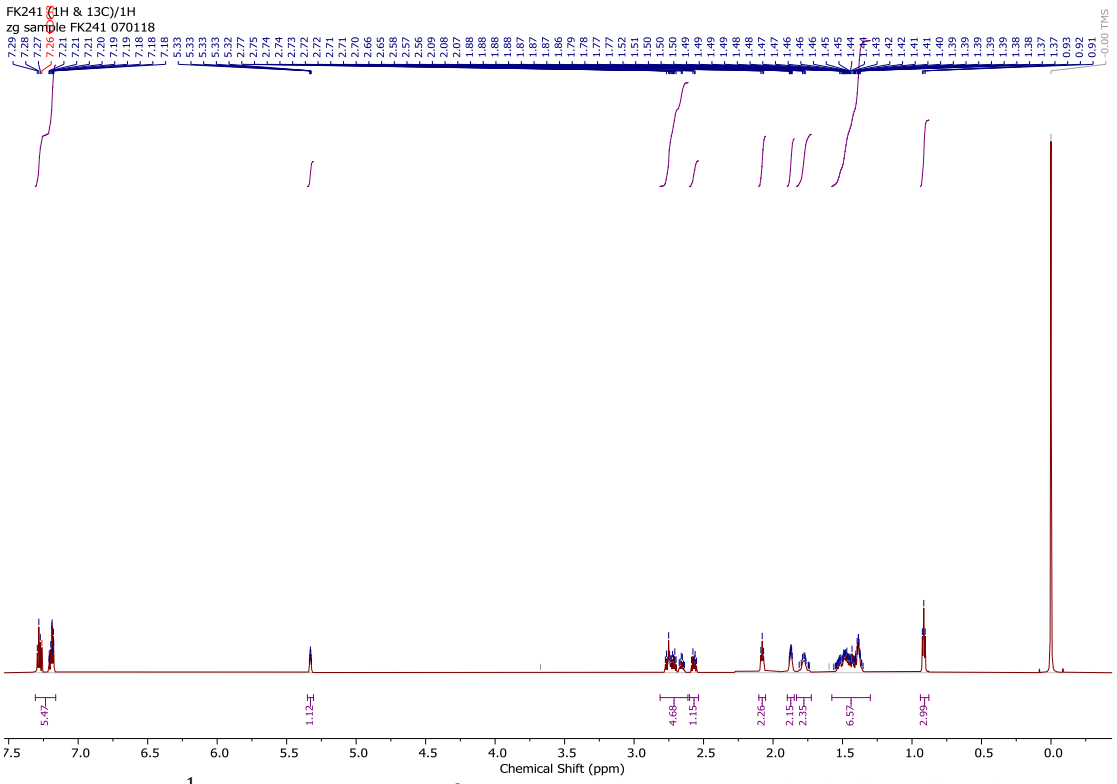


Figure S148. ^{1}H NMR spectrum of *N*-(2-(cyclohex-1-en-1-yl)ethyl)-1-phenylpentan-2-amine (**215f**) ($CDCl_3$, 700 MHz)

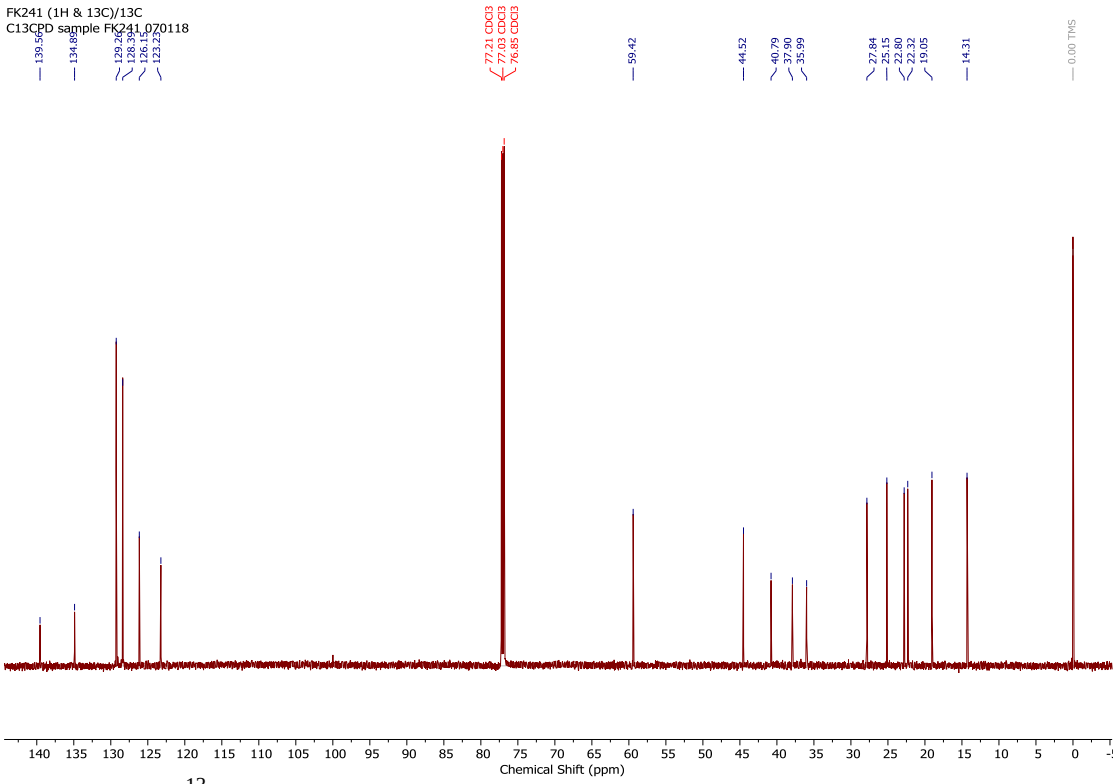


Figure S149. ^{13}C NMR spectrum of *N*-(2-(cyclohex-1-en-1-yl)ethyl)-1-phenylpentan-2-amine (**215f**) ($CDCl_3$, 175 MHz)

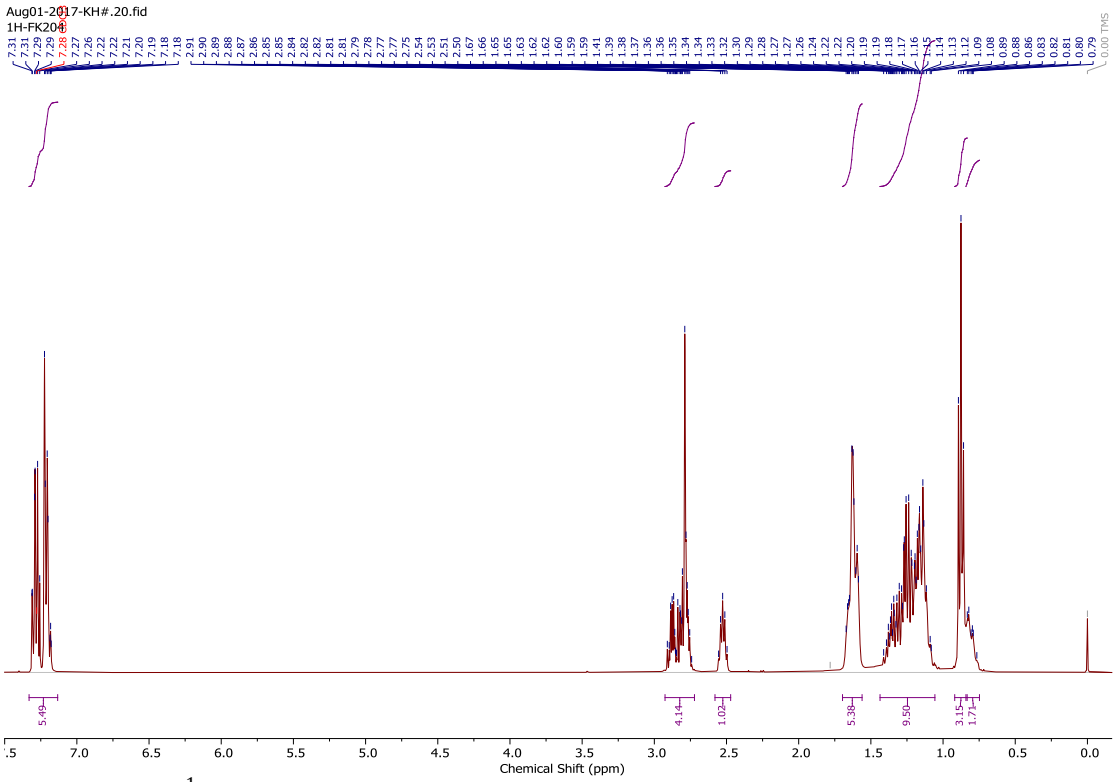


Figure S150. ^{1}H NMR spectrum of 1-cyclohexyl-*N*-phenethylpentan-2-amine (**215g**) ($CDCl_3$, 400 MHz)

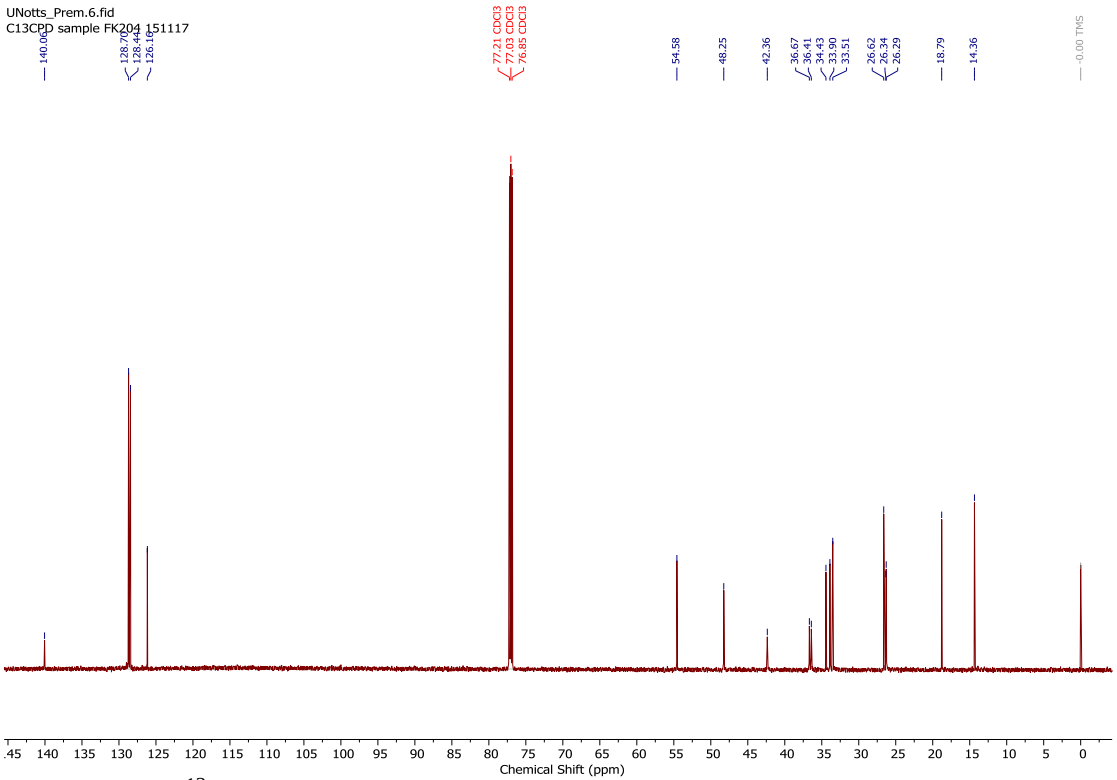


Figure S151. ^{13}C NMR spectrum of 1-cyclohexyl-*N*-phenethylpentan-2-amine (**215g**) ($CDCl_3$, 175 MHz)

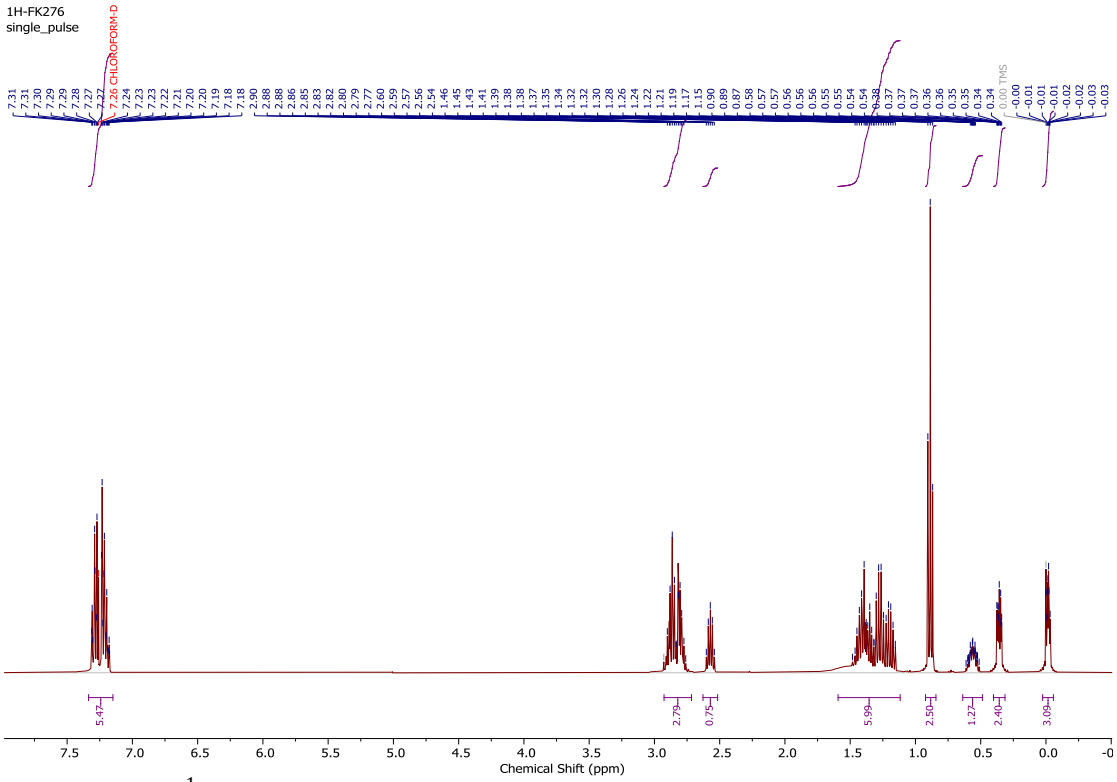


Figure S152. ^{1}H NMR spectrum of 1-cyclopropyl-*N*-phenethylpentan-2-amine (**215h**) ($CDCl_3$, 400 MHz)

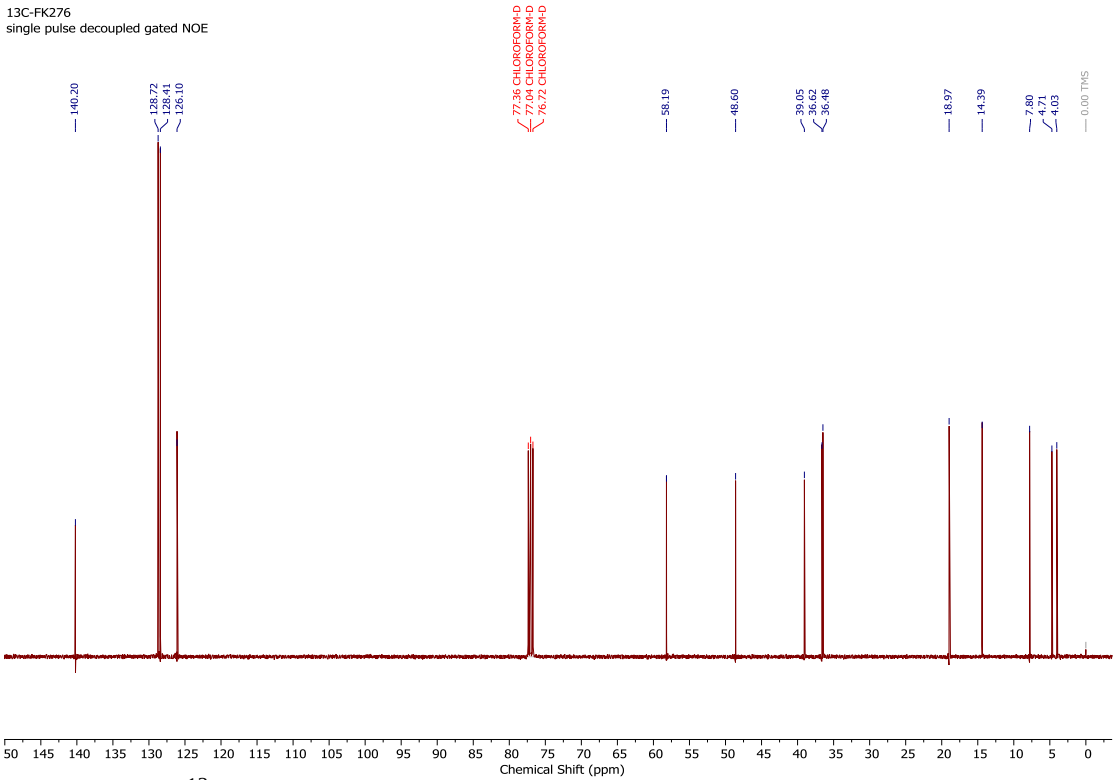


Figure S153. ^{13}C NMR spectrum of 1-cyclopropyl-*N*-phenethylpentan-2-amine (**215h**) ($CDCl_3$, 100 MHz)

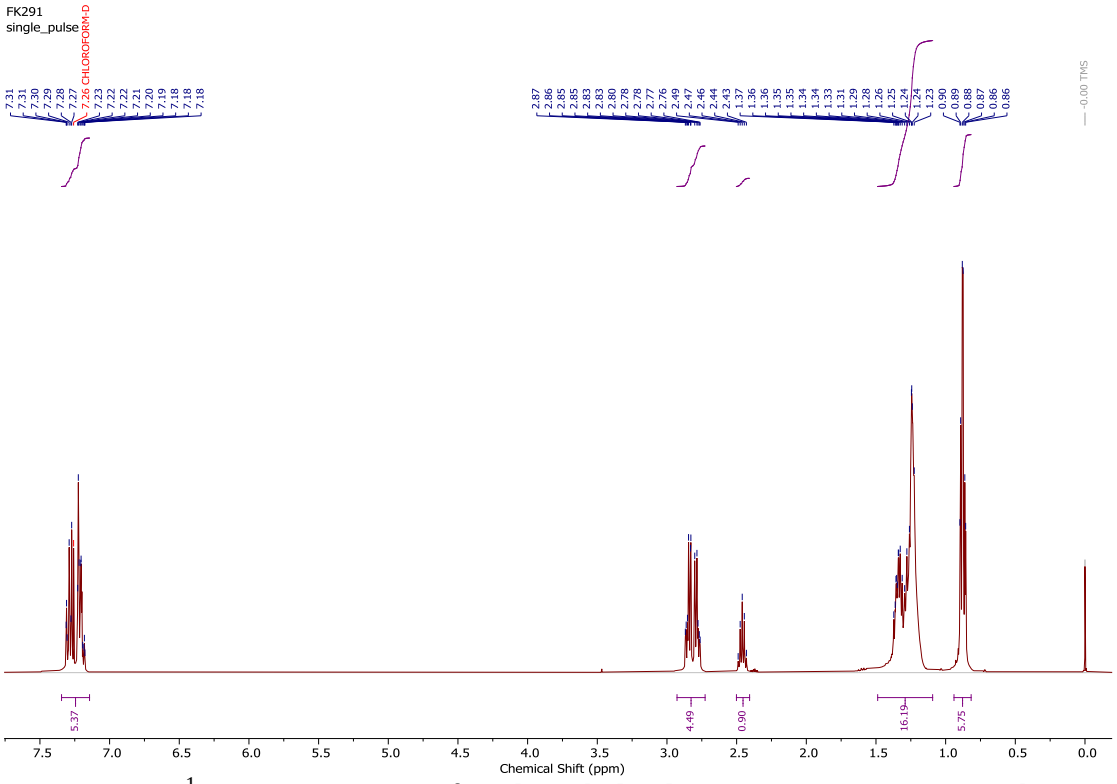


Figure S154. ^{1}H NMR spectrum of *N*-phenethylundecan-4-amine (**215i**) ($CDCl_3$, 400 MHz)

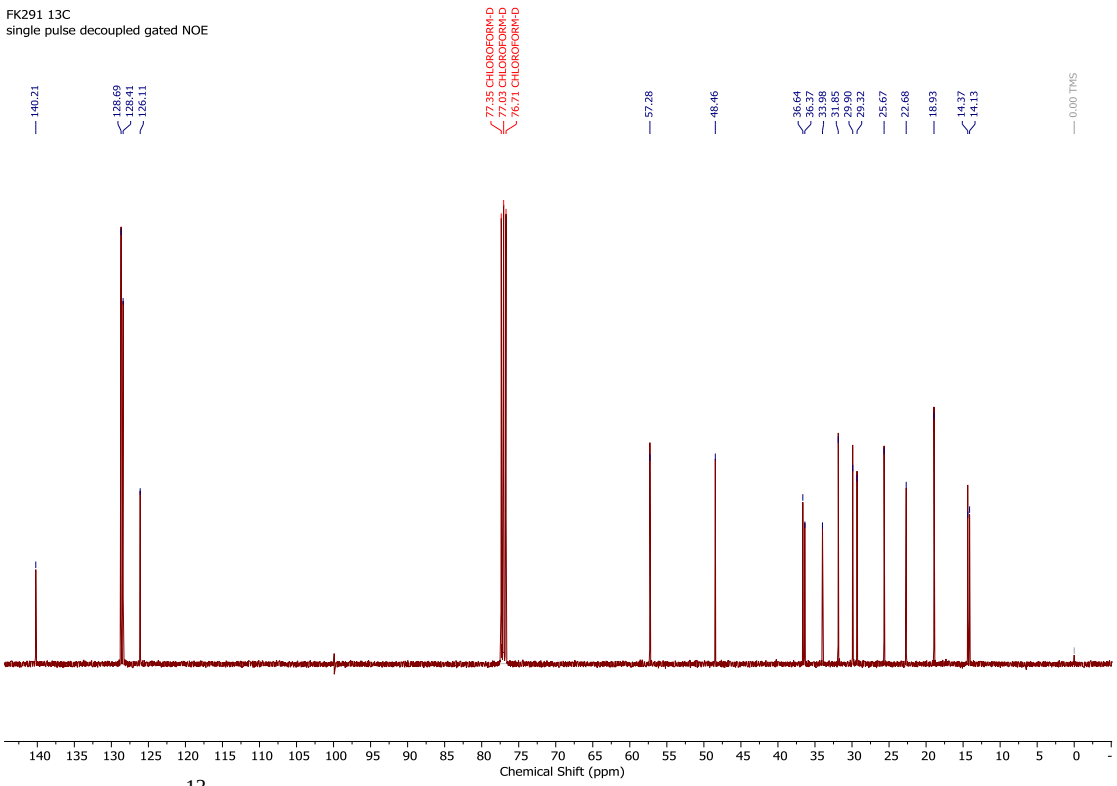


Figure S155. ^{13}C NMR spectrum of *N*-phenethylundecan-4-amine (**215i**) ($CDCl_3$, 100 MHz)

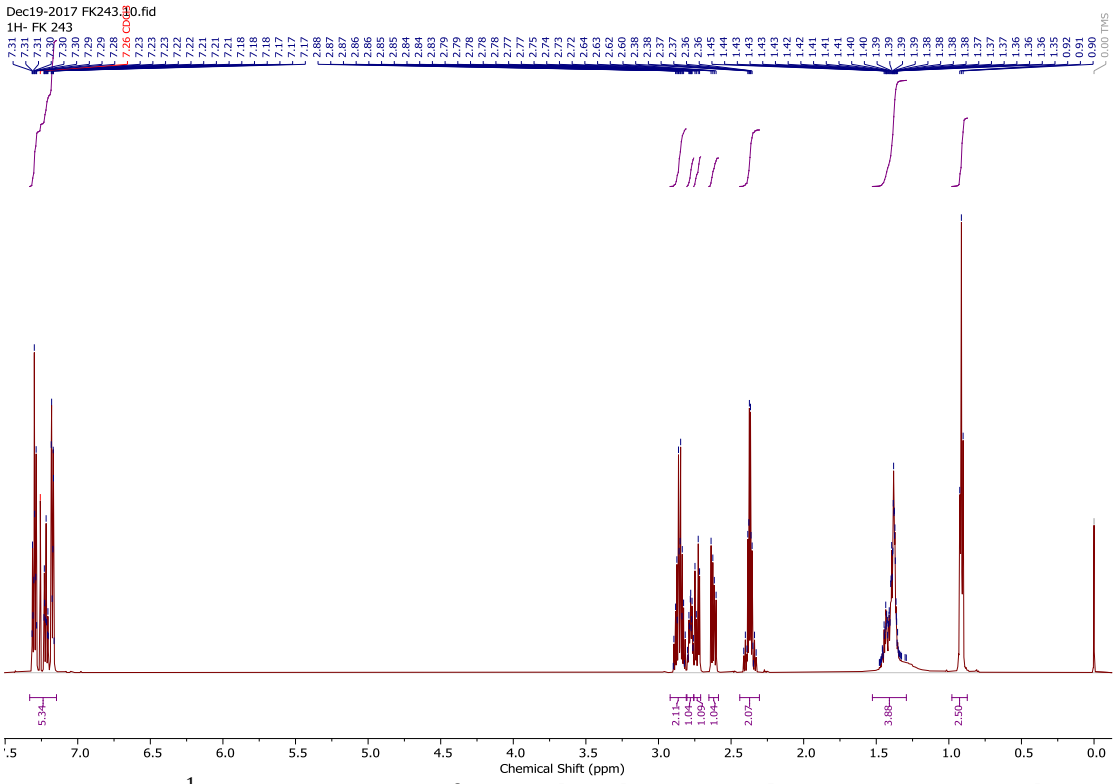


Figure S156. ^{1}H NMR spectrum of 3-((1-phenylpentan-2-yl)amino)propanenitrile (**215j**) ($CDCl_3$, 600 MHz)

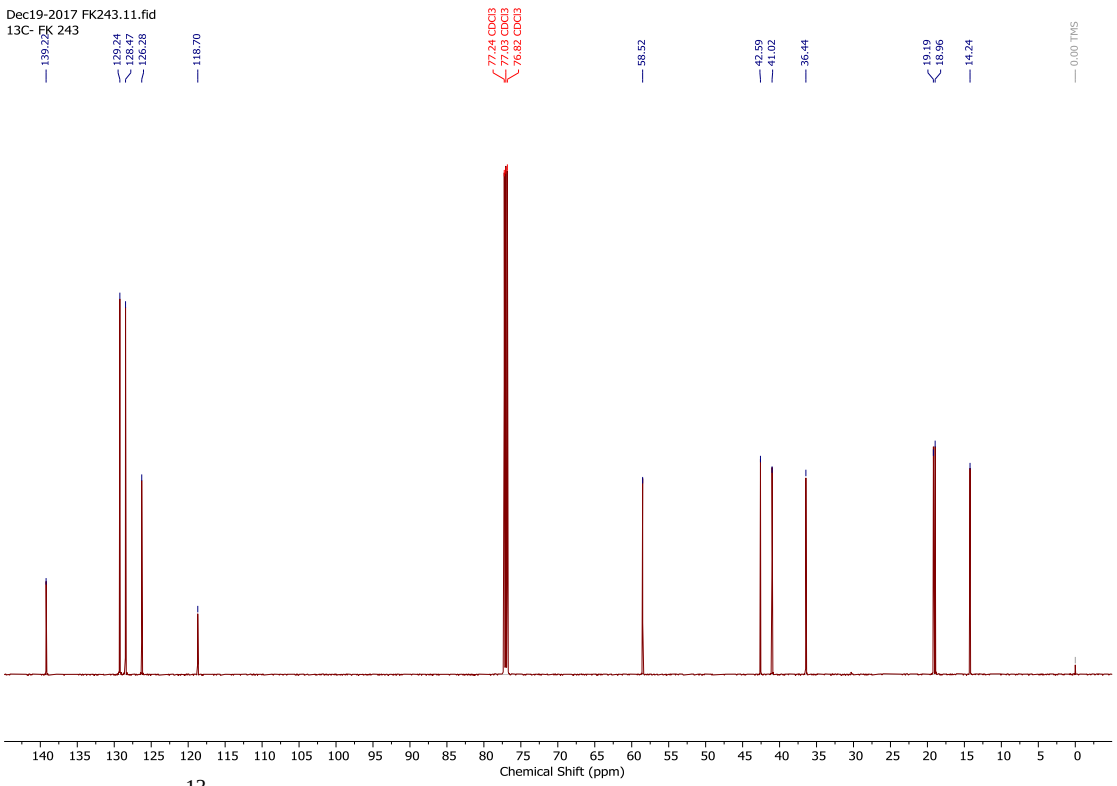


Figure S157. ^{13}C NMR spectrum of 3-((1-phenylpentan-2-yl)amino)propanenitrile (**215j**) ($CDCl_3$, 150 MHz)

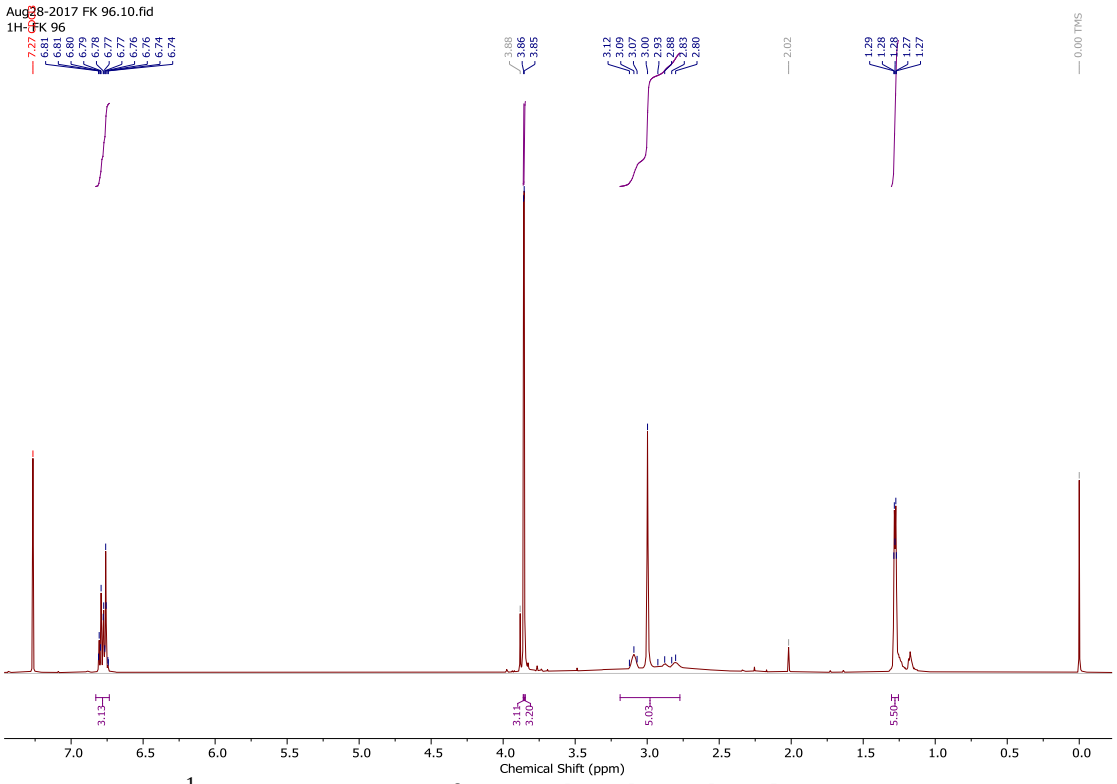


Figure S158. ^{1}H NMR spectrum of 2-(3,4-dimethoxyphenyl)-1-(isopropylamino)ethane (**215k**) ($CDCl_3$, 600 MHz)

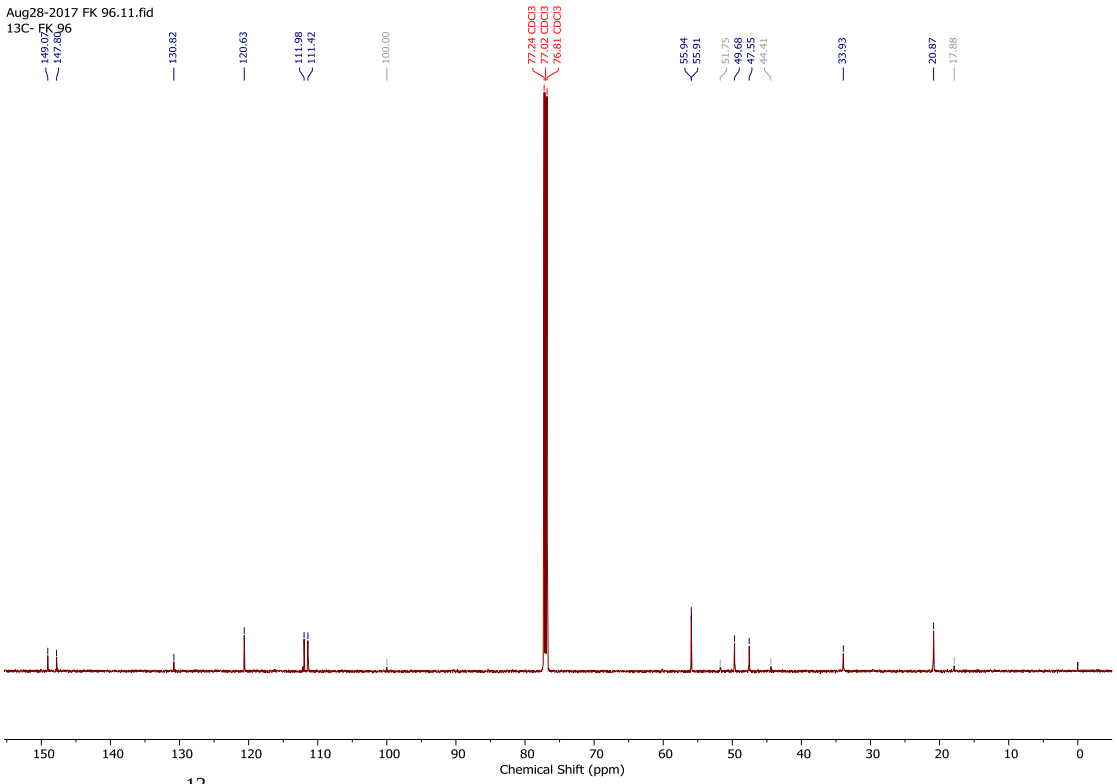


Figure S159. ^{13}C NMR spectrum of 2-(3,4-dimethoxyphenyl)-1-(isopropylamino)ethane (**215k**) ($CDCl_3$, 150 MHz)

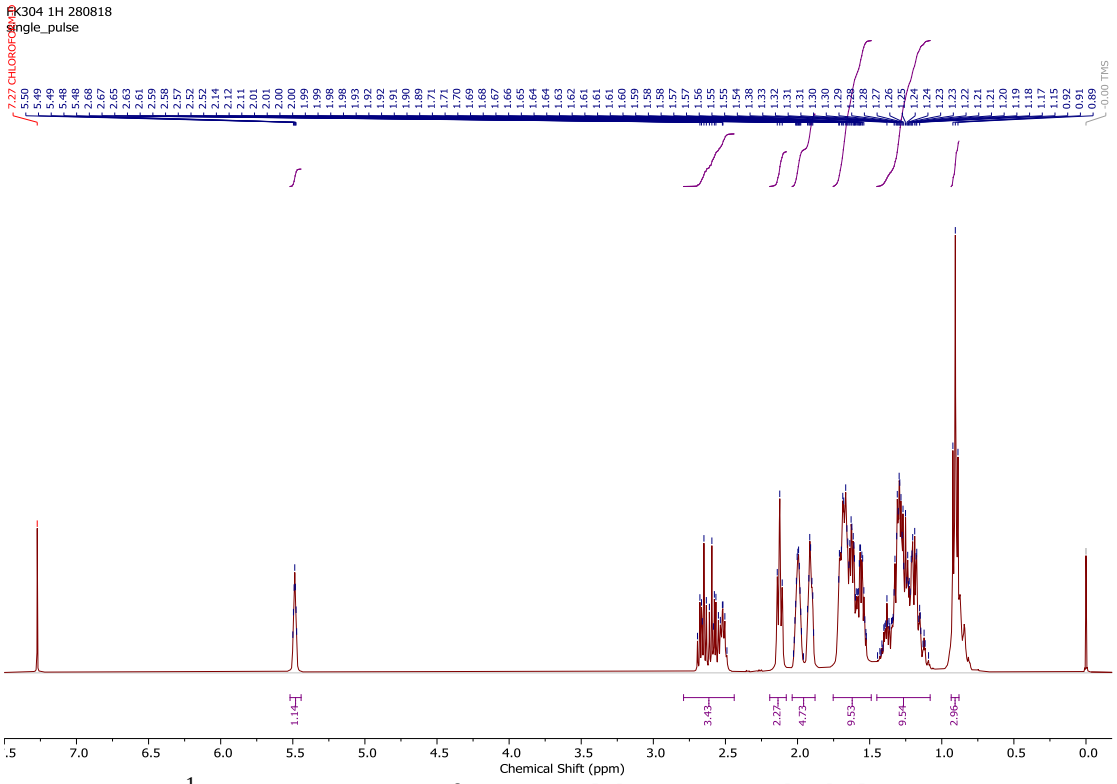


Figure S160. ^{1}H NMR spectrum of *N*-(2-(cyclohex-1-en-1-yl)ethyl)-1-cyclohexylpentan-2-amine (**215l**) ($CDCl_3$, 400 MHz)

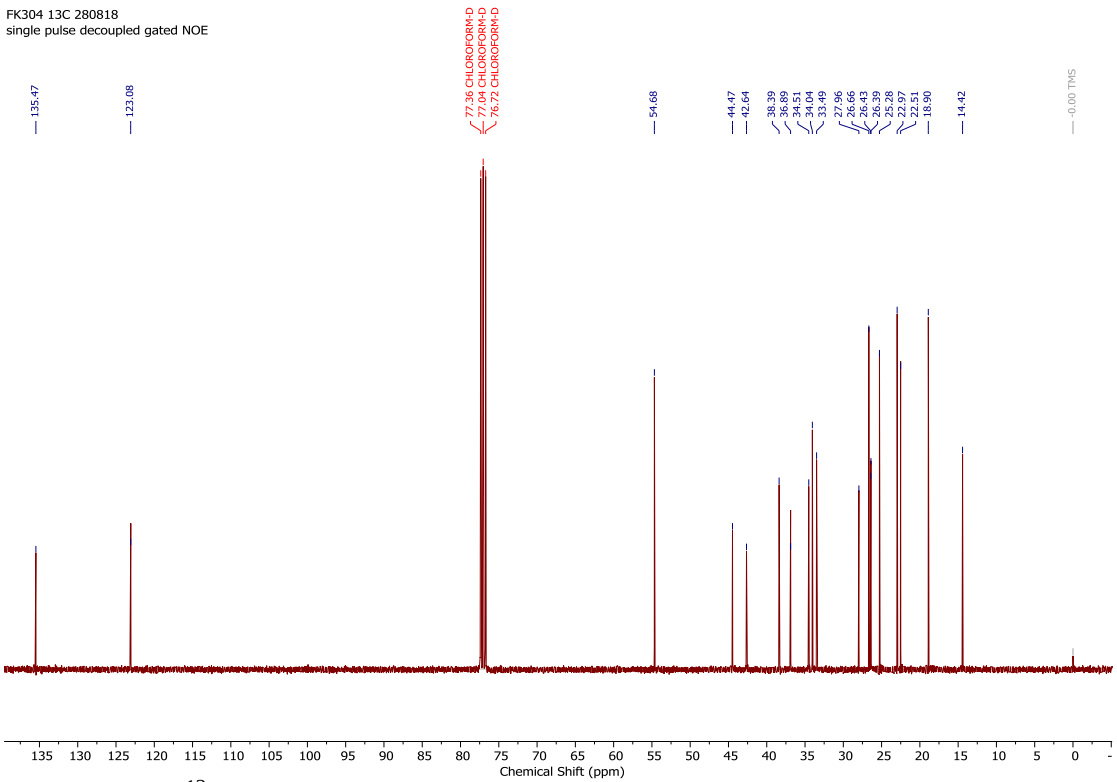


Figure S161. ^{13}C NMR spectrum of *N*-(2-(cyclohex-1-en-1-yl)ethyl)-1-cyclohexylpentan-2-amine (**215l**) ($CDCl_3$, 100 MHz)

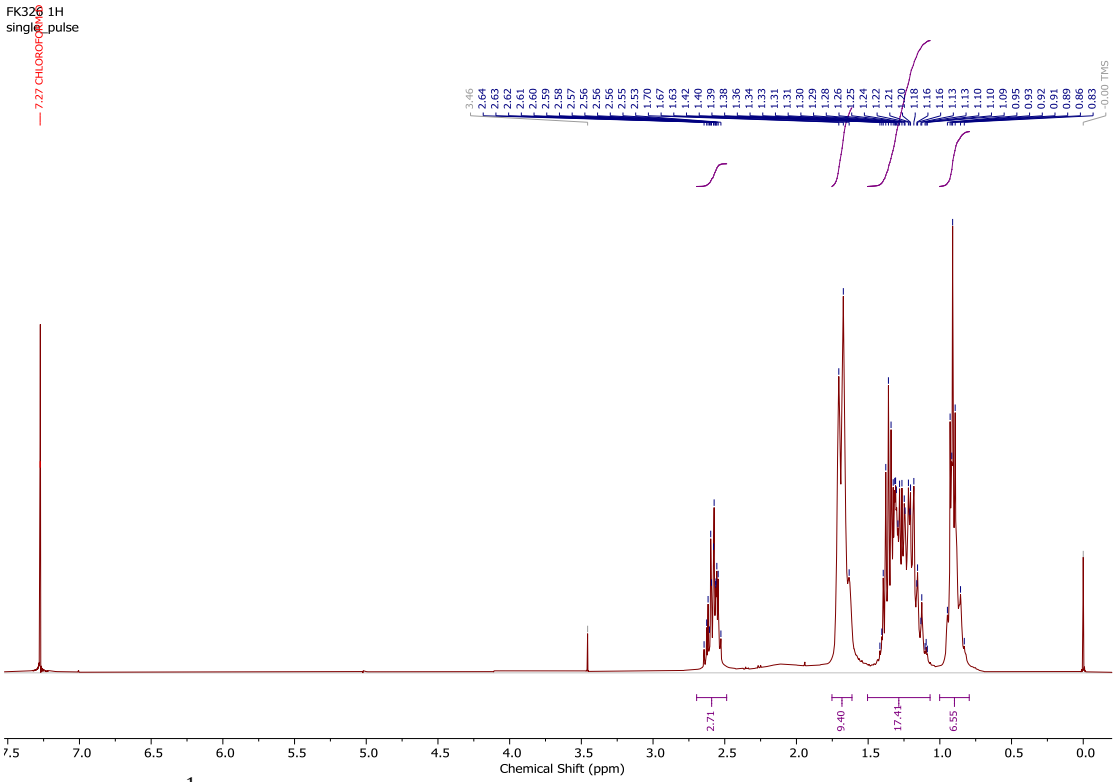


Figure S162. ^{1}H NMR spectrum of 1-cyclohexyl-*N*-(2-cyclohexylethyl)pentan-2-amine (**215m**) ($CDCl_3$, 400 MHz)

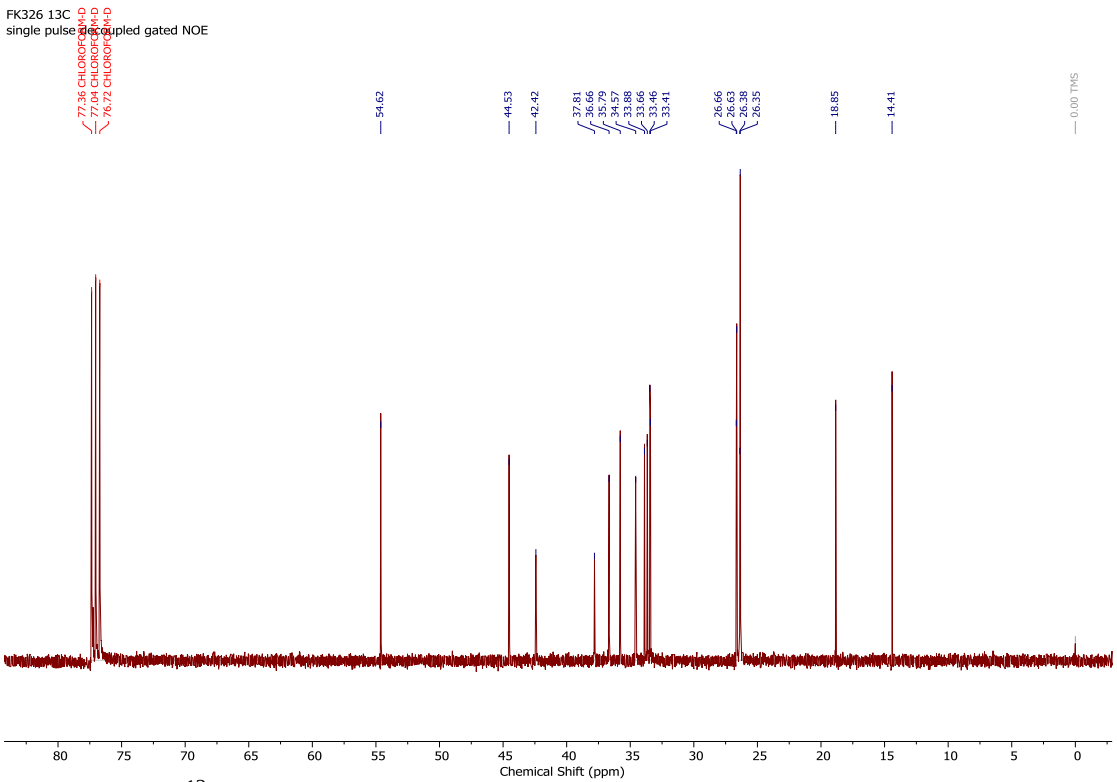


Figure S163. ^{13}C NMR spectrum of 1-cyclohexyl-*N*-(2-cyclohexylethyl)pentan-2-amine (**215m**) ($CDCl_3$, 100 MHz)

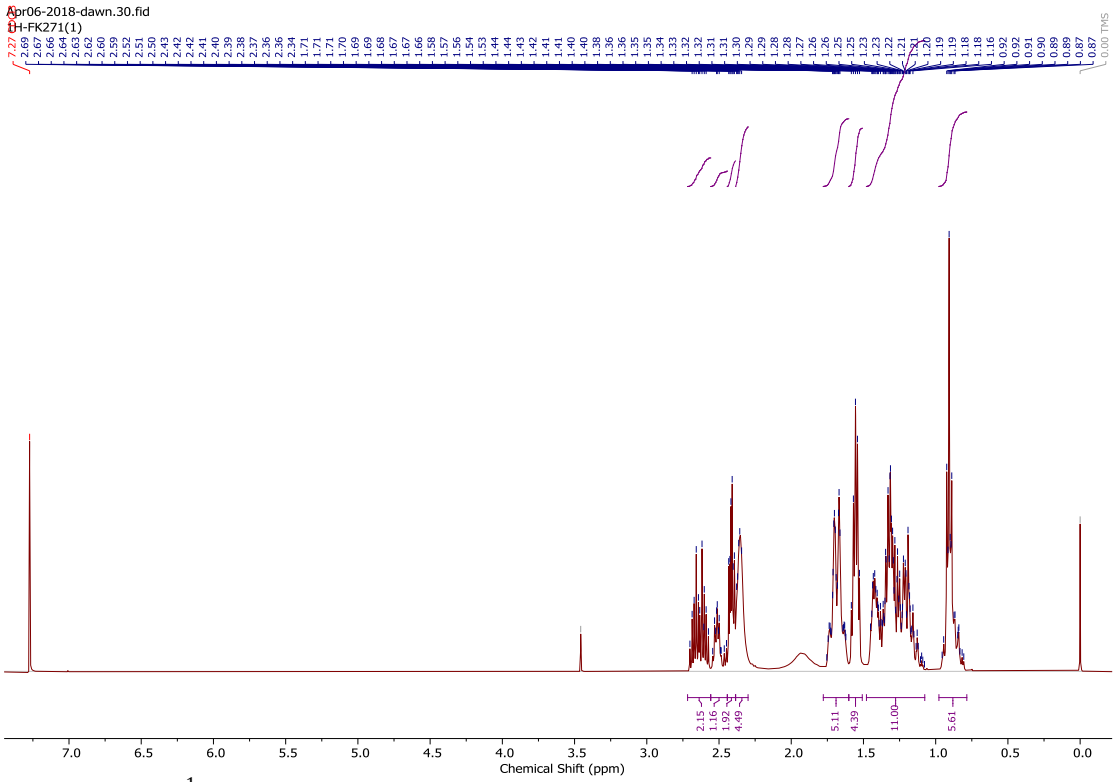


Figure S164. ^{1}H NMR spectrum of 1-cyclohexyl-*N*-(2-(piperidin-1-yl)ethyl)pentan-2-amine (**215n**) ($CDCl_3$, 400 MHz)

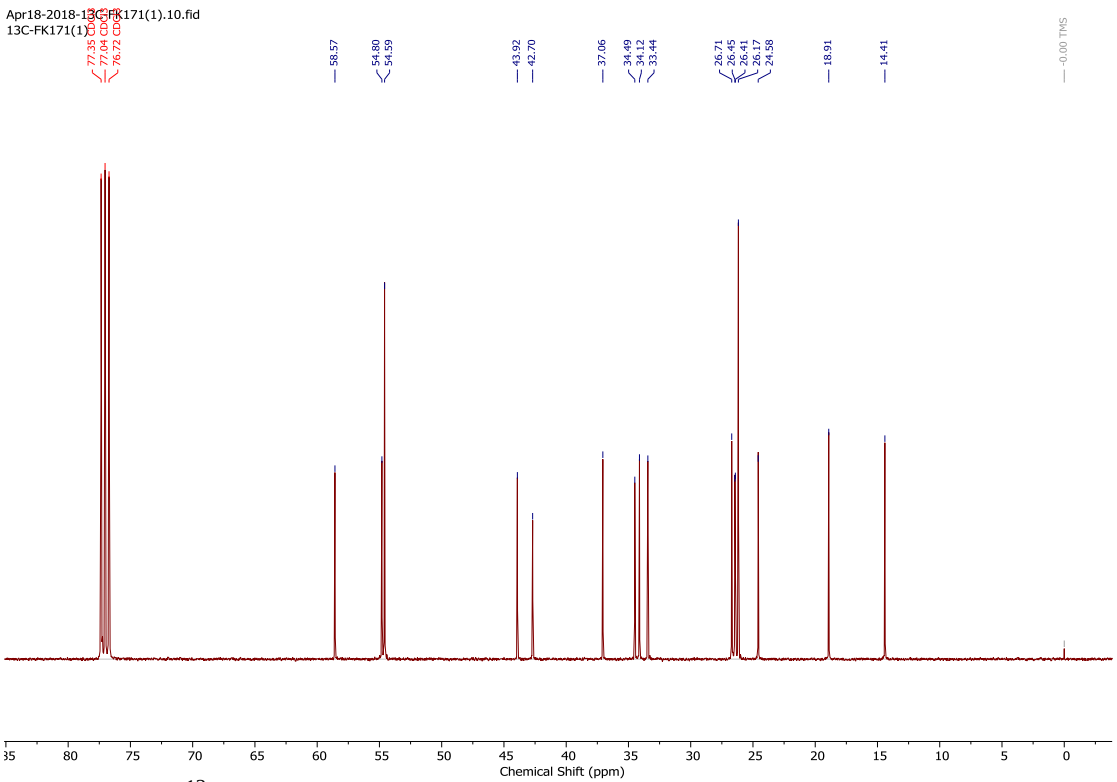


Figure S165. ^{13}C NMR spectrum of 1-cyclohexyl-*N*-(2-(piperidin-1-yl)ethyl)pentan-2-amine (**215n**) ($CDCl_3$, 100 MHz)

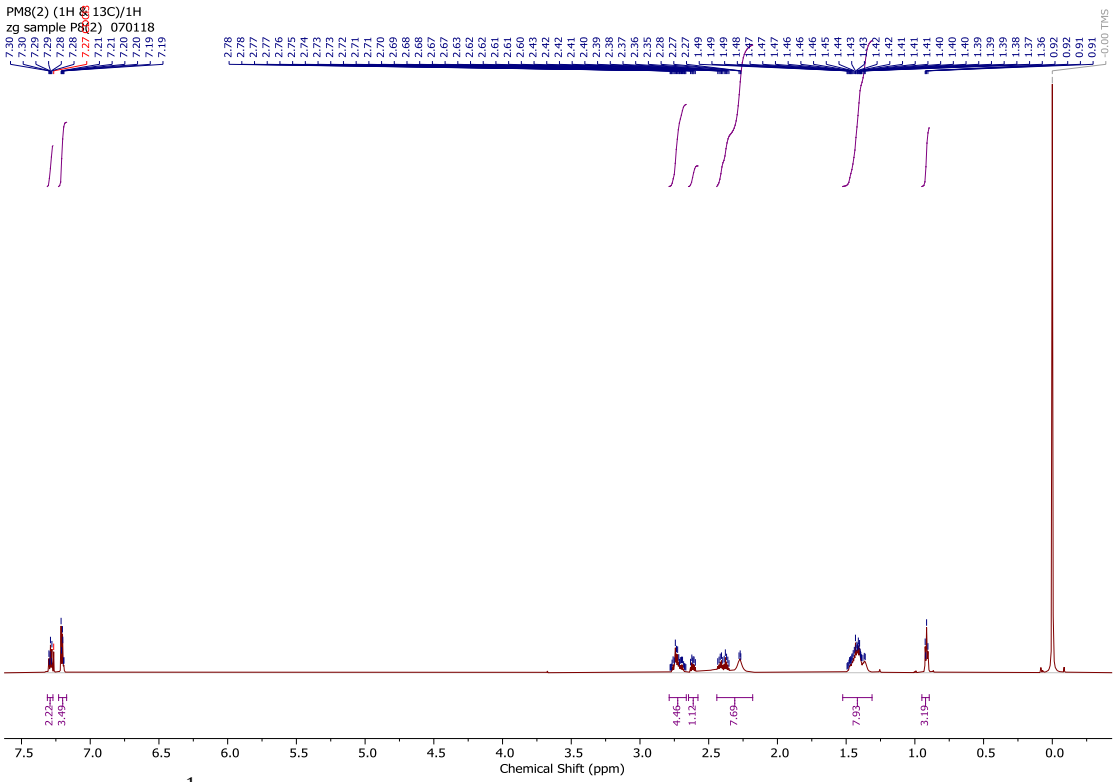


Figure S166. ^{1}H NMR spectrum of 1-phenyl-*N*-(2-(piperidin-1-yl)ethyl)pentan-2-amine (**215o**) ($CDCl_3$, 700 MHz)

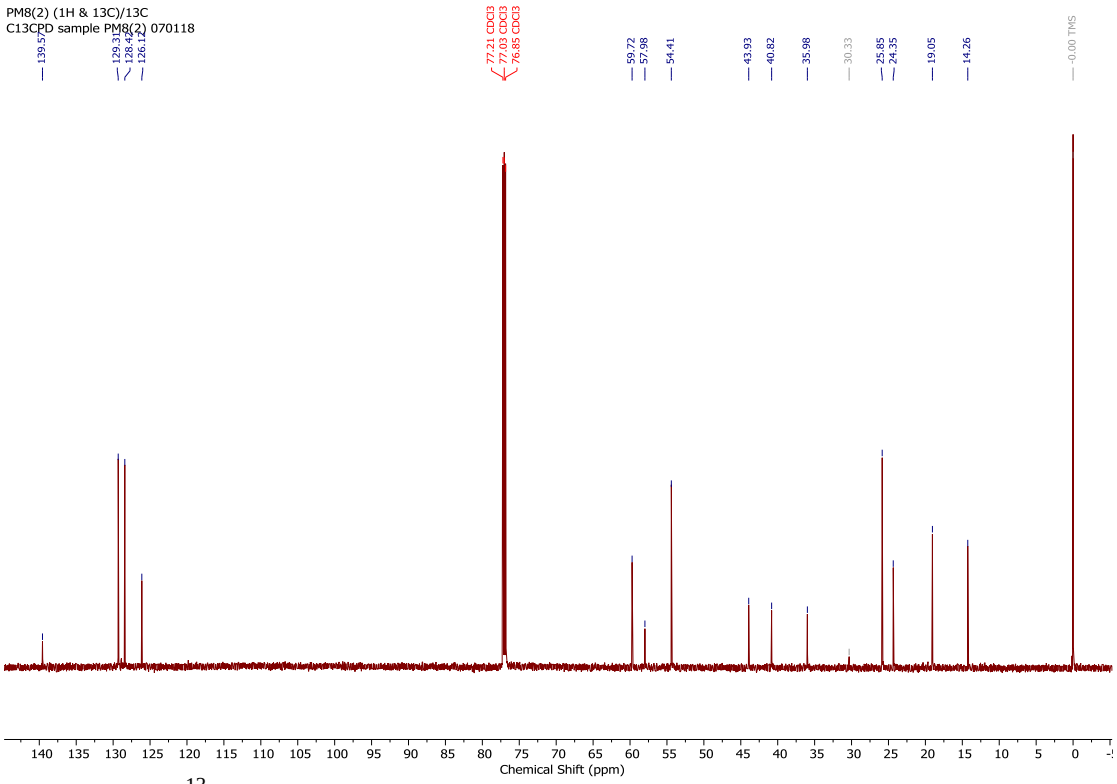


Figure S167. ^{13}C NMR spectrum of 1-phenyl-*N*-(2-(piperidin-1-yl)ethyl)pentan-2-amine (**215o**) ($CDCl_3$, 175 MHz)

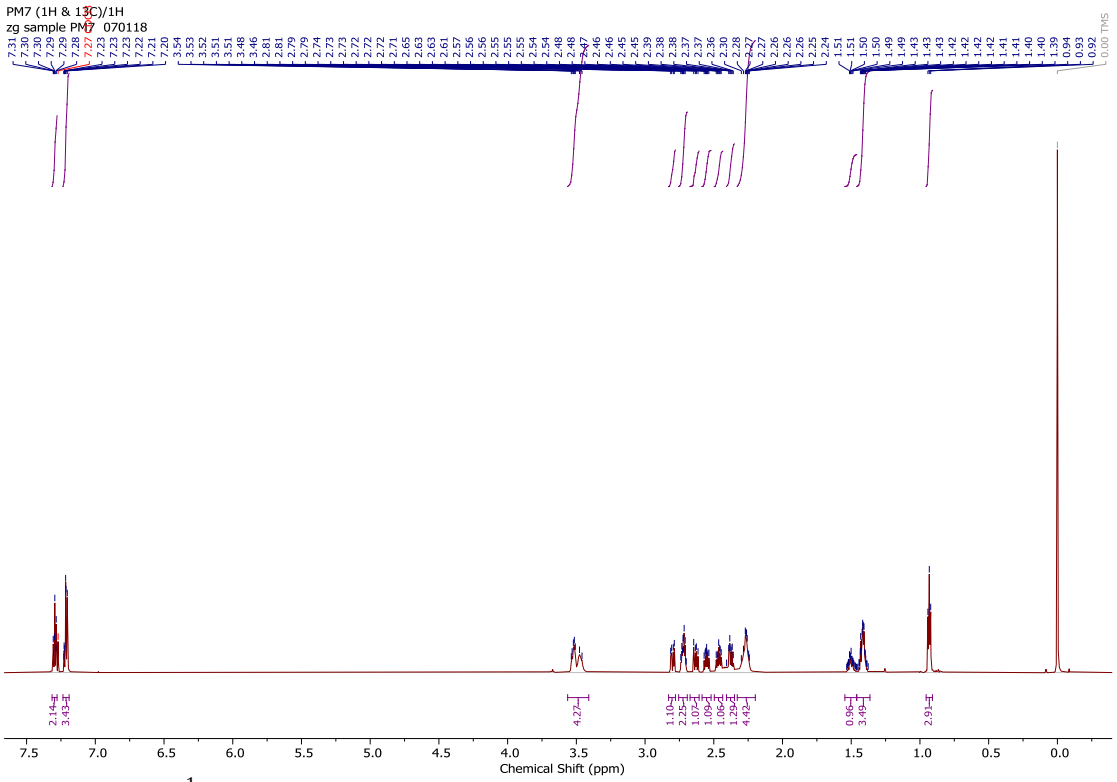


Figure S168. ^{1}H NMR spectrum of *N*-(2-morpholinoethyl)-1-phenylpentan-2-amine (**215p**) ($CDCl_3$, 700 MHz)

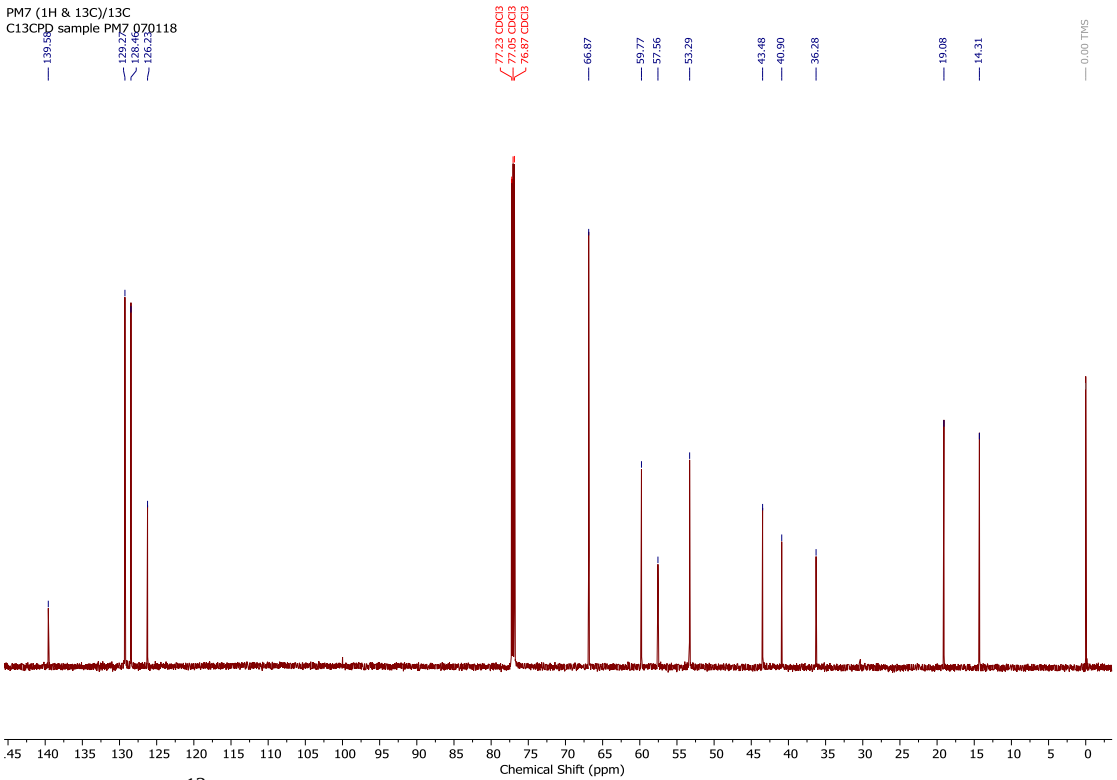


Figure S169. ^{13}C NMR spectrum of *N*-(2-morpholinoethyl)-1-phenylpentan-2-amine (**215p**) ($CDCl_3$, 175 MHz)

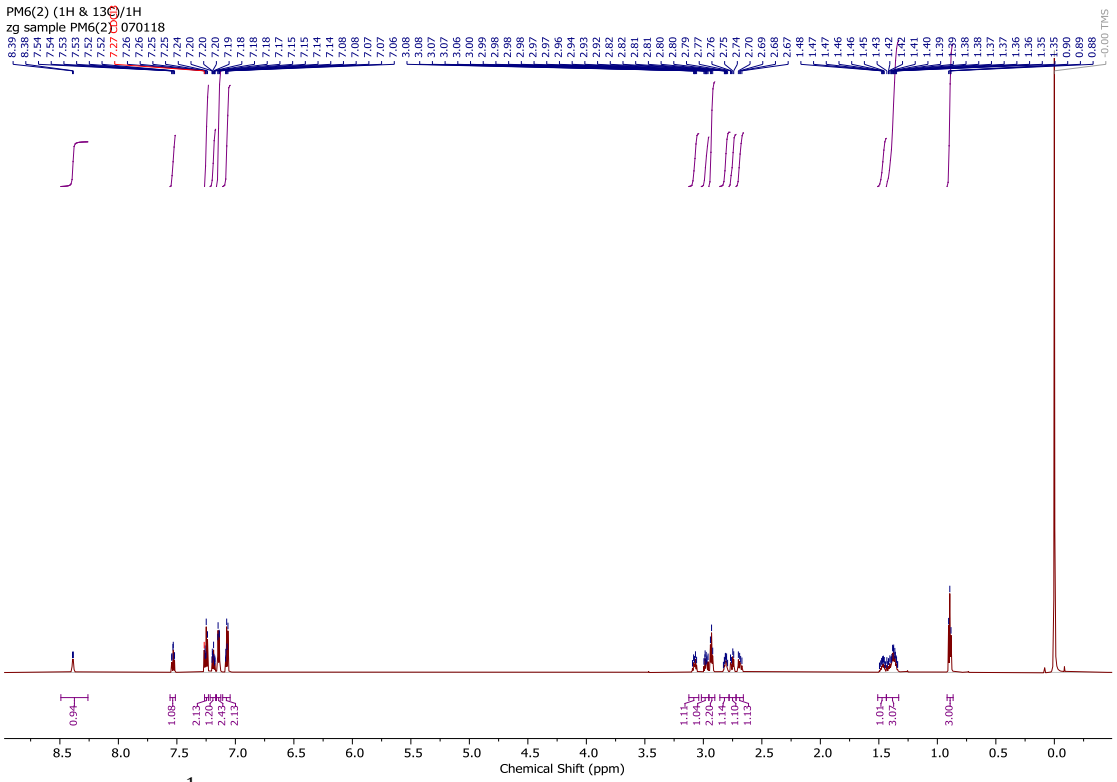


Figure S170. ^{1}H NMR spectrum of 1-phenyl-*N*-(2-(pyridine-2-yl)ethyl)pentan-2-amine (**215q**) ($CDCl_3$, 700 MHz)

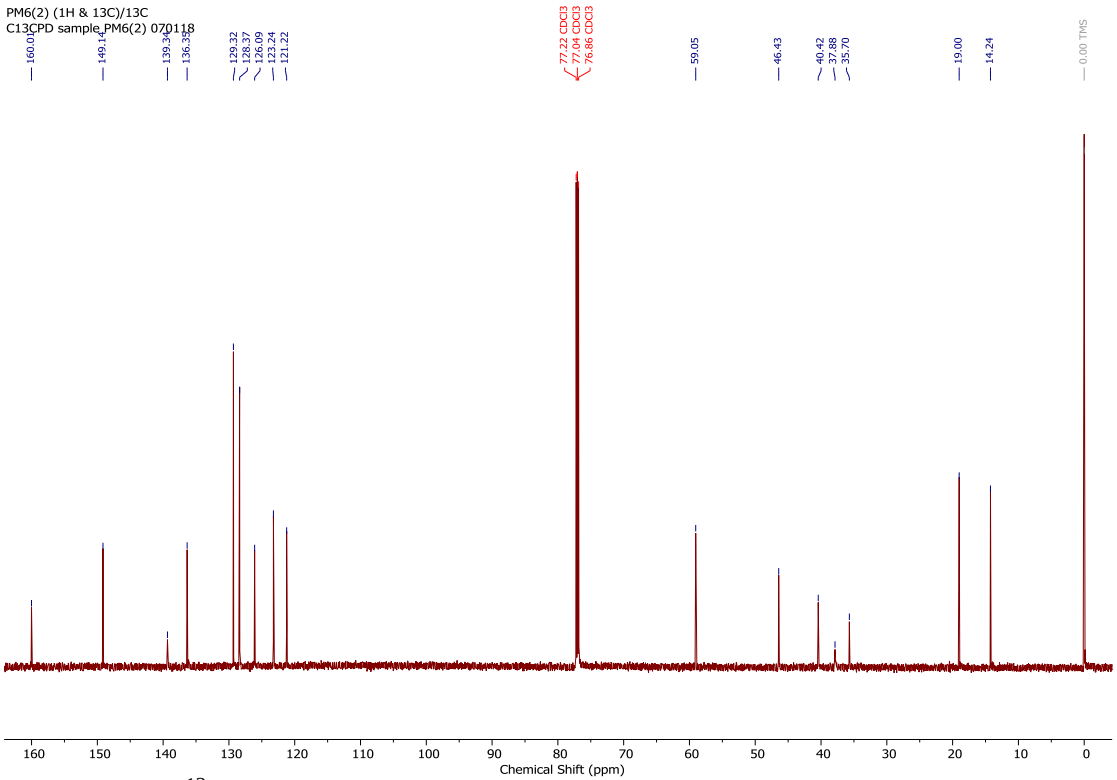


Figure S171. ^{13}C NMR spectrum of 1-phenyl-*N*-(2-(pyridine-2-yl)ethyl)pentan-2-amine (**215q**) ($CDCl_3$, 175 MHz)

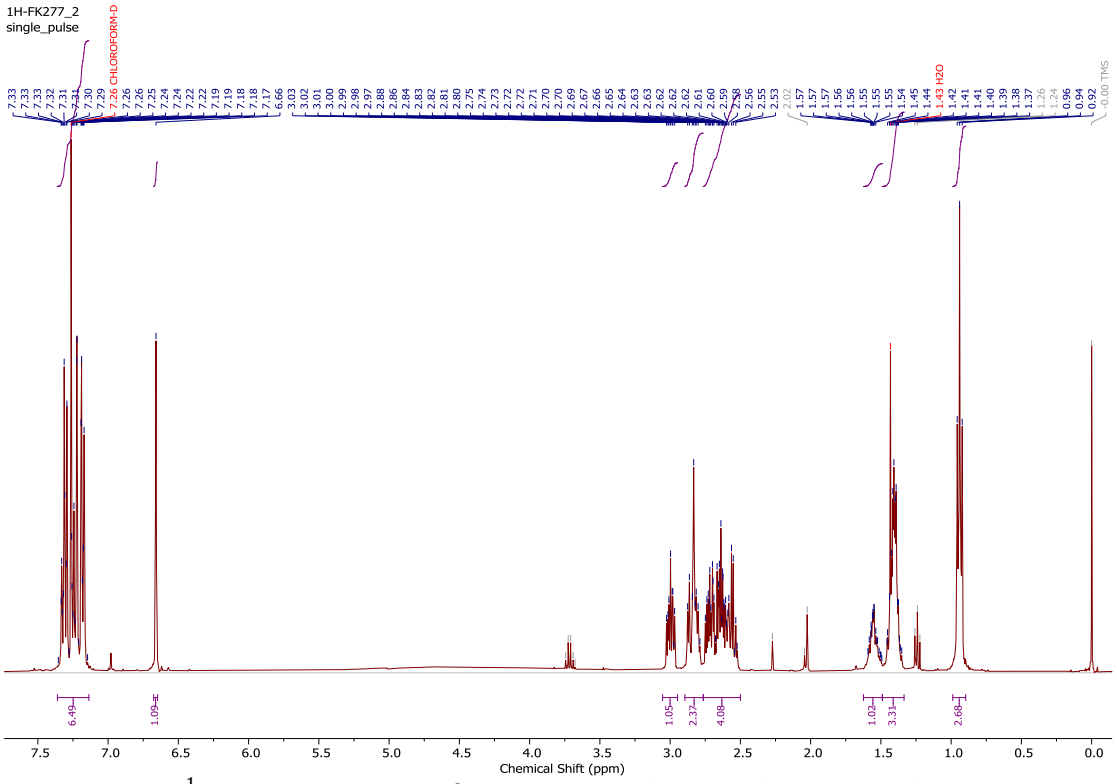


Figure S172. ^{1}H NMR spectrum of *N*-(2-(1*H*-imidazol-4-yl)ethyl)-1-phenylpentan-2-amine (**215r**) ($CDCl_3$, 400 MHz)

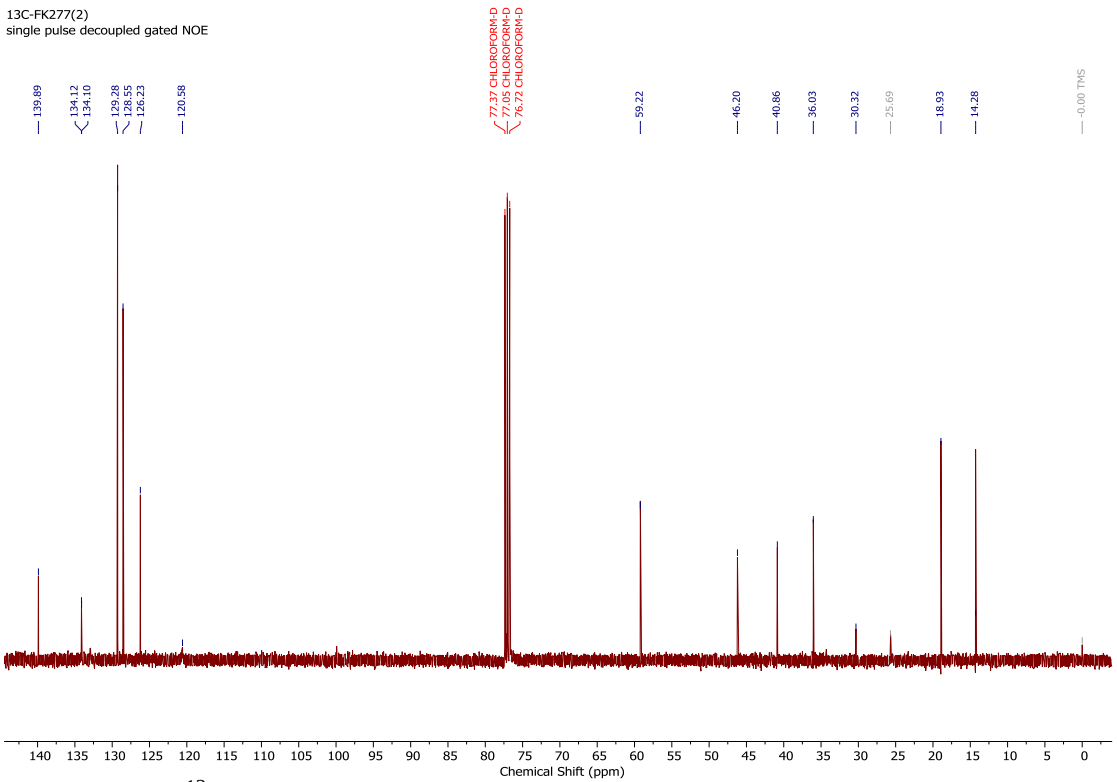


Figure S173. ^{13}C NMR spectrum of *N*-(2-(1*H*-imidazol-4-yl)ethyl)-1-phenylpentan-2-amine (**215r**) ($CDCl_3$, 100 MHz)

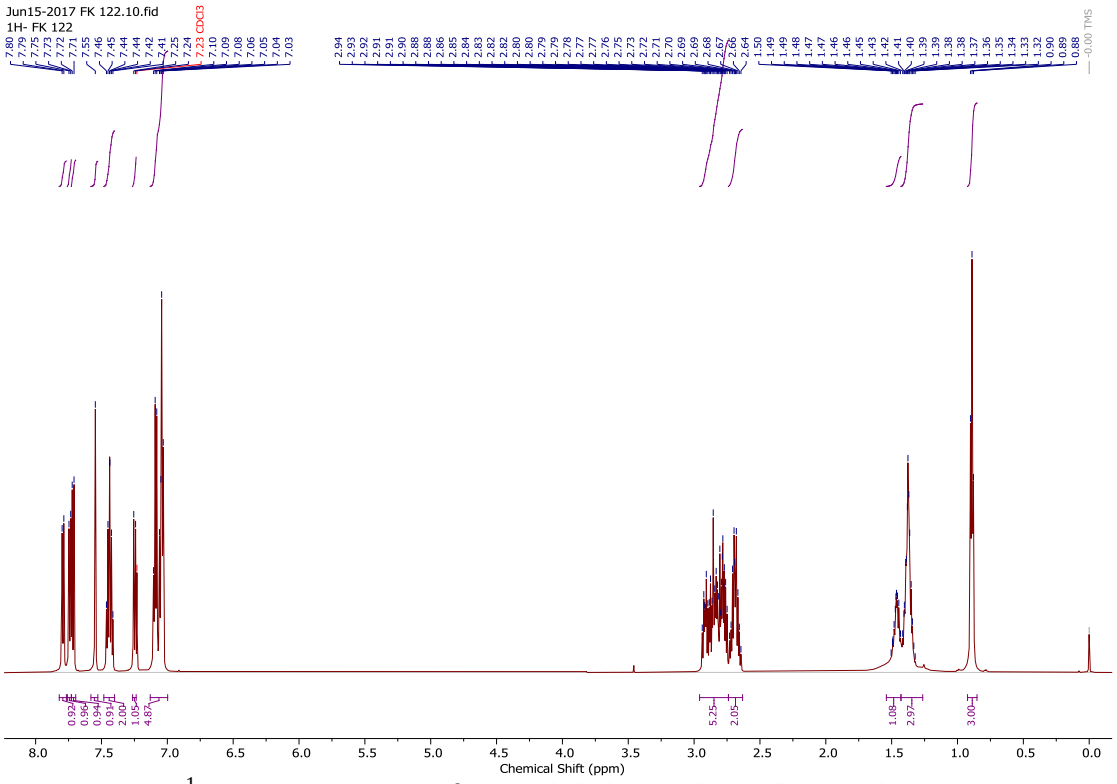


Figure S174. ^{1}H NMR spectrum of 1-(naphthalen-2-yl)-*N*-phenethylpentan-2-amine (**215s**) ($CDCl_3$, 600 MHz)

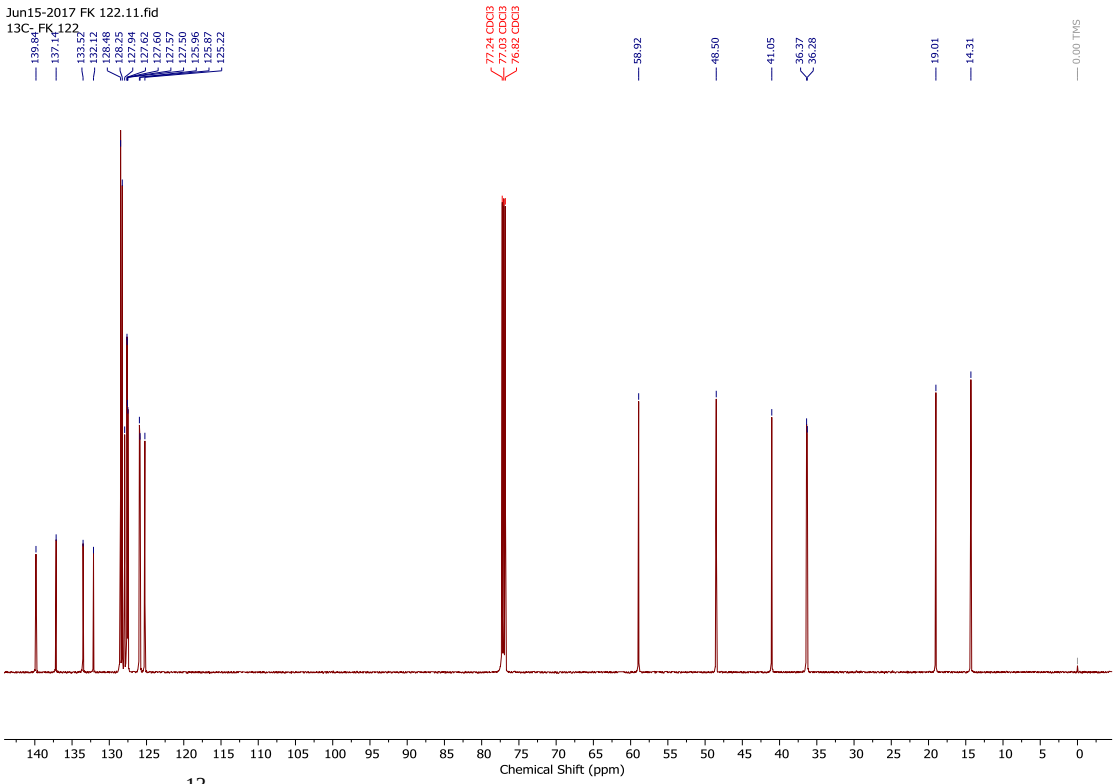


Figure S175. ^{13}C NMR spectrum of 1-(naphthalen-2-yl)-*N*-phenethylpentan-2-amine (**215s**) ($CDCl_3$, 150 MHz)

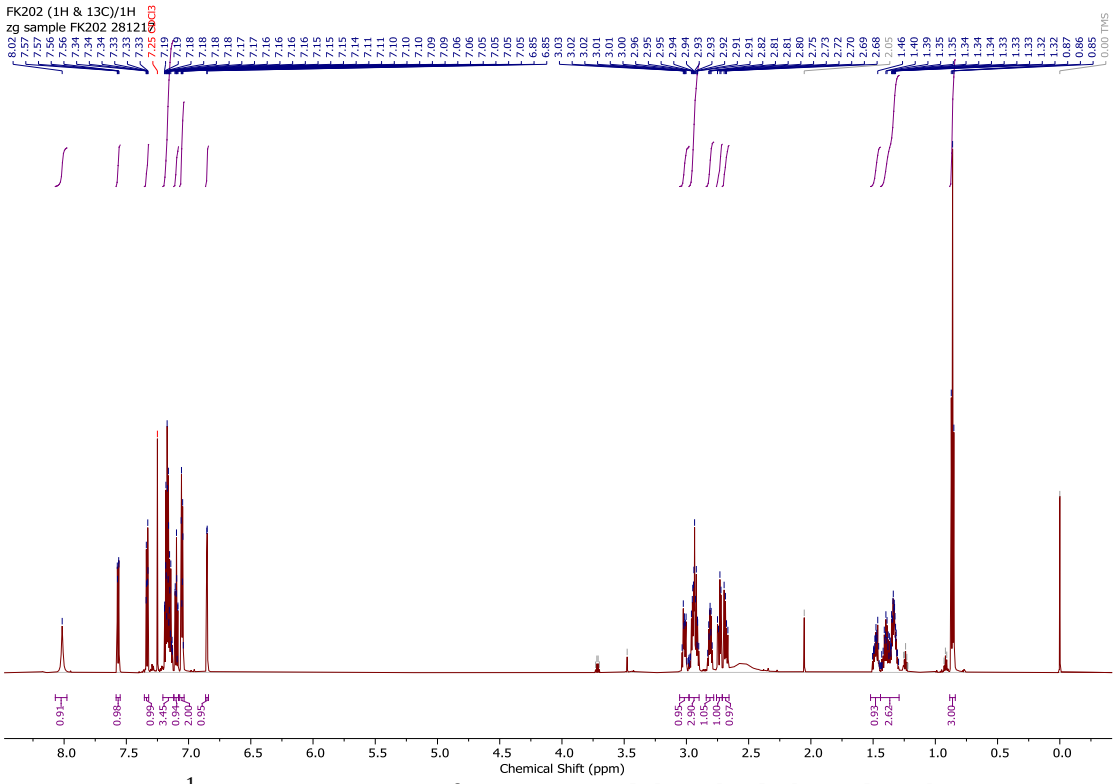


Figure S176. ^{1}H NMR spectrum of *N*-(2-(1*H*-indol-3-yl)ethyl)-1-phenylpentan-2-amine (**215t**) ($CDCl_3$, 700 MHz)

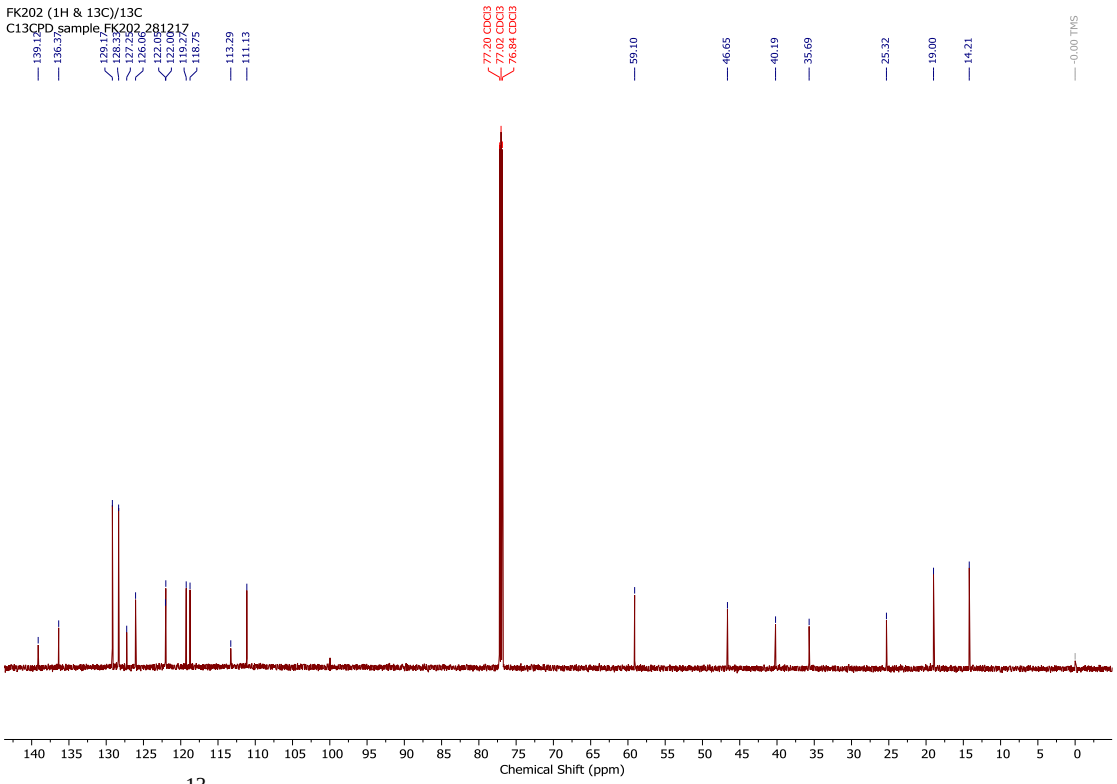


Figure S177. ^{13}C NMR spectrum of *N*-(2-(1*H*-indol-3-yl)ethyl)-1-phenylpentan-2-amine (**215t**) ($CDCl_3$, 175 MHz)

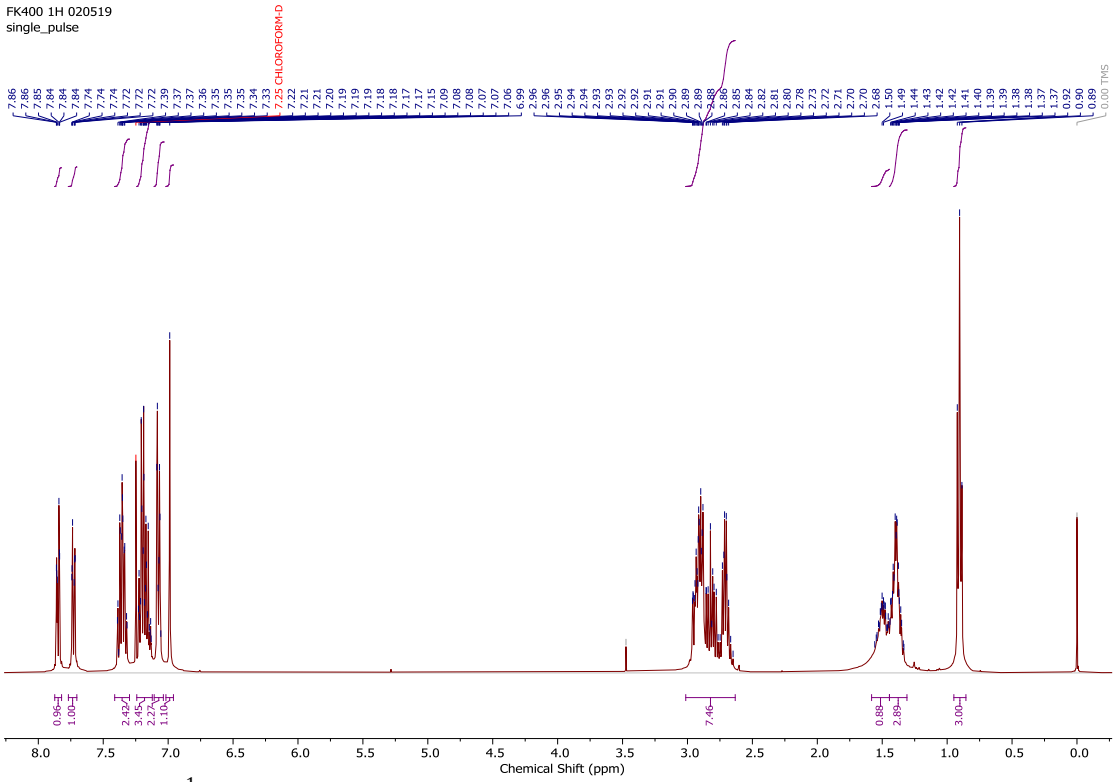


Figure S178. ^{1}H NMR spectrum of 1-(benzo[*b*]thiophen-3-yl)-*N*-phenethylpentan-2-amine (**215u**) ($CDCl_3$, 400 MHz)

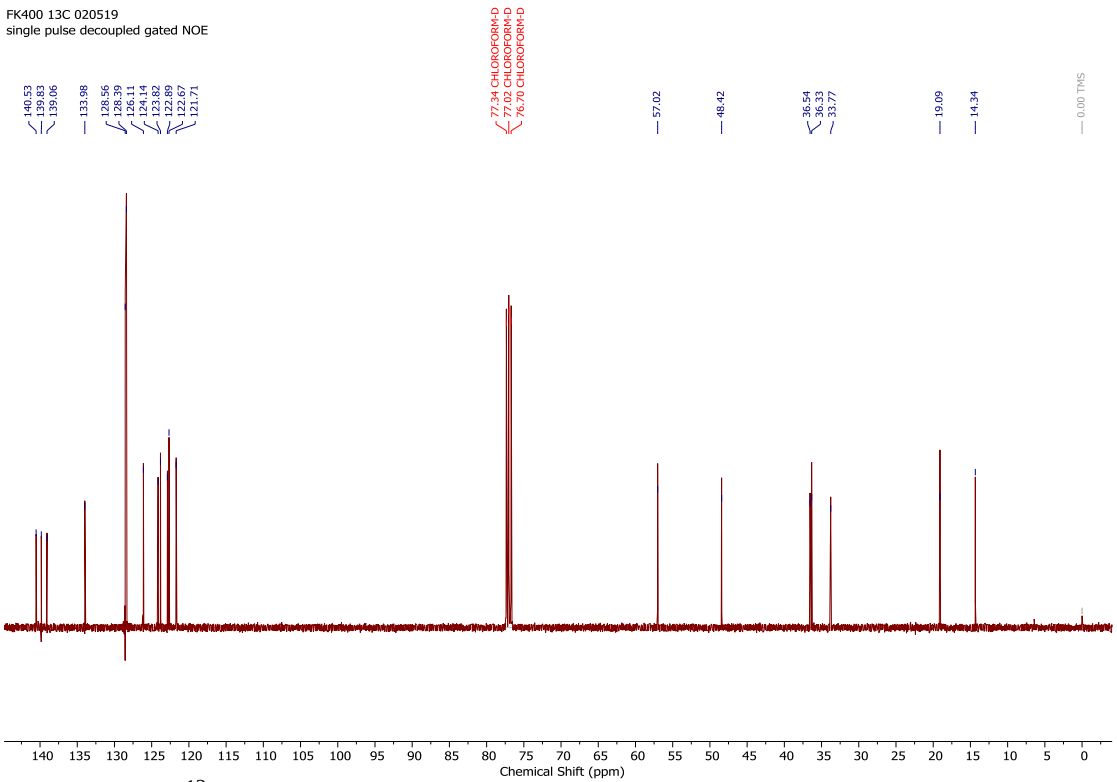


Figure S179. ^{13}C NMR spectrum of 1-(benzo[*b*]thiophen-3-yl)-*N*-phenethylpentan-2-amine (**215u**) ($CDCl_3$, 100 MHz)

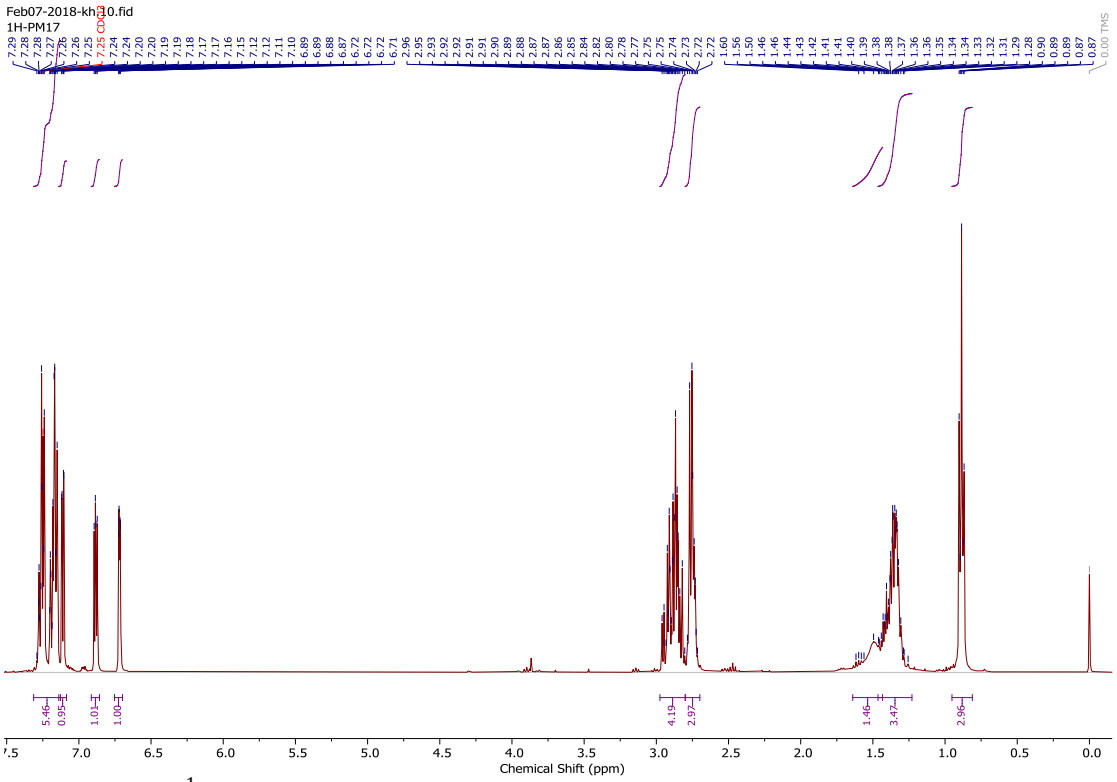


Figure S180. ^{1}H NMR spectrum of *N*-phenethyl-1-(thiophen-2-yl)pentan-2-amine (**215v**) ($CDCl_3$, 400 MHz)

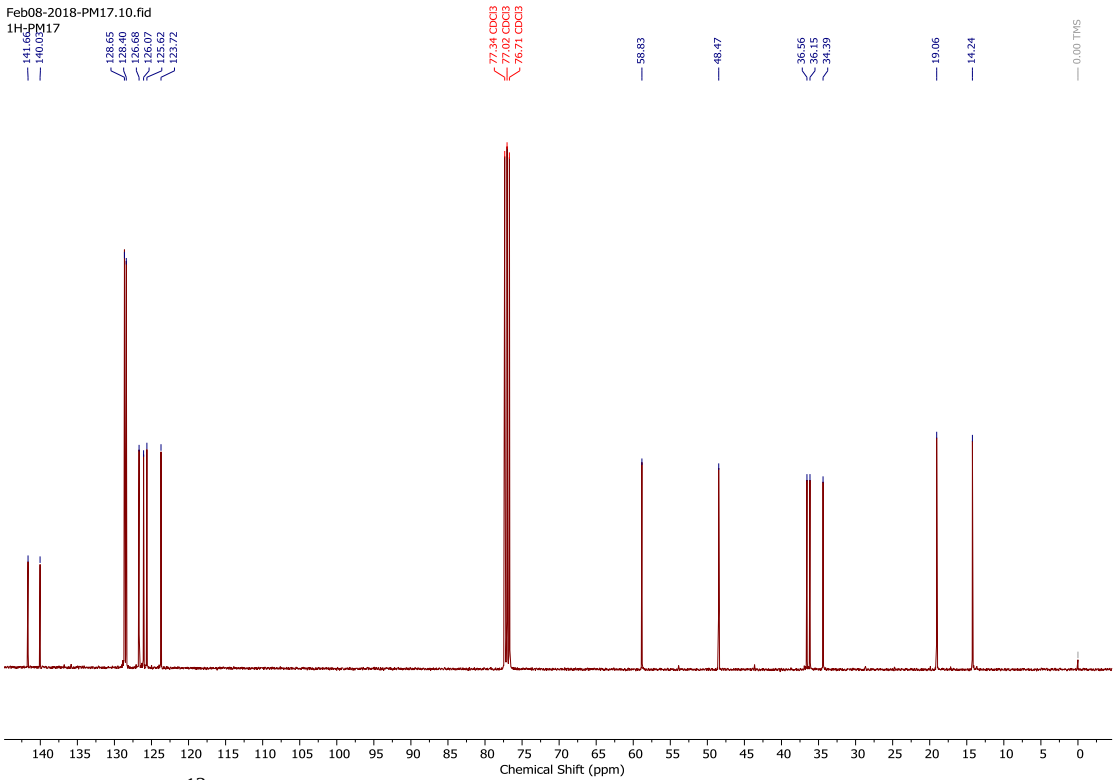


Figure S181. ^{13}C NMR spectrum of *N*-phenethyl-1-(thiophen-2-yl)pentan-2-amine (**215v**) ($CDCl_3$, 100 MHz)

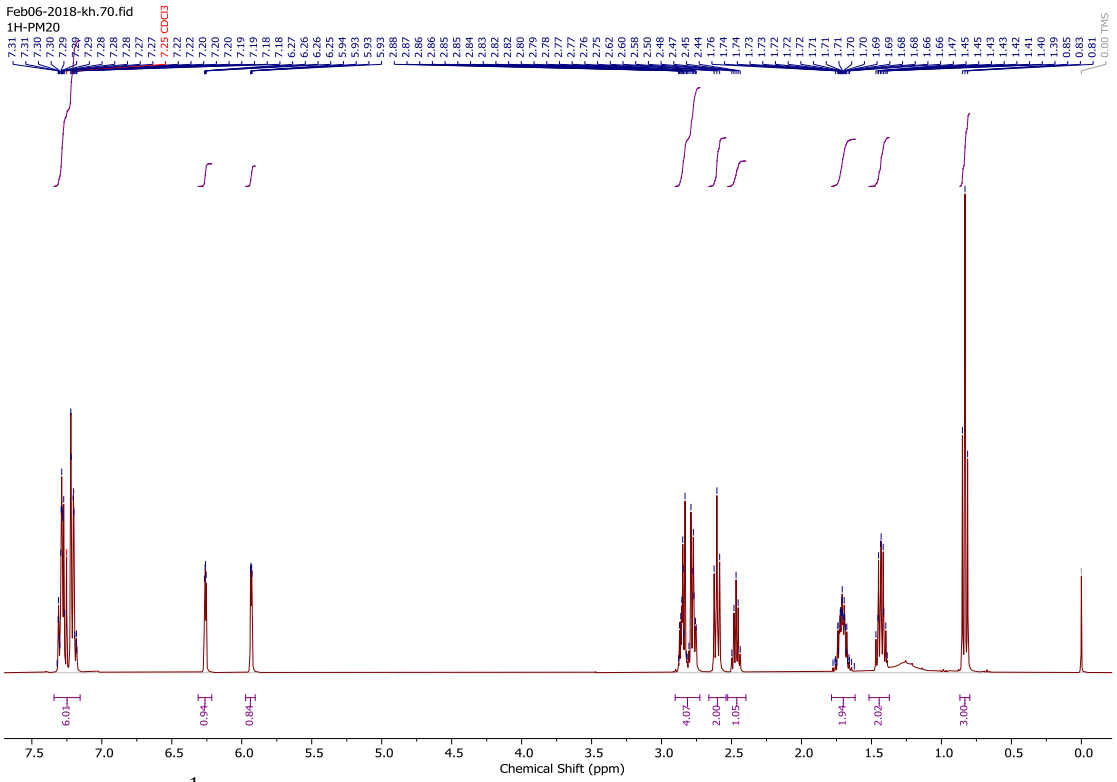


Figure S182. ^{1}H NMR spectrum of 1-(furan-2-yl)-*N*-phenethylpentan-3-amine (**215w**) ($CDCl_3$, 400 MHz)

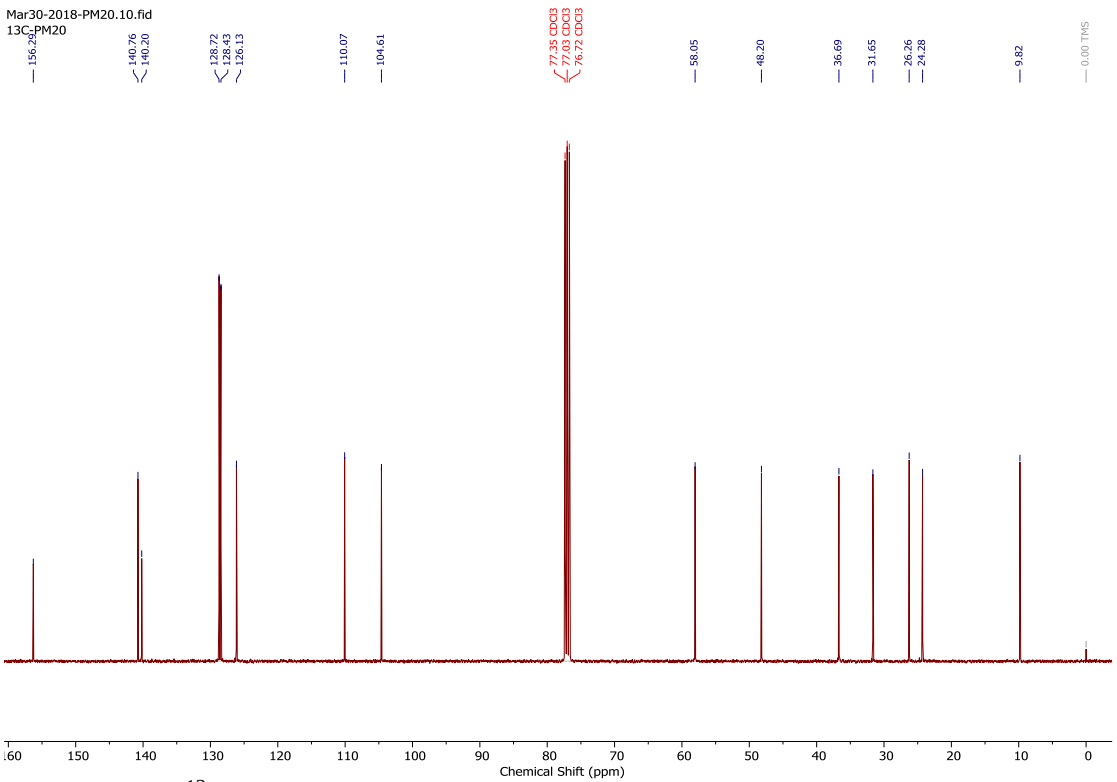


Figure S183. ^{13}C NMR spectrum of 1-(furan-2-yl)-*N*-phenethylpentan-3-amine (**215w**) ($CDCl_3$, 100 MHz)

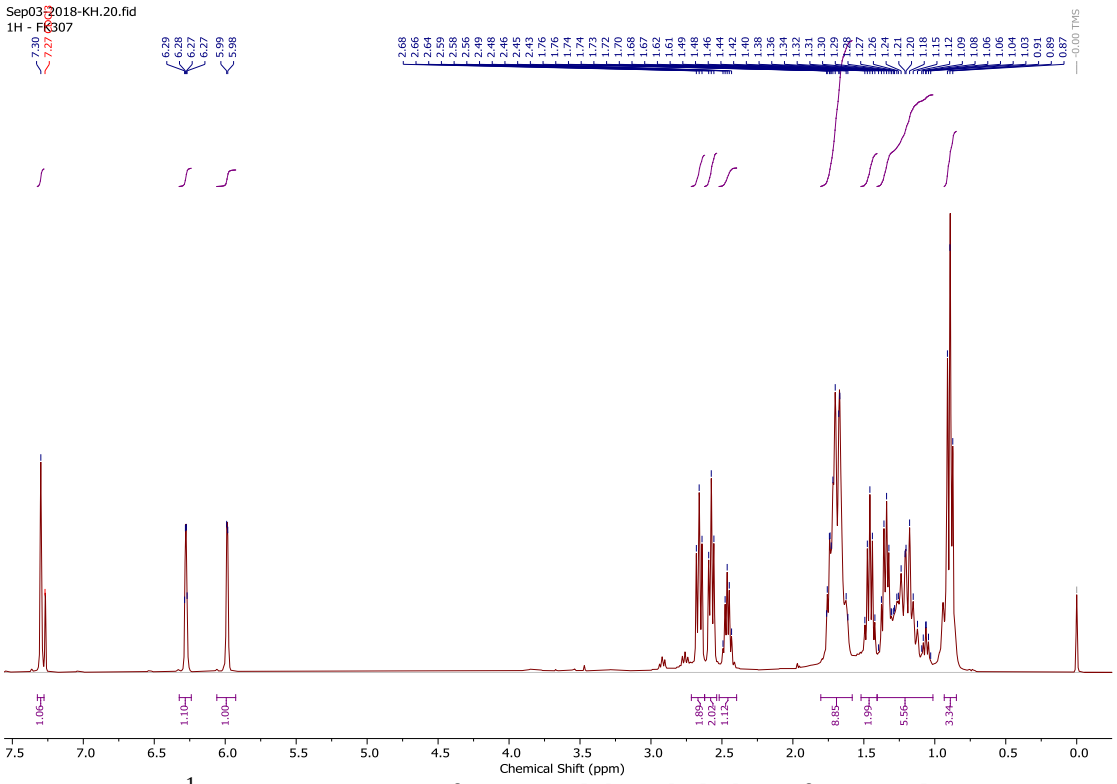


Figure S184. ^{1}H NMR spectrum of *N*-(2-cyclohexylethyl)-1-(furan-2-yl)pentan-3-amine (**215x**) ($CDCl_3$, 400 MHz)

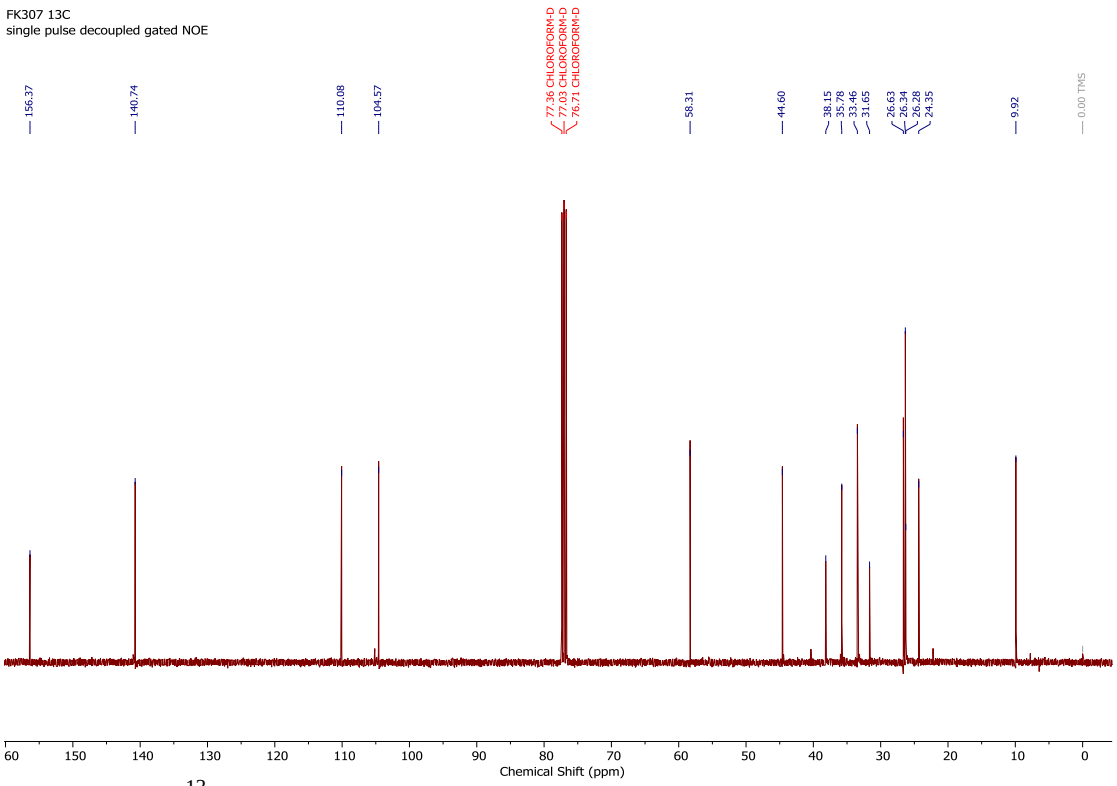


Figure S185. ^{13}C NMR spectrum of *N*-(2-cyclohexylethyl)-1-(furan-2-yl)pentan-3-amine (**215x**) ($CDCl_3$, 100 MHz)

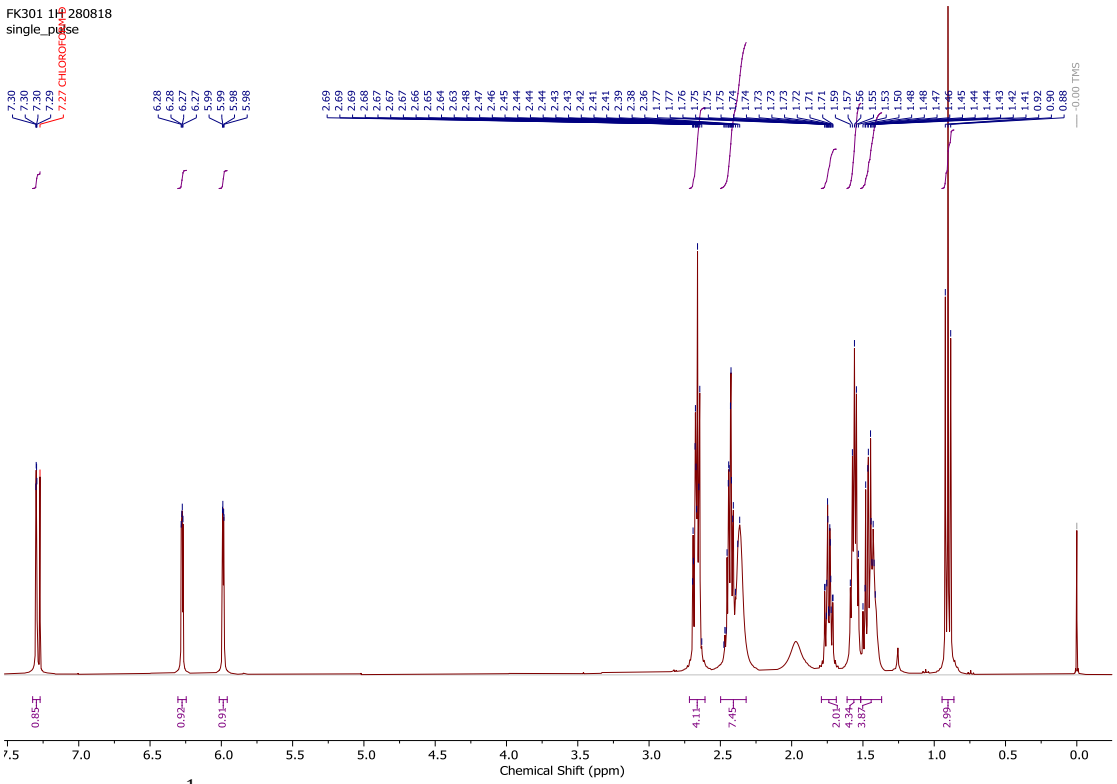


Figure S186. ^{1}H NMR spectrum of 1-(furan-2-yl)-*N*-(2-(piperidin-1-yl)ethyl)pentan-3-amine (**215y**) ($CDCl_3$, 400 MHz)

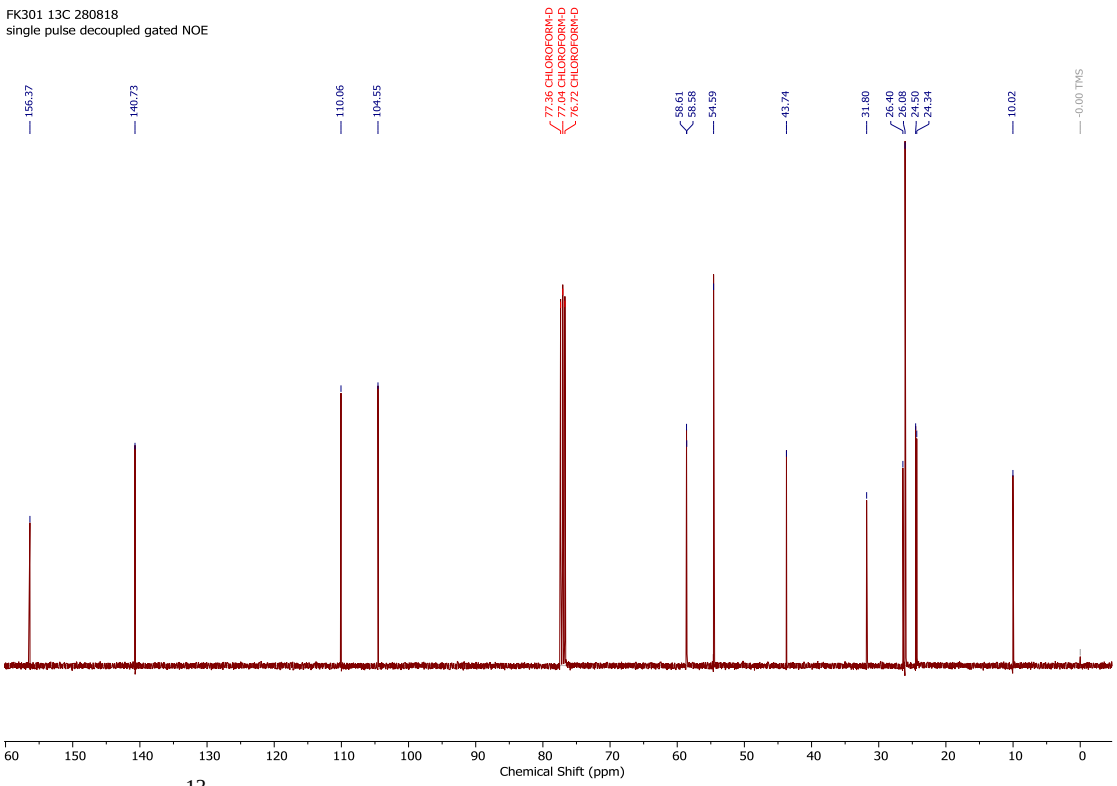


Figure S187. ^{13}C NMR spectrum of 1-(furan-2-yl)-*N*-(2-(piperidin-1-yl)ethyl)pentan-3-amine (**215y**) ($CDCl_3$, 100 MHz)

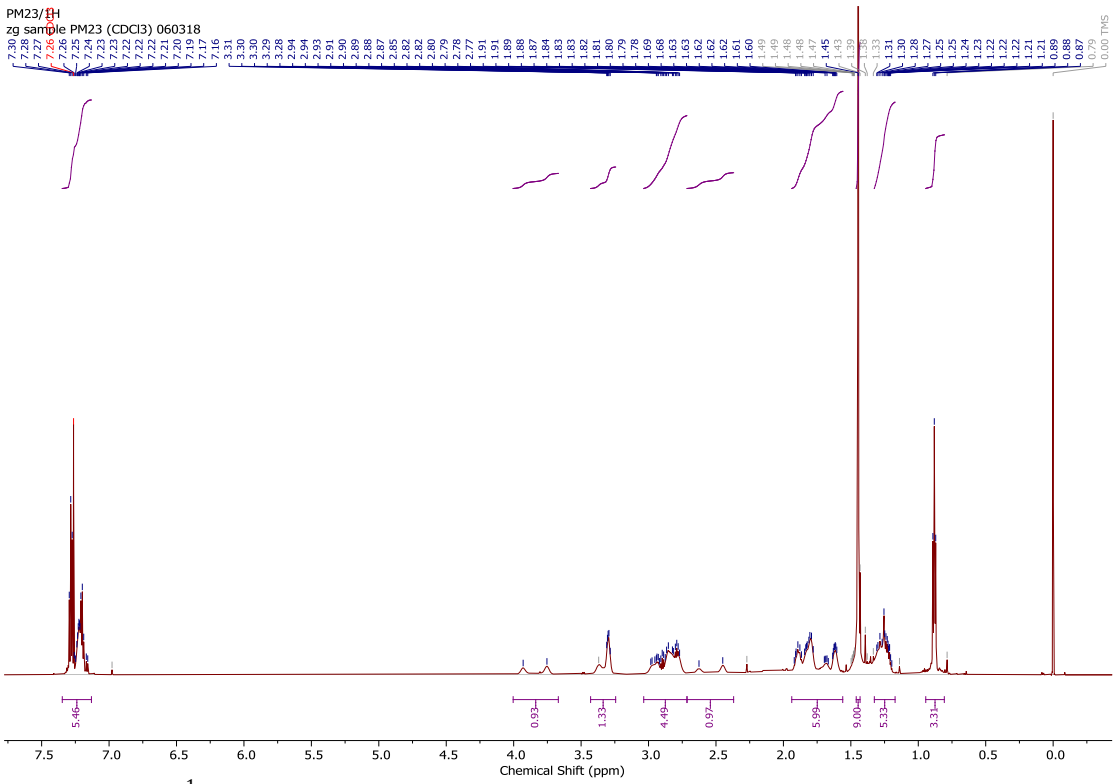


Figure S188. ^{1}H NMR spectrum of (2*S*)-*tert*-butyl 2-(2-(phenethylamino)pentyl)pyrrolidine-1-carboxylate (**215z**) ($CDCl_3$, 700 MHz)

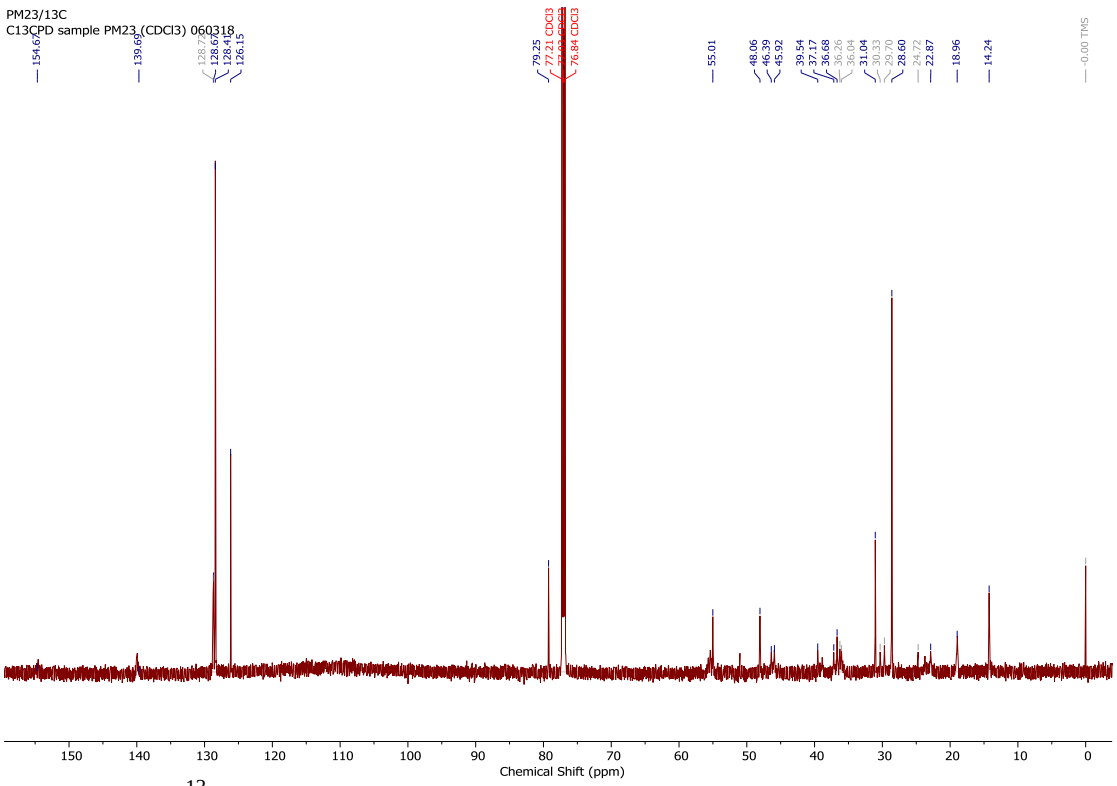


Figure S189. ^{13}C NMR spectrum of (2*S*)-*tert*-butyl 2-(2-(phenethylamino)pentyl)pyrrolidine-1-carboxylate (**215z**) ($CDCl_3$, 175 MHz)

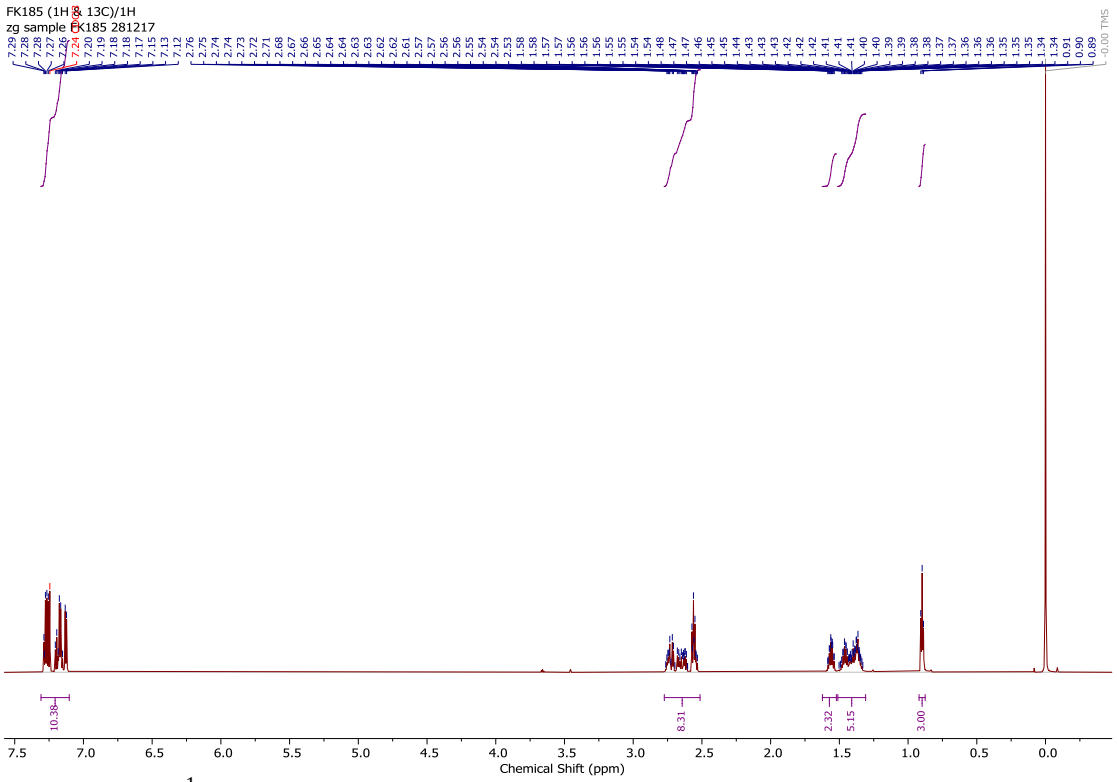


Figure S190. ^{1}H NMR spectrum of 1-phenyl-*N*-(4-phenylbutyl)pentan-2-amine (**215za**) ($CDCl_3$, 700 MHz)

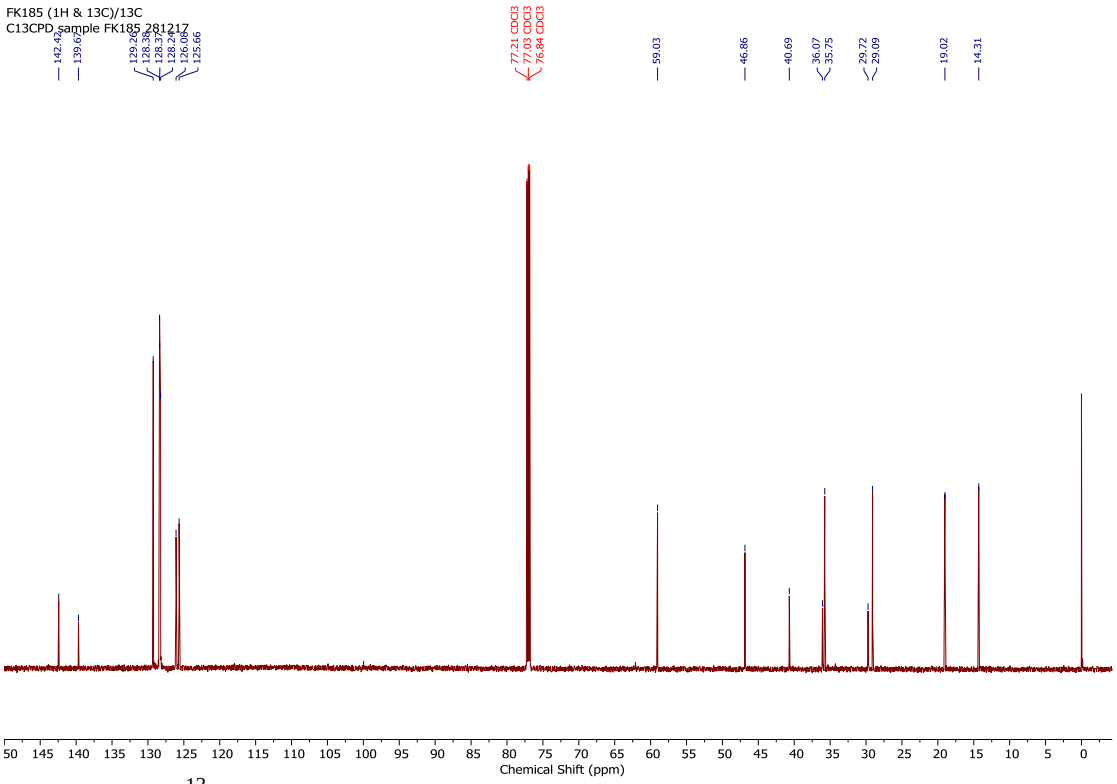


Figure S191. ^{13}C NMR spectrum of 1-phenyl-*N*-(4-phenylbutyl)pentan-2-amine (**215za**) ($CDCl_3$, 175 MHz)

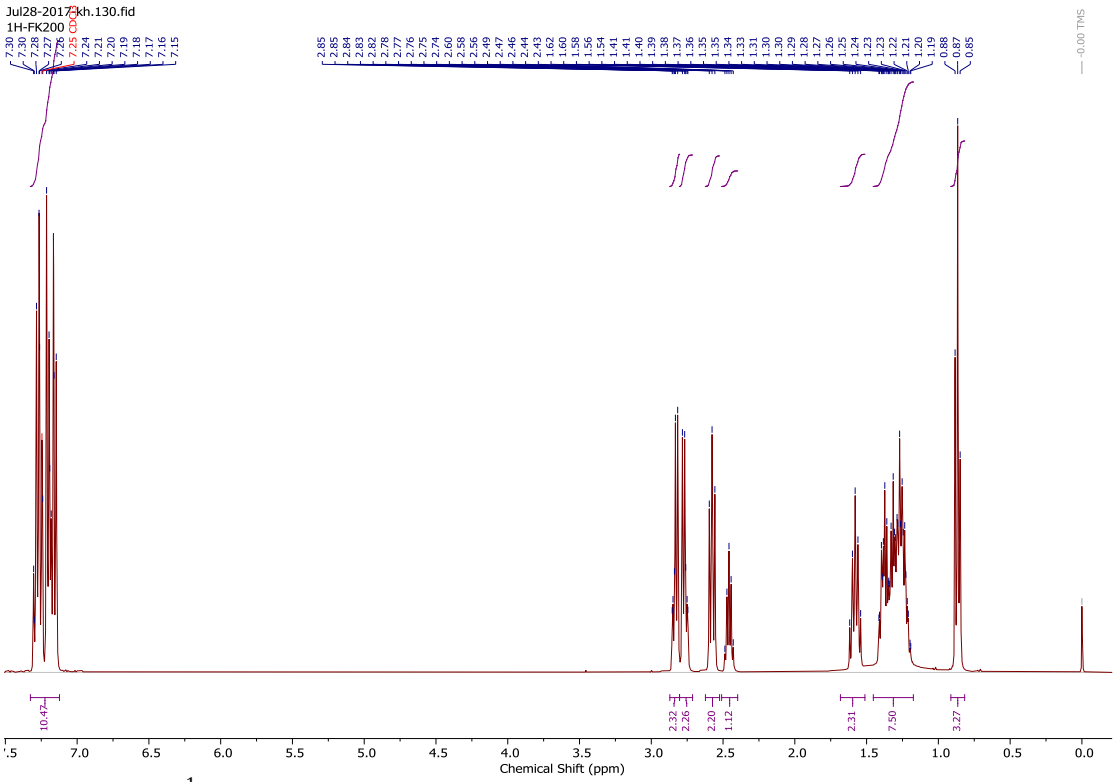


Figure S192. ^{1}H NMR spectrum of *N*-phenethyl-8-phenyloctan-4-amine (**215zb**) ($CDCl_3$, 400 MHz)

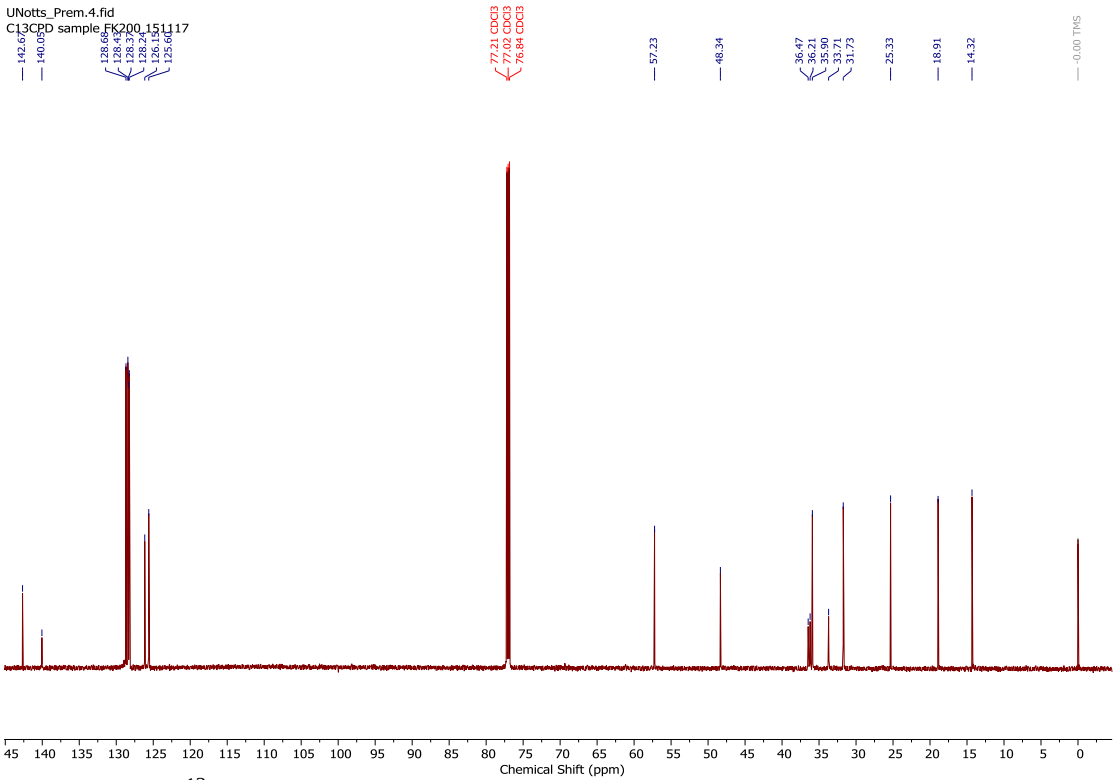


Figure S193. ^{13}C NMR spectrum of *N*-phenethyl-8-phenyloctan-4-amine (**215zb**) ($CDCl_3$, 175 MHz)

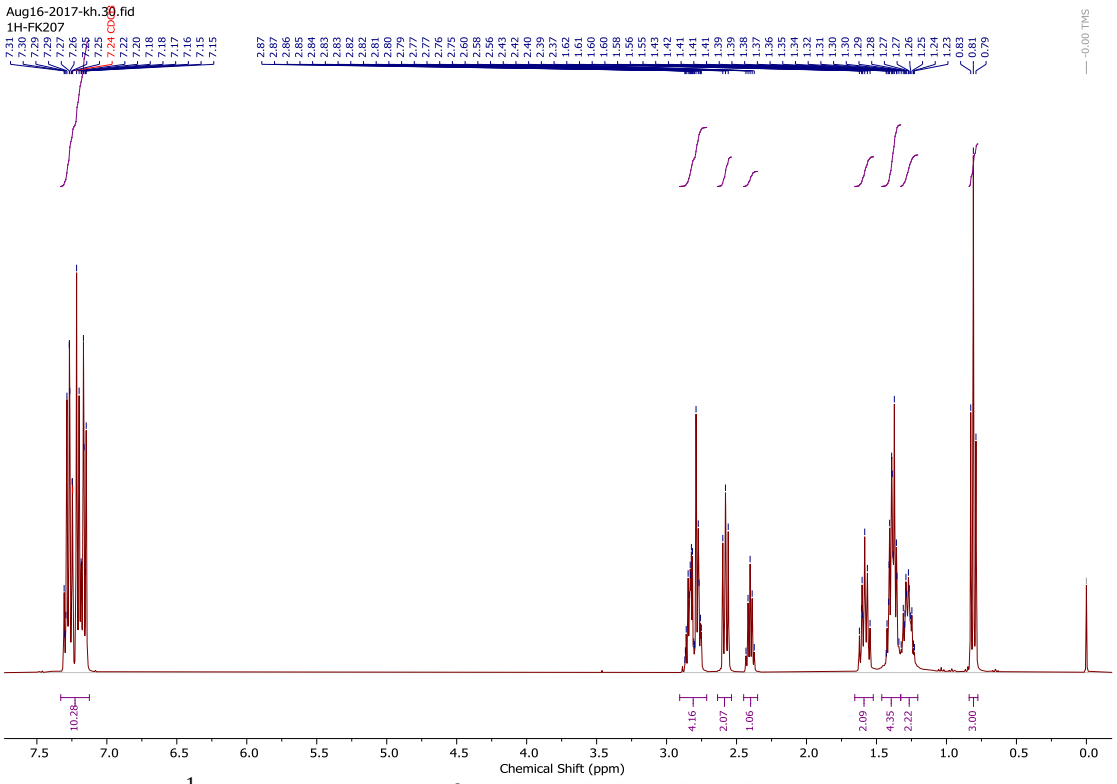


Figure S194. ^{1}H NMR spectrum of *N*-phenethyl-7-phenylheptan-3-amine (**215zc**) ($CDCl_3$, 400 MHz)

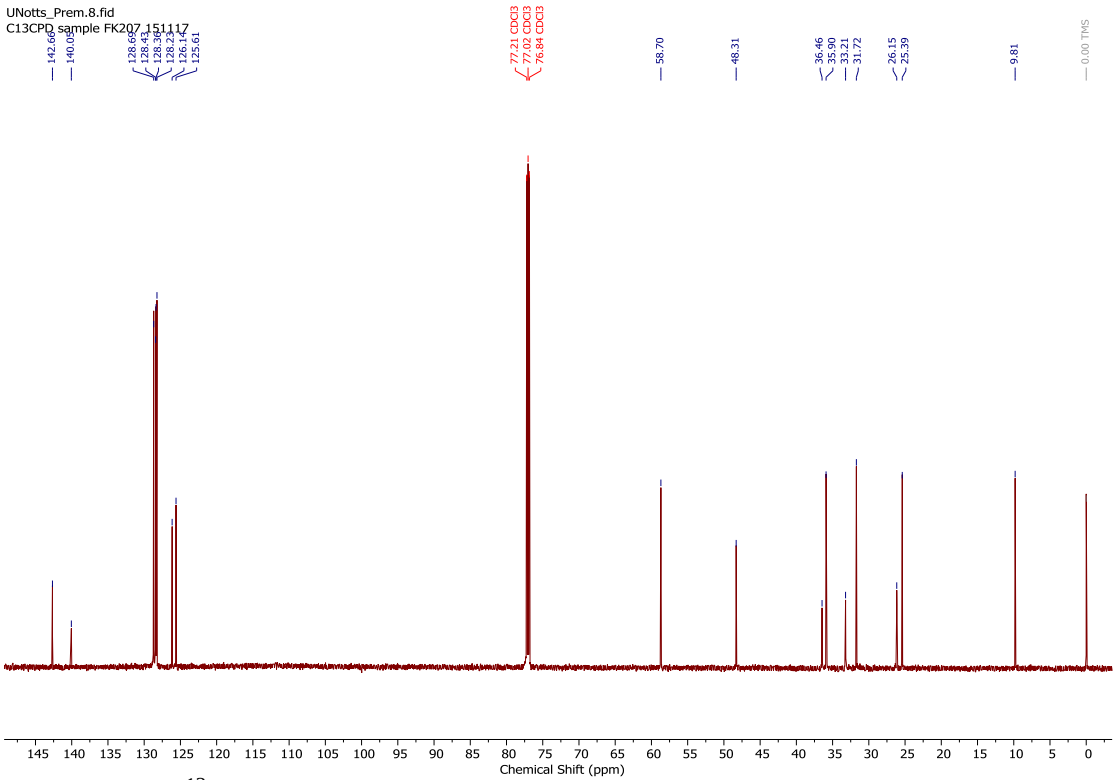


Figure S195. ^{13}C NMR spectrum of *N*-phenethyl-7-phenylheptan-3-amine (**215zc**) ($CDCl_3$, 175 MHz)

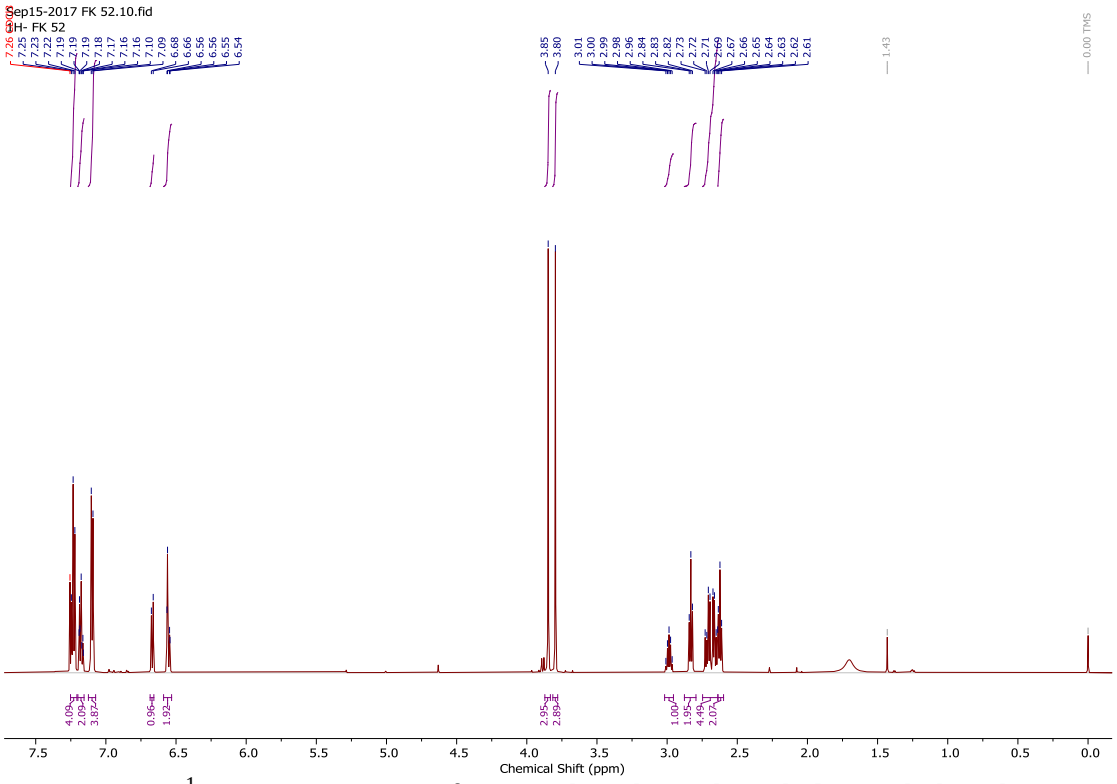


Figure S196. ^{1}H NMR spectrum of *N*-(3,4-dimethoxyphenethyl)-1,3-diphenylpropan-2-amine (**215zd**) ($CDCl_3$, 600 MHz)

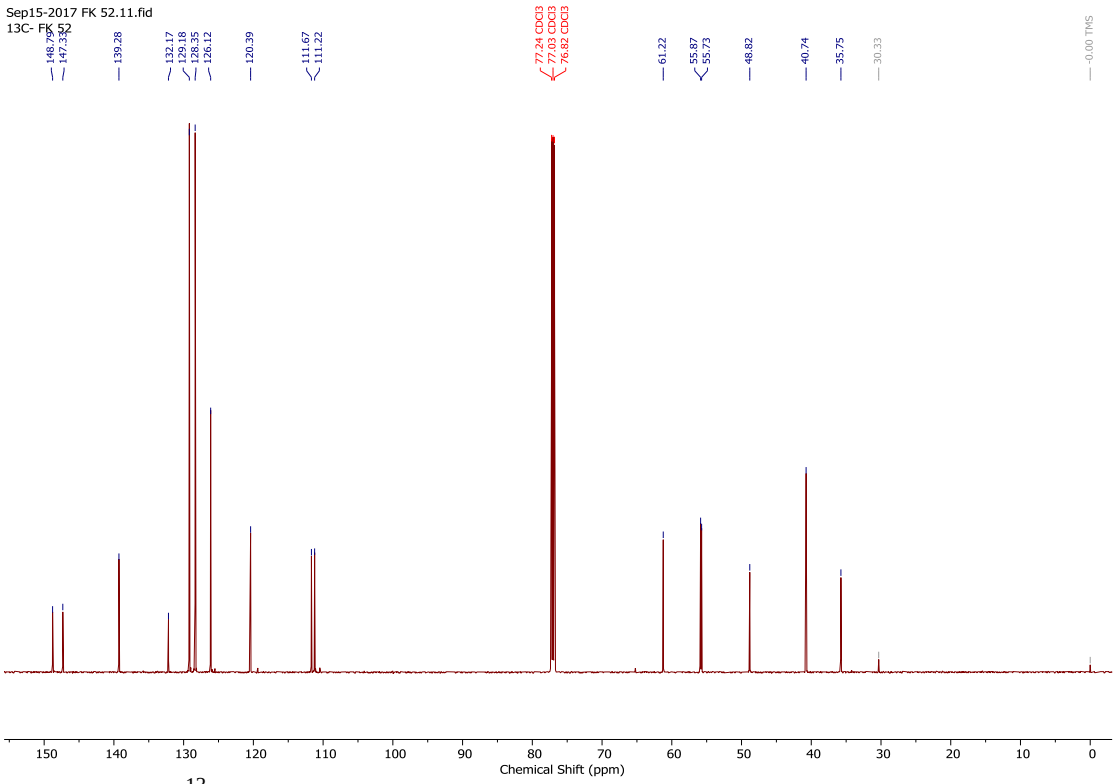


Figure S197. ^{13}C NMR spectrum of *N*-(3,4-dimethoxyphenethyl)-1,3-diphenylpropan-2-amine (**215zd**) ($CDCl_3$, 150 MHz)

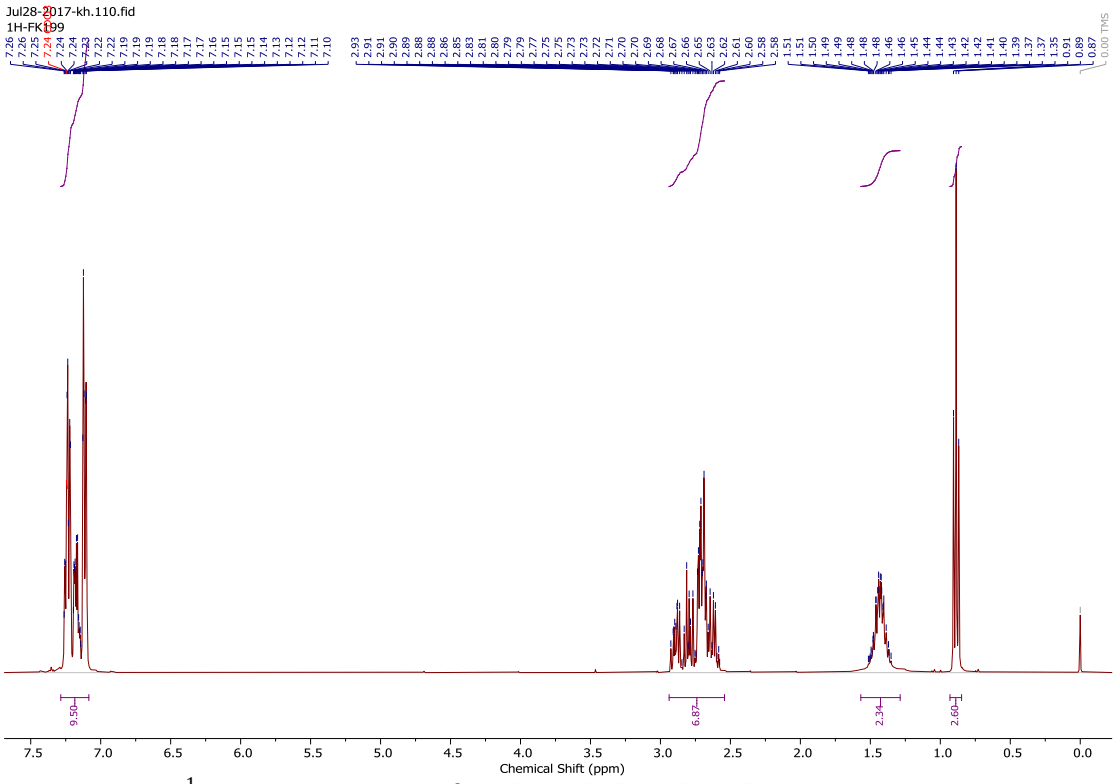


Figure S198. ^{1}H NMR spectrum of *N*-phenethyl-1-phenylbutan-2-amine (**215ze**) ($CDCl_3$, 400 MHz)

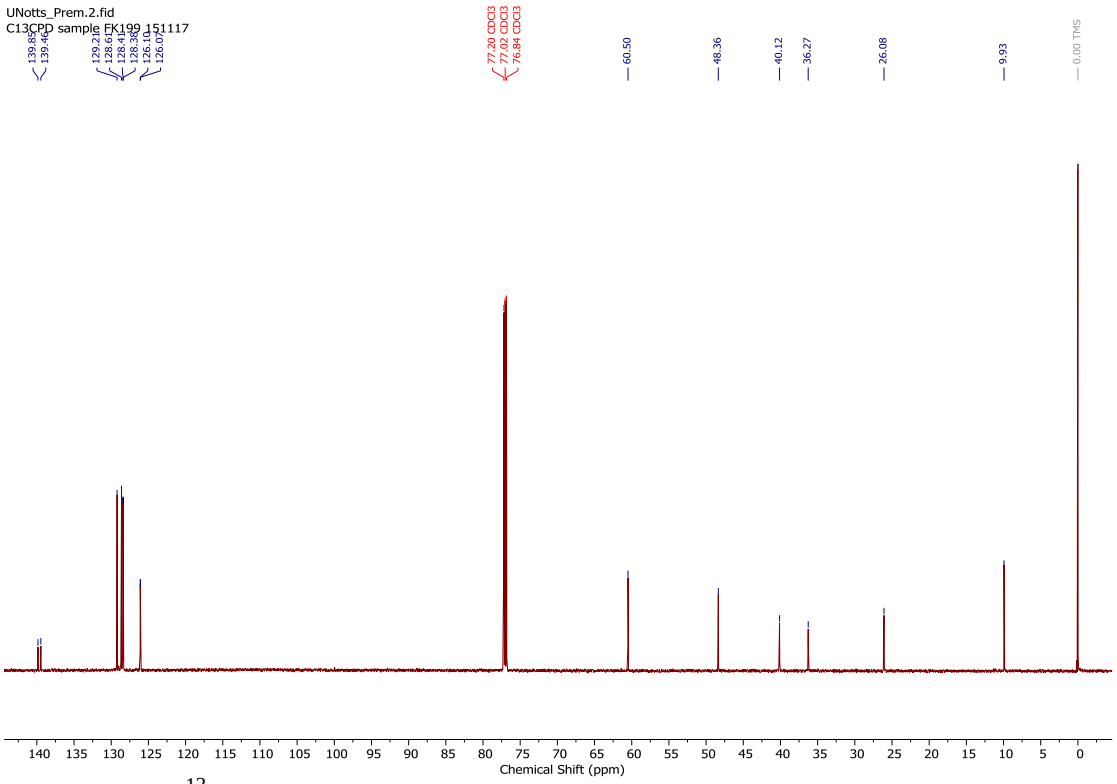


Figure S199. ^{13}C NMR spectrum of *N*-phenethyl-1-phenylbutan-2-amine (**215ze**) ($CDCl_3$, 175 MHz)

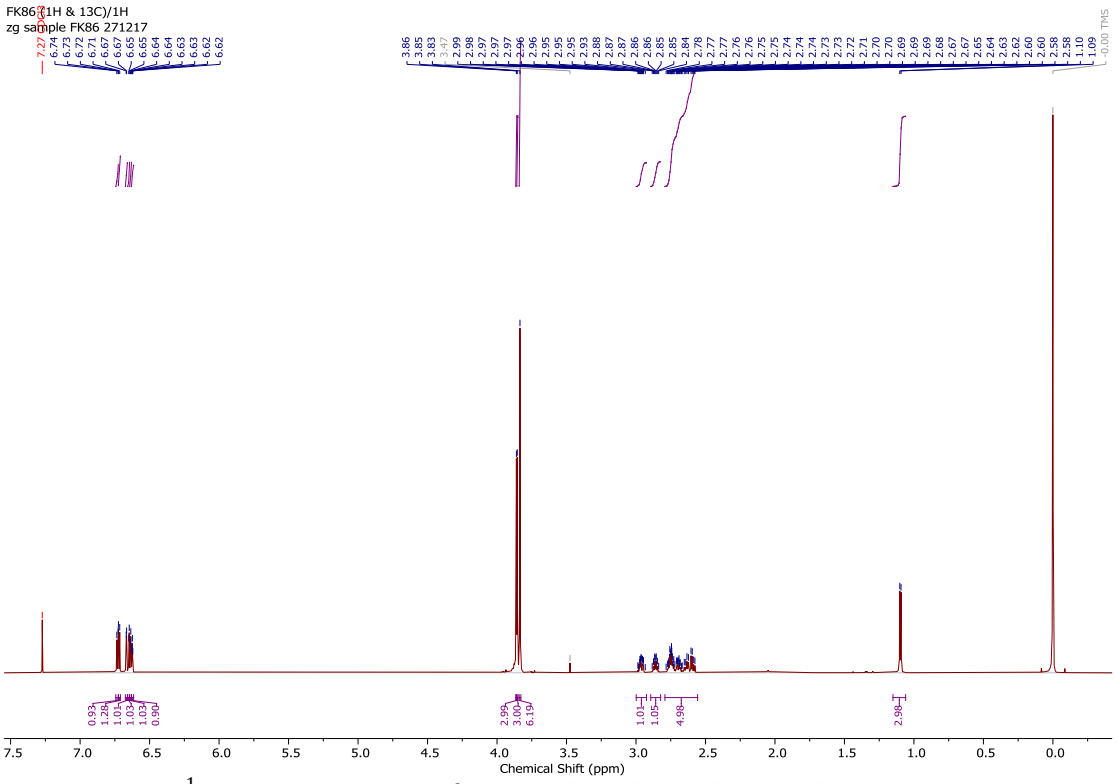


Figure S200. ^{1}H NMR spectrum of *N*-(3,4-dimethoxyphenethyl)-1-(3,4-dimethoxyphenyl)-propan-2-amine (**215zf**) ($CDCl_3$, 700 MHz)

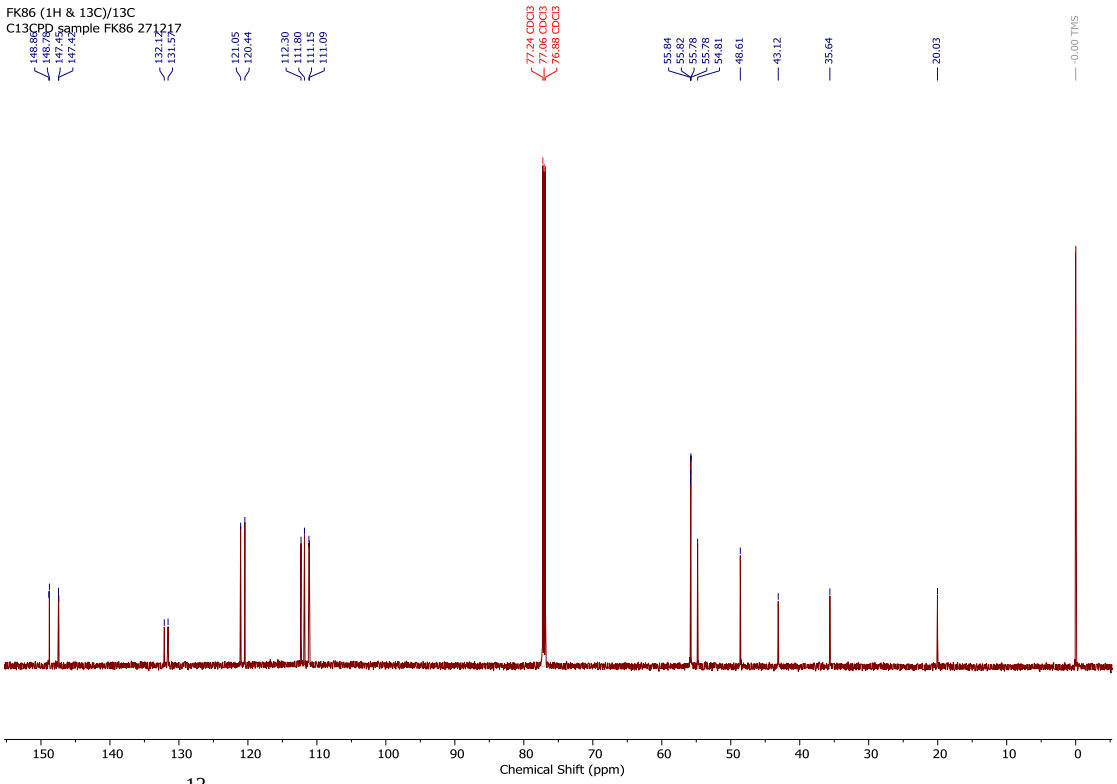


Figure S201. ^{13}C NMR spectrum of *N*-(3,4-dimethoxyphenethyl)-1-(3,4-dimethoxyphenyl)-propan-2-amine (**215zf**) ($CDCl_3$, 175 MHz)

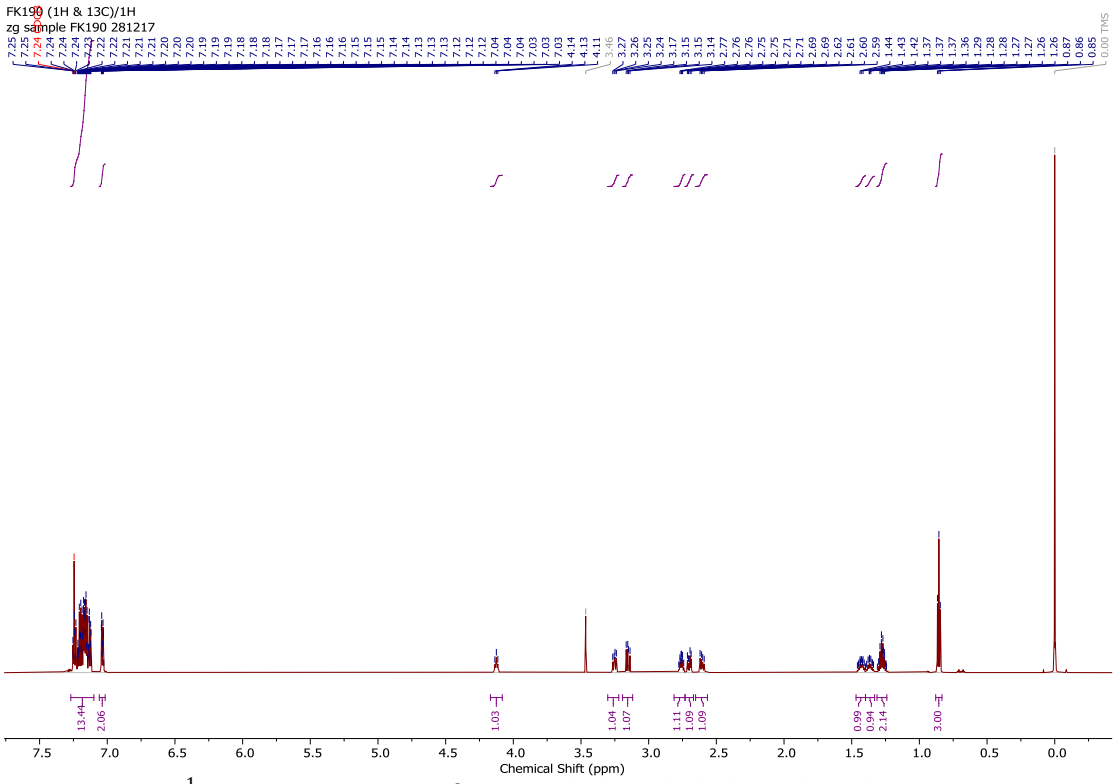


Figure S202. ^{1}H NMR spectrum of *N*-(2,2-diphenylethyl)-1-phenylpentan-2-amine (**215zg**) ($CDCl_3$, 700 MHz)

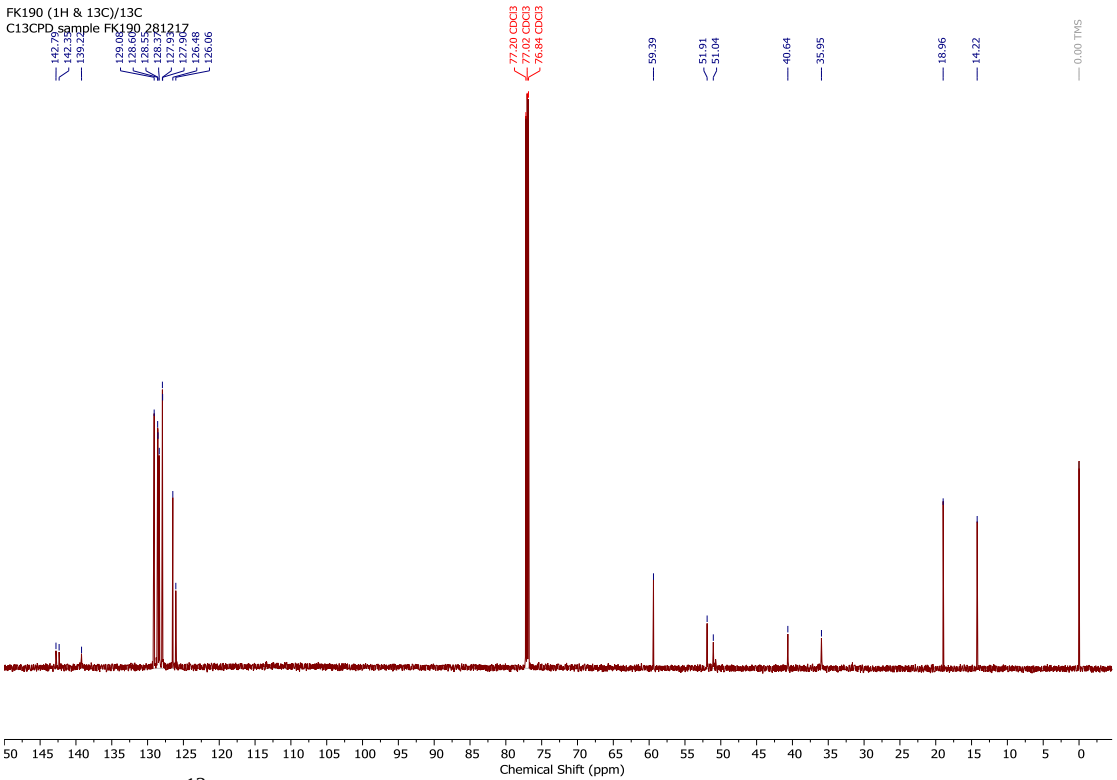


Figure S203. ^{13}C NMR spectrum of *N*-(2,2-diphenylethyl)-1-phenylpentan-2-amine (**215zg**) ($CDCl_3$, 175 MHz)

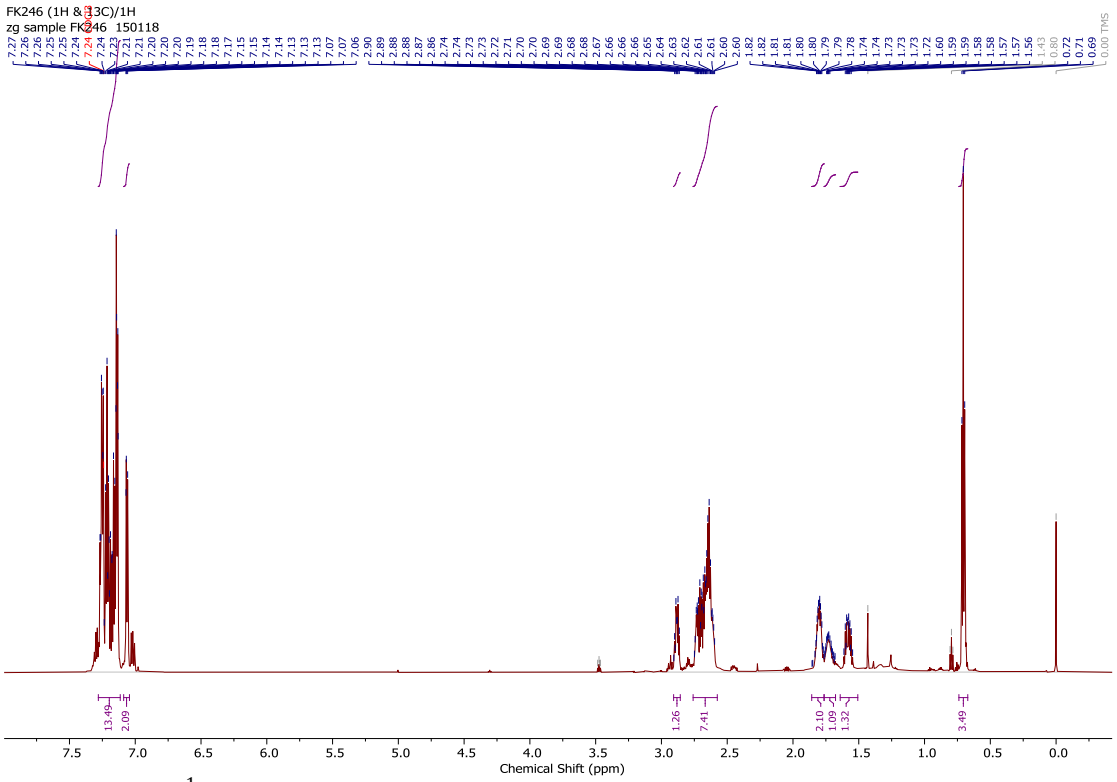


Figure S204. ^{1}H NMR spectrum of *N*-phenethyl-1,4-diphenylhexan-3-amine (**215zh**) ($CDCl_3$, 700 MHz)

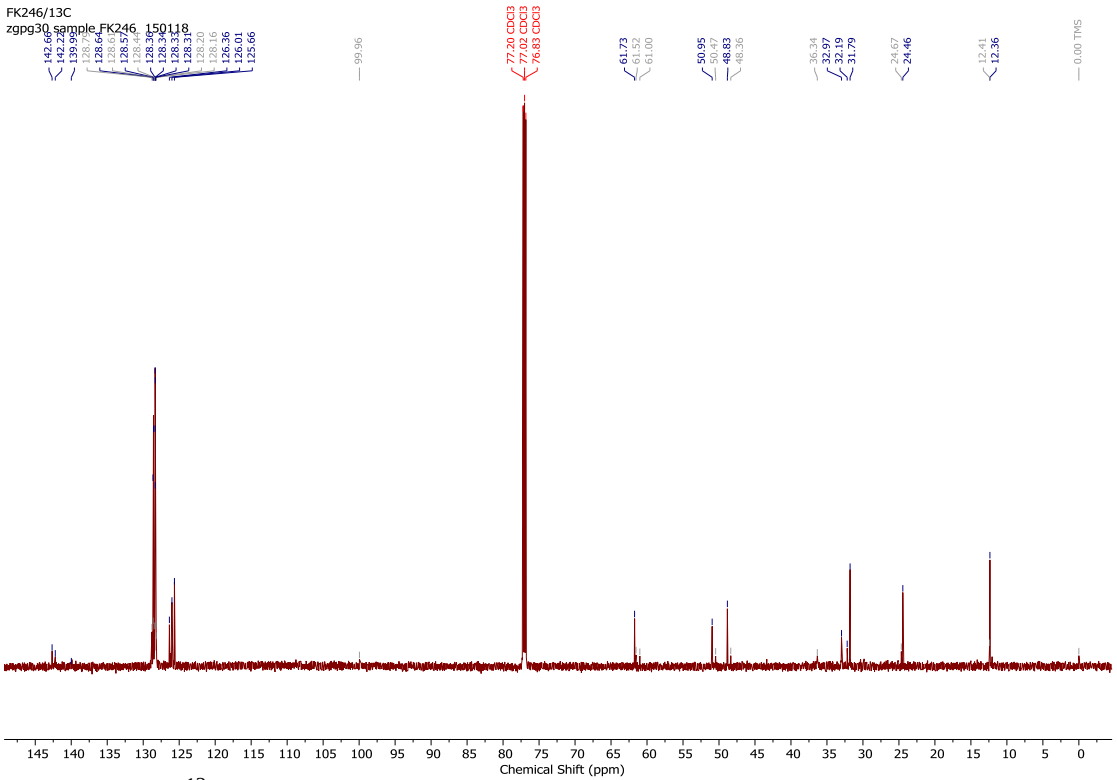


Figure S205. ^{13}C NMR spectrum of *N*-phenethyl-1,4-diphenylhexan-3-amine (**215zh**) ($CDCl_3$, 175 MHz)

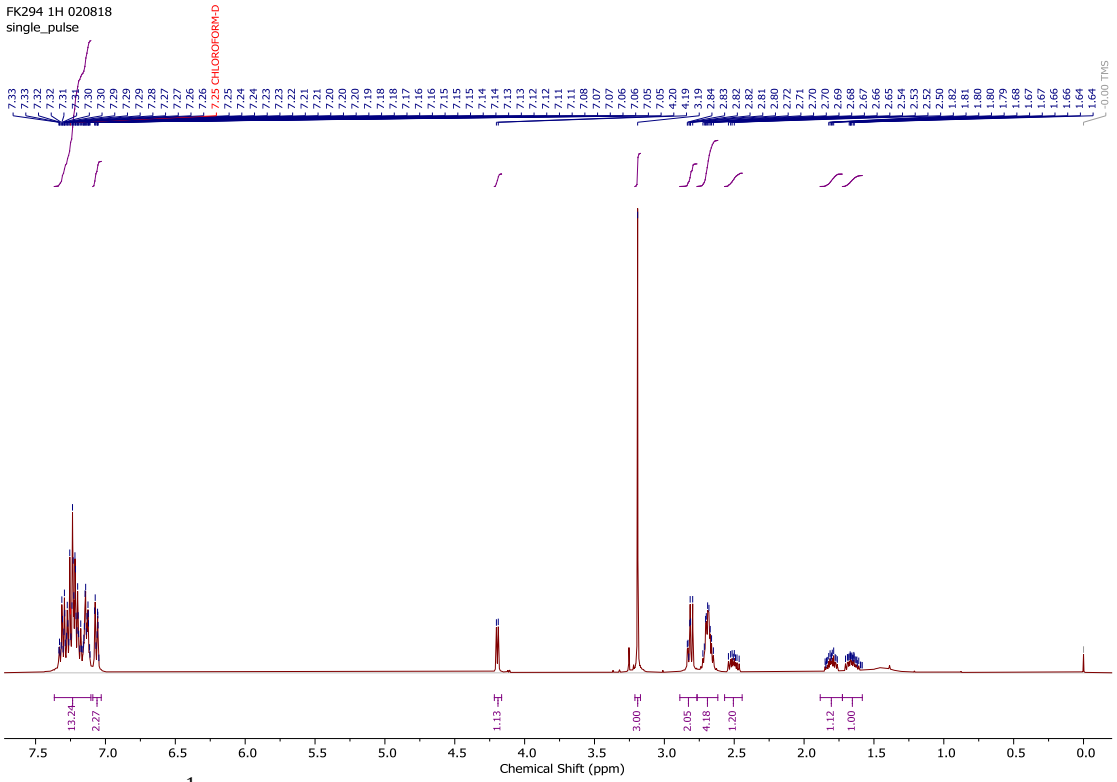


Figure S206. ^{1}H NMR spectrum of 1-methoxy-*N*-phenethyl-1,4-diphenylbutan-2-amine (**215zi**) ($CDCl_3$, 400 MHz)

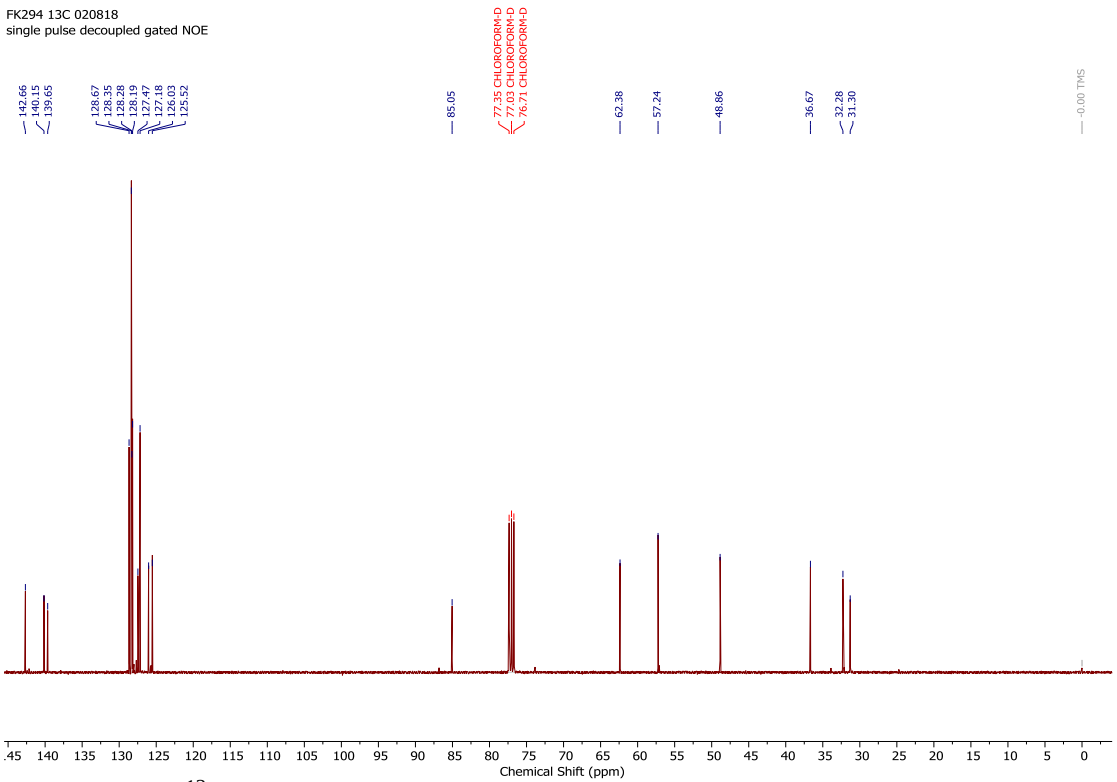


Figure S207. ^{13}C NMR spectrum of 1-methoxy-*N*-phenethyl-1,4-diphenylbutan-2-amine (**215zi**) ($CDCl_3$, 100 MHz)

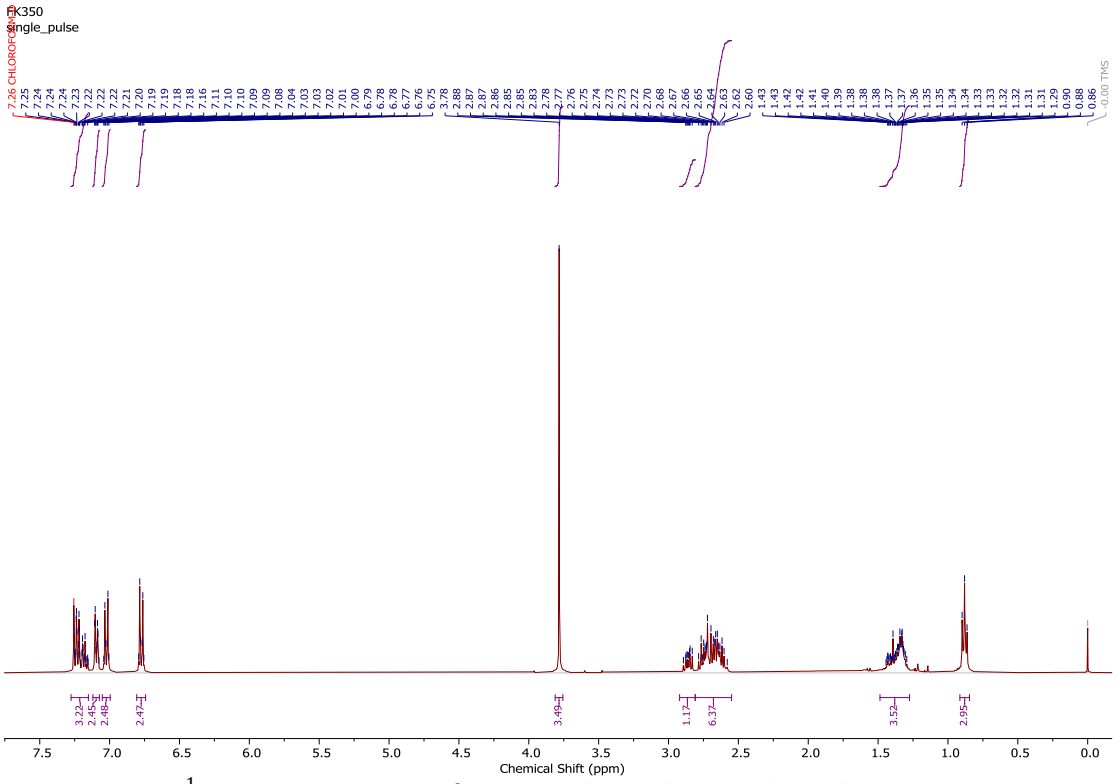


Figure S208. ^{1}H NMR spectrum of *N*-(4-methoxyphenethyl)-1-phenylpentan-2-amine (**215zj**) ($CDCl_3$, 400 MHz)

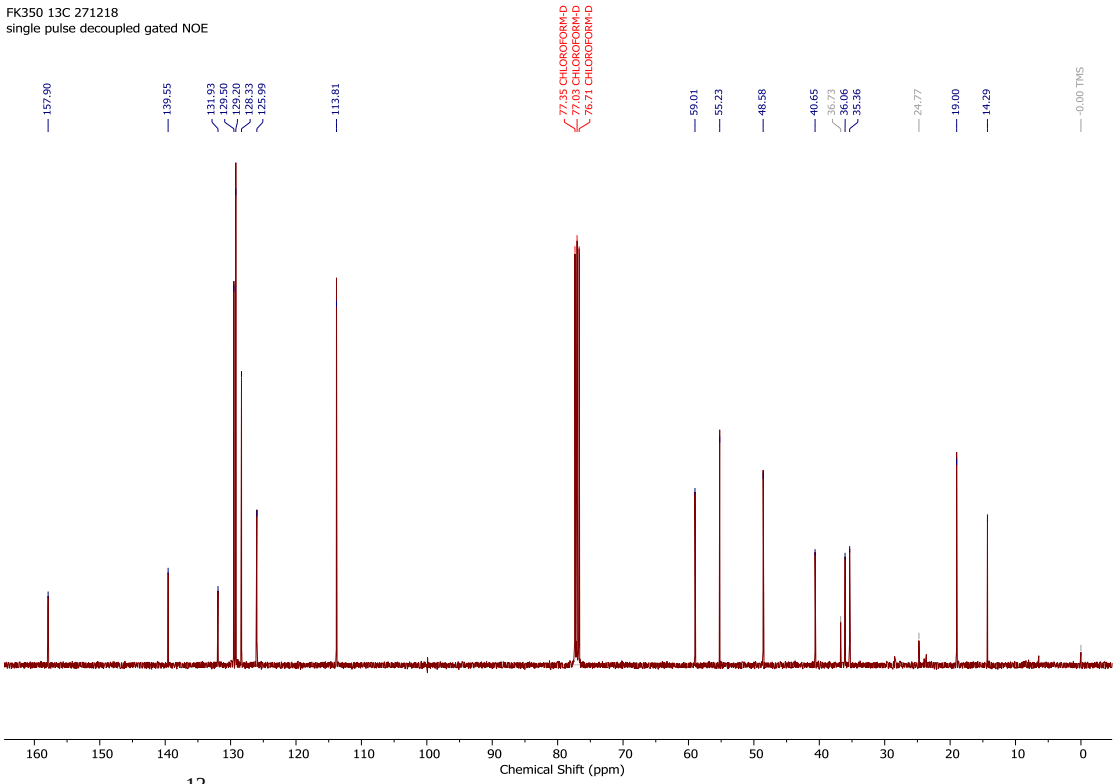


Figure S209. ^{13}C NMR spectrum of *N*-(4-methoxyphenethyl)-1-phenylpentan-2-amine (**215zj**) ($CDCl_3$, 100 MHz)

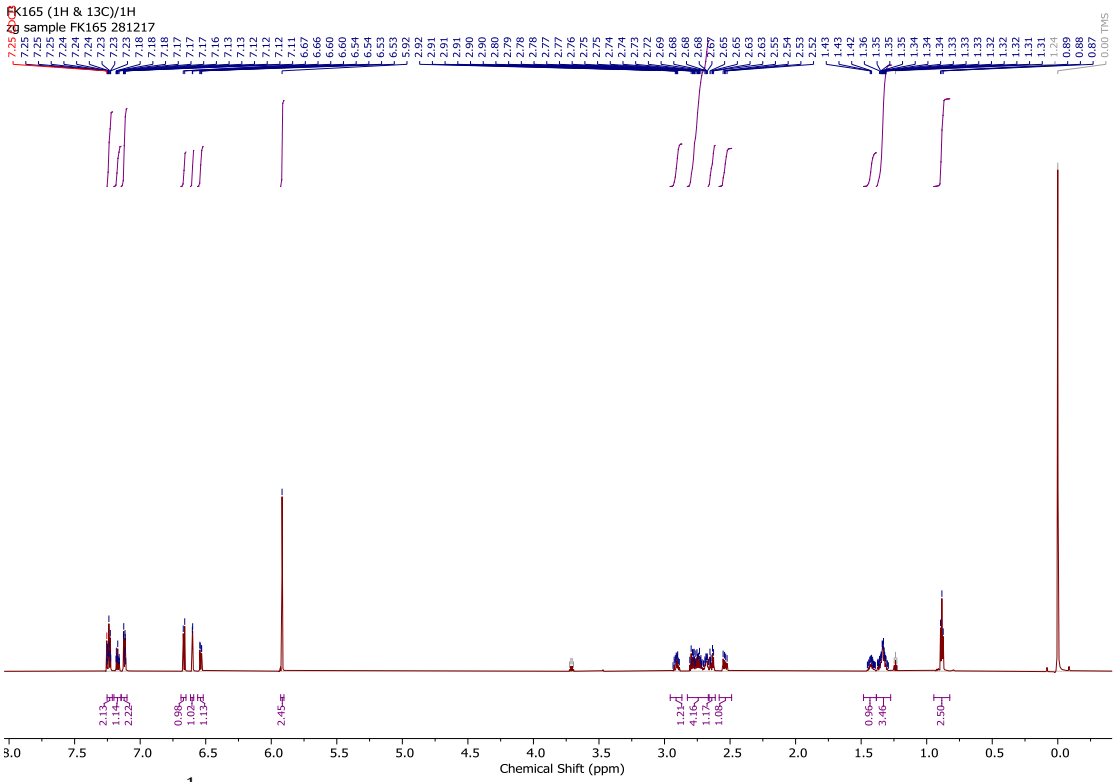


Figure S210. ^{1}H NMR spectrum of 1-(benzo[*d*][1,3]dioxol-5-yl)-*N*-phenethylpentan-2-amine (**215zk**) ($CDCl_3$, 700 MHz)

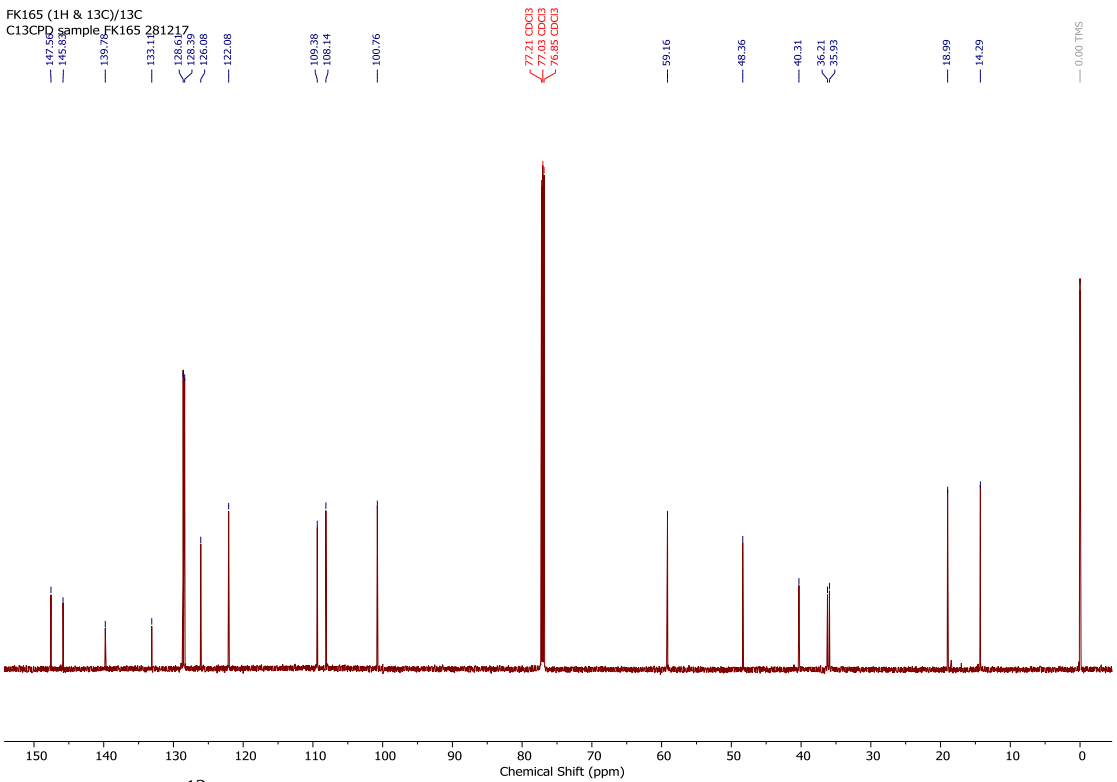


Figure S211. ^{13}C NMR spectrum of 1-(benzo[*d*][1,3]dioxol-5-yl)-*N*-phenethylpentan-2-amine (**215zk**) ($CDCl_3$, 175 MHz)

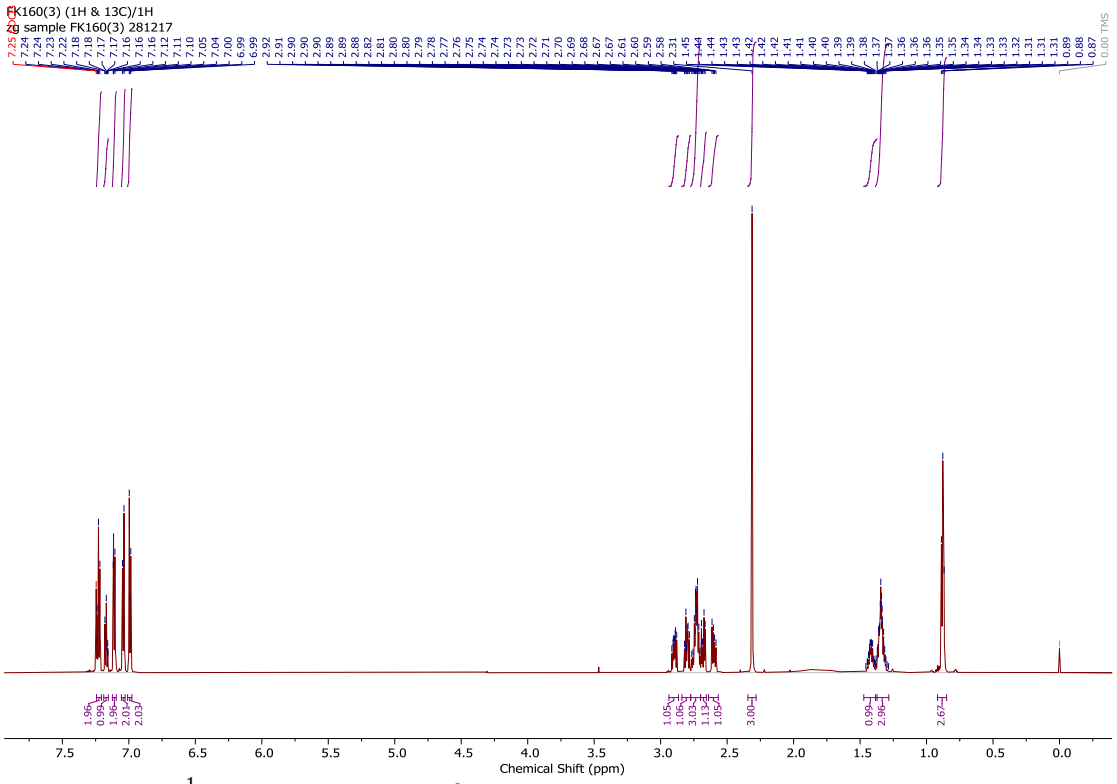


Figure S212. ^{1}H NMR spectrum of *N*-phenethyl-1-(*p*-tolyl)pentan-2-amine (**215zl**) ($CDCl_3$, 700 MHz)

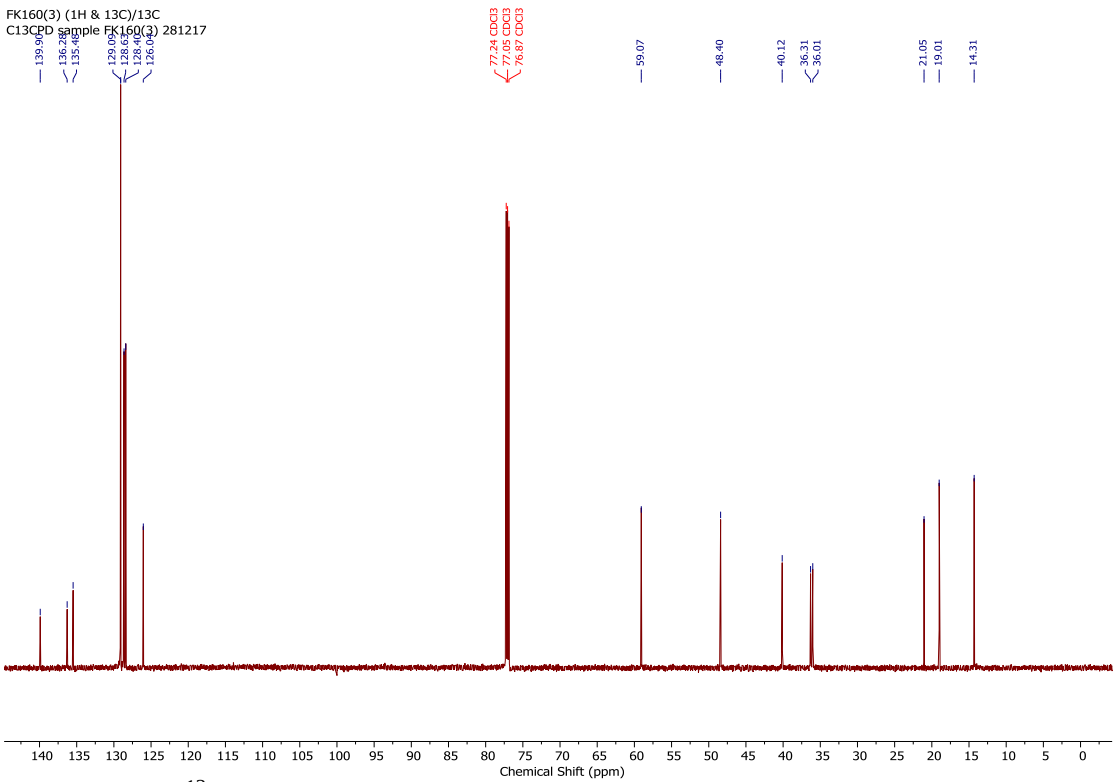


Figure S213. ^{13}C NMR spectrum of *N*-phenethyl-1-(*p*-tolyl)pentan-2-amine (**215zl**) ($CDCl_3$, 175 MHz)

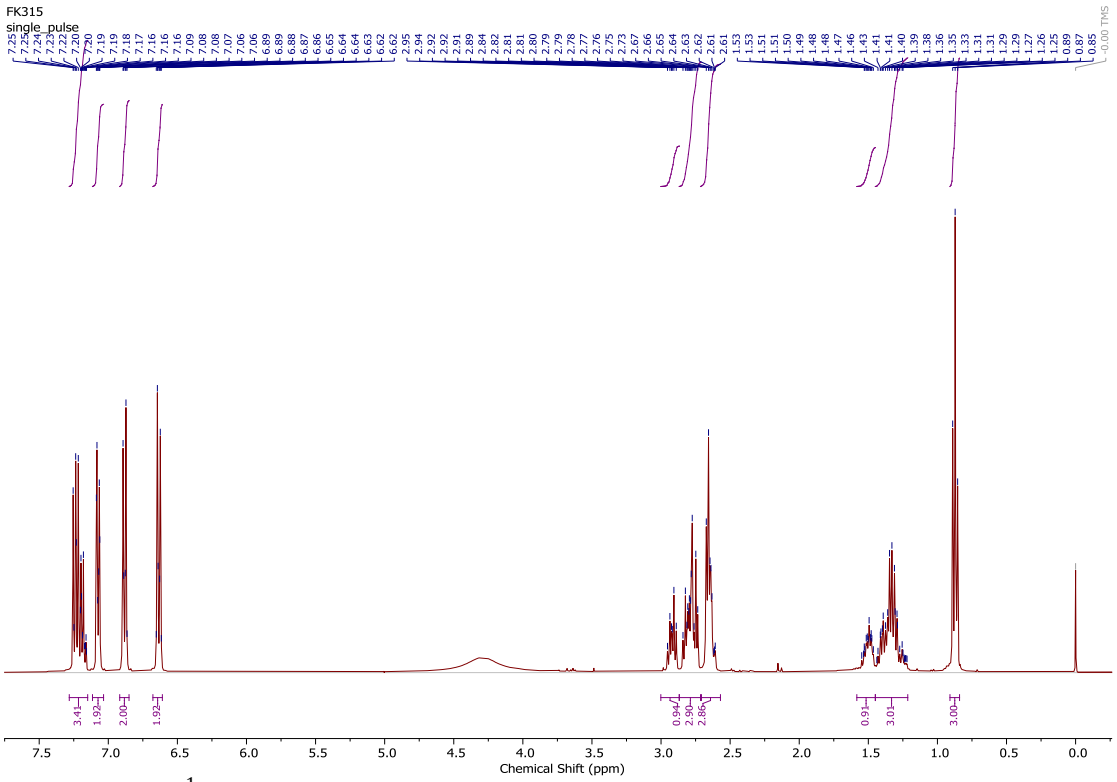


Figure S214. ^{1}H NMR spectrum of 4-(2-((1-phenylpentan-2-yl)amino)ethyl)phenol (**215zm**) ($CDCl_3$, 400 MHz)

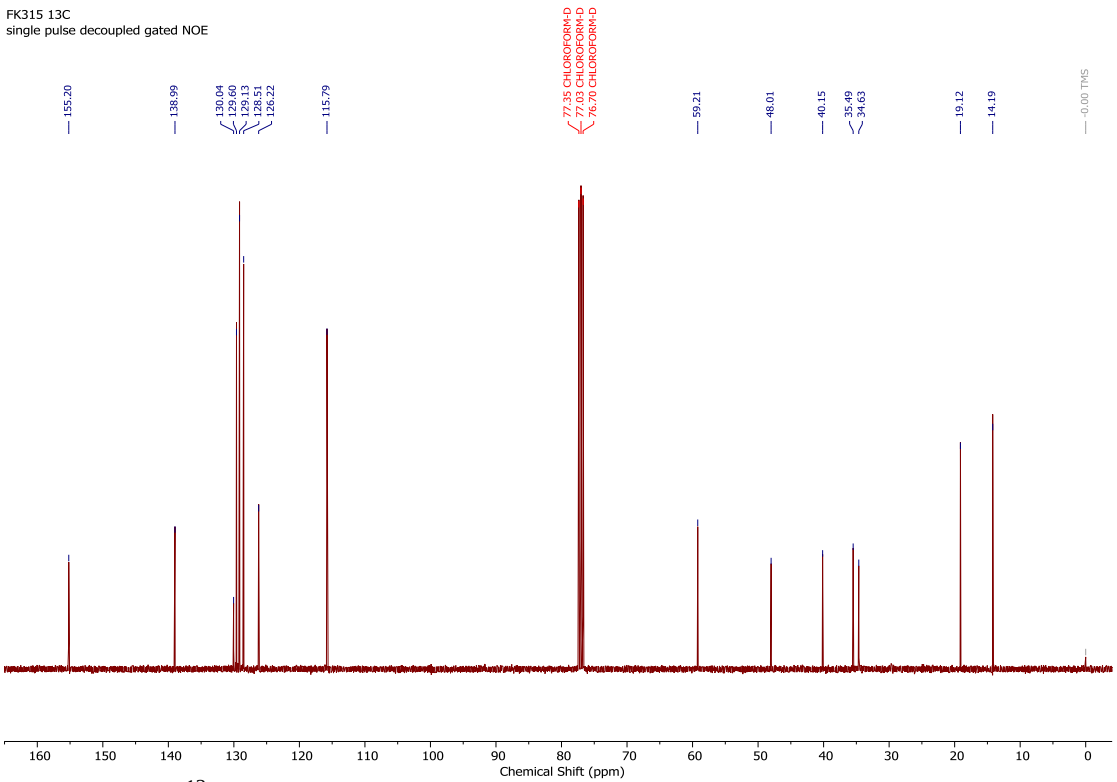


Figure S215. ^{13}C NMR spectrum of 4-(2-((1-phenylpentan-2-yl)amino)ethyl)phenol (**215zm**) ($CDCl_3$, 100 MHz)

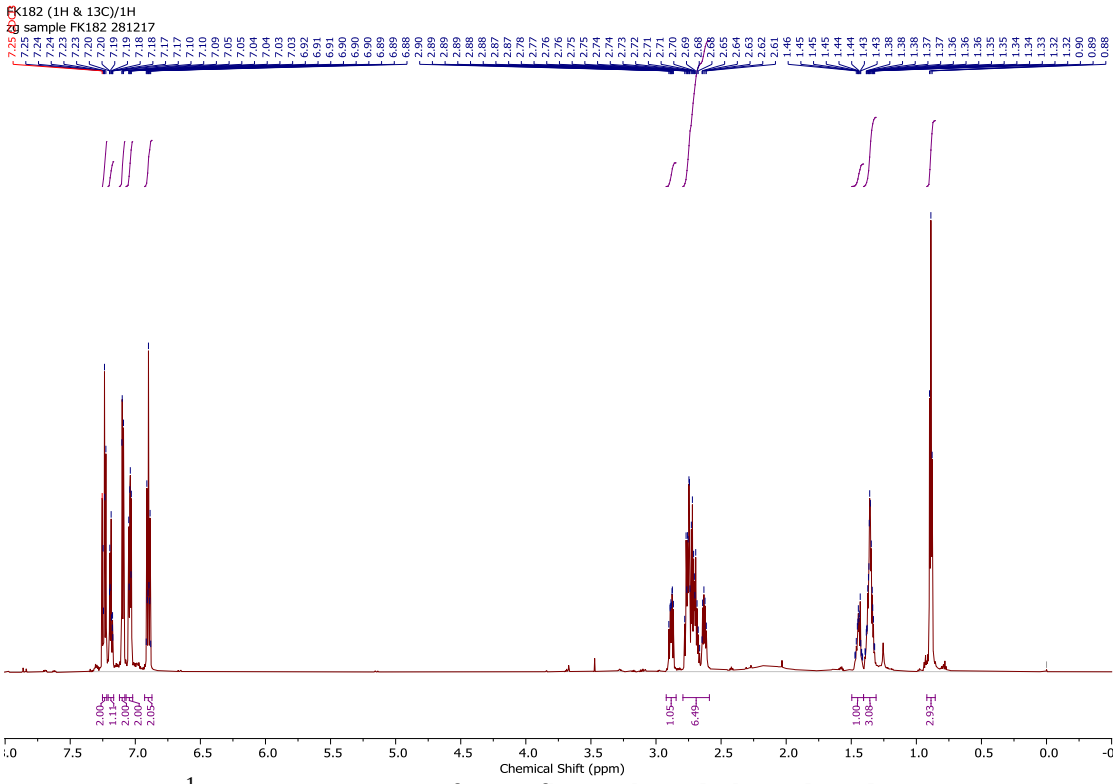


Figure S216. ^{1}H NMR spectrum of *N*-(4-fluorophenethyl)-1-phenylpentan-2-amine (**215zn**) ($CDCl_3$, 700 MHz)

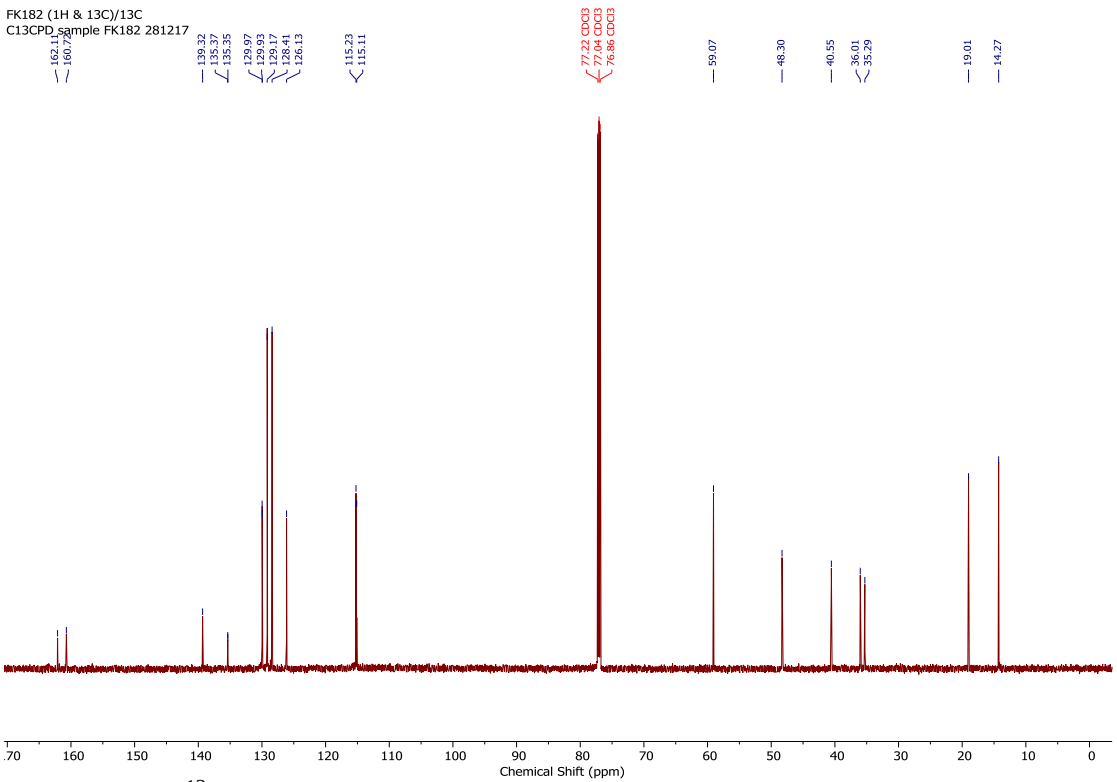


Figure S217. ^{13}C NMR spectrum of *N*-(4-fluorophenethyl)-1-phenylpentan-2-amine (**215zn**) ($CDCl_3$, 175 MHz)

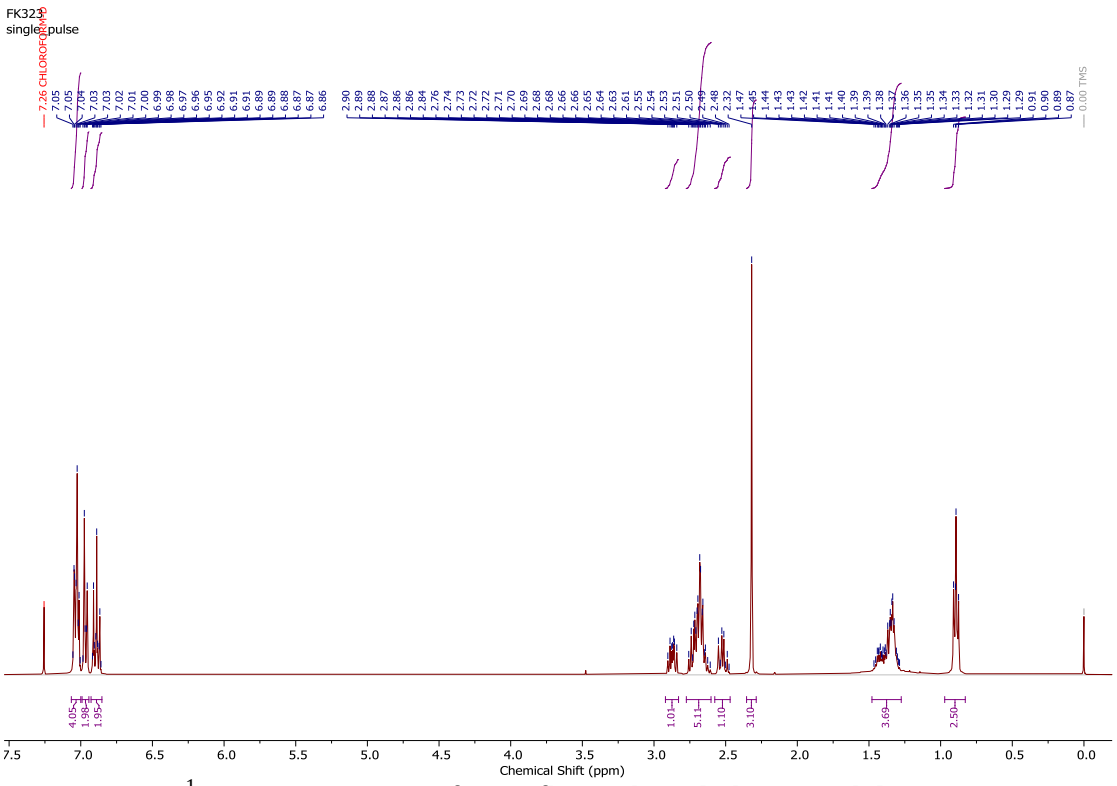


Figure S218. ^{1}H NMR spectrum of *N*-(4-fluorophenethyl)-1-(*p*-tolyl)pentan-2-amine (**215zo**) ($CDCl_3$, 400 MHz)

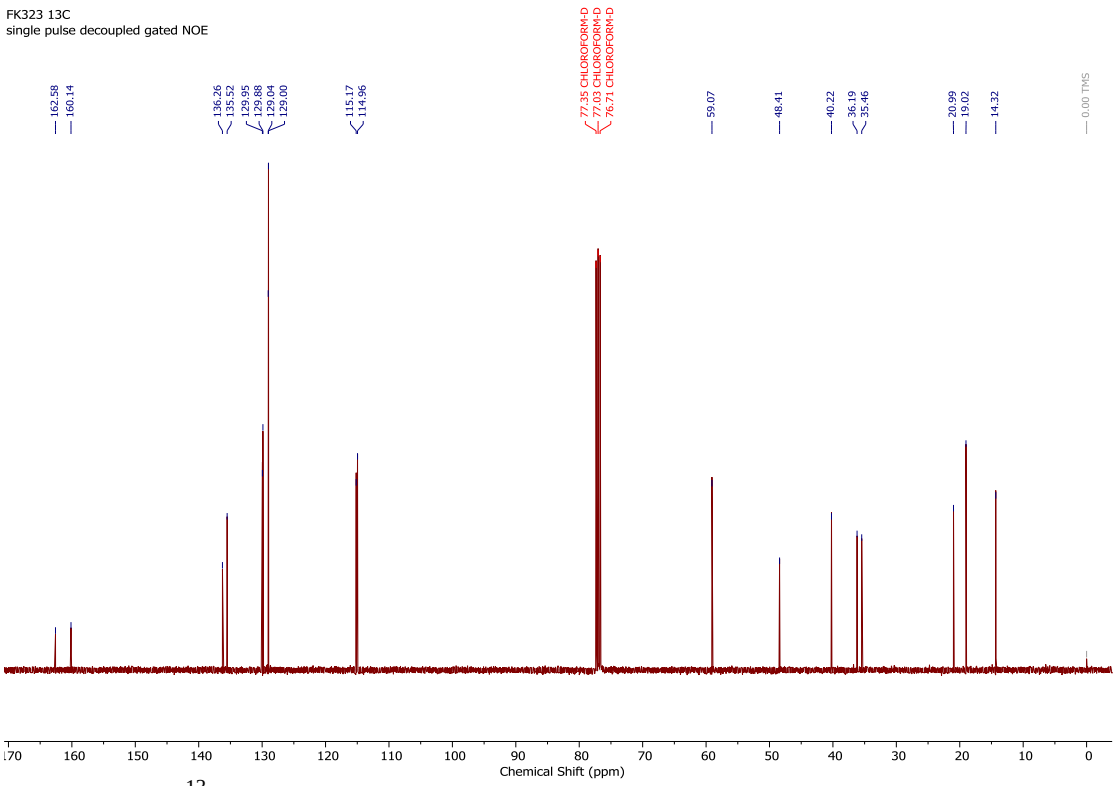


Figure S219. ^{13}C NMR spectrum of *N*-(4-fluorophenethyl)-1-(*p*-tolyl)pentan-2-amine (**215zo**) ($CDCl_3$, 100 MHz)

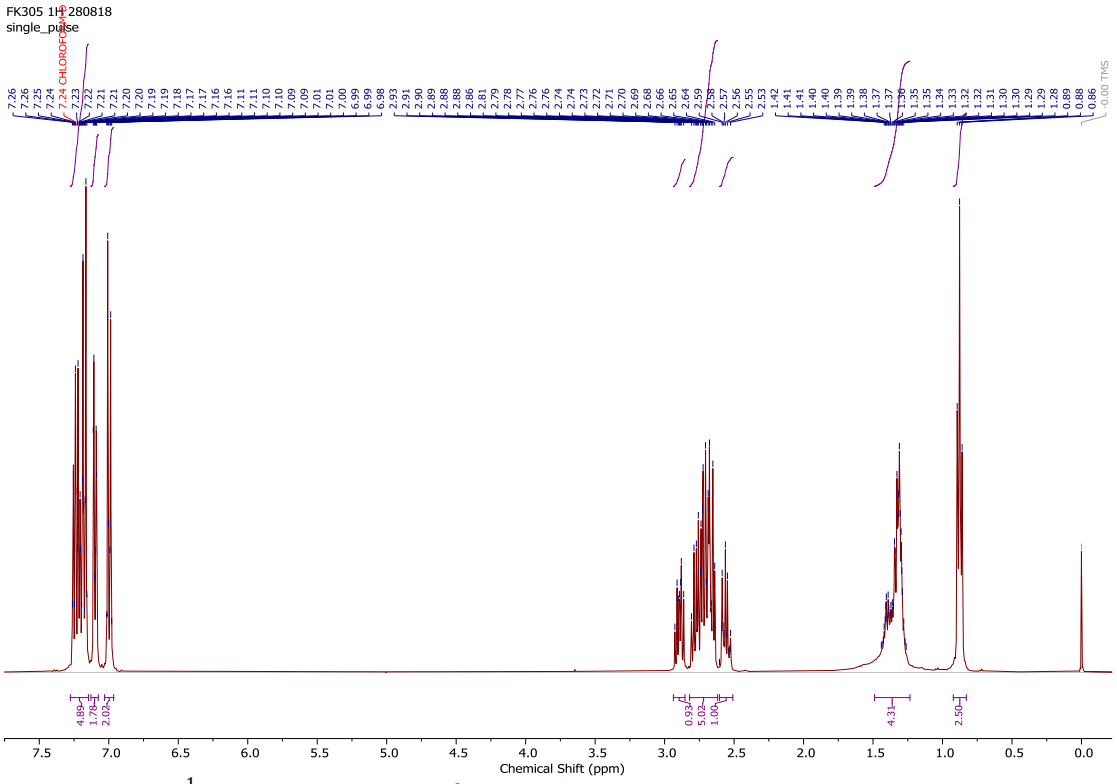


Figure S220. ^{1}H NMR spectrum of 1-(4-chlorophenyl)-*N*-phenethylpentan-2-amine (**215zp**) ($CDCl_3$, 400 MHz)

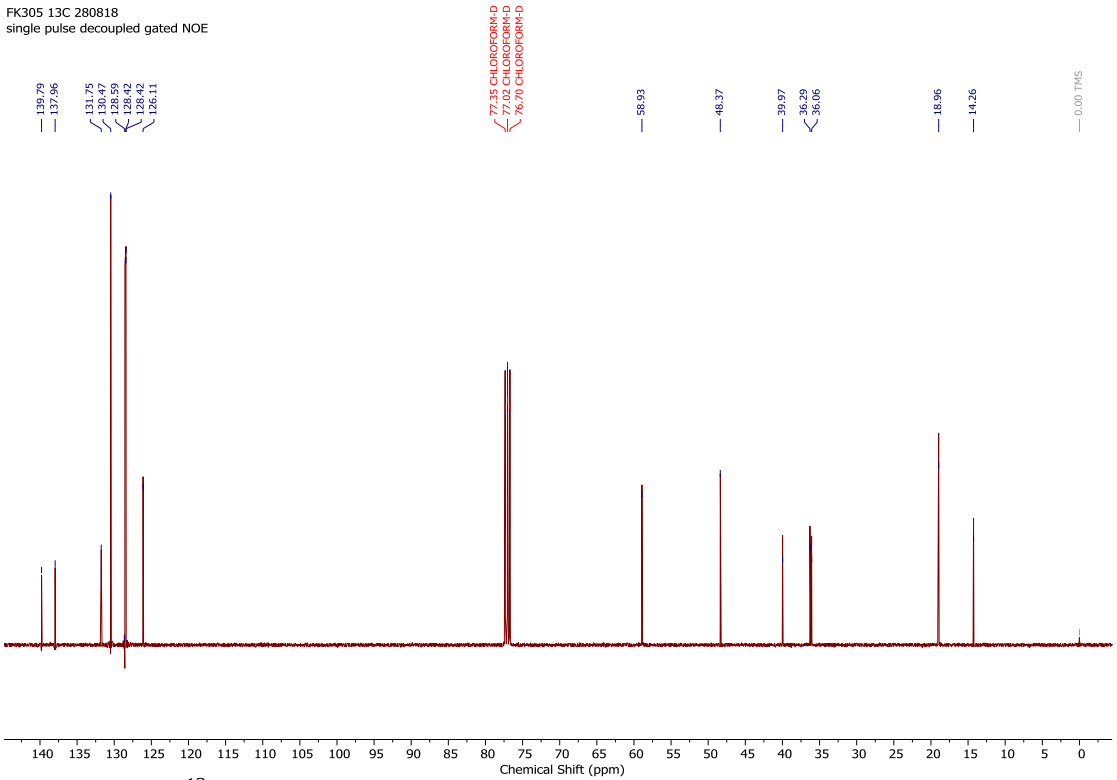


Figure S221. ^{13}C NMR spectrum of 1-(4-chlorophenyl)-*N*-phenethylpentan-2-amine (**215zp**) ($CDCl_3$, 100 MHz)

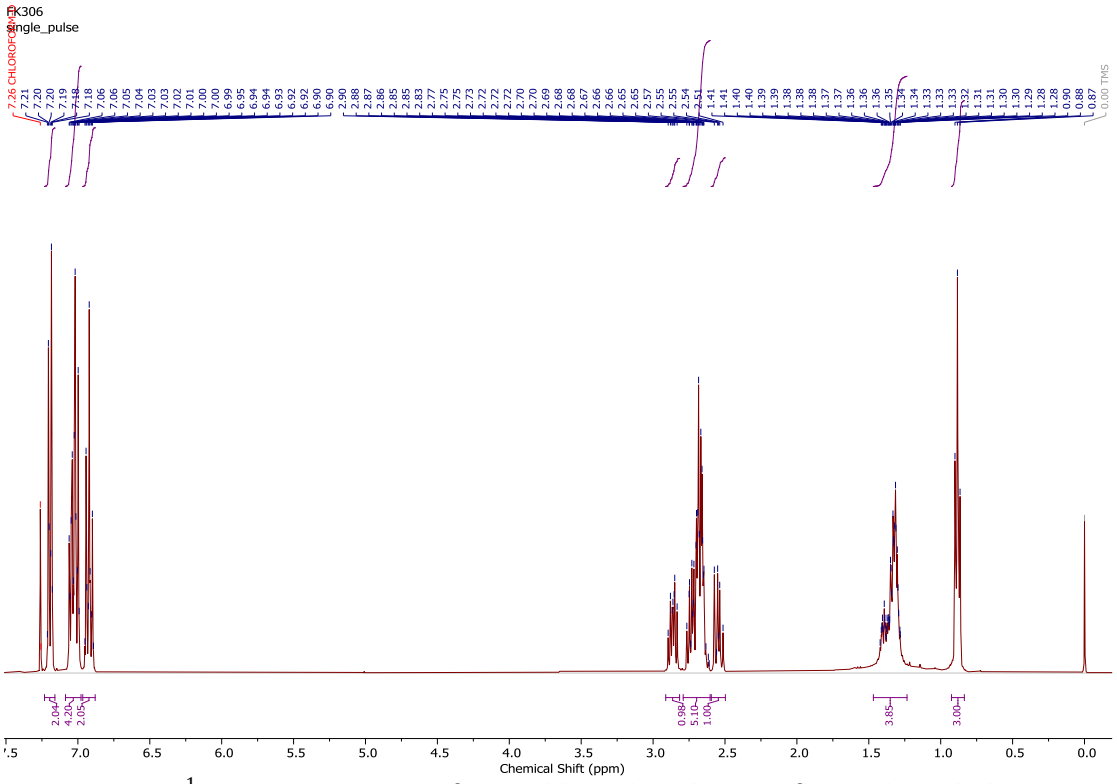


Figure S222. ^{1}H NMR spectrum of 1-(4-chlorophenyl)-*N*-(4-fluorophenethyl)pentan-2-amine (**215zq**) ($CDCl_3$, 400 MHz)

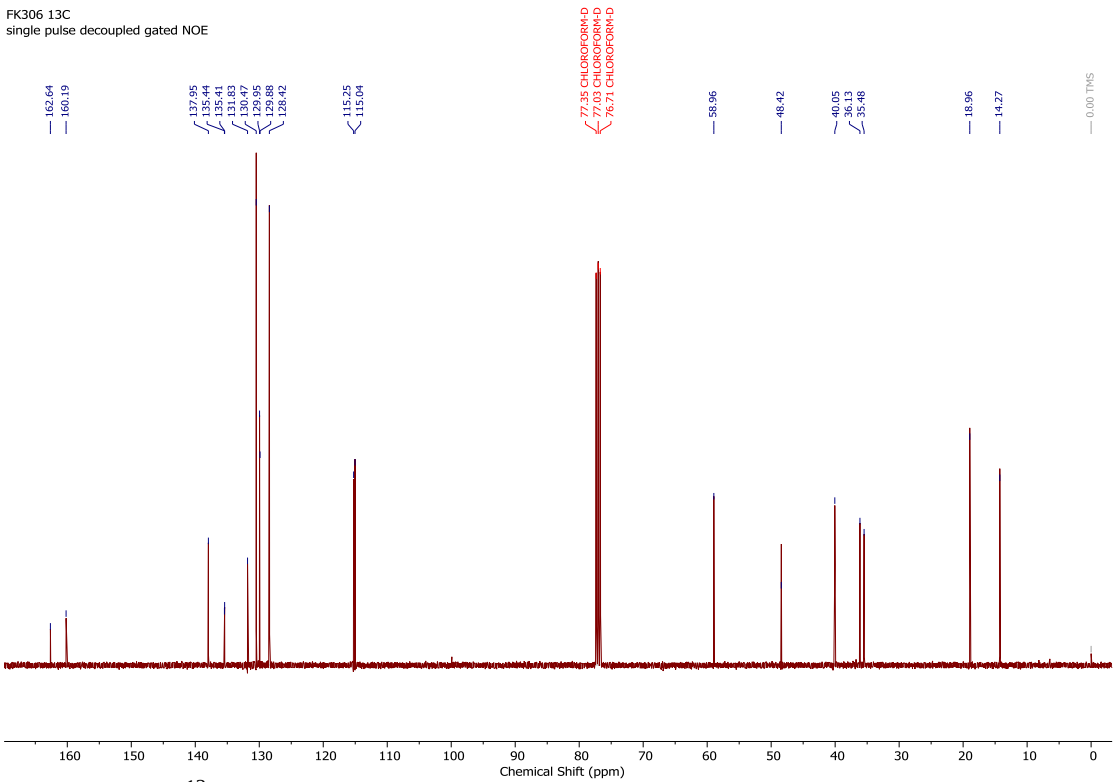


Figure S223. ^{13}C NMR spectrum of 1-(4-chlorophenyl)-*N*-(4-fluorophenethyl)pentan-2-amine (**215zq**) ($CDCl_3$, 100 MHz)

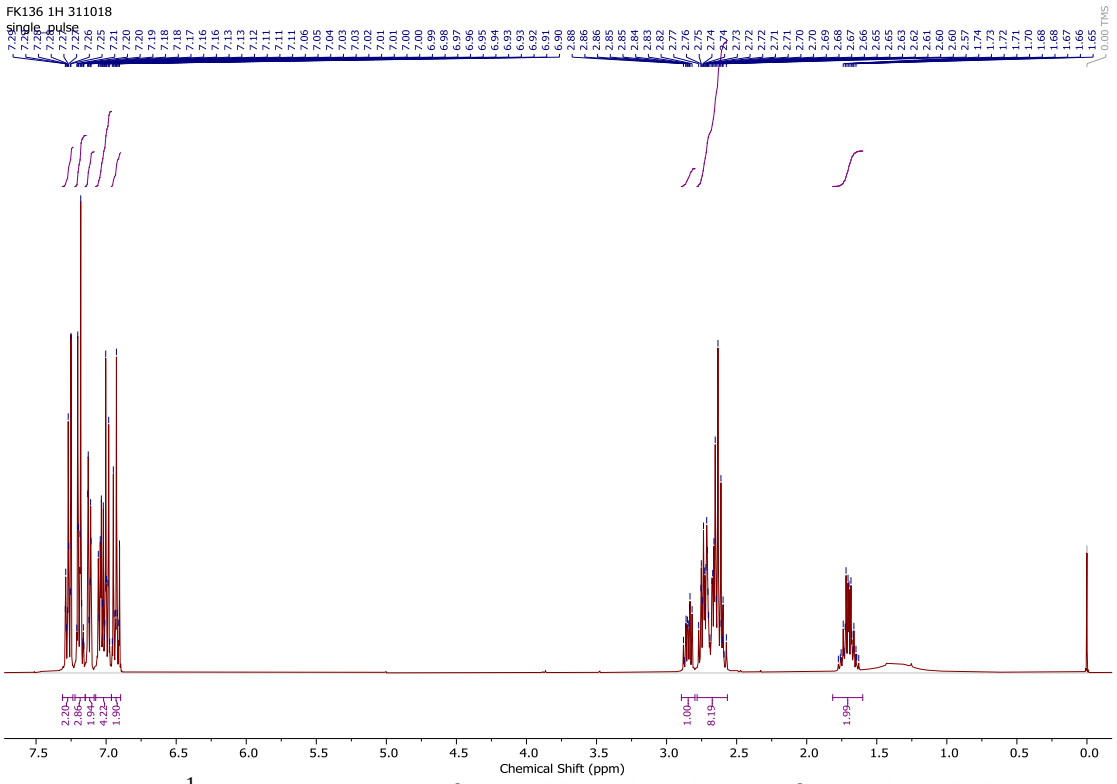


Figure S224. ^{1}H NMR spectrum of 1-(4-chlorophenyl)-*N*-(4-fluorophenethyl)-4-phenylbutan-2-amine (**215zr**) ($CDCl_3$, 400 MHz)

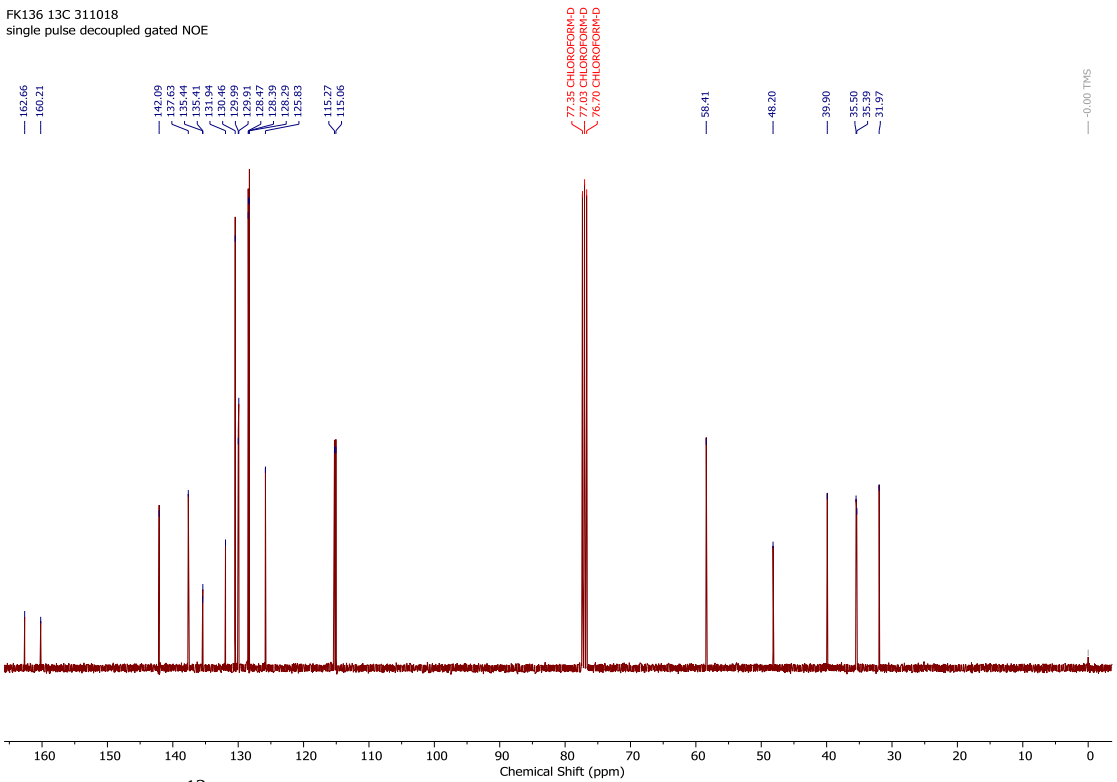


Figure S225. ^{13}C NMR spectrum of 1-(4-chlorophenyl)-*N*-(4-fluorophenethyl)-4-phenylbutan-2-amine (**215zr**) ($CDCl_3$, 100 MHz)

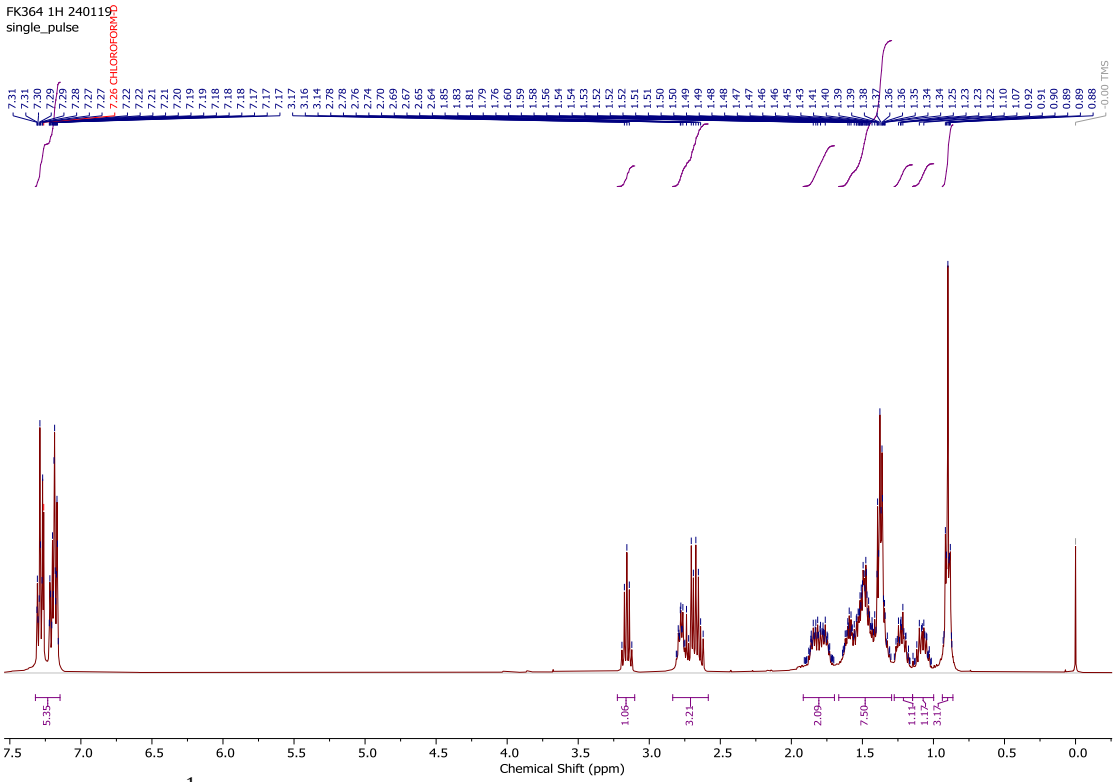


Figure S226. ^{1}H NMR spectrum of *N*-(1-phenylpentan-2-yl)cyclopentanamine (**216a**) ($CDCl_3$, 400 MHz)

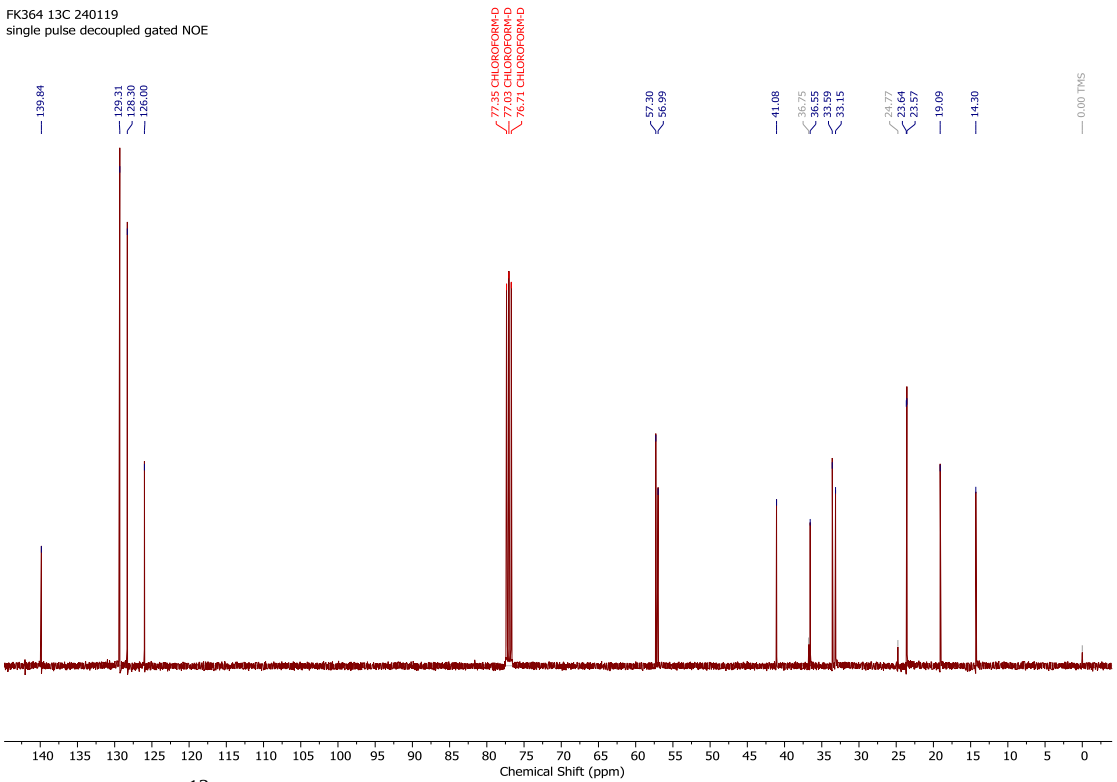


Figure S227. ^{13}C NMR spectrum of *N*-(1-phenylpentan-2-yl)cyclopentanamine (**216a**) ($CDCl_3$, 100 MHz)

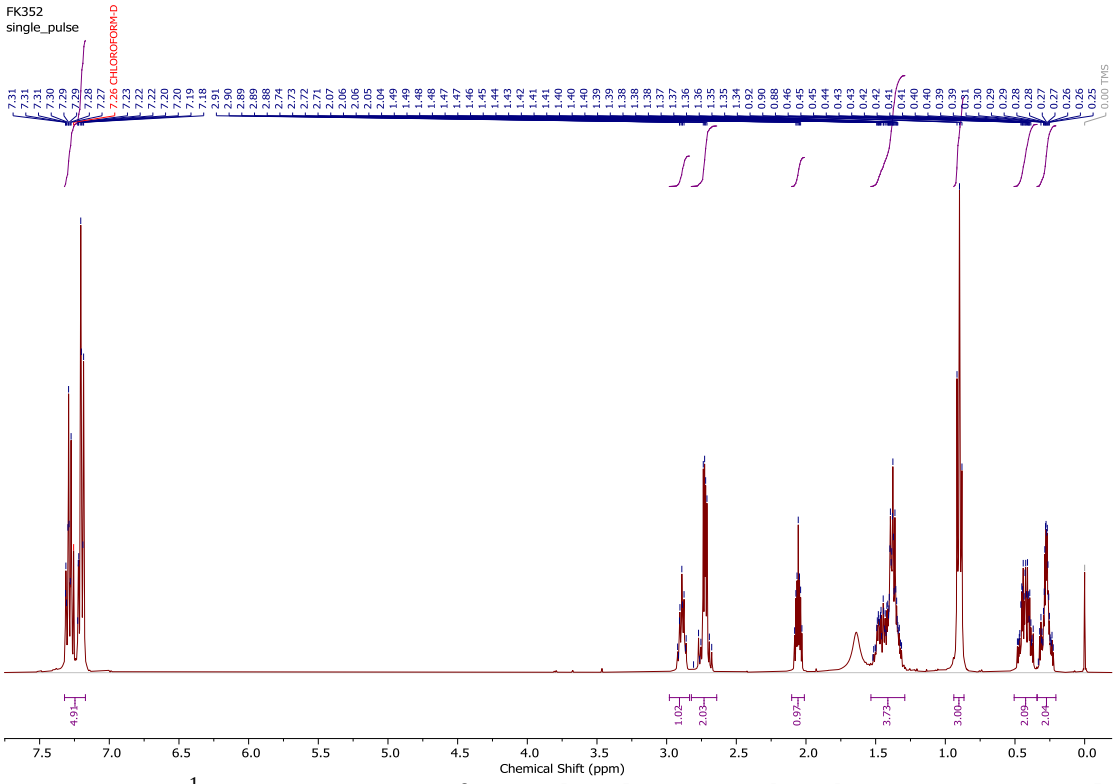


Figure S228. ^{1}H NMR spectrum of *N*-(1-phenylpentan-2-yl)cyclopropanamine (**216b**) ($CDCl_3$, 400 MHz)

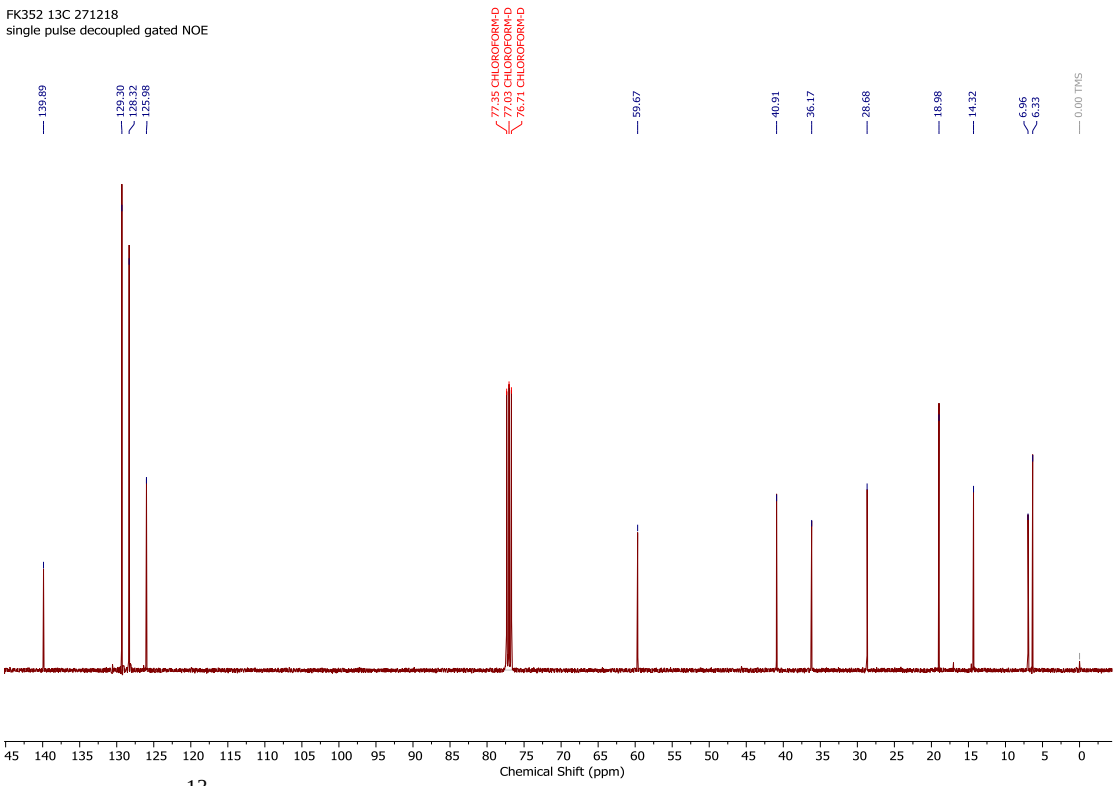


Figure S229. ^{13}C NMR spectrum of *N*-(1-phenylpentan-2-yl)cyclopropanamine (**216b**) ($CDCl_3$, 100 MHz)

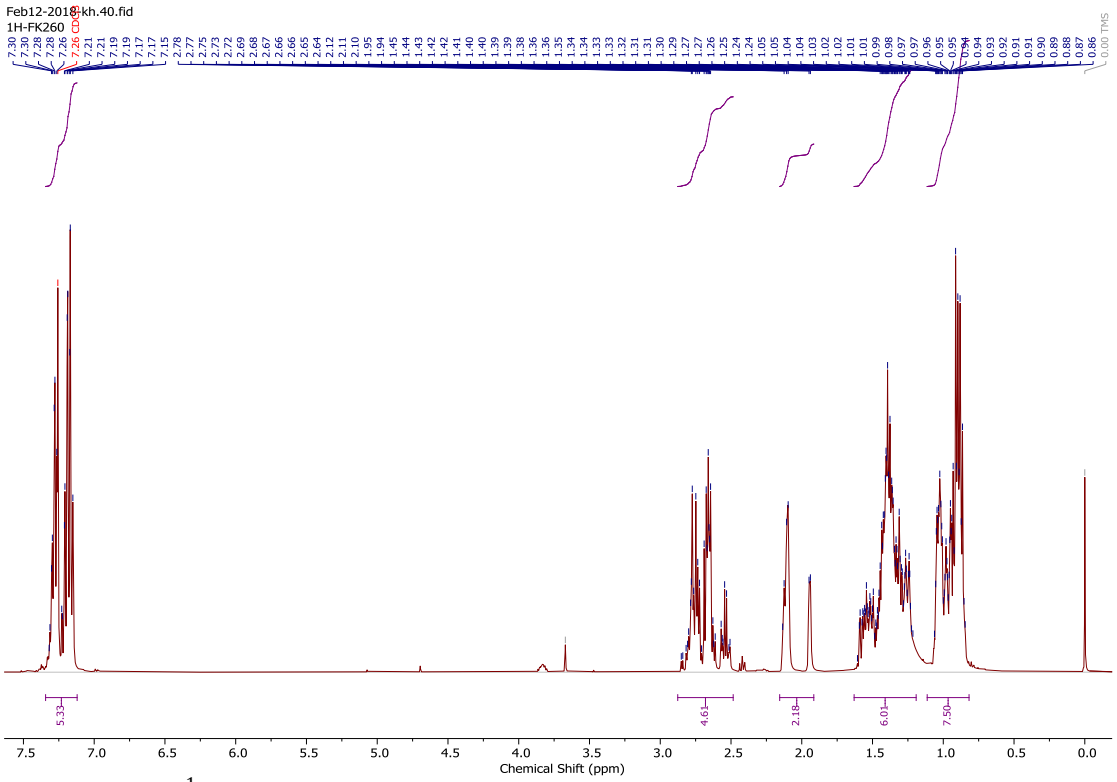


Figure S230. ^{1}H NMR spectrum of *N*-(1-phenylpentan-2-yl)bicyclo[2.2.1]heptan-2-amine (**216c**) ($CDCl_3$, 400 MHz)

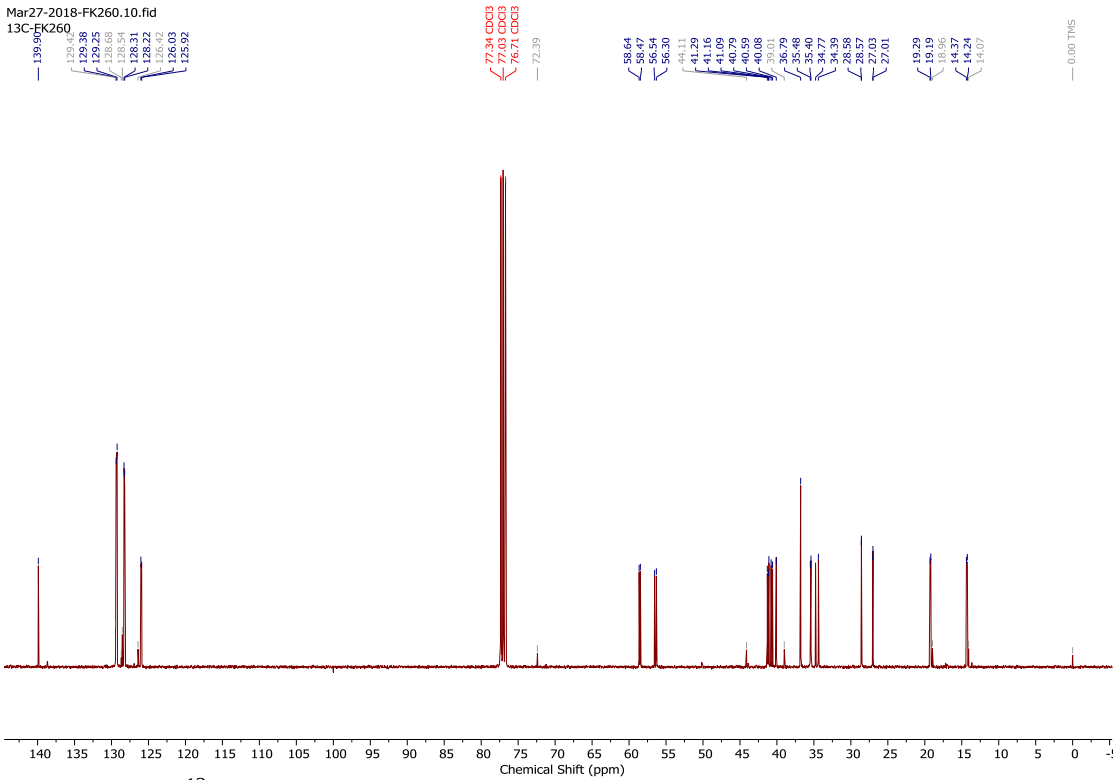


Figure S231. ^{13}C NMR spectrum of *N*-(1-phenylpentan-2-yl)bicyclo[2.2.1]heptan-2-amine (**216c**) ($CDCl_3$, 100 MHz)

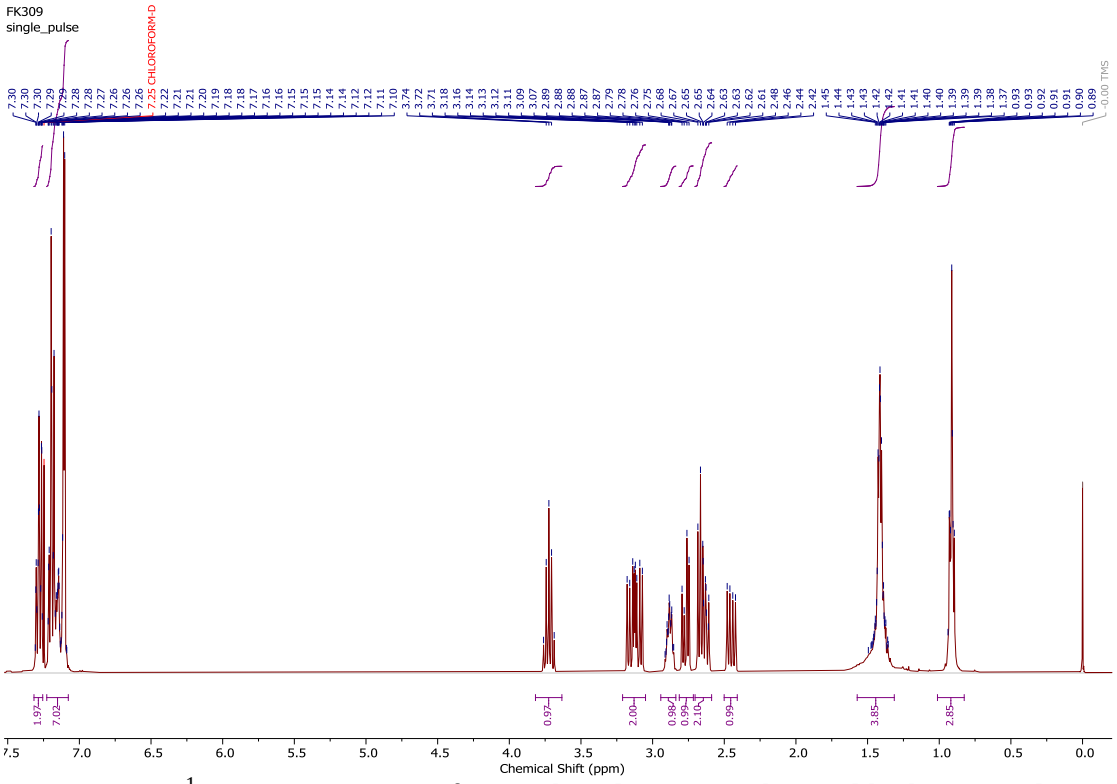


Figure S232. ^{1}H NMR spectrum of *N*-(1-phenylpentan-2-yl)-2,3-dihydro-1*H*-inden-2-amine (**216d**) ($CDCl_3$, 400 MHz)

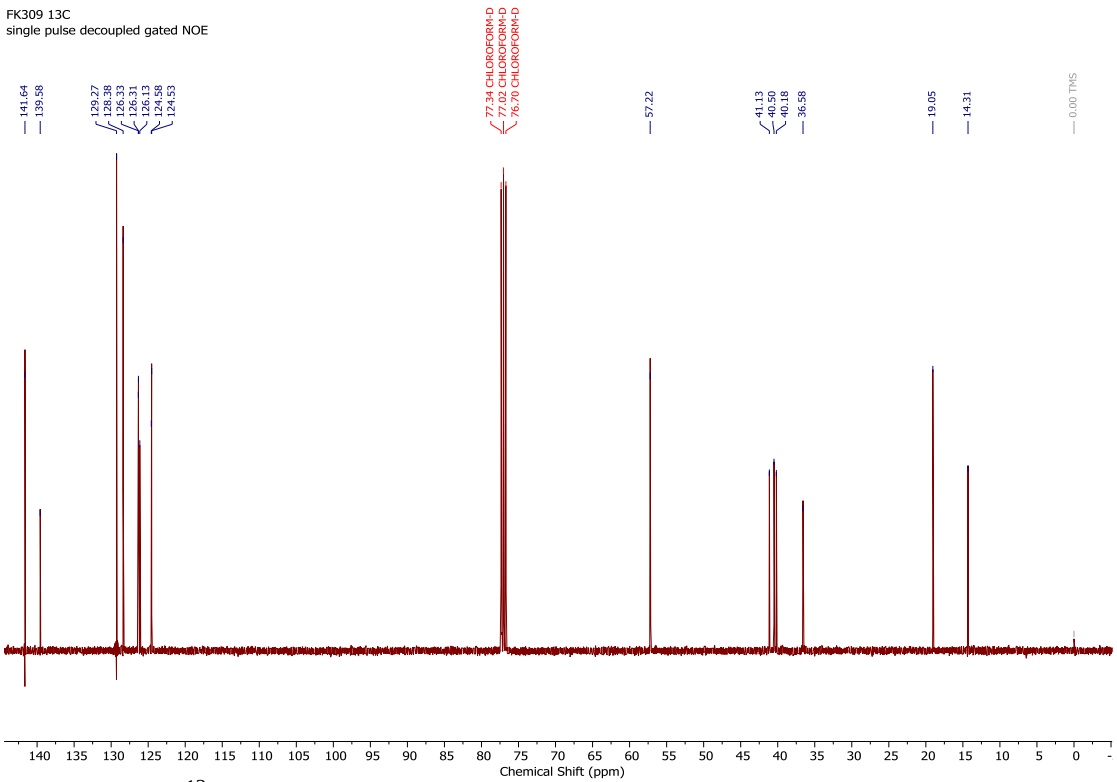


Figure S233. ^{13}C NMR spectrum of *N*-(1-phenylpentan-2-yl)-2,3-dihydro-1*H*-inden-2-amine (**216d**) ($CDCl_3$, 100 MHz)

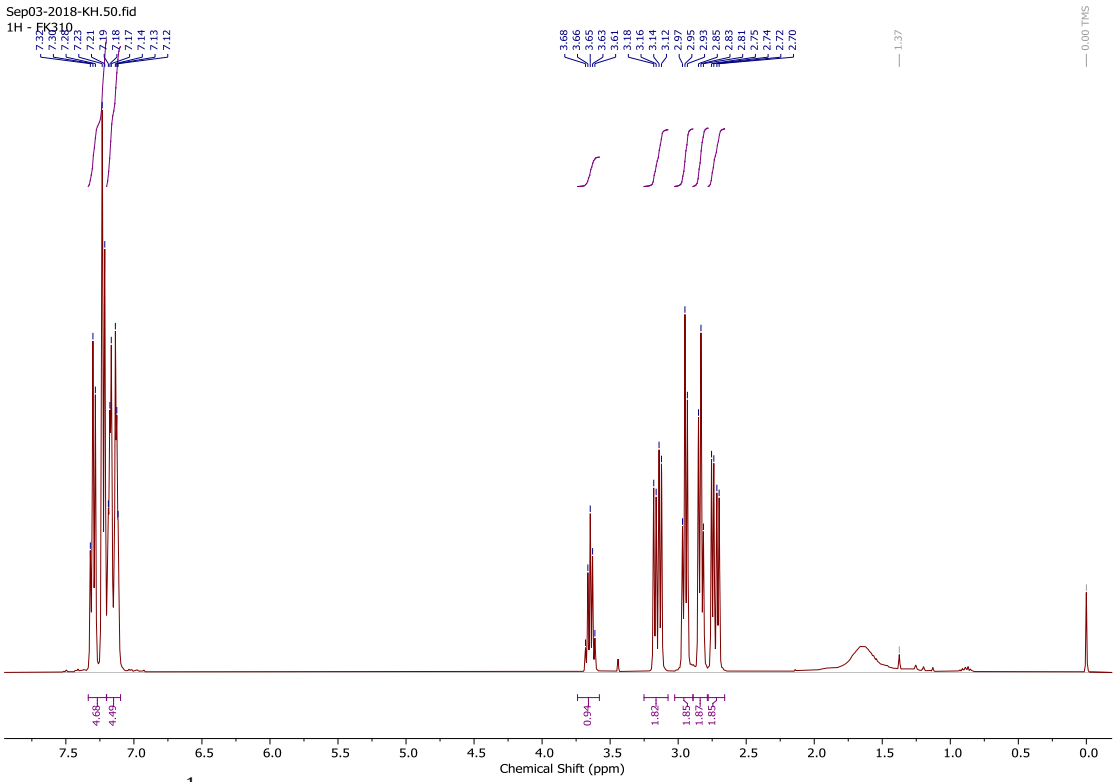


Figure S234. ^{1}H NMR spectrum of *N*-phenethyl-2,3-dihydro-1*H*-inden-2-amine (**217a**) ($CDCl_3$, 400 MHz)

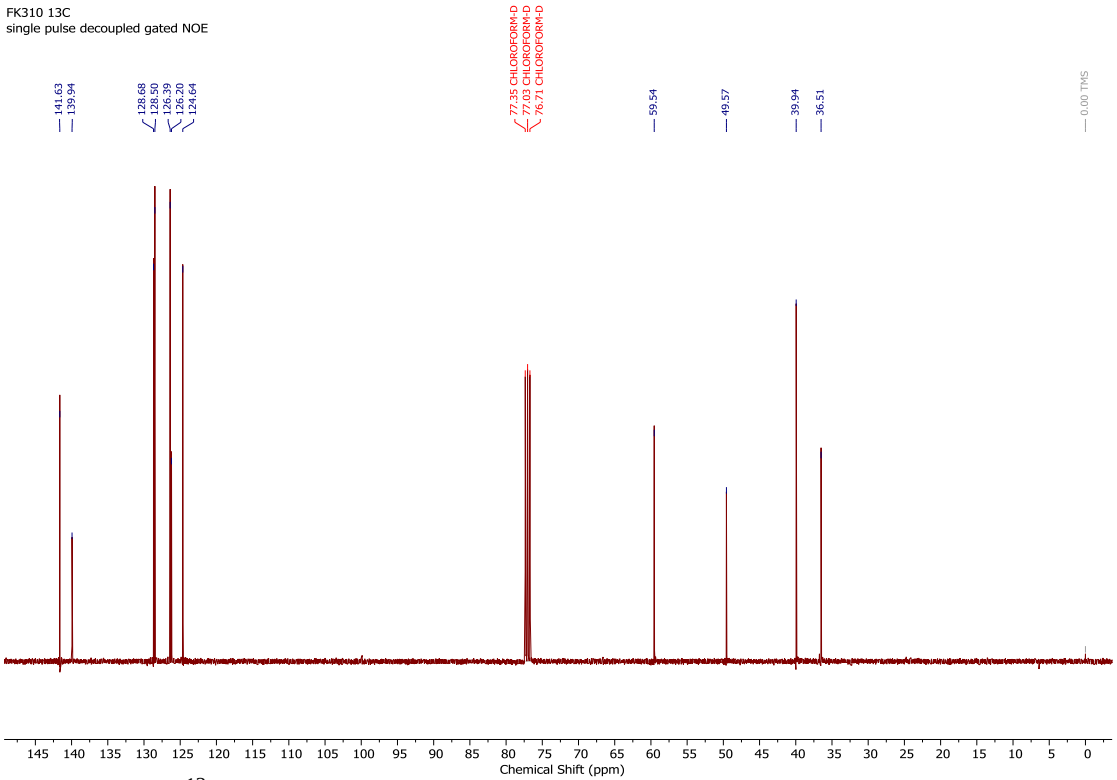


Figure S235. ^{13}C NMR spectrum of *N*-phenethyl-2,3-dihydro-1*H*-inden-2-amine (**217a**) ($CDCl_3$, 100 MHz)

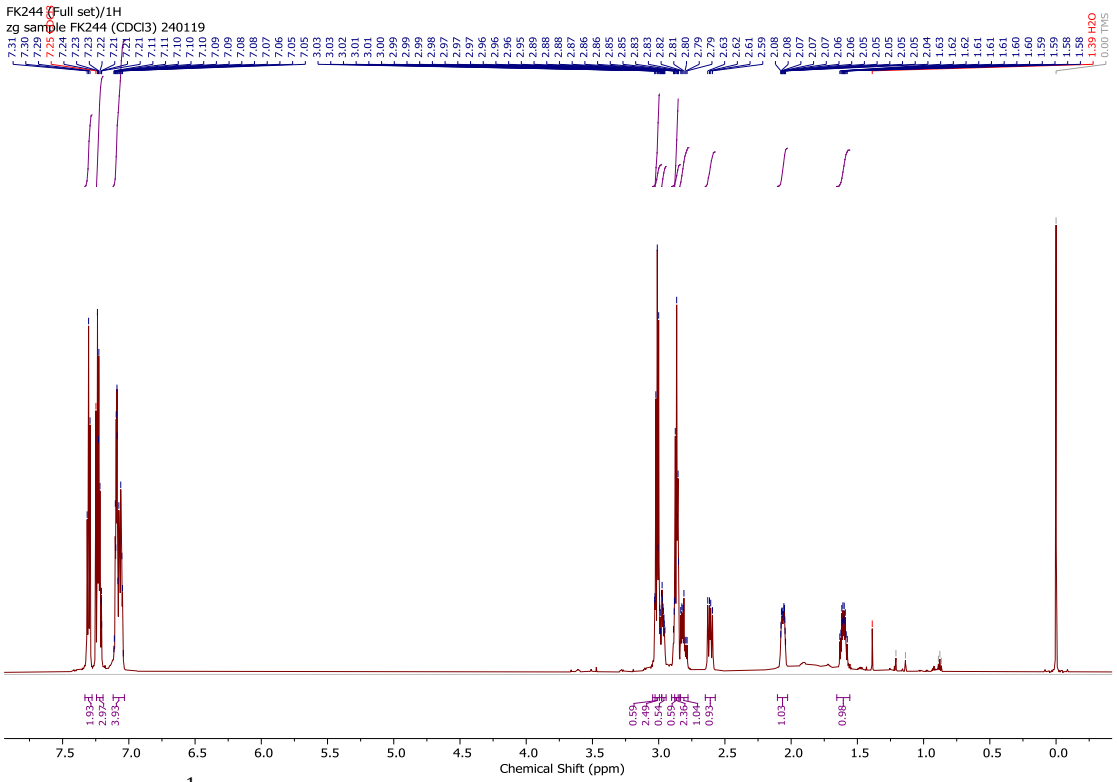


Figure S236. ^{1}H NMR spectrum of *N*-phenethyl-1,2,3,4-tetrahydronaphthalen-2-amine (**217b**) ($CDCl_3$, 700 MHz)

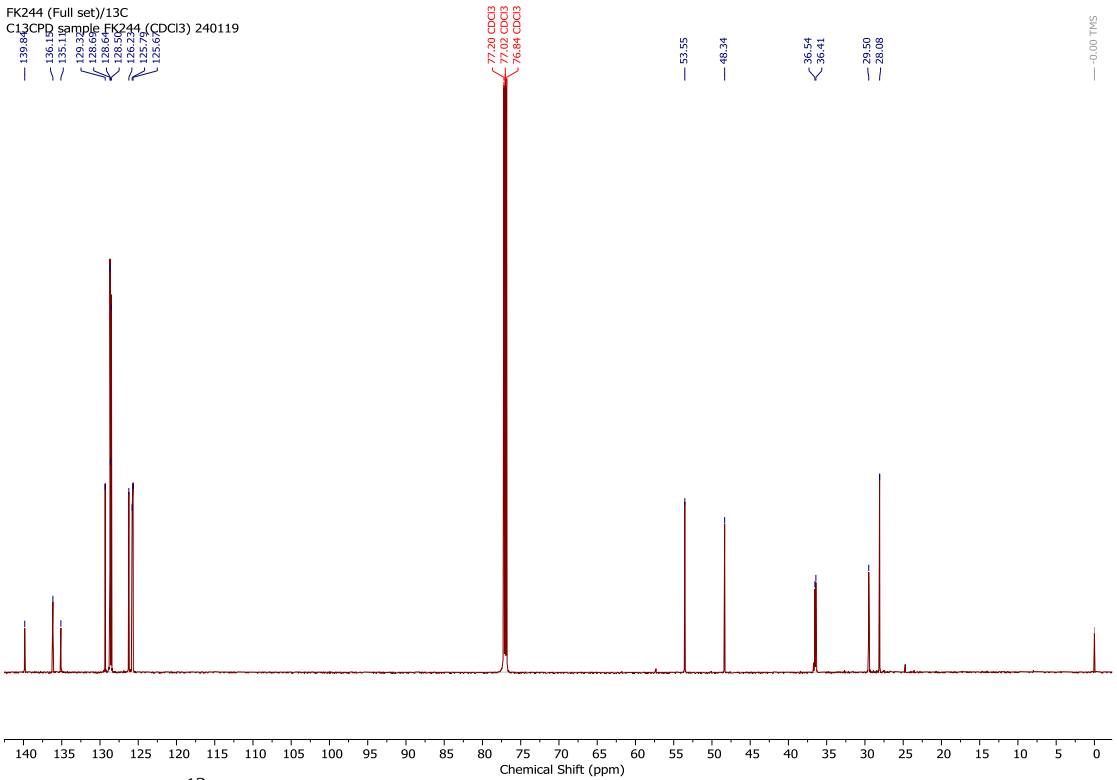


Figure S237. ^{13}C NMR spectrum of *N*-phenethyl-1,2,3,4-tetrahydronaphthalen-2-amine (**217b**) ($CDCl_3$, 175 MHz)

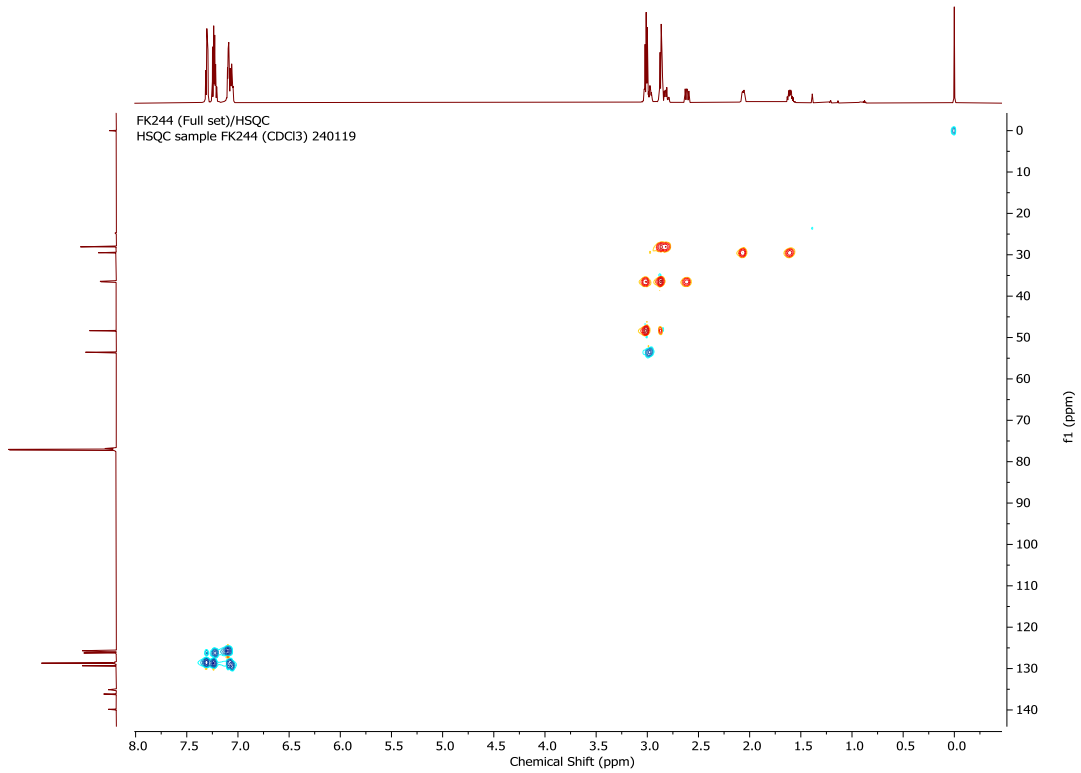


Figure S238. HSQC spectrum of *N*-phenethyl-1,2,3,4-tetrahydronaphthalen-2-amine (**217b**) ($CDCl_3$, 700 MHz)

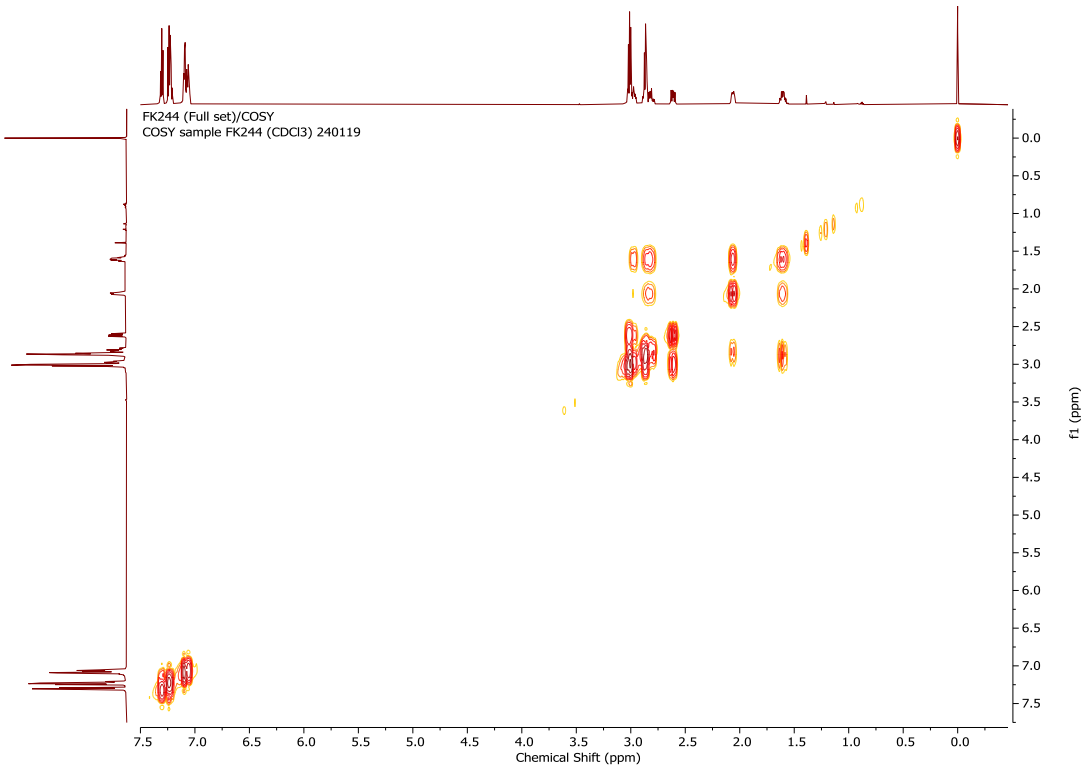


Figure S239. COSY spectrum of *N*-phenethyl-1,2,3,4-tetrahydronaphthalen-2-amine (**217b**) ($CDCl_3$, 700 MHz)



Figure S240. HMBC spectrum of *N*-phenethyl-1,2,3,4-tetrahydronaphthalen-2-amine (**217b**) ($CDCl_3$, 700 MHz)

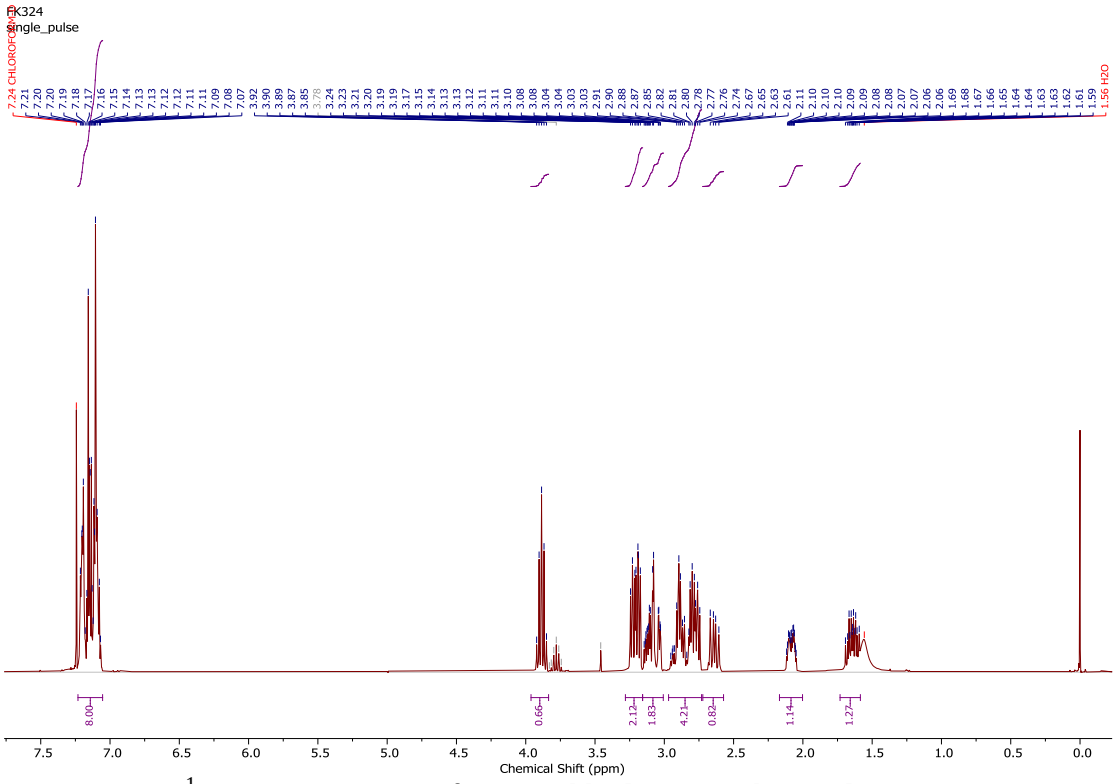


Figure S241. ^{1}H NMR spectrum of *N*-(2,3-dihydro-1*H*-inden-2-yl)-1,2,3,4-tetrahydronaphthalen-2-amine (**218**) ($CDCl_3$, 400 MHz)

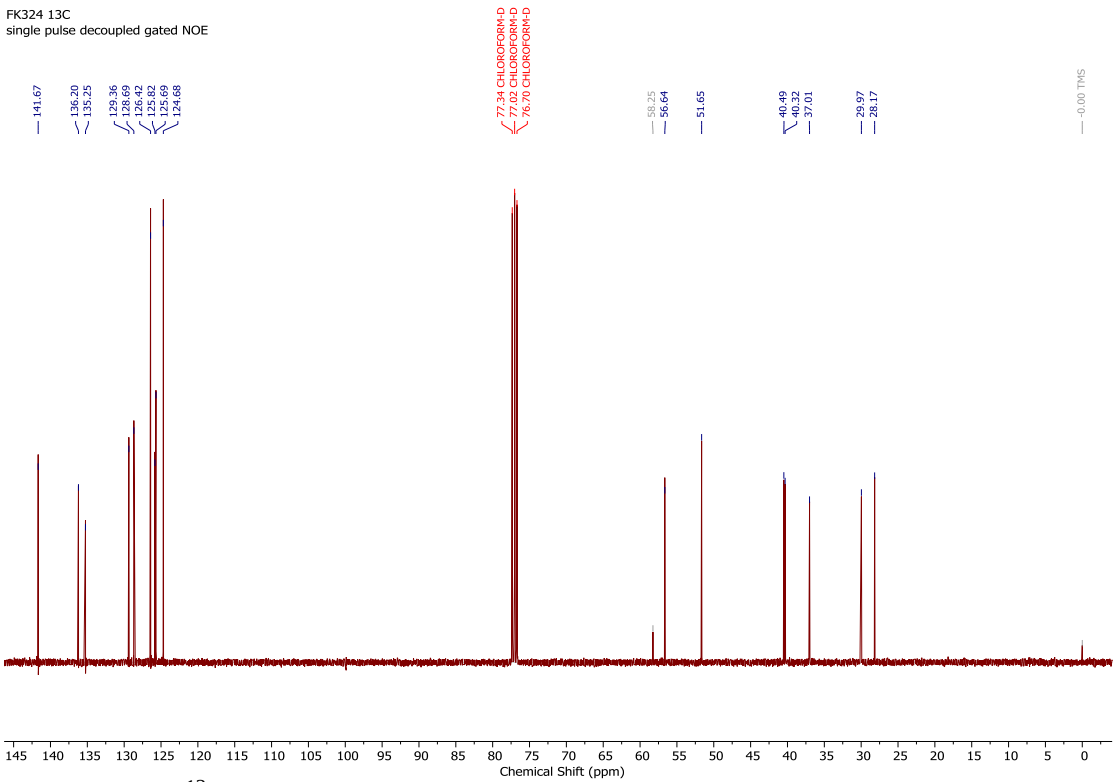


Figure S242. ^{13}C NMR spectrum of *N*-(2,3-dihydro-1*H*-inden-2-yl)-1,2,3,4-tetrahydronaphthalen-2-amine (**218**) ($CDCl_3$, 100 MHz)

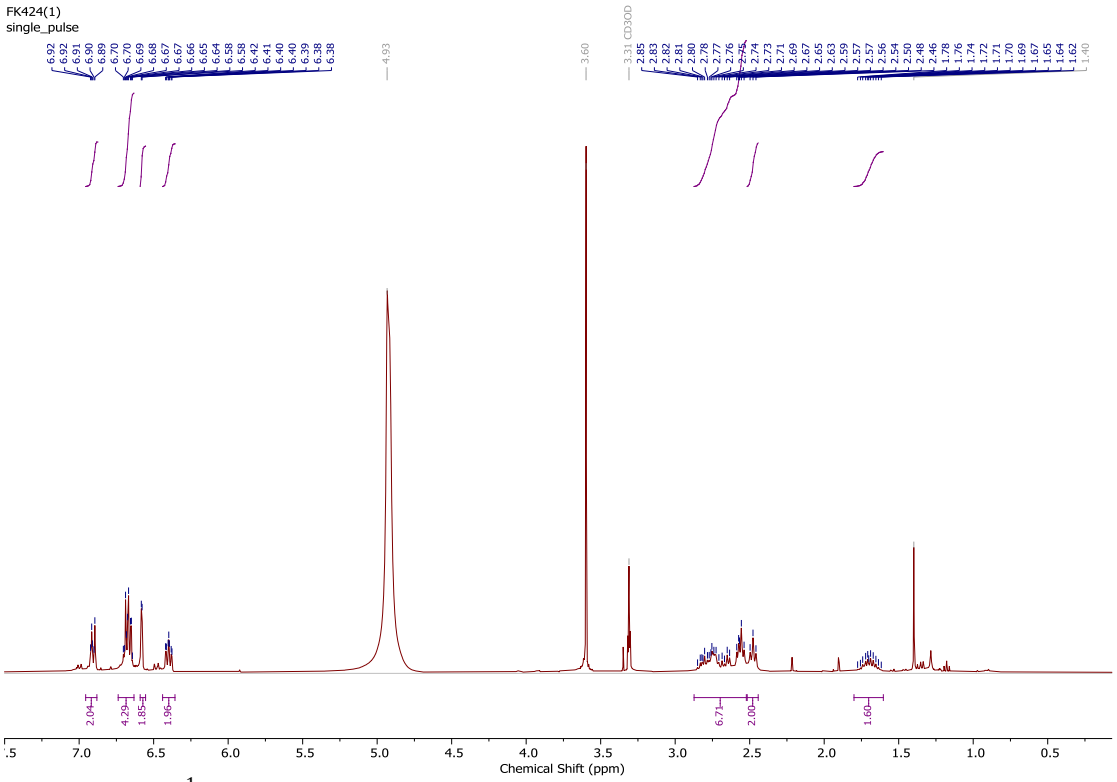


Figure S243. ^{1}H NMR spectrum of 4-(2-((3,4-dihydroxyphenethyl)amino)-4-(4-hydroxyphenyl)butyl)benzene-1,2-diol (**219**) (CD_3OD, 400 MHz)

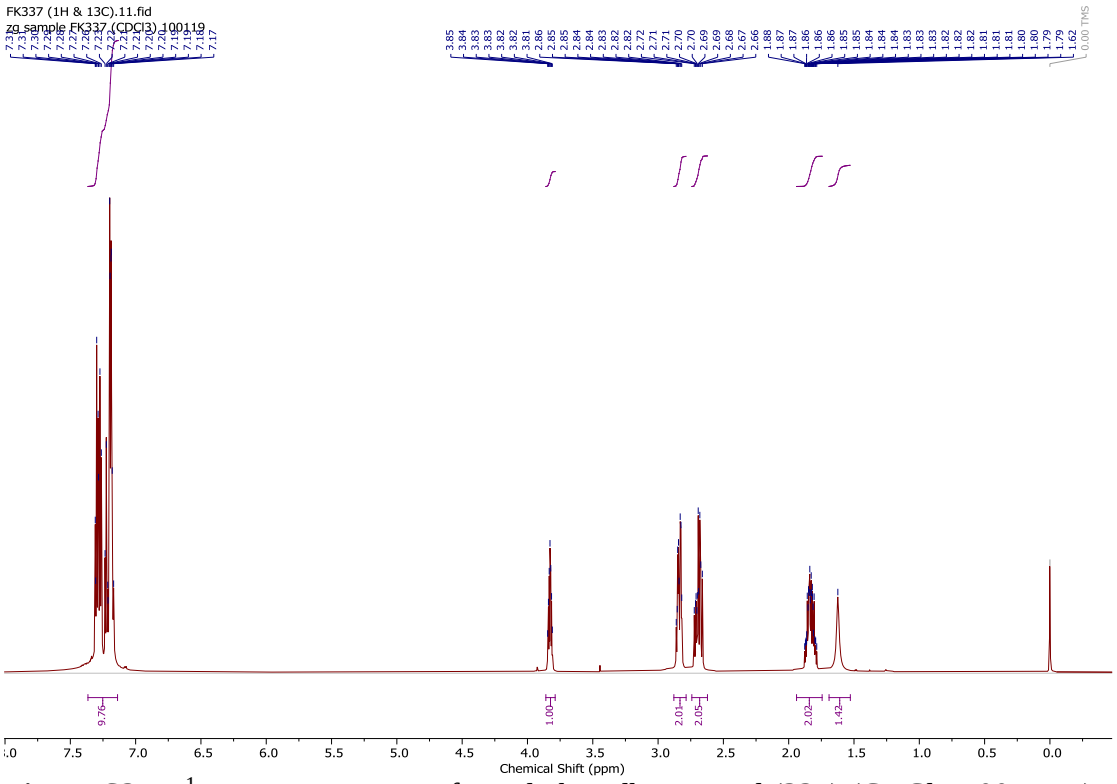


Figure S244. ^{1}H NMR spectrum of 1,4-diphenylbutan-2-ol (**221**) ($CDCl_3$, 700 MHz)

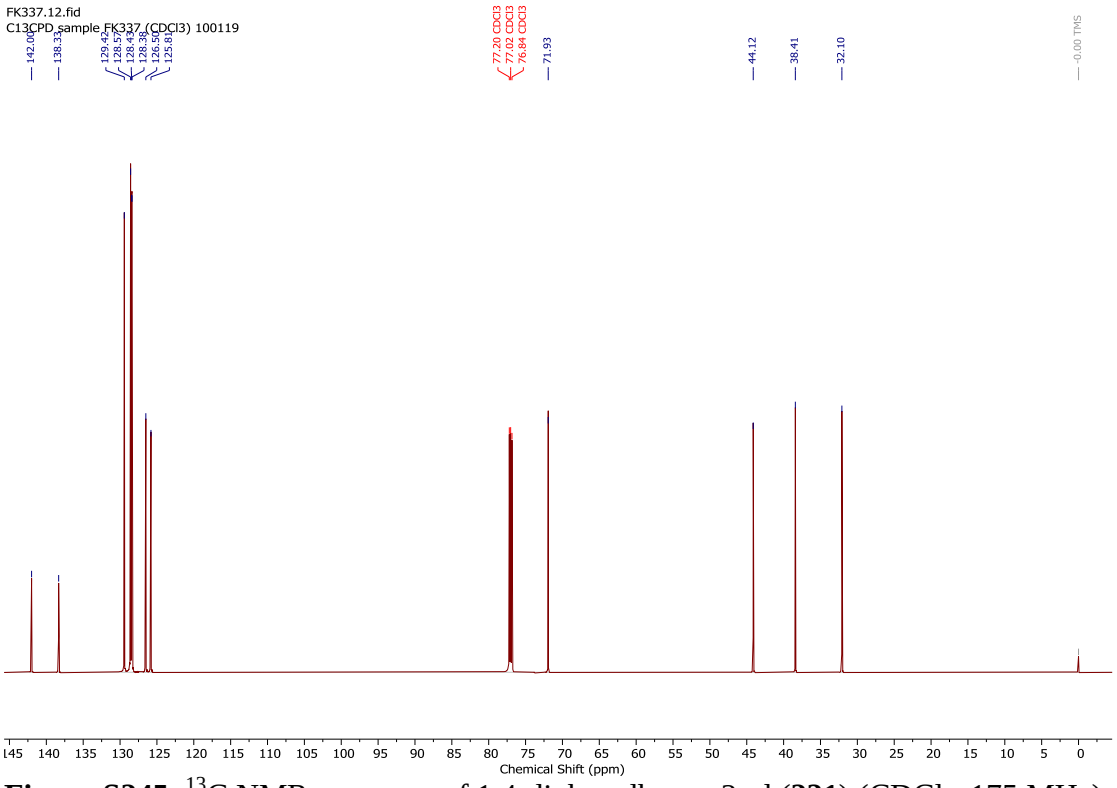


Figure S245. ^{13}C NMR spectrum of 1,4-diphenylbutan-2-ol (**221**) ($CDCl_3$, 175 MHz)

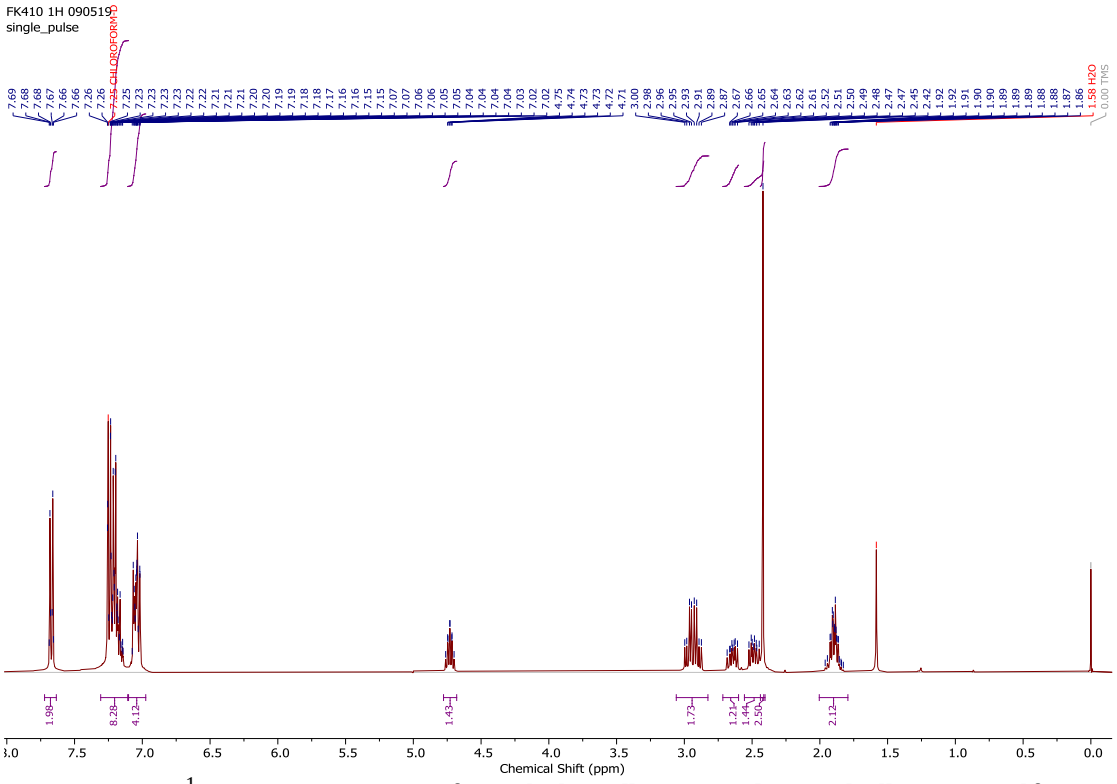


Figure S246. ^{1}H NMR spectrum of 1,4-diphenylbutan-2-yl 4-methylbenzenesulfonate (**224**) ($CDCl_3$, 400 MHz)

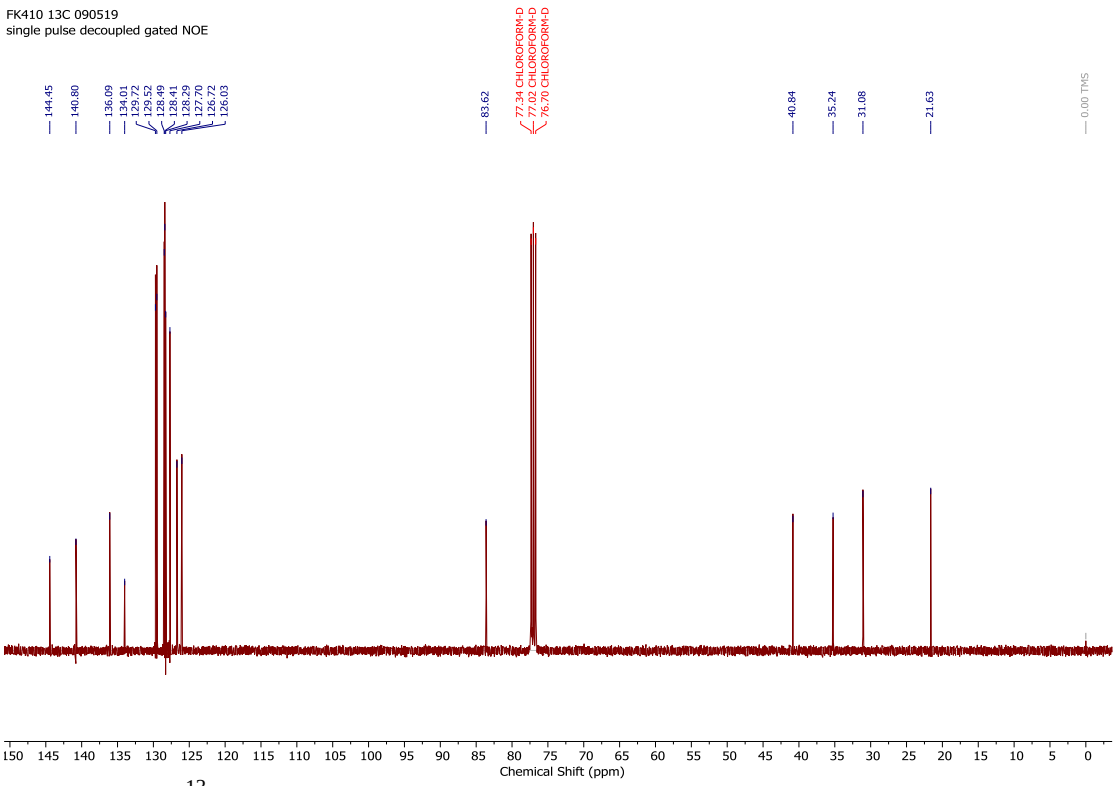


Figure S247. ^{13}C NMR spectrum of 1,4-diphenylbutan-2-yl 4-methylbenzenesulfonate (**224**) ($CDCl_3$, 100 MHz)

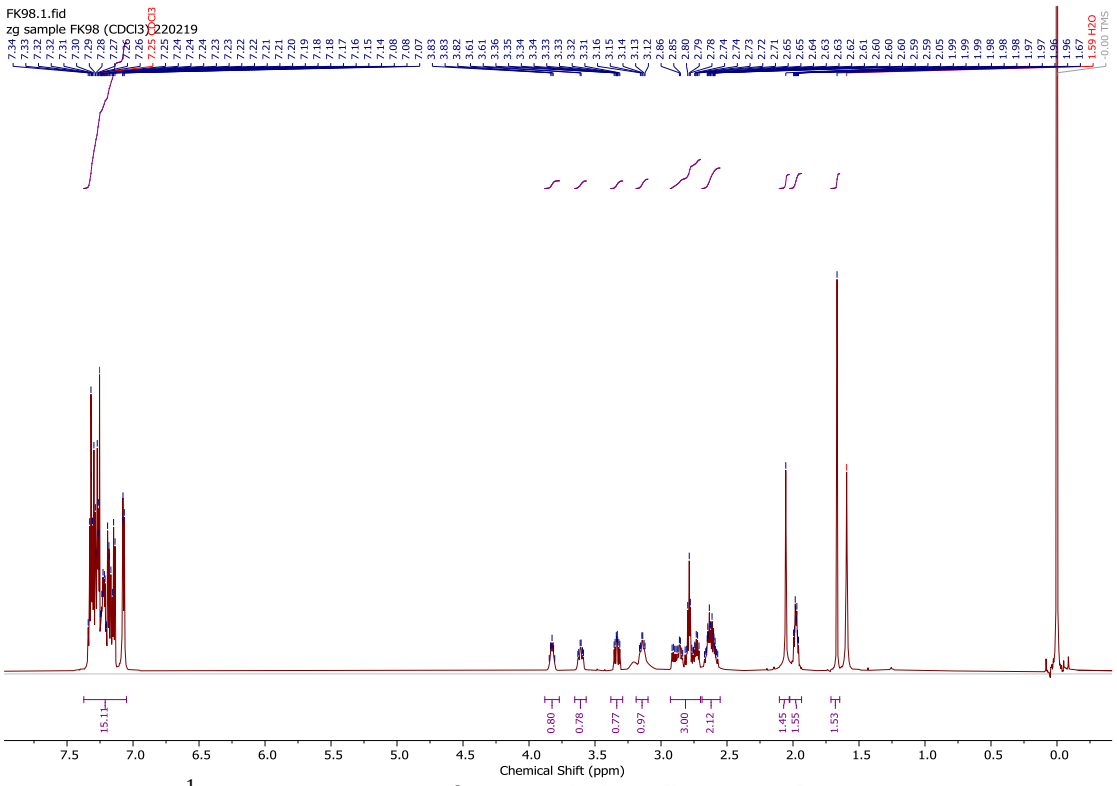


Figure S248. ^{1}H NMR spectrum of *N*-(1,4-diphenylbutan-2-yl)-*N*-phenethylacetamide (**230a**) ($CDCl_3$, 700 MHz)

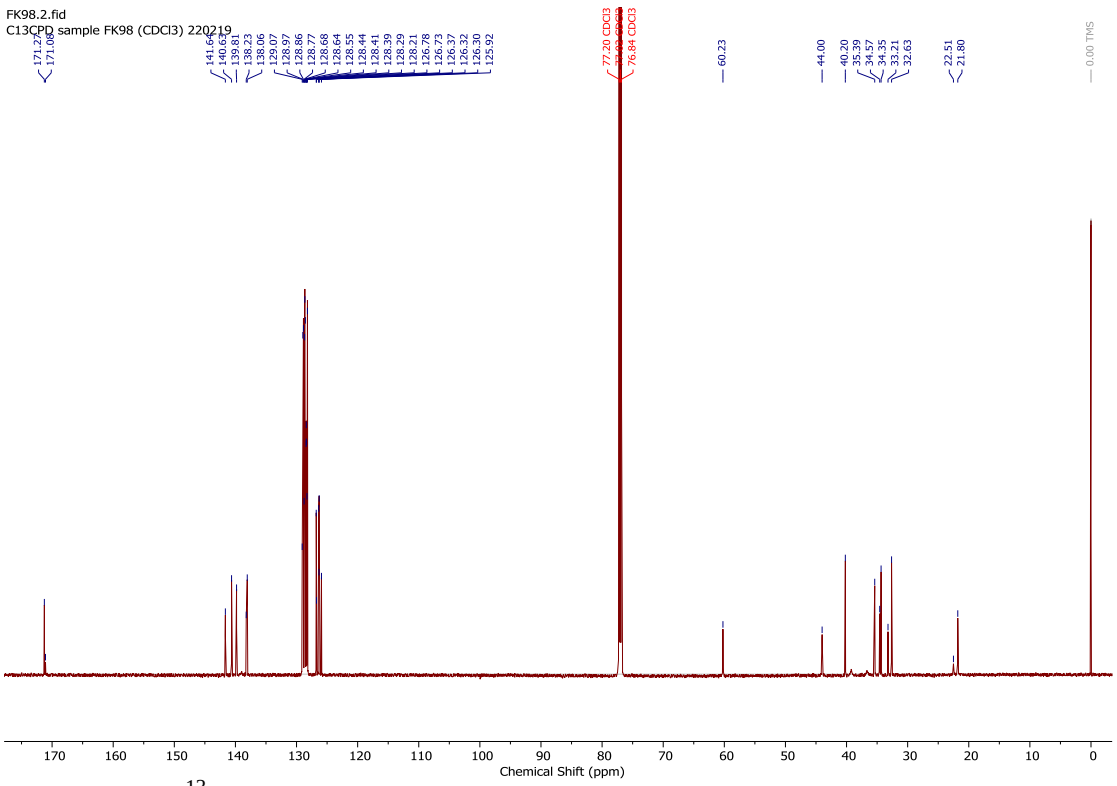


Figure S249. ^{13}C NMR spectrum of *N*-(1,4-diphenylbutan-2-yl)-*N*-phenethylacetamide (**230a**) ($CDCl_3$, 175 MHz)

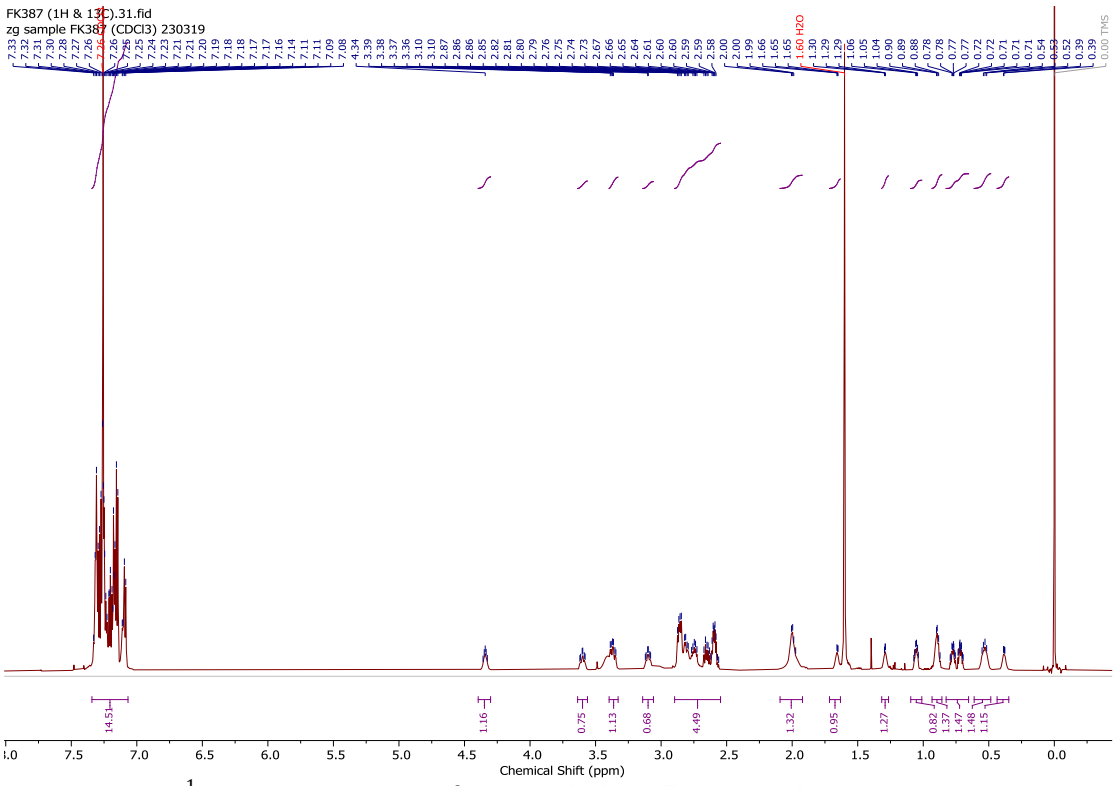


Figure S250. ^{1}H NMR spectrum of *N*-(1,4-diphenylbutan-2-yl)-*N*-phenethylcyclopropanecarboxamide (**230b**) ($CDCl_3$, 700 MHz)

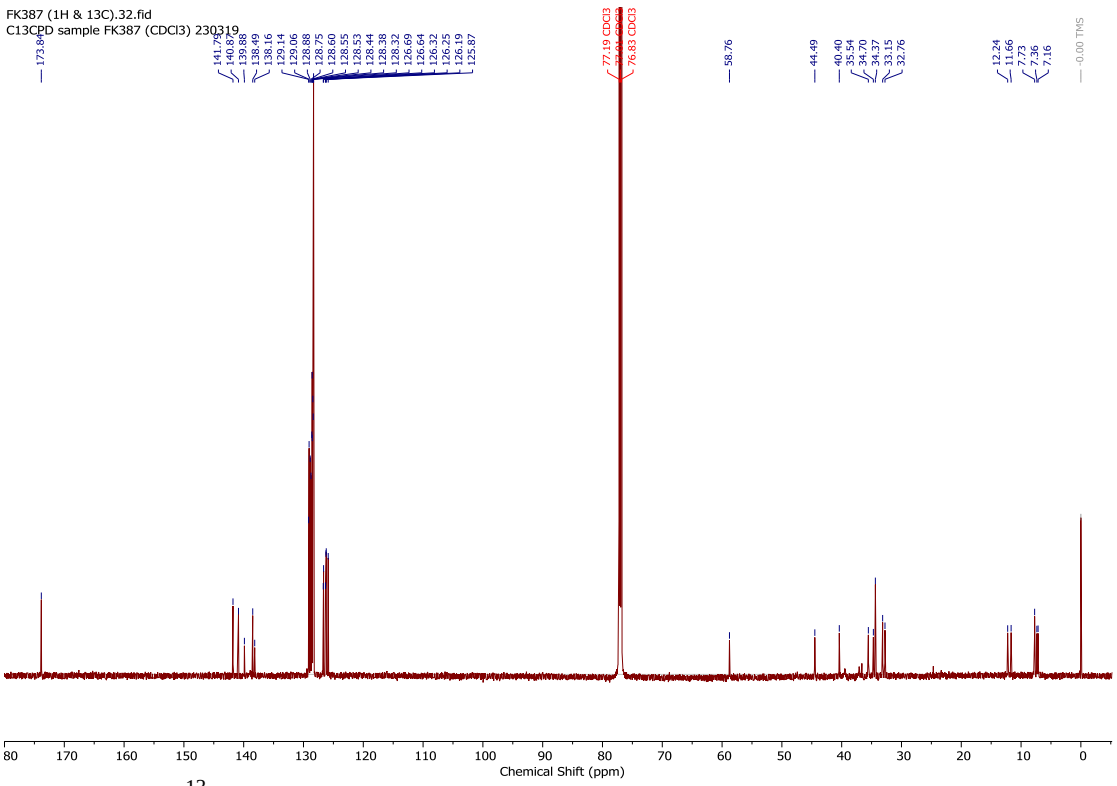


Figure S251. ^{13}C NMR spectrum of *N*-(1,4-diphenylbutan-2-yl)-*N*-phenethylcyclopropanecarboxamide (**230b**) ($CDCl_3$, 175 MHz)

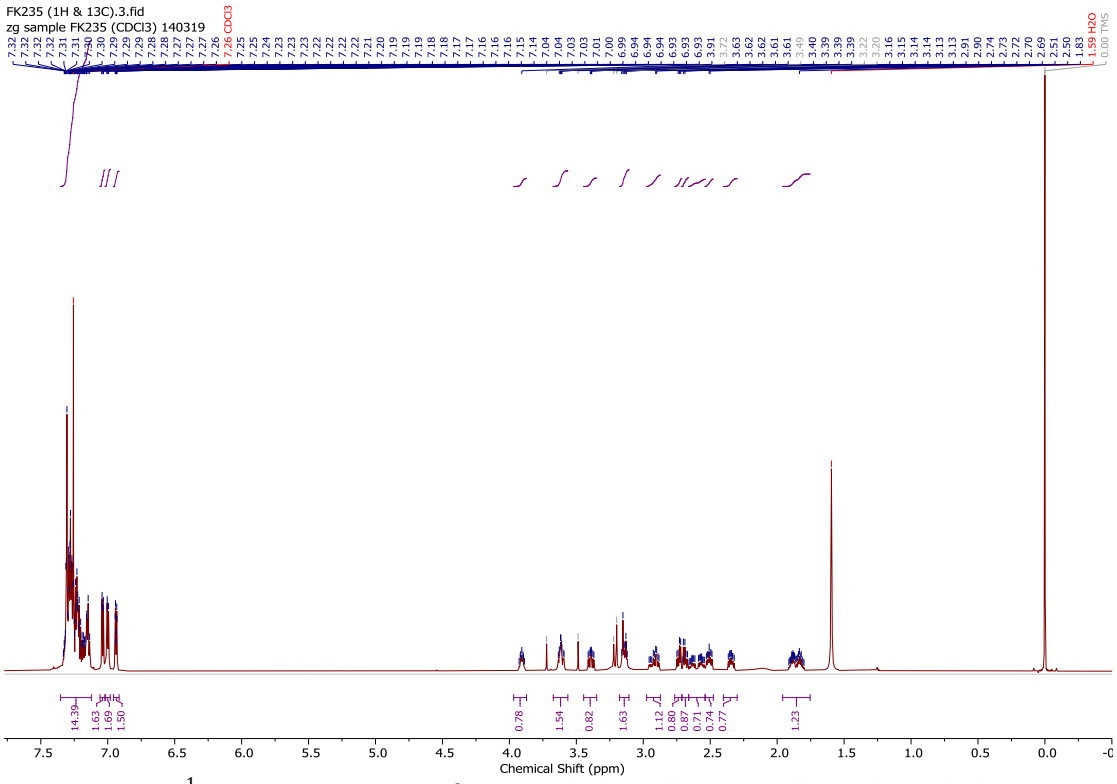


Figure S252. ^{1}H NMR spectrum of *N*-(1,4-diphenylbutan-2-yl)-*N*-phenethyl-2-phenylacetamide (**230c**) ($CDCl_3$, 700 MHz)

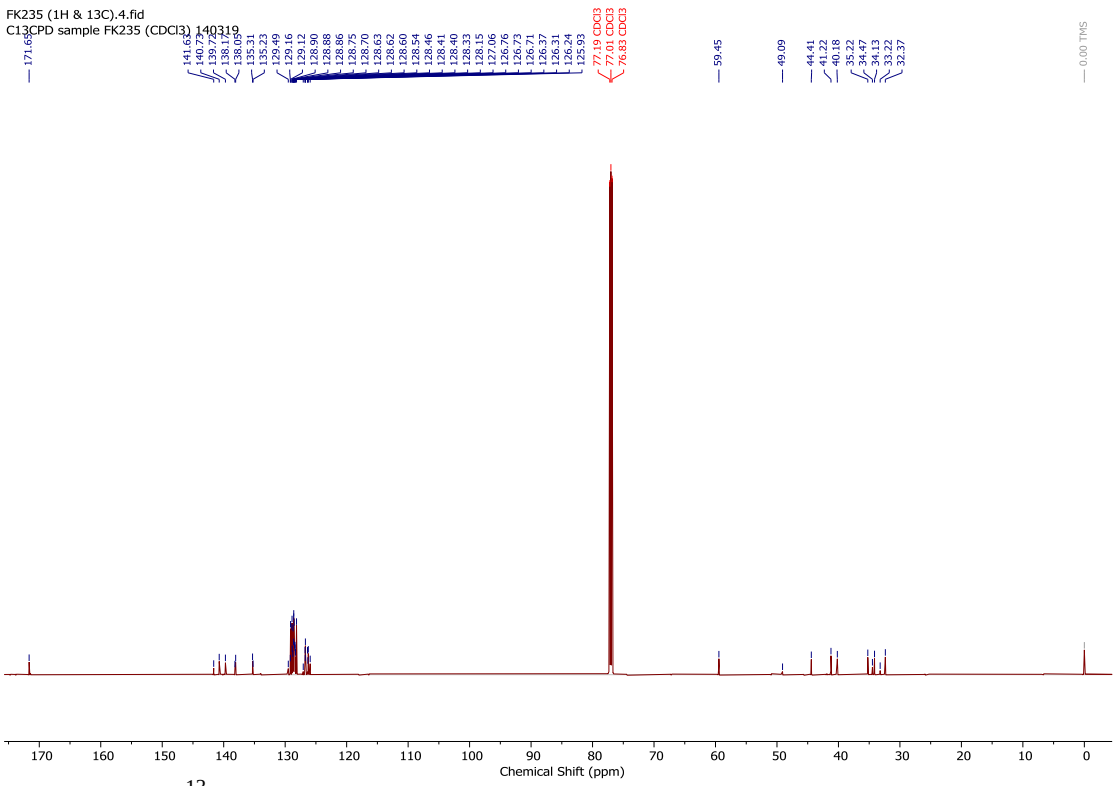


Figure S253. ^{13}C NMR spectrum of *N*-(1,4-diphenylbutan-2-yl)-*N*-phenethyl-2-phenylacetamide (**230c**) ($CDCl_3$, 175 MHz)

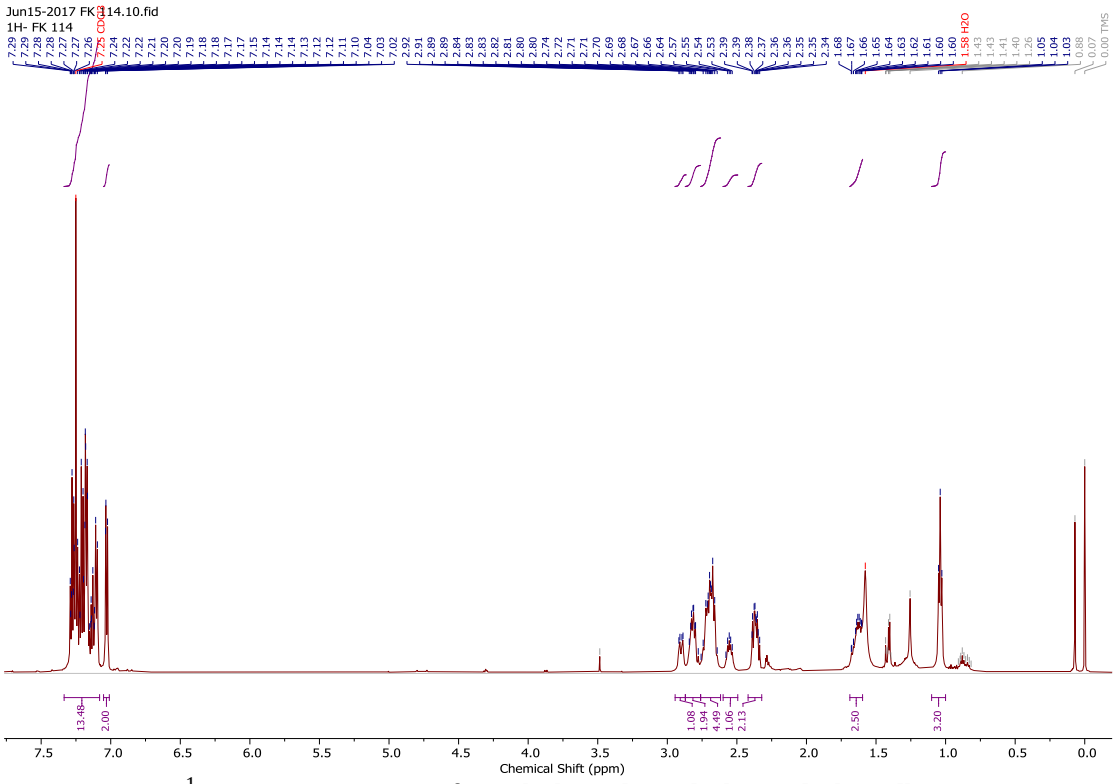


Figure S254. ^{1}H NMR spectrum of *N*-ethyl-*N*-phenethyl-1,4-diphenylbutan-2-amine (**231a**) ($CDCl_3$, 600 MHz)

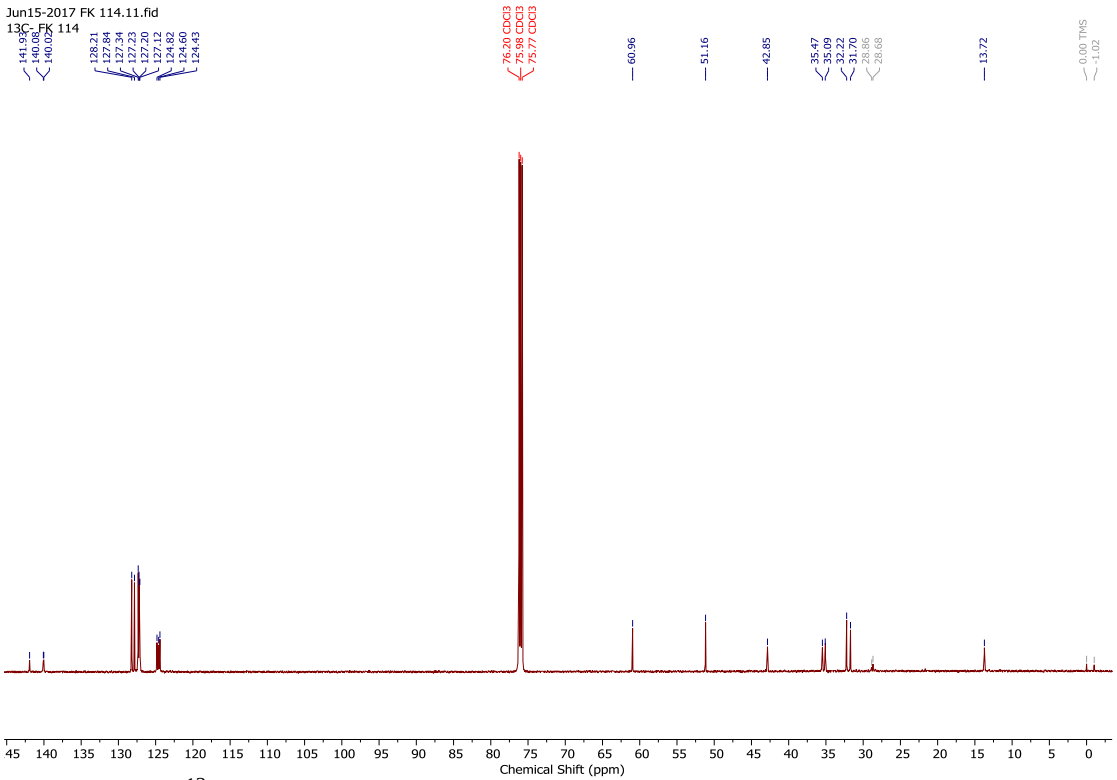


Figure S255. ^{13}C NMR spectrum of *N*-ethyl-*N*-phenethyl-1,4-diphenylbutan-2-amine (**231a**) ($CDCl_3$, 150 MHz)

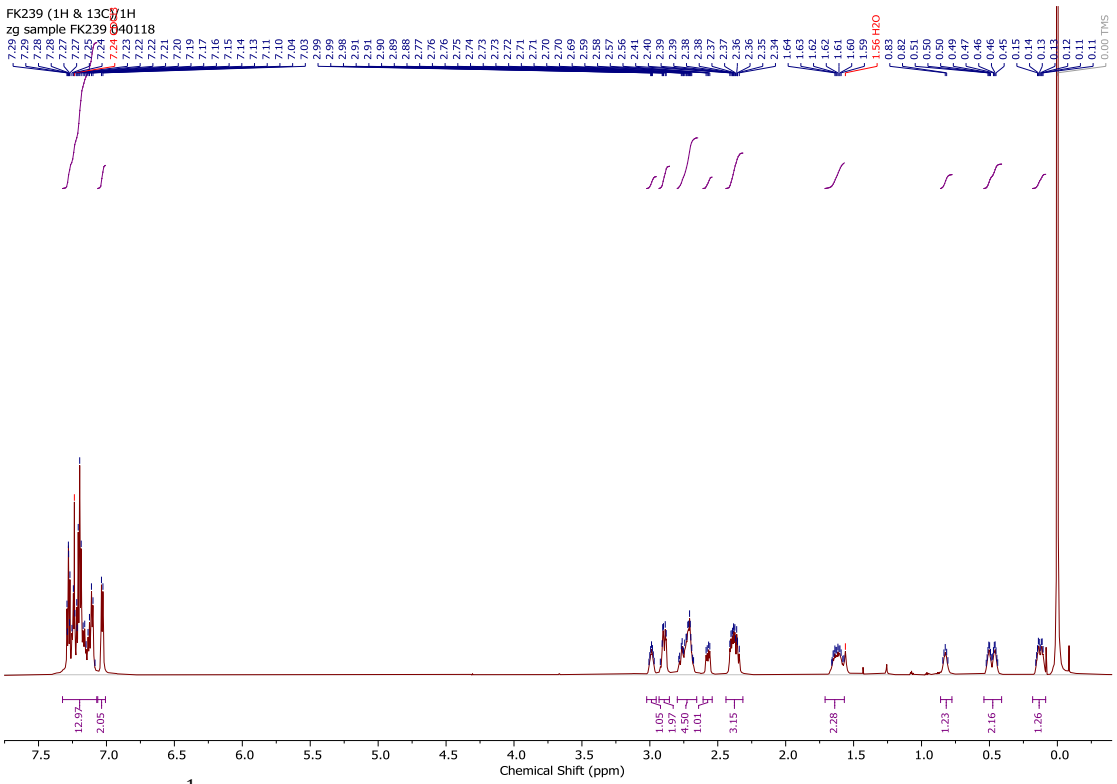


Figure S256. ^{1}H NMR spectrum of *N*-(cyclopropylmethyl)-*N*-phenethyl-1,4-diphenylbutan-2-amine (**231b**) ($CDCl_3$, 700 MHz)

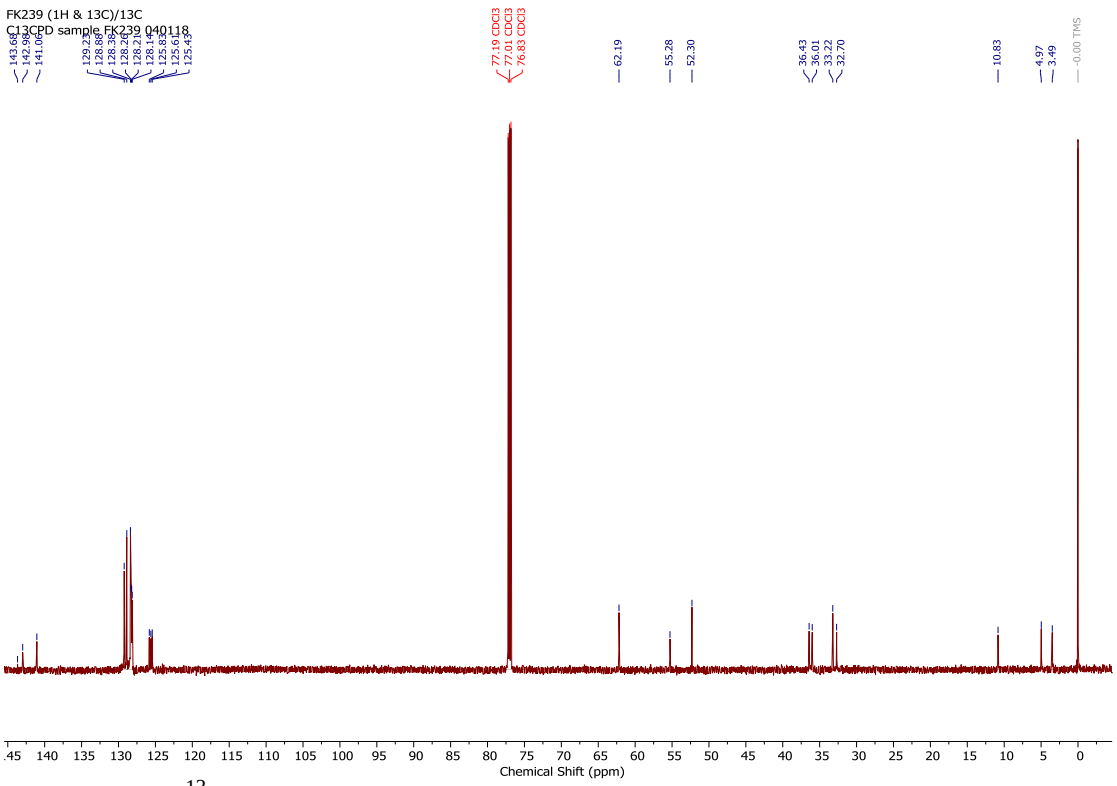


Figure S257. ^{13}C NMR spectrum of *N*-(cyclopropylmethyl)-*N*-phenethyl-1,4-diphenylbutan-2-amine (**231b**) ($CDCl_3$, 175 MHz)

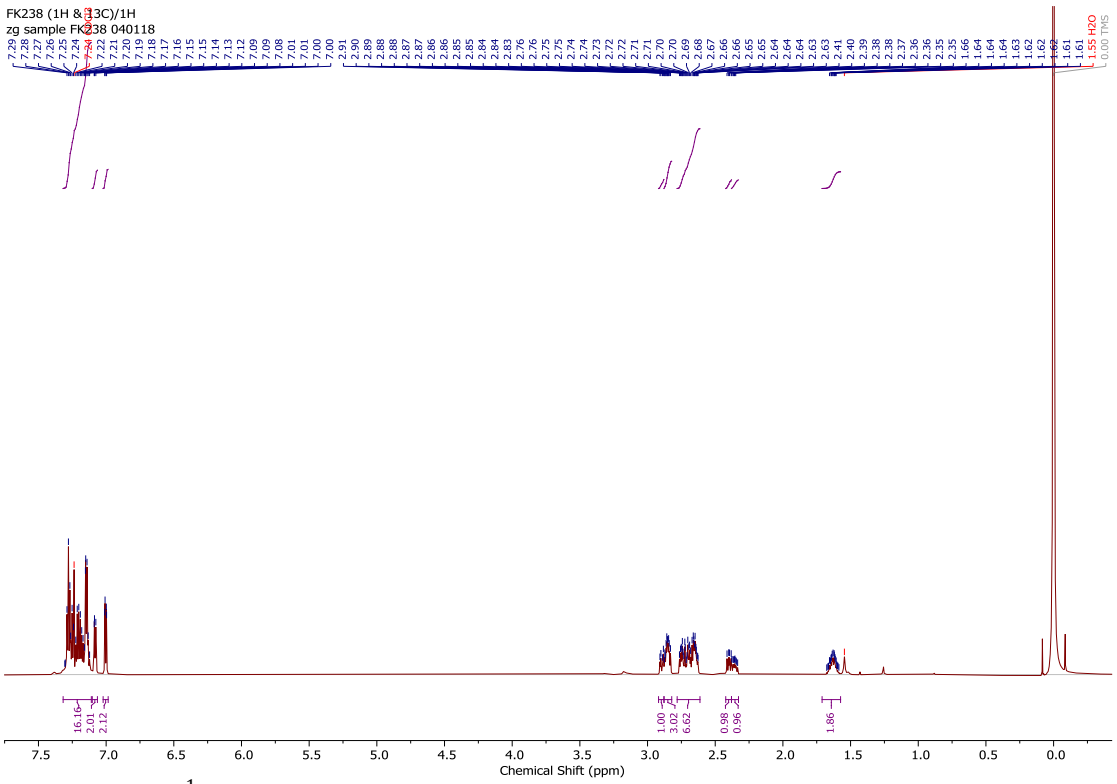


Figure S258. ^{1}H NMR spectrum of *N*,*N*-diphenethyl-1,4-diphenylbutan-2-amine (**231c**) ($CDCl_3$, 700 MHz)

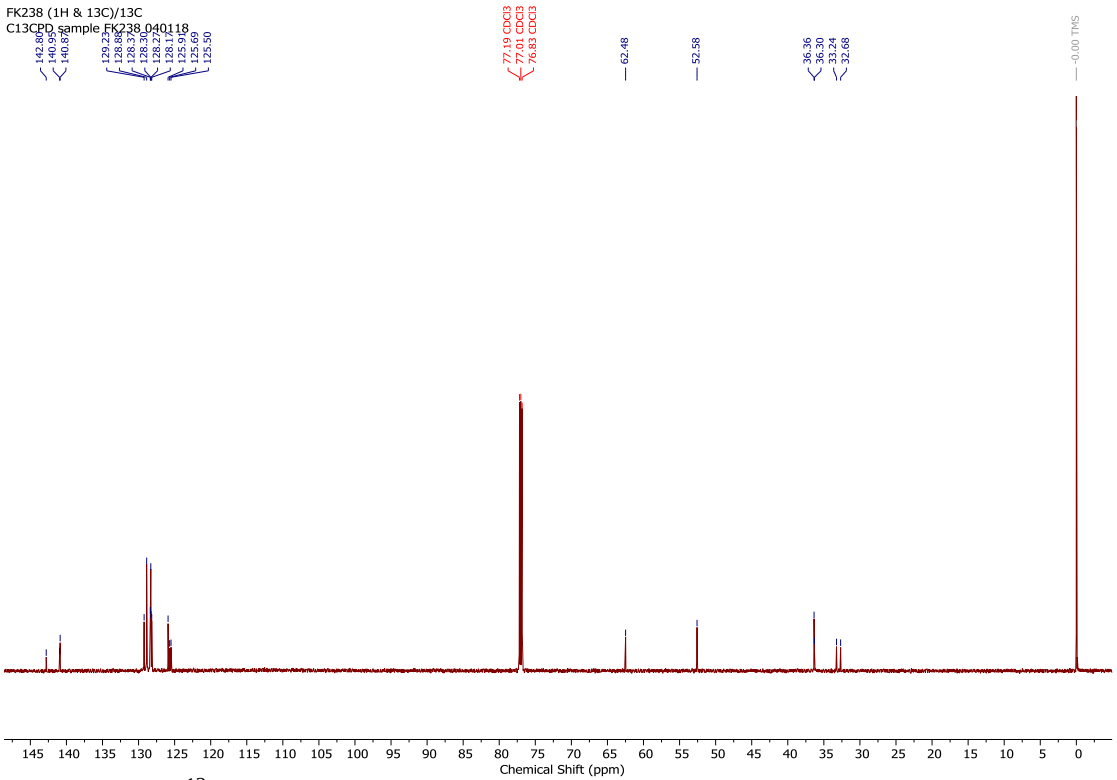


Figure S259. ^{13}C NMR spectrum of *N*,*N*-diphenethyl-1,4-diphenylbutan-2-amine (**231c**) ($CDCl_3$, 175 MHz)

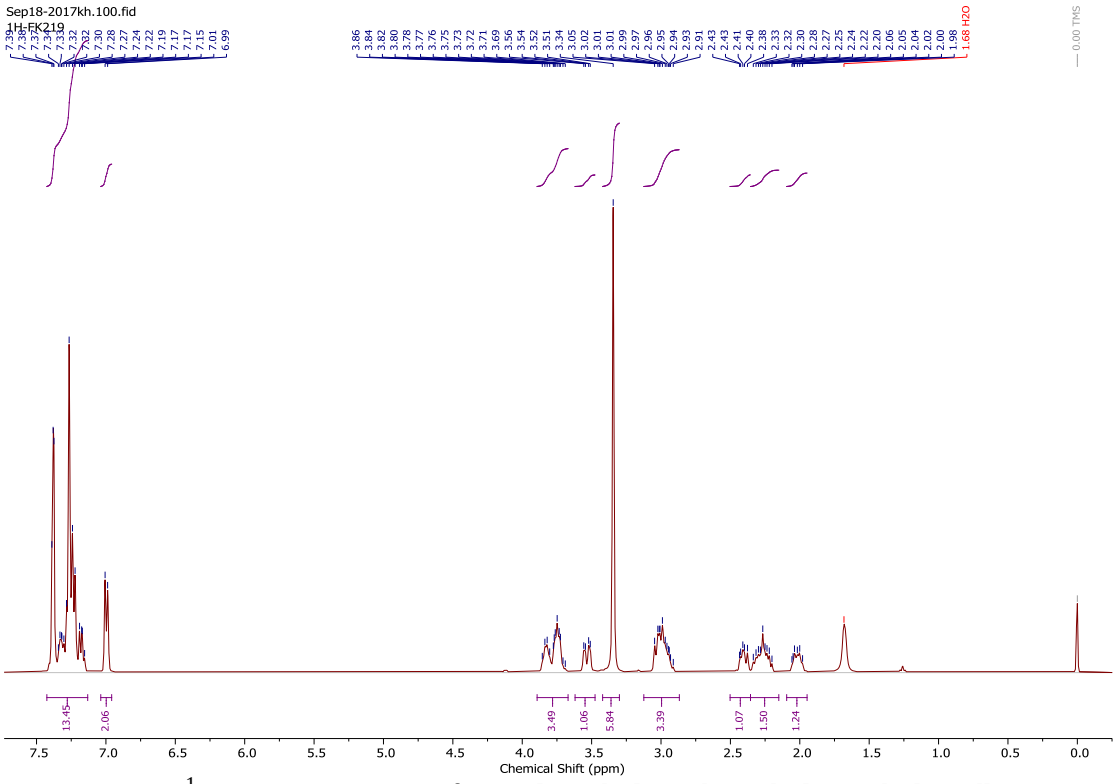


Figure S260. ^{1}H NMR spectrum of *N*,*N*-dimethyl-*N*-phenethyl-1,4-diphenylbutan-2-aminium iodide (**232**) ($CDCl_3$, 400 MHz)

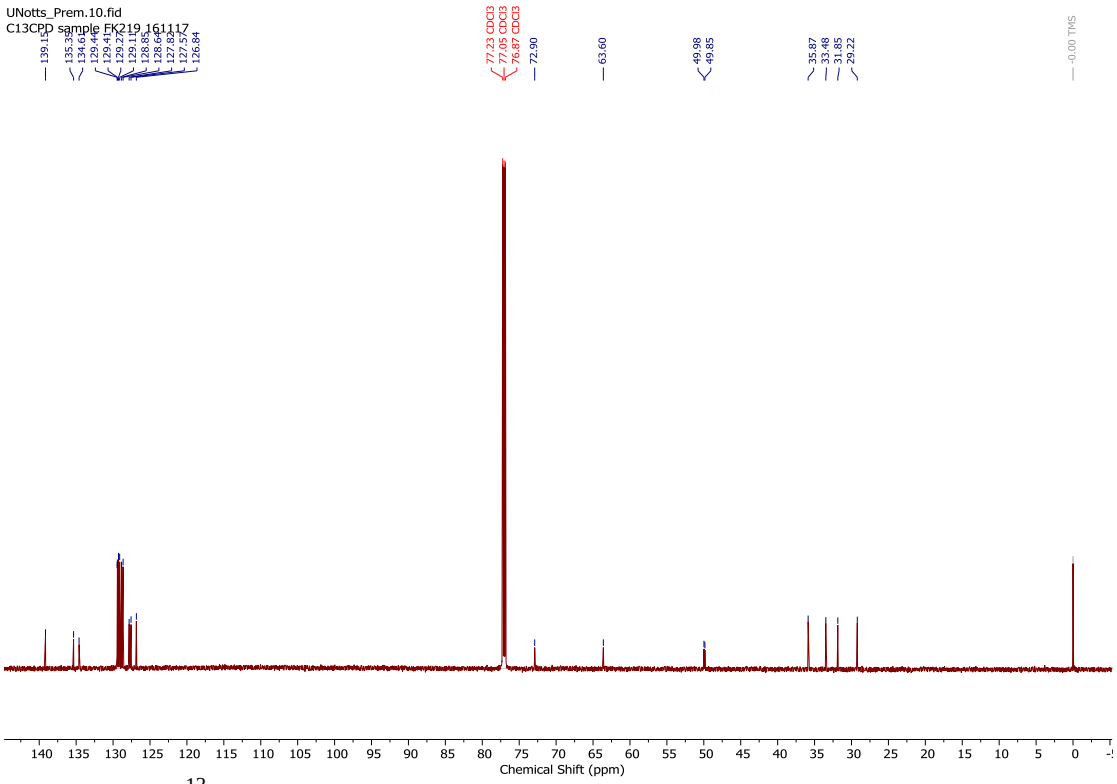


Figure S261. ^{13}C NMR spectrum of *N*,*N*-dimethyl-*N*-phenethyl-1,4-diphenylbutan-2-aminium iodide (**232**) ($CDCl_3$, 175 MHz)

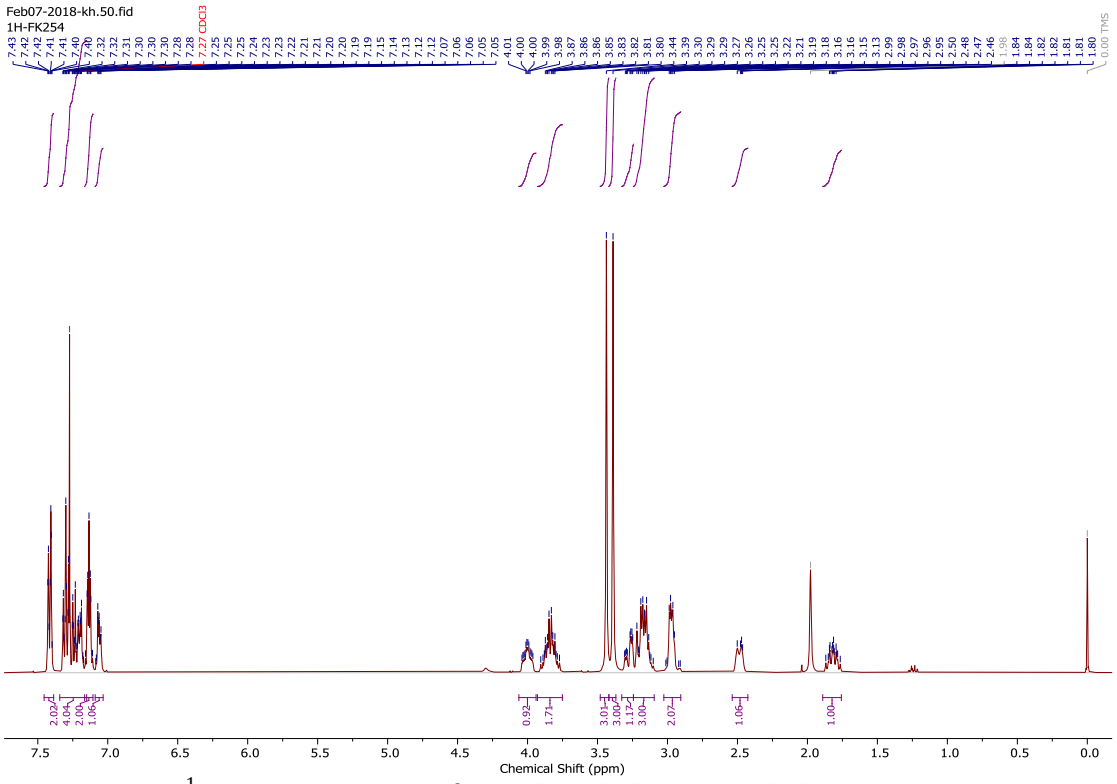


Figure S262. ^{1}H NMR spectrum of *N*,*N*-dimethyl-*N*-phenethyl-1,2,3,4-tetrahydronaphthalen-2-aminium iodide (**233**) ($CDCl_3$, 400 MHz)

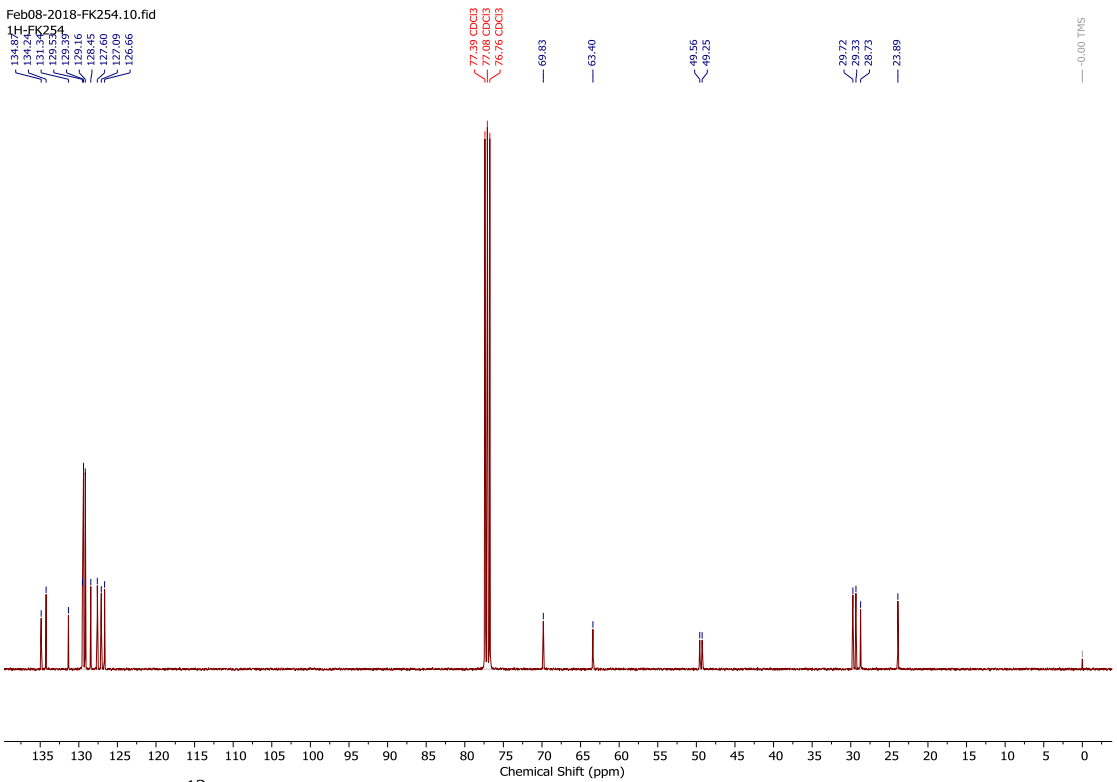


Figure S263. ^{13}C NMR spectrum of *N*,*N*-dimethyl-*N*-phenethyl-1,2,3,4-tetrahydronaphthalen-2-aminium iodide (**233**) ($CDCl_3$, 100 MHz)

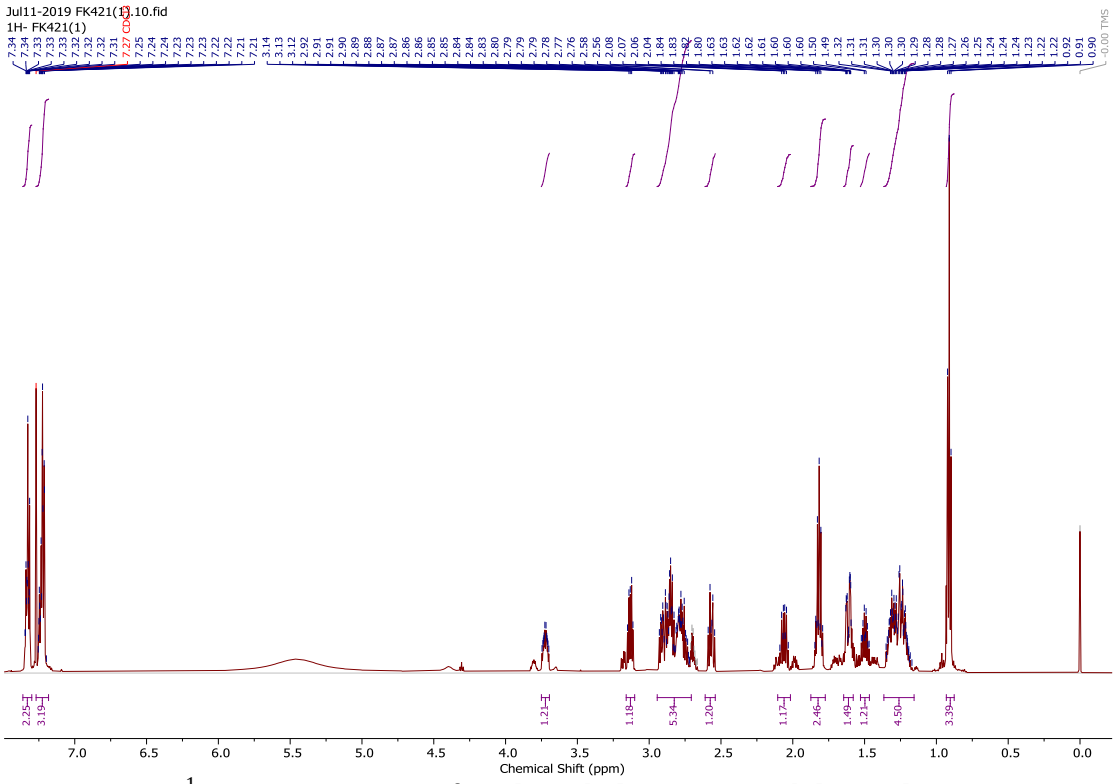


Figure S264. ^{1}H NMR spectrum of *N*-phenethyl-1-((*S*)-pyrrolidin-2-yl)pentan-2-amine (diastereomer 1 of **239**) ($CDCl_3$, 600 MHz)

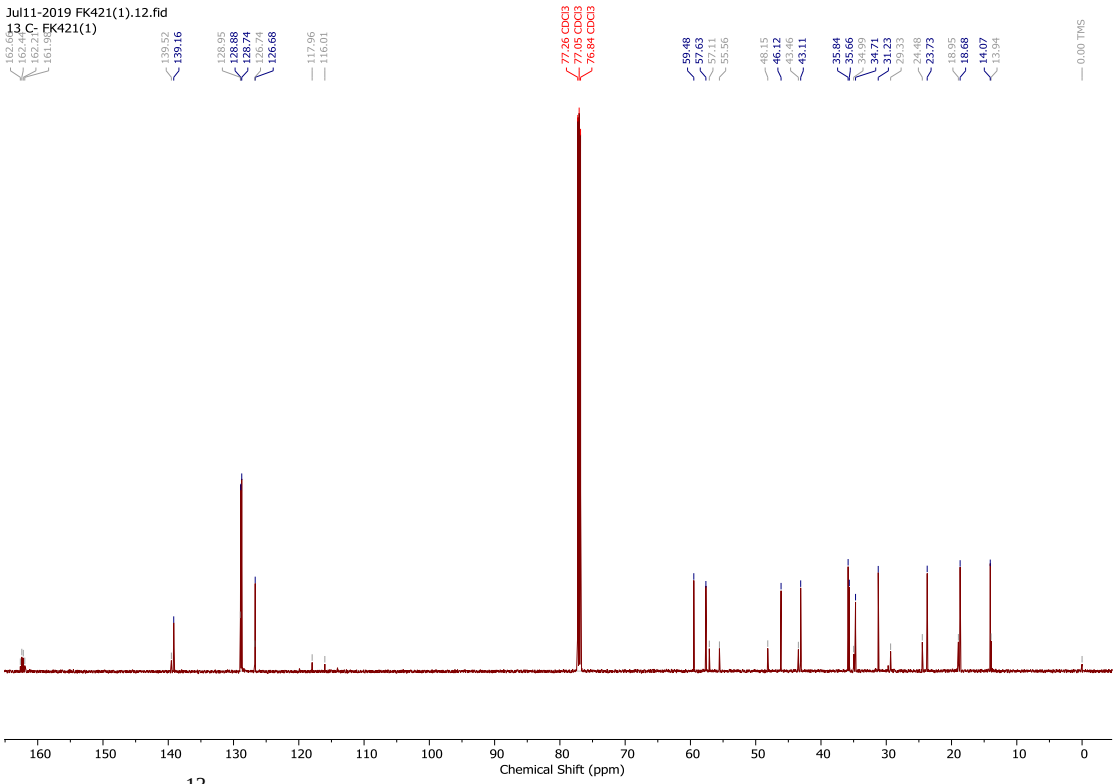


Figure S265. ^{13}C NMR spectrum of *N*-phenethyl-1-((*S*)-pyrrolidin-2-yl)pentan-2-amine (diastereomer 1 of **239**) ($CDCl_3$, 150 MHz)

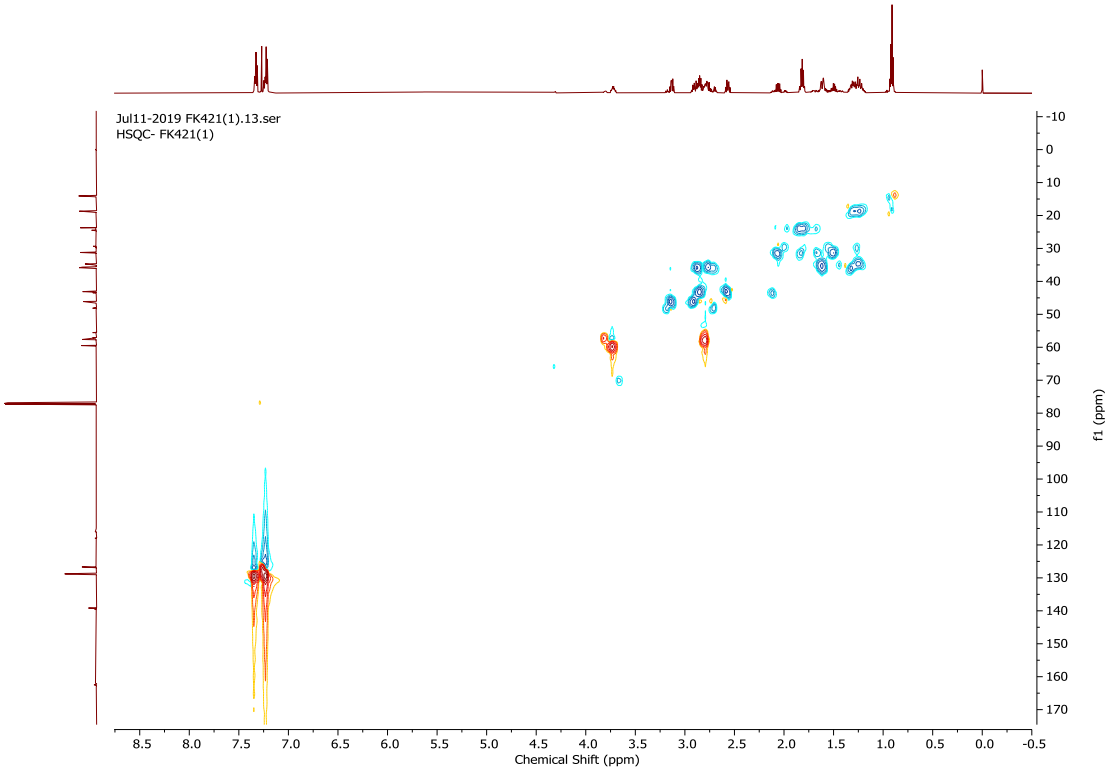


Figure S266. HSQC spectrum of *N*-phenethyl-1-((*S*)-pyrrolidin-2-yl)pentan-2-amine (diastereomer 1 of **239**) ($CDCl_3$, 600 MHz)

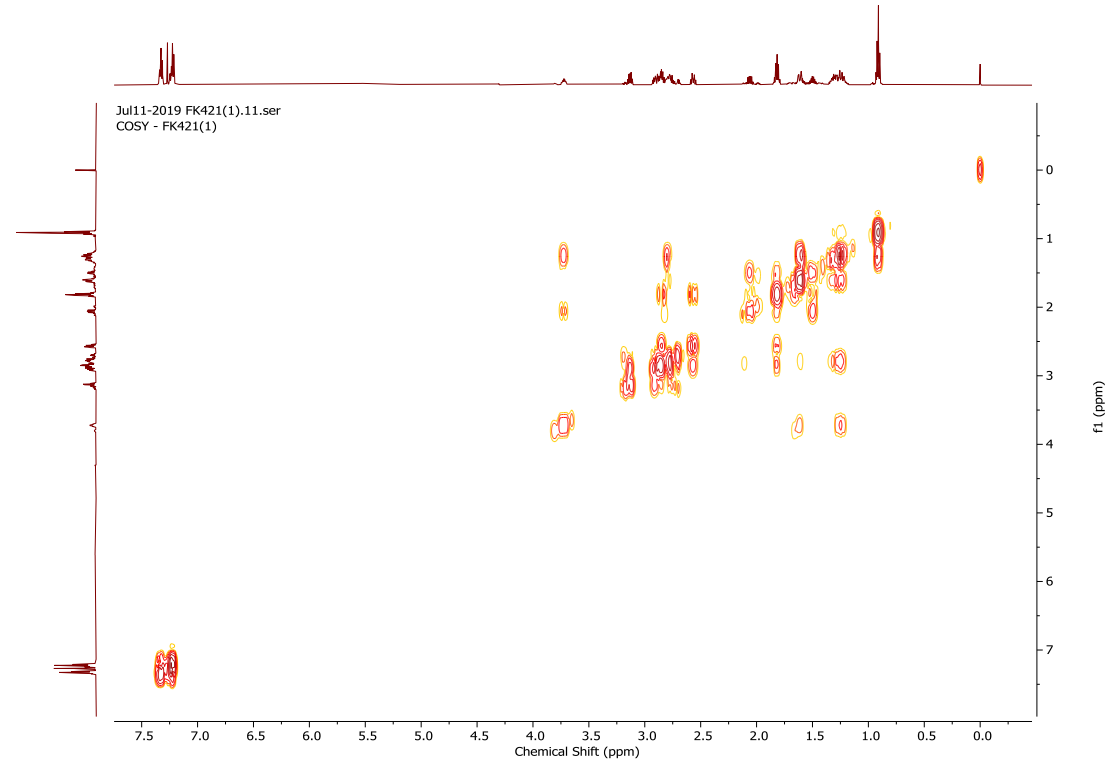


Figure S267. COSY spectrum of *N*-phenethyl-1-((*S*)-pyrrolidin-2-yl)pentan-2-amine (diastereomer 1 of **239**) ($CDCl_3$, 600 MHz)

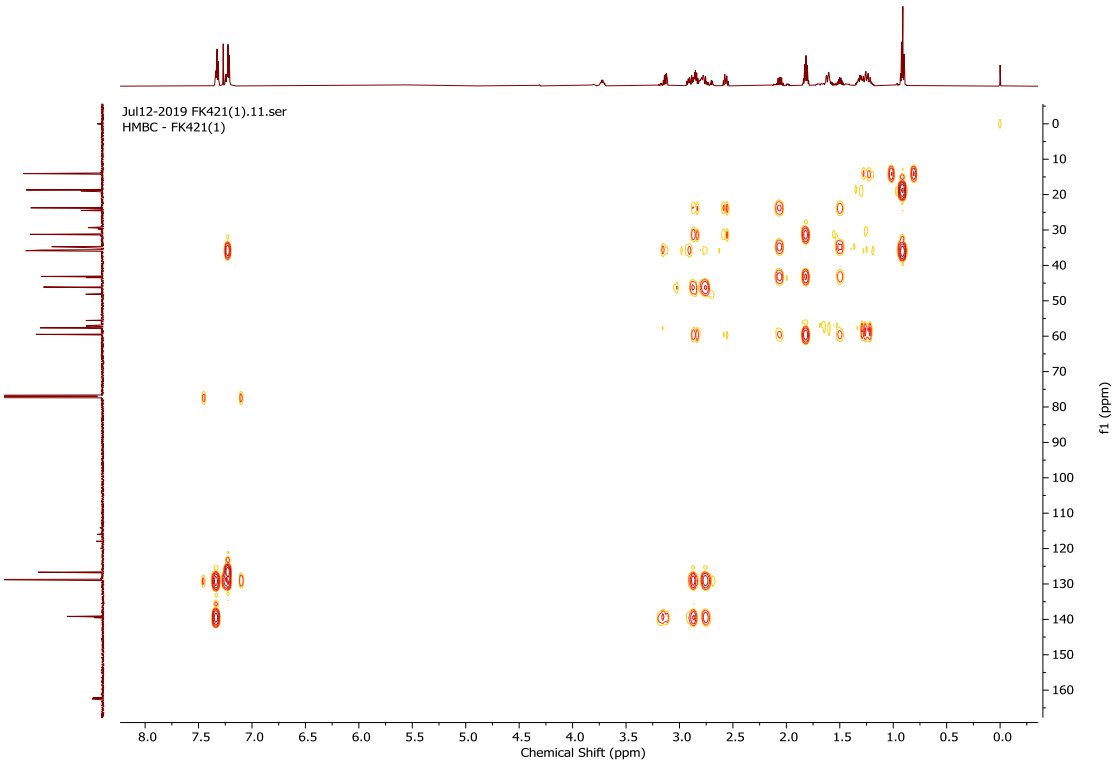


Figure S268. HMBC spectrum of *N*-phenethyl-1-((*S*)-pyrrolidin-2-yl)pentan-2-amine (diastereomer 1 of **239**) ($CDCl_3$, 600 MHz)

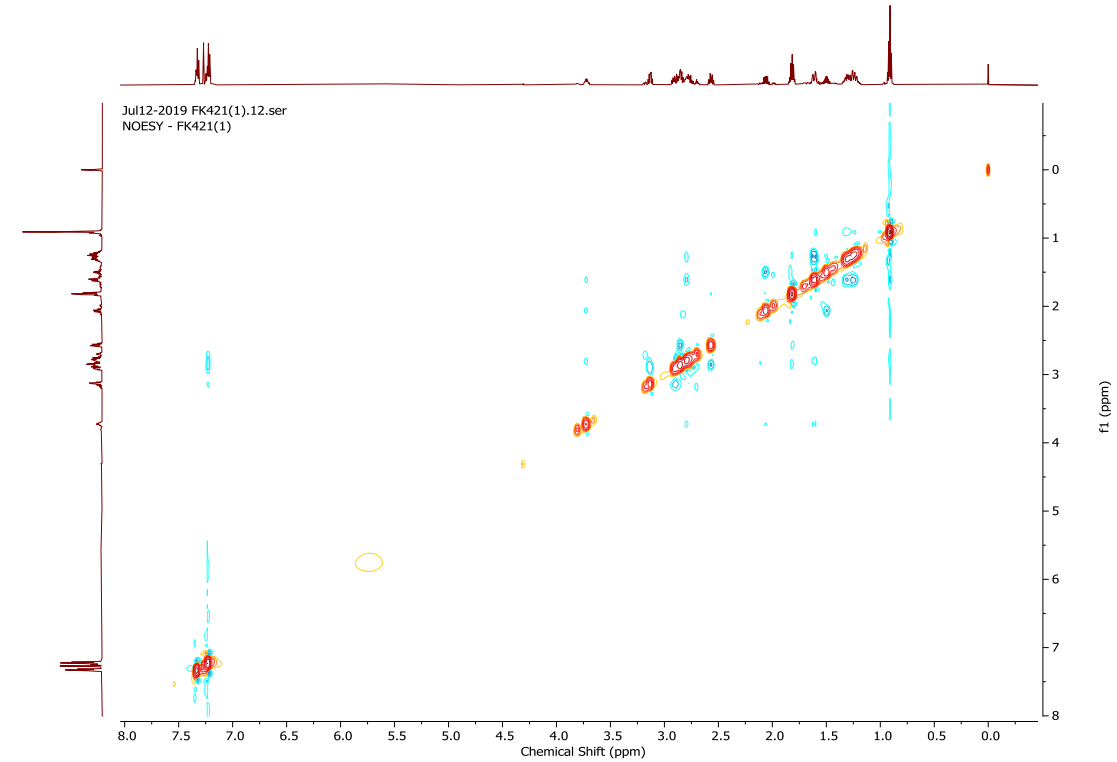


Figure S269. NOESY spectrum of *N*-phenethyl-1-((*S*)-pyrrolidin-2-yl)pentan-2-amine (diastereomer 1 of **239**) ($CDCl_3$, 600 MHz)

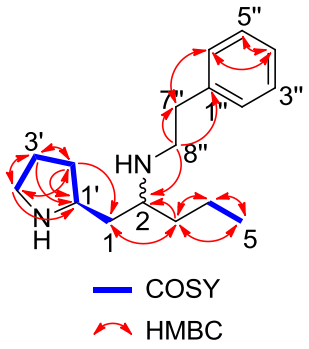


Figure S270. COSY and HMBC correlations of *N*-phenethyl-1-((*S*)-pyrrolidin-2-yl)pentan-2-amine (diastereomer 1 of **239**)

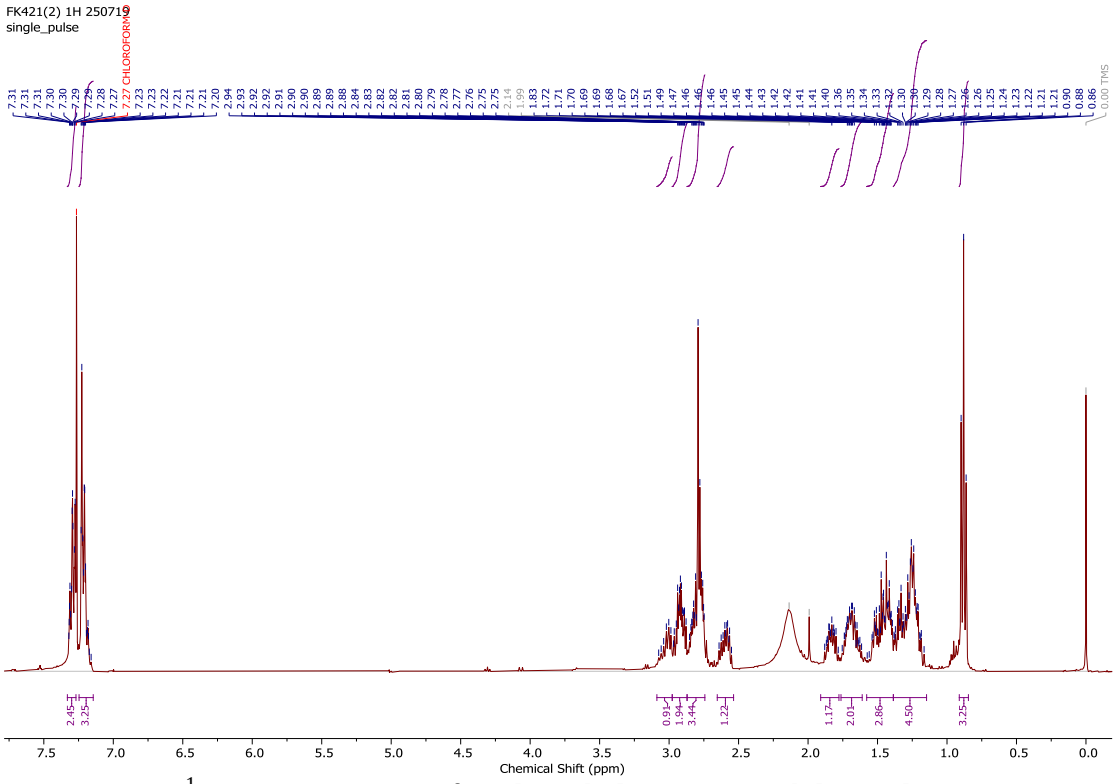


Figure S271. ^{1}H NMR spectrum of *N*-phenethyl-1-((*S*)-pyrrolidin-2-yl)pentan-2-amine (diastereomer 2 of **239**) ($CDCl_3$, 400 MHz)

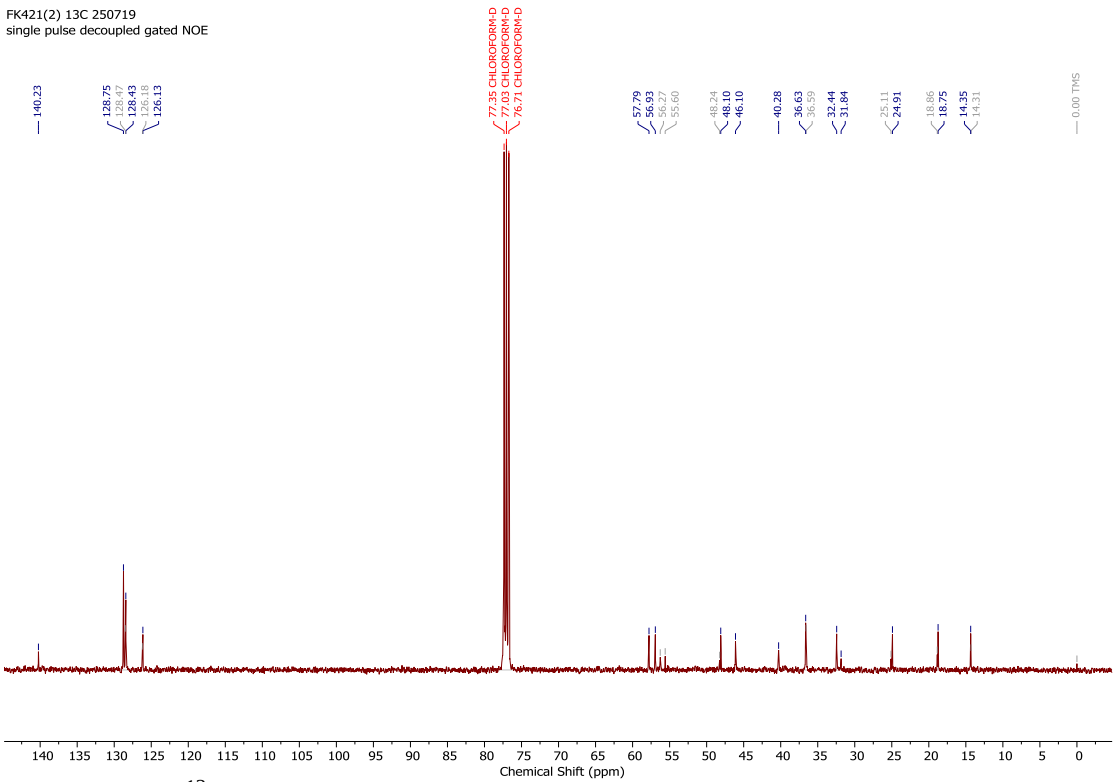


Figure S272. ^{13}C NMR spectrum of *N*-phenethyl-1-((*S*)-pyrrolidin-2-yl)pentan-2-amine (diastereomer 2 of **239**) ($CDCl_3$, 100 MHz)

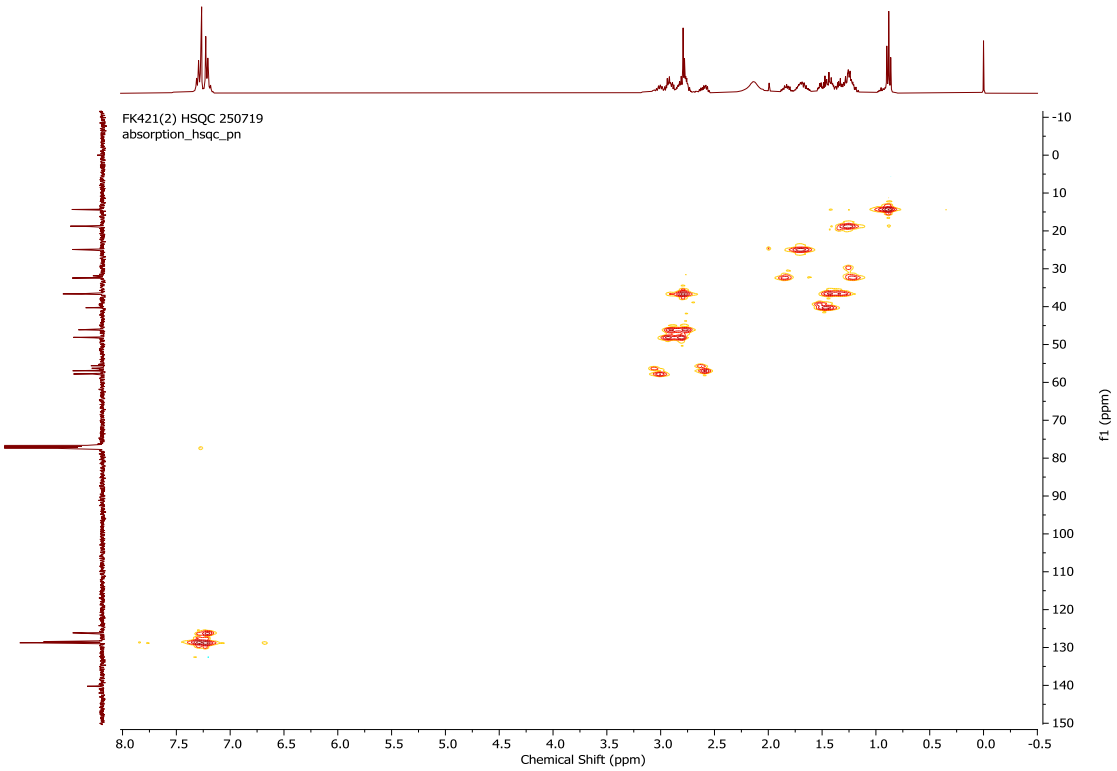


Figure S273. HSQC spectrum of *N*-phenethyl-1-((*S*)-pyrrolidin-2-yl)pentan-2-amine (diastereomer 2 of **239**) ($CDCl_3$, 400 MHz)

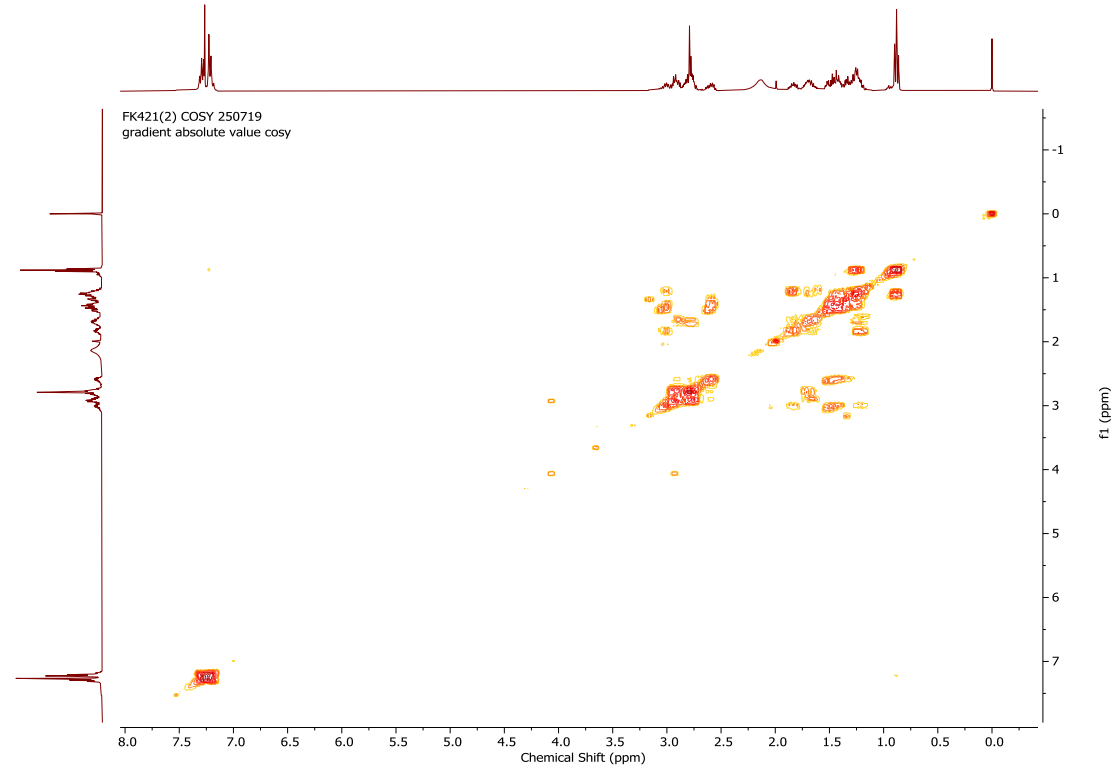


Figure S274. COSY spectrum of *N*-phenethyl-1-((*S*)-pyrrolidin-2-yl)pentan-2-amine (diastereomer 2 of **239**) ($CDCl_3$, 400 MHz)

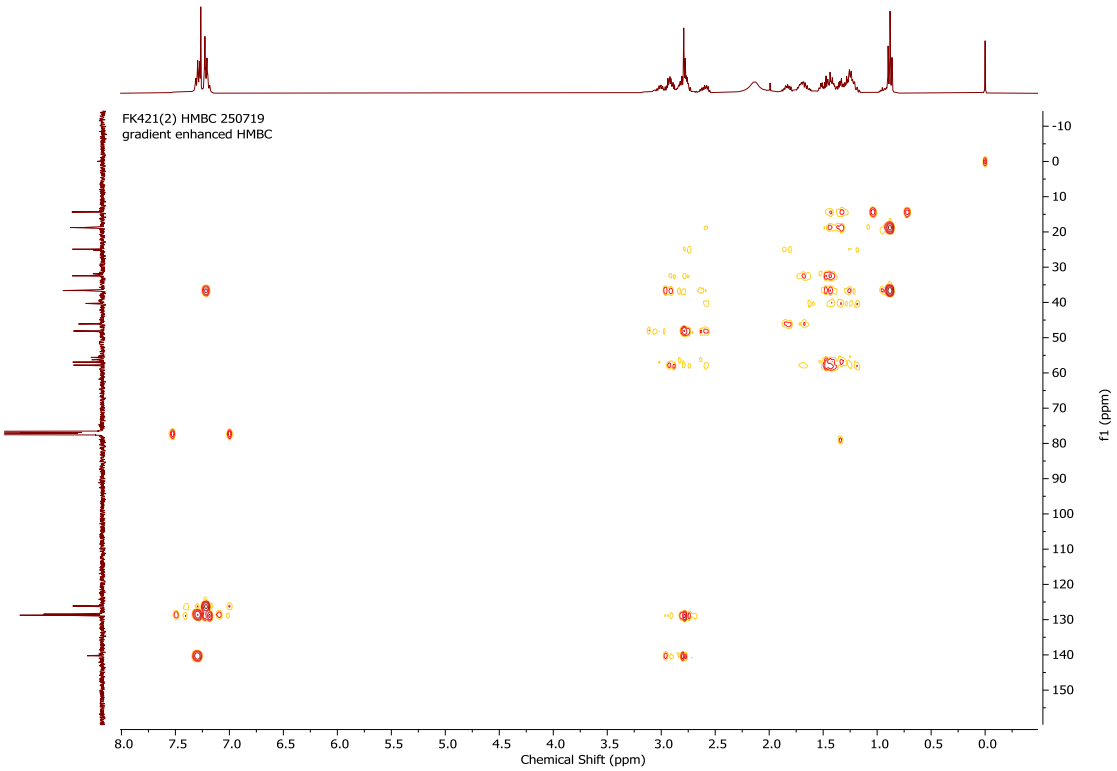


Figure S275. HMBC spectrum of *N*-phenethyl-1-((*S*)-pyrrolidin-2-yl)pentan-2-amine (diastereomer 2 of **239**) ($CDCl_3$, 400 MHz)

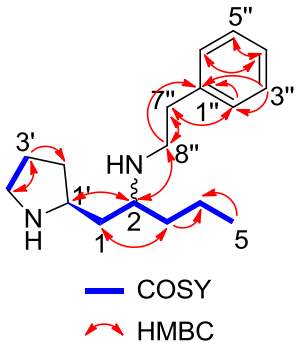


Figure S276. COSY and HMBC correlations of *N*-phenethyl-1-((*S*)-pyrrolidin-2-yl)pentan-2-amine (diastereomer 2 of **239**)

Animal Welfare and Ethical Review Body

Cover Form applicable to the use of animals in non-regulated procedures

Title of Study: **Investigation on the effect of natural product extracts and compounds on the isolated rat smooth muscles**

Name of Applicant: **Kang Nee TING**

School: **Life Sciences (Malaysia Campus)**

AWERB REF: UNMC12

1. Requests to use animals in non-regulated procedures must incorporate the information required below in the format requested for project licence applicants. The completed form should be returned electronically to the bsu@nottingham.ac.uk. When approved a protocol reference number will be provided to the applicant and must be used when ordering animals for use in the non-regulated study.

Its purpose is to highlight the key points in the proposed programme of work and to provide an executive summary in non-technical language accessible to the lay members of the Animal Welfare and Ethical Review Body.

Your application must be accompanied by this summary written in non-technical terms. You should complete this summary template. We expect that, for all but the most complex of studies, you will be able to provide a satisfactory summary using 500 to 1,000 words.

Study Title (max. 50 characters)	In-vitro organ bath experiments investigating effects of natural product extracts and isolated compounds on rat smooth muscles.		
Key Words (max. 5 words)	Isolated tissues; aorta; bladder; airway		
Expected duration of the study (yrs)	4 years (this is formed part of PhD projects, BSc Biomedical Sciences, MPharm year 4 research projects and a grant application to be submitted to the Malaysia government)		
Purpose of the study	Basic research	**Yes**	
	Translational and applied research		No
	Regulatory use and routine production		No
	Protection of the natural environment in the interests of the health or welfare of humans or animals		No
	Preservation of species		No
	Higher education or training	**Yes**	
	Forensic enquiries		No
	Maintenance of colonies of genetically altered animals[1]		No

Describe the objectives of the study (e.g. the scientific unknowns or scientific/clinical needs being addressed)	This application is divided into two main objectives: 1. MPharm year 3 and BSc Biomedical Sciences research projects: To enable students to further understand the pharmacology of smooth muscles including understanding the process of research in natural product drug discovery. 2. PhD projects: This forms part of the research skills training. In vitro organ bath technique will be one of the methodology to be included in the thesis. There are currently 3 students under my supervision using this technique of experiments
What are the potential benefits likely to derive from this study (how science could be advanced or humans or animals could benefit from the project)?	1. Students will gain a better understanding of the pharmacology of the smooth muscles in different vascular beds where technical skills will be gained as part of their training in undergraduate or postgraduate level. 2. These experiments will provide new information on the effect of active extracts and compounds isolated from the natural flora on isolated smooth muscles from the airways, bladder and aorta. We are moving to test new compounds synthesize based on the skeletal structure of novel compounds isolated from local plant species. 3. In Malaysia, the skills on isolated organ bath are limited and this forms part of an important technique for drug discovery.
What species and approximate numbers of animals do you expect to use over what period of time?	Adult rats will be utilised for these experiments. With the current set up, it is estimated about 3 to 4 animals will be used weekly.
What procedures will be conducted?	All animals will be sacrificed by an experienced animal technician according to the methods described in Schedule 1 of the UK Animals (Scientific Procedures) Act 1986.
In the context of what you propose to do to the animals, what are the expected adverse effects and the likely/expected level of severity? What will happen to the animals at the end?	No treatments will be carried out on living animals. After humane killing, the tissues will be removed for isolated organ bath experiments.

Application of the 3Rs	
1. Replacement State why you need to use animals and why you cannot use non-animal alternatives	The study of some of the pharmacology can only be meaningful when carried out in complex integrated tissues from animals. We have tried carrying out some experiments on primary smooth muscle cell lines and to date this has not been successful. Cell lines only provide limited information on the effects of the compounds and extracts that we have been working with. Answering a direct question, for example whether a compound would dilate the airway is only possible from investigations on the isolated smooth muscle rings.
2. Reduction Explain how you will assure the use of minimum numbers of animals	The maximum number of different organs from each animal will be utilised. For example, the aorta, bladder and airways (bronchus and trachea) will be used from each rat.
3. Refinement Explain the choice of species and why the animal model(s) you will use are the most refined, having regard to the objectives. Explain the general measures you will take to minimise welfare costs (harms) to the animals.	At present no other sources of animal tissues are available but, for future planning, sourcing animal tissues from sheep obtained from local slaughter houses will be considered to minimise the use of rats in these experiments.
4. Housing and Care Please confirm that animals will be housed and cared for according to the requirements of the UK Animals (Scientific Procedures) Act 1986 draft Code of Practice for the care and accommodation of animals (February 2013) **or** provide details and justification for alternative housing and care standards.	Animals will be purchased from the animal facilities in University Putra Malaysia (UPM) and University Kebangsaan Malaysia (UKM) Both of these animal facilities are governed by their own institutional animal care and use committee (IACUC). They adhere to the Malaysian code of practice for the care and use of animals for scientific purposes which are consistent with the UK Home Office regulations. Information on the facility can be found here http://www.vet.upm.edu.my/eiacuc.html (UPM) http://www.kkl.ukm.my:8080/laru/wp-content/uploads/2013/03/UKMAEC-GUIDELINE-2007.pdf (UKM)

5. Humane Killing Please confirm that animals will be humanely killed using an appropriate method of humane killing detailed in Schedule 1 of the UK Animals (Scientific Procedures) Act 1986 **or** provide details and justification for alternative methods of killing.	Animals will be killed by concussion of the brain and/or exposure to carbon dioxide gas. Death is confirmed by dislocation of the neck.
For Office Use Only	
Will the study be subject to Retrospective Assessment?	Yes | No | Date due:

Committee use only

Comments by NACWO:

The proposed project appears appropriate with no welfare issues providing animals are humanely killed by trained and competent staff.
Neil Yates
05.09.13

Amendment 07/12/16
The request to source animals from an additional University is reasonable and confirmation has been received that both animal providers adhere to the Malaysian Code of Practice. However additional information on actual standards of animal care has been requested as the standards in place are not clear from the web links provided.
Neil Yates
07/12/16

Confirmation received - OK to proceed.
NY 13/03/17

Comments by NVS:

This would appear to be satisfactory, although an approximation for the total number of rats to be used per year or over the lifetime of the project should be given. Users should be trained to a level of competency that will ensure humane euthanasia is achieved at all times.

Ewan McNeill 05-09-13

I am happy with the information provided.
E. McNeil 13/3/17

We have contacted the animal house at UPM. The technician confirms that the rats are kept between 18 and 20 C. Reply from Kang Nee Ting 15/2/17

Dear Annemarie

Please find attached the requested information on benefits accrued from this work.

From our record we have used 318 rats between September 2014 until now. Many thanks.
Best wishes
Kang Nee

Update on research output following the approval of
UNMC2kn Publication list

PhD thesis of Bi Juin Loong 2016: Development of a functional bioassay to study the mechanism of action of a novel phenylethylamine alkaloid, schwarzinicine

BJ Loong, KH Lim, Y Mbaki and KN Ting: Calcium mobilisation and relaxant properties of a novel phenyethylamine alkaloid, schwarzinicine A (In preparation)

Mei-Kee Lee, Kuan-Hon Lim, Chon-Seng Tan, Szu-Ting Ng, Sue-Mian Then, Suresh Kumar Mohankumar, Kang-Nee Ting: Bronchodilator effects of *Lignosus rhinocerotis* extract on rat isolated airways is linked to the blockage of calcium entry (Submitted to Journal of Phytomedicine).

Jun-Lee Lim, Kae-Shin Sim, Kien-Thai Yong, Bi-Juin Loong, Kang-Nee Ting, Siew-Huah Lim, Yun-Yee Low, Toh-Seok Kam: Biologically active vallesamine, strychnan, and rhazinilam alkaloids from Alstonia: Pneumatophorine, a nor-secovallesamine with unusual incorporation of a 3-ethylpyridine moiety. *Phytochemistry* 09/2015; 117.

Suet-Pick Wong, Chew-Yan Gan, Kuan-Hon Lim, Kang-Nee Ting, Yun-Yee Low, Toh-Seok Kam: Arboridinine, a Pentacyclic Indole Alkaloid with a New Cage Carbon–Nitrogen Skeleton Derived from a Pericine Precursor. *Organic Letters* 07/2015; 17(14):3628-3631.

B J Loong, J H Tan, K H Lim, Y Mbaki, K N Ting: Contractile function of smooth muscle retained after overnight storage. *Naunyn-Schmiedeberg's Archives of Pharmacology* 06/2015; 388(10):1061-1067.

Veronica Alicia Yap, Bi-Juin Loong, Kang-Nee Ting, Sandy Hwei-San Loh, Kien-Thai Yong, Yun-Yee Low, Toh-Seok Kam, Kuan-Hon Lim: Hispidacine, an unusual 8,4'-oxyneolignan-alkaloid with vasorelaxant activity, and hispiloscine, an antiproliferative phenanthroindolizidine alkaloid, from Ficus hispida Linn. *Phytochemistry* 01/2015; 109:96-102.

Choy-Eng Nge, Chew-Yan Gan, Kuan-Hon Lim, Kang-Nee Ting, Yun-Yee Low, Toh-Seok Kam: ChemInform Abstract: Criofolinine and Vernavosine, New Pentacyclic Indole Alkaloids Incorporating Pyrroloazepine and Pyridopyrimidine Moieties Derived from a Common Yohimbine Precursor. *Organic Letters* 12/2014; 46(21).

Students trained

Bi Juin Loong PhD, graduated 2016
Mei Kee Lee, 3rd year PhD
Kayatri Govindaraju, 2nd year PhD
Fong Kai Lee, 1st year PhD
Undergraduates (final year projects for MPharm and BSc Biomedical Sciences & summer placements) > 10

Justification for extension of the work

At present, we have 3 active PhD students (see the list above) using the post mortem tissues for their organ bath experiments. We have also completed a grant from the Ministry of Higher Education entitled "Mechanism of action of Lignosus rhinocerus (Tiger Milk Mushroom) on airway smooth muscle contractility and mast cells degranulation". We are currently preparing two proposals to be submitted to Newton Senior Fellowship and Wellcome Fellowship for the extension of the Tiger Milk Mushroom work. In addition, we have just submitted two grant

applications to the Ministry of Higher Education to study a series of novel compounds with vasorelaxation effects.
These are our justification for requesting extension of the ethics application for another 4 years from Sept 2017 to August 2021.

Comments by primary reader for the Committee (if applicable):

Comments by Lay Person (If applicable):

Committee decision: Approved

Communicated to applicant (date): 13/3/17

Animal Welfare and Ethical Review Body

Cover Form applicable to the use of animals in non-regulated procedures

Title of Study: **Investigation on Schwarzinicine A (Sch A), a novel pheylethylamine alkaloid, and its derivatives on their effects in isolated tissues obtained from spontaneous hypertensive rats (SHR)**

Name of Applicant: **Kang Nee TING**

School: **Life Sciences (Malaysia Campus)**

AWERB REF: UNMC18

1. Requests to use animals in non-regulated procedures must incorporate the information required below in the format requested for project licence applicants. The completed form should be returned electronically to the bsu@nottingham.ac.uk. When approved a protocol reference number will be provided to the applicant and must be used when ordering animals for use in the non-regulated study.

Its purpose is to highlight the key points in the proposed programme of work and to provide an executive summary in non-technical language accessible to the lay members of the Animal Welfare and Ethical Review Body.

Your application must be accompanied by this summary written in non-technical terms. You should complete this summary template. We expect that, for all but the most complex of studies, you will be able to provide a satisfactory summary using 500 to 1,000 words.

Study Title (max. 50 characters)	Investigation on Schwarzinicine A (Sch A), a novel pheylethylamine alkaloid, and its derivatives on their effects in isolated tissues obtained from spontaneous hypertensive rats (SHR)		
Key Words (max. 5 words)	Isolated tissues; aorta; bladder; airway		
Expected duration of the study (yrs)	3 years (this forms part of three/four PhD projects and three research proposals awarded in 2017 by the Ministry of Higher Education and Toray Foundation)		
Purpose of the study	Basic research	**Yes**	
	Translational and applied research		No
	Regulatory use and routine production		No
	Protection of the natural environment in the interests of the health or welfare of humans or animals		No
	Preservation of species		No
	Higher education or training	**Yes**	
	Forensic enquiries		No

	Maintenance of colonies of genetically altered animals[1]		No

Describe the objectives of the study (e.g. the scientific unknowns or scientific/clinical needs being addressed)	The objectives of the study are: 1. To compare the effectiveness and the potency of a series of newly synthesised compounds based on the phamacophore of Sch A in the isolated aorta of SHRs. We have some data from previous work to show that these compounds are more efficacious in SHR when compared to normotensive rats (see Appendix 1). 2. To further understand the mechanism of action of Sch A (and derivatives) in SHR. We have data to support the role of calcium entry and and interference of Gq-coupled activation of receptor are affected by Sch A (see Appendix 2). 3. To study the selectivity of Sch A (and derivatives) on other smooth muscle tissues such as bladder and trachea. All the experiments will be carried out in organ bath experiments set up.
What are the potential benefits likely to derive from this study (how science could be advanced or humans or animals could benefit from the project)?	1. Students will gain a better understanding of the pharmacology of the smooth muscles in different rat species where technical skills will be gained as part of their PhD training. 2. These experiments will provide new information on the effect of these active compounds on isolated smooth muscles from the airways, bladder and aorta in SHR. 3. In Malaysia, the skills on isolated organ bath are limited and this forms part of an important technique for drug discovery. 4. We are able to understand the mechanism of action of Sch A (and derivatives) potentially file a patent of their applications for treatment of hypertension. We have some data to support the action via TRPC channels. This would be a novel target for treatment of hypertension.
What species and approximate numbers of	Adult rats will be utilised for these experiments. With the current set up, it is estimated about 4

animals do you expect to use over what period of time?	animals will be used for a period of 5 to 6 weeks in a year. An estimate of not more than 80 SHRs to be used for the next 3 years.
What procedures will be conducted?	All animals will be sacrificed by an experienced animal technician according to the methods described in Schedule 1 of the UK Animals (Scientific Procedures) Act 1986.
In the context of what you propose to do to the animals, what are the expected adverse effects and the likely/expected level of severity? What will happen to the animals at the end?	No treatments will be carried out on living animals. After humane killing at the University of Monash (Malaysia campus) animal facility, the tissues will be removed for isolated organ bath experiments.
Application of the 3Rs	
1. Replacement State why you need to use animals and why you cannot use non-animal alternatives	The study of some of the pharmacology can only be meaningful when carried out in complex integrated tissues from animals. We have tried carrying out some experiments on primary smooth muscle cell lines and to date this has not been successful. Cell lines only provide limited information on the effects of the compounds and extracts that we have been working with. Answering a direct question, for example whether a compound would dilate the airway is only possible from investigations on the isolated smooth muscle rings. We have a series of data on the functional responses in normotensive rats and we would like to investigate if the SHRs will be more sensitive to our compounds with smooth muscle relaxant activities.
2. Reduction Explain how you will assure the use of minimum numbers of animals	The maximum number of different organs from each animal will be utilised. For example, the aorta airways (bronchus and trachea) will be used from each rat for two different projects. The extra tissues will be frozen for staining and protein expression work subsequently.
3. Refinement Explain the choice of species and why the animal model(s) you will use are the most refined, having regard to the objectives. Explain the general measures you will take to	At present no other sources of animal tissues are available but, for future planning, sourcing animal tissues from sheep obtained from local slaughter houses will be considered to minimise the use of rats in these experiments.

minimise welfare costs (harms) to the animals.	
4. Housing and Care Please confirm that animals will be housed and cared for according to the requirements of the UK Animals (Scientific Procedures) Act 1986 draft Code of Practice for the care and accommodation of animals (February 2013) **or** provide details and justification for alternative housing and care standards.	Animals will be purchased from the animal facilities in a local university (University of Monash Malaysia) This animal facility is governed by its own institutional animal care and use committee (IACUC). They adhere to the guidelines prepared by the Expert Working Group of the Animal Welfare Committee of the National Health and Medical Research Council, Australia (see attached guidelines).
5. Humane Killing Please confirm that animals will be humanely killed using an appropriate method of humane killing detailed in Schedule 1 of the UK Animals (Scientific Procedures) Act 1986 **or** provide details and justification for alternative methods of killing.	Animals will be killed by concussion of the brain and/or exposure to carbon dioxide gas. Death is confirmed by dislocation of the neck.
For Office Use Only	
Will the study be subject to Retrospective Assessment?	Yes | No | Date due:

Committee use only

Comments by Experimental Officer:
A relatively small number of SHR rats have been proposed over the 3 yr period. No *in vivo* work will take place. The rats will be culled by a S1 method and a range of tissues removed. A comparable approach have been used in the past involving normotensive and SHR rats (UNMC 2, UNMC6 and UNMC12).

- **Could you provide a brief experimental plan to explain how you will meet the objectives** (e.g. what data will be required, use of controls. NY 10/04/18). Response: See Annex 1

- **Please provide the same assurances are in place as before regarding:**
  a) checking that the rats are hypertensive before culling takes place
  b) the competency of the person carrying out the humane killing of the rats and
  c) the ability to transport the tissues in a manner which does not affect the viability of the tissues.

Response: The rats will be obtained and killed at the animal facility of University of Monash which is about 40km away from the Nottingham Campus. The required tissues will be removed immediately at Monash and transported back to Nottingham in ice cold Krebs. This protocol has been used previously and the results obtained did not show any loss of tissue viability. A trained technician in Monash University will take the blood pressure using the tail cuff method a day before the sacrificing of the rats by humane killing. He will supply adult rats that registered systolic blood pressure of between 170mmHg and 210mmHg.

A.Kelly 13/3/18

Comments by NVS:

This would appear to be a reasonable request and the applicant has stated specific aims for the study. Can you confirm;

- **No normal rats are required as controls for comparison studies?**

  Response: We have done a series of work on normal rats as control (Sprague Dawley rats under the approved applications UNMC2kn and UNMC12). The current work will be to compare our observations in SD and SHR tissues.

- **There will be no more than 80 SHRs used over the 3 year period (I was unsure how this links to '4 animals will be used for a period of 5 to 6 weeks in a year').**
  (If presumed that this is 4 rats over a 5 week period giving 10 periods per year = 40 rats per year for 3 years then approximately 120 rats and not 80 rats in total could be used over the 3 years of this study – clarification required. NY 10/04/18)

  Response: We plan to use 4 rats per week for a short period of 6 weeks or 6 rats per week for 5 weeks. For the first phase of work we will order 30 rats. Phase two or three will be carried out with the remaining rats in the next two years if we have newer compounds to test in SHR or to clarify the mechanism of these compounds in SHR tissues. We do not plan to use more than 80 rats in total for a period of 3 years.

Ewan McNeill 09-04-18

Comments by primary reader for the Committee (if applicable):

Comments by Lay Person (If applicable):

Committee decision:

Approved following Clarification – NY 13/04/18

Communicated to applicant (date): 13/04/18